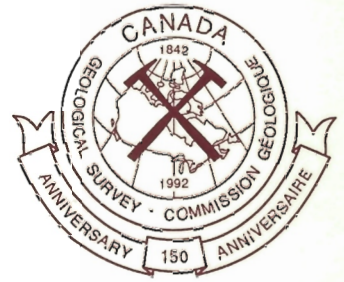


**GEOLOGICAL SURVEY
OF CANADA
MEMOIR 420**



This document was produced
by scanning the original publication.

Ce document est le produit d'une
numérisation par balayage
de la publication originale.

The Late Cenozoic Mount Edziza Volcanic Complex, British Columbia



J.G. Souther

1992

GEOLOGICAL SURVEY OF CANADA
MEMOIR 420

**THE LATE CENOZOIC MOUNT EDZIZA
VOLCANIC COMPLEX, BRITISH COLUMBIA**

J.G. Souther

1992

© Minister of Supply and Services Canada 1992

Available in Canada through
authorized bookstore agents and other bookstores

or by mail from

Canada Communication Group - Publishing
Ottawa, Canada K1A 0S9

and from

Geological Survey of Canada offices:

601 Booth Street
Ottawa, Canada K1A 0E8

3303-33rd Street N.W.,
Calgary, Alberta T2L 2A7

100 West Pender Street
Vancouver, B.C. V6B 1R8

A deposit copy of this publication is also available for reference
in public libraries across Canada

Cat. No. M46-420E
ISBN 0-660-14407-7

Price subject to change without notice

Critical Reader

J.A. Roddick

Author's address

*Cordilleran Division
100 West Pender Street
Vancouver, B.C.
V6B 1R8*

Cover photo description

For cover photo description see Frontispiece description, page x.

*Original manuscript received: 1985-01
Final version approved for publication: 1987-02*

Preface

The Mount Edziza Volcanic Complex is one of several volcanic terranes in the Cordilleran region which are located along linear belts related to the modern tectonic environment. The complex is the product of episodic eruptions which began in the Late Miocene and continued into Recent time, producing a host of overlapping volcanic shields, central volcanoes, and small calderas. It was selected for detailed study because of its longevity, diverse lithology and exceptional exposures of both volcanic and subvolcanic units provided by deeply incised valleys. Precise mapping and detailed stratigraphy are combined with petrographic and chemical data, geochronology, and geomorphology to document the history of the complex from the petrogenesis of its diverse magmas to the rapidly changing landscape resulting from the interaction of successive volcanoes with glaciers and rivers.

The complex is a bimodal assemblage of alkaline, shield-forming basalts and a lesser volume of mostly peralkaline oversaturated rocks which form domes and composite central volcanoes. The suite is analogous to that associated with continental rift zones and thus has important implications with respect to the neotectonic setting of the northern Cordillera and the genesis of peralkaline magma. The history and nature of recent activity provide criteria for assessing the probability and impact of future eruptions and the potential for an associated geothermal resource.

The dramatic examples of both ancient and modern volcanic structures and landforms exposed in the Mount Edziza Volcanic Complex have led to its designation as a Provincial Park. In response to this use as a natural history resource the author has augmented the scientific documentation, contained in the main report, with an extensive summary designed to help nontechnical readers and park visitors appreciate the complex history of volcanic and glacial events which shaped the present landscape.

Elkanah A. Babcock
Assistant Deputy Minister
Geological Survey of Canada

Préface

Le complexe volcanique de Mount Edziza est un de plusieurs terrains volcaniques de la région de la Cordillère qui sont situés le long de zones linéaires associées à l'environnement tectonique contemporain. Le complexe est le produit d'éruptions épisodiques qui ont débuté à la fin du Miocène et se sont poursuivies durant la période holocène, produisant une série de boucliers volcaniques chevauchants, de volcans centraux et de petites caldeiras. Il a été choisi pour faire l'objet d'une étude détaillée à cause de sa longévité, de sa lithologie variée et de l'exposition exceptionnelle d'unités volcaniques et sous-volcaniques découvertes dans les vallées profondément encaissées. Un travail de cartographie précis et une étude stratigraphique détaillée, combinés aux données pétrographiques, chimiques, géochronologiques et morphologiques disponibles, révèlent l'histoire du complexe depuis la pétrogénèse de ces divers magmas jusqu'au paysage actuel dont l'évolution rapide est le produit de l'interaction des volcans successifs avec des glaciers et des cours d'eau.

Le complexe est une association bimodale de basaltes alcalins formant boucliers et d'un volume moindre de roches sursaturées, en grande partie hyperalcalines, qui forment des dômes et des strato-volcans centraux. L'ensemble est analogue à celui qui est associé aux zones d'effondrement continentales et a donc des répercussions importantes au niveau du cadre néotectonique du nord de la Cordillère et sur la genèse du magma hyperalcalin. L'histoire et la nature de l'activité récente du complexe fournissent des critères d'évaluation de la probabilité et de l'incidence des éruptions futures ainsi que de la possibilité d'utiliser le complexe comme ressource géothermique.

Les exemples exceptionnels de structure et de relief volcaniques tant anciens que contemporains que révèle le complexe volcanique du Mount Edziza ont contribué à sa désignation comme parc provincial. En raison donc de l'élévation du complexe à l'état de ressource d'un grand intérêt dans le domaine de l'histoire naturelle, l'auteur a ajouté à la documentation scientifique contenue dans le rapport principal, un long résumé dont l'objet est d'aider les lecteurs et les visiteurs des parcs ne possédant pas de connaissances techniques à apprécier l'histoire complexe des épisodes volcaniques et glaciaires qui ont modelé le paysage actuel.

Elkanah A. Babcock
Sous-ministre adjoint
Commission géologique du Canada

CONTENTS

1	Abstract/Résumé
2	Summary/Sommaire
31	INTRODUCTION
31	Location and access
31	Physiography
33	Drainage and glaciation
36	Previous investigations and present study
37	Field and laboratory methods
37	Acknowledgments
39	TECTONIC SETTING
39	Major tectonic elements
39	Stikine Volcanic Belt
41	BASEMENT GEOLOGY
41	Structural setting
41	Paleozoic rocks
41	Mesozoic rocks
43	Tertiary rocks
44	Pre-Edziza tertiary erosion surface
47	RASPBERRY FORMATION
47	General geology
47	Flow morphology and depositional environment
47	Regional variations in flow morphology
51	Subaqueous facies
51	Stratigraphy
53	Petrography
54	Aphyric and slightly feldsparphyric basalt (types 1 and 2)
55	Highly feldsparphyric basalt (type 3)
56	Pyroxene-phyric basalt (type 4)
57	Amygdules
58	Chemistry
61	LITTLE ISKUT FORMATION
61	General geology
61	Introduction
61	Lower unit
61	Upper unit
64	Subvolcanic structures
64	Origin
66	Petrography
69	Chemistry
71	ARMADILLO FORMATION
71	General geology
71	Felsic rocks
71	Cartoona Ridge centre
76	Armadillo caldera
78	Tadedá centre
79	IGC centre
81	Distal facies
83	Armadillo basalt
83	Stratigraphy
83	Petrography
83	Basalts

84	Felsic rocks
84	Holocrystalline rocks
86	Vitreous rocks
89	Ash flows
89	Intrusive rocks
90	Chemistry
93	NIDO FORMATION
93	General geology
93	Introduction
93	Tenchen Member
93	Alpha peak
98	Beta peak
99	Palagonite lake
101	Gamma peak
104	Kounugu Member
105	Swarm peak
106	Vanished peak
106	Lost peak
108	Exile hill
108	Petrography
112	Chemistry
113	SPECTRUM FORMATION
113	General geology
113	Main lava dome
115	Flow morphology
115	Soda rhyolite and comendite
117	Pantelleritic trachyte
119	Pyroclastic deposits
119	Flow mechanics
119	Yeda Peak eruptive centre
120	Fumarolic alteration
120	Subvolcanic intrusions and caldera collapse
120	Satellitic vents
122	Kitsu Member
123	Petrography
123	Felsic rocks
123	Kitsu basalt
125	Chemistry
125	Felsic rocks
128	Kitsu basalt
129	PYRAMID FORMATION
129	General geology
129	Introduction
129	Basal pyroclastic member
129	Basalt member
132	The Pyramid
134	Sphinx dome
135	Pharaoh dome
137	Tut lake volcanoclastic deposits
141	Petrography
143	Chemistry
145	ICE PEAK FORMATION
145	General geology
145	Introduction
145	Pre-Ice Peak surface
147	Lower assemblage
149	Ice-contact deposits

150	Upper assemblage
150	Central cone and proximal deposits
152	Subvolcanic intrusions
154	Satellitic centres
154	The neck
155	Ornostay and Koosick centres
155	Distal flows
156	Subordinate centres
159	Petrography
159	Basalt
162	Intermediate rocks
162	Trachyte
163	Cumulate inclusions
163	Chemistry
165	PILLOW RIDGE FORMATION
165	General geology
165	Introduction
165	Pillow Ridge
172	Tsekone Ridge
172	Accidental inclusions
173	Petrography
174	Chemistry
175	EDZIZA FORMATION
175	General geology
175	Introduction
175	Pre-Edziza surface
175	Central composite cone
177	Satellitic vents
179	Lava domes
182	Lava flows
184	Subvolcanic intrusions
184	Hydrothermal alteration
185	Lava lakes
185	Petrography
185	Trachyte and comenditic trachyte
187	Inclusions
190	Chemistry
191	KLASTLINE FORMATION
191	General geology
197	Petrography
197	Chemistry
199	ARCTIC LAKE FORMATION
199	General geology
199	Introduction
199	Preglacial phase
200	Intraglacial stage
200	Late glacial stage
205	Petrography
205	Chemistry
207	KAKIDDI FORMATION
207	General geology
207	Introduction
207	Flows and pyroclastic deposits
207	Eruptive centres
210	Petrography
212	Chemistry

213	BIG RAVEN FORMATION
213	General geology
213	Introduction
213	Desolation Lava Field
216	Sleet Cone (DLF-1) and Storm Cone (DLF-2)
219	Triplex Cones (DLF-3 to DLF-5)
219	Sidas Cone (DLF-6) and Twin Cone (DLF-7)
222	Moraine Cone (DLF-8)
222	Eve Cone (DLF-9) and Williams Cone (DLF-10)
224	Kana Cone
226	East slope centres
228	Snowshoe Lava Field
230	Subglacial centres (SLF-1 to SLF-3)
231	Transitional centres (SLF-4 to SLF-8)
232	Subaerial centres (SLF-9 to SLF-12)
234	Walkout Creek centres
235	Mess Lake Lava Field
235	Arctic Plateau
236	Sheep Track Member
237	Petrography
238	Chemistry
241	THERMAL SPRINGS
241	Elwyn Hotsprings
241	Taweh Hotsprings
241	Mess Lake Hotsprings
242	Mess Creek Hotsprings
242	Geochemistry of thermal waters
245	GEOCHRONOLOGY
245	Potassium-argon
245	Fission-track
252	Paleomagnetism
253	Radiocarbon
255	PETROCHEMISTRY
255	Introduction
255	Mineral chemistry
256	Feldspar
256	Pyroxene
257	Olivine
257	Amphibole
258	Aenigmatite
259	Iron-titanium oxides
260	Whole-rock chemistry
260	Major elements
262	Minor elements
262	Minor-element distribution
262	Rare-earth elements
264	Rb, Sr and Sr isotopes
267	PETROGENESIS
267	Major-element model
268	Alkali olivine basalt-trachybasalt-trachyte-comendite
268	Alkali olivine basalt-trachyte-comendite
270	Alkali olivine basalt-trachybasalt-comendite
271	Alkali olivine basalt to hawaiiite
275	CONCLUSIONS
277	REFERENCES

Appendices

281	1. Mineral chemistry from microprobe analysis
314	2. Whole-rock chemistry
315	3. Rare-earth elements
316	4. Hotspring data
318	5. Source of geographic names

Map 1623A. Geology, Mount Edziza Volcanic Complex, British Columbia, scale 1:50 000. (*in pocket*)



View looking northeast across the Kitsu and Big Raven plateaus at the central, ice-covered dome of Mount Edziza. Flat-lying flows of the Late Tertiary Raspberry, Armadillo and Nido formations are exposed along Mess Creek Escarpment (foreground). Low, conical hills around the lower edge of the ice-cap are Quaternary pyroclastic cones of the Big Raven Formation.

THE LATE CENOZOIC MOUNT EDZIZA VOLCANIC COMPLEX, BRITISH COLUMBIA

Abstract

The Mount Edziza Volcanic Complex lies about 100 km inland from the continental margin in north-central British Columbia. It includes a group of overlapping basaltic shields, felsic composite volcanoes, domes and small calderas which range in age from at least 7.5 Ma to less than 2000 B.P. During this long period of intermittent volcanic activity the ebb and flow of local and regional glaciations resulted in a complex assemblage of subaerial and subglacial volcanic landforms.

The volcanic assemblage is chemically bimodal, comprising voluminous alkali olivine basalt and hawaiite, a felsic suite of mainly peralkaline trachyte and comendite, and a relatively small volume of intermediate rocks (trachybasalt, tristanite, mugearite, benmoreite). The complex is the product of five cycles of magmatic activity, each of which began with alkali basalt and culminated with the eruption of felsic magma. Petrogenetic modelling suggests that the felsic rocks formed by fractionation of observed phenocryst and cumulate mineral phases from a common alkali olivine basalt parent magma.

The chemical diversity and longevity of the Mount Edziza Volcanic Complex are attributed to its location over a zone of crustal extension where mantle-derived basalt, trapped in large high-level reservoirs, has undergone prolonged fractionation. Incipient rifting associated with the volcanic activity is probably related to dextral transcurrent movement between North America and the Pacific Plate, a tectonic regime that has persisted throughout the life of the complex.

Résumé

Le complexe volcanique de Mount Edziza est situé à 100 km environ vers l'intérieur, à partir de la marge continentale dans le centre nord de la Colombie-Britannique. Il comprend un groupe de boucliers basaltiques chevauchants, de strato-volcans felsiques, de dômes et de petites caldeiras dont l'âge varie d'au moins 7,5 Ma à il y a moins de 2000 ans. Pendant cette longue période d'activité volcanique intermittente, le flux et le reflux des glaciations locales et régionales ont produit un ensemble complexe de topographies volcaniques de nature subaérienne et sous-glaciaire.

L'ensemble volcanique est chimiquement bimodal, comprenant une grande masse d'hawaiites et de basaltes alcalins à olivine, une série felsique de comendites et de trachytes principalement hyperalcalines et un volume relativement petit de roches intermédiaires (trachybasalte, tristanite, mugéarite, benmoreite). Le complexe est le produit de cinq cycles d'activité magmatique, chacun ayant débuté avec du basalte alcalin et culminé avec l'éruption de magma felsique. La modélisation pétrogénétique semble indiquer que les roches felsiques se sont formées par cristallisation fractionnée des phases minérales observées à phénocristaux et cumulats, dérivées d'un même magma original de basalte alcalin à olivine.

La diversité chimique et la longévité du complexe volcanique de Mount Edziza s'expliquent par son emplacement sur une zone d'extension crustale dans laquelle le basalte provenant du manteau, piégé dans de grands réservoirs proches de la surface, a subi une cristallisation fractionnée prolongée. Un fossé d'effondrement naissant, associé à l'activité volcanique, est probablement lié au mouvement de décrochement dextre survenu entre les plaques nord-américaines et pacifiques, lequel régime tectonique a persisté pendant toute la vie du complexe.

SUMMARY

In presenting the results of this study an attempt has been made to treat the geology of the Mount Edziza Volcanic Complex from an historical perspective, to describe not only the rocks as we see them today but also to recreate the physical setting into which they were erupted. An effort has also been made to clearly distinguish between data, based on field and laboratory observations, and interpretation, based on modern analogues.

Rocks predating the Mount Edziza Volcanic Complex are referred to collectively as basement. The complex itself is subdivided into 13 formations, each the product of a distinct stage of volcanic activity. The upper and lower surfaces of each formation have been contoured to produce a series of paleogeological maps depicting the changing landforms that resulted from construction and erosion of the myriad volcanoes whose remnants comprise the present complex. This summary presents an interpretation of the geological history and the physical setting of the period during which each formation was deposited. The summary and paleogeological maps contain the essence of this work and the casual reader may not wish to go farther.

Details of the stratigraphy, structural relationships, petrography and chemistry are documented for each formation in the main body of the text. The final chapters (Geochronology, Petrochemistry, Petrogenesis) treat special aspects of the study in the broader context of the Mount Edziza Volcanic Complex as a whole, and its relationship to other Cordilleran volcanoes.

Tectonic setting and basement geology. The Mount Edziza Volcanic Complex is underlain by Late Paleozoic and Mesozoic sedimentary and volcanic rocks, including oceanic tholeiites and calc-alkaline arc assemblages, which were accreted to the continental margin during the Late Mesozoic. These older rocks are cut by numerous Mesozoic and Early Tertiary plutons which range in composition from quartz monzonite to diorite and which were emplaced both before and after amalgamation of the accreted terranes.

The youngest rocks exposed beneath the Mount Edziza Volcanic Complex are calc-alkaline volcanics and related subvolcanic plutons of the Early Tertiary Sloko Group. These subaerial, intermontane rocks were tilted, cut by normal faults, and deeply eroded before the first flows of the Mount Edziza Volcanic Complex were erupted in the Late Miocene. The resulting mature, gently rolling Tertiary erosion surface forms the present unconformity at the base of the Mount Edziza pile.

SOMMAIRE

Dans la présentation des résultats de la présente étude, on a tenté de traiter la géologie du complexe volcanique de Mount Edziza d'un point de vue historique, afin de décrire non seulement les roches telles qu'on les voit aujourd'hui, mais aussi de recréer le cadre physique dans lequel elles ont fait éruption. On a aussi tenté d'établir une distinction nette entre les données, basées sur des observations faites sur le terrain et en laboratoire, et les interprétations, basées sur des situations analogues de nature contemporaine.

Les roches antérieures au complexe volcanique de Mount Edziza sont qualifiées collectivement de socle. Le complexe lui-même est subdivisé en 13 formations chacune étant le produit d'une étape distincte de l'activité volcanique. Les surfaces supérieures et inférieures de chaque formation ont été délimitées de façon à produire une série de cartes paléogéologiques décrivant les topographies changeantes qui ont résulté de la construction et de l'érosion de la myriade de volcans dont les vestiges représentent le complexe actuel. Le présent sommaire constitue une interprétation de l'histoire géologique et du cadre physique de la période correspondant à la mise en place de chaque formation. Le sommaire et les cartes paléogéologiques représentent l'essentiel de ce travail, et il se peut que le lecteur moyen s'en satisfasse.

La stratigraphie, les relations structurales, la pétrographie et la chimie de chaque formation sont approfondies dans le corps du texte. Les derniers chapitres (géochronologie, pétrochimie, pétrogenèse) traitent d'aspects particuliers de l'étude dans le contexte plus général de l'ensemble du complexe volcanique de Mount Edziza et de ses liens avec d'autres volcans de la Cordillère.

Cadre tectonique et géologique du socle. Le complexe volcanique de Mount Edziza repose sur des roches sédimentaires et volcaniques du Paléozoïque supérieur et du Mésozoïque, y compris des tholéiites océaniques et des ensembles d'arcs calco-alkalins, dont la mise en place s'est produite sur la marge continentale pendant le Mésozoïque supérieur. Ces roches plus anciennes sont recoupées par de nombreux plutons du Mésozoïque et du Tertiaire inférieur dont la composition varie de monzonites quartzifères à des diorites; la mise en place de ces plutons a eu lieu avant et après l'amalgamation des terranes formés par accréation.

Les roches les plus récentes, exposées sous le complexe volcanique de Mount Edziza, sont des roches volcaniques calco-alkalines et des plutons subvolcaniques connexes du groupe de Sloko du Tertiaire inférieur. Ces roches intermontagnardes de nature subaérienne ont été inclinées, recoupées par des failles normales et fortement érodées avant l'éruption des premières coulées du complexe volcanique de Mount Edziza à la fin du Miocène. Il en est résulté une surface d'érosion tertiaire évoluée et faiblement ondulée qui constitue la discordance actuelle présente à la base de l'amas de Mount Edziza.

The Mount Edziza Volcanic Complex is part of the Stikine Volcanic Belt, a broad arcuate belt of Miocene and younger volcanoes which runs roughly parallel to the continental margin through northwestern British Columbia and southern Yukon. Vents within the belt are concentrated in a series of north-trending en echelon segments which bear no obvious structural relationship to the basement geology. Eruptive centres of the Mount Edziza Volcanic Complex define the southern segment of the Stikine Volcanic Belt which lies about 100 km inland from the present northwesterly trending transcurrent boundary between the North American and Pacific plates. This same tectonic regime is believed to have persisted during the entire history of the volcanic complex. A close association between the volcanoes and north-trending Cenozoic normal faults suggests an extensional tectonic environment, possibly due to incipient rifting of the adjacent continental margin in response to dextral movement on the northwesterly trending transcurrent boundary between North America and the Pacific Plate.

Raspberry Formation. Evolution of the Mount Edziza Volcanic Complex began about eleven million years ago with eruption of the Raspberry basalt. The first flows issued from an unidentified vent, or cluster of vents in the Central Highlands of the late Miocene landscape, near what is now Raspberry Pass. Showers of tephra, thrown out in the initial burst of activity blanketed the surrounding surface and choked the rivers and streams with ash and cinders. Shortly thereafter streams of fluid basaltic lava coursed down valleys from the Central Highlands and spread out into thick, fan-shaped lobes on the adjacent lowlands. As the lava advanced it buried gravel bars, soil and colluvium along with the charred remains of the Miocene forest. The duration of this first stage is not known but there is no evidence of any prolonged break in activity during Raspberry time. Instead, successive flows appear to have followed one another in rapid succession until more than 83 km³ of lava had spilled out onto the surface. Near their source the flows piled up to a depth of more than 300 m whereas the distal, amoeba-like lobes that welled into depressions on the periphery of the pile were only a few metres thick. By the end of Raspberry time at least 775 km² of the late Miocene surface had been flooded by lava, transforming it from a mature upland of rolling hills and broad, forested valleys to a sprawling, treeless wasteland of black, drifting ash and clinkery lava fields. On the western edge of the Highlands the symmetrical summit of Raspberry volcano rose to an elevation of nearly 7000 ft (2100 m) while clusters of lesser cones dotted the surface of broad lava domes to the north and south (Fig. 20). The original drainage was disrupted. Lakes, ponded behind lava dams, spilled out across the newly formed surface and rivers, displaced by lava, began to etch out new valleys along the margins of the encroaching pile of basalt. The fragile cinder cones and ash

Le complexe volcanique de Mount Edziza fait partie de la zone volcanique de Stikine, large zone arquée de volcans miocènes et plus récents qui traverse, plus ou moins parallèlement à la marge continentale, le nord-ouest de la Colombie-Britannique et le sud du Yukon. Les cheminées volcaniques au sein de cette zone sont concentrées dans une série de segments en échelon orientés vers le nord qui ne présentent aucune affinité structurale évidente avec la géologie du socle. Les centres éruptifs du complexe volcanique de Mount Edziza définissent le segment sud de la zone volcanique de Stikine qui se situe à environ 100 km à l'intérieur des terres par rapport à la limite actuelle de décrochement de direction nord-ouest séparant les plaques nord-américaine et pacifique. Ce même régime tectonique aurait persisté pendant toute l'histoire du complexe volcanique. Une association étroite entre les volcans et les failles normales de direction nord et d'âge cénozoïque semble indiquer l'existence d'un milieu tectonique d'extension, qui serait peut-être dû à un début d'effondrement de la marge continentale adjacente en réponse à un mouvement dextre survenu à la limite de décrochement de direction nord-ouest qui sépare l'Amérique du nord de la plaque du Pacifique.

Formation de Raspberry. L'évolution du complexe volcanique de Mount Edziza a débuté il y a environ onze millions d'années, avec l'éruption des laves basaltiques de Raspberry. Les premières coulées provenaient d'un cratère ou d'un groupe de cratères non identifiés dans les hautes-terres centrales présentes à l'époque du Miocène supérieur, près du col actuel de Raspberry. D'abondantes quantités de tephra, projetées durant la phase initiale d'activité, ont recouvert la surface environnante et engorgé les fleuves et rivières de cendres et de scories. Peu après, des flots de lave basaltique fluide ont suivi le cours des vallées des hautes-terres centrales et se sont étalés en formant d'épais lobes en forme d'éventail dans les basses-terres adjacentes. À mesure que progressaient les laves, elles ont enseveli les bancs de graviers, le sol et les colluvions en même temps que les restes carbonisés de la forêt miocène. On ne connaît pas la durée de cette première phase, mais il ne semble pas qu'il y ait eu d'interruption prolongée de l'activité volcanique durant l'intervalle de temps correspondant à la formation de Raspberry. Au contraire, il semble qu'il y ait eu une succession rapide de coulées, qui ont recouvert la surface de plus de 83 km³ de laves. Près de leur source, les coulées ont formé une accumulation de laves de plus de 300 m d'épaisseur tandis que les lobes distaux amiboïdes qui ont occupé les dépressions à la périphérie de l'accumulation volcanique, n'avaient que quelques mètres d'épaisseur. Vers la fin de l'intervalle de Raspberry, la surface existant au Miocène supérieur avait été submergée sur au moins 775 km² par des laves; ces dernières ont transformé ces hautes-terres matures composées de collines onduleuses et de grandes vallées boisées en un immense désert totalement dépourvu d'arbres, et couvert de cendres noires mouvantes et de champs de laves scoriacées. Sur le bord ouest des hautes-terres, s'élevait le sommet symétrique du volcan Raspberry jusqu'à presque 7000 pi (2100 m), tandis que des groupes de cônes de moindre hauteur parsemaient la surface de vastes dômes de lave au nord et au sud (fig. 20). Le réseau

fields of the source area were rapidly eroded away and the main edifice of Raspberry volcano itself was deeply dissected before the next stage of volcanic activity began. But the thick piles of basalt flows that flooded the valleys and lowlands remained to become the foundation on which much of the present edifice of Mount Edziza and the Spectrum Range were subsequently built.

Little Iskut Formation. During the waning stages of Raspberry activity a large lake was ponded in upper Little Iskut Valley, behind a lava dam formed by flows from South craters (Fig. 30). By the time the last Raspberry eruption had died, the lake had already reached its maximum size and its level had begun to fall as the outlet stream deepened its channel around the eastern edge of the lava barrier. At about this time a new surge of volcanic activity began and, by a strange coincidence, it began beneath the waters of Raspberry lake. Thus, as the rising column of magma forced its way toward the surface it opened fractures that were immediately flooded with water. At first this may have done no more than cause the formation of hot springs and fumeroles on the lake bottom, but as increasing volumes of water came into contact with hot or molten rock it ultimately flashed to steam and produced violent phreatic explosions. Water above the developing vent was churned into a seething mixture of suspended debris settling against a turbulent current of rising steam and gas bubbles. The larger explosions produced towering black spires of water that rose high above the surface and fell back, carrying with them suspended ash and granular particles torn from the quenched outer surface of the rising magma column. This suspended material gradually settled over much of the lake floor, forming a layer of ash and fine breccia that forms the lowermost beds of the Little Iskut shield volcano.

The Little Iskut lava is mainly trachybasalt which differs from the Raspberry alkali olivine basalt both chemically, having more silica and alkalis, and also in its physical properties, due partly to its lower content of dissolved volatiles. Thus the first Little Iskut lava that issued onto the floor of Raspberry lake (Fig. 35) did not form the typical assemblage of pillows, tuff-breccia and quenched lava toes that are characteristic of the Raspberry and other, more basic, subaqueous flows. Instead the lava was quenched and fractured without being torn apart by the expansion of dissolved gases. Once water was expelled from the conduit system, phreatic explosions became less

hydrographique originel a été perturbé. Sur la surface nouvellement formée, sont apparus des lacs retenus derrière des barrages naturels de lave, et les cours d'eau, détournés par les laves, ont commencé à creuser de nouvelles vallées le long des marges de l'accumulation de basaltes. Les fragiles cônes de scories et étendues de cendres de la région source ont été rapidement érodés, et le volcan Raspberry a été lui-même profondément disséqué, avant le commencement de la phase suivante d'activité volcanique. Mais les épaisses accumulations de coulées basaltiques qui ont recouvert les vallées et les basses-terres ont subsisté, et constituent le fondement de la structure actuelle du mont Edziza et du chaînon Spectrum, qui se sont formés par la suite.

Formation de Little Iskut. Durant les dernières phases d'activité du volcan Raspberry, un vaste lac s'est formé dans la vallée supérieure de la rivière Little Iskut, derrière un barrage naturel de lave formé par les coulées des cratères South (fig. 30). Au moment où la dernière éruption du volcan Raspberry venait de se terminer, le lac avait déjà atteint ses dimensions maximales, et son niveau avait commencé à tomber, à mesure que le cours d'eau lui servant de canal de décharge approfondissait son lit sur le bord est de la barrière de lave. A peu près à cette époque, a débuté une nouvelle phase d'activité volcanique, qui par une coïncidence étrange, a commencé à se manifester au-dessous des eaux du lac Raspberry. Ainsi, en même temps que la colonne ascendante de magma se frayait un chemin vers la surface, elle ouvrait des fissures qui se remplissaient immédiatement d'eau. Tout d'abord, ce phénomène peut n'avoir eu comme effet que la formation de sources chaudes et de fumerolles au fond du lac, mais les quantités de plus en plus grandes d'eau venant en contact avec la roche brûlante ou en fusion se sont transformées tout d'un coup en vapeur et ont fini par produire de violentes explosions phréatiques. L'eau se trouvant au-dessus du cratère en formation a été transformée par agitation en un mélange bouillonnant de débris en suspension, que rencontrait un courant ascendant et turbulent de vapeurs et bulles de gaz. Les plus fortes explosions ont produit d'immenses colonnes noires d'eau qui se sont élevées bien au-dessus de la surface et sont retombées en entraînant des cendres en suspension et des particules granulaires arrachées à la surface extérieure, brusquement refroidie, de la colonne ascendante de magma. Ces produits en suspension se sont graduellement déposés sur une grande étendue du fond du lac, de façon à former une couche de cendres et de brèches fines, qui constituent les couches de la base du volcan en bouclier de Little Iskut.

Les laves de Little Iskut se composent principalement de trachybasaltes qui diffèrent chimiquement des basaltes alcalins à olivine de Raspberry, puisqu'ils contiennent plus de silice et de produits alcalins, et aussi du point de vue de leurs propriétés physiques, en raison de leur plus faible teneur en composants volatiles dissous. Ainsi, les premières laves de Little Iskut qui se sont répandues sur le fond du lac Raspberry (fig. 35) n'ont pas formé l'assemblage typique de laves en coussins, de brèches tufacées et de lobes de lave brusquement refroidies et fissurées, sans être fragmentées par l'expansion des gaz dissous. Une fois l'eau chassée du réseau de conduits volcaniques, les explosions phréatiques sont devenues moins fréquentes, et le

frequent and the growing lava dome on the lake bed expanded relatively quietly, insulated from the surrounding water by a porous mantle of breccia and escaping steam. Fractures, induced by thermal shock, fragmented the rock into a mass of small polygonal blocks. These were continuously sloughed from the outer surface of the growing dome and accumulated as chaotic piles of marginal breccia. Within the cores of both domes and flows similar fracturing occurred but there the blocks retained their original relative positions to form a "crackle breccia" of closely fitted pieces.

The summit of Little Iskut volcano rapidly grew above the surface of Raspberry lake, appearing first as a small, steaming island and later growing into a broad conical mountain that overlapped the northern shoreline and displaced much of the original lake with breccia. Lava issuing from its summit crater spread down the gentle east and south slopes into the shrinking remnants of Raspberry lake (Fig. 30). As each successive flow entered the water it was quenched and fractured to form a subaqueous "crackle breccia" similar to that formed in the early stages of activity. On the west side of the shield highly mobile Little Iskut lava poured directly onto the old surface of Raspberry basalt to form a lobe of lava that extended west almost to Mess Creek. In contrast to the rough, clinkery, surface of the Raspberry flows, the Little Iskut lava flows were covered with a mantle of smooth, fracture-bounded blocks. Nor was the eruption of Little Iskut lava accompanied by spectacular fire fountaining and ash falls. Instead each pulse of activity produced a large volume of highly mobile lava that welled rapidly from a central vent. As it spread and cooled, a solid crust repeatedly formed, fractured and reformed until the pasty, molten core was covered by a mantle of shifting blocks. When the last Little Iskut flow finally ground to a halt its blocky surface merged imperceptibly with the sprawling fields of older blocks that covered the entire surface of the newly formed shield.

Armadillo Formation Six million years ago, the harsh barren landscape formed by the eruption of Raspberry basalt had been greatly subdued by erosion. The layer of black ash that blanketed the Central Highlands had been eroded away, as had most of the cinder cones that dotted its surface three million years earlier. Flows of Raspberry basalt surrounding the Highlands still retained their larger features, the sinuous network of levies and overlapping lobes of lava with their concentric ridges still contrasted with the smooth rolling landscape of the Highlands, but the blocky lava surface was now mantled with a thin veneer of broken rock and sediment. Streams, seeking a route across its irregular surface had begun to etch out tiny box

dôme de lave croissant sur le fond du lac s'est développé de façon relativement tranquille, puisqu'il était isolé de l'eau environnante par un manteau poreux de brèches et par les vapeurs se dégageant des fissures. Les fractures produites par le choc thermique ont fragmenté la roche en une masse de petits blocs polygonaux. Ces derniers se sont continuellement détachés de la surface extérieure du dôme durant la croissance de celui-ci et, en s'accumulant, ont formé des empilements chaotiques de brèches marginales. Au cœur des dômes et des coulées, sont apparues des fractures similaires, mais cette fois, les blocs ont conservé leur position relative les uns par rapport aux autres, et ont formé une « brèche de dislocation » formée de morceaux étroitement ajustés les uns aux autres.

Le sommet du volcan Little Iskut s'est rapidement élevé au-dessus de la surface du lac Raspberry, et a tout d'abord pris la forme d'un îlot fumant, et plus tard d'une large montagne conique qui a empiété sur le littoral nord, et a déplacé une grande partie du lac originel en le comblant avec des brèches. Les laves émises par son cratère sommital se sont étalées sur les pentes douces est et sud jusqu'aux vestiges de plus en plus réduits du lac Raspberry (fig. 30). À mesure que chaque coulée successive a pénétré dans l'eau, elle a subi un refroidissement brusque, et la lave s'est fracturée pour donner une « brèche de dislocation » subaquatique, semblable à celle formée au cours des premières phases d'activité volcanique. Du côté ouest du bouclier, les laves très fluides de Little Iskut se sont directement déversées sur l'ancienne surface du basalte de Raspberry, en créant un lobe de lave qui se prolongeait à l'ouest presque jusqu'au ruisseau Mess. Contrairement à la surface rugueuse et scoriacée des coulées de Raspberry, la surface des coulées de Little Iskut a été recouverte d'un manteau de blocs lisses limités par des fractures. Aucuns phénomènes spectaculaires, comme des fontaines de feu et des chutes de cendres n'ont accompagné l'éruption des laves du volcan Little Iskut. Au contraire, chaque épisode d'activité a produit un vaste volume de laves très fluides, qui ont rapidement surgi d'un événement central. À mesure que les laves se sont étalées et refroidies, une croûte solide s'est à plusieurs reprises formée, fracturée et reformée jusqu'à ce que le noyau de lave pâteuse en fusion ait été recouvert d'un manteau de blocs mouvants. Lorsque la dernière coulée de lave de Little Iskut a fini par s'immobiliser, sa surface blocailleuse s'était imperceptiblement fondue avec les immenses champs d'anciens blocs de lave qui recouvraient toute la surface du bouclier nouvellement formé.

Formation d'Armadillo. Il y a six millions d'années, le rude paysage désert formé par l'éruption du basalte de Raspberry avait été grandement adouci par l'érosion. La couche de cendres noires qui recouvrait les hautes-terres centrales avait été enlevée par l'érosion, de même que la plupart des cônes de scories qui parsemaient sa surface trois millions d'années auparavant. Les coulées du basalte de Raspberry environnant les hautes-terres conservaient encore leurs grands traits topographiques, c'est-à-dire le réseau sinueux de levées naturelles et de lobes de lave chevauchants dont les crêtes concentriques se détachaient encore nettement de la topographie doucement ondulée des hautes-terres, mais la surface de lave blocailleuse se trouvait recouverte d'un mince placage de fragments

MOUNT EDZIZA

canyons along the old lava troughs and around the margins of flow lobes. Where they entered depressions or spread out onto flat bench land their load of sediment was deposited as small alluvial fans and lacustrine deposits and there, pioneer vegetation, rooted in the sparse layer of new-formed soil began to spread from the swampy lowlands and stream banks to the lava itself.

On the southern edge of the old Raspberry shield, a plume of vapour and small periodic bursts of ash and lava, still issued from the low black cone of Little Iskut volcano and the surrounding fields of lava still had a fresh blocky surface devoid of vegetation.

As activity subsided on Little Iskut volcano, a new and different phenomenon began to appear farther north. Warm springs in the eastern Highlands, near what is now Armadillo Peak, began to increase rapidly in temperature and the region was soon dotted with great steaming scars where the bedrock shale was bleached white and altered to brightly coloured clay by hot acid water and vapours rising to the surface through fractures. Beneath the fields of boiling mud pots, geysers, and fumaroles, a large body of magma, forcing its way slowly upward, caused the overlying rock to dome and fracture. Earthquakes occurred with increasing frequency and intensity and finally the first eruption of Armadillo trachyte burst from the surface.

The Armadillo stage of activity (Fig. 40) began with the explosive discharge of gas and pumice from a vent near Cartoona Ridge, on the northern edge of the rising basement dome, nearly 8 km north of the main body of intrusive magma. Light frothy pumice, along with particles of shale, torn from the walls of the vent, were thrown hundreds of metres into the air, falling back to form a blanket of loose, white, air-fall pumice several hundred square kilometres in extent. Near its source, the pumice reached a thickness of more than 150 m, and 32 km west of its source the basal ash layer is still up to 15 m thick. No sooner had it fallen than wind and running water began to redistribute it, washing it from the Highlands into the adjacent lowlands where it was deposited along with normal sediments.

The column of gas and pumice that produced the air-fall deposits was accompanied by periodic outbursts of gas-charged magma that overflowed the crater rim and swept down the slopes as glowing avalanches. Welded ash flow deposits formed in this way are found as much as 10 km from their source. Although periodic discharges

rocheux et de sédiments. Les cours d'eau, en se frayant un chemin à travers cette surface irrégulière, avaient commencé à creuser de petits canyons rectangulaires le long des anciennes dépressions de la lave, et à la lisière des lobes des coulées. Lorsque ces cours d'eau pénétraient dans des dépressions ou s'épandaient sur des cuestas subhorizontales, ils déposaient leur charge de sédiment sous forme de petits cônes de déjection et de dépôts lacustres, et là, une végétation pionnière, enracinée dans la très mince couche de sol nouvellement formée, a commencé à se propager des basses-terres marécageuses et des rives des cours d'eau jusqu'aux laves elles-mêmes.

Sur le bord sud de l'ancien bouclier de Raspberry, s'échappait encore un panache de vapeur, tandis que le cône noir et peu élevé du volcan Little Iskut produisait encore de petites éruptions périodiques de cendres et de laves, et les champs de lave environnants présentaient encore une surface blocailleuse et fraîche, dépourvue de végétation.

À mesure que diminuait l'activité du volcan Little Iskut, un phénomène nouveau et différent commençait à se manifester plus au nord. La température des sources chaudes des hautes-terres de l'est, près du pic Armadillo actuel, avait commencé à s'élever rapidement, et la région était bientôt parsemée de grandes cicatrices fumantes à l'emplacement desquelles le schiste argileux du soubassement était blanchi ou altéré en argile vivement colorée par l'eau chaude acide et la vapeur remontant jusqu'à la surface par l'entremise des fractures. Au-dessous des champs de sources volcaniques boueuses, de geysers et fumerolles, l'important volume de magma, qui se frayait lentement un chemin vers le haut, provoquait le bombement et la fracturation des roches sus-jacentes. Des séismes de fréquence et d'intensité croissantes se sont manifestés, et la première éruption du trachyte d'Armadillo a finalement eu lieu.

La phase d'activité d'Armadillo (fig. 40) a commencé avec le dégagement explosif de gaz et de pierre ponce à partir d'un événement situé à proximité de la crête de Cartoona, sur le bord nord du dôme formé par le soulèvement de la roche de fond, à presque 8 km au nord de la masse principale de magma intrusif. De la pierre ponce légère et bulleuse, en même temps que des particules de schiste argileux arrachées aux parois de l'événement, ont été projetées à des centaines de mètres en altitude, et leur retombée a formé un manteau de pierre ponce dispersée, blanche et très légère, couvrant plusieurs centaines de kilomètres carrés. Près de sa source, la pierre ponce a atteint une épaisseur de plus de 150 m; à 32 km à l'ouest de sa source, la couche basale de cendres atteint encore 15 m d'épaisseur. Immédiatement après avoir atteint le sol, les pierres ponces et cendres ont été redistribuées par le vent et les eaux courantes, qui les ont entraînées des hautes-terres dans les basses-terres adjacentes, où elles se sont accumulées en même temps que les sédiments habituels.

Le jaillissement de la colonne de gaz et de pierre ponce responsable de cette dispersion des dépôts, a été accompagné d'éruptions périodiques de magma chargé de gaz qui a débordé du bord du cratère, et a dévalé les pentes sous forme de coulées de cendres incandescentes. On rencontre des dépôts d'ignimbrites ainsi formés jusqu'à 10 km de distance de leur source.

of pumice continued throughout the Armadillo stage of activity, their volume was dwarfed by the immense upwelling of trachyte and rhyolite lava that followed the initial explosive eruptions. The first viscous lava piled up into steep sided, overlapping domes above the vent area, but as the pile grew the gradient steepened and successive flows moved farther out from their source, eventually covering most of the southeastern Highlands in bulbous mounds of trachyte and rhyolite. Withdrawal of magma from the shallow reservoir beneath the Armadillo basement dome allowed the roof to collapse and an elliptical cauldron about 3 km across formed on the crest of the dome. As its floor subsided, trachyte magma welled up along the fractures in the roof and formed a succession of lava lakes ponded within the depression. An even larger volume of lava overflowed the caldera rim and spread westward in great composite lobes of viscous trachyte and rhyolite flows nearly 13 km long and up to 460 m thick.

Armadillo caldera and Cartoona Ridge were not the only vents through which Armadillo trachyte and rhyolite were erupted. Tadedá, on the northwest side of the basement dome and IGC vent farther west both produced pumice and lava, and rhyolitic dykes, exposed at several places cutting basement rocks, suggest that magma may have welled out of other vents now hidden beneath the lavas or destroyed by later erosion.

Nor were rhyolite and trachyte the only materials erupted during Armadillo time. Flows of highly fluid basalt issued from several vents around the periphery of the main Armadillo pile. The main centre lay northwest of the growing pile of rhyolite domes, near the northern edge of the older Raspberry shield. Most of the lava from this source flowed west into the Mess Creek lowlands. However, along its southern edge thin black sheets of basalt periodically spread across the white, desert-like apron of pumice and fine rhyolitic sand that flanked the main cluster of Armadillo rhyolite domes. These and other smaller streams of basalt from isolated centres within the Highlands, were subsequently covered by showers of rhyolite pumice from vents farther south. Thus as the two adjacent piles grew in a series of eruptive spasms, encroaching first one way and then the other across their shifting boundary, they produced a thick intervening zone in which thin wedges of basalt and rhyolite are interlayered. Little Iskut shield volcano, buried by the first showers of air-fall pumice and overridden by ash flows that swept down the southern slope of Armadillo caldera, also remained active during Early Armadillo time. Trachybasalt flows

Bien que des émissions périodiques de pierre ponce aient eu lieu pendant toute la phase d'activité du volcan Armadillo, leur volume était minimal par rapport aux immenses jaillissements de laves trachytiques et rhyolitiques qui ont suivi la série initiale d'éruptions explosives. Les premières laves visqueuses se sont accumulées sur des dômes chevauchants à parois raides et situés au-dessus de la région des bouches volcaniques, mais à mesure qu'augmentait l'accumulation des laves, la pente s'accroissait également, et les coulées successives se sont répandues de plus en plus loin de leur source; elles ont finalement recouvert la majeure partie des hautes-terres du sud-est, en formant des monticules d'aspect mamelonné, composés de trachytes et de rhyolites. Le retrait du magma du réservoir peu profond qui se trouvait sous le dôme basal du volcan Armadillo, a provoqué l'effondrement du toit, phénomène qui a donné suite à l'apparition d'une caldeira elliptique d'environ 3 km de diamètre sur la crête du dôme. À mesure que s'affaissait le plancher, le magma trachytique est remonté le long des fractures du toit, et a formé une succession de lacs de lave retenus à l'intérieur de la dépression. Un volume encore plus grand de lave a débordé de la caldeira et s'est répandu vers l'ouest en formant de grands lobes composites de trachyte visqueux et des coulées rhyolitiques atteignant presque 13 km de longueur et 460 m d'épaisseur.

La caldeira d'Armadillo et la crête de Cartoona n'étaient pas les seuls événements d'où aient jailli les trachytes et rhyolites d'Armadillo. Le volcan Tadedá, du côté nord-ouest du dôme basal et l'évent IGC situé plus à l'ouest, ont tous deux émis de la pierre ponce et de la lave, et la présence de dykes rhyolitiques, exposés en plusieurs endroits où ils recoupent les roches du soubassement, semble indiquer que le magma a pu s'échapper d'autres événements maintenant dissimulés sous les laves ou détruits par l'érosion subséquente.

Les éruptions survenues pendant l'intervalle d'Armadillo n'ont pas émis que des rhyolites et trachytes. Des coulées de basalte très fluide ont été émises par plusieurs événements situés à la périphérie de la structure principale d'Armadillo. La partie centrale se trouvait au nord-ouest de l'empilement croissant de dômes rhyolitiques, près du rebord septentrional du bouclier plus ancien de Raspberry. La plupart des laves provenant de cette source se sont écoulées vers l'ouest dans les basses-terres du ruisseau Mess. Toutefois, sur le bord sud du Bouclier, de minces nappes noires de basalte se sont périodiquement répandues sur l'épandage, blanc et d'aspect désertique, de pierre ponce et de sable rhyolitique fin jouxtant le principal groupe de dômes rhyolitiques d'Armadillo. Ces nappes, et d'autres épanchements moins abondants de basalte provenant de cratères isolés situés à l'intérieur des hautes-terres, ont été ensuite recouverts par des pluies de pierre ponce rhyolitique émises par des événements situés plus au sud. Ainsi, à mesure que les deux édifices adjacents augmentaient de taille durant une série d'épisodes éruptifs, en empiétant tantôt dans un sens, tantôt dans l'autre sur leur limite mouvante, ils ont créé une épaisse zone intermédiaire caractérisée par des interstratifications de minces prismes de basalte et de rhyolite. Le volcan en bouclier Little

issuing from near its summit flowed northwesterly across the early formed fields of pumice until, like Little Iskut volcano itself, they were eventually buried beneath the expanding pile of Armadillo rhyolite.

By the end of Armadillo time, some five million years ago, all traces of the old Raspberry and Little Iskut shield volcanoes had vanished beneath an unbroken layer of grey and white trachyte and rhyolite. On Armadillo Mountain, Tadedá, and Cartoona Ridge, spires of steaming rock, altered red and yellow by fumarolic gases, rose above the rolling grey and white surface of flows and domes which now formed a cluster of low mountains and ridges in the eastern Highlands. Beyond these mountains stretched a vast, wind-sculptured desert of shifting pumice, crossed only by the dry beds of intermittent streams. During periods of flood, pumice-laden water coursed through these channels to the edge of the pile and spread out across broad alluvial fans. There the apron of sediment encroached steadily on the edge of the living forest, burying it along with the charred skeletons of pre-Armadillo trees that still projected through the thin peripheral layer of ash.

Nido Formation. The events that followed the first eruption of Nido basalt are shrouded in complexity. The activity was not confined to an isolated eruption or even a series of closely related eruptions, but rather a long episode ensued during which a multitude of individual, widely separated centres flared into eruption and died, leaving piles of basalt and tephra that were subsequently buried beneath the products of yet another active centre. At least six major volcanoes were active during Nido time as well as uncounted smaller cones whose only remaining record is preserved as highly oxidized lenses of bombs and agglutinated tephra sandwiched between the lava flows. Although the precise sequence of events is not known, a generalized picture of Nido volcanism can be surmised from the juxtaposition of volcanic products and fluvial gravel that continued to pour out of the Armadillo Highlands and the surrounding basement terrane throughout Nido time. The highly mobile, fluid basaltic lava which was common to all the Nido centres flowed rapidly into the newly formed valleys, burying lag gravels and outwash from the Highlands, disrupting the drainage, and ponding numerous lakes behind lava dams. Near the end of Nido time the picture was further complicated by the appearance of glacier ice.

Iskut, enfoui sous les premières pluies de pierre ponce et submergé par des coulées de cendres qui ont dévalé la pente sud de la caldeira d'Armadillo, est aussi resté actif durant le début de l'intervalle d'Armadillo. Les coulées de trachybasalte émises à proximité de son sommet se sont dirigées vers le nord-ouest, en traversant les champs déjà existants de pierre ponce, jusqu'à ce que, à l'instar du volcan Little Iskut, l'accumulation de plus en plus vaste de rhyolite d'Armadillo les ait finalement recouvertes.

Vers la fin de l'intervalle d'Armadillo, il y a environ cinq millions d'années, toute trace des anciens volcans en bouclier, le volcan Raspberry et le volcan Little Iskut, avait disparu, enfouie sous une couche continue de trachyte et de rhyolite gris et blancs. Sur le pic Armadillo, sur le volcan Tadedá et sur la crête de Cartoona, sont apparues des aiguilles de roche fumante, que l'altération due aux gaz fumeroliens a coloré rouge et jaune, au-dessus de la surface onduleuse grise et blanche des coulées et dômes qui maintenant formaient un groupe de montagnes et crêtes peu élevées dans les hautes-terres de l'est. Au-delà de ces montagnes s'étendait un vaste désert, sculpté par le vent, composé de dunes mouvantes de pierre ponce, et traversé seulement par les lits secs des oueds. Durant les périodes d'inondation, les cours d'eau torrentiels chargés de pierre ponce parcouraient ces chenaux jusqu'au bord de l'amas volcanique, et se répandaient ensuite sur de vastes cônes alluviaux plats. Là, la nappe alluviale a continuellement gagné du terrain sur la forêt vivante, et l'a peu à peu ensevelie en même temps que les squelettes carbonisés des arbres qui poussaient avant l'éruption d'Armadillo et émergeaient encore de la mince couche périphérique de cendres.

Formation de Nido. Les événements qui ont fait suite à la première éruption du basalte de Nido demeurent obscurs, en raison de leur complexité. L'activité ne s'est pas limitée à une éruption isolée, ou même à une série d'éruptions très rapprochées; il s'est agi plutôt d'un long épisode, durant lequel une multitude de centres volcaniques distincts, très éloignés les uns des autres, sont entrés en éruption, puis se sont éteints, en laissant des amas de basaltes et de projections volcaniques, que les produits d'un autre centre d'activité volcanique ont par la suite complètement recouverts. Au moins six grands volcans ont été actifs durant l'intervalle de Nido, ainsi que d'innombrables cônes de petite taille, dont les seules traces actuelles sont la présence de lentilles fortement oxydées, constituées de bombes volcaniques et de tephra agglutinés, intercalées entre les coulées de lave. Bien que l'on ne connaisse pas avec précision la séquence des événements, on peut se faire une idée générale du volcanisme de Nido, d'après la juxtaposition des produits volcaniques et des graviers fluviaux que les hautes-terres d'Armadillo et les terrains constituant le soubassement environnant n'ont pas cessé de fournir pendant tout l'intervalle de Nido. Les laves basaltiques très mobiles et fluides qu'émettaient tous les centres volcaniques de Nido, se sont rapidement écoulées dans les vallées nouvellement formées, en recouvrant les pavages désertiques et les épandages fluvio-glaciaires en provenance des hautes-terres, perturbant ainsi le réseau hydrographique et créant de nombreux lacs derrière des barrages de lave. Un peu avant la fin de l'intervalle de Nido, l'apparition des glaces de glacier est venue compliquer cette situation.

A chain of three composite volcanoes developed north of Armadillo Peak along the eastern edge of the Central Highlands (Fig. 65). The oldest of these, Alpha peak and its satellites, gradually diverted and eventually completely blocked the streams flowing north from the Highlands. The first flows buried river gravels and ponded shallow lakes in which thin layers of fine silt and sand accumulated along with thick deltaic wedges of gravel. These deposits were themselves buried beneath later flows from the same volcano. Where flows entered bodies of water, plumes of steam rose from the lakes and drifted across the streams of lava. Beneath the surface, the molten lava was quenched and fractured, producing clusters of small lava toes, pillows, and irregular globules of lava surrounded by chaotic piles of glassy fragments spalled from the quenched surface of the advancing flow. Pods of this subaqueous tuff-breccia, formed in small transient lakes, are found throughout the dissected edifice of Alpha peak but, on the south side of the mountain, a lake must have persisted from the inception of the volcano until its final stages of activity (Fig. 69). The level of the lake rose as the volcano itself grew higher, and as successive batches of lava entered the lake and accumulated as tuff-breccia, the water was displaced upward until finally a pile of tuff-breccia more than 335 m thick formed on the southern flank of Alpha peak.

During the late stages of Alpha activity, lava began to issue from a second centre 12 km farther south (Fig. 67). Pulses of lava rose through fractures to a summit crater where expanding gases, dissolved in the magma, produced an incandescent column of lava that sent up showers of frothy tephra which fell back as bombs and spatter to form a loosely welded pile of pyroclastic debris from which the cone is built. This fire fountaining, accompanied by periodic outpouring of lava built a composite cone, Beta peak, which rose at least 365 m above the surrounding surface. Lava flows of fluid basalt coursed down the slopes of the growing cone and into the adjacent valleys, their distal ends extending at least 13 km north of the main cone, overlapping the southern edge of the Alpha pile and burying gravel from the Armadillo Highlands as well as colluvium and slide debris derived from the basaltic cones themselves. Still farther south, Gamma volcano flared into eruption on the western flanks of Cartoona Ridge and spread thin flows of basalt across the gently sloping alluvial fans that flanked Armadillo Highlands on the north and west.

Long before Beta and Gamma peaks had grown to their final heights their black clinkery surfaces were dusted with more or less permanent snow. Alpine glaciers

Une chaîne de trois stratovolcans s'est formée au nord du pic Armadillo, le long du bord est des hautes-terres centrales (fig. 65). Le plus ancien de ces volcans, le mont Alpha et ses satellites, a graduellement détourné et finalement complètement bloqué les rivières qui s'écoulaient vers le nord à partir des hautes-terres. Les premières coulées de lave ont recouvert les graviers fluviaux et formé des barrages naturels, créant des lacs peu profonds dans lesquels de fines couches de limon et de sable fin se sont accumulées en même temps que d'épais dépôts de gravier deltaïques en biseau. Ces dépôts ont eux-mêmes été ensevelis sous des coulées ultérieurement émises par le même volcan. Lorsque les coulées ont pénétré dans des plans d'eau, des panaches de vapeur se sont élevés des lacs et ont été emportés par le vent au-dessus des coulées de lave. Au-dessous de la surface, les laves en fusion ont été brusquement refroidies et se sont fracturées en produisant des groupes de petits lobes de lave, des coussins, et des globules irréguliers de lave entourés d'entassements chaotiques d'éclats vitreux qui se sont détachés de la surface brusquement refroidie de la coulée, durant l'avancée de cette dernière. On rencontre des lentilles allongées de cette brèche tufacée de nature subaquatique, formée dans de petits lacs transitoires, dans tout l'édifice disséqué du mont Alpha mais, du côté sud de la montagne, a dû exister un lac de la naissance du volcan à ses derniers stades d'activité (fig. 69). Le niveau du lac a monté au fur et à mesure de la croissance du volcan; alors que des coulées successives de lave pénétraient dans le lac et s'accumulaient sous forme de brèches tufacées, les eaux ont été déplacées vers le haut, jusqu'à ce que finalement un amas de brèche tufacée dépassant 335 m d'épaisseur se soit formé sur le flanc sud du volcan Alpha.

Durant les dernières phases d'activité du volcan Alpha, à 2 km plus au sud, un second centre éruptif a commencé à émettre des laves (fig. 67). À travers des fractures, ont eu lieu plusieurs émissions de lave, jusqu'à un cratère sommital où les gaz en expansion dissous dans le magma ont donné naissance à une colonne incandescente de lave; le tephra écumeux ainsi projeté en l'air est retombé sous forme de bombes et de débris volcaniques qui, en s'accumulant, ont formé la masse de débris pyroclastiques plus ou moins bien soudés entre eux dont le cône se compose. Ces fontaines incandescentes, accompagnées d'écoulements périodiques de lave, ont édifié un stratovolcan, le pic Beta, qui domine d'au moins 365 m la surface environnante. Les coulées basaltiques fluides ont dévalé les pentes du cône en formation, et pénétré dans les vallées adjacentes; elles se terminaient à au moins 13 km au nord du cône principal, et recouvraient en partie le bord septentrional de l'amas volcanique Alpha, tout en ensevelissant les graviers des hautes-terres d'Armadillo, de même que les colluvions et le matériel éboulé provenant des cônes basaltiques eux-mêmes. Encore plus au sud, le volcan Gamma est entré en éruption sur les flancs ouest de la crête de Cartoona, et a déversé de minces coulées de basalte sur les cônes alluviaux aux pentes faiblement inclinées qui bordaient les hautes-terres d'Armadillo au nord et à l'ouest.

Bien avant que les pics Beta et Gamma aient atteint leur altitude finale, leur surface noire, d'aspect scoriacé, était couverte d'une couche de neige plus ou moins permanente. Les

forming on the higher surrounding peaks sent tongues of ice into adjacent valleys choking rivers and streams with glacial-fluvial sediment that accumulated in broad outwash plains. The waxing and waning of glacial ice over a period of several thousand years was punctuated by further eruptions of Nido basalt. At times Beta peak was nearly enveloped by tributary glaciers flowing northward from an ice cap that mantled the Armadillo Highlands and ultimately covered the broad shield of Gamma peak (Fig. 67c).

Basalt erupted during periods of glacial advance was quenched against the ice or accumulated as piles of pillows and tuff-breccia in meltwater ponds thawed along the contact between lava and ice. During periods of glacial recession, lava flows spread over the scoured surface, burying moraines and outwash left by the retreating glaciers.

The last series of eruptions from Beta peak took place during such a recession. Retreating glaciers had left deep scars on the sides of the cone and deposited a thin veneer of outwash gravel and moraine on its lower slopes. The final surge of lava to issue from the battered cone of Beta peak flowed across the truncated remnants of earlier flows and spread out across the glacial deposits, filling outwash channels and piling up against abandoned morainal ridges. The lava, unlike the sparsely porphyritic basalt of earlier eruptions, was a partly crystalline mush containing up to 60% large feldspar crystals. Fire fountaining of this material produced a frothy black scoria from the molten lava, whereas much of the enclosed feldspar was blown free to form a mixed tephra of cinders and clear, glassy crystals. The extinct but still fuming cone of Beta peak lay near the northern edge of the Armadillo ice cap, from which meltwater streams cut meandering courses across the blanket of newly deposited black ash. Locally, wind and running water winnowed away the light, porous scoria leaving behind pockets of clear feldspar crystals on the surface of small floodplains and river bars.

Beneath the ice cap itself new life was beginning to stir in the frozen remains of Gamma volcano. A small steaming lake appeared on the sagging surface of Armadillo ice cap above the active fumeroles issuing from the dormant crater. A short time later lava began to pour from a vent in the bottom of the lake. Unlike the incandescent fire fountains that accompanied earlier eruptions of Gamma volcano, the vent was now completely shrouded in billowing clouds of white steam pierced by jagged columns of black, water-saturated ash that rose and fell with each successive explosion (Fig. 77). The lake was rapidly enlarged and before eventually draining from beneath the edge of the ice cap it extended for more than 5 km west

glaciers alpins qui se sont formés sur les pics environnants plus élevés, ont émis des langues de glace dans les vallées adjacentes, et ont engorgé les fleuves et rivières de sédiments fluvio-glaciaires qui se sont accumulés dans de vastes plaines d'épannage fluvio-glaciaires. Les processus de croissance et de disparition de la glace de glacier, pendant une période de plusieurs milliers d'années, ont été marqués par d'autres épisodes d'éruption du basalte de Nido. Parfois, le pic Beta a été presque totalement enveloppé par des glaciers tributaires avançant vers le nord à partir d'une calotte glaciaire qui recouvrait entièrement les hautes-terres d'Armadillo, et qui a finalement occupé le vaste bouclier du pic Gamma (fig. 67c).

Les basaltes produits par des éruptions durant des périodes d'avancée glaciaire ont été brusquement refroidis par contact avec la glace, et se sont accumulés sous forme de coussins et de brèches tufacées dans les mares d'eau de fonte formées dans la région de contact entre la glace et la lave. Durant les périodes de recul glaciaire, les coulées de lave se sont épanchées sur la surface affouillée, en ensevelissant les moraines et les épanages fluvio-glaciaires laissés par les glaciers en retraite.

La dernière série d'éruptions du pic Beta a eu lieu durant une période de recul. Les glaciers, en se retirant, ont laissé de profondes cicatrices sur les versants du cône et ont déposé un mince placage de graviers fluvio-glaciaires et de moraine au bas des pentes. La dernière émission de laves provenant du cône ruiniforme du pic Beta s'est répandue sur les restes tronqués des anciennes coulées, et a recouvert les dépôts glaciaires, tout en comblant les chenaux fluvio-glaciaires et en s'entassant contre des crêtes morainiques abandonnées. Contrairement aux basaltes faiblement porphyriques des éruptions antérieures, les laves constituaient une masse spongieuse partiellement cristalline, contenant jusqu'à 60% de macrocristaux de feldspath. Les laves en fusion de ce type, projetées par les fontaines de feu, ont donné en se refroidissant des scories noires et écumeuses, mais la plupart des feldspaths, projetés à l'écart, ont formé des tephra composés d'un mélange de cendres et de cristaux vitreux et clairs. Le cône éteint mais encore fumant du pic Beta se situait près de la limite nord de la calotte glaciaire d'Armadillo, où prenaient leur source les torrents d'eau de fonte qui creusaient leur méandres dans la couverture de cendres noires nouvellement déposées. Par endroits, le vent et les eaux courantes ont entraîné les scories légères et poreuses, en laissant sur place des amas isolés de cristaux clairs de feldspath à la surface de petites plaines d'inondation et de bancs fluviaux.

Au-dessous de la calotte glaciaire elle-même, la vie a recommencé à s'installer dans les ruines glacées du volcan Gamma. Un petit lac fumant est apparu à la surface déprimée de la calotte glaciaire d'Armadillo, au-dessus des fumerolles actives émises par le cratère inactif. Un peu plus tard, un événement situé au fond du lac a commencé à émettre des laves. Alors qu'auparavant des fontaines de laves incandescentes accompagnaient les éruptions du volcan Gamma, le cratère se trouvait maintenant complètement enveloppé par d'épaisses volutes de vapeur blanche, traversées par des colonnes déchiquetées de cendres noires saturées d'eau, que chaque explosion successive (fig. 77) faisait monter et retomber. Le lac s'est rapidement agrandi jusqu'à s'étendre sur plus de 5 km à l'ouest de l'évent

of the main vent. Each surge of lava produced large chunks of basalt that sank rapidly to the bottom of the lake, as well as smaller fragments that settled more slowly to form a series of bedded and crudely graded deposits of tuff-breccia. Primary ejecta and the quenched lobes of subaqueous flows were mixed with debris originally thrown onto the ice and later slumped into the lake as it continued to enlarge.

Before the final surge of lava issued from Gamma volcano the meltwater lake had drained. The black ash-covered glacial ice had wasted away beyond the limits of the volcano and subsequent flows of subaerial basalt partly covered and lapped against the piles of older tuff-breccia and were themselves covered by patches of glacial fluvial gravel spreading from the retreating ice.

Activity continued with a massive effusion of olivine basalt from the summit crater of Gamma peak. Near its source the lava clung tenaciously to steep slopes of the older cone, covering the fragile pile of tuff-breccia with a resistant mantle of hard rock up to 90 m thick, while thin distal lobes spread westward for more than 6.5 km. Unlike the final, feldspar-rich lava that issued from Beta peak, the culminating flows from Gamma volcano carried large crystals of olivine, clusters of olivine, pyroxene and feldspar and lherzolite nodules torn from a source area within the Earth's mantle.

Eruption of Nido basalt was not confined to the area north of Armadillo Highlands (Fig. 65). Magma, forcing its way upward through swarms of north-trending fractures, cut through the extinct cone of Little Iskut volcano and erupted to form Swarm peak. Lava poured down the western and southern flanks of the old shield and spread across alluvial fans and gravel bars flanking the southern edge of Armadillo Highlands. Still farther south, along this same zone of fractures, a major eruption flared in the high mountains at least 10 km beyond the outermost limits of the old Raspberry and Little Iskut flows. Fire fountains, playing above the vent, built a lopsided unstable pyroclastic cone, Vanished peak, against the steeply sloping surface, but most of the lava flowed north and west, coursing rapidly down a narrow valley that led from the flanking mountains onto the rolling surface of Spectrum Plateau. There the lava spread in thin sheets, coalescing with flows streaming down the flanks of Little Iskut volcano and welling out across the boulder-strewn surface of the plateau.

At least two additional centres, Exile hill and Lost peak, erupted on the plateau itself. Exile hill on the extreme western edge, was a small, subaerial pyroclastic cone that was almost completely inundated by younger flows from the south and east. Lost peak, on the southern

principal, avant de finalement se drainer en s'échappant sous le bord de la calotte glaciaire. Chaque éruption de lave a projeté de gros morceaux de basalte qui ont rapidement coulé au fond du lac, ainsi que des fragments plus petits qui se sont lentement déposés et ont formé une série de dépôts lités et grossièrement triés, composés de brèches tufacées. Les projections primaires et les lobes rapidement refroidis des coulées subaquatiques, se sont mélangés aux débris initialement projetés sur la glace, et ont ensuite glissé dans le lac à mesure que ce dernier continuait à croître.

Avant la dernière éruption des laves émises par le volcan Gamma, le lac formé par les eaux de fonte s'était vidé. La glace de glacier recouverte de cendres noires s'était retirée au-delà des limites du volcan, et des coulées ultérieures de basalte subaérien avaient partiellement enseveli ou effleuré les amas d'anciennes brèches tufacées, et avaient elles-mêmes été recouvertes d'étendues de graviers fluvio-glaciaires, provenant des glaciers en retraite.

L'activité volcanique s'est poursuivie avec une effusion massive de basalte à olivine à partir du cratère sommital du pic Gamma. Près de leur source, les laves sont restées solidement accrochées aux pentes raides du cône ancien, et ont recouvert l'amas fragile de brèches tufacées d'un manteau résistant de roche dure atteignant parfois 90 m d'épaisseur, tandis que de minces lobes distaux se sont étalés vers l'ouest sur plus de 6,5 km. Contrairement aux dernières laves riches en feldspath émises par le pic Beta, les coulées culminantes du volcan Gamma ont entraîné de gros cristaux d'olivine, des groupes de cristaux d'olivine, de pyroxène et de feldspath, et des nodules de lherzolite arrachés à une zone source du manteau terrestre.

Les effets de l'éruption du basalte de Nido ne se sont pas fait sentir que dans la région située au nord des hautes-terres d'Armadillo (fig. 65). Le magma, se frayant un passage à travers des essaims de fractures d'orientation nord, a entaillé le cône éteint du volcan Little Iskut, s'est déversé le long des flancs ouest et sud de l'ancien bouclier, et s'est étalé à travers des cônes alluviaux plats et bancs de gravier longeant le bord sud des hautes-terres d'Armadillo. Encore plus au sud, le long de cette même zone de fractures, une importante éruption s'est produite dans les hautes montagnes à au moins 10 km au-delà des limites extérieures des anciennes coulées de Raspberry et de Little Iskut. Les fontaines incandescentes, jaillissant au-dessus de l'évent, ont édifié un cône pyroclastique instable et asymétrique, le pic Vanished, sur la surface en pente raide, mais la majeure partie des laves se sont écoulées vers le nord et l'ouest, et ont rapidement descendu une étroite vallée allant des monts qui les bordaient, à la surface ondulée du plateau Spectrum. À cet endroit, les laves se sont étalées en minces nappes, et ont fusionné avec des coulées qui descendaient des flancs du volcan Little Iskut, en s'épanchant sur la surface blocailleuse du plateau.

Au moins deux cratères supplémentaires, les cratères Sigma et Epsolon, ont produit des éruptions sur le plateau lui-même. Des coulées plus récentes, provenant du sud et de l'est, ont presque complètement inondé le cône Sigma, petit cône pyroclastique subaérien, qui se dresse à l'extrémité ouest du

edge of the plateau is a composite pyroclastic dome consisting of both subaerial and subaqueous ejecta. A pile of tuff-breccia and quenched flow tongues forms a complex waterlain pile more than 300 m thick on the western flanks of the dome, whereas the eastern flank consists of normal subaerial flows and scoria. The lake in which these deposits accumulated was probably ponded between the growing volcano and a lobe of glacier ice encroaching on the plateau from the high mountains farther south. Other glaciers had already advanced northward, overriding the breached cone of Vanished peak and grinding down the sinuous network of lava levees that led to Spectrum Plateau, and for a short time the fiery showers of tephra and streams of molten lava ceased. By the time the last eruption of Nido basalt had sputtered to an end new ice caps had begun to grow on the volcanoes themselves. The stark, black landscape that they had formed was soon lost beneath a silent mantle of ice and snow that gave no hint of the pent-up energy trapped in a new mass of magma forming beneath the Spectrum Plateau.

Spectrum Formation. About two million years ago, the battered remains of basaltic cones formed during the long episode of Nido activity began to emerge from the receding ice. As the glaciers withdrew still farther, the vast lava fields which spread from Vanished and Swarm peaks were again exposed, their mantle of black scoria now stripped off, leaving a scoured pavement of solid basalt strewn with erratic boulders and isolated morainal ridges left by the receding ice. Alluvial fans and lag gravels, carried in from the adjacent highlands, began to accumulate around the edges of the old lava fields. On the south, streams flowing out of the Hickman massif deposited gravels composed of dioritic, andesitic and sedimentary clasts derived from the pre-Tertiary basement rocks. Farther south, streams from the Armadillo Highlands deposited an apron of rhyolitic gravel on the surrounding fields of Nido basalt. This fluvial cover had only begun to accumulate when the first explosive discharge of Spectrum rhyolite burst through the surface and deposited a layer of pumice and ash across the entire southern half of the old pile of Nido basalt.

The initial Spectrum vent was subsequently buried beneath thousands of metres of rhyolite and trachyte lavas that still conceal its exact location and form (Fig. 87). However, there is considerable evidence that much of the Spectrum activity was centred near what is now Yeda Peak (Fig. 88). This towering spire of explosion breccia, near the centre of the Spectrum Range, is flanked by subvolcanic, intrusive dykes and alteration zones which extend

plateau. Le cône Epsilon, un dôme pyroclastique composite, situé à l'extrémité sud du plateau, comprend à la fois des projections volcaniques subaériennes et subaquatiques. Un amas de brèches tufacées et de langues de lave brusquement refroidies forme un édifice complexe mis en place dans l'eau et atteignant plus de 300 m d'épaisseur sur les flancs ouest du dôme, tandis que le flanc est se compose de coulées et scories subaériennes normales. Le lac dans lequel se sont accumulés ces dépôts a probablement été créé par un barrage naturel entre le volcan en développement et un lobe de glace de glacier qui empiétait sur le plateau à partir des hautes montagnes situées plus au sud. D'autres glaciers avaient déjà progressé vers le nord, chevauché le cône fracturé du pic Vanished, et abattu le réseau sinueux de levées naturelles de lave aboutissant au plateau Spectrum; pendant un court intervalle, les pluies incandescentes de tephra et les écoulements de lave fondue avaient cessé. Alors que venaient de prendre fin les dernières phases de l'éruption du basalte de Nido, de nouvelles calottes glaciaires avaient commencé à se développer sur les volcans eux-mêmes. Le paysage noir et désolé qui s'était formé avait été rapidement enseveli sous un épais manteau de glace et de neige; ce dernier dissimulait complètement l'énergie latente, piégée dans une nouvelle masse de magma en formation sous le plateau Spectrum.

Formation de Spectrum. Il y a environ deux millions d'années, les restes ruiniformes des cônes basaltiques formés durant le long épisode d'activité du volcan Nido avaient commencé à émerger des glaces en recul. À mesure que se retiraient encore les glaciers, les vastes champs de lave qui s'étendaient à partir des pics Vanished et Swarm avaient de nouveau été exposés, maintenant dénudés de leur manteau de scories noires, et leur surface se présentait comme un dallage affouillé, composé de basalte solide, et parsemé de blocs erratiques et crêtes morainiques isolées, abandonnés par les glaces en recul. Les cônes alluviaux et pavages désertiques, formés de matériaux entraînés à partir des hautes-terres adjacentes, avaient commencé à s'accumuler sur les bords des anciens champs de lave. Au sud, des cours d'eau s'écoulant du massif Hickman avaient déposé des graviers composés de fragments dioritiques, andésitiques et sédimentaires dérivés du soubassement prétertiaire. Plus au sud, des cours d'eau provenant des hautes-terres d'Armadillo avaient formé une plaine d'épandage couverte de graviers rhyolitiques, sur les champs environnants des laves basaltiques de Nido. Cette couverture de sédiments fluviaux avait seulement commencé à s'accumuler, lorsque la première éruption explosive des laves rhyolitiques de Spectrum a surgi de la surface; cette éruption a déposé une couche de pierre ponce et de cendres sur toute la moitié sud de l'ancien amas du basalte de Nido.

L'événement initial de Spectrum a par la suite été enseveli sous des milliers de mètres de laves rhyolitiques et trachytiques, qui dissimulent encore sa position et sa configuration exactes (fig. 87). Toutefois, d'après les nombreux indices observés, il semble bien qu'une grande partie de l'activité du volcan Spectrum se soit concentré près du pic Yeda actuel (fig. 88). Cette impressionnante aiguille formée de brèches d'explosion volcanique, proche du centre du chaînon Spectrum, est bordée de

more than 300 m below the old surface of the Vanished Peak lava field on which the Spectrum Range lavas were deposited. Thus, the voluminous outpouring of rhyolite and trachyte must have been accompanied by collapse and foundering of part of the surface onto which it was poured (Fig. 89).

The history of the Spectrum Range began long before the first ash eruptions broke through the surface. The body of magma which fed the eruptions had begun to accumulate in a deep chamber many hundreds of years earlier, probably during the period of Nido volcanism. As the volume of magma increased, it began to migrate upward, enlarging its reservoir and fracturing and doming the roof rocks until, by the time Nido volcanism had ceased, a column of magma more than 9 km across and at least 1 km high lay beneath the extinct basaltic lava fields of Spectrum plateau. With each upward surge, pressure within the chamber decreased and volatile constituents, dissolved in the magma, streamed into the upper part of the reservoir. This process, prolonged over hundreds of years, produced a stratified column of magma with the lighter, more volatile constituents at the top and denser, less volatile magma in the lower part of the chamber.

Hydrothermal activity, localized along fractures in the domed roof of the magma chamber, almost certainly preceded the first eruption. It may have been sufficiently intense to maintain an ice-free area of steaming ground during the period of pre-Spectrum glaciation. At first the boiling springs and geysers were fed by meteoric water that seeped into fractures around the periphery of the thermal zone and, after being heated by the hot rocks above the magma chamber, rose to the surface by convection or flashed to steam and discharged in fumaroles. Later the convecting meteoric water was joined by the direct discharge of volatiles from the underlying body of magma. This gradual degassing of the magma through fractures in the roof of the chamber must have continued for a very long period and, by the time the first magma reached the surface, most of its explosive, volatile pressure had been dissipated.

The initial burst of Spectrum activity produced a relatively small volume of pumice and ash which settled onto the bare, glacially scoured surface of the Kounugu flows. This was followed almost immediately by the rapid upwelling of an enormous volume of rhyolitic magma from the upper part of the magma chamber. Individual flows up to 150 m thick and 13 km long were discharged in a single pulse of activity. Near its source the hot viscous lava was covered by a thin glassy rind that spalled off the steep front of the flow in showers of incandescent scales to form a thin, vitreous pavement on which the molten

dykes subvolcaniques et intrusifs, et de zones d'altération qui s'étendent à plus de 300 m sous l'ancienne surface du champ de lave du pic Vanished, sur laquelle s'étaient déposées les laves du chaînon Spectrum. Ainsi, les volumineux épanchements de rhyolite et de trachyte avaient sans doute été accompagnés de l'effondrement et de l'affaissement d'une partie de la surface sur laquelle s'étaient écoulées les laves (fig. 89).

L'histoire du chaînon Spectrum a commencé bien avant que les premières éruptions de cendres n'aient surgies de la surface. Le corps magmatique qui alimentait les éruptions avait commencé à s'accumuler dans une chambre profonde de nombreux siècles auparavant, probablement durant la période du volcanisme de Nido. À mesure qu'augmentait le volume de magma, ce dernier avait commencé à migrer vers le haut, à agrandir son réservoir, à fracturer et à soulever les roches du toit en les arquant, de sorte qu'au moment où pris fin le volcanisme de Nido, une colonne de magma de plus de 9 km de large et d'au moins 1 km de haut s'était constituée au-dessous des champs éteints de laves basaltiques du plateau Spectrum. À chaque nouvelle éruption, la pression diminuait à l'intérieur de la chambre, et les composants volatils dissous dans le magma montaient dans la partie supérieure du réservoir. Ce processus, qui a duré des centaines d'années, a produit une colonne magmatique stratifiée dans laquelle les composants les plus légers et volatils se trouvaient au sommet, et le magma plus dense et moins volatil se trouvait dans la partie inférieure de la chambre.

L'activité hydrothermale, localisée le long des fractures du toit arqué de la chambre magmatique, avait presque certainement précédé la première éruption. Il est possible qu'elle ait été suffisamment intense pour maintenir une surface libre de glace, d'où s'échappait de la vapeur durant la période de glaciation antérieure à la formation du plateau Spectrum. Tout d'abord, les sources bouillonnantes et les geysers avaient été alimentés par les eaux météoriques qui s'infiltraient dans les fractures, à la périphérie de la zone d'activité hydrothermale et qui, après avoir été réchauffées par les roches brûlantes au-dessus de la chambre magmatique, remontaient à la surface par convection, ou étaient transformées en vapeur et se dégageaient sous forme de fumaroles. Plus tard, les eaux météoriques circulant par convection avaient été accompagnées de dégagements directs de produits volatils issus du corps magmatique sous-jacent. Ce dégazage graduel du magma par des fractures du toit de la chambre s'est sans doute poursuivi pendant un temps très long, et à l'époque où le magma avait atteint la surface pour la première fois, la majeure partie de sa force explosive, créée par la pression des produits volatils, s'était dissipée.

La première manifestation d'activité du volcan Spectrum avait produit un volume relativement faible de pierre ponce et de cendres, qui s'étaient déposées sur la surface nue, affouillée par les glaces, des coulées de Kounugu. La remontée rapide d'un énorme volume de magma rhyolitique issu de la partie supérieure de la chambre magmatique avait presque immédiatement suivi cet épisode. Des coulées individuelles pouvant atteindre 150 m d'épaisseur et 13 km de long avaient eu lieu durant une phase unique d'activité. Près de sa source, la lave visqueuse et chaude était recouverte d'une mince croûte vitreuse qui se détachait du front fortement incliné de la coulée

lava advanced (Fig. 92). Farther from their source, where cooling and partial crystallization had increased the viscosity of the lava, sluggishly moving flows were covered by a thick mantle of solid blocks. These were carried forward, as though on a slowly moving conveyor belt, and dumped into the path of the slowly expanding distal lobes around the periphery of the pile. One flow followed another until a broad dome of lava, more than 20 km across and at least 750 m thick at its centre, covered almost the entire southern half of the old Nido basalt lava fields (Fig. 93). As predominantly rhyolitic magma was drawn from the upper part of the magma chamber, successively deeper parts of the reservoir were tapped and the lava changed from rhyolite to trachyte. Also, at some point during the withdrawal of magma, the roof of the chamber began to collapse, carrying with it the early formed flows at the base of the Spectrum pile. During collapse and foundering of the roof, some magma was injected into the lower part of the overlying edifice, where it cooled and crystallized in small, high-level chambers without reaching the surface.

At least 90% of the Spectrum pile was emplaced as flows. However, its relatively quiet effusion was punctuated by episodic bursts of pumice. Some of this, thrown high into the atmosphere, fell back as solid particles to form loose beds of air-fall tephra. More often, the pumice, along with accidental fragments torn from the vent, swept down the flanks of the growing domes as clouds of gas-charged, incandescent particles. Most of these were directed northward from a source that lay either on the north slope of the dome, or from an asymmetrical summit vent with a low northern rim over which the frothy magma repeatedly spilled.

The explosive eruption of Yeda Peak near the end of Spectrum activity produced a gaping central crater near the crest of the lava dome (Fig. 89). Angular and rounded blocks torn from the conduit walls were thrown out along with particles of incandescent pumice and fine ash. Part of this ejecta piled up in a low breccia cone around the vent, while more volatile, pumice-rich phases sped down the slopes as ash flows. The conduit itself was a column of loose debris about 500 m across that extended from the surface at least 1000 m down to the magma chamber. Blocks in this breccia pipe are up to 2 m across and include chunks of pre-Tertiary basement rocks as well as clasts derived from the underlying Nido basalt and rhyolite from the lower parts of the Spectrum pile. Many of

en pluies d'écaillés incandescentes, et formait ainsi un mince dallage vitreux sur lequel avançait la lave en fusion (fig. 87). Plus loin de leur source, où le refroidissement et la cristallisation partielle avaient accru la viscosité de la lave, les coulées plus lentes étaient recouvertes d'un épais manteau de blocs solides. Ces derniers avaient été entraînés comme sur un tapis roulant de faible vitesse, puis avaient abandonnés sur le trajet des lobes distaux qui s'élargissaient peu à peu à la périphérie de l'amas volcanique. Les coulées s'étaient succédées, jusqu'à ce qu'un vaste dôme de lave, de plus de 20 km de large et d'au moins 750 m d'épaisseur en son centre, eût presque entièrement recouvert la moitié sud des anciens champs de laves basaltiques de Nido (fig. 93). À mesure que le magma de nature principalement rhyolitique s'échappait de la partie supérieure de la chambre magmatique, les produits du réservoir, et la composition des laves était passée de rhyolitique à trachytique. Aussi, à un moment donné, durant le retrait du magma, le toit de la chambre avait commencé à s'effondrer, entraînant avec lui les coulées précédemment formées à la base de l'amas volcanique de Spectrum. Durant l'effondrement et l'affaissement du toit, une partie du magma avait été injectée dans la partie inférieure de l'édifice sus-jacent, où il s'était refroidi et avait cristallisé dans de petites chambres plus proches de la surface, mais sans atteindre cette dernière.

Au moins à 90 %, la mise en place de l'amas volcanique de Spectrum avait eu lieu sous forme de coulées. Toutefois, l'effusion relativement calme des laves avait été occasionnellement marquée par des épisodes de projections de pierre ponce. Une partie de cette pierre ponce, projetée à grande altitude, était retombée sous forme de particules solides qui avaient créé des lits non consolidés, composés de tephra. Plus souvent, la pierre ponce, en même temps que quelques fragments arrachés au cratère, était retombée le long des flancs des dômes en développement, sous forme de nuées de particules incandescentes à haute teneur en gaz. La plupart de ces nuages étaient dirigés vers le nord, et issus d'une source qui se trouvait soit sur le versant nord du dôme, soit sur un cratère sommital asymétrique, dont la bordure nord plus basse avait laissé s'échapper à plusieurs reprises le magma écumeux.

L'éruption explosive du pic Yeda, vers la fin de l'époque d'activité du volcan Spectrum, avait créé un cratère central béant près de la crête du dôme de lave (fig. 89). Des blocs anguleux et arrondis arrachés aux parois de la cheminée volcanique avaient été éjectés en même temps que des particules de pierre ponce incandescente et de cendres fines. En partie, ces projections s'étaient accumulées en formant un cône bréchi que peu élevé autour du cratère, tandis que les phases plus volatiles, riches en pierre ponce, avaient dévalé les pentes sous forme de coulées de cendres incandescentes. La cheminée elle-même était une colonne composée de débris meubles, d'environ 500 m de large, qui s'étendait de la surface jusqu'à au moins 1000 m de profondeur dans la chambre magmatique. Les blocs que l'on trouve dans cette cheminée bréchi que atteignent 2 m

the clasts were rounded by abrasion during violent gas explosions that churned, fractured and refractured the enormous mass of broken rock within the conduit.

Eight kilometres west of the Yeda Peak vent, a similar, but much smaller eruption built Exile Hill (Fig. 94), a satellitic cone near the edge of the main Spectrum lava dome. The first explosive discharge of gas formed a breccia pipe about 200 m across through which trachyte lava was later forced to the surface. At least three separate surges of lava issued from the vent to produce a small, satellitic dome about 100 m high.

A plume of sulphurous steam continued to rise from the Spectrum dome long after the effusion of lava had stopped. Much of this issued from fumaroles in and around Yeda Peak crater where violent jets of steam discharged directly from the deep recesses of the old, collapsed magma chamber. Thousands of smaller fumaroles, originating from vapours within the cooling flows themselves, dotted the surface of the surrounding dome. Each cluster of steaming vents was surrounded by a patch of bright red and yellow stain, produced by the reaction of hot sulphurous gases and acid waters on the rock.

During the Spectrum stage of activity, more than 100 km³ of rhyolite and trachyte were erupted. Successive flows poured out in rapid succession, filling potential valleys before an integrated drainage pattern could become incised. A few streams etched small transient valleys into the growing edifice, and spread thin fans of rhyolitic gravel onto the flanks of the dome. Near the end of Spectrum time basaltic lava began to erupt from several new summit vents. During this brief interval of Kitsu activity thin streams of black basalt coursed down the white flanks of Spectrum dome, covering and preserving a few remnants of the original surface and its mantle of fluvial gravel.

Pyramid Formation. For at least a million years following the final burst of ash from Spectrum dome the volcanoes of the Edziza complex lay dormant while streams and glacier ice cut deeply into their slopes. Spectrum dome itself was dissected by a system of radial drainage and the ever-widening valleys of trunk streams along the eastern and western sides of the complex encroached steadily on the edges of the old basaltic shields. The uplands, formed by Raspberry, Little Iskut and Nido volcanoes were

de large, et comprennent des fragments de roches du soubassement prétertiaire, ainsi que des fragments de roches dérivés du basalte sous-jacent de Nido et de la rhyolite des parties inférieures de l'amas volcanique de Spectrum. Un grand nombre de ces fragments avaient été arrondis par l'abrasion durant les violentes éruptions explosives qui avaient brassé, fracturé et refracturé l'énorme masse de roches broyées à l'intérieur de la cheminée volcanique.

À huit kilomètres à l'ouest de l'évent du pic Yeda, une éruption similaire, mais de bien plus faible envergure, avait édifié la colline Exile (fig. 94); il s'agit d'un cône satellite situé à proximité du bord du dôme de lave principal de Spectrum. La première éruption explosive avait formé une diatrème d'environ 200 m de large, au moyen de laquelle des laves trachytiques s'étaient ensuite frayées un passage jusqu'à la surface. Il a fallu au moins trois éruptions successives de laves émises par le cratère pour créer un petit dôme satellite d'environ 100 m de haut.

Un panache de vapeurs sulfureuses avait continué à s'élever du dôme Spectrum bien après la fin de l'épanchement des laves. Une grande partie de cette vapeur a été émise par des fumaroles à l'intérieur et autour du cratère du pic Yeda, duquel de violents jets de vapeur s'étaient directement échappés des recoins profonds de l'ancienne chambre magmatique effondrée. Des milliers de fumaroles plus petites, qui avaient pour origine les vapeurs libérées par le refroidissement des coulées elles-mêmes, parsemaient la surface du dôme environnant. Chaque groupe d'évents produisant de la vapeur était entouré d'une surface de couleur rouge vif et jaune, produite par la réaction des gaz sulfureux chauds et des eaux acides au contact de la roche.

Durant la phase d'activité du volcan Spectrum, plus de 100 km³ de rhyolite et de trachyte avaient été libérés par des éruptions. Les coulées s'étaient déversées en succession rapide, et avaient comblé l'espace de vallées potentielles, avant même qu'un réseau hydrographique intégré n'ait pu se constituer. Quelques cours d'eau avaient incisé de petites vallées transitoires dans l'édifice qui se formait, et étalé de minces cônes alluviaux de graviers rhyolitiques sur les flancs du dôme. Vers la fin de l'intervalle de Spectrum, des laves basaltiques avaient commencé à s'échapper de plusieurs nouveaux cratères sommitaux. Durant ce bref intervalle d'activité volcanique du Kitsu, de minces coulées de basalte noir avaient dévalé les flancs décolorés du dôme Spectrum, puis recouvert et préservé quelques vestiges de la surface originale et de sa couverture de graviers fluviaux.

Formation de Pyramid. Pendant au moins un million d'années après la dernière éruption de cendres du dôme Spectrum, les volcancs du complexe d'Edziza sont restés inactifs, tandis que les cours d'eau et les glaciers ont sans relâche incisé leurs versants. Le dôme Spectrum lui-même a été profondément disséqué par un réseau radial de drainage, et les vallées de plus en plus larges des fleuves principaux, le long des versants est et ouest du complexe, ont continuellement gagné du terrain sur les bords des anciens boucliers basaltiques. Les

soon bounded by low escarpments cut into their flanks and tributary streams began to erode small box canyons into the outer edge of the volcanic plateau. At higher elevations, where drainage was not yet incised, small glacier-fed streams meandered across the gently sloping plateau, depositing outwash fans of fluvial gravel, reworked cinders and ash. During this period of dormancy the waxing and waning of the central ice cap spread glacial-fluvial and morainal deposits over much of the upland surface.

One million years ago the long period of quiet ended with the explosive discharge of pumice, gas and rock fragments from a vent near the northeastern edge of the complex. This violent eruption, accompanied by pyroclastic surges (Fig. 101) and phreatic explosions, marked the beginning of Pyramid activity (Fig. 100). It was followed by the relatively quiet effusion of basalt (Fig. 102) which spread in thin flows across the surface of the surge deposits and entered the valley of a north-flowing glacial stream. Layers of lag gravel being carried north by this stream were buried by successive flows and a small lake was ponded on the southern edge of the growing basalt pile (Fig. 111).

The basaltic stage of volcanism was short-lived and the small lava field it produced was rapidly buried beneath felsic flows and domes that issued during the main pulse of Pyramid activity that followed (Fig. 111). This began with eruption of the Pyramid, probably from the same vent that discharged the precursor, pyroclastic surge deposits. The magma that formed this first Pyramid dome was already partly crystalline before it reached the surface. With up to 40% of its volume consisting of solid feldspar crystals the lava was too viscous to form flows. Instead it welled out above the vent into a bulbous dome 1 km across and 400 m high. Scale and slabs spalled off the steaming surface of the growing dome and formed a peripheral apron of brown, oxidized debris. Part of this was buried beneath the expanding mass, but no true lava flows advanced beyond the edge of the dome.

A period of quiescence intervened between the eruption of the Pyramid dome and the next major pulse of Pyramid activity. During this time, detritus eroded from the Pyramid was spread by local streams onto the surface of the surrounding plateau (Fig. 106) and, farther south a major ice field began to advance out of the Armadillo Highlands. By the time volcanic activity resumed with eruption of Sphinx dome the ice front had advanced almost as far north as Pyramid dome and the first Sphinx

hautes-terres formées par les volcans Raspberry, Little Iskut et Nido ont rapidement été limitées par des escarpements peu élevés, entaillés dans leurs flancs; les cours d'eau tributaires ont commencé à éroder de petits canyons rectangulaires dans le rebord extérieur du plateau volcanique. À plus grande altitude, là où le réseau hydrographique n'avait pas encore réussi à inciser le terrain, de petits cours d'eau alimentés par les glaciers ondulèrent à travers le plateau en pente douce, en créant des plaines d'épandage fluvio-glaciaire couvertes de graviers fluviaux, de cendres et de scories remaniées. Durant cette période d'inactivité volcanique, la croissance et la disparition de la calotte glaciaire centrale ont contribué à déposer des sédiments fluvio-glaciaires et morainiques sur une grande partie de la surface des hautes-terres.

Il y a un million d'années, la longue période de calme a été interrompue par l'émission explosive de pierre ponce, de gaz et de fragments rocheux à partir d'une bouche volcanique situé à proximité du bord nord-est du complexe. Cette violente éruption, accompagnée de montées de matériaux pyroclastiques (fig. 101) et d'explosions phréatiques, a marqué le début de l'activité du volcan Pyramid (fig. 100). Elle a été suivie de l'effusion, dans des conditions relativement calmes, de basaltes (fig. 102) qui se sont répandues en minces coulées sur la surface des dépôts pyroclastiques, et ont pénétré dans la vallée d'un torrent glaciaire dont l'écoulement se faisait en direction du nord. Les couches de pavage désertique, entraînées vers le nord par ce cours d'eau, ont été ensevelies par des coulées successives, et un petit lac de barrage naturel s'est constitué sur le bord sud de l'édifice basaltique en formation (fig. 111).

La phase basaltique du volcanisme a duré peu de temps, et le petit champ de laves qu'elle a créé a été rapidement enseveli par des coulées et dômes de couleur claire créés durant la période suivante, soit la phase principale d'activité du volcan Pyramid (fig. 111). Cette seconde phase a commencé avec l'éruption du volcan Pyramid, probablement à partir du même cratère qui avait émis les dépôts pyroclastiques précurseurs. Le magma qui avait édifié ce premier dôme du volcan Pyramid avait déjà un caractère partiellement cristallin avant d'atteindre la surface. Étant donné qu'à presque 40% de son volume, il était composé de cristaux feldspathiques solides, les laves étaient trop visqueuses pour engendrer des coulées. Au lieu de se répandre, les laves ont dû sourdre de l'évent pour former un dôme de 1 km de large et de 400 m de haut. Des écailles et plaques se sont détachées de la surface fumante du dôme en formation, et ont créé une nappe alluviale périphérique composée de débris oxydés de couleur brune. Une partie de ces dépôts ont été ensevelis sous la masse en expansion, mais aucune vraie coulée de lave n'a progressé au-delà des bords du dôme.

Une période de tranquillité a marqué la période entre l'éruption du dôme Pyramid et la principale phase suivante d'activité du volcan Pyramid. Durant cette époque, des débris arrachés par l'érosion au volcan Pyramid ont été étalés par des cours d'eau locaux à la surface du plateau environnant (fig. 106) et plus au sud, un grand champ de glace a commencé à progresser en dehors des hautes-terres d'Armadillo. Au moment où l'activité volcanique a repris, et où s'est manifestée l'éruption du dôme Sphinx, le front glaciaire avait progressé

magma may have erupted under ice. As the Sphinx dome was enlarged by successive effusions of viscous rhyolite, a body of water, Tut lake, was ponded between the growing dome and the ice field along its southern margin (Fig. 109). Extrusion of lava was accompanied by minor bursts of pyroclastic activity during which pumice, incandescent blocks, and lapilli were discharged. Part of this material fell into Tut lake and settled to form evenly bedded, and graded lacustrine deposits. Much of the pumice that fell onto surrounding areas of land and ice was also flushed by running water into the lake, where it accumulated in chaotic deposits, mixed with foreign blocks, pebbles and boulders stripped from the old plateau surface. Molten globules of magma, thrown into the lake or onto adjacent ice, were quenched to a dense, uniform glass with closely spaced thermal shock fractures. Disintegration of these "crackled" vitreous globules released polygonal, fracture-bounded granules of obsidian 1-2 cm across. These accumulated in lenses and thin beds throughout the lacustrine deposits.

By the time Sphinx activity ceased, the dome had grown to an elongated ridge of rhyolite over 5 km across and 800 m high. Its northeastern edge lapped against and partly covered the older dome of The Pyramid and a broad delta of pumice and alluvial deposits extended from the southern slope of the dome to the shores of Tut lake. South of the lake rhyolite magma began to issue from a new vent beneath the growing mantle of glacier ice. As this new pile expanded to form Pharaoh dome its outer edge was quenched in the moat of meltwater separating it from the surrounding ice and in the remnants of Tut lake ponded along its northern edge (Fig. 111). Where the rhyolite lava entered water it fractured and spalled into glassy fragments and blocks to form a chaotic pile of tuff-breccia churned by violent boiling and phreatic steam explosions. Later flows spread out over the peripheral pile of tuff-breccia and ultimately built Pharaoh dome above the level of the surrounding ice.

For a short time after its final eruption Pharaoh dome stood as a steaming nunatak projecting above the surface of a vast ice field, but ultimately it too was buried by ice. As glaciers of the Central Highlands expanded and merged with lobes of ice flowing out of the Coast Mountains the region entered a major period of glaciation, a period during which the dormant volcanoes of the Mount Edziza Volcanic Complex would yield to the eroding power of a regional ice sheet.

vers le nord, jusqu'au dôme du volcan Pyramid, et il se peut que l'émission de magma du volcan Sphinx se soit produite au-dessous de la glace. Alors que des effusions successives de rhyolite visqueuse agrandissaient le dôme du volcan Sphinx, un plan d'eau, le lac Tut, a été formé par le barrage naturel existant entre le dôme qui se développait, et le champ de glace bordant sa marge sud (fig. 109). L'extrusion des laves a été accompagnée de manifestations peu importantes d'activité pyroclastique, durant lesquelles ont été émis de la pierre ponce, des blocs incandescents et des lapilli. Ces matériaux sont retombés en partie dans le lac Tut, où ils ont formés, en se déposant, des sédiments lacustres uniformément lités et granulés. Une grande partie de la pierre ponce retombée dans la région environnante, soit au sol, soit sur la glace, a aussi été entraînée par les eaux courantes jusque dans le lac, où elle s'est accumulée sous forme de dépôts chaotiques, mêlés à des blocs, galets et pierres de grande taille arrachées à la surface de l'ancien plateau. Des globules fondus de magma, projetés dans le lac ou sur la glace adjacente, ont été brusquement refroidis, et ont donné un verre dense et uniforme caractérisé par des fractures de choc thermique, très rapprochées. La désagrégation de ces globules vitreux « disloqués » a libéré des granules palagonitiques d'obsidienne, limités par des fractures, et dont la taille atteignait de 1 à 2 cm. Ces granules se sont accumulés en formant des lentilles et de minces couches dans l'ensemble des dépôts lacustres.

À l'époque où l'activité du volcan Sphinx a pris fin, le dôme avait grandi jusqu'à devenir une crête allongée de rhyolite de plus de 5 km de large et 800 m de haut. Son bord nord-est effleurait ou couvrait partiellement l'ancien dôme du volcan Pyramid, et un vaste delta de dépôts de pierre ponce et dépôts alluviaux s'étendait de la pente sud du dôme jusqu'aux rives du lac Tut. Au sud du lac, un magma rhyolitique a commencé à s'échapper d'un nouvel événement situé au-dessous du manteau de plus en plus épais de glace de glacier. À mesure que ce nouvel amas s'élargissait pour donner le dôme Pharaoh, son bord extérieur a été brusquement refroidi dans le fossé rempli d'eau de fonte qui le séparait de la glace environnante, et dans les vestiges du lac Tut, endigué le long de son bord septentrional (fig. 111). Là où la lave rhyolitique avait pénétré dans l'eau, elle s'était fracturée et débitée en fragments vitreux et désagrégée en blocs, formant ainsi un amas chaotique de brèche tufacée, agité par des bouillonnements violents et par des explosions phréatiques. Plus tard, les coulées se sont répandues sur l'amas périphérique de brèche tufacée, et ont fini par édifier le dôme Pharaoh au-dessus du niveau de la glace environnante.

Pendant un certain temps après son éruption finale, le dôme Pharaoh accusait la forme d'un nunatak fumant qui émergeait de la surface d'un vaste champ de glace, mais les glaces ont finalement réussi à lui aussi l'ensevelir. À mesure que les glaciers des hautes-terres centrales s'agrandissaient et fusionnaient avec des lobes de glace s'écoulant des chaînons côtiers, la région a commencé à connaître une grande période de glaciation, durant laquelle les volcans inactifs du complexe volcanique de Mount Edziza allaient être soumis aux forces d'érosion exercées par un inlandsis régional.

Ice Peak Formation. The regional ice sheet which covered the volcanic complex in post-Pyramid time had started to recede long before the onset of Ice Peak volcanism. Large areas of the old plateau were ice-free, covered by till, recessional moraine and glacial-fluvial gravel, deposited behind the retreating ice. The first Ice Peak lava issued from a vent on the south flank of Sphinx dome, where residual ice still mantled the upper ridges and eastern slopes. During this early phase of activity glacial meltwater, mixed with newly erupted pyroclastic debris, glacial deposits and older colluvium, produced debris flows or lahars. These highly mobile slurries, carrying suspended blocks of solid rock, sped down radial valleys and deposited chaotic debris flows on the eastern side of the complex.

With each eruption the central edifice of Ice volcano was enlarged and successive flows spread farther and farther across the old glaciated surface (Fig. 118). Where glaciers were encountered, narrow meltwater lakes formed between the ice and the advancing lava front. Lava entering these lakes was quenched to form pillow lava and tuff-breccia, displacing the meltwater pond and the ice front progressively farther down slope (Fig. 122). But most of the Ice Peak activity was subaerial and centred around a cluster of vents near the present summit of Ice Peak. During its long period of activity Ice volcano erupted a variety of lava types. Viscous lava of intermediate composition piled up around the vent area in thick flows and domes which form the steep, upper part of the cone (Fig. 119). More fluid, basaltic lava streamed down the steeper slopes and spread in thin sheets across the gently sloping surface of the surrounding plateau. Periods of activity were separated by periods of dormancy during which glaciers formed on the upper slopes and meltwater streams spread alluvial fans of gravel and redeposited tephra onto the surrounding shield. At the zenith of its growth Ice volcano was a beautifully symmetrical composite cone that rose to a small summit crater over 8000 ft (2400 m) high. Three thick, steep-sided lobes of blocky trachytic lava extended from satellitic domes on its western flank and beyond them sinuous flows of ropy basalt formed the barren surface of the surrounding shield.

South of Ice volcano, in the deeply dissected terrain west of Armadillo Highlands, two much smaller volcanoes, Camp Hill and Cache Hill (Fig. 118), were formed during Ice Peak time. Camp Hill, like Ice volcano itself, first erupted when remnants of glacier ice still covered parts of the plateau (Fig. 132). A circular meltwater pond formed in the ice above the vent and lava entering it was quenched, fractured and churned by repeated phreatic explosions. The resulting debris built a broad, circular tuff-cone which eventually grew above the level of the ponded

Formation d'Ice Peak. L'inlandsis régional qui recouvrait le complexe volcanique après l'intervalle de Pyramid avait commencé à reculer bien avant le commencement du volcanisme du pic Ice. De vastes zones de l'ancien plateau étaient libres de glaces et recouvertes de till, d'une moraine de retrait et de graviers fluvio-glaciaires, déposés au fur et à mesure que reculait la glace. Les premières laves du pic Ice ont été émises par un événement volcanique situé sur le flanc sud du dôme Sphinx, où de la glace résiduelle enveloppait encore les crêtes les plus hautes et les versants orientés vers l'est. Durant cette phase initiale d'activité, les eaux de fonte des glaciers, mêlées à des débris pyroclastiques nouvellement émis, à des dépôts glaciaires et à des colluvions anciennes, ont produit des coulées de débris ou lahars. Ces boues très mobiles, qui entraînaient des blocs de roche solide, ont dévalé les pentes des vallées radiales et ont laissé des coulées de débris chaotiques sur le versant est du complexe.

À chaque éruption, l'édifice central du volcan Ice s'est agrandi, et les coulées successives se sont répandues de plus en plus loin sur l'ancienne surface recouverte par les glaces (fig. 118). Là où ces coulées ont rencontré les glaciers, des lacs étroits d'eau de fonte se sont constitués entre la glace et le front des laves en progression. Les laves pénétrant dans ces lacs ont été soudainement refroidies, et ont ainsi formé des laves en coussins et des brèches tufacées, et déplacé la mare d'eau de fonte et le front glaciaire progressivement plus en aval de la pente (fig. 122). Toutefois, la majeure partie de l'activité volcanique dans la région du pic Ice était de nature subaérienne, et centrée sur un groupe de cratères proches du sommet actuel du pic Ice. Durant sa longue période d'activité, le volcan Ice a émis divers types de laves. Des laves visqueuses de composition intermédiaire se sont accumulées autour du cratère en épaisses coulées et dômes qui constituent la partie fortement inclinée et supérieure du cône (fig. 119). Des laves basaltiques plus fluides, se sont écoulées le long des pentes les plus raides, et se sont étalées en nappes sur la surface doucement inclinée du plateau environnant. Les périodes d'activité volcanique ont été interrompues par des périodes d'inactivité, durant lesquelles les glaciers formés sur les pentes supérieures et les torrents d'eau de fonte ont créé des cônes alluviaux de graviers et redéposé des tephra sur le bouclier environnant. Au zénith de sa croissance, le volcan Ice présentait un cône composite parfaitement symétrique, qui s'élevait jusqu'à un petit cratère sommital dépassant 8000 pi. (2 400 m) d'altitude. Trois lobes épais, à pentes raides et composés de laves trachytiques blocailleuses, portaient de dômes satellites construits sur son flanc ouest et au-delà, des coulées sinueuses de basalte cordé couvraient la surface désolée du bouclier environnant.

Au sud du volcan Ice, dans le terrain fortement disséqué situé à l'ouest des hautes-terres d'Armadillo, deux volcan beaucoup plus petits, ceux de la colline Camp et de la colline Cache (fig. 118), ont pris naissance durant l'époque d'activité volcanique du pic Ice. La colline Camp, comme le volcan Ice lui-même, a fait éruption pour la première fois alors que la glace de glacier résiduelle recouvrait encore des parties du plateau (fig. 132). Une mare circulaire d'eau de fonte s'est formée dans la glace au-dessus de l'événement, et les laves pénétrant dans

water. Subsequent eruption of subaerial fire fountains built a relatively steep-sided pyroclastic cone on top of the tuff ring. Before Camp Hill activity ceased, the surrounding ice had receded and lava flows spread in thin sheets to build a small shield on top of the glacial deposits.

By the time Camp Hill erupted, glacier ice had retreated into the highlands, and gravel, carried by swift melt-water streams, was being deposited on thick alluvial fans and aggrading bars in the more gently sloping main valleys. The first Cache Hill lava issued from a vent in the broad valley of a northwesterly flowing river on the west side of Armadillo Highlands. The flows spread across the valley, damming the river and ponding a small lake above the lava dam. Later, southeasterly directed flows entered the lake forming pillow lava and tuff-breccia, whereas northwesterly directed flows spread in thin sheets across dry gravel bars below the dam. Cache Hill activity continued until a small, intermontane shield filled the old valley and forced the river into a new, more westerly, course.

The long period of Ice Peak volcanism was accompanied by the waxing and waning of alpine glaciers which cut deep cirques into the summit of Ice volcano even during its active period. By the time Ice Peak activity ceased, between 0.5 and 1 million years ago, the advancing summit glaciers of Ice volcano had merged with those of the Armadillo Highlands and spread out across the low shields of Cache Hill and Camp Hill. The culmination of this glacial advance was part of a regional Pleistocene ice sheet and, once again, the volcanoes of the Mount Edziza Volcanic Complex were shrouded in a thick mantle of glacier ice.

Pillow Ridge Formation. The symmetrical cone of Ice volcano was already sheathed in a mantle of glacier ice when the final surge of lava issued from satellitic vents on its western flank. The thick, ice-ponded flows of this climactic eruption momentarily held back the advancing glaciers and then, they too were enveloped by the rising tide of ice. At the climax of their advance, about a million years ago, the glaciers had merged into a vast, regional ice sheet. Only the highest peaks rose above its nearly flat surface which stood at an elevation of at least 7500 ft (2285 m)

cette mare ont été brusquement refroidies, fracturées et brisées par des explosions phréatiques répétées. Les débris résultants ont édifié un vaste cône circulaire composé de tufs, qui a fini par s'élever au-dessus du niveau des eaux endiguées. Les éruptions ultérieures de fontaines de laves incandescentes, au-dessous de la surface de l'eau, ont édifié un cône pyroclastique à versants relativement raides au sommet de l'anneau de tufs. Avant les dernières phases d'activité de la colline Camp, les glaces environnantes avaient reculé et les coulées de lave s'étaient étalées en minces nappes, qui ont construit un bouclier de faible étendue au sommet des dépôts glaciaires.

Au moment de l'éruption du volcan de la colline Camp, la glace de glacier s'était retirée jusque dans les hautes-terres, et les graviers, entraînés par les torrents d'eau de fonte, se sont déposés sur d'épais cônes alluviaux et bancs alluviaux, dans les vallées principales à pente plus douce. Les premières laves du volcan de la colline Cache ont été émises par un événement situé dans la vaste vallée d'un cours d'eau s'écoulant vers le nord-ouest, du côté ouest des hautes-terres d'Armadillo. Les coulées se sont répandues dans la vallée, bloquant le cours d'eau et permettant la formation d'un petit lac au-dessus d'un barrage naturel de lave. Plus tard, des coulées de direction sud-est ont pénétré dans le lac en formant des laves en coussins et brèches tufacées, tandis que des coulées de direction nord-ouest se sont étalées en minces nappes sur des bancs de gravier secs, au-dessous du barrage naturel. L'activité du volcan de la colline Cache s'est poursuivie jusqu'à ce qu'un petit bouclier d'entremont ait comblé l'ancienne vallée, et dévié le cours d'eau dans une nouvelle direction, plus à l'ouest.

La longue période d'activité volcanique du pic Ice a été accompagnée de l'avancée et du recul des glaciers alpins qui ont entaillé de profonds cirques dans le sommet du volcan Ice, même durant la période d'activité de ce volcan. Au moment où l'activité volcanique du pic Ice a pris fin, soit il y a entre 0,5 et 1 million d'années, les glaciers sommitaux en progression du volcan Ice avaient fusionné avec ceux des hautes-terres d'Armadillo, et s'étaient étalés sur les boucliers peu élevés des collines Cache et Camp. Le point culminant de cette avancée glaciaire correspond à l'apparition d'un inlandsis régional d'âge pléistocène qui, une fois encore, a enseveli les volcans du complexe volcanique du mont Edziza sous un épais manteau de glace de glacier.

Formation de Pillow Ridge. Le cône symétrique du volcan Ice était déjà enveloppé d'un manteau de glace de glacier, lorsqu'a eu lieu la dernière émission de lave à partir d'événements satellites situés sur le flanc ouest de ce volcan. Les coulées épaisses, obstruées par les glaces, de cette ultime éruption ont momentanément empêché la progression des glaciers, puis ont été, elles aussi, submergées par la crue des glaciers. Au point culminant de leur avancée, il y a environ 1 million d'années, les glaciers avaient fusionné en un vaste inlandsis régional. Seuls les pics les plus élevés se dressaient au-dessus de sa surface presque plane, qui atteignait une altitude d'au moins 7500 pi (2285 m).

The dormant summit of Ice volcano was, for a time, the only visible evidence of the volcanic complex that lay sealed beneath the ice sheet. But deep in the earth's crust, far below the ice-covered volcanoes, a column of basaltic magma was rising through fractures toward the surface. The ice sheet was still near its maximum thickness when the first of this magma issued from a vent on the north slope of Ice volcano. Molten basalt, at a temperature of over 1000°C was injected into the base of the ice sheet and the quenched lava was ripped apart by violent steam explosions. As the shattered debris accumulated around the vent to form a growing pile of tuff-breccia a meltwater cavity was thawed at the base of the ice (Fig. 138, 144). At the surface the first eruption was heralded by a burst of steam from crevasses on the ice and later by surges of black, ash-laden water as meltwater was replaced and forced to the surface by basalt entering subglacial cavities. As the tuff-breccia pile and enclosing meltwater cavity grew larger the ice above them sagged to form a water-filled depression at the surface. The resulting lake, filled with floating blocks of ice and churned by violent phreatic explosions must ultimately have grown to a length of over 4 km. Within it, the pile of tuff-breccia and pillow lava continued to enlarge with each successive eruption until its summit rose above the lake surface. And for a brief period, near the end of Pillow Ridge activity, this small island, in a lake surrounded by ice, was the site of incandescent fire fountains and lava flows.

Not all of the magma in the deep conduit system was expelled during the initial series of eruptions that built Pillow Ridge. The remaining portion, modified by partial crystallization, was erupted later to form the small, nearby pile of Tsekone Ridge (Fig. 138, 139). The ice sheet still stood at least 215 m above the plateau when Tsekone Ridge erupted. There is no evidence that it ever grew above the ice surface but its history and eruptive environment were otherwise similar to Pillow Ridge.

Edziza Formation. The ice sheet that covered the entire Stikine region during the Pillow Ridge and Tsekone eruptions had receded, at least from the upper slopes and surrounding plateau of the volcanic complex, before the next major episode of volcanic activity. The glacially scoured slopes of Ice volcano lay bare beneath its craggy, crescent-shaped summit where a deep cirque opened into the eastern side of the breached crater. On the north side of Ice volcano the narrow black crest of Pillow Ridge sloped down toward the plateau, almost to the base of the isolated, 600 ft (180 m) high mound of Tsekone Ridge. High on the north slope of Ice volcano, near the southeastern

Le sommet inactif du volcan Ice a été pendant un certain temps le seul indice visible de l'existence du complexe volcanique qui gisait enseveli sous l'inlandsis. Mais au sein de la croûte terrestre, bien au-dessous des volcans couverts par les glaces, une colonne de magma basaltique remontait le long des fractures jusqu'à la surface. L'inlandsis atteignait encore presque son épaisseur maximale, lorsque la première émission de ce magma a eu lieu à partir d'un événement situé sur le versant nord du volcan Ice. Du basalte en fusion dont la température dépassait 1000 °C s'est trouvé injecté dans la base de l'inlandsis, et la lave ainsi brutalement refroidie a été fragmentée par de violentes explosions phréatiques. À mesure que s'accumulaient les débris de l'explosion autour de l'événement, en formant un amas de plus en plus élevé de brèches tufacées, une cavité remplie d'eau de fonte s'est formée à la base de la glace (fig. 138, 144). À la surface, la première explosion s'est manifestée par un jaillissement de vapeur issu des crevasses traversant la glace, et plus tard par des torrents d'eau noire chargée de cendres, à mesure que l'eau de fonte était remplacée et repoussée en surface par le basalte pénétrant dans des cavités sous-glaciaires. À mesure que croissaient l'édifice de brèche tufacée et la cavité environnante occupée par les eaux de fonte, la glace sus-jacente s'affaissait de façon à former une dépression superficielle remplie d'eau. Le lac ainsi formé, plein de blocs de glace flottante et agité par de violentes explosions phréatiques, a sans doute fini par atteindre une longueur de plus de 4 km. À l'intérieur de ce dernier, l'amas de brèches tufacées et de laves en coussins a continué à s'agrandir chaque fois que se produisait une éruption, jusqu'à ce que son sommet émerge de la surface du lac. Pendant un court intervalle de temps, alors que l'activité du volcan de la crête Pillow tirait à sa fin, cet îlot, situé dans un lac entouré de glaces, a été embrasé par des jaillissements de produits incandescents et des coulées de lave.

Une partie du magma se trouvant dans le profond réseau de conduits volcaniques n'a pas été éjectée durant la série initiale d'éruptions qui ont édifié la crête Pillow. Le reste du magma, modifié par cristallisation fractionnée, a plus tard été libéré par une éruption qui a formé l'édifice proche et de petite taille de la crête Tsekone (fig. 138, 139). L'inlandsis dominait encore d'au moins 215 m le plateau, lorsqu'a eu lieu l'éruption du volcan de la crête Tsekone. Il ne semble pas que ce volcan ait jamais émergé de la surface des glaces, mais son évolution et le milieu dans lequel se sont déroulées ces éruptions étaient par ailleurs semblables à ceux caractérisant le volcan de la crête Pillow.

Formation d'Edziza. L'inlandsis qui recouvrait toute la région de Stikine durant les éruptions des volcans des crêtes Pillow et Tsekone avait reculé, du moins des pentes supérieures du complexe volcanique et du plateau environnant, avant l'importante manifestation ultérieure d'activité volcanique. Les pentes du volcan Ice affouillées par les glaces, et d'aspect désolé, étaient dominées par son sommet rocaillieux, en forme de croissant, au niveau duquel un cirque profond s'ouvrait sur le versant est du cratère érodé. Du côté nord du volcan Ice, l'étroite crête noire du volcan de la crête Pillow descendait en pente vers le plateau, presque jusqu'à la base du monticule de 600 pi (180 m) d'altitude que constituait la crête Tsekone; sur

end of Pillow Ridge, a bulge of steaming rubble heralded the birth of a new volcano. Viscous trachyte magma, forcing its way into the base of the bulge, about 900,000 years ago, was the first of many surges of trachyte that ultimately built the present, symmetrical cone of Mount Edziza (Fig. 150). During its long history of activity the effusion of trachyte flows and steep-sided domes was punctuated by vent-clearing explosions. Blocks torn from the conduit were thrown, along with tephra and bombs, onto the flanks of the growing cone and later buried by flows that welled over the crater rim. Most of this activity was concentrated in the summit area but at least two satellite vents erupted near the base. A small pyroclastic cone on the northwest flank was the source of a relatively fluid trachyte flow that spread onto the plateau, burying the lower slopes of Pillow Ridge and nearly surrounding Tsekone Ridge. Similar trachyte issued from a vent on the northeast flank and spread in thin flows across the gently sloping plateau (Fig. 164). This vent was later occupied by a plug of viscous trachyte that welled out to form the steep-sided monolith of Glacier Dome (Fig. 163, 164).

At the zenith of its growth Mount Edziza rose to a small crater at least 2000 ft. (610 m) higher than the present 3 km wide, basin-shaped summit. The original summit was probably destroyed during a violent, climactic eruption—part of it was shattered and blown onto the flanks of the truncated cone and part of it foundered into the newly formed crater (Fig. 156). The summit collapse was followed by a prolonged period of hydrothermal activity. Steam, sulphurous gases and hot, acidic water streamed through the broken rocks of the central conduit, altering them to clay and other secondary minerals. The plume of vapour that rose from the summit was punctuated by minor phreatic explosions that fractured and refractured the rocks of the central conduit.

During the waning stages of hydrothermal activity a final surge of lava issued from a vent on the southeast crater rim. Part of it spread onto the outer surface of the cone, building the circular mound of Nanook Dome (Fig. 158), and part of it flowed into the crater and was ponded in lava lakes that sealed the fuming vent (Fig. 155). Soon after the summit lava had consolidated a small phreatic explosion blew away a portion of the eastern crater rim, providing a new vent for escaping gases, and opening the initial scar that erosion would gradually enlarge into the present immense amphitheatre of Tenchen cirque (Fig. 152).

le haut du versant nord du volcan Ice, près de l'extrémité sud-est de la crête Pillow, un monticule de débris fumants annonçait la naissance d'un nouveau volcan. Un magma trachytique visqueux, se frayant un chemin dans la base de ce monticule, il y a environ 900 000 années, a donné lieu à la première des nombreuses émissions de trachyte, qui ont fini par édifier le cône actuel et symétrique du mont Edziza (fig. 150). Durant sa longue histoire d'activité volcanique, l'effusion de coulées trachytiques et la formation de dômes à versants raides ont été parfois marquées par des explosions qui ont dégagé les événements. Les blocs arrachés à la cheminée volcanique ont été projetés, en même temps que des tephra et bombes volcaniques, sur les flancs du cône en développement, et plus tard ensevelis par des coulées qui ont débordé du cratère. La majeure partie de cette activité se concentrait dans la région sommitale, mais au moins deux événements satellites ont fait éruption près de la base. Un petit cône pyroclastique situé sur le flanc nord-ouest a été la source d'une coulée trachytique relativement fluide qui s'est déversée sur le plateau, ensevelissant les pentes inférieures de la crête Pillow et entourant presque complètement la crête Tsekone. Un événement situé sur le flanc nord-est a émis un trachyte similaire, qui s'est répandu en minces coulées sur le plateau en pente douce (fig. 164). Cet événement a plus tard été comblé par un bouchon de trachyte visqueux, qui a formé, en s'épanchant, le monolithe à versants raides du dôme Glacier (fig. 163, 164).

Au zénith de sa croissance, le mont Edziza s'est agrandi jusqu'à former un petit cratère d'au moins 2000 pi (610 m) plus élevé que le sommet actuel en forme de bassin de 3 km de large. Le sommet original a probablement été détruit durant une éruption climatique particulièrement violente — une partie du sommet a été détruite, la violence de l'explosion projetant les fragments sur les flancs du cône tronqué, tandis que le reste du sommet s'effondrait dans le cratère nouvellement formé (fig. 156). L'effondrement du sommet a été suivi d'une période prolongée d'activité hydrothermale. De la vapeur, des gaz sulfureux et des eaux chaudes et acides circulaient à travers les roches fragmentées du conduit central, en les transformant en argile et en autres minéraux secondaires. Le panache de vapeur qui s'est élevé du sommet a été parfois interrompu par des explosions phréatiques mineures qui ont fracturé et refracturé les roches du conduit volcanique central.

Durant les dernières phases d'activité hydrothermale, a eu lieu une émission finale de lave à partir d'un événement situé sur le bord sud-est du cratère. Cette lave s'est en partie étalée sur la surface extérieure du cône, en édifiant le monticule circulaire du dôme Nanook (fig. 158); elle s'est en partie écoulée dans le cratère, où elle a formé des lacs de lave qui ont obturé l'événement fumant (fig. 155). Peu après la consolidation des laves du sommet, une petite explosion phréatique a détruit et projeté une partie du bord est du cratère, créant ainsi un nouvel événement par où pouvaient s'échapper les gaz, et ouvrant la cicatrice initiale qui, agrandie par l'érosion, allait devenir l'immense amphithéâtre que constitue maintenant le cirque Tenchen (fig. 152).

Klastline formation. The newly formed cone of Mount Edziza lay dormant beneath a mantle of alpine glaciers when basaltic lava of the Klastline Formation began to pour from vents along its northern flank. The present drainage system had already been established and the massive effusion of lava was channelled into the valleys of Kakiddi Creek and Klastline River, and onto the hummocky bottomland around Buckley Lake (Fig. 172). At least three, and possibly as many as six separate centres were active during Klastline time and each pulse of activity produced a surge of fluid magma which spread in thick flows up to 25 km long. The effusion of lava was accompanied by minor fire fountaining and construction of small pyroclastic cones around subaerial vents on the lower shield. But one vent, near an alpine glacier at the head of Pyramid Creek (Fig. 174), was repeatedly flooded by meltwater. The resulting steam produced phreatic explosions that threw out towering columns of ash and small cinders. This material, saturated with water from the condensing steam, accumulated around the vent to form a broad, complexly bedded tuff cone. Lava from this same vent coursed down into Kakiddi Valley, damming the creek and flowing north across the dry gravel bars to the confluence with Klastline Valley. There a second lava dam temporarily blocked Klastline River and ponded a large, shallow lake in the upper part of the valley. But more lava continued to pour from the vent. Part of it spilled off the eastern edge of the lava dam and was quenched in the ponded water to form pillow structures and breccia. Most of it streamed west and advanced for at least another 19 km down the narrow valley of Klastline River.

Arctic Lake Formation. At about the same time that lava began streaming into Klastline Valley from vents north of Mount Edziza two small volcanoes were born far to the south, on Arctic Plateau (Fig. 177). This nearly flat upland surface, perched between the deep canyon of Mess Creek on the west and the precipitous front of the Spectrum Range on the east, had been dormant for almost two million years when lava began to issue from the new centres. At the extreme northern end of the plateau, basaltic lava poured from a fountaining vent near the western edge of the Spectrum Range (Fig. 177). Westerly flowing streams were blocked by the growing pile of lava and bombs, which ultimately rose more than 1000 ft (300 m) above the plateau surface to form the composite cone of Outcast Hill (Fig. 178). A temporary lake was ponded against its eastern side and lava entering this was quenched to form pillows and tuff-breccia. Most of the lava from Outcast Hill flowed west, across alluvial fans, toward Mess Creek Escarpment.

Formation de Klastine. Le cône nouvellement formé du mont Edziza ne donnait aucun signe d'activité sous le manteau de glaciers alpins qui le recouvrait, lorsque les laves basaltiques de la formation de Klastine ont commencé à s'échapper d'événements situés le long de son flanc nord. Le réseau hydrographique actuel était déjà bien établi, et les effusions massives de lave ont été canalisées dans les vallées du ruisseau Kakiddi et de la rivière Klastine, et dans la plaine d'inondation d'aspect bosselé qui environne le lac Buckley (fig. 172). Au moins trois et peut-être même six centres volcaniques distincts étaient actifs durant l'intervalle de Klastine, et chaque manifestation d'activité a produit un épanchement de magma fluide qui s'est étalé en épaisses coulées pouvant atteindre 25 km de long. L'effusion de laves a été accompagnée de petites fontaines de laves incandescentes, et de l'édification de petits cônes pyroclastiques autour des événements subaériens du bouclier inférieur. Mais un événement, proche d'un glacier alpin à la source du ruisseau Pyramid (fig. 174), a été à plusieurs reprises inondé par des eaux de fonte. La vapeur ainsi produite a donné lieu à des explosions phréatiques qui ont projeté des colonnes gigantesques de cendres et petites scories. Ces produits, saturés d'eau par la condensation de la vapeur, se sont accumulés autour de l'événement et ont formé un large cône de tufs à litage complexe. Les laves provenant du même événement se sont rapidement déversées dans la vallée du ruisseau Kakiddi, obstruant ce ruisseau et s'écoulant vers le nord à travers les bancs de gravier secs, jusqu'à la confluence du ruisseau Kakiddi et de la vallée de la rivière Klastine. À cet endroit, un second barrage de lave a temporairement endigué la rivière Klastine, et créé un vaste lac peu profond dans la partie supérieure de la vallée. Mais l'événement a continué à déverser encore plus de lave. Une partie de cette lave a débordé à l'est de l'endiguement et, brusquement refroidie dans le lac de barrage naturel, a formé des structures en coussins et des brèches. La majeure partie de la lave s'est dirigée vers l'ouest et a progressé sur au moins 19 km de plus, suivant le cours de l'étroite vallée de la rivière Klastine.

Formation d'Arctic Lake. À peu près à l'époque où les laves ont commencé à s'écouler dans la vallée de la rivière Klastine à partir d'événements situés au nord du mont Edziza, deux petits volcancs sont apparus loin au sud, sur le plateau Arctique (fig. 177). Cette surface élevée, presque plane, perchée entre le canyon profond du ruisseau Mess à l'ouest et le front abrupt du chaînon Spectrum à l'est, était demeurée inactive pendant presque deux millions d'années, lorsque les laves ont commencé à s'échapper des nouveaux centres d'éruptions. Tout à fait à l'extrémité nord du plateau, des laves basaltiques ont jailli d'un événement proche du bord ouest du chaînon Spectrum (fig. 177). Des cours d'eau orientés vers l'ouest ont été obstrués par l'amas grandissant de lave et de bombes volcaniques, qui finalement s'est dressé plus de 1000 pi (300 m) au-dessus de la surface du plateau, et a ainsi mené à la formation du cône composite de la colline Outcast (fig. 178). Un lac temporaire de barrage naturel a pris naissance contre son versant est, et les laves qui s'y déversaient, brutalement refroidies, ont formé des coussins et des brèches tufacées. La majeure partie des laves provenant de la colline Outcast se sont écoulées vers l'ouest, en traversant des cônes de déjection, en direction de l'escarpement dominant le ruisseau Mess.

Four kilometres south of Outcast Hill a second vent opened near the crest of a small hill on the plateau. The old hill, a 600 ft. (180 m) high erosional remnant of Spectrum trachyte, was almost completely buried by the younger composite cone of Tadekho Hill which was built over it. The Tadekho flows spread onto the plateau, forming a small shield that overlapped the distal flows from Outcast Hill.

The eruptions that built Outcast Hill and Tadekho Hill were the first in a long series of eruptions from many different centres on Arctic Plateau. When the activity began the plateau was relatively ice-free, but shortly thereafter the final advance of Pleistocene glaciation began. Glaciers, advancing out of the Spectrum Range, merged with ice from the Coast Mountains covering Arctic Plateau, along with Outcast and Tadekho hills, beneath at least 300 m of ice. At the height of this glacial advance a small volume of basaltic magma issued from a vent near the centre of Arctic Plateau. It thawed a meltwater cavity at the base of the ice sheet where it accumulated to form Wetalth Ridge, a steep-sided pile of quenched pillow lava and tuff-breccia. For a short time a depression formed on the surface of the ice above the Wetalth vent and ash may have been thrown out by phreatic explosions. But the steady, northwesterly flow of ice soon carried away the surface scar and began to erode the hidden pile of Wetalth lava.

Before the ice receded at least three more centres erupted on the Arctic Plateau (Fig. 177). Knob 1 and knob 2 are small mounds of pillow lava which probably erupted beneath the ice during the waning stages of glaciation. When only a thin lobe of ice remained in the central part of the plateau a massive effusion of lava issued from a vent at Source hill. The vent itself lay west of the ice margin, but flows spreading east impinged on the ice and as the broad lobe of lava advanced the ice was melted back. The resulting torrent of meltwater was channelled south along the advancing lava front. Finally the lava itself converged into the narrow valley of More Creek, along which it advanced for another 4.5 km.

Glacier ice melted by the Source hill lava was re-established on the flows after the cessation of volcanic activity. It advanced almost to the western edge of the plateau before stagnating and finally wasting away, leaving the scoured surface of the flows covered with moraine, drumlins and glacial-fluvial gravel. During this final period of ice stagnation a small eruption on the east side of the plateau built Thaw cone (Fig. 179). The eruption may have produced a flood of meltwater which escaped northwesterly, across the rock-strewn surface of the stagnating ice.

À 4 km au sud de la colline Outcast, est apparu un second événement près de la crête d'une petite colline qui émergeait du plateau. L'ancienne colline, inselberg de 600 pi (180 m) de haut composé de trachyte de Spectrum, a été presque entièrement ensevelie par le cône composite plus récent de la colline Tadekho, qui s'est construit au-dessus d'elle. En se répandant sur le plateau, les coulées de Tadekho ont formé un bouclier de petite taille qui a partiellement recouvert les coulées distales en provenance de la colline Outcast.

Les éruptions qui ont édifié la colline Outcast et la colline Tadekho ont été les premières d'une longue série provenant de divers centres éruptifs situés sur le plateau Arctique. Lorsque l'activité a commencé à se manifester, le plateau était relativement libre de glaces, mais peu après, a débuté l'avancée finale de la glaciation du Pléistocène. Les glaciers, qui progressaient à partir du chaînon Spectrum, ont fusionné avec les glaces provenant de la chaîne Côtière, et ont recouvert le plateau Arctique, en même temps que les collines Outcast et Tadekho, d'une couche de glace d'au moins 300 m d'épaisseur. À l'apogée de cette avancée glaciaire, un petit volume de magma basaltique a été émis par un événement proche du centre du plateau Arctique. En faisant fondre la glace, ce magma basaltique a créé une cavité d'eau de fonte à la base de l'inlandsis et a formé, en s'y accumulant, la crête de Wetalth, édifice à versants raides, composé de brèches tufacées et de laves en coussins formées par refroidissement brutal. Pendant un court intervalle de temps, est apparue une dépression à la surface de la glace au-dessus de l'évent de Wetalth, et il est possible que des cendres aient été éjectées par des explosions phréatiques. Mais l'écoulement continu de glace en direction du nord-ouest a effacé la cicatrice de surface, et commencé à éroder l'amas dissimulé des laves de Wetalth.

Avant le recul des glaces, au moins trois centres éruptifs supplémentaires se sont manifestés sur le plateau Arctique (fig. 177). Le monticule 1 et le monticule 2, petites éminences de laves en coussins, ont probablement été émises sous la glace durant les derniers stades de la glaciation. Alors qu'il ne restait qu'un mince lobe de glace dans la partie centrale du plateau, un événement situé sur la colline Source a émis une quantité considérable de lave. L'événement lui-même se trouvait à l'ouest de la marge glaciaire, mais les coulées qui s'étaient vers l'est ont empiété sur les glaces, et à mesure que progressait le vaste lobe de lave, la glace reculait en fondant. Le torrent d'eau de fonte ainsi produit s'est dirigé vers le sud le long du front des laves en progression. Finalement, les laves elles-mêmes ont convergé dans l'étroite vallée du ruisseau More, dans laquelle elles ont continué à avancer sur 4,5 km.

Les glaces de glacier qu'avaient fait fondre les laves de la colline Source se sont reconstituées sur les coulées, lorsqu'a pris fin l'activité volcanique. Les glaces ont progressé presque jusqu'au bord ouest du plateau, avant de devenir stationnaires et finalement de disparaître, en abandonnant sur la surface des coulées qu'elles avaient affouillée, des moraines, drumlins et graviers fluvio-glaciaires. Durant cette période finale de stagnation des glaces, a eu lieu une petite éruption sur le versant est du cône Thaw, édifié sur le plateau (fig. 179). Il est possible que l'éruption ait produit une crue d'eaux de fonte, qui se sont

MOUNT EDZIZA

Narrow, deeply incised channelways, cut into the ice by the initial surge of meltwater from Thaw cone, continued to serve as the main corridors of meltwater discharge during the final period of glacial wasting.

By the time the last ice had melted from Arctic Plateau, Thaw cone itself had been slightly modified by glacial scouring (Fig. 180). A network of converging eskers extended from the quenched base of the cone northwesterly across the plateau. Formed of sand and gravel that had accumulated within the old meltwater channels, these sinuous ridges were deposited on the plateau when the enclosing ice melted. Their northwesterly course has been abandoned by the present southerly-flowing streams. But the eskers, lava flows and eroded cinder cones remain, the relics of a dynamic, rapidly changing landscape.

Kakiddi Formation. About half a million years ago an immense, rubble-covered lava flow, almost 1 km wide and 60-90 m thick, advanced slowly down the ancestral valley of Sorcery Creek and entered the hummocky lowlands of Kakiddi Valley (Fig. 181). There its expanding terminal lobe, fed by a continuing supply of lava, welled out onto the flat valley bottom until it covered an area of more than 20 km². If an observer could have followed the lava stream west toward its source, he would have come to several junctions where the stream of lava divided into tributary streams, each flowing from somewhere still higher on the mist-shrouded slopes of Ice Peak. Unable to see farther our imaginary observer could report only that several enormous streams of lava were coursing down valleys on the east side of Ice Peak. Their source remains a mystery. The fragile tephra cones that may have formed around the vents were rapidly eroded from the steep terrane on which they formed. Except for a few scattered remnants, even the upper parts of the lava flows are gone. They were probably deposited on unconsolidated tephra, talus and debris fans that filled the upper part of the valleys. As this foundation of loose material was undercut by torrential streams the lava itself collapsed and was gradually eroded away.

We can only speculate on the source of the Kakiddi lava flows. Those in the south forks of Tennaya Creek probably issued from vents in or near the valleys containing them. The main flow that descended Tennaya Creek must have issued from a vent, now covered by glaciers, near the summit of Ice Peak (Fig. 182). Some of it may have issued from Nanook Dome on the southeast rim of Mount Edziza and a relatively small lobe spread onto the plateau from a vent at Punch cone (Fig. 187) on the west

dirigées vers le nord-ouest, en traversant la surface rocailleuse de la glace stagnante. Des chenaux étroits et profondément encaissés, entaillés dans la glace par la crue initiale des eaux de fonte en provenance du cône Thaw, ont continué à canaliser la majeure partie des eaux de fonte durant la période finale de disparition des glaces.

Alors que les dernières glaces du plateau Arctique finissaient de fondre, le cône Thaw lui-même avait déjà été légèrement modifié par l'affouillement glaciaire (fig. 180). Un réseau d'eskers convergents s'étendait de la base du cône couverte de laves brusquement refroidies par l'eau, vers le nord-ouest, en travers du plateau. Constituées de sables et de graviers qui s'étaient accumulés à l'intérieur des anciens chenaux d'eau de fonte, ces crêtes sinueuses se sont déposées sur le plateau, lorsque la glace qui les recouvrait a fondu. Le cours nord-ouest des eaux de fonte a été abandonné par les cours d'eau actuels, qui se dirigent vers le sud. Mais les eskers, les coulées de lave et les cônes de scories érodés subsistent, vestiges d'un paysage dynamique, en évolution rapide.

Formation de Kakiddi. Il y a environ un demi-million d'années, une immense coulée de lave couverte de débris, d'environ 1 km de large et de 60 à 90 m d'épaisseur, a lentement descendu la vallée ancestrale du ruisseau Sorcery et a pénétré dans les basses-terres bosselées de la vallée de la rivière Kakiddi (fig. 181). Là, son lobe frontal en expansion, alimenté par un apport continu de lave, s'est répandu sur le fond plat de la vallée, jusqu'à couvrir une superficie de plus de 20 km². Si un observateur avait pu suivre l'écoulement de lave à l'ouest, en remontant jusqu'à sa source, il aurait rencontré plusieurs points de confluence, où cet écoulement de lave se subdivisait en tributaires, l'origine de chaque coulée se situant encore un peu plus haut sur les versants enveloppés de brume du pic Ice. Au-delà, la visibilité étant nulle, l'observateur imaginaire aurait seulement pu indiquer que plusieurs flots de lave très volumineux descendaient les vallées du côté est du pic Ice. La source de ces écoulements de lave demeure un mystère. Les fragiles cônes de tufs qui ont pu se former autour des événements ont été rapidement érodés sur les versants raides où ils étaient apparus. Sauf quelques vestiges épars, même les parties supérieures des coulées de lave ont disparu. Les laves s'étaient probablement déposées sur des tephra non consolidés, des talus d'éboulis, et des cônes de déjection qui comblaient la partie amont des vallées. À mesure que ce substrat de matériaux meubles a été sapé par les torrents, la lave elle-même s'est effondrée et a été graduellement enlevée par l'érosion.

On ne peut que spéculer à propos de la source des coulées de lave de Kakiddi. Les laves présentes dans les bras sud du ruisseau Tennaya ont probablement été émises par des événements situés à l'intérieur ou à proximité des vallées qui les ont canalisées. La principale coulée qui a suivi le cours de la vallée du ruisseau Tennaya, provenant probablement d'un événement maintenant couvert par les glaciers et proche du sommet du pic Ice (fig. 182). Une partie de cette coulée provenait peut-être du dôme Nanook, situé sur le bord sud-est du mont Edziza, et un

side of Ice Peak. Whatever its source, the massive effusion of Kakiddi lava was a landmark in the history of the Mount Edziza Volcanic Complex—the last major eruption of intermediate (trachyte) lava from a central vent.

Big Raven Formation. During the final waning of Pleistocene glaciation the volcanoes of the Mount Edziza Volcanic Complex began to assume their present form. At first the plateau, grooved, striated and strewn with glacial debris, began to emerge from beneath the ice. As the central ice cap retreated into the highlands turbulent melt-water streams spread their load of silt and gravel on thick alluvial fans along the upper edge of the plateau. For a time after the plateau was ice-free the stagnant remnants of valley glaciers lingered in Mess Creek and Kakiddi valleys, but these too wasted rapidly away in the steadily warming climate. As the supporting ice receded from valley walls the oversteepened slopes, burdened with unstable deposits of marginal moraine, collapsed in a series of great landslides that swept down the newly exposed escarpments into the major valleys. There the ancestral shrubs and trees of the present forest took root and spread to form a protective mat of roots and soil over the barren landscape that emerged from under the ice. Alpine willow and cariboo moss thrived on a mature tundra that extended across the plateau almost to the edge of the retreating central ice cap. Then, about 2600 years ago, the warming trend ceased and the shrunken glaciers again began to advance during Neoglaciation (Porter and Denton, 1967). From the summit areas of Mount Edziza, Ice Peak and the highlands of Armadillo and the Spectrum Range, the growing alpine glaciers expanded to new positions along the upper edge of the plateau. There they fluctuated between minor episodes of retreat and advance during the remainder of Neoglacial time, building furrowed terminal moraines which stand up to 18 m above the plateau and form the trimlines of the present alpine glaciers. The end of Neoglaciation in the early 20th century heralded the present trend toward more moderate climate and the rapid recession of alpine glaciers. Terminal moraines formed during Neoglacial advances now lie up to 2 km beyond the glaciers that formed them. So rapidly has the ice receded that no vegetation has yet been established on the barren, rocky ground between the trimline and the ice.

The waxing and waning of post-Pleistocene alpine glaciers was punctuated by the sporadic eruption of basalt from numerous satellitic cones throughout the Mount Edziza Volcanic Complex, and by a single climactic eruption of pumice from the south slope of Ice Peak. Together,

lobe relativement peu étendu s'est étalé sur le plateau à partir d'un événement situé sur le cône Punch (fig. 187) du côté ouest du pic Ice. Peu importe sa source, l'épanchement volumineux des laves de Kakiddi a été un événement marquant dans l'évolution du complexe volcanique de Mount Edziza, soit la dernière éruption importante de laves intermédiaires (trachytes) émises par un événement central.

Formation de Big Raven. Au cours de l'étape finale de disparition des glaciers du Pléistocène, les volcans du complexe volcanique de Mount Edziza ont commencé à prendre leur forme actuelle. Tout d'abord le plateau, sillonné de cannelures, de stries et de débris glaciaires, a commencé à émerger d'au-dessous de la glace. À mesure que la calotte glaciaire centrale se retirait dans les hautes-terres, les torrents d'eau de fonte ont déposé leur charge de limons et graviers sur d'épais cônes de déjection le long du bord supérieur du plateau. Pendant un certain temps après la disparition des glaces du plateau, les vestiges stagnants de glaciers de vallée ont subsisté un certain temps dans les vallées du ruisseau Mess et de la rivière Kakiddi, mais ceux-ci ont aussi rapidement fondu, étant donné les conditions de réchauffement continu. Au fur et à mesure que les glaces qui les soutenaient s'éloignaient des parois des vallées, les pentes très fortement inclinées, chargées des dépôts instables de moraines marginales, se sont écroulées en une succession de grands glissements de terrain qui ont déferlé le long des escarpements nouvellement exposés jusqu'au cœur des vallées principales. Là, les buissons et arbres vétustes de la forêt actuelle se sont installés et propagés en formant un tapis protecteur de racines et de sol sur le paysage désolé qui émergeait des glaces. Le saule alpin et la cladonie des rennes ont prospéré sur une toundra mature qui s'étendait sur tout le plateau, presque jusqu'au bord de la calotte glaciaire centrale en retraite. Ensuite, il y a environ 1400 années, a pris fin la tendance au réchauffement, et les glaciers amenuisés ont recommencé à progresser durant le Petit âge glaciaire. À partir des régions du sommet du mont Edziza, du pic Ice et des hautes-terres d'Armadillo et du chaînon Spectrum, les glaciers alpins en développement ont gagné de nouvelles positions le long du bord supérieur du plateau. Là, ils sont restés plus ou moins stables pendant le reste du Petit âge glaciaire, et ont édifié des moraines frontales parcourues de sillons, qui atteignaient 18 m au-dessus du plateau et constituent les zones de transition forestière déterminées par les glaciers alpins actuels. La fin du Petit âge glaciaire a annoncé la tendance actuelle vers un climat plus modéré, ainsi que le rapide recul des glaciers alpins. Les moraines frontales formées durant le Petit âge glaciaire se situent maintenant jusqu'à 2 km au-delà des glaciers qui leur ont donné naissance. La glace a si rapidement reculé, qu'aucune végétation n'a encore eu le temps de s'établir sur le terrain désolé et rocailleux situé entre la zone de transition forestière et la glace.

La croissance et la disparition de glaciers alpins ultérieurs au Pléistocène ont été marqués par des éruption sporadiques de basaltes produites par de nombreux cônes satellites, dans l'ensemble du complexe volcanique du mont Edziza, et par une unique éruption climacique de pierre ponce issue du versant

MOUNT EDZIZA

the products of this activity comprise the Big Raven Formation which includes the only volcanic landforms in the complex that have escaped glacial erosion (Fig. 189). The pristine cinder cones, wind-sculptured ash fields and blocky lava flows of the Big Raven Formation have remained almost unchanged since they were formed.

Tennena Cone, high on the west side of Ice Peak, was among the first Big Raven centres to erupt. Basaltic magma began to issue from its vent beneath the central ice cap during the height of the Neoglacial advance, and its steep-sided, pyramid-shaped edifice was built entirely of quenched pillow lava and pahoehoe toes that accumulated within a depression melted in the ice. A thin lava flow coursed down a meltwater channel thawed from the base of the cone to the western edge of the ice. There the violently steaming mixture of water and lava spilled over the terminal moraine and spread onto the tundra-covered plateau beyond the ice.

At least thirty basaltic centres flared into eruption and died during Big Raven time, and each event reacted in its own unique way with the surface environment. On the deeply dissected eastern side of Mount Edziza, basaltic magma forced its way to the surface through a thick pile of talus and glacial moraine, engulfing loose debris within the molten rock. The mixture of lava and scavenged fragments was ponded against stagnant ice to form the Cinder Cliff in the north fork of Tenchen Valley. Farther south, a small cinder cone was built on an active landslide moving slowly off the escarpment into Raspberry Pass. Other isolated vents erupted at various places throughout the complex: at the Ash Pit a towering fire fountain burst from the steep cliffs of Mess Creek Escarpment and deposited a plume of fine black ash across the adjacent plateau, and on Arctic Plateau tiny Nahta Cone erupted from the top of a glacially-scoured limestone hill and sent a narrow stream of lava into Nahta Creek. But most of the Big Raven activity was concentrated in two areas: one on the north flank of Mount Edziza and one on the west flank of Ice Peak where the lava from multiple centres coalesced into composite lava fields.

The Desolation Lava Field, on the north slope of Mount Edziza, issued from at least ten separate vents, most of which are clustered close to the northern trimline of the central ice cap. Some of the eruptions encroached on the edge of the ice and initially formed low tuff-rings of quenched breccia, but as these eruptions progressed the ice and meltwater were displaced and the fountaining vents produced normal subaerial cinder cones and lava flows.

sud du pic Ice. Considérés tous ensemble, les produits de cette activité constituent la formation de Big Raven qui inclut les seules formes de topographie volcanique du complexe qui aient échappé aux ravages de l'érosion glaciaire (fig. 189). Les cônes de scories intacts, les champs de cendres sculptés par le vent et les coulées de laves blocailleuses de la formation de Big Raven sont restés presque inchangés depuis leur formation.

Le cône Tennena, perché haut sur le versant ouest du pic Ice, a été l'un des premiers centre éruptifs de Big Raven à se manifester. Un magma basaltique a commencé à s'échapper de son événement, au-dessous de la calotte glaciaire centrale, durant l'apogée du Petit âge glaciaire, et sa structure pyramidale, à parois raides, a été entièrement construite par des laves en coussins brusquement refroidies par l'eau, et par des lobes de pahoehoe qui se sont accumulés dans une dépression créée par la fonte des glaces. Une mince coulée de lave s'est déversée dans un chenal d'eau de fonte glaciaire, s'étendant de la base du cône jusqu'au bord ouest du glacier. Là, un mélange bouillonnant et fumant d'eau et de lave s'est déversé sur la moraine frontale, et s'est étendu sur le plateau couvert par la toundra, au-delà des glaces.

Au moins 30 centres d'éruptions basaltiques se sont éveillés et éteints durant l'intervalle de Big Raven, et chaque éruption a eu un effet particulier sur les terrains de surface. Sur le versant est profondément disséqué du mont Edziza, le magma basaltique s'est frayé un chemin jusqu'à la surface à travers un épais amas composé de talus d'éboulis et de moraines glaciaires, en engloutissant sur son passage les débris meubles. Le mélange de laves et de fragments absorbés s'est immobilisé contre la glace stagnante, formant ainsi les falaises de cendres (Cinder Cliffs) dans le bras nord de la vallée Tenchen. Plus au sud, un petit cône de scories a pris forme sur un terrain animé d'un glissement lent qui se déplaçait progressivement de l'escarpement au col de Raspberry. D'autres événements isolés sont entrés en éruption en divers endroits dans tout le complexe: à l'endroit appelé « puits de cendres » (Ash Pit), une immense fontaine de produits incandescents a jailli des falaises abruptes de l'escarpement qui dominait le ruisseau Mess, et a déposé sur le plateau adjacent un panache de cendres noires et fines; sur le plateau Arctique, le minuscule cône Nahta est entré en éruption au sommet d'une colline calcaire affouillée par les glaces, et a émis un étroit flot de lave qui s'est écoulé dans le ruisseau Nahta. Toutefois, la majeure partie de l'activité du volcan Big Raven s'est concentrée dans deux régions: l'une sur le flanc nord du mont Edziza, l'autre sur le flanc ouest du pic Ice, où les laves provenant de centres multiples ont fusionné et constitué des champs de laves composites.

Le champ de laves Desolation, sur le versant nord du mont Edziza, provient d'au moins dix événements séparés, dont la plupart sont concentrés à proximité de la zone nord de transition forestière déterminée par la calotte glaciaire centrale. Quelques-unes des éruptions ont empiété sur le bord des glaces, et ont initialement formé des anneaux tufacés de brèches brusquement refroidies par l'eau, mais à mesure que progressaient ces éruptions, les glaces et les eaux de fonte ont été détournées,

The beautifully symmetrical cone and summit crater of Eve Cone (Fig. 201), near the centre of the Desolation Lava Field, must have been formed by a towering, vertical fire fountain, whereas Sidas Cone, on the northern edge of the field, is the product of two simultaneous fire fountains issuing in different directions from adjacent vents. Williams Cone (Fig. 203), the youngest centre in the Desolation Field, is still partly covered with fine black cinders and ash that blanket its eastern flank and extend in an elongated lobe across the plateau east to Kakiddi Valley. The column of ash from which this material fell must have been driven by a strong westerly wind throughout the eruption. Near the end of its activity the western rim of Williams Cone collapsed and was swept away by a massive stream of lava that welled out of its central crater. This flow, one of the largest in the Desolation Lava Field, moved steadily north for over 12 km into Klastline Valley where its distal lobe formed a temporary dam across Klastline River. The surface of the Desolation Lava Field is a jumble of loose, jagged slabs (Fig. 200); the broken crust from scores of lava flows, piled in chaotic windrows along the sinuous, branching levees that once bounded molten streams of lava.

The Snowshoe Lava Field issued from at least twelve separate vents on the west flank of Ice Peak. Like the Desolation vents they are clustered near the trimline of the central ice cap and the first material to erupt was quenched by ice and meltwater. The subsequent construction of Coffee and Cocoa craters and the other subaerial cinder cones was accompanied by a massive effusion of basaltic lava that flooded the plateau surface and sent tongues of lava into Taweh and Sezill valleys. Not all of the eruptions were accompanied by fire fountaining and the construction of cinder cones. One of the youngest flows in the Snowshoe Field issued quietly from a fissure on the divide south of Tencho Glacier. Tongues of lava flowed east into Shaman Creek and west into Taweh Creek but the only evidence of its source is a low, circular mound of lava, "The Saucer", bounded by concentric ridges of broken slabs. The surface features of the Snowshoe and Desolation lava fields are similar and their activity almost certainly overlapped in time.

Near the end of Big Raven time, probably before the eruption of The Saucer, a small but violent eruption of trachyte pumice burst from the southwestern flank of Ice Peak. Frothy, granular chunks the size of snowballs fell over an area of several square kilometres around the vent

et les événements d'où jaillissaient des fontaines de produits incandescents ont créé des cônes de scories et coulées de lave normaux de nature subaérienne. Le cône parfaitement symétrique et le cratère sommital du cône Eve (fig. 201); près du centre du champ de laves Desolation, ont sans doute été édifiés par une impressionnante fontaine verticale de produits incandescents, tandis que le cône Split, du côté nord du champ de laves, résulte de l'action simultanée de deux fontaines de produits incandescents qui jaillissaient dans des directions différentes à partir d'événements adjacents. Le cône Williams (fig. 203), le plus récent centre éruptif du champ de Desolation, est encore partiellement couvert de scories et de cendres fines et noires qui recouvrent son flanc est, et se prolongent à travers le plateau sans forme de lobe allongé, de l'est jusqu'à la vallée de la rivière Kakiddi. La colonne de cendres dont provient ce matériau a sans doute, pendant toute la durée de l'éruption, été poussée par un fort vent d'ouest. Vers la fin de son activité, le bord ouest du cône Williams s'est effondré, et a été balayé par un flot volumineux de laves qui ont jailli de son cratère central. Cette coulée, l'une des plus vastes du champ de Desolation, s'est uniformément déplacée vers le nord sur plus de 12 km jusque dans la vallée de la rivière Klastline, où son lobe distal a formé un barrage temporaire obstruant la rivière Klastline. La surface du champ de laves de Desolation est un chaos de dalles disjointes, aux bords déchiquetés (fig. 200); la croûte brisée par des dizaines de coulées de lave, est empilée en amas chaotiques grossièrement triés le long des levées sinueuses et ramifiées qui autrefois limitaient les écoulements de laves.

Les laves du champ de laves de Snowshoe ont été émises par au moins douze événements séparés, situés sur le flanc ouest du pic Ice. Comme les événements du champ de Desolation, ils se concentrent près de la zone de transition forestière déterminée par la calotte glaciaire centrale, et les premiers produits émis par l'éruption ont été brusquement refroidis par la glace et les eaux de fonte. L'édification ultérieure des cratères Coffee et Cocoa, et d'autres cônes subaériens de scories, a été accompagnée d'une effusion volumineuse de laves basaltiques qui ont submergé la surface du plateau et émis des langues de lave dans les vallées des cours d'eau Taweh et Sezill. Le jaillissement de fontaines de produits incandescents et l'édification de cônes de scories n'ont pas accompagné quelques-unes des éruptions. L'une des coulées les plus récentes du champ de laves de Snowshoe s'est tranquillement échappée d'une fissure située sur la ligne de partage, au sud du glacier Tencho. Des langues de lave se sont écoulées à l'est dans le ruisseau Shaman et à l'ouest dans le ruisseau Taweh, mais le seul indice de leur source demeure un monticule bas et circulaire de lave, appelé « The Saucer » (la soucoupe), et limité par des crêtes concentriques formées de dalles brisées. Les détails topographiques des champs de laves de Snowshoe et de Desolation se ressemblent, et l'activité volcanique de ces deux régions fait presque certainement preuve de contemporanéité.

Vers la fin de l'intervalle de Big Raven, probablement avant l'éruption du monticule appelé « The Saucer », une éruption de pierre ponce trachytique de faible étendue mais violente, a eu lieu sur le flanc sud-ouest du pic Ice. Les fragments rocheux granulaires, vésiculeux et de la dimension de boules

and pea-sized tephra blanketed a circular area at least 10 km in diameter. This loose, air-fall tephra comprises the Sheep Track Member of the Big Raven Formation (Fig. 220). Originally it covered all but the youngest flows and cones of the Snowshoe Lava Field but rain and wind have since removed it from the steeper slopes. Along the western edge of Tencho Glacier beds of coarse, Sheep Track pumice are up to 2 m thick but their source is hidden somewhere beneath the ice.

Geochronology, petrochemistry, and petrogenesis.

Four independent dating methods: potassium-argon, fission-track, radiocarbon, and paleomagnetism; were employed to establish the absolute age of rocks within the Mount Edziza Volcanic Complex. The K-Ar dates, which range from 11.4 to 0.28 Ma, are mostly consistent with the observed stratigraphic succession (Table 26). A few anomalously old K-Ar ages appear to be the result of contamination of lava with crustal rocks. In two such cases fission-track dates, on apatite from partly fused granitic inclusions in contaminated basalt, are in good agreement with the stratigraphy. The fission-track method was also used to date obsidians at the base of thick comendite and trachyte flows (Table 27). Although several of these dates are in good agreement with K-Ar dates, it is clear that their precision is greatly influenced by the uranium content and the post-depositional history of individual samples. Annealing at relatively low temperature and loss of uranium by diffusion from the noncrystalline glasses limit the reliability of the method. Charred willow twigs from under basaltic tephra associated with flows too young to date by the K-Ar method have yielded a ^{14}C date of 1340 B.P. Paleomagnetic polarity profiles on thick stratigraphic sections record a maximum of six reversals, far fewer than the number known to have occurred during the history of the Complex (Fig. 232). Thus no unique correlation with the standard magnetozones is possible.

The petrography and chemistry of rocks from the Mount Edziza Volcanic Complex are typical of bimodal, alkaline suits associated with continental rifting. Sequences of basic flows, mainly alkali olivine basalt and lesser hawaiite, alternate with complex piles of felsic rocks, many of which are peralkaline (Fig. 240 to 242). Most of the basic rocks are porphyritic, containing varying proportions of phenocrystic plagioclase, olivine and clinopyroxene in a groundmass of the same minerals plus

de neige, sont retombés sur une superficie de plusieurs kilomètres carrés autour de l'événement, et des tephra de la taille d'un pois ont recouvert une région circulaire d'au moins 10 km de diamètre. Ces tephra meubles comprennent le membre de Sheep Track, qui appartient à la formation de Big Raven (fig. 220). À l'origine, ils couvraient toutes les coulées et tous les cônes, sauf les plus récents, du champ de laves de Snowshoe, mais depuis, les pluies et le vent les ont entraînés des pentes les plus raides. Le long du rebord ouest du glacier Tencho, des couches de pierre ponce grossière du membre de Sheep Track atteignent jusqu'à 2 m d'épaisseur, mais leur source est dissimulée quelque part sous la glace.

Géochronologie, pétrochimie et pétrogenèse. Quatre méthodes indépendantes de datation, soit la radiochronologie basée sur le couple potassium et argon, la méthode des traces de fission, la datation au carbone radioactif et le paléomagnétisme, ont été utilisées dans le but d'établir l'âge absolu de roches faisant partie du complexe volcanique du mont Edziza. La datation par la méthode au K-Ar a fourni des âges entre 11,4 et 0,28 Ma. qui sont généralement compatibles avec la séquence stratigraphique observée (tableau 26). Une contamination de la lave par la roche encaissante semble être à l'origine de quelques âges anormalement élevés qui ont été obtenus par la méthode de datation au K-Ar; dans deux de ces cas, on a eu recours à la méthode des traces de fission pour dater l'apatite tirée d'inclusions granitiques partiellement fusionnées que contenait du basalte contaminé. Les dates ainsi obtenues sont en accord avec la stratigraphie. Cette dernière méthode a aussi servi à déterminer l'âge d'obsidiennes trouvées à la base d'épaisses coulées de comendite et de trachyte (tableau 27). Plusieurs de ces dates sont comparables à celles obtenues par la méthode de datation au K-Ar; cependant, il est évident que la teneur en uranium des échantillons et que l'histoire de la roche suivant sa mise en place ont beaucoup d'effet sur la précision des résultats obtenus par la méthode des traces de fission. La recuisson à des températures relativement basses et la perte par diffusion de l'uranium contenu dans les roches vitreuses non cristallines limitent la fiabilité de cette méthode. Des brindilles carbonisées de saule ont été prélevées sous du tephra basaltique associé à des coulées trop récentes pour être soumises à la méthode au K-Ar; par datation au ^{14}C , on a établi que l'âge de ces brindilles se situait à 1340 B.P. Des profils paléomagnétiques de la polarité ont été effectués dans des coupes structurales profondes et on y a relevé six inversions magnétiques au plus, soit un nombre bien inférieur au nombre d'inversions déjà connues dans l'histoire du complexe (fig. 232). Par conséquent, il n'existe pas de corrélation unique entre ces profils et les périodes paléomagnétiques (« magnetozones »).

La pétrographie et la chimie des roches du complexe volcanique du mont Edziza représentent de façon typique les cortèges alcalins bimodaux associés au « rifting » (création de fossé) continental. On retrouve en alternance des séquences de coulées basiques, formées surtout de basalte alcalin à olivine et d'une petite quantité d'hawaiite, et des amas complexes de roches siliceuses dont plusieurs sont hyperalcalines (fig. 240 à 242). La plupart des roches basiques sont porphyriques : elles renferment une proportion variable de plagioclase, d'olivine et

disseminated opaque oxides and devitrified glass. The felsic rocks range in composition from trachyte to comendite. The trachyte is a nearly pure alkali feldspar rock containing only trace amounts of sodic pyroxene or amphibole. With the appearance of interstitial quartz the trachyte grades into sodic rhyolite and the shift to peralkaline compositions is manifest in the appearance of sodium-rich mafic minerals, aenigmatite, arfvedsonite and aegirine. Rocks intermediate in composition between basalt and trachyte (trachybasalt, tristanite) are present locally in very small volumes but there is a distinct compositional gap between 52 and 62 % silica. Chemical variation in major element abundances between the two end members is uniform and characterized by moderate iron-enrichment followed by extreme alkali-enrichment up to a maximum in rocks with about 66 % silica. Minor element abundances, including the rare earths, reflect the major-element variation and appear to be controlled by crystal/liquid partition coefficients (Fig. 243, 244). Rb-Sr isotopes suggest a complex origin involving both contamination of mantle-derived mafic magma and prolonged fractionation in crustal reservoirs.

Petrogenesis of the Mount Edziza volcanic suite is consistent with a crystal fractionation process (Fig. 249). Using a multi-stage model in which the cumulate assemblage changes as fractionation progresses, it is possible to derive significant volumes of the more evolved rocks from a parent alkali olivine basalt magma. Initial fractionation of olivine, titanite, magnetite and plagioclase in the proportions observed in cumulate inclusions produces a residual trachyte liquid. Subsequent removal of relatively large amounts of alkali-feldspar drives the residual liquid toward a peralkaline composition. Additional enrichment in alkalis and silica may have resulted from volatile transfer. The scarcity of intermediate rocks is probably a function of eruption dynamics which favour the initial rise of fluid basalt and of the very low density siliceous residual liquids.

The volume of lava erupted within the Mount Edziza Volcanic Complex has decreased with each successive episode of magmatic activity (Table 29) but there is no compelling evidence that the cycle of eruptions has come to an end.

de clinopyroxène à phénocristaux logée dans une matrice de ces mêmes minéraux auxquels s'ajoutent çà et là des oxydes opaques et du verre dévitrifié. La composition des roches siliceuses va du trachyte à la comendite. Le trachyte est presque entièrement formé de feldspath alcalin et ne contient qu'une quantité négligeable de pyroxène ou d'amphibole sodiques. Avec l'apparition de quartz interstitiel, le trachyte se transforme en rhyolite sodique et ce passage à une composition hyperalkaline se manifeste par la formation de minéraux mafiques riches en sodium, soit l'aenigmatite, l'arfvedsonite et l'aegyrine. Des roches dont la composition se situe entre celle du basalte et celle du trachyte, soit le trachybasalte et la tristanite, sont présentes à certains endroits, en très petite quantité; cependant, il est évident qu'il n'existe pas de roches renfermant entre 52 % et 62 % de silice. La proportion des principaux éléments varie uniformément entre les deux termes finaux et cette variation est caractérisée par un enrichissement modéré en fer, suivi d'un enrichissement extrême en métaux alcalins qui atteint son maximum lorsque les roches renferment environ 66 % de silice. La proportion d'éléments accessoires, y compris les terres rares, est parallèle à celle des principaux éléments et semble être contrôlée par les coefficients de partage entre les cristaux et les liquides (fig. 243 et 244). Les isotopes du couple Rb-Sr attestent de l'évolution complexe des roches qui aurait été marquée par la contamination du magma mafique dérivé du manteau et par une longue différenciation au sein de chambres situées dans la croûte.

La pétrogenèse de l'ensemble volcanique du mont Edziza correspond à celle due au processus de la cristallisation fractionnée (fig. 249). À l'aide d'un modèle à étapes multiples dans lequel le cumulat se transforme à mesure que la cristallisation se déroule, on peut obtenir des volumes considérables de roches plus évoluées à partir d'un magma parent formé de basalte alcalin à olivine. Au départ, la cristallisation fractionnée de l'olivine, de la titano-augite, de la magnétite et du plagioclase dans des rapports observés dans les cumulats produit un magma résiduel de composition trachytique. Le retrait, par la suite, de quantités relativement grandes de feldspath alcalin pousse la composition du magma résiduel vers un état d'hyperalkalinité. Le dégagement de composants volatiles du magma peut avoir entraîné un enrichissement supplémentaire en minéraux alcalins et en silice. La rareté des roches intermédiaires s'explique probablement du fait que l'éruption a favorisé la montée initiale de basalte fluide et de magma résiduel silicieux à très faible densité.

Le volume de lave émis par le complexe volcanique du mont Edziza a diminué avec chaque nouvelle période de magmatisme (tableau 29) mais rien ne prouve avec certitude que le cycle d'éruptions soit terminé.

INTRODUCTION

LOCATION AND ACCESS

The Mount Edziza Volcanic Complex occupies about 1000 km² of upland plateau between the Stikine and Iskut River valleys in north-central British Columbia. It is visible from the road leading south from Dease Lake along Stikine Valley to Telegraph Creek, and from the Cassiar-Stewart Highway, in Iskut Valley, south of Dease Lake (Fig. 1,2). There are no roads into the area, but horse trails, maintained by local outfitters, provide access from Kinaskan Lake to the Raspberry Pass area, and from the village of Iskut, west along Klastline Valley. The old "Telegraph Trail", built in the early 1900s to service the Northwest Telegraph Line, swings west from Iskut River valley across the centre of the volcanic complex at Raspberry Pass and hence along Mess Creek valley to Telegraph Creek. Although the telegraph line and trail were used and maintained until 1936 they are now largely overgrown and only short segments of the trail are still passable.

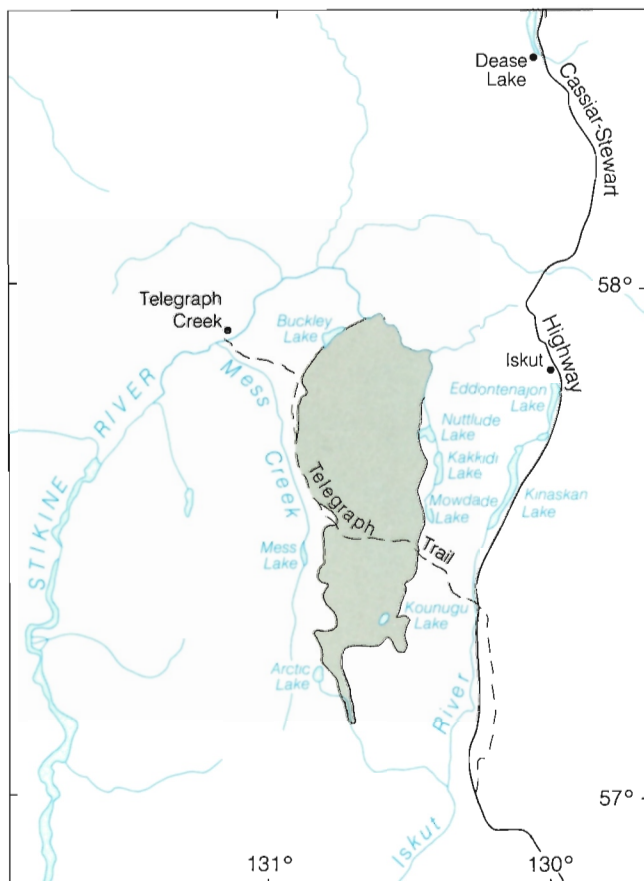


Figure 1. Index map, showing access routes and settlements in the vicinity of the Mount Edziza Volcanic Complex, which is shaded.



Figure 2. The north slope of Mount Edziza from the Cassiar-Stewart Highway, south of Stikine crossing. GSC 202468-A.

Several lakes (Buckley, Nuttlude, Kakkidi, Mowdade, Kounugu, 180, Arctic, and Mess) on and adjacent to the complex, are large enough to be used by float-equipped aircraft. In 1974 an access road was built from a landing site on Nuttlude Lake to a mineral exploration camp at an elevation of 5000 ft. (1525 m) on the east side of Mount Edziza. Both float planes and helicopters are available for charter at Dease Lake and Iskut.

Travel on foot is relatively easy in the western part of the area, where the rolling upland surface is mainly above timberline. The bounding escarpments and steep-sided box canyons which cut the plateau impose local barriers, but they can easily be avoided by alternate routes. In contrast the eastern side of the complex is bounded by precipitous unstable cliffs, nearly vertical cirques, and deeply crevassed icefalls. Those travelling in this part of the area should have mountaineering experience and come equipped for challenging climbing.

PHYSIOGRAPHY

The Mount Edziza Volcanic Complex forms a rolling upland plateau, flanked on the west by rugged granitic peaks of the Coast Mountains (Fig. 3), and on the east by the more subdued Skeena Mountains and Klastline Plateau. A diversity of physical features within the Mount Edziza Volcanic Complex reflect its prolonged and varied volcanic history. The older elements of the complex have been deeply dissected and, in places, all but a few remnants of once large volcanoes have been eroded away during the millions of years since they were formed. Successively younger volcanoes have suffered less erosion, and although deeply dissected, those formed during the last 3 to 4 million years still

MOUNT EDZIZA



Figure 3. View looking west from the volcanic plateau, across Mess Creek valley, to granitic peaks of the Coast Mountains. GSC 202468-B.

retain the gross features of their original form. At the youngest end of the scale are pristine-looking cinder cones and lava fields where erosion of even surficial ash is only now beginning. In addition to differences in age the physical features vary according to the type of material erupted and the surface on which it was deposited. Because of its low viscosity basaltic lava spread in thin flows to build broad shields with gently sloping upper surfaces. More viscous, felsic lava built steep-sided domes, composite cones, and thick, stubby flows.

The history of the Mount Edziza Volcanic Complex spans several periods of glacial advance and retreat. Lava erupted during periods of ice cover accumulated in melt-water ponds, giving rise of very different landforms than those formed under subaerial conditions.

The north-south axis of the volcanic complex is defined by four, composite, central volcanoes in various stages of dissection (Fig. 4). The Spectrum Range (Fig. 5), at the southern end, is a composite rhyolite dome of which only a few small remnants of the original surface are preserved on the summits of the higher peaks. A crudely radial drainage pattern extends outward from the central part of the range. The deeply incised valleys are flanked by largely felsenmeer- and talus-covered slopes which rise at the angle of repose to broad, rounded crests of the interfluvial ridges.

North of the Spectrum Range, is Armadillo Peak whose precipitous slopes rise to a broad, rounded summit at 7218 ft. (2200 m) elevation. Originally a caldera surrounded by satellitic domes, the present topography of Armadillo is due entirely to deep dissection that totally altered its original, circular form.

North of Cartoona Ridge, one of the satellitic centres of Armadillo Caldera, the topography rises gradually to the 8200 ft. (2500 m) summit of Ice Peak (Fig. 6), a pyramid-shaped horn, bounded on all sides by steep-walled active cirques. Ice Peak is a glacially modified composite volcano

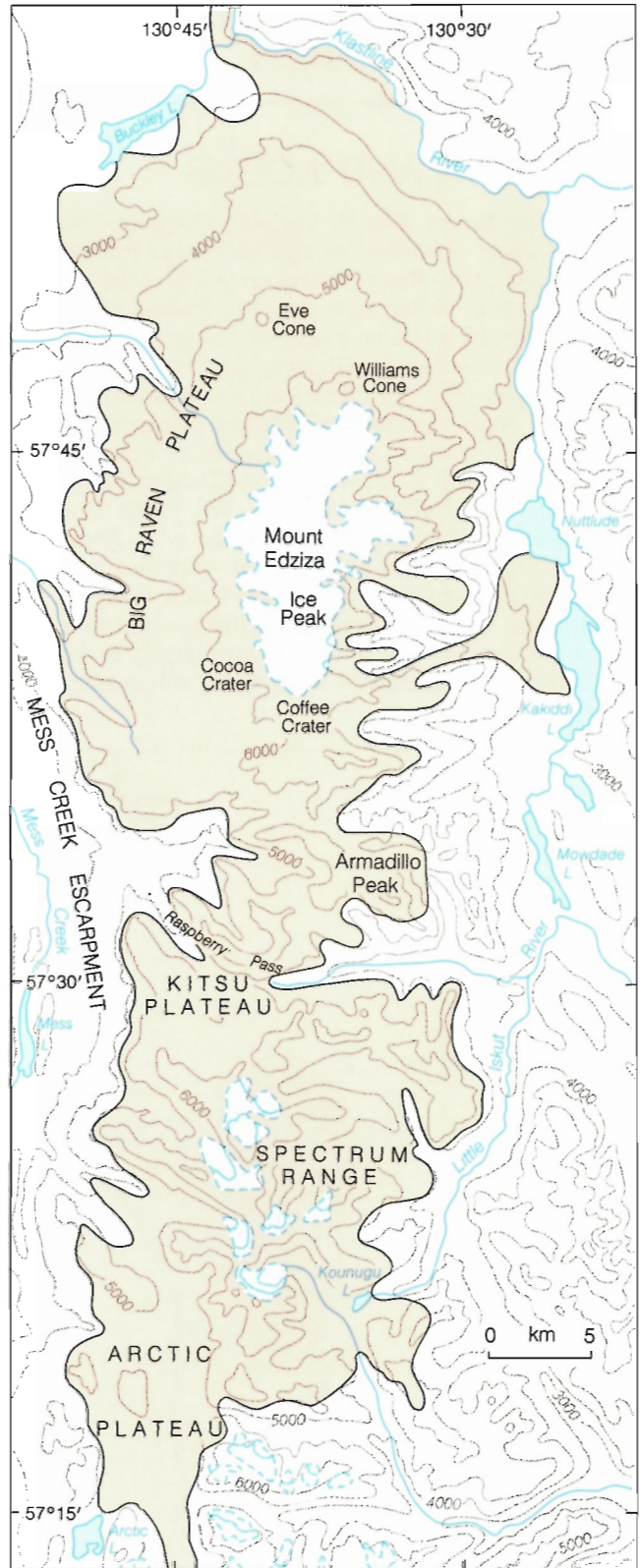


Figure 4. Principal physiographic elements of the Mount Edziza Volcanic Complex.



Figure 5. *Felsenmeer-covered ridges of the central Spectrum Range, brightly-coloured erosional remnants of a rhyolite dome complex. GSC 202468-C*



Figure 6. *The south slope of Ice Peak and nunataks on the south rim of the summit crater of Mount Edziza. GSC 202468-D.*

whose original profile is approximately preserved on its glacier-covered south and west flanks. Its eastern flank has been largely destroyed by headward erosion of glacial valleys, and its northern slope is buried beneath the younger edifice of Mount Edziza.

Mount Edziza (Fig. 7), the youngest and most northerly of the four central composite volcanoes, rises to a circular ice-filled crater about 2 km in diameter, at an elevation higher than 8500 ft. (2590 m). A narrow cirque, eroded into the east side of the volcano, is bounded by near-vertical headwalls which breach the eastern rim of the summit crater (Fig. 8). Elsewhere the crater rim and the flanking upper slopes of the composite cone are only moderately dissected by a system of radial meltwater channels.

The four central volcanoes that lie along the axis of the complex are flanked on the west by a broad, gently west-sloping lava plateau at an elevation of 5000 to 6000 ft. (1500-1800 m). It is bounded on the west by a steep escarpment which exposes, in step-like terraces, the myriad thin

flows of basalt and distal ash flows from which it is built (Fig. 9). From the edge of the escarpment a few youthful, fast-flowing streams have cut V-shaped canyons eastward, almost to the lower slopes of the central volcanoes. Most of the plateau surface is a mature alpine tundra, covered by tufts of grass, alpine willow and cariboo moss. Locally ice polygons and other patterned ground indicate the presence of permafrost on the upper part of the plateau.

East of the central volcanoes, only a few remnants of the original flanking shield are preserved on interfluves between the deeply incised, east-flowing glacial streams. The upper parts of most of the valleys are occupied by active cirques and the intervening, sharp-crested spurs and ridges are all that remain of the once extensive eastern part of the complex (Fig. 10).

Most of the north slope of the volcanic complex, and large parts of the western plateau, are covered by postglacial cinder cones, fields of blocky lava, and unconsolidated beds of basaltic tephra and rhyolitic pumice (Fig. 11). Within those areas of very young lava, stream drainage is mainly through subsurface channels. As a result, the original lava surfaces show little evidence of erosion or sediment cover.

DRAINAGE AND GLACIATION

The Mount Edziza Volcanic Complex is drained entirely by tributaries of Stikine River. Mess Creek, a north-flowing, locally aggrading stream, occupies a broad valley parallel to the bounding escarpment on the west side of the volcanic complex (Fig. 3). Its west-flowing tributaries, short high-gradient streams which occupy steep-sided canyons cut into the volcanic plateau, provide the principal drainage for the western half of the complex. The precipitous eastern side of the volcanic complex faces a broad hummocky lowland on a drainage divide between Kakiddi Creek, flowing north into the Klastline drainage and streams flowing south, via Little Iskut River into Iskut River proper. East-flowing tributaries of Kakiddi Creek are choked with glacial and landslide debris from the rapidly eroding headwalls and steep spurs on the east side of the volcanic complex. Where these streams enter Kakiddi Valley, large alluvial fans have been built, behind which several lakes (Nuttlude, Kakiddi, Mowdade, Mowchilla) have been ponded (Fig. 12). The youthful north slope of Mount Edziza is drained by small, shallowly incised streams which flow north into Klastline River.

With the exception of the youngest cinder cones and associated lava flows all the elements of the Mount Edziza Volcanic Complex have been modified by local and regional glaciation. Evidence of regional glaciation is well preserved on the western plateau where drumlinoid ground, grooving, and striations indicate north-northwest ice movement (Fig. 13). At lower elevations, particularly on the slope south of Buckley Lake, evidence of ice stagnation is seen in morainal ridges, kame and kettle topography, eskers and outflow channels.

MOUNT EDZIZA

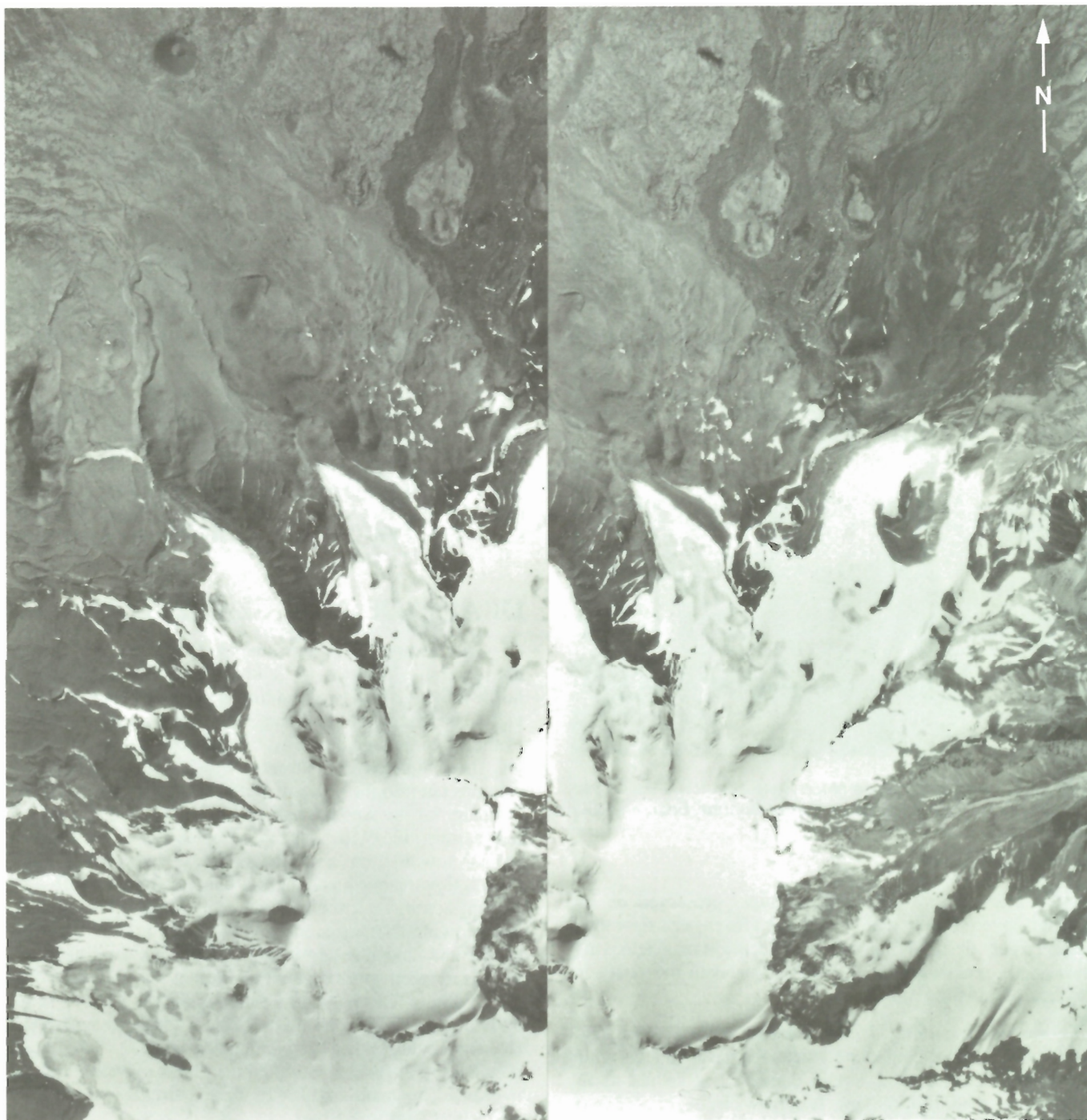


Figure 7. Summit crater of Mount Edziza, a circular, ice-filled depression 2 km across. Stereoscopic pair. Province of British Columbia photos BC 5607-143, 144.

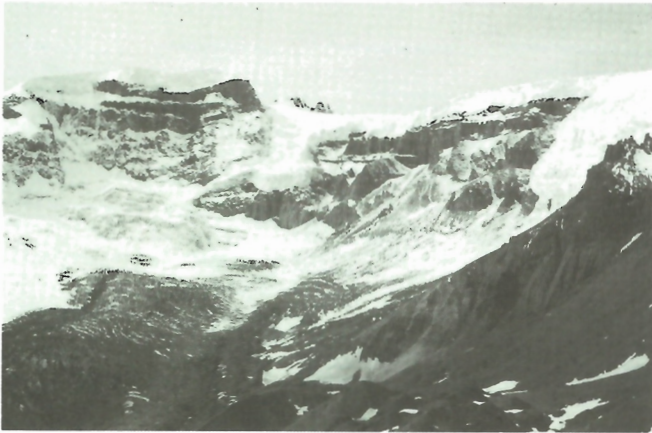


Figure 8. Precipitous headwall of an active cirque that breaches the east side of the summit crater and central conduit system of Mount Edziza. GSC 202468-E



Figure 9. Volcanic plateau and escarpment on the west side of the Mount Edziza Volcanic Complex. Flat-lying flows which underlie the plateau are mainly basalt, whereas rhyolite and trachyte form the relatively steep slopes of Ice Peak and Mount Edziza central volcanoes in the background. GSC 202468-F.



Figure 10. Steep interfluvial ridges and deeply incised valleys on the east side of the Mount Edziza Volcanic Complex. GSC 202468-G.



Figure 11. Young pyroclastic cones and blocky lava flows on the north slope of Mount Edziza. GSC 125601.



Figure 12. Kakiddi and Nuttlude lakes, two of several lakes ponded behind rapidly aggrading alluvial fans being deposited by debris-choked streams draining the precipitous, east slope of the Mount Edziza Volcanic Complex. GSC 202468-H.

During the final stages of deglaciation, as the supporting ice receded from unstable, oversteepened valley walls the debris-covered cliffs collapsed in a series of landslides. The low-yield strength of the highly fractured, poorly consolidated rocks of the volcanic complex resulted in numerous such landslides, particularly along the Mess Creek Escarpment.

At high elevations evidence of regional glaciation has been obliterated by younger alpine glaciers. Active glaciers occupy cirques on most peaks over 7000 ft (2130 m). In the Spectrum Range, Armadillo and adjacent peaks, the ice is

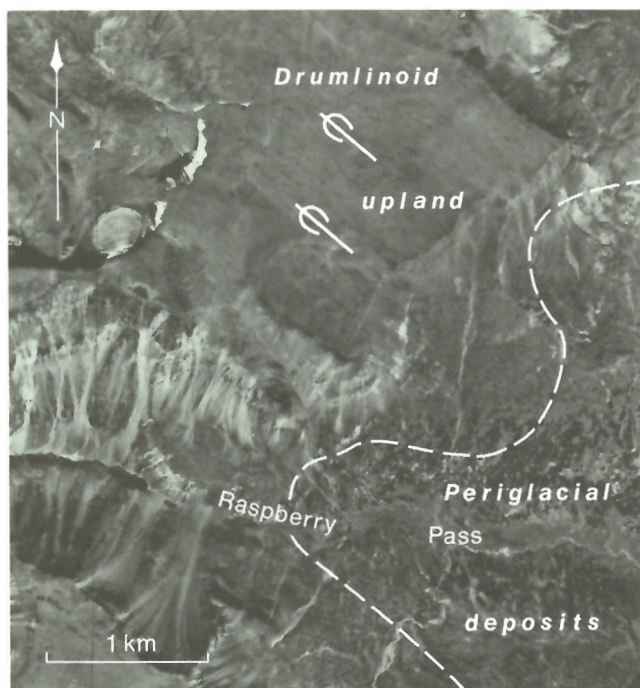


Figure 13. Fluted, drumlinoid ground, showing the north-northwesterly direction of ice movement across the western volcanic plateau, north of Raspberry Pass. Province of British Columbia photo BC 1374-6.

restricted to relatively small separate glaciers but Ice Peak and Mount Edziza are covered by a small ice cap (Fig. 6) with an area of approximately 70 km². Distributary glaciers from the ice cap extend down the steep east side of the complex and are characteristically broken by ice falls (Fig. 14), whereas west-flowing glaciers have spread in broad lobes onto the upper part of the plateau (Fig. 15). All glaciers in the area have receded from prominent, unvegetated trimlines which are commonly from 1 to 2 km beyond the present ice front.

PREVIOUS INVESTIGATIONS AND PRESENT STUDY

Remnants of basalt flows, resting on river gravels in Stikine Valley near Telegraph Creek, were described by Kerr (1948), who speculated correctly that the flows had entered Stikine Valley from the Klastline drainage. Although he did not trace them back to their origin he cited local reports of a vast area of lavas up Klastline River to the southeast, where undestroyed, well-formed craters, hot springs, and other evidence of recent volcanism suggested to him that the Stikine Valley lava flows had originated there and flowed some 83 km to their present location.

No further work was done on the Mount Edziza Volcanic Complex until 1956, when the boundaries of the volcanic pile were mapped in conjunction with regional reconnaissance by the Geological Survey of Canada (1957)



Figure 14. Icefalls and deeply cravassed ice, typical of glaciers on the east side of the Mount Edziza Volcanic Complex. GSC 202468-I.



Figure 15. Broad, unfractured distributary lobes of ice spreading from the central icefield onto the western plateau surface. GSC 202468-J.

during Operation Stikine. J.G. Souther carried out additional work on the volcanic complex in the course of preparing a 1:250 000 geological map of the Telegraph Creek area (Souther, 1972a).

The present study was begun in 1965 and continued through the summers of 1966 and 1967. The author revisited the area briefly during the summers of 1968, 1969, 1972, 1973 and 1976. Results of this work have been published in several general summary papers (Souther, 1967, 1968, 1969, 1972a,b) and in topical papers dealing with specific aspects of the study. The latter include: fission-track dating of volcanic glass (Aumento and Souther, 1973), stratigraphy and paleomagnetism (Souther and Symons, 1974), mineralogy (Yagi and Souther, 1974), volcanic hazards (Souther, 1981a,b), geochronology (Souther et al, 1984), and chemistry and petrogenesis (Souther and Hickson, 1984).

FIELD AND LABORATORY METHODS

The complex was mapped at a scale of 1:25 000. Because the pile is essentially flat-lying, emphasis was placed on obtaining detailed stratigraphic sections with precision. Elevations were measured with a surveying altimeter, and corrected for diurnal variation by closing traverses on bench marks of known elevation. In key sections each of the flow-units was sampled. Locations were plotted on air photographs and transferred optically to the map.

Petrographic work included the examination of over 800 thin sections which provided the basis for selecting representative samples for whole-rock and microprobe analysis.

Whole-rock chemical analyses were made by the Geological Survey of Canada, under the direction of S. Abbey and J.A. Maxwell. X-ray fluorescence (XRF) was used for SiO₂, Al₂O₃, total Fe as Fe₂O₃, CaO, MgO, K₂O, TiO₂, MnO, NiO and Cr₂O₃. Total H₂O, CO₂, P₂O₅, Na₂O, and FeO were measured by rapid chemical means. Sulphur was determined by conventional chemical methods and Fe₂O₃ by difference. Three groups of minor element analyses were run on the same powders prepared for the major element analyses. The first group of 96 samples was analysed by Acme Analytical Laboratories of Vancouver for 26 elements, using an inductively coupled argon plasma (ICP) method. A second group of 19 samples was analyzed by C. Hickson, University of British Columbia, for Ba, Rb, Y, Ni, Zr, and Sr using XRF spectrometry. Ten samples were analyzed by neutron activation for the rare-earth elements La, Ce, Nd, Sm, Eu, Tb, Yb, and Lu by Nova Track Analysts of Vancouver.

Microprobe analyses were performed by L.C. Pigage on the University of British Columbia ARL SEMQ microprobe, using 10 2-s counting periods for each element.

K-Ar dates were determined by R.K. Wanless at the Geological Survey of Canada in Ottawa, and by R.L. Armstrong at the University of British Columbia. K was determined in duplicate by atomic absorption using a Techtron AA4 spectrophotometer, and Ar by isotope dilution using an AEI MS-10 mass spectrometer and high purity ³⁸Ar spike.

ACKNOWLEDGMENTS

To the following geology students the writer extends his appreciation for satisfactory and, more often, excellent assistance in the field: in 1965—M.B. Lambert, L.A. Burgess, N. Lockwood; in 1966—M.B. Lambert, R.G. Friesen, G.L. Haszard, R.D. Cruickshank; in 1967—L.G. Charlebois; in 1972—B.A. Griffin; in 1973—G.B. Mitchell; and in 1976—B.C. Souther; R.G. Anderson assisted with the petrographic work and C.J. Hickson assisted with compilation and synthesis of the chemical data. Special thanks are extended to the GSC cartography staff in Ottawa for preparation of the map and figures, to Bev Vanlier for typing and proof reading the manuscript, and to J.A. Roddick whose careful review lead to many improvements in the original text.

The writer is indebted to many residents of the area for their hospitality and help. Special thanks are extended to Mr. and Mrs. R.S. Hyland of Kiniskan Lake, Mr. and Mrs. D. Blanchard of Telegraph Creek and Mr. and Mrs. T. Black of Eddontenajon for their assistance and many courtesies. Fieldwork was greatly facilitated through the unselfish co-operation of many mining and exploration companies, particularly Heckla Mining Corporation, Conwest, Silver Standard, Kennco, and Amax.

For their wise council in the field, and their encouragement during the early stages of the study the writer is indebted to his friend and colleague Ken Yagi of Hokkaido University, and to the late Prof. H. Kuno of the University of Tokyo.

TECTONIC SETTING

MAJOR TECTONIC ELEMENTS

The Mount Edziza Volcanic Complex lies within Stikinia, the largest segment of the Insular Superterrane, a composite terrane thought to have been accreted to the continental margin in the Jurassic (Monger, 1984). West of Stikinia the Coast Plutonic Complex, a linear belt of intense deformation, metamorphism and granitic intrusion, separates Stikinia from the Intermontane Superterrane, which was accreted probably during the Cretaceous and forms the present continental margin (Fig. 16).

Post-accretion deformation of the Stikine Terrane was dominated, during Late Cretaceous-Early Tertiary time, by

transpression that probably reflected oblique convergence between oceanic crust and the accreted continental margin. Calc-alkaline magmatism was accompanied by dextral movement on major northwesterly trending faults, and by development of horst and graben structures bounded by synvolcanic north-trending normal faults.

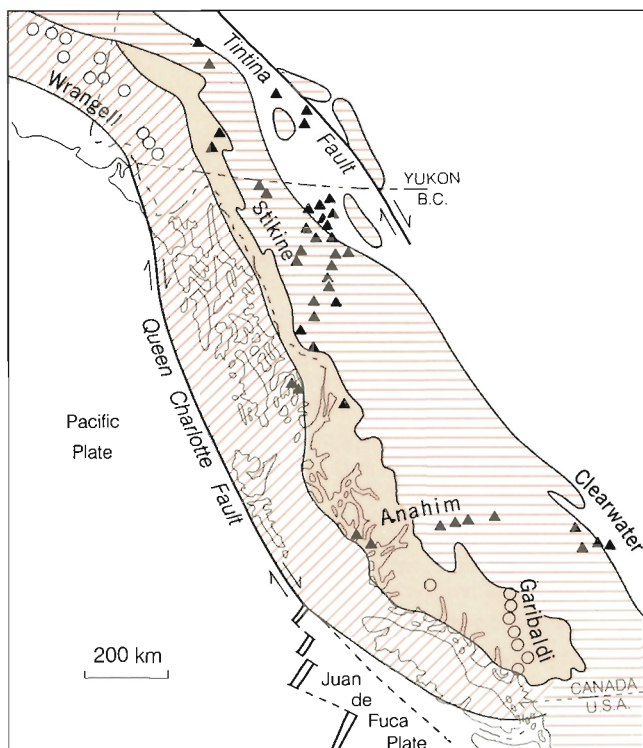
By Late Miocene, when the oldest units of the Mount Edziza Volcanic Complex were erupted, the tectonic regime was similar to that of the present. Convergence and accompanying calc-alkaline volcanism had ceased and the continent was bounded by a right-lateral, transform margin.

STIKINE VOLCANIC BELT



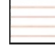
Stikine Volcanic Belt is defined by a north-northwesterly trending group of late Cenozoic volcanoes that extends through the northern Coast Mountains into the Intermontane Belt of northern British Columbia and southern Yukon. It is superimposed on the pre-existing collage of terranes, crossing from the Coast Plutonic Complex onto Stikinia, across the Atlin Terrane, and into the Omineca Crystalline Belt without any apparent regard for old suture zones (Fig. 17). The belt itself appears to comprise a series of short, north-trending, en echelon segments. The most southerly of these includes the Mount Edziza Volcanic Complex, Hoodoo Mountain and scores of smaller composite and monogenetic cones. It is fairly linear and extends from the Aiyansh centre, in the central Coast Mountains (Sutherland Brown, 1969), north to Dease Lake in the Intermontane Belt.

The north trend within the more northerly segments of Stikine Volcanic Belt is less clearly defined. Level Mountain (Hamilton, 1981), the largest and oldest centre in the belt, is bounded on the south by a cluster of monogenetic cones, and on the north by a group of cones and erosional remnants of Cenozoic basalt flows which occupy a broad zone extending north across the Atlin Terrane into the Omineca Crystalline Belt in southern Yukon. A crude north-south orientation is also seen in other clusters of eruptive centres such as those near Atlin, Miles Canyon and related basalts of Whitehorse area, and Recent cones near Fort Selkirk.

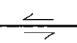
North-trending normal faults appear to be the dominant late Cenozoic structure within the Stikine Volcanic Belt. Some of these faults cut flat-lying lavas of the Mount Edziza Volcanic Complex and are clearly synvolcanic. Many of them, however, undoubtedly were formed during the earlier, Cretaceous and Early Tertiary, episode of transpression and later reactivated. Northerly trending faults and dyke swarms of Early Tertiary age (Eocene) are associated with volcanics of the Sloko Group in Telegraph Creek map



TERRANES

-  Insular superterrane
-  Coast plutonic complex
-  Intermontane superterrane

Geological boundary ~~~~~

- Fault (arrow indicates relative movement) 
- Neogene volcano
- Calc-alkaline basalt, andesite, dacite, rhyolite ○
- Alkaline basalt, trachyte, comendite ▲
- Volcanic belt Stikine

MOUNT EDZIZA

area (Souther, 1972a), and in Tulsequah map area (Souther, 1971). Also, extensive, north-trending swarms of Early Tertiary feldspar porphyry dykes are exposed north of Klunane Lake at the extreme northwestern end of the Stikine Volcanic Belt.

It seems probable that all of these northerly trending, Early Tertiary structures originated where northwesterly directed transcurrent motion along major faults resulted in a couple with an east-west component of extension. During

the Early Tertiary episode of oblique subduction these extensional zones in the upper plate became the loci of calc-alkaline volcanism that produced the Sloko and related rocks (Fig. 18). Subsequently, when subduction and associated calc-alkaline volcanism ceased in the mid-Tertiary, the extensional zones, driven by continued transcurrent motion at the continental margin, were propagated into the lower crust becoming the conduits for the rise of more primitive, mantle-derived alkaline magmas, which are characteristic of the Upper Tertiary Stikine Volcanic Belt.

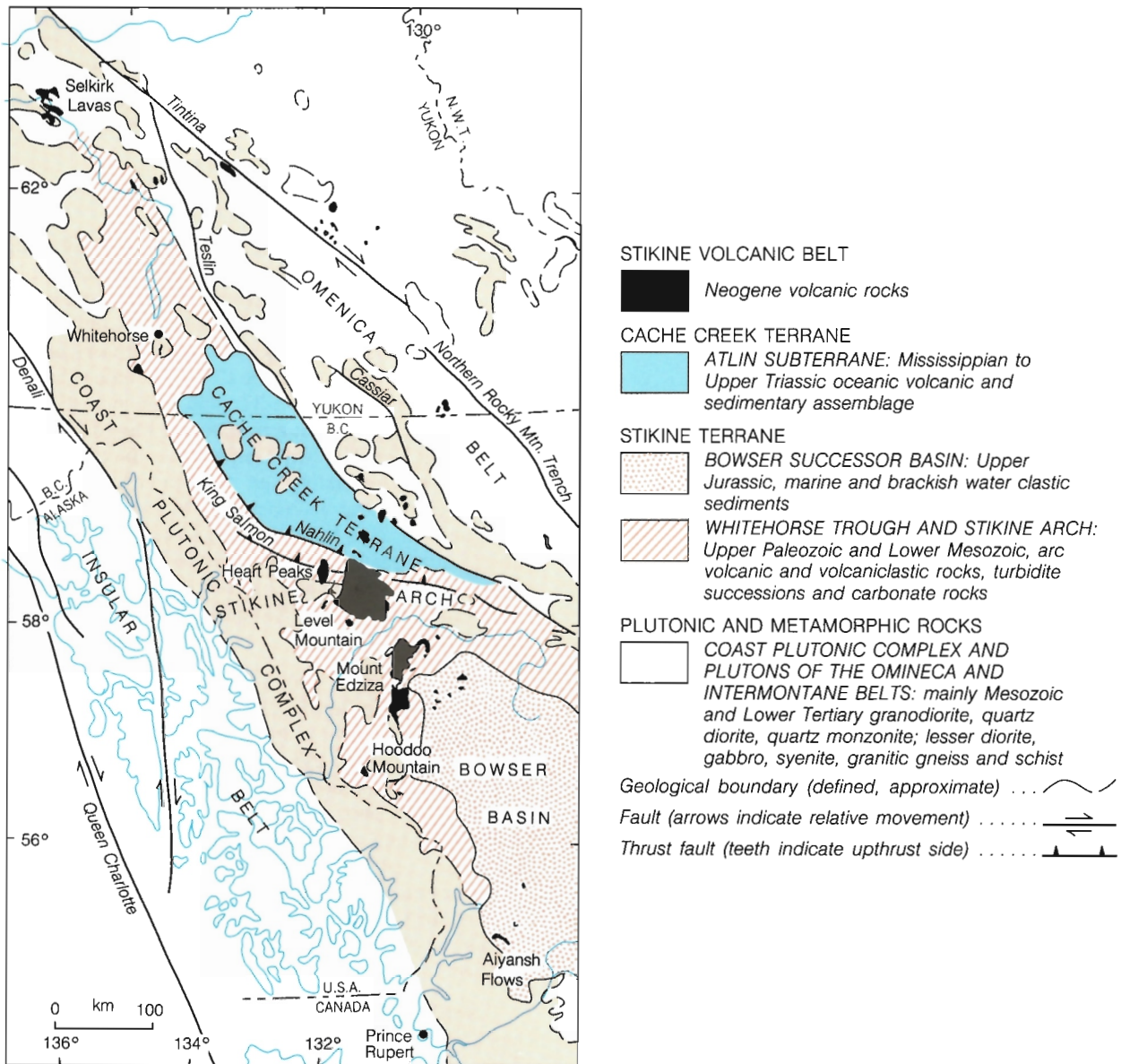


Figure 17. Distribution of late Miocene and younger eruptive centres within the Stikine Volcanic Belt, showing the structural setting of the Mount Edziza Volcanic Complex. North-south, en echelon segments of the belt are parallel to early Tertiary dyke swarms and faults.

BASEMENT GEOLOGY

STRUCTURAL SETTING

The Mount Edziza Volcanic Complex lies on the Stikine Arch near its eastern contact with Bowser Basin (Souther, 1972a,b). Stikine Arch (Fig. 17) is a north-easterly trending lobe on the east side of the Coast Plutonic Complex that has remained relatively positive throughout much of Mesozoic time. It is underlain by a metamorphic core zone which is locally exposed beneath a thick succession of late Paleozoic and Mesozoic volcanic and sedimentary rocks. All rocks within the Arch are cut by Mesozoic and Early Tertiary plutons and batholiths.

On the east, Stikine Arch is bounded by the Upper Jurassic to Lower Cretaceous, Bowser, successor basin, and on the north by an extension of the Whitehorse Trough (Wheeler, 1961; Souther 1971) in which volcanic and clastic sedimentary rocks were deposited during Late Triassic and Early Jurassic time.

Limestone and thin-bedded clastic sediments of the Paleozoic succession are locally intensely folded, but faulting is the predominant structural style within the massive Mesozoic units which underlie most of the Stikine Arch. The north-south valleys of Iskut River and Mess Creek, which flank the Mount Edziza Volcanic Complex on the east and west, are controlled by major fault zones which have undergone repeated movement (Fig. 18). Between these two major zones of dislocation the basement rocks that extend under the volcanic complex are cut by numerous additional north-south faults and by a conjugate set of northwest- and northeast-trending faults. Some of the latter are clearly cut by a younger north-south set whereas others change direction and merge with the north-south fault zones. Most of the faults are near vertical and exhibit normal displacement, but an anomalous east-trending, steeply south-dipping reverse fault crosses Klastline Plateau and extends under the northern part of the volcanic complex. Cinder cones on Klastline Plateau lie along the trace of this fault and young cinder cones on the north flank of Mount Edziza lie above its projected western extension beneath the volcanic pile.

The present distribution of faults probably developed during the Early Tertiary when numerous normal faults accompanied east-west extension, intrusion of plutons, and eruption of Sloko volcanics and deposition of associated intermontane sediments. Remnants of Lower Tertiary strata, preserved at different elevations on different fault slices, indicate that profound vertical displacements continued after their deposition in the Eocene. Some of the bounding faults remained active through Late Tertiary time and may have exerted some control on the distribution of Neogene eruptive centres.

PALEOZOIC ROCKS

Paleozoic rocks (Fig. 18) underlie the southern and western part of the Mount Edziza Volcanic Complex and are particularly well exposed on and adjacent to Arctic Plateau, west of the Spectrum Range. Fossiliferous Mississippian and Permian strata include massive limestone units interbedded with fine clastic sediments, bedded tuff, and intermediate volcanic rocks. Devonian conodonts have been recovered from pre-Mississippian strata at a single locality south of the Spectrum Range (P. Read, pers. comm., 1987). Elsewhere the pre-Carboniferous rocks of Stikine Arch have yielded no fossils, and the predominantly fine grained clastic sediments and volcanics are commonly metamorphosed to schist and gneiss.

MESOZOIC ROCKS

Mesozoic volcanic and sedimentary rocks, cut locally by granitic plutons, underlie most of the Mount Edziza Volcanic Complex. They are unmetamorphosed, and range from Upper Triassic to Cretaceous.

The Upper Triassic succession (Fig. 18) is at least 2440 m thick and comprises about equal proportions of augite andesite, derived volcanoclastic rocks, and clastic sediments. The volcanic rocks are mostly massive breccias but the succession includes lavas, locally pillowed, bedded tuff, and a profusion of dykes and subvolcanic intrusions. Upper Triassic sedimentary rocks, exposed on the south and east sides of the Mount Edziza Volcanic Complex, constitute an interbedded succession of volcanic sandstone, greywacke, graded siltstone, chert, carbonaceous shale, and discontinuous lenses of limestone.

The Upper Triassic rocks east of Mess Creek are overlain unconformably by Lower to Middle Jurassic clastic sediments (Fig. 18). A basal conglomerate contains volcanic clasts from the underlying Upper Triassic strata and sparse granitic clasts derived from unroofing of the Upper Triassic Hickman Batholith farther west. South of the Spectrum Range on Ball Creek the basal conglomerate is overlain by at least 1200 m of Lower Jurassic, tuffaceous siltstone, sandstone and grit interbedded with fragmental volcanic rocks including thick sections of calcareous, basaltic andesite breccia (peperite). The Lower Jurassic succession is overlain conformably by about 1050 m of friable black shale (Fig. 18) which contains fossils of late Early and early Middle Jurassic age. South of Little Iskut River the shale is overlain conformably by a massive pile of basaltic andesite pillow lava, minor flows and associated dykes and sills (Fig. 18). This volcanic pile appears to thin northward and, on

MOUNT EDZIZA

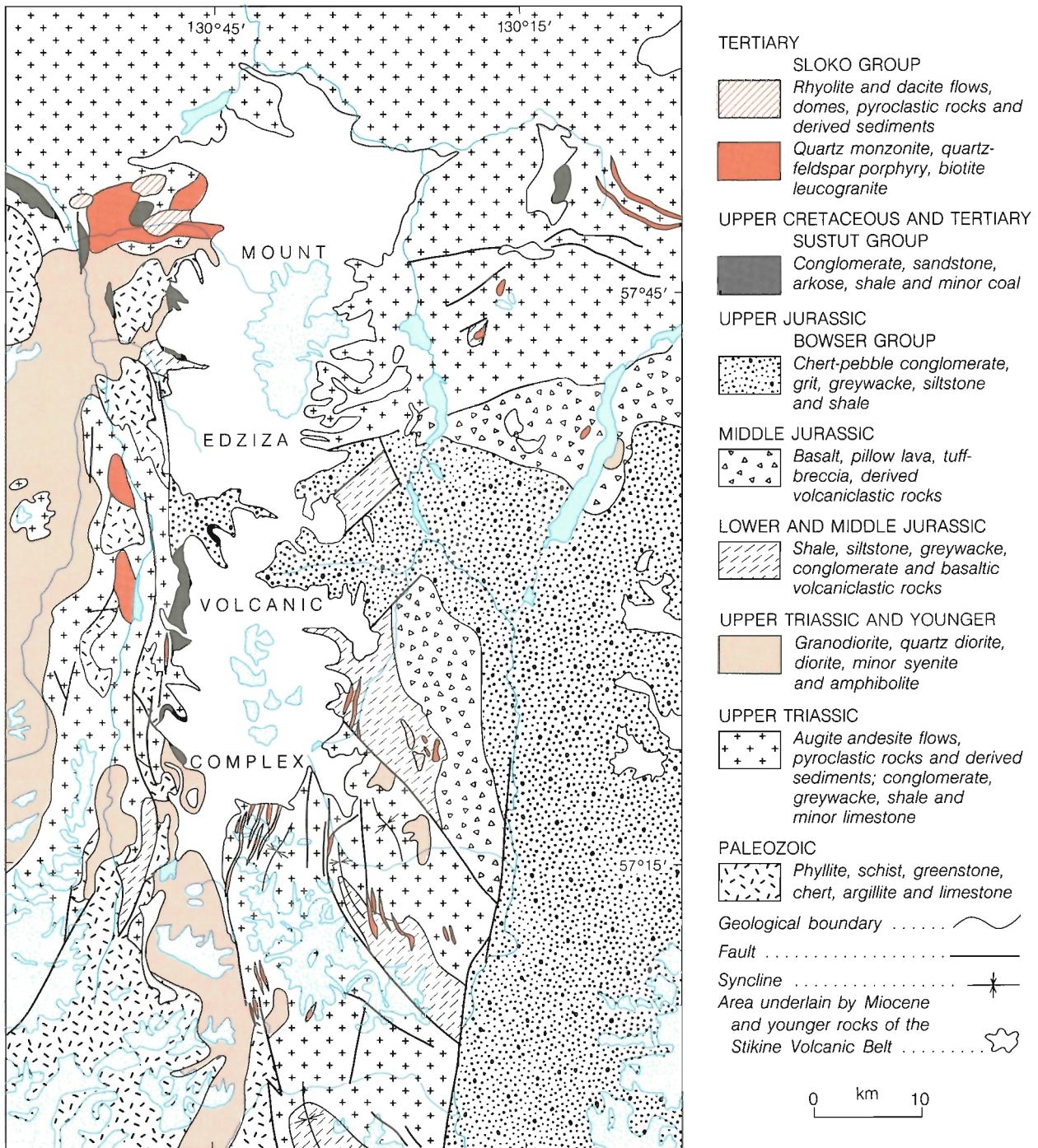


Figure 18. Geological map showing the distribution of basement rocks and structures surrounding the Mount Edziza Volcanic Complex.

Klastline Plateau, the same stratigraphic interval is occupied by 100 m of basaltic andesite, volcanoclastic conglomerates and pillow breccias.

Upper Jurassic clastic sediments of the Bowser Group (Fig. 18) underlie a vast area within the Hazelton Mountains, east of Iskut River, and a small apophysis of similar rocks extends west, across southern Klastline Plateau beneath the eastern edge of the Mount Edziza Volcanic Complex. The succession east of Iskut River includes at least 1500 m of interbedded greywacke, grit, siltstone, shale and chert-pebble conglomerate. The proportion of conglomerate and the average clast size increase westward, suggesting that the western apophysis is a fluvial, deltaic facies near the northwestern margin of the basin.

Cretaceous sediments of the Sustut Group (Fig. 18) are preserved on the mountains west of Mess Creek and in downfaulted blocks along Mess Creek Valley. West of Mess Lake, and in the canyons of Sezill and Kadeya creeks, as much as 300 m of gently tilted strata are preserved beneath the basal lavas of the Mount Edziza Volcanic Complex. The Sustut rocks are moderately to poorly indurated, interbedded sandstone, carbonaceous siltstone, polymict conglomerate, and friable carbonaceous shale, locally with thin seams of coal, carbonized stems, and plant debris.

Intrusive rocks of Triassic and younger age (Fig. 18) are widely exposed in the Coast Mountains west of Mess Creek and smaller, probably coeval bodies, are exposed farther east, around the periphery of the Mount Edziza Volcanic Complex.

The Late Triassic Hickman Batholith underlies an area of about 260 km² west of Mess Creek. It is a crudely zoned body which ranges from pyroxene diorite in the interior to biotite granodiorite in the exterior.

The Jurassic-Cretaceous intrusions range in composition from diorite, which is confined to relatively small bodies, to larger bodies of hornblende-biotite granodiorite, and hornblende-quartz diorite. The younger, Cretaceous to Tertiary, intrusions are mostly coarse grained biotite-hornblende quartz monzonite.

TERTIARY ROCKS

A complex of Early Tertiary intrusive (Fig. 18), extrusive and clastic sedimentary rocks is exposed in the rolling terrain south of Buckley Lake and in the nearby canyons of Elwyn and Kadeya creeks. The principal intrusive body is Elwyn Creek Pluton, which is at least 5 km across and consists of uniformly fine grained, slightly porphyritic leucogranite with phenocrysts of sodic plagioclase and small euhedra of hornblende and biotite. The rock has a uniform, closely spaced rectangular joint system which, near contacts,

resembles columnar jointing at right angles to the cooling surface. Also, most contacts have fine grained selvages, suggesting that the body was intruded and quenched at a shallow depth. It exhibits both intrusive and fault contacts with Cretaceous, Sustut, conglomerate and sandstone (Fig. 18).

Peripheral to Elwyn Creek Pluton the gently tilted Sustut strata are invaded by a network of dykes, sills and apophyses with well developed rectangular jointing at right angles to their contacts. These are slightly finer grained, but otherwise similar to rocks of the parent body and are believed to be part of a distributary system to overlying volcanic rocks.

Genetically related andesitic, dacitic and rhyolitic extrusive rocks (Fig. 18) include remnants of domes, thick lava flows and pyroclastic breccia deposits. The flows and domes vary in texture from aphanitic to porphyritic and, like their intrusive equivalents, are characterized by small hornblende and biotite euhedra. Contorted flow layering is a common feature of the flows and domes. The associated pyroclastic breccia, unlike that in the overlying Mount Edziza Volcanic Complex, has been zeolitized and chloritized. The matrix is commonly pale to bright green (celadonite), and vesicles are completely filled with silica, zeolites, and carbonate.

The extrusive rocks are associated with thick deposits of epiclastic breccia (Fig. 18) comprising a chaotic mixture of volcanic and basement clasts in a poorly indurated earthy matrix. The breccia is clast-supported and exhibits no sorting or stratification. Most clasts are volcanic, derived from the associated extrusive units, but they are intimately mixed with well rounded cobbles and boulders incorporated from the underlying Sustut conglomerate, and with angular blocks of older basement rock, including biotite leucogranite from the Elwyn Creek Pluton. Clast size ranges from small pebbles to blocks 2-3 m across. Like the associated extrusive rocks, the epiclastic breccia is cut by a profusion of biotite-bearing andesite and dacite dykes and is thus clearly synvolcanic. Its large volume and wide extent suggest that Early Tertiary volcanism here, as in many other parts of the western Cordillera, was accompanied by large scale vertical movement which generated repeated landslides and debris flows.

Potassium-argon dating of biotite from the Elwyn Creek Pluton and from a nearby extrusive dome gave dates of 53.1 ± 2.4 Ma and 49.8 ± 2.4 Ma respectively. This Eocene age records the youngest documented igneous event prior to eruption of the first Edziza lavas in the Late Miocene. Between these two events the Elwyn Creek Pluton was bevelled by a gently west-sloping erosion surface that appears to be truncated abruptly, west of Mess Creek Valley, by the precipitous eastern ranges of the Coast Mountains.

PRE-EDZIZA TERTIARY EROSION SURFACE

The surface onto which the first flows of the Mount Edziza Volcanic Complex issued almost ten million years ago bore little resemblance to the present rugged topography. Where the old surface is preserved beneath the volcanic complex its trace is defined by the basal flows, and these are commonly exposed on steep cliffs at elevations of 4000 to 5000 ft. (1200 to 1500 m), and from 1500 to 2000 ft. (450 to 600 m) above the adjacent valley floors. Only a

few small remnants of the old erosion surface are preserved beyond the limits of the volcanic complex. East of Kinaskan Lake, flat-lying basalt flows cap broad, 6000 ft. (1800 m), concordant summits in the western Skeena Mountains, and similar basalt remnants are preserved at an elevation of 5000 ft. (1500 m) on the southern Klastline Plateau (Fig. 18). Together these remnants define a mature, gently rolling upland of moderate relief that extended as far west as Mess Creek. Farther west no obvious remnants of the pre-Edziza surface are preserved on the sharp-crested summits of the Coast Mountains where the present rugged topography is due largely to post-Early Miocene uplift and erosion.

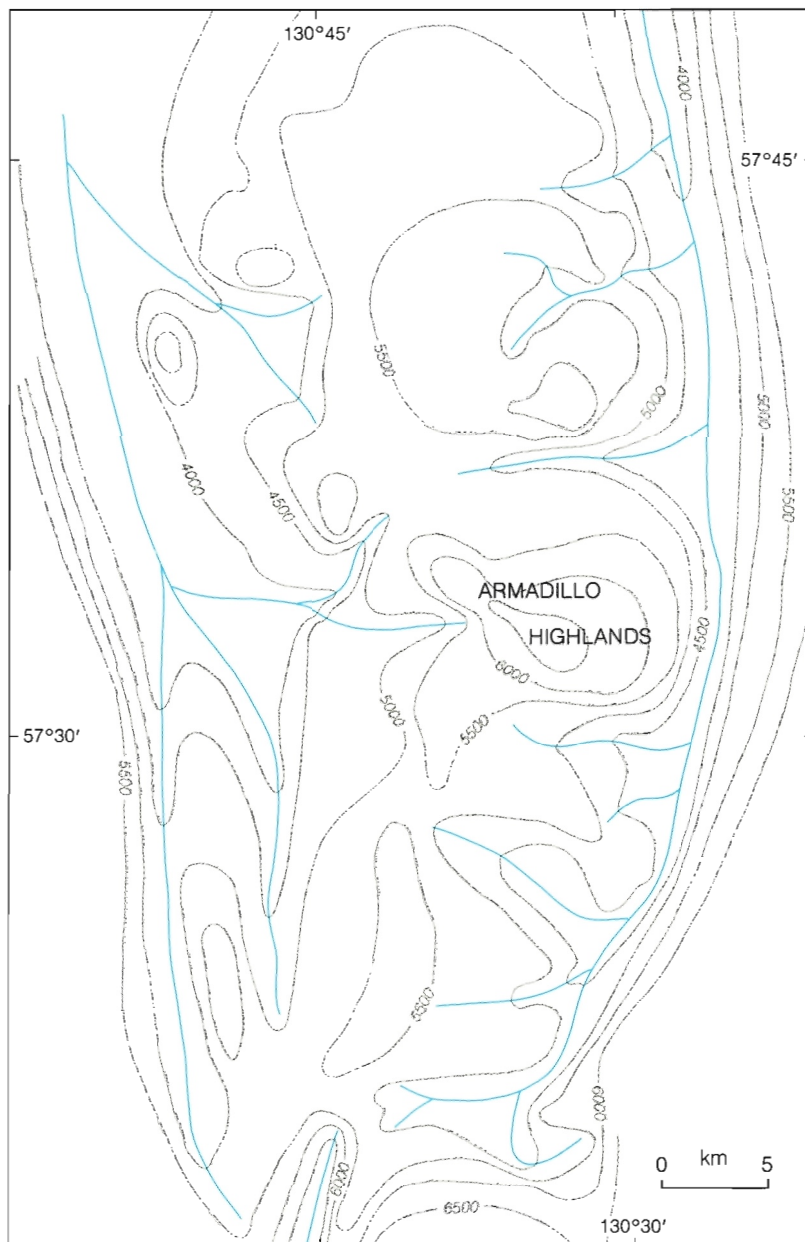


Figure 19. Paleogeographic map of the region underlain by the Mount Edziza Volcanic Complex, showing relief and inferred drainage of the pre-Late Miocene erosion surface.

The type of material preserved beneath the basal lavas varies from place to place. Locally, as in the Armadillo Highlands (Fig. 19), the lava rests directly on bedrock which is only slightly discoloured by preburial weathering. Elsewhere, paleosols, developed on fossil colluvium several metres thick, lie between the basal flows and weathered bedrock. Fluvial gravel underlies most of the distal remnants in Skeena Mountains, and is also present at several places under basal lavas of the Mount Edziza Volcanic Complex. Carbonized wood, found at several localities beneath the basal flows of Mess Creek Escarpment, suggests that the prevolcanic surface was at least partly covered by mature forest.

A paleogeographic map (Fig. 19), reconstructed by contouring the base of the volcanic pile, suggests that the

area now underlain by the Mount Edziza Volcanic Complex was a topographically high region, even before the volcanic edifice was built. The Armadillo Highlands and several lesser hills rose up to 1000 ft. (300 m) above a broad, northerly trending upland plateau, bounded on the east and west by the ancestral valleys of Mess Creek and the Little Iskut-Kakiddi Creek drainage. When the first lavas were erupted onto this intermontane plateau in latest Miocene time, the fault-controlled valley of ancestral Mess Creek was probably already flanked on the west by scarps bounding the actively rising and rapidly eroding terrain of the present Coast Mountains. Thus, while part of the old erosion surface was being preserved beneath the growing volcanic edifice, the adjacent parts were being destroyed by erosion.

RASPBERRY FORMATION

GENERAL GEOLOGY

Flat-lying, rusty, brown weathering flows of Raspberry basalt and interlayered reddish-brown to yellow or orange scoria are exposed at the base of prominent escarpments on the east and west sides of both Mount Edziza and Spectrum Range (Fig. 21, Map 1623A, in pocket). They rest directly on pre-Edziza basement rocks and their distribution reflects the topography of the late Miocene, pre-volcanic surface (Fig. 20). The elevation of the base of the pile varies from 5700 ft. (1740 m) above sea level on the east, near Armadillo Peak, to less than 4300 ft. (1310 m) above sea level along Mess Creek Escarpment. Thicknesses vary from more than 300 m in the southeastern part of the pile to only a few metres along its northern and eastern margins where narrow, valley-filling flows are exposed in cross-section. South of Bourgeaux Creek, basalt of the Raspberry Formation is overlain by trachybasalt of the Little Iskut Formation, deposited as a small shield that originally covered only the extreme southeastern corner of the Raspberry pile. Elsewhere, the Raspberry Formation is separated from overlying Armadillo and younger members by an erosion surface.

Regardless of their source or stratigraphic position the Raspberry flows are monotonously uniform. Throughout most of the pile the rock is a fine- to medium-grained brownish to greenish-grey basalt, either aphyric or with sparse phenocrysts of clear, glassy feldspar and less commonly, of black, lustrous pyroxene. Olivine is rarely visible without the aid of a lens. The only significant variation in lithology is in phenocryst content. A few flows contain up to 5% pyroxene phenocrysts and there is an abrupt increase in the size and number of plagioclase phenocrysts in some of the uppermost flows. This is particularly marked along the western side of the pile where the upper one or two flows contain 50% or more large glassy, yellow-weathering feldspar phenocrysts. Individual cooling units, both highly porphyritic as well as aphyric flows, can be traced for kilometres without any appreciable change in thickness, indicating a high degree of mobility despite initial dips commonly of only 1-2°.

Profound erosion has removed much of the outer portion of the Raspberry pile, and the central part has been largely covered by younger Formations. However, from the thickness, morphology, and elevation of exposed flow sequences it is clear that the Raspberry Formation originated as a composite shield, comprising overlapping lobes of lava from at least three source areas in the Central Highlands (Fig. 20). Most of the thick flows exposed along Mess Creek Escarpment originated from Raspberry volcano itself, whereas the small, valley-filling flows exposed on and around Cartoona Ridge must have issued from a centre

(North craters) farther to the northeast, on or east of the height of land. The extensive flows exposed in upper Little Iskut Valley must have originated from a centre (South craters) on the southeastern side of the Central Highlands. In reality, each of the three centres shown on the paleogeological map (Fig. 20) was probably itself a composite of many separate vents. Throughout Raspberry time the sites of activity undoubtedly migrated from place to place within the Highlands.

Flow morphology and depositional environment

Most of the Raspberry flows have three parts, a central core of dense columnar or crudely columnar basalt, an upper skin of clinkery blocks, rafted bombs and tephra, and a basal part of loosely agglutinated scoria. The structure and relative thickness of these three parts varies with the distance of the flow from its source and the rate and type of flow motion (Fig. 22). Rapidly flowing, distributary streams of fluid lava, confined by old valleys or by natural levees, rest directly on the underlying surface or have a relatively thin mat of basal scoria. In many cases the fluid basalt was quenched against the old surface and now displays a thin, fine grained to glassy selvage. Boulders or tree stumps on the old surface may be encased directly in the solid basalt. Similarly, the upper layer of such flows is relatively thin and may consist only of a shiny black, ropy surface or thin vesicular crust.

In accumulation areas, where the lava welled out in thick, expanding lobes on flat or gently sloping surfaces the lava front advanced more slowly and built up to a greater height depending on the viscosity of the lava. There, a thick crust formed, fractured and reformed on the slowly moving surface to produce a jumbled mass of broken slabs, clinker, and granular debris on top of the molten core. This superincumbent load was continually being sloughed off along with semimolten lava from the oversteepened lava front and buried by the advancing flow. In addition to debris derived from the surface of the flow itself the basal scoria layer may include airborne tephra, bombs and spatter deposited ahead of, and overridden by the flow, or deposited on the flow itself, and ultimately carried forward to the flow front and sloughed off into the path of the advancing lava.

Regional variations in flow morphology

On the northeast slope of the Highlands, near North craters, individual flow units are from 3-9 m thick. Each unit is mainly dense, crudely columnar basalt with only a thin upper rind of vesicular, clinkery slabs and a relatively

MOUNT EDZIZA

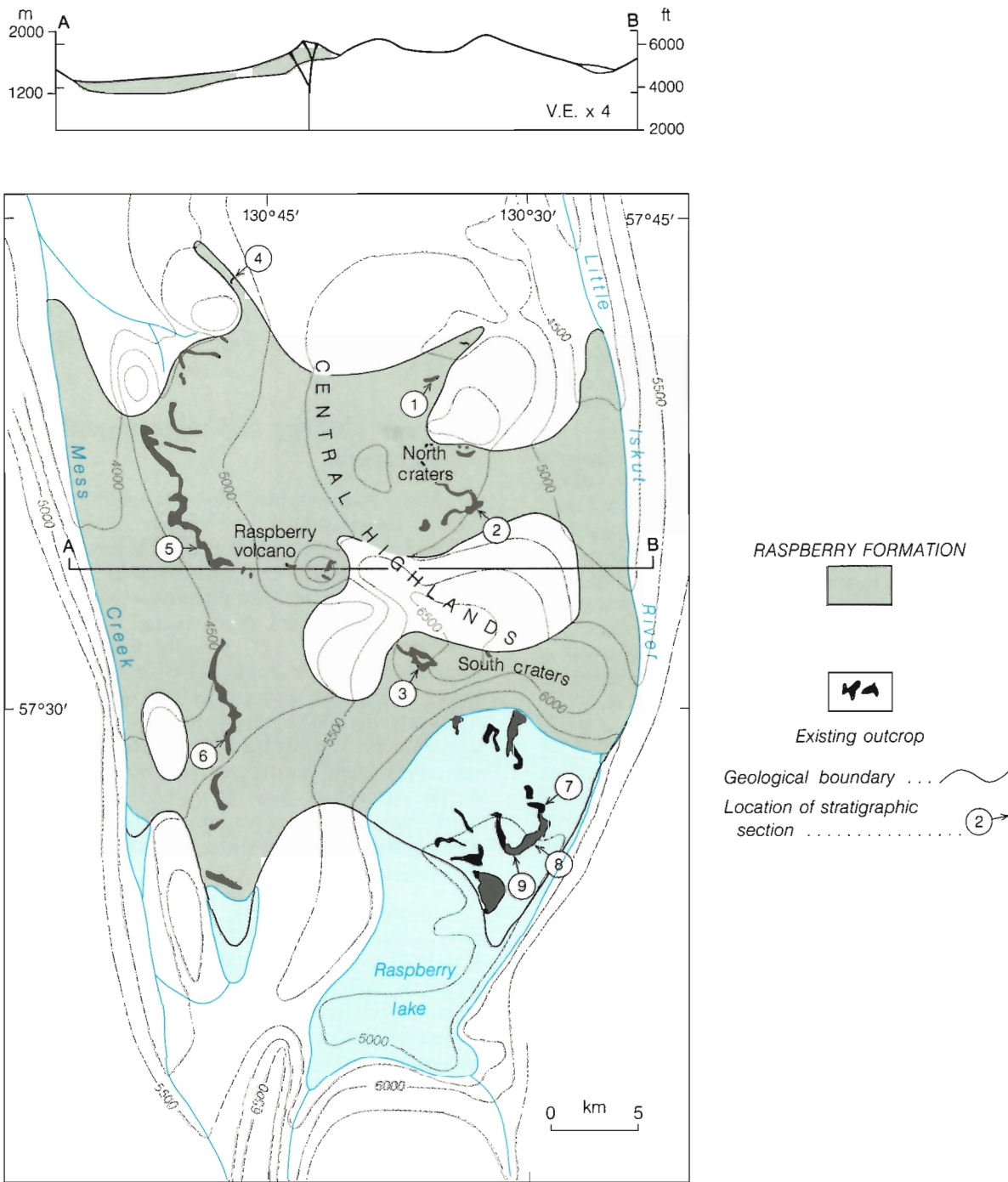


Figure 20. Paleogeological map and schematic cross-section showing the inferred maximum extent of Raspberry basalt at the end of Raspberry time. Stratigraphic sections are shown in Figure 24.

thin, uniform mat of underlying scoria. The scoria is commonly bright red, orange or yellow and comprises broken rubble spalled from the flow front as well as a high proportion of bombs, spatter and spindle-shaped lapilli obviously deposited directly from a fountaining vent. Similar flows of columnar basalt in the vicinity of South craters are inter-layered with beds of loose black, evenly sized lapilli and ash. In both places the base of the pile is more than 5000 ft. (1525 m) above sea level and rests on the surface of the

late Miocene, Central Highlands. These exposures are believed to be the only erosional remnants of the proximal facies of the Raspberry Formation. The exposures north of the Highlands were close enough to one of the vents to include oxidized bombs and spatter thrown out of the fire fountain, whereas those on the south side lay on the flanks of the volcano where fields of fine airborne tephra accumulated downwind from the vent area.

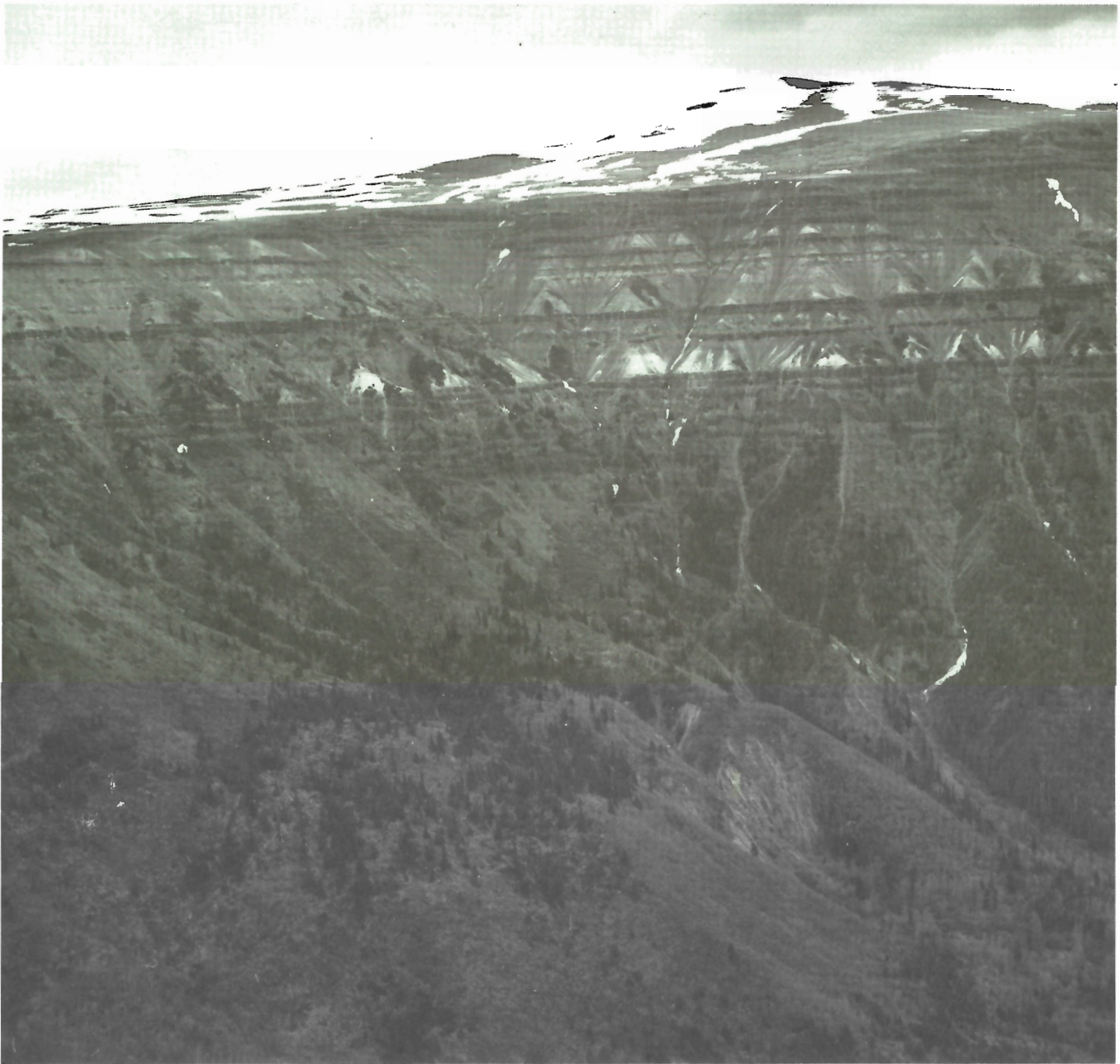


Figure 21. Mess Creek Escarpment showing typical section of thick, distal flows of Raspberry basalt overlain by Armadillo ash and fluvial deposits (white, recessive unit). Thin flows of intra-Armadillo basalt form discontinuous lenses within the fluvial unit. GSC 125 602

Cross-sections of distributary flows are well exposed north and east of North craters where basalt with radiating clusters of columns is quenched to a thin glassy rind directly against the base and sides of steep-walled bedrock canyons cut into Jurassic shale. The dark grey shale is bleached to a rusty white adjacent to the flow. A much larger distributary flow exposed in upper Walkout Creek rests directly on old gravel deposits. The basalt is molded around individual boulders, some of which have cracked from the heat.

In the more distal parts of the shield, particularly in sections along Mess Creek Escarpment, individual flow units are over 30 m thick and contain 30 to 50% basal scoria and blocky flow-top breccia. The cores of crudely columnar basalt pinch and swell between irregular lobes of scoria and breccia. In some places piles of debris, spalled off the flow front, were too large to be overridden and the lava has either divided and streamed around the obstruction or, more commonly, enveloped it and carried it along as a pocket within

MOUNT EDZIZA

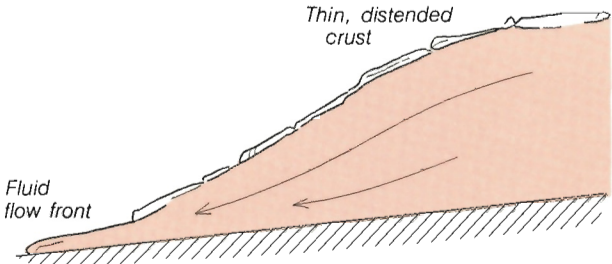
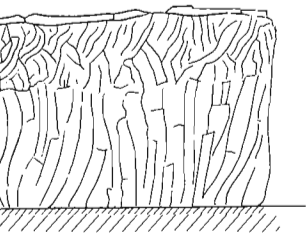
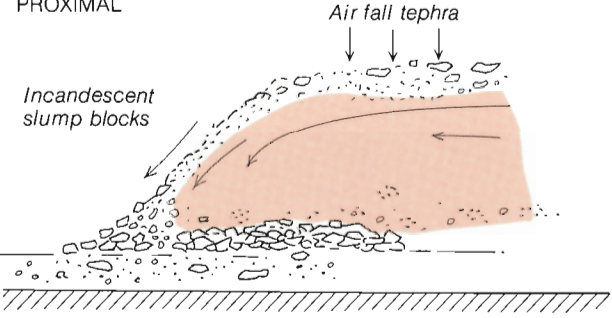

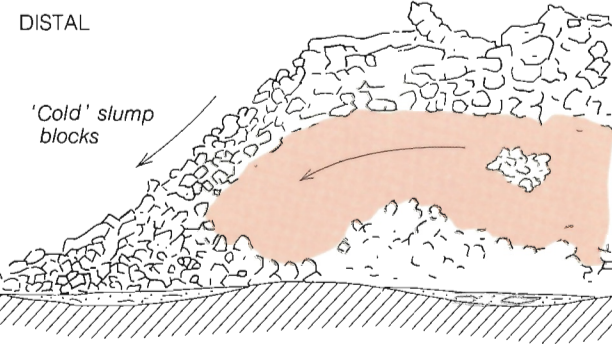
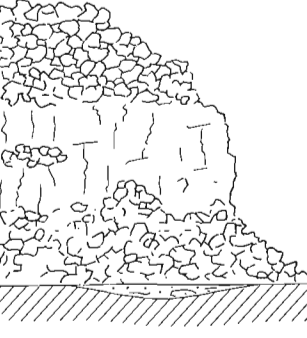
INFERRED DEPOSITIONAL ENVIRONMENT	VARIATIONS IN FLOW MORPHOLOGY	
<p>DISTRIBUTARY</p>  <p>Thin, distended crust</p> <p>Fluid flow front</p>		<p>Narrow cross-section and steep initial dip</p> <p>Crust of thin discontinuous slabs having ropy surfaces</p> <p>Prominent colonnade with long, slender or radiating columns; complexly jointed entablature</p> <p>Quenched flow base</p> <p>Thermal alteration of underlying surface</p>
<p>PROXIMAL</p>  <p>Air fall tephra</p> <p>Incandescent slump blocks</p>		<p>Flow-top breccia of mixed clinker, slabs, bombs and tephra</p> <p>Colonnade of stout, irregular columns; random or flaggy jointing in upper third of flow</p> <p>Remnant of deformed and partly remelted fragments in lower part of flow</p> <p>Basal breccia of flattened and agglutinated fragments resting on mat of primary tephra, spatter and bombs</p>
<p>DISTAL</p>  <p>'Cold' slump blocks</p>		<p>Thick flow-top breccia of large clinker and blocks</p> <p>Flow core highly irregular, pinches and swells, contains pockets of clinkery breccia</p> <p>Random or crudely columnar jointing</p> <p>Thick basal breccia of loose, uncompacted clinkery blocks</p> <p>Commonly underlain by pockets of fine, wind or waterlain tephra</p>

Figure 22. Relationship between depositional environment and morphology of Raspberry flows.

the flow. The scoria in this part of the pile consists almost entirely of reddish or yellowish-brown and grey broken debris derived from the flows themselves. Thin pockets of black ash and cinders were noted in a few places but no red, oxidized bombs or spatter were found. The enormous thickness of these flow units, their high proportion of flowtop breccia and absence of primary pyroclastic debris suggest that they accumulated at a considerable distance from their source. The base of the pile along Mess Creek Escarpment is less than 4500 ft. (1370 m) above sea level and corresponds to the western lowlands of the late Miocene surface. It was there that the distributary streams of lava from the Central Highlands welled out into thick lobes that advanced slowly across the nearly flat surface.

Along the outer margins of the pile small tongues of lava protruded into depressions on the old surface. Cross-sections of such flows are exposed in Kedeya and Shaman creeks. They are characterized by a thick irregular mat of scoria and locally by pockets of talus and slide debris from the old valley wall. An open lava tube on Kedeya Creek formed when fracturing at the toe of the flow allowed the last vestige of molten lava to drain out of the core. Unlike the fast-moving distributary flows of the Highlands, these distal tongues and lobes moved sluggishly into depressions around the accumulating pile, cooling and fracturing until, by the time all motion has ceased, the flow was reduced largely to rubble.

Only near their source in the Central Highlands and in distributary channels where molten lava came in direct contact with the old surface is there evidence of appreciable thermal alteration. The bleached bedrock and thermally fractured boulders noted in distributary channels are not found beneath flows more distant from their source. The base of the pile is well exposed at several places along Mess Creek Escarpment and in the escarpment facing Little Iskut River. There the old bedrock surface is commonly overlain by a regolith of fractured and weathered blocks and a thin layer of soil, in some places with rooted tree stumps. Locally the soil is overlain by bedded, fluvial sand composed mostly of basaltic ash, broken crystals of feldspar and less commonly pyroxene and olivine. This material, derived from the initial falls of tephra was carried from its source in the Central Highlands by ash-choked streams and deposited in the lowlands ahead of the first flows. Locally the old regolith has a few centimetres of reddish discolouration, but in most exposures the only visible change is due to groundwater leaching rather than thermal alteration, probably because the thick blanket of porous, basal breccia effectively insulated the underlying surface.

Contacts between successive flows of Raspberry basalt are remarkably sharp. In a few places pockets of windblown ash or waterlain basaltic sand have sifted in amongst the jumbled blocks of flow surfaces. A thin layer of granitic pebbles is present between some of the flows exposed in Mess Creek Escarpment but the vast majority of contacts show no erosion or intraflow sedimentation. The basal scoria of one flow rests directly on the clinkery surface of the flow beneath, suggesting that the Raspberry episode of activity was a rapid, nearly continuous event that ended as suddenly as it began.

Subaqueous facies

It is reasonable to assume that the local drainage was thoroughly disrupted by the rapid effusion of Raspberry basalt but direct evidence is surprisingly rare. The damming of Mess Creek on the west must have ponded a long shallow lake in the upper part of the valley although no trace of lacustrine deposits has survived later erosion. If lava entered the lake to form aquagene deposits they too have been removed by erosion. More direct evidence of damming is found on the east side of the pile where Little Iskut Valley was dammed by a thick sequence of flows that entered it from a tributary valley on the west (Fig. 23). The southern edge of the tributary valley is well exposed on the south end of Artifact Ridge where the lower flows lap against the steeply rising basement surface. About 0.8 km farther north, near what was the confluence of the western tributary and Little Iskut Valley, the three lower subaerial flows are overlain by a 90 m thick section with obvious water contact features. It is a massive, cliff-forming unit of complexly jointed flows and irregular pockets of tuff-breccia. Here and there the breccia has weathered out leaving shallow caves, spires and ribs of columnar basalt and overhanging cliffs of

yellowish-brown sideromelane breccia. Discontinuous flow masses coalesce into single thick cooling units with slender, curving columns more than 30 m long. Quenched lava tongues, with pillow-shaped cross-sections 1.5-15 m across, exhibit radial jointing and huge masses of complexly jointed basalt, detached from their parent flow, are completely surrounded by piles of tuff-breccia. The tuff-breccia is intimately mixed with the flows throughout the unit. It consists of a lustrous brown matrix of palagonitized sideromelane granules surrounding irregular masses and polygonal or wedge-shaped blocks from broken pillows or quenched lava toes. The irregular masses commonly have an altered glassy selvage of yellowish-brown sideromelane 1-2 cm thick.

The relationship of this aquagene deposit to the old, pre-volcanic surface suggests that Little Iskut Valley was initially dammed by a series of subaerial flows that entered it from the west (Fig. 23). Raspberry lake, ponded behind the dam, was entered by later flows which formed the deposit of tuff-breccia and quenched lava tongues. Water, discharged from the lake, followed a new course along the eastern edge of the encroaching pile of lava where the flows sloped down against the opposite valley wall. There the displaced river etched out a new valley whose easterly deflected course is preserved in the present easterly bend of Little Iskut River.

STRATIGRAPHY

The basal flow in most Raspberry sections displays well developed columnar jointing as do the narrow flows in distributary valleys and in tongues and lobes around the perimeter of the pile. The columns are commonly long and curved, or form radiating, sheaf-like clusters and rosettes that reflect the uneven cooling surface onto which the lava flowed. Cross-sections of small, valley-filling flows exposed in Kedeya Creek and on Cartoona Ridge, west of Kakiddi Lake, display perfect sets of radial columns normal to the valley cross-sections. At Kedeya Creek the central part of the flow is a small open lava tube around which the radial columns form a complete circular rosette about 12 m in diameter.

Flows higher in the section commonly have crude columnar or random subvertical joints. Individual flow units range in thickness from a few metres to more than 30 m. Most of them have a basal mat of loosely agglutinated, porous scoria, a central core of dense, columnar basalt, and an upper rind of flowtop breccia. Together the basal scoria and flowtop breccia form recessive benches which alternate with near-vertical cliffs formed by the columnar flow-cores to give the sections a prominent terraced aspect (Fig. 21).

Outcrops of Raspberry basalt are universally weathered to a deep reddish-brown rind from less than 1 mm thick on steep, newly exposed cliff surfaces to more than 5 cm thick on spheroidally weathered joint surfaces of stable slopes. Beneath this surface the rock is medium grey to greenish or

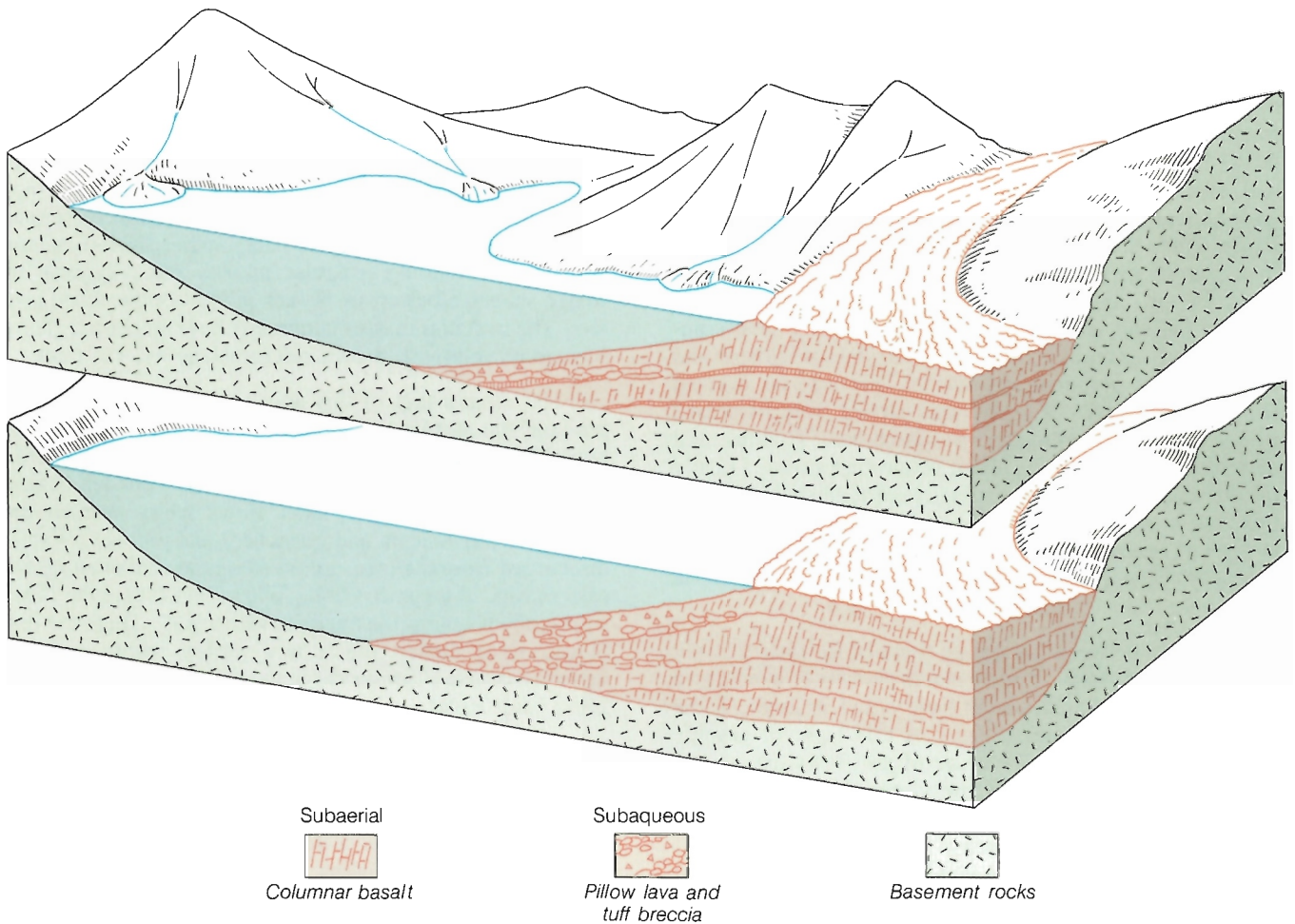


Figure 23. Schematic block diagram showing two stages in the damming of Little Iskut River by lava flows descending a tributary valley from the west.

brownish black. In most stratigraphic sections the megascopic texture and mineralogy of successive flows are monotonously uniform, but locally variations in the phenocryst content provide a basis for subdivision (Fig. 24). Four fairly distinctive types are recognized:

1. Aphyric basalt
2. Slightly feldsparphyric (1 to 10% plagioclase phenocrysts)
3. Highly feldsparphyric (> 30% plagioclase phenocrysts)
4. Pyroxene-phyric (1-5% pyroxene phenocrysts).

The first two types comprise by far the greater volume. Flows in the lower half of the pile are mostly aphyric, whereas those higher in the section commonly contain 1-10% phenocrysts of clear, glassy or amber feldspar. The aphyric basalt varies from a greyish-black subvitreous rock to dark grey medium grained basalt in which groundmass feldspars and pyroxene, but rarely olivine, are visible without the aid of a lens. Feldspar phenocrysts in the slightly

porphyritic flows (type 2) are flat, tabular and usually randomly oriented. They commonly range in size from 1-10 mm across, though sparse, isolated crystals up to 4 cm are widely distributed. In most stratigraphic sections the percentage of phenocrysts increases systematically from older to younger flows.

The highly feldsparphyric flows (type 3) are confined to one or two cooling units in the upper part of the pile. In most places they form the uppermost unit, however, they are locally overlain by one or two aphyric flows. Most of them contain 30-60% clear glassy or amber, randomly oriented, tabular phenocrysts of plagioclase from 1-5 cm long and 1-10 mm thick. Locally phenocrysts make up to 80% of the rock and the associated scoria consists mostly of broken feldspar crystals. The change from aphyric or slightly porphyritic flows to the highly porphyritic type is usually abrupt and only rarely do flows of intermediate phenocryst content intervene.

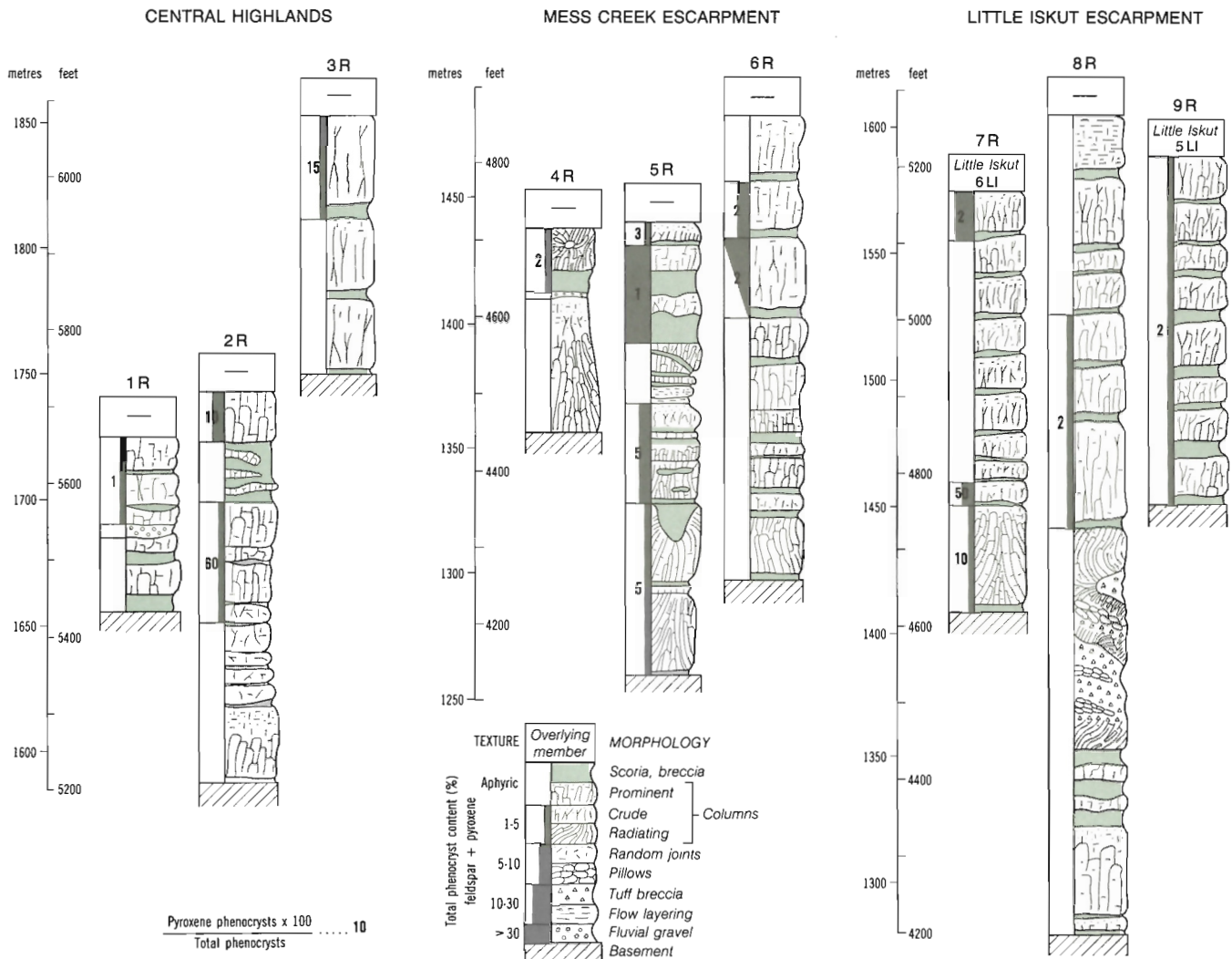


Figure 24. Typical stratigraphic sections of the Raspberry Formation showing variations in morphology and phenocryst content. Section numbers (1-9) refer to locations shown on the paleogeological map (Fig. 20). R, Raspberry Formation; LI, Little Iskut Formation.

Basalt with pyroxene as well as feldspar phenocrysts (type 4) forms a distinct, relatively young facies, that is confined to the central and eastern part of the Raspberry pile. The rock is commonly brownish grey and contains 1-5% phenocrysts of black pyroxene up to 5 mm across. Associated feldspar phenocrysts are similar to those in the feldsparphyric types and may be either more or less abundant than the pyroxene.

PETROGRAPHY

Thin sections of Raspberry basalt exhibit the simple mineralogy typical of alkali olivine basalts. The major silicate minerals are plagioclase, titaniferous augite, and olivine, and megascopic variations in the basalt are due solely

to variations in the relative amounts of these three minerals in the groundmass and phenocrystic phases. The opaque oxides, magnetite, ilmenite and hematite, are ubiquitous but vary widely in amount and mode of occurrence. Twenty-one microprobe analyses of the principal minerals are plotted on Figure 25 and five representative analyses are listed in Table 1. Minor minerals include apatite and alkali feldspar, which are widely and fairly uniformly distributed, rare biotite, analcite and fluorite. With the exception of water-quenched flows, the Raspberry basalts are essentially holocrystalline and, what little glass was present has been altered to green or brown chlorophaeite. In addition many thin sections reveal a pervasive alteration of the matrix to carbonate, chlorite, and zeolites.

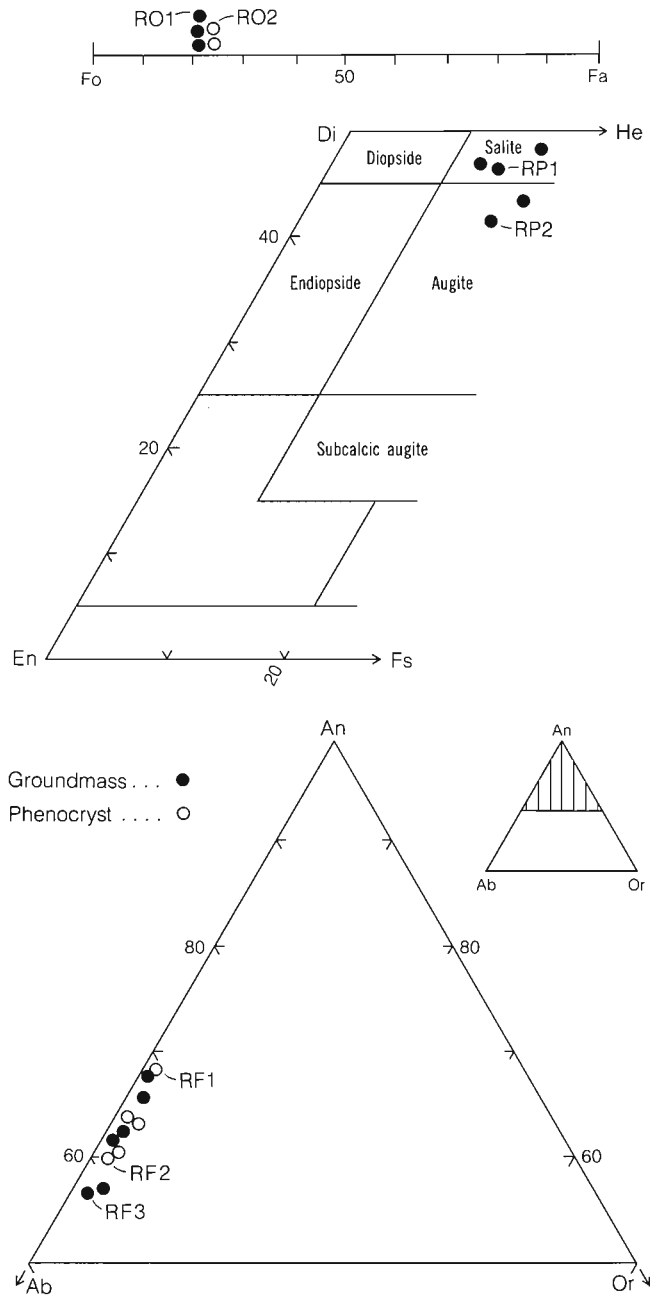


Figure 25. End-member plots showing compositions of feldspar, pyroxene and olivine in Raspberry basalt, based on 21 microprobe analyses. Five representative analyses, identified by numbers (RO1, RF2 etc.) are listed in Table 1.

Aphyric and slightly feldsparphyric basalt (types 1 and 2)

The texture and composition of the aphyric flows (type 1; Fig. 26a) is similar to the groundmass of the slightly feldsparphyric flows (type 2; Fig. 26c). Euhedral to subhedral laths of zoned plagioclase form 50 to 70% of the rock. The feldspars may be either randomly, or strongly oriented to

give the rock a trachytic fabric. Flat stage optical determinations indicate a range of compositions from An₄₃₋₇₀. In any given section there is a rough correlation between core composition and grain size, the larger laths being slightly more calcic (Fig. 27). Six microprobe analyses of the groundmass feldspar give a range of core compositions from An₅₆₋₆₇.

Plagioclase phenocrysts, where present, are either euhedral or slightly corroded and embayed by the groundmass. Most of them have complex twinning, usually albite combined with carlsbad and less commonly with pericline. The cores of most phenocrysts are slightly more calcic than the groundmass feldspar. Some of the large phenocrysts exhibit oscillatory or reverse zoning. However, zoning is commonly confined to a narrow outer rim, across which the composition changes rapidly from that of the core to that of the groundmass feldspar. Whereas the inner core of most phenocrysts is relatively free of inclusions, the outer strongly zoned rim commonly includes tiny circular or elliptical blebs of glass, fluid inclusions, and microlites of pyroxene.

Strongly pigmented, purplish-brown titanite is confined, in most Raspberry basalts, to interstitial spaces between the plagioclase laths. In rapidly cooled flows, such as the basal flow along Mess Creek Escarpment and the water-quenched flows of Little Iskut Escarpment, the titanite occurs as skeletal, bladed or dendritic crystals in an interstitial mesostasis of iron-rich glass. Elsewhere it commonly forms ophitic or subophitic plates that enclose or are interstitial to the groundmass plagioclase. Rarely it occurs as granular, subhedral interstitial crystals, particularly in those rocks with a well developed trachytic texture.

Titanite in the Raspberry basalt has a relatively narrow range of composition near the salite-augite boundary (Fig. 25).

Olivine (Fa₂₂₋₂₄) forms from less than 1 to about 3% of most Raspberry basalt. In the aphyric and slightly porphyritic rocks it occurs as sparse, prismatic microphenocrysts and subhedral granules (Fig. 26b). The amount and size of olivine phenocrysts increases in the slightly feldsparphyric rocks. Rarely it occurs in glomeroporphyritic clusters with magnetite and, where a trachytic texture developed, the flow layers wrap around both olivine and early formed magnetite. No reaction is evident between olivine phenocrysts and matrix.

Titanomagnetite occurs as euhedral microphenocrysts; as tiny evenly dispersed granules; and as irregular space fillings between the groundmass feldspars. The microphenocrysts are commonly associated with olivine and are most abundant in aphyric basalt having a pronounced trachytic texture. Deflection of the flow layering around both olivine and titanomagnetite indicates that they were the first minerals to crystallize. A second generation of titanomagnetite crystallized after the groundmass feldspar. It occurs as tiny granules dispersed throughout the ophitic plates of titanite. Most of the granules appear to have crystallized before the augite and are enclosed by it. In some

Table 1. Selected microprobe analyses and structural data for feldspar, pyroxene and olivine from the Raspberry basalt.

	Feldspar			Pyroxene		Olivine			
	Phenocrysts		Ground-mass	Groundmass		Ground-mass	Pheno-cryst		
	RF1	RF2	RF3	RP1	RP2	RO1	RO2		
SiO ₂	50.79	52.43	52.89	48.45	49.30	38.19	38.46		
Al ₂ O ₃	31.09	29.56	28.95	3.93	2.96	0.31	0.0		
TiO ₂	0.0	0.0	0.0	2.60	2.00	0.03	0.01		
Cr ₂ O ₃	0.0	0.0	0.0	0.03	0.0	0.0	0.0		
Fe ₂ O ₃	0.53	0.63	0.71	1.98	2.06	0.0	0.0		
FeO	0.0	0.0	0.0	8.28	10.83	20.66	22.20		
MnO	0.0	0.0	0.0	0.20	0.24	0.25	0.25		
MgO	0.0	0.0	0.0	12.91	12.57	40.37	39.44		
NiO	0.0	0.0	0.0	0.0	0.0	0.13	0.13		
CaO	14.12	12.27	11.96	20.83	19.69	0.31	0.29		
Na ₂ O	3.56	4.36	4.85	0.45	0.44	0.0	0.0		
K ₂ O	0.13	0.24	0.30	0.0	0.0	0.0	0.0		
H ₂ O	0.0	0.0	0.0	0.0	0.0	0.0	0.0		
F	0.0	0.0	0.0	0.0	0.0	0.0	0.0		
Total	100.22	99.49	99.66	99.66	100.09	100.25	100.78		
	No. of ions on basis of 8 (0)			No. of ions on basis of 6 (0)		No. of ions on basis of 4 (0)			
Si	2.3112	2.3919	2.4113	Si	1.8270	1.8641	Si	0.9851	0.9931
Al	1.6673	1.5893	1.5555	Al	0.1730	0.1319	Al	0.0	0.0
Cr	0.0	0.0	0.0	Ti	0.0	0.0040	Cr	0.0	0.0
Fe ⁺³	0.0181	0.0216	0.0244	Fe	0.0	0.0	Fe ⁺³	0.0	0.0
				Cr	0.0	0.0			
Al	0.0	0.0	0.0	Al	0.0016	0.0	Al	0.0094	0.0
Cr	0.0	0.0	0.0	Ti	0.0737	0.0529	Cr	0.0	0.0
Ti	0.0	0.0	0.0	Fe ⁺³	0.0561	0.0585	Ti	0.0006	0.0002
Fe ⁺³	0.0	0.0	0.0	Cr	0.0009	0.0	Fe ⁺³	0.0	0.0
Ni	0.0	0.0	0.0	Ni	0.0	0.0	Ni	0.0027	0.0027
Fe ⁺²	0.0	0.0	0.0	Fe ⁺²	0.2611	0.3425	Fe ⁺²	0.4457	0.4794
Mn	0.0	0.0	0.0	Mn	0.0064	0.0077	Mn	0.0055	0.0055
Mg	0.0	0.0	0.0	Mg	0.7256	0.7084	Mg	1.5521	0.5179
				Ca	0.8416	0.7977			
				Na	0.0329	0.0323			
				K	0.0	0.0			
Ca	0.6884	0.5998	0.5842				Ca	0.0086	0.0080
Na	0.3141	0.3857	0.4287				Na	0.0	0.0
K	0.0075	0.0140	0.0174				K	0.0	0.0

rocks, however, both minerals form large irregular, ophitic or subophitic plates that enclose the groundmass feldspar and have sharp common boundaries. Thus crystallization of titanomagnetite appears to have continued during crystallization of the interstitial titanite.

Accessory minerals include apatite, which is uniformly distributed as tiny acicular crystals, minor potassium feldspar and rare biotite as small intergranular crystals. Analcite is found as primary, euhedral crystals and as a void-filling with calcite in a few sections.

Highly feldsparphyric basalt (type 3)

The highly feldsparphyric basalt contains 30-80% phenocrysts of plagioclase up to 3 cm long (Fig. 26e). These are of two distinct types: an older generation of relatively small, partly resorbed crystals; and a younger generation of unaltered crystals. The resorbed phenocrysts form only 10 to 15% of the total. They are ragged, deeply embayed or rounded crystals of strongly zoned plagioclase in which the calcic cores have been partly or wholly resorbed and display coarse sieve structure. In contrast, the younger crystals are

unzoned, except for a thin outer rim of more sodic plagioclase and rarely of potassium feldspar. They show no evidence of reaction with the liquid. Contacts with the groundmass are sharp, formed by either euhedral crystal boundaries or, more commonly, fracture surfaces. The high proportion of broken crystals in the porphyritic rocks indicates that considerable cataclasis took place during the final stages of flow.

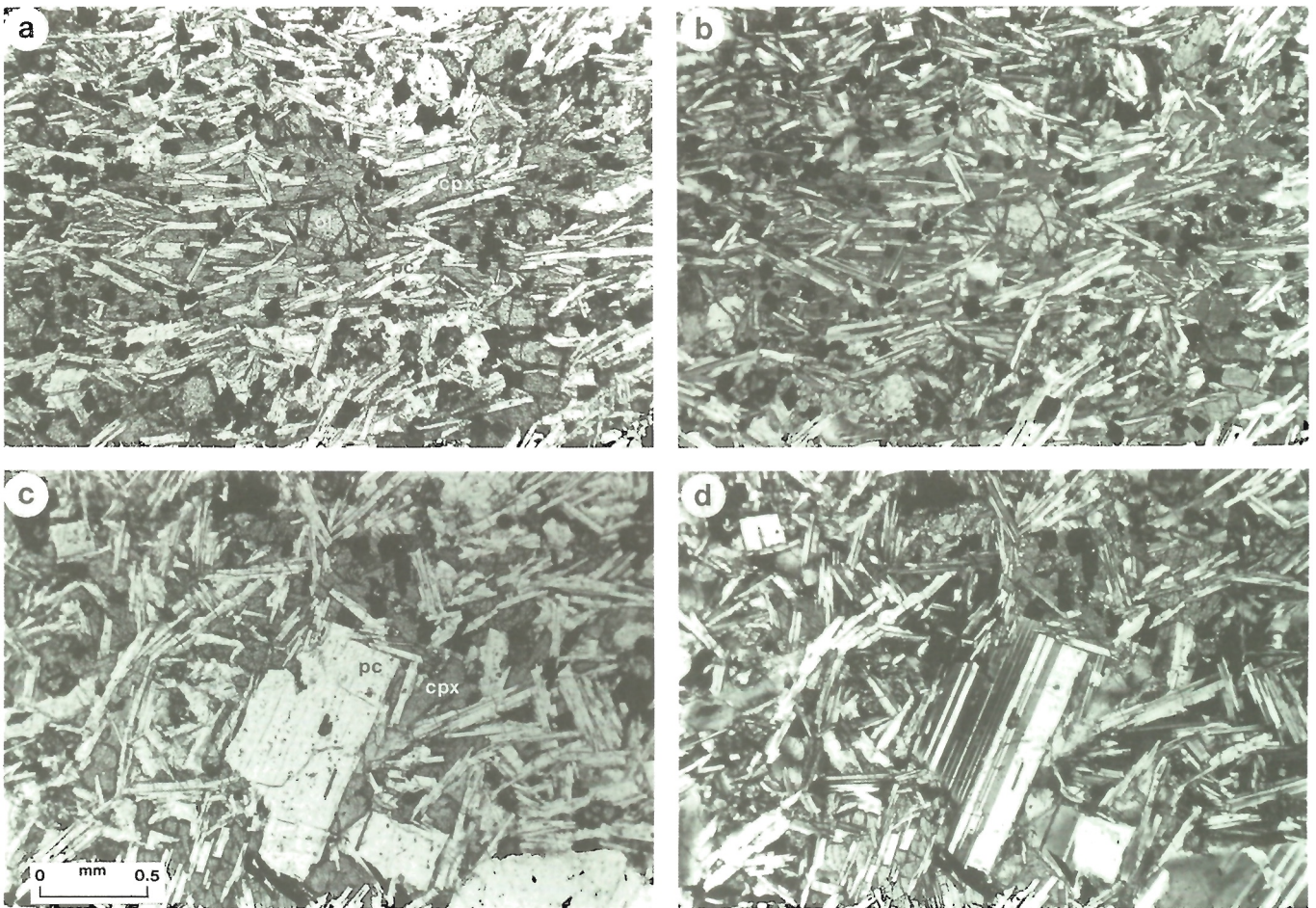
In addition to plagioclase, the highly feldsparphyric basalt contains rare phenocrysts and fairly abundant microphenocrysts of both olivine and titanomagnetite. A reaction rim of green amphibole and opaque oxides commonly mantles the larger olivines.

The groundmass comprises oriented laths of plagioclase, and small granules of olivine and titanomagnetite enclosed by ophitic plates of titanaugite. It differs from that of the slightly feldsparphyric basalt in having a much lower ratio of pyroxene to feldspar. Whereas titanaugite may form 20 to 50% of the groundmass of slightly feldsparphyric basalts, it rarely exceeds 10% in the groundmass of highly porphyritic types.

Pyroxene-phyric basalt (type 4)

This relatively minor facies of the Raspberry basalt is characterized by augite phenocrysts 1-10 mm across, which form up to 5% of the rock (Fig. 26g). The phenocrysts lack the strong purplish-brown pigmentation of the ophitic titanaugite in types 1 to 3. They comprise equant, pale brown, strongly zoned and usually twinned crystals, most of which are deeply embayed and surrounded by porous reaction rims. Many have been so completely resorbed that only a skeletal outline remains and the crystal interior is crowded with a mosaic of feldspar and opaque oxides. Co-existing olivine phenocrysts, which are commonly smaller but at least as abundant as the pyroxene, show little or no evidence of reaction. The groundmass, like that of the other Raspberry basalts, consists mainly of well oriented laths of plagioclase (An_{50-60}) and interstitial titanaugite. The groundmass pyroxene, however, forms tiny prismatic to subhedral grains rather than large ophitic plates.

Augite, similar to that in the phenocrysts, is also present in small rounded, cognate inclusions. These appear to be cumulate clusters in which augite is the dominant mineral, associated with minor olivine and magnetite.



a,b — Aphyric alkali olivine basalt (a, plane light; b, crossed polarizers).

c,d — Sparsely porphyritic hawaiiite (c, plane light; d, crossed polarizers).

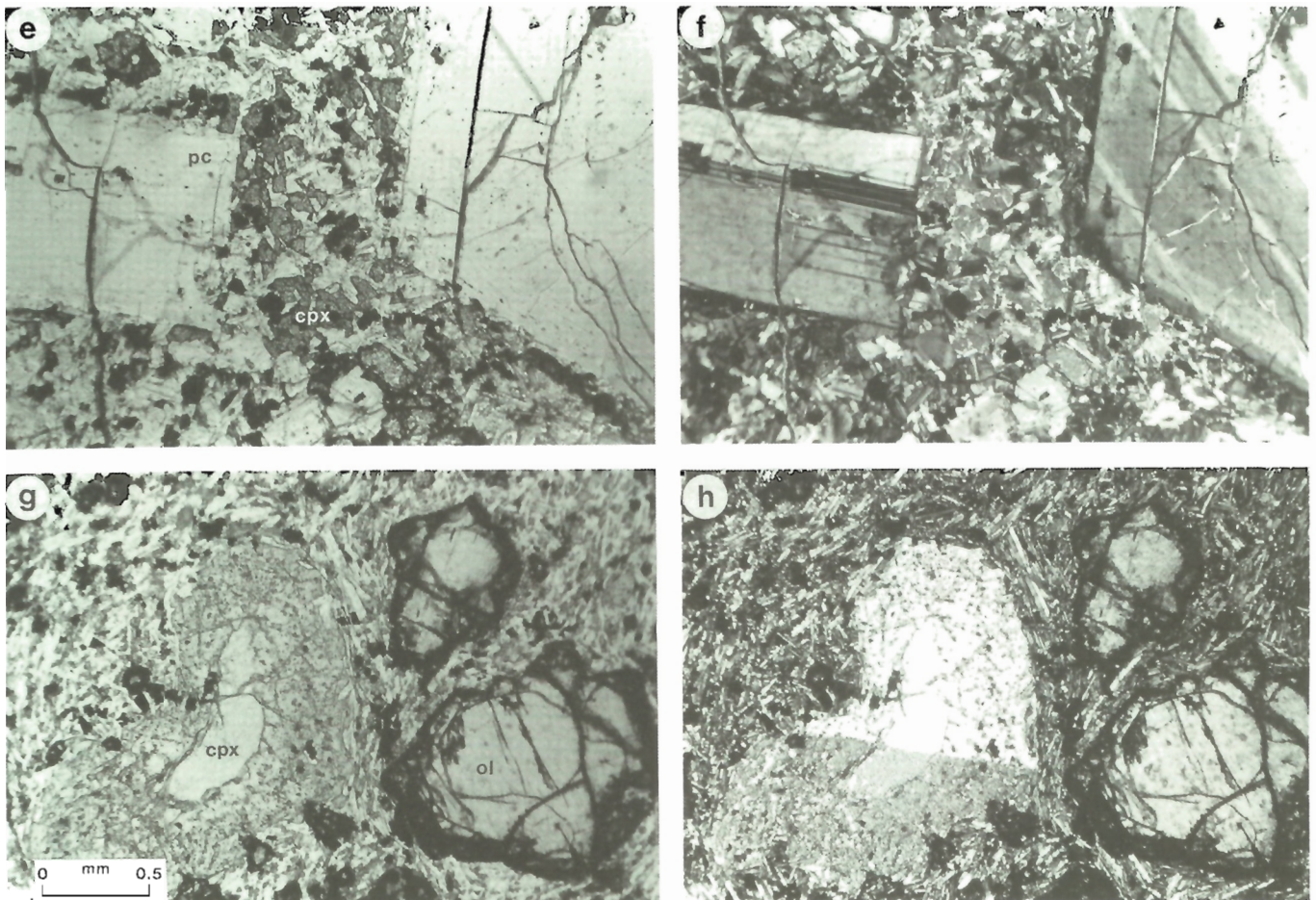
Figure 26. Photomicrographs of Raspberry basalt; scale bar 0.5 mm. (pc, plagioclase; ol, olivine; cpx, clinopyroxene; tia, titanaugite).

Amygdules

Open vesicles are rare in the Raspberry basalt, but nearly every flow contains at least a few amygdules, either randomly distributed, or concentrated in subparallel layers in the upper part. Amygdule minerals include aragonite, calcite, ankerite, goethite, hematite, limonite, fluorite, chlorite, several different zeolites, and various forms of quartz, chalcedony and opal. Usually more than one mineral is present, and the first to form in most cases is an iron oxide. This commonly occurs as a dark botryoidal rind, lining the interior of the cavity and forming a thin discoloured halo in the adjacent rock. Concentrically banded aragonite and calcite are the most common and often the only fillings.

Calcite, fluorite and the zeolites were usually the last to crystallize and, where present, they form a relatively small part of the amygdule.

No attempt has been made to make a rigorous study of the amygdules, but the occurrence of different types is apparently not random. Although their mineralogy varies from place to place within the volcanic pile, it is fairly consistent over large areas. Amygdules in the thick flows of the Mess Creek Escarpment, for example, are mainly carbonate, whereas those in the central part of the complex, near Armadillo Peak, are mainly chalcedony and opal. The former formed in flows that were ponded in an accumulation area several kilometres from their source and presumably the solutions that gave rise to the aragonite amygdules were relatively low-temperature carbonate waters. In contrast, the flows exposed in the central part of the complex are close to their source where the relatively hot solutions circulating through them would be expected to have a higher silica content. Also silica, rather than carbonate amygdules tend to occur in flows that are overlain directly by thick rhyolite



e,f — Highly porphyritic mugearite (e, plane light; f, crossed polarizers).

g,h — Pyroxene-phyric alkali olivine basalt (g, plane light; h, crossed polarizers).

Figure 26 (Cont.)

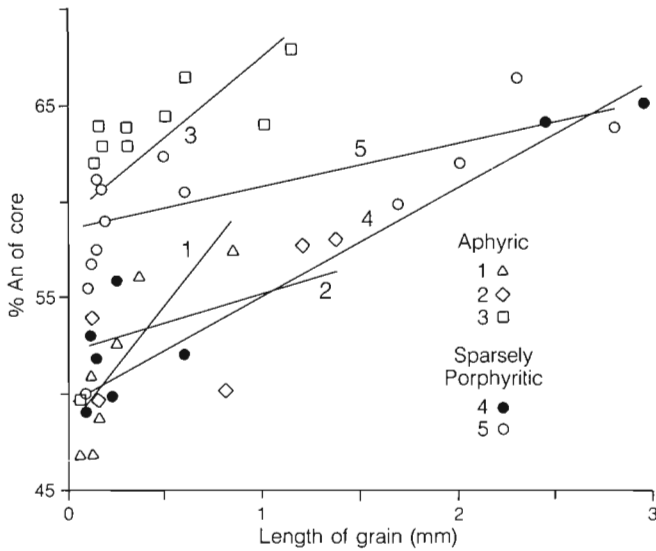


Figure 27. Plot showing the relationship of grain size to core composition of groundmass feldspar in five Raspberry basalts. Lines are least squares regression lines calculated for each data set.

units. Thus silica amygdules predominate in the uppermost Raspberry flow where it is overlain by the Armadillo Formation, whereas carbonate fillings are more common in the lower part of the pile and in distal flows that were never buried by more acid members.

CHEMISTRY

Twenty-one major-element analyses of Raspberry basalt (Appendix 2, Table 2) indicate a very narrow range of compositions. Over 80% of the silica values fall between 45 and 48% and all other oxides exhibit a similarly narrow range (Fig. 28). Quartz does not appear in any of the norms. Sixteen of the analyzed specimens are hypersthene normative and the remaining five contain a trace (< 1.2%) of normative nepheline. The AFM plot (Fig. 29a) shows a relatively strong iron enrichment. In the Irving-Baragar (1971) classification most of the Raspberry analyses plot within the alkaline field of the SiO₂ vs. Na₂O + K₂O diagram (Fig. 29b) and either in, or very close to the sodic field of the Ab'-An-Or ternary (Fig. 29a). Thus the chemistry, like the mineralogy, indicates that the Raspberry basalt

Table 2. Representative chemical analyses of Raspberry basalts.

Spec. no.	Alkali olivine basalt			Hawaiite			Mugearite	
	2657	36	52	80	79	54	78	2875
SiO ₂	47.00	45.00	47.60	46.00	46.50	46.00	49.40	47.30
Al ₂ O ₃	16.00	16.20	16.50	17.00	15.90	16.40	18.30	14.40
Fe ₂ O ₃	2.50	3.60	3.30	2.80	3.00	5.52	4.00	8.00
FeO	10.00	9.60	8.00	8.90	9.60	7.70	6.50	7.00
MgO	5.80	6.41	6.66	4.84	6.67	3.24	2.89	3.40
CaO	8.40	8.23	8.96	8.97	8.10	8.10	7.83	6.40
Na ₂ O	3.00	3.00	3.10	3.20	3.20	3.90	4.10	4.30
K ₂ O	1.10	1.31	1.11	1.26	1.26	1.39	1.67	1.90
TiO ₂	2.65	3.36	2.49	2.84	2.96	3.01	2.30	2.80
P ₂ O ₅	0.44	0.46	0.40	0.47	0.47	0.62	0.81	1.30
MnO	0.17	0.17	0.15	0.18	0.20	0.21	0.16	0.23
S	0.0	0.06	0.07	0.09	0.08	0.07	0.06	0.0
NiO	0.0	0.01	0.01	0.01	0.0	0.01	0.0	0.0
Cr ₂ O ₃	0.0	0.0	0.0	0.0	0.0	0.0	0.0	0.0
CO ₂	0.30	0.0	0.0	2.10	0.10	2.70	1.20	1.40
H ₂ O	1.60	2.60	1.00	2.10	2.60	1.30	1.00	1.70
Total	99.56	99.65	100.25	100.76	100.64	99.78	100.20	99.92

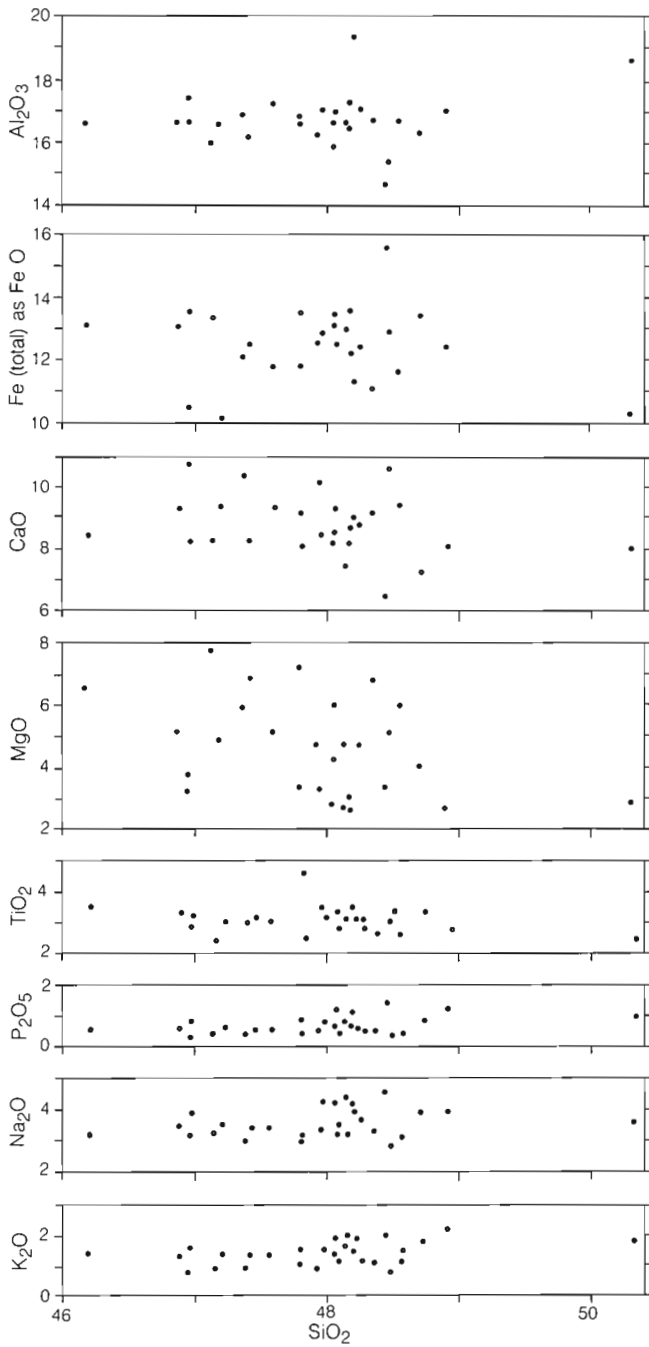


Figure 28. Harker diagram showing the chemical variation in weight per cent of 21 analyzed Raspberry basalts with respect to silica.

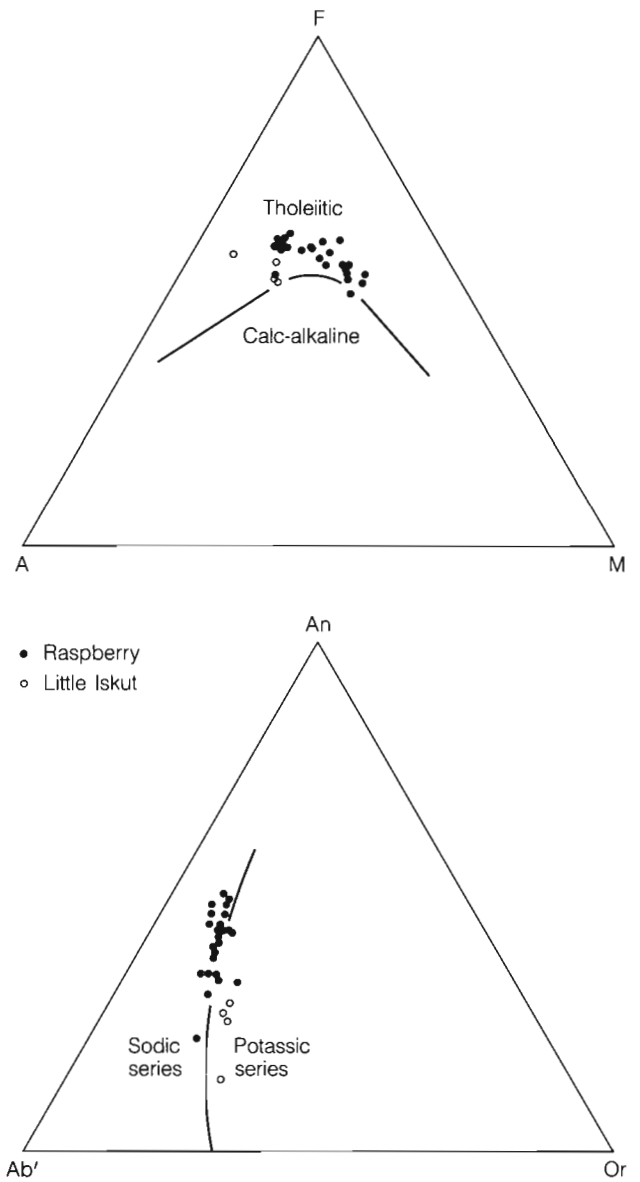


Figure 29a. AFM and Ab'-An-Or plots of Raspberry basalt and Little Iskut trachybasalt. ($A = Na_2O + K_2O$; $F = FeO + 0.8998 Fe_2O_3$; $M = MgO$; $Ab' = Ab + 5/3Ne$.)

MOUNT EDZIZA

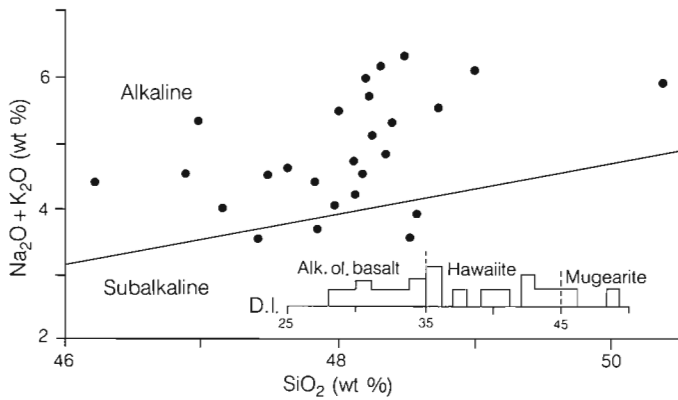


Figure 29b. Total alkali vs. silica plot showing the distribution of 21 Raspberry basalts relative to the Irvine- Baragar (1971) boundary between alkaline and subalkaline rocks. Inset shows frequency distri- bution of differentiation index (D.I.) values.

forms a sodic suite within the alkali olivine basalt series. A further subdivision, using the Thornton and Tuttle (1960) differentiation index (D.I.) according to the scheme proposed by Thompson et al. (1972) indicates about equal numbers of alkali olivine basalts (9) and hawaiites (10), and two mugearites (Fig. 29b). The shift to higher D.I. values is clearly due to an increase in the percentage of feldspar phenocrysts. The two mugearites (D.I. > 45) are from the highly porphyritic (> 50% feldspar phenocrysts) unit at the top of the Raspberry section along Mess Creek Escarpment. Thus the trend toward mugearite in these data does not necessarily reflect a liquid line of descent, but rather a shift in bulk composition caused by removal of an iron-rich liquid residue from a mush of early formed plagioclase phenocrysts. In fact the most notable feature of the Raspberry basalt is the absence of any well defined chemical trend. The lavas appear to be the product of a fairly uniform batch of primitive magma. If part of the batch did evolve into more highly fractionated end members, no evidence that any of them erupted during Raspberry time exists.

LITTLE ISKUT FORMATION

GENERAL GEOLOGY

Introduction

Little Iskut flows and breccia are confined to a relatively small area about 10 km across, in the north-eastern Spectrum Range (Fig. 30; Map 1623A, in pocket). They form prominent cliffs around the eastern end of both Artifact and Stewpot ridges (Fig. 31) but, except for two relatively thin flows in Mess Creek Escarpment, they do not appear in more distal sections. The pile rests conformably on Raspberry basalt and is overlain conformably by Armadillo trachyte and rhyolite. It has a maximum thickness of about 300 m near the centre of Artifact Ridge and thins rapidly from that point, decreasing to only 90 m on Stewpot Ridge.

The succession is subdivided into a lower, light coloured unit comprising pyroclastic and aquagene breccias and an upper unit of thick dark grey subaerial lava flows and associated flow breccia (Fig. 32). Both the geometry of the pile and the presence of coalescing dyke swarms and alteration pipes along the north side of Artifact Valley suggest that the Little Iskut pile was a small, symmetrical shield, whose central vent lay near the bend in Artifact Valley (Fig. 30). Its total volume is estimated to have been about 14.3 km³.

Lower unit

The lower part of the Little Iskut pile forms a distinctive, light coloured recessive unit 15-140 m thick that contrasts with massive columnar flows of the underlying Raspberry basalt and dark irregular flows of trachybasalt in the upper part of the Little Iskut pile. The most abundant rock type is a "crackle breccia" comprising closely fitted polygonal chunks of trachybasalt from the size of coarse lapilli up to about 20 cm across. The bounding faces of adjacent polygons are commonly smooth, gently curving or planar fracture surfaces. In most outcrops no evidence of relative movement along these surfaces is seen, but locally the precisely fitted polygons are disrupted along zones of secondary fracturing. Within these zones the polygons have been more or less rotated to produce an open breccia in which the interstitial voids are lined with secondary minerals. In many of these fracture zones, the larger polygons are surrounded by a matrix of smaller polygons cemented by iron-manganese oxide.

Pervasive alteration of the "crackle breccia" has changed the normally dark grey trachybasalt to shades of pale yellow or brown. A small core of fine grained, nonporphyritic pale grey trachybasalt can be found in the centre of a few of the largest polygons, but even that has been altered. The cores of most polygons are a pale brown that

grades to a nearly white outer rind. Bounding fractures are commonly coated with yellowish-brown iron-manganese oxide.

The "crackle breccia" is associated with varying amounts of pumice, crystal tuff and explosion breccia. The more northerly exposures, in Raspberry Pass, have 1.5-4.5 m of well sorted and bedded white, sand- to lapilli-sized pumice at the base (Fig. 33). Locally this is overlain by a few metres of black vitrophyre containing conspicuous white weathering fiamme up to 2 cm long. Both the pumice and vitrophyre are slightly porphyritic, but they are commonly overlain by a crystal tuff of lightly welded fine yellowish-white ash containing abundant crystals of clear, white tabular feldspar up to 5 mm long. This material is overlain by 60-90 m of "crackle breccia" with isolated lenses and pockets of similar crystal tuff and bedded pumice.

Both the basal pumice and the crystal tuff contain small angular accidental clasts of basalt. Along the northern edge of the pile these are rarely more than 2 cm across and form less than 1% of most beds. Their size and number increase rapidly northward and locally, along the southeast end of Artifact Ridge, accidental basalt blocks up to 1.2 m across form up to 50% of the basal ash deposit. The angularity and size of these blocks, as well as the intense oxidation of the red and yellow enclosing pumiceous ash, suggest that the deposit is the proximal facies of an explosion breccia.

Still farther south, on Stewpot Ridge, the lower unit is poorly developed. "Crackle breccia" is present in isolated lenses that grade laterally into normal flow breccia, crystal tuff and ash. The ash forms laminated beds of fine white pumice containing only a few small accidental clasts of basalt.

Upper Unit

The entire upper part of the Little Iskut pile consists of trachybasalt lava flows (Fig. 34). Most are highly irregular, with varying proportions of lava and flow breccia within a single cooling unit. Viewed from a distance the section appears to be made up of discontinuous lenses of lava in a rubbly pile of rusty breccia that contrasts with the regular succession of uniform flows in the underlying Raspberry basalt. Individual cooling units are 9-18 m thick and include about equal amounts of crudely jointed, dark brown weathering lava and yellowish-brown flow breccia. With one exception, the flows are aphanitic, dark grey to greenish-grey, flow banded trachybasalt, either nonporphyritic or with a few small feldspar phenocrysts. The exception is a single abundantly feldsparphyric flow exposed near the centre of the thickest part of the pile on Artifact Ridge.

MOUNT EDZIZA

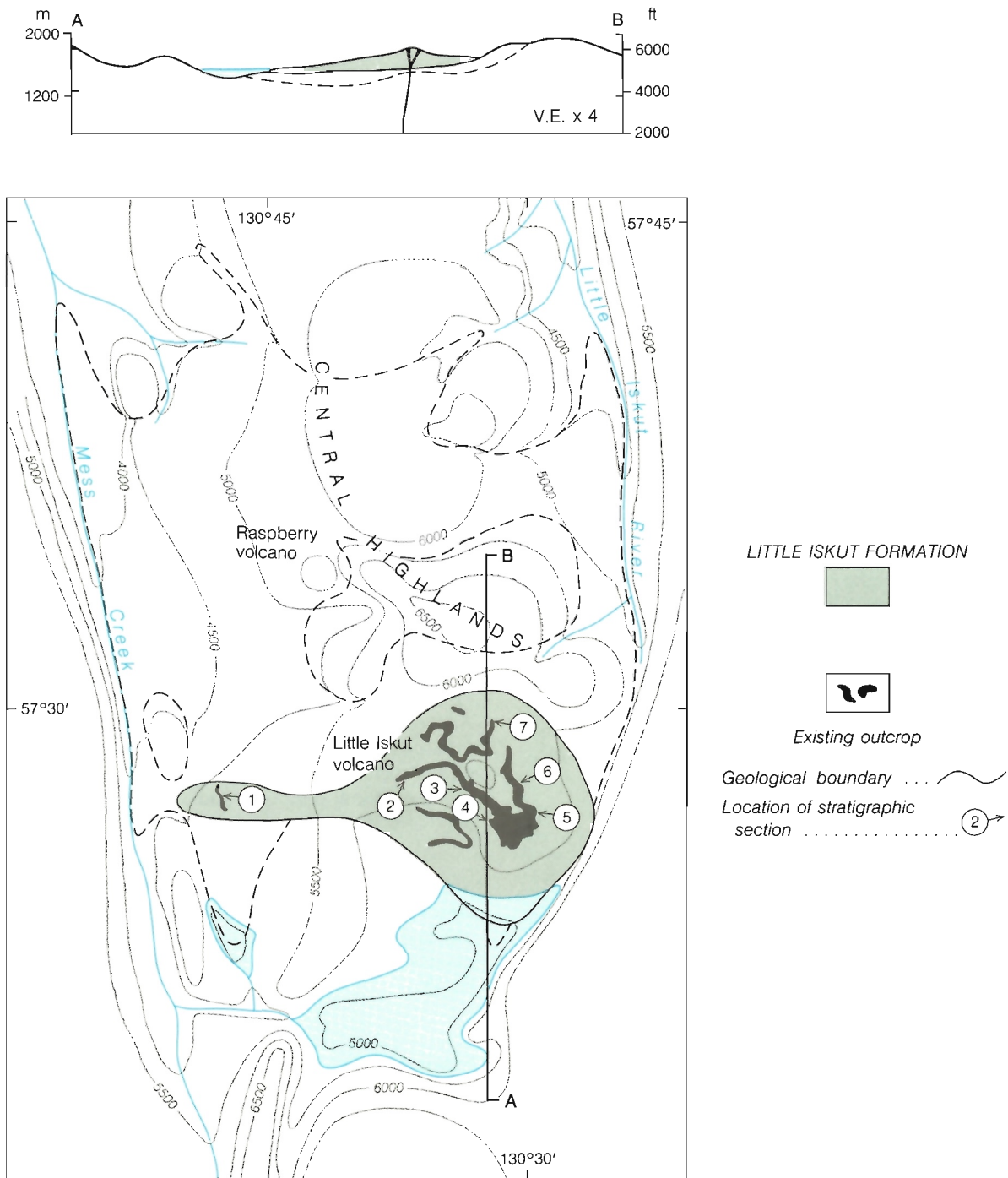


Figure 30. Paleogeological map and schematic cross-section showing the inferred maximum extent of Little Iskut trachybasalt at the end of Little Iskut time, and the outer limits of the older Raspberry pile (dashed line). Stratigraphic sections are shown in Figure 32.

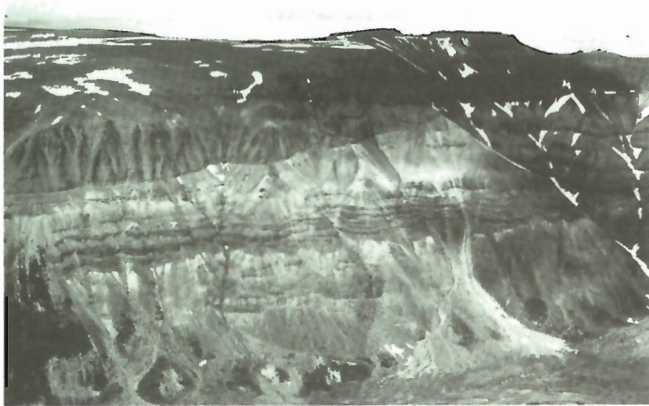


Figure 31. Artifact Ridge, looking north from Obsidian Ridge. Thick irregular flows of Little Iskut trachybasalt form the lower part of the section (no. 3LI, Fig. 32), and are overlain by light coloured Armadillo rhyolite. GSC 202468-K.

The flow breccia, unlike the hackly scoria common to basaltic lavas, consists mainly of discreet, fracture-bounded blocks and fragments up to 10 cm across. Many have the same equant, polygonal form that characterizes the lower “crackle breccia”, but unlike the latter the flow breccia particles are completely disaggregated to form a loose, randomly stacked mass. Nor has the flow breccia been bleached and altered to the same extent as the “crackle breccia”. The larger clasts are medium grey and only slightly lighter coloured than the massive trachybasalt in the flows. Even the smallest particles have been only moderately altered to a pale greenish grey.

Fracture and joint surfaces in both the flows and flow breccia are covered with a deep brown resinous to iridescent varnish of iron-manganese stain. On stable slopes, where deep weathering has produced spheroidal surfaces on the flows, the iron-rich weathering rind is up to 2 cm thick. Iron-manganese oxides are also the dominant vesicle and fracture filling, nearly every opening being lined with botryoidal encrustations of manganiferous goethite.

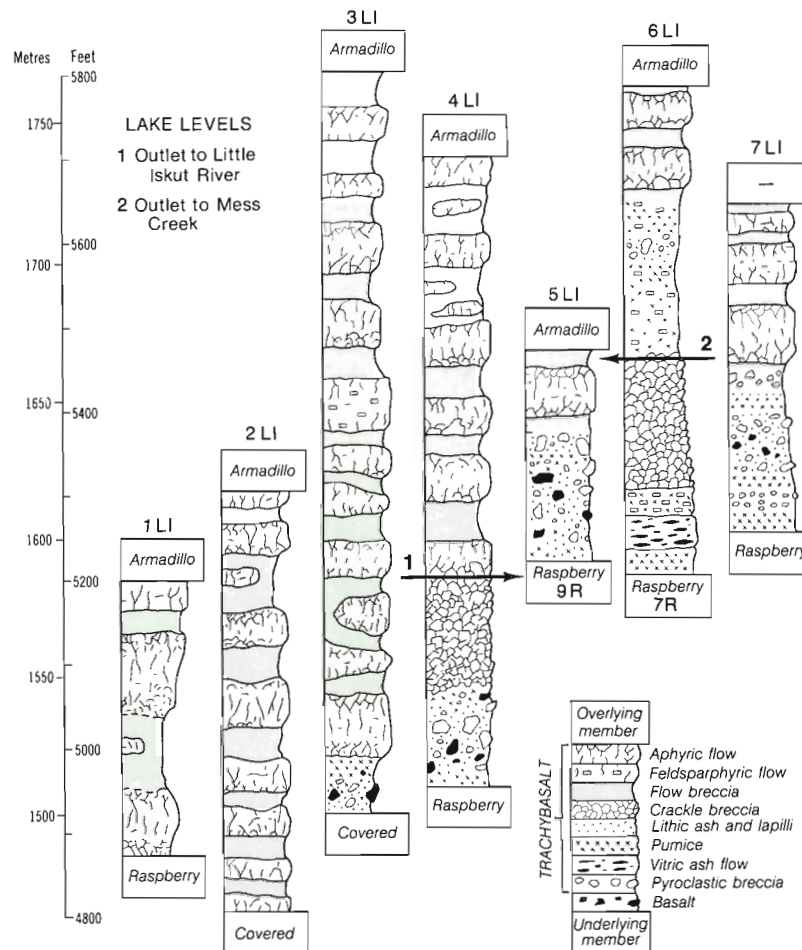


Figure 32. Typical stratigraphic sections of Little Iskut trachybasalt showing variations in morphology and the relationship of the lower “crackle breccia” to changing lake levels. Section numbers (1-7) refer to locations shown on the paleogeological map (Fig. 30). LI, Little Iskut Formation; R, Raspberry Formation.

Subvolcanic structures

Two poorly exposed, low, northeasterly trending ridges of trachybasalt along the break in slope on the north side of Artifact Creek are believed to be coalescing dykes or small irregular intrusions that were probably part of the Little Iskut conduit system. A third feature, also at the base of the section, on the north side of Artifact Creek, appears to be part of a conduit through which a large volume of gas and particles was discharged. The basal "crackle breccia", and overlying trachybasalt flows are cut by a group of irregular, funnel-shaped bodies of explosion breccia 1-10 m

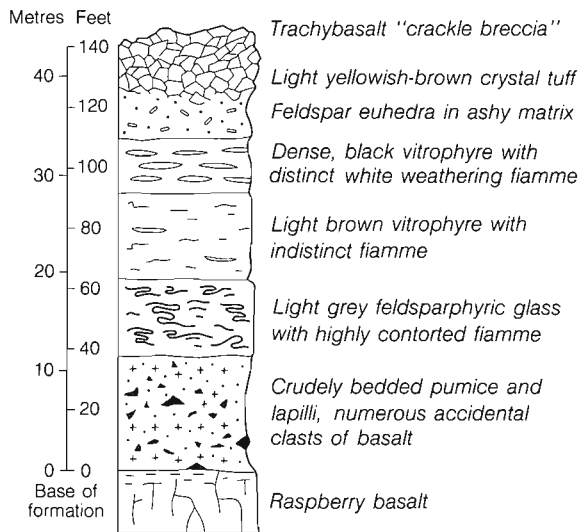


Figure 33. Sketch of pyroclastic and lacustrine beds at the base of the Little Iskut succession in Raspberry Pass (section 6LI, Fig. 32).

across. Within the funnels an aggregate of highly oxidized, red, scoriaceous pyroclastic debris has been cemented into a cohesive mass. Locally melting has produced irregular pockets and veinlets of interstitial lava. Both the explosion breccia and the surrounding wall rock have been bleached nearly white for about 5 cm adjacent to all fractures, indicating that fumarolic gases continued to flow through them after formation of the breccia funnels.

Origin

The absence of fluvial deposits beneath the Little Iskut pile suggests that it was erupted soon after Raspberry activity ceased. It occupies approximately the same area as that believed to have been flooded by water ponded behind Raspberry basalt which dammed the ancestral Little Iskut River. The initial activity that produced the basal pumice may have begun as a subaqueous eruption within this lake (Fig. 35). The thick pile of angular explosion breccia at the base of the pile in Artifact Valley has several features that suggest such an origin. The pumice, in which the large angular accidental blocks of basalt are suspended, has undergone much more intense hydrothermal alteration than pumice elsewhere in the pile. Also, it retains traces of deformed laminar bedding. The lake could not have been more than a few hundred metres deep and the subaqueous pile of breccia must soon have grown above its surface. Showers of pumice thrown from the emergent vent fell back into the lake and settled to form the graded laminar beds that occur at the base of most sections in the distal parts of the pile. The small volume of ash and pyroclastic deposits in the Little Iskut pile indicates that the initial explosive activity was short lived. It was followed by rapid effusion of a large volume of trachybasalt lava from one or more vents near the centre of the shield. Where these entered lake water, around

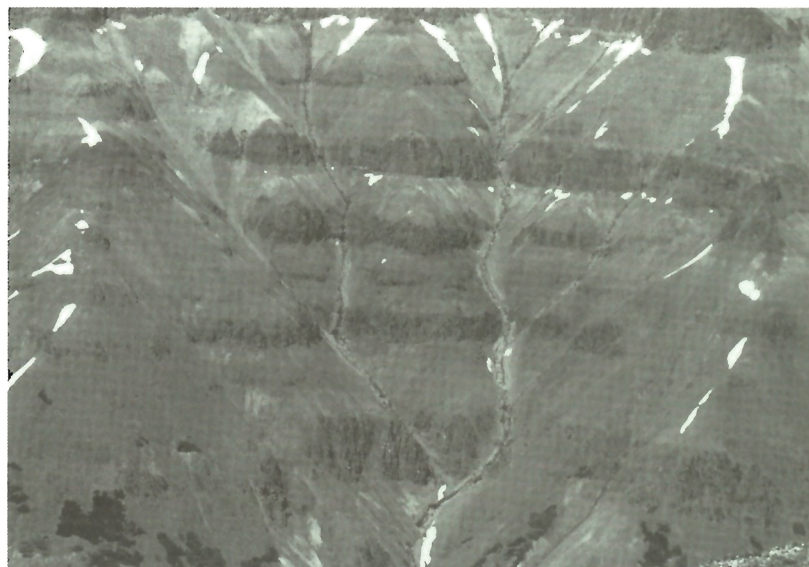


Figure 34. Irregular flows of Little Iskut trachybasalt with characteristically thick flow-top and basal breccia. GSC 204627-B.

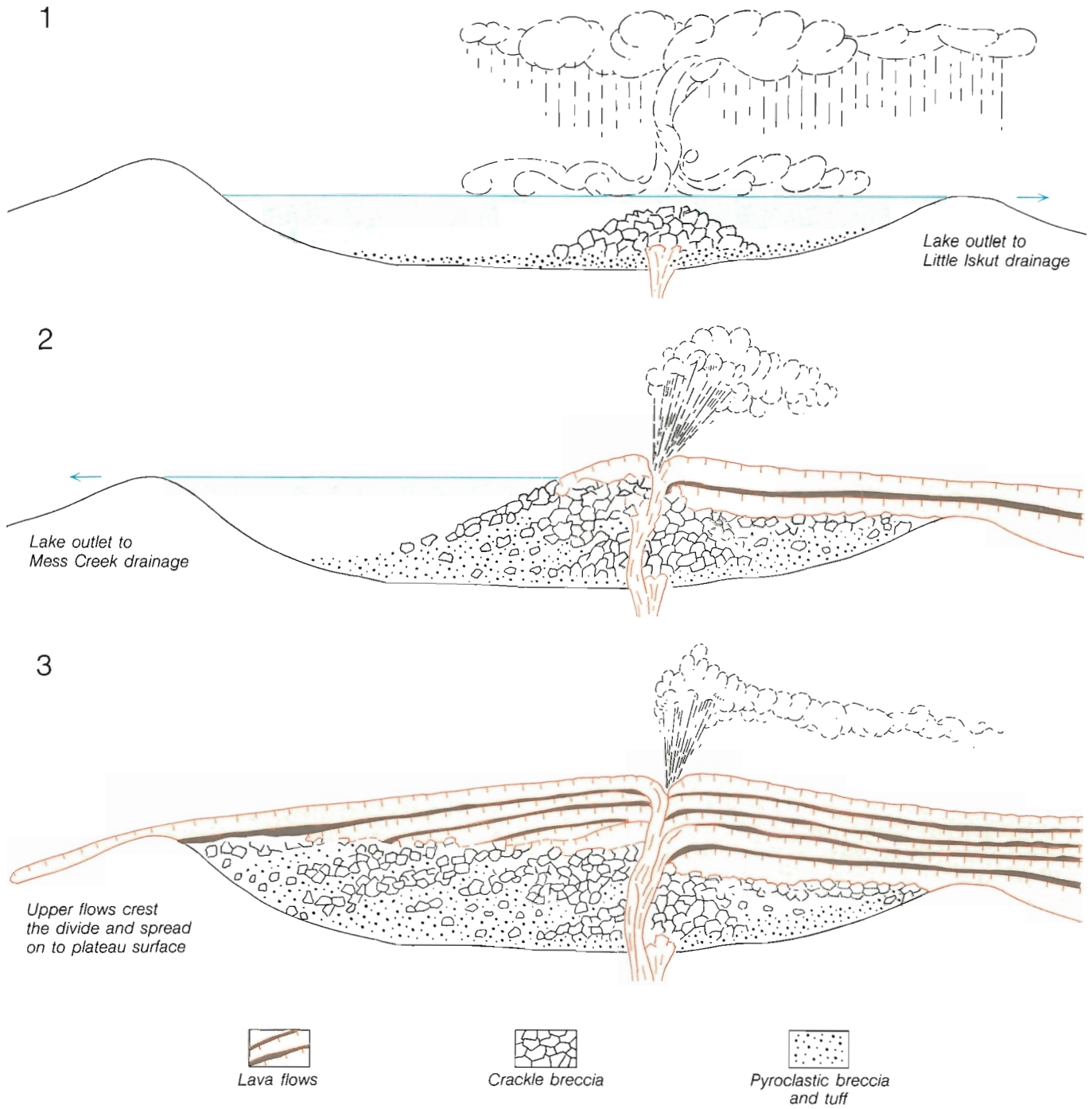
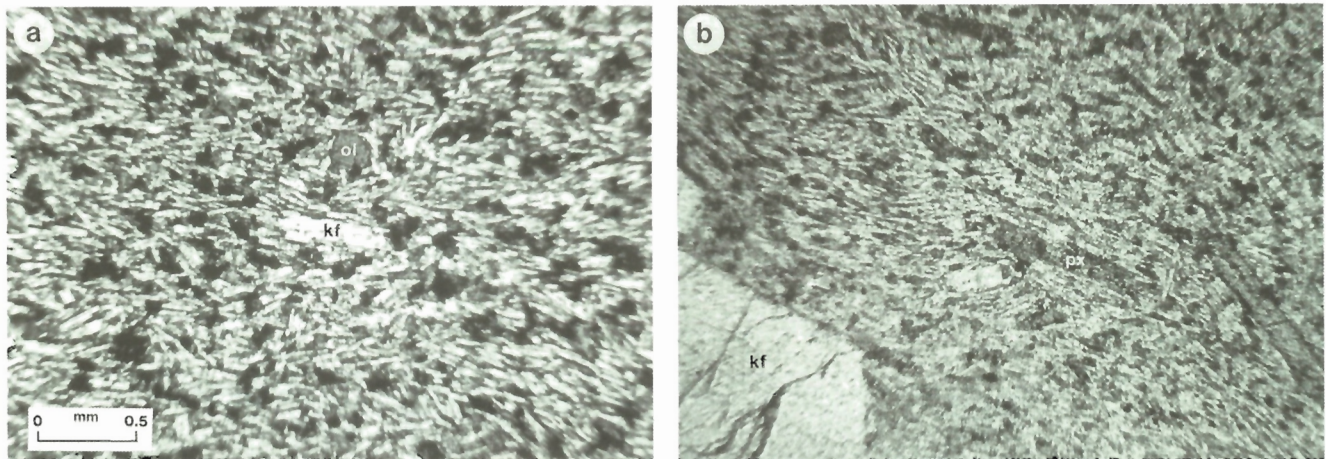


Figure 35. Schematic cross-sections showing the relationship of the upper and lower members of the Little Iskut Formation to the progressive displacement of Raspberry lake by lava.



a — Fine grained phase with sparse microphenocrysts of olivine (ol) and alkali feldspar (kf) (plane light)

b — Porphyritic phase with large euhedral phenocrysts of alkali feldspar (kf) and microphenocrysts of titaniferous ferroaugite (px) with rims of green ferrohedenbergite (plane light)

Figure 36. Photomicrographs of Little Iskut trachybasalt; scale bar 0.5 mm.

the periphery of the growing pile, they were quenched and shattered to form the “crackle breccia” of the lower unit. Thus, except for the basal pumice, the lower unit is probably not the product of a widespread early eruptive event. It is more likely a diachronous, subaqueous facies that developed along the margins of the pile where the distal ends of successive flows entered the lake. As the edifice grew each flow advanced slightly farther covering the quenched margins of preceding flows and, on entering the lake itself, adding a new wedge of “crackle breccia” to the outer margins of the pile.

Variations in the elevation of the top of the “crackle breccia” suggest that the original outlet of the lake into Little Iskut River was dammed by early flows and that its level rose during construction of the shield (Fig. 32). In several sections the transition from subaqueous breccia to subaerial flows occurs at an elevation of about 5200 ft. (1585 m) whereas a transition at about 5500 ft. (1675 m) is common to several others. These are interpreted to be, respectively, the initial and maximum lake levels. The latter was probably controlled by the elevation of the divide between Little Iskut River and Mess Creek drainage. Once the lake rose to that level it began to drain west into Mess Creek.

Ultimately the lake water was displaced by lava and a few of the uppermost flows spread far beyond its original shores. Two of these are exposed in Mess Creek Escarpment about 14.5 km from the centre of the Little Iskut shield.

Throughout most of its active life, Little Iskut volcano produced a very uniform, nonporphyritic trachybasalt lava. Although each surge of activity yielded a very large volume of lava, it appears to have issued quietly in the form of massive flows with little related fire fountaining or explosive

activity and hence, little associated tephra. Many of the pyroclastic deposits in the pile contain a high proportion of feldspar crystals suggesting that they may be related to the relatively small volume of porphyritic flows within the upper succession. This may have originated as nonporphyritic trachybasalt magma that became trapped and underwent fractionation in high level reservoirs where feldspar crystallization was accompanied by separation of a volatile-rich phase. This more highly evolved magma would thus tend to erupt more explosively than the more primitive parent magma and hence generate proportionally more tephra.

PETROGRAPHY

The Little Iskut trachybasalt flows are holocrystalline, very fine grained rocks with pronounced eutaxitic textures (Fig. 36). Potassic anorthoclase and ferruginous clinopyroxene (Fig. 37, Table 3) are the dominant minerals in both groundmass and phenocrystic phases. Aenigmatite is present in the groundmass of some flows and iron-rich olivine forms abundant microphenocrysts in a few others. Opaque oxides are extremely fine grained and are confined to the groundmass.

The groundmass feldspars, though strongly oriented, occur as stout, feathery laths having sinuous, often interlocking common boundaries. The absence of interstitial glass in such highly foliated rock suggests that crystallization of the feldspars began early and continued during the final cooling of the lava, after the flows had come to rest. Sparse feldspar phenocrysts, commonly less than 3 mm long, occur in about half of the sections examined. They comprise euhedral laths of anorthoclase having simple pericline or crosshatched twinning and displaying sharp

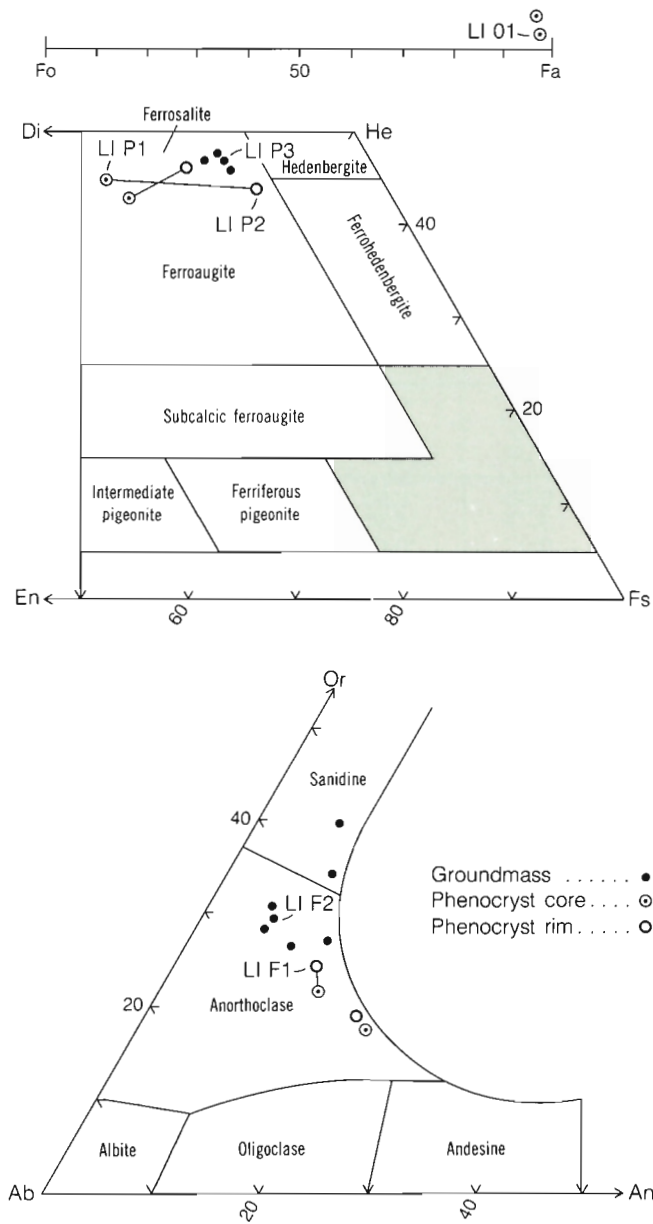


Figure 37. End-member plots showing compositions of feldspar, pyroxene, and olivine in Little Iskut trachybasalt, based on 21 microprobe analyses. Six representative analyses, identified by numbers (LIO1, LIP2 etc.) are listed in Table 3.

crystal boundaries against the foliated groundmass (Fig. 36b). They are slightly less potassic than the groundmass feldspar (Fig. 37) but little or no internal zoning is apparent from either optical or microprobe data.

The groundmass pyroxene occurs as tiny irregular, intergranular prisms of pale yellow to deep green, pleochroic ferrohedenbergite. Pyroxene phenocrysts and microphenocrysts are mainly less than 1 mm long. They have a slender, spindle-shaped habit and are commonly

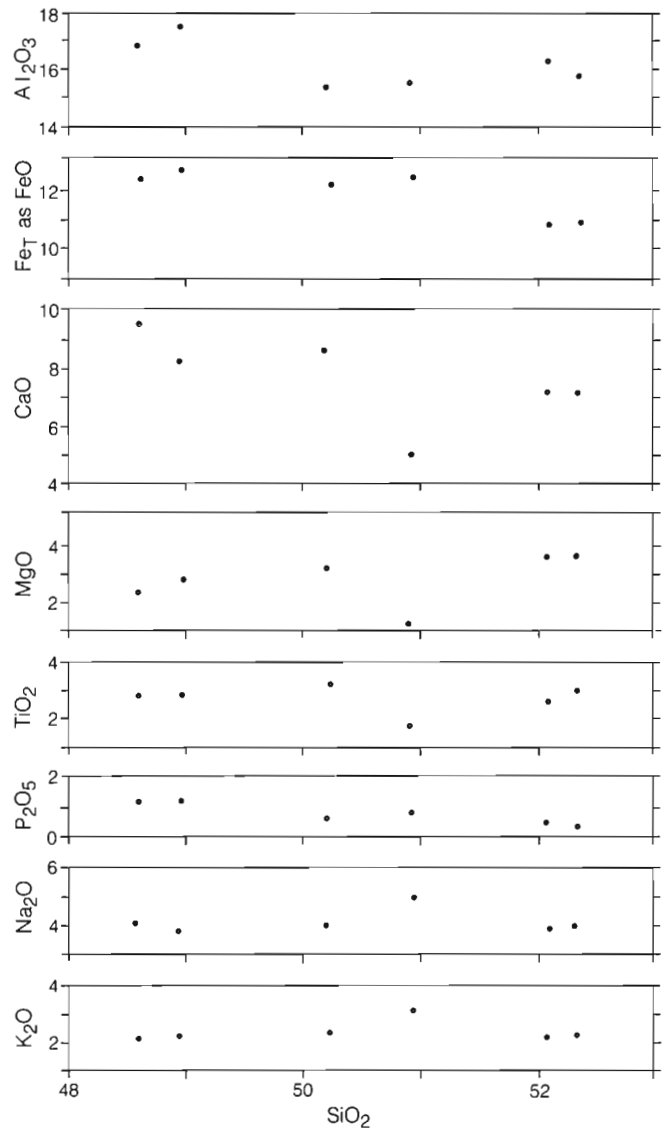


Figure 38. Harker diagram showing chemical variation in weight per cent for 6 analyzed specimens of Little Iskut trachybasalt.

strongly zoned from cores of purplish-brown titaniferous ferroaugite to deep green rims approaching ferrohedenbergite in composition (Fig. 37).

Microphenocrysts of fayalite (Fe_3) occur in several flows throughout the Little Iskut pile. Where present, they tend to be fairly abundant, forming up to 50% of the total phenocrysts. The equant, pale yellow crystals, mostly less than 0.5 mm across, are evenly dispersed throughout the rock. They are commonly associated with, and may partly enclose, pale green euhedral microphenocrysts of ferrosalite of about the same size. The pyroxene in the olivine-bearing rocks, though similar chemically, differs from that in other Little Iskut trachybasalts in its tendency to be unzoned and to form stout prisms rather than slender spindle-shaped crystals.

Table 3. Selected microprobe analyses and structural data for feldspar, pyroxene and olivine from the Little Iskut trachybasalt.

	Feldspar		Pyroxene			Olivine		
	Pheno-cryst	Ground-mass	Pheno core		Ground-mass	Pheno-cryst		
			cryst rim					
	LI F1	LI F2	LI P1	LI P2	LI P3	LI O1		
SiO ₂	62.36	65.48	48.27	47.61	47.81	30.04		
Al ₂ O ₃	21.98	19.55	2.67	1.83	1.35	0.0		
TiO ₂	0.05	0.02	1.28	1.37	0.64	0.08		
Cr ₂ O ₃	0.0	0.0	0.0	0.0	0.0	0.0		
Fe ₂ O ₃	1.11	0.63	2.19	2.27	2.86	0.0		
FeO	0.0	0.0	16.74	24.34	21.45	65.25		
MnO	0.03	0.01	0.67	0.99	0.93	3.03		
MgO	0.0	0.0	7.97	3.71	4.16	1.03		
NiO	0.0	0.0	0.0	0.0	0.0	0.0		
CaO	4.90	1.36	19.55	19.00	20.50	0.54		
Na ₂ O	7.11	7.12	0.42	0.38	0.36	0.0		
K ₂ O	2.18	4.87	0.08	0.03	0.0	0.0		
H ₂ O	0.0	0.0	0.0	0.0	0.0	0.0		
F	0.0	0.0	0.0	0.0	0.0	0.0		
Total	99.72	99.04	99.84	101.53	100.06	99.97		
	No. of ions on basis of 8 (0)		No. of ions on basis of 6 (0)			No. of ions on basis of 4 (0)		
Si	2.7954	2.9472	Si	1.8867	1.8975	1.9197	Si	1.0059
Al	1.1612	1.0370	Al	0.1133	0.0860	0.0639	Al	0.0
Cr	0.0	0.0	Ti	0.0	0.0165	0.0165	Cr	0.0
Fe ³⁺	0.0374	0.0213	Fe	0.0	0.0	0.0	Fe ³⁺	0.0
			Cr	0.0	0.0	0.0		
Al	0.0	0.0	Al	0.0097	0.0	0.0	Al	0.0
Cr	0.0	0.0	Ti	0.0376	0.0246	0.0029	Cr	0.0
Ti	0.0017	0.0007	Fe ³⁺	0.0644	0.0680	0.0863	Ti	0.0020
Fe ³⁺	0.0	0.0	Cr	0.0	0.0	0.0	Fe ³⁺	0.0
Ni	0.0	0.0	Ni	0.0	0.0	0.0	Ni	0.0
Fe ²⁺	0.0	0.0	Fe ²⁺	0.5472	0.8113	0.7203	Fe ²⁺	1.8273
Mn	0.011	0.0004	Mn	0.0222	0.0334	0.0316	Mn	0.0859
Mg	0.0	0.0	Mg	0.4643	0.2204	0.2490	Mg	0.0514
			Ca	0.8187	0.8114	0.8819		
			Na	0.0318	0.0294	0.0280		
			K	0.0040	0.0015	0.0		
Ca	0.2353	0.0656					Ca	0.0194
Na	0.6180	0.6214					Na	0.0
K	0.1247	0.2796					K	0.0

Finely disseminated opaque oxides form less than one volume percent of the rock. Accessory minerals are apatite, which is ubiquitous; aenigmatite, which occurs as small aggregates within the groundmass of some flows; and reddish-brown biotite, which appears to be a late, vapour phase mineral.

Vesicles are either still open or only partly filled with manganiferous iron oxides and rarely lined with carbonate and analcime. The pervasive, carbonate alteration, that is so widespread in the underlying Raspberry basalt, is not

present. Except for oxidation along minute fractures the Little Iskut flows are fresh. Extending a few millimetres into the adjacent rock from these fractures are bleached, rusty zones, within which the pyroxene has been replaced by hematite and amphibole and some of the feldspar has been recrystallized.

Thin sections of "crackle breccia" from the lower unit reveal a texture and mineralogy that resembles the fracture-controlled alteration zones in the flows of the upper unit. Surprisingly even the smallest polygons from the "crackle

Table 4. Selected chemical analyses of typical Little Iskut trachybasalts.

Trachybasalt			
Spec. no.	55	48	58
SiO ₂	48.00	51.20	51.90
Al ₂ O ₃	15.10	16.10	15.80
Fe ₂ O ₃	5.60	4.40	5.20
FeO	6.80	6.60	6.00
MgO	3.09	3.50	3.54
CaO	8.29	6.92	6.92
Na ₂ O	4.00	4.00	4.10
K ₂ O	2.29	2.21	2.22
TiO ₂	3.08	2.54	2.72
P ₂ O ₅	0.77	0.61	0.59
MnO	0.26	0.20	0.18
S	0.10	0.09	0.10
NiO	0.0	0.0	0.0
Cr ₂ O ₃	0.0	0.0	0.0
CO ₂	1.00	0.0	0.0
H ₂ O	1.00	1.70	1.40
Total	100.18	100.07	100.67

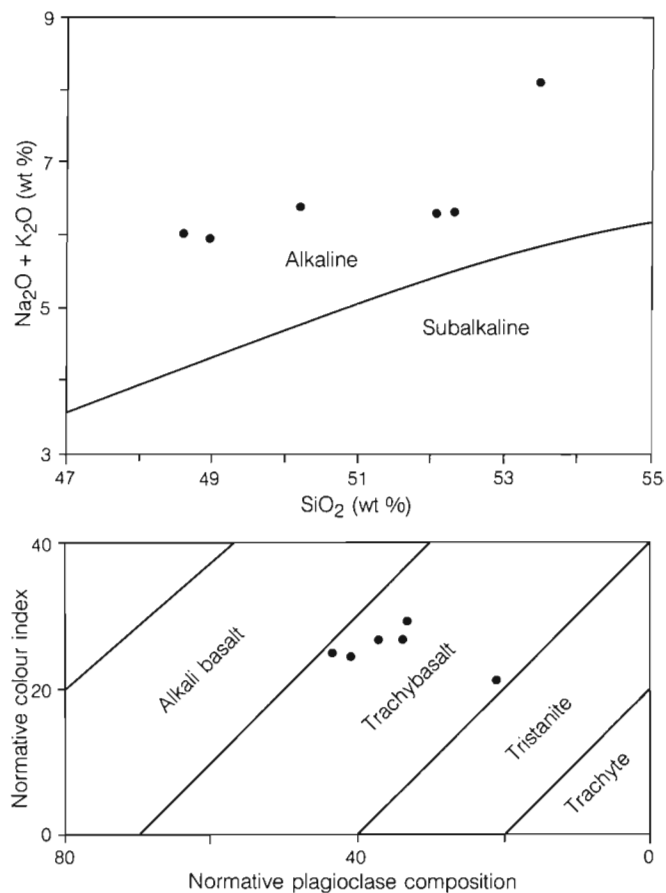


Figure 39. Plots of Little Iskut trachybasalt on the total alkali vs. silica, and normative colour index vs. normative plagioclase composition diagrams of Irvine and Baragar (1971).

breccia'' are holocrystalline. Interlocking anorthoclase laths form more than 90% of the rock, the remainder being very fine, irregular shreds of amphibole and patches of hydrous iron oxide which appear to be pseudomorphous after early formed, iron-rich pyroxene and olivine. The latter minerals, surrounded by rusty oxidation haloes, are still preserved in the less severely altered cores of the largest polygons of the "crackle breccia".

CHEMISTRY

Six major-element analyses of Little Iskut trachybasalt were run (Fig. 38) of which three superior analyses are

listed in Table 4. They range from 48.6 to 52.5% silica and from slightly quartz normative to slightly nepheline normative.

On both the SiO₂ vs. alkali and AFM diagrams (Fig. 39 and 29a) the Little Iskut analyses plot close to the Raspberry basalt field but show a distinct bias toward higher SiO₂, total alkalis and iron. Similarly the Ab'-An-Or plot (Fig. 29a) shows a significant shift toward Or as compared with the Raspberry basalts. Whereas the latter plot almost entirely within the field of Irvine and Baragar's (1971) sodic series, all the Little Iskut analyses plot in the trachybasalt field of the potassic series.

ARMADILLO FORMATION

GENERAL GEOLOGY

The Armadillo Formation (Fig. 40, Map 1623A, in pocket) includes both felsic and basic lavas and pyroclastic rocks that issued from separate centres during a long period of bimodal volcanism. The felsic rocks, which include comenditic rhyolite and trachyte flows, domes and pyroclastic deposits, were erupted from a cluster of vents on and around Armadillo Peak. The basic centres are less clearly defined, but major, long-lived basaltic volcanoes must have developed both north and south of the felsic lava complex and spread thick lobes of flows west into the Mess Creek lowlands. In addition several small, short-lived basaltic centres erupted within the main area of felsic volcanism, producing isolated basaltic flows which are now buried within the rhyolite-trachyte succession.

Felsic rocks

Eruption of felsic rocks during the Armadillo stage of activity produced two distinct facies: a proximal facies comprising a felsic lava complex and a distal facies comprising a peripheral apron of mainly ash and sediment. The eastern third of the pile has been removed by erosion, but deeply dissected remnants of the central and western part provide excellent exposures of both extrusive facies, as well as several vents and subvolcanic structures. Pale green to dark olive-green, rusty weathering trachyte and white, green or purple rhyolite flows of the central lava complex underlie Armadillo Peak and cap most of the surrounding ridges. In the Highlands, the basal flows rest directly on pre-Tertiary basement that stood above the level flooded by Raspberry basalt. The contacts are sharp, in most cases lacking any intervening layer of clastic or pyroclastic debris, or they are separated by only a thin layer of ash, and less than a metre of colluvium deposited on the old basement surface. At lower elevations, where the Armadillo rests on Raspberry basalt, it is commonly underlain by a thin layer of colluvium or fluvial sediment deposited on the Raspberry flows. In contrast, contacts with Little Iskut trachybasalt show no evidence of pre-Armadillo erosion or deposition of sediment. Armadillo ash and pumice have in fact been sifted into irregularities in a blocky upper surface of fresh Little Iskut flows.

Individual cooling units vary from small bulbous domes from 6-9 m thick and a few hundred metres across to comendite flows more than 150 m thick that are exposed for nearly 6.5 km along the north side of Raspberry Pass (Fig. 41). The thickest flows commonly have a composite structure. A basal zone of vitreous, welded spatter with eutaxitic textures is overlain by a few metres of granular or flow-banded obsidian. Above this, the lower half of most flows is a

dense, uniform dark green to greenish grey, blocky to crudely columnar massive rock, whereas the upper half is commonly a light green to purple platy rock with pronounced flow structure, often displaying complex flow folds with amplitudes of a few millimetres up to several tens of metres. Grooves and striations parallel to the direction of flow and transverse chattermarks indicate that the highly viscous flows continued to move until they were almost solid. In most stratigraphic sections the lava flows are separated by relatively thin partings of loose pumice, lightly welded ash flows, or by pockets of fluvial sand and gravel. An exception is found on Armadillo Peak where a thick sequence of dark, greenish grey, porphyritic trachyte flows are stacked one on another without any clastic or pyroclastic partings.

At the summit of Raspberry Pass, the Armadillo flows have a composite thickness of more than 460 m but, 6.5 km farther west, they end abruptly and are flanked by a relatively thin apron of clastic and pyroclastic deposits interbedded with the thin, distal ends of basaltic flows that lapped against the edge of the steep-sided felsic pile (Fig. 42). On the northern edge of the felsic lava complex more than 300 m of comendite and trachyte flows, exposed on Cartoona Ridge, thin to less than 90 m 3 km farther north and to less than 30 m of ash and gravel within another 1.5 km. Similarly, the southern margin thins from 150 m of lava flows on the north side of Artifact Creek to a single 9 m ash flow on the south side. Thus, the original form of the felsic lava complex was that of an irregular cluster of overlapping, steep-sided lobes that coalesced to form a thick, amoeboid mass of lava more than 19 km across.

The felsic lava complex is a composite pile that originated from several separate vents, four of which have been recognized: Armadillo caldera is believed to be the principal centre of activity whereas Cartoona Ridge, Tadedea Peak, and IGC Dome are satellitic vents (Fig. 40). The order in which these centres erupted is not known, nor can the flows from any one vent be recognized where they merge with those from another. Hence, no attempt is made to map the precise distribution of flows from the different centres. Nevertheless, the eruptive products surrounding each vent display subtle differences that indicate a unique history for each.

Cartoona Ridge centre

Cartoona Ridge is a pie-shaped remnant of Armadillo lava and pyroclastic deposits about 8 km north of Armadillo caldera (Fig. 43). At the narrow eastern end of the ridge a complex vent area about 0.5 km across is exposed on two sides. Breccias, small overlapping domes, crosscutting

MOUNT EDZIZA

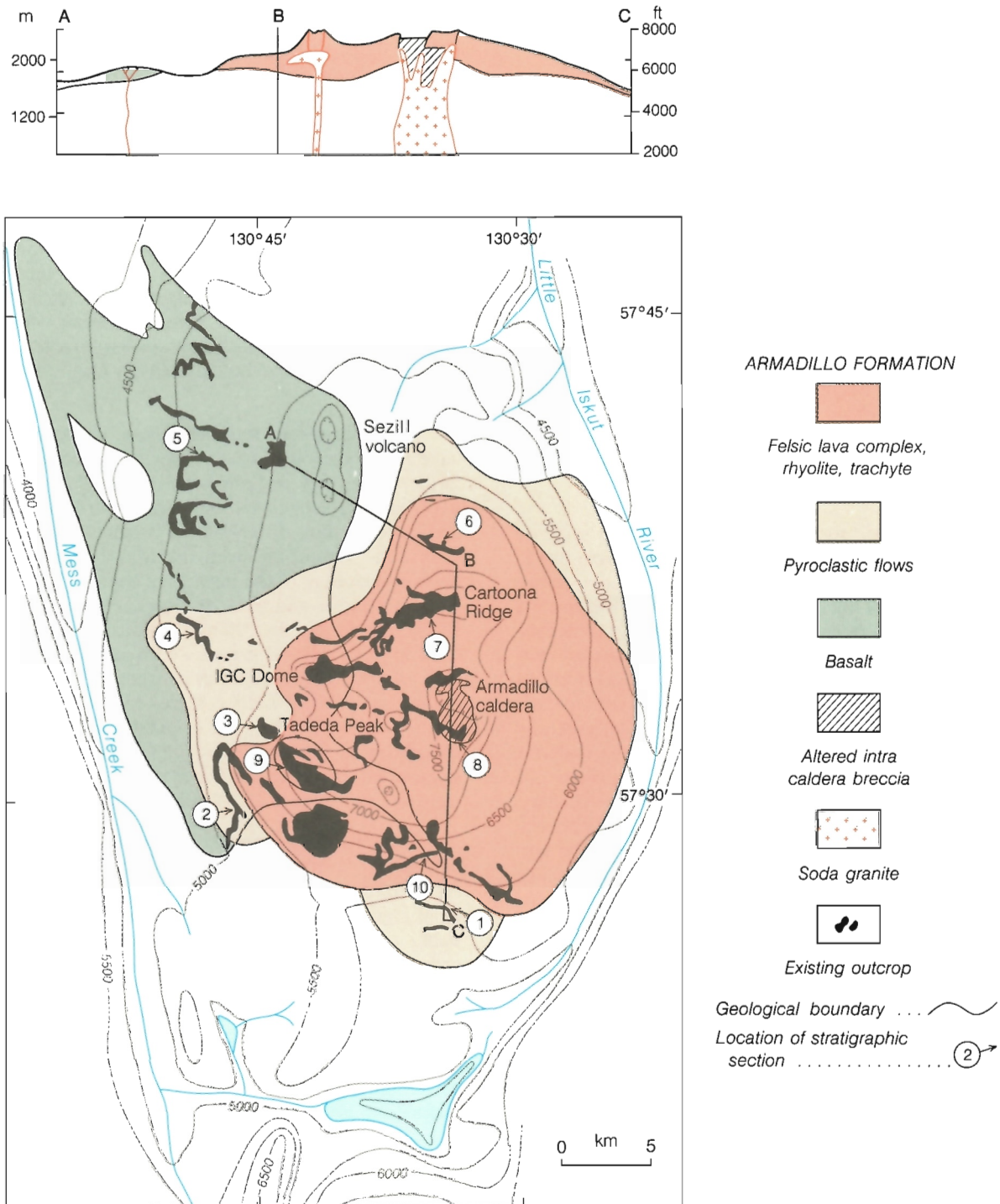


Figure 40. Paleogeological map showing the inferred maximum extent of the Armadillo Formation at the end of Armadillo time, and schematic cross-section through Armadillo caldera. Stratigraphic sections are shown in Figure 55.



Figure 41. Looking northeast across Raspberry Pass at the south slope of Gnu Butte. Gently dipping, Early Tertiary sandstone and conglomerate beds in foreground are overlain unconformably by Raspberry basalt flows in the lower part of the Butte. Upper part of Butte is interlayered Armadillo basalt, comendite, and epiclastic deposits derived from thick comendite flows that form ridge at upper right. (see Fig. 42) GSC 125 603.

MOUNT EDZIZA

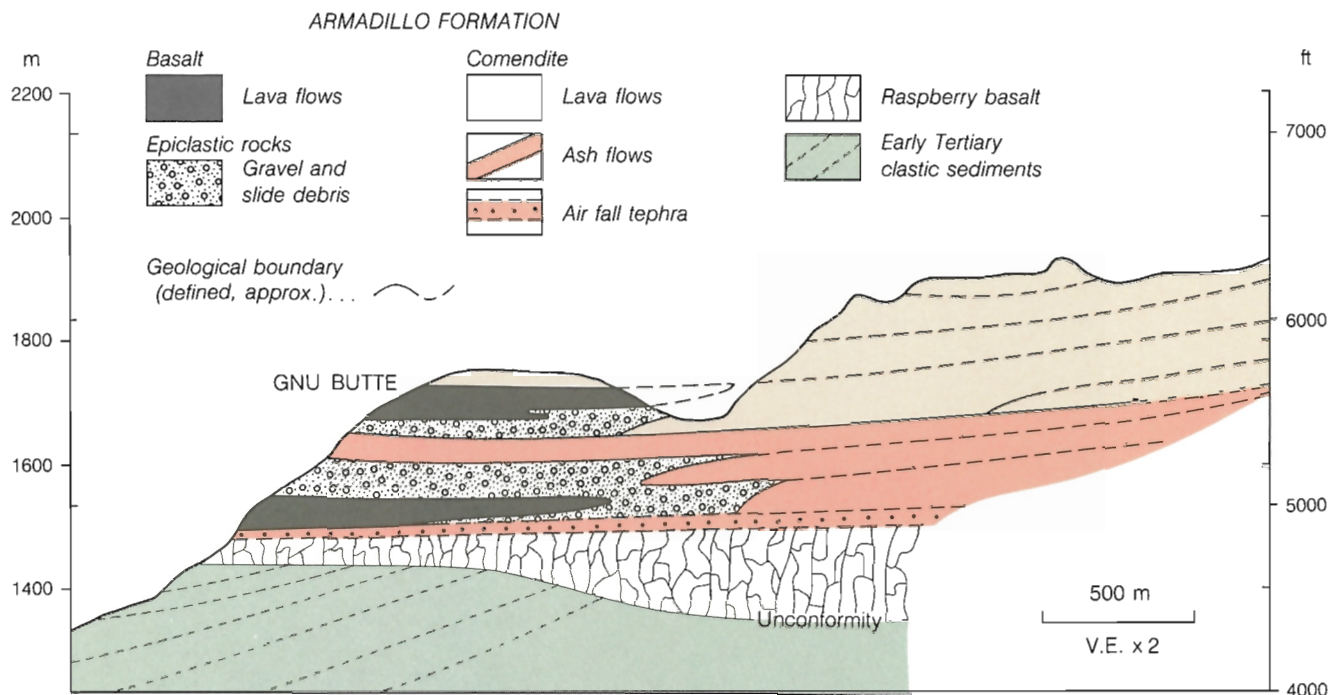


Figure 42. Cross-section through Gnu Butte, showing the relationship between comendite and basalt flows near the western edge of the Armadillo felsic pile.

feeder pipes and swarms of dykes in and around the vent area have all been more or less altered by hydrothermal action. The breccia fragments, particularly, are bleached to a chalky white and coated with a thin yellow, ochre or iridescent manganese-iron rind that contrasts with green, greenish-grey weathering of more distal trachyte flows which form the western part of the ridge.

The Cartoona Ridge lavas are underlain by a layer of unconsolidated pumice and crystal ash interlayered with a few highly welded ash flows as well as finely laminated silt, sand and pebble layers composed of reworked pumice, trachyte and rhyolite. Many of the sediments contain small granules of obsidian whereas others are rich in crystals of feldspar and quartz. Small chips of shale, presumably torn from the conduit wall, are present in the air-fall pumice, and charred wood and plant debris are present in the basal layer. Near the vent this unconsolidated layer is about 150 m thick. It thins and becomes finer grained toward the north and west, and is missing completely beneath the flows that cap the ridges south of Chakima Creek. Whether the pumice of this basal layer was erupted from the Cartoona Ridge vent or simply preserved by later burial beneath the Cartoona Ridge lavas is uncertain. In any case, the high proportion of tuffaceous sediments in the basal layer indicates that a considerable interval of time elapsed between the first explosive discharge of pumice and extrusion of the first lavas from the Cartoona Ridge centre. The pumice unit occupies a topographic depression on the south side of the Armadillo basement-dome which surrounds the caldera, and much of the tuffaceous sediment was probably flushed

off these adjacent Highlands and redeposited in the Cartoona Ridge basin. It is apparent from the map and cross-section (Fig. 43) that distribution of the pumice unit corresponds almost exactly with the distribution of Raspberry basalt which was channelled into the same topographic depression two to three million years earlier. It seems probable that this basal, unconsolidated layer is of composite origin, derived from the initial pyroclastic eruptions of several nearby centres, including Armadillo caldera.

The first major discharge of Armadillo lava is believed to have erupted from the Cartoona Ridge centre (Fig. 44) since it is only beneath these lavas that the extensive air-fall pumice is preserved. The vent area, exposed near the eastern end of Cartoona Ridge is about 0.5 km across and consists mainly of hydrothermally altered explosion breccia made of angular, loosely fitted blocks of bleached rhyolite and trachyte up to 2 m across. On the south side, the breccia is exposed down to basement rocks and clearly cuts the overlying Raspberry basalt and basal pumice layer as well as the lower Armadillo flows. Rocks adjacent to the breccia are themselves highly fractured and altered for about 100 m around the breccia. Fracture surfaces are stained with iron-manganese oxide and the adjacent rock is bleached white. The northern side of the ridge exposes a group of mushroom-shaped lava domes and feeder pipes surrounded by vent breccia (Fig. 45) and the entire vent complex is cut by north-trending green trachyte dykes with glass selvages. At least six thick flows of comendite were extruded from the Cartoona Ridge centre in fairly rapid succession (Fig. 43). Each cooling unit includes a basal part of dense green

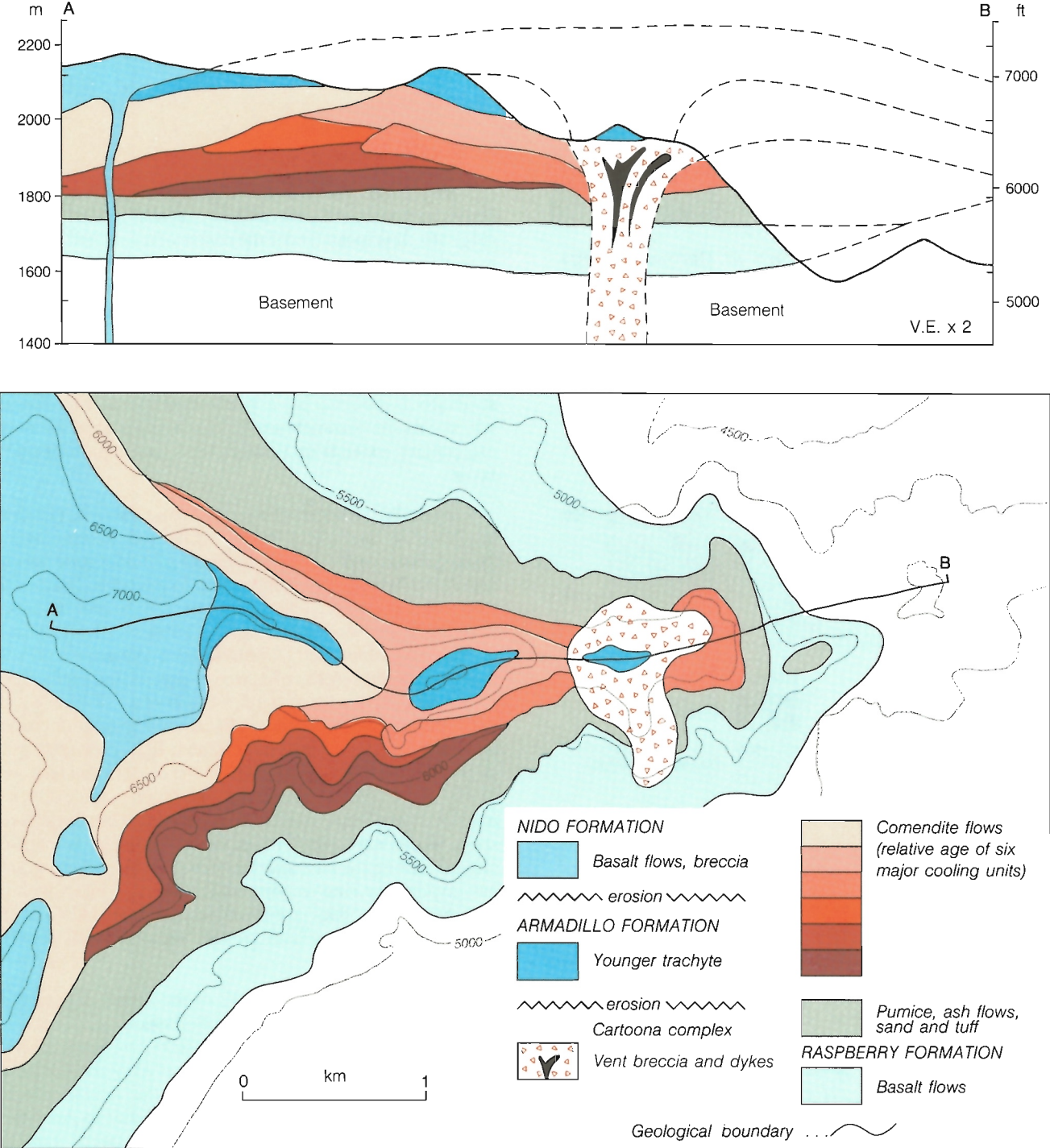


Figure 43. Map and schematic cross-section of the Cartoona Ridge eruptive centre.



Figure 44. View looking north at Cartoona Ridge. Hydrothermally altered explosion breccia, deposited around the eruptive vent, forms the right end of the ridge, whereas thick flow lobes form the central and left portion. Central dome of Mount Edziza in background. GSC 202468-L.

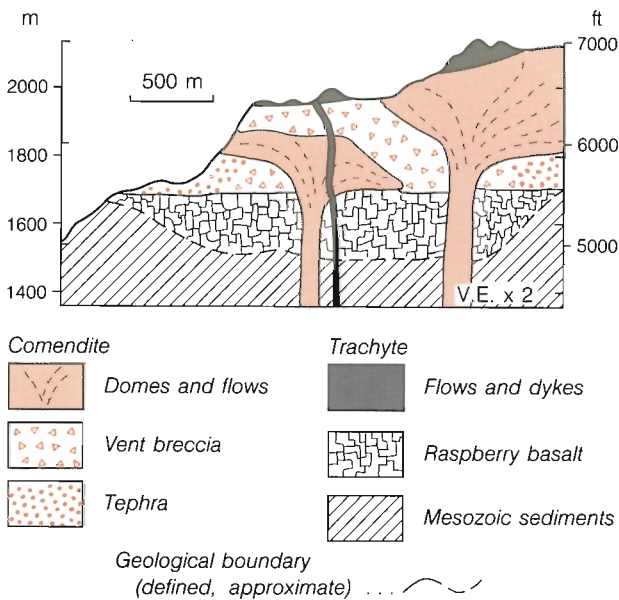


Figure 45. Sketch of nested lava domes on the north side of Cartoona Ridge.

porphyritic lava with small (2-3 mm) randomly oriented equant feldspar phenocrysts. This is overlain successively by purplish or greenish-white porous, flow banded rock, and finally by a frothy, glass-bearing, flow-top breccia.

On the western part of the ridge the six flows have a composite thickness of 365 m and a remnant of similar lava extends southwest, thinning to less than 60 m in about 5 km. The earlier flows are overlapped successively by younger flows toward the west. Initial dips of 10-15° are common, but the basal surface of most flows is highly irregular, in places lapping against the steep margins of underlying flows.

The Cartoona Ridge comendite flows and vent breccia are overlain by remnants of a 9-18 m thick younger trachyte flow which rests on an east-dipping erosion surface. It is not underlain by gravel, nor is there channelling, weathering or other evidence of extensive erosion of the underlying rocks prior to its extrusion. It is lithologically similar to acmite-bearing trachytes surrounding Armadillo caldera and may have been erupted from a satellitic vent during that stage of activity.

Armadillo caldera

Armadillo caldera is an elliptical structure about 5 km across its north-south axis and 3 km across its east-west axis (Fig. 46). It is located near the centre of an ancient basement high that predates the eruption of Raspberry basalt. Post-Armadillo erosion has removed almost all of the original deposits which formerly covered its surface and cut deeply into the subvolcanic regime, exposing more than 900 m of vertical section. Except for the northwest corner, which is covered by glacial ice, moraine and recent lava flows, the structure is defined by a fairly continuous ring-fracture which cuts the basement rocks and, along part of the northern contact, extends up through the superincumbent pile of lavas.

Inside the structure the rocks below 6500 ft. (1975 m) in elevation include a highly fractured assemblage of trachyte lavas and breccias that have all undergone varying degrees of hydrothermal alteration. In the central part of the structure, alteration appears to be controlled by north-northwesterly trending fractures. These vertical zones of fractured and bleached, limonitic rock alternate with relatively unaltered screens of massive, green, fine grained porphyritic rhyolite and trachyte. This same north-northwesterly trend is reflected in irregular or crudely tabular intrusions of medium grained, light grey soda granite that cut the altered rocks within the caldera and less commonly form dykes cutting the basement outside the ring fracture. The granite itself is relatively fresh but the adjacent rock, whether trachyte or basement sediments, is intensely altered. Along the east and western margins, where granite has invaded the ring fracture and comes in contact with the basement rocks, dark grey to black Jurassic shale and siltstone are altered to a pale greyish white hornfels for 9-12 m from the contact.

Overlying the altered rocks of the lower caldera complex and forming most of Armadillo Peak (Fig. 47) is a 180 m section of relatively thin (3-9 m) dark olive-green trachyte flows. Seen from a distance the pile has a regular horizontal layering but on close examination the actual contacts between individual cooling units are difficult to determine. There is little or no pyroclastic material between them and rarely any textural or colour change indicative of cooling or alteration of flow boundaries. Most of the rock is porphyritic and some phases have up to 2% equant feldspar phenocrysts 5-10 mm across. The texture of these rocks is similar to that of porphyritic dykes in the lower part of the

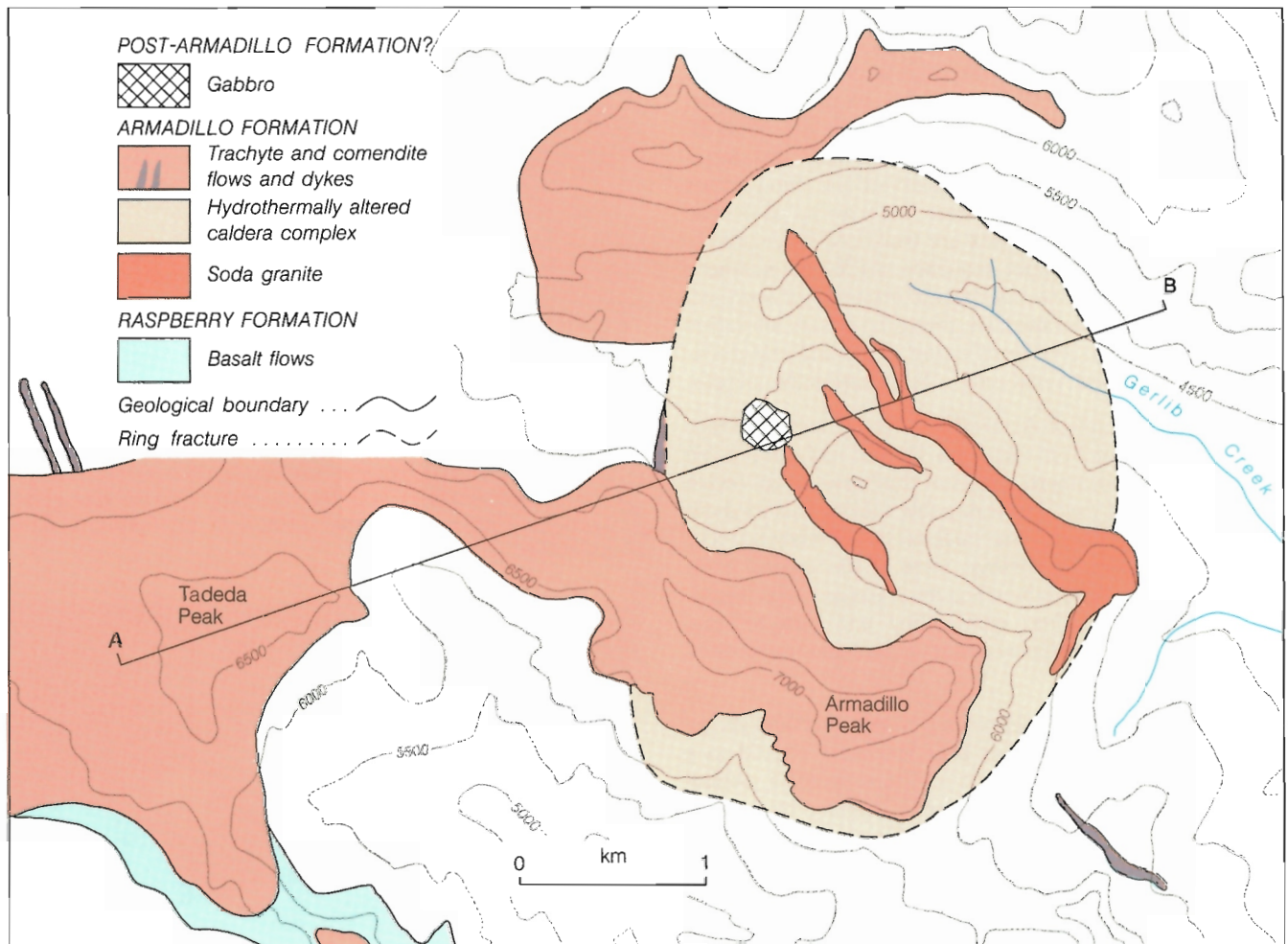
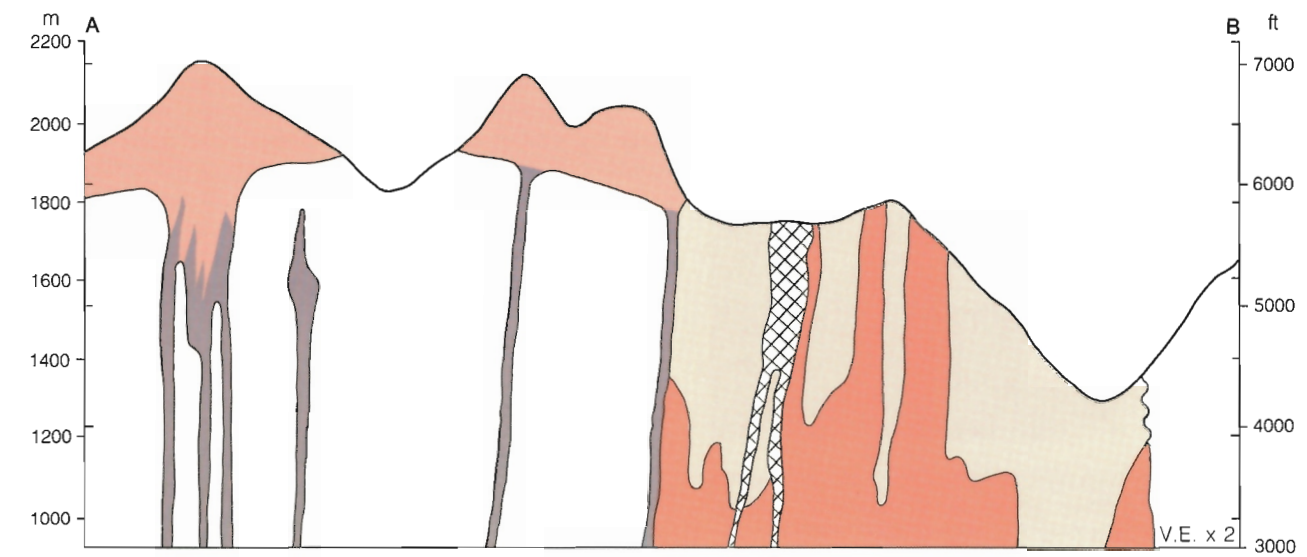


Figure 46. Map and schematic cross-section through Armadillo caldera and Tadedo Peak, two of the principal Armadillo eruptive centres. Blank areas are Mesozoic basement.



Figure 47. View looking west at Armadillo Peak, a thick pile of flat-lying trachyte flows which were originally ponded within Armadillo caldera (see Fig. 44). GSC 202468-M.

cauldron succession, except that the groundmass of the latter is finely crystalline whereas that of the lavas is aphanitic. The contact between the lower caldera complex and the superincumbent pile of lavas appears to be planar and horizontal, conforming almost exactly with the 6500 ft. (1980 m) contour. In detail it is gradational, showing a gradual upward decline in the intensity of alteration across a distance of 15 to 30 m. However, local zones of intense alteration in the lower complex are truncated by relatively unaltered lavas of the upper sequence. Along the southern edge of the caldera a few porphyritic granite dykes project up into the lower part of the lava, imposing a rusty alteration on the trachyte flows and terminating in a branching stock-work of dykelets and veins only a few centimetres across.

Near the summit of Armadillo Peak the lava sequence is overlain by about 30 m of coarse, bedded tuff and breccia with angular to subrounded clasts of light grey to yellowish white trachyte and rhyolite from a few millimetres to about 10 cm across. Although some beds are a few metres thick, and display little or no sorting, most of the section comprises 5-10 cm thick beds in which the clasts are well sorted, often displaying grading, channelling and crossbedding which suggest that they have been reworked and redeposited in a body of water.

The bounding ring-fracture is a zone of vertical shearing along which the rock has been intensely altered to a hard, siliceous, limonitic gouge and microbreccia. Along much of the contact the fracture zone is defined by a series of jagged, dark reddish brown spires and stacks which have remained standing after the less resistant surrounding rock was eroded away (Fig. 48). Trachyte dykes are present along short intervals of the contact but no extensive ring dykes were recognized. Similarly, the granite bodies, while confined largely to the interior of the structure, do not appear to have been channelled along the bounding fracture.

Remnants of lava from Armadillo caldera are exposed almost continuously for about 13 km toward the southwest. Originally these were part of two great lobes of trachyte and rhyolite that overflowed the relatively low western rim of the caldera. A remnant of the smaller and more northerly lobe caps IGC Ridge and is up to 210 m thick. The much larger southern lobe, exposed on the north side of Raspberry Pass, is locally more than 460 m thick and must once have flanked the entire southwest quadrant of the caldera in a continuous sheet of lava extending more than 10 km from its source.

Tadedea center

Tadedea Peak is a steep, bright red and yellow pyramidal horn, flanked by a nearly continuous apron of talus, felsenmeer and landslide deposits which cover all but the uppermost slopes (Fig. 49). Precipitous spires and narrow



Figure 48. View north into the central part of Armadillo caldera. Arcuate rib across central ridge is an erosional remnant of silicified microbreccia in the bounding ring-fracture zone. Cartoona Ridge and Mount Edziza in background. GSC 202468-N.

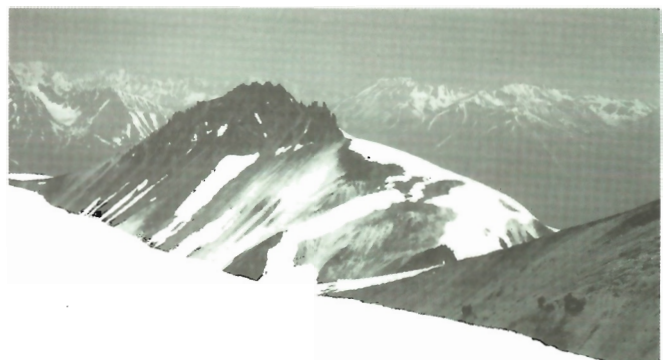


Figure 49. Looking west at the summit area of Tadedea Peak, a satellitic, Armadillo eruptive centre. GSC 202468-O.

serrated ridges of the summit area consist almost entirely of trachyte breccia, shattered trachyte flows, and swarms of dykes. The breccia and highly fractured lava are intensely altered, the fractures filled with secondary hydrothermal minerals. These include chalcedony, opal, minor calcite, iron-manganese oxides and pyrite which occurs both as veinlets and as disseminations of tiny cubes in the bleached, nearly white rock fragments.

The only clue to the underlying structure of Tadedea Peak is provided by an exposure on the northwest side of the mountain, 1800 ft. (550 m) below the summit. There basement rocks of Jurassic shale are cut by a 300 m long swarm of north-northwesterly trending rhyolite dykes. The projection of this swarm passes under the vent and is parallel with the trend of both fractures and granitic dykes in and around Armadillo caldera farther east. No estimate of the amount of material erupted from the Tadedea centre is possible but it was certainly the site of prolonged and vigorous fumarolic activity.

IGC centre

The IGC centre is a single vent on the extreme western edge of the felsic lava complex, about 10 km from Armadillo caldera (Fig. 50). The vent area has been almost completely isolated by erosion, providing a beautifully

exposed cross-section almost directly through the centre of the conduit (Fig. 51). The basal vent breccia rests on a nearly flat erosion surface that truncates an older pyroclastic cone of Raspberry basalt comprising steeply dipping basaltic tephra, agglutinated spatter and thin basalt flows. The basal IGC explosion breccia is a crudely bedded, chaotic mixture of fine rhyolitic ash, fragments of altered rhyolite, and small globular masses of granular obsidian, surrounding loosely stacked accidental clasts of the underlying basalt and pre-Tertiary basement rocks torn from the conduit walls. Most of the clasts are angular and from less than 1 cm to more than 1 m across, but a few well rounded cobbles and boulders are probably from fluvial deposits incorporated in the vent breccia.

The vent breccia is overlain by an asymmetrical dome of green comendite which forms a 120 m thick remnant on the west end of the ridge. The eastern, partly covered contact, is nearly vertical, whereas the western end, truncated by erosion, rests on a nearly flat surface. The slope of the cooling surface is mimicked by cryptic flow layers and widely spaced joints in the dome. Long slender columns form a spectacular fan normal to this surface (Fig. 52).

The base of the dome is defined by a layer of black, granular obsidian. Along the steep eastern contact the glass layer is about 2 m thick and in direct contact with the basal vent breccia on one side and with flow banded trachyte on

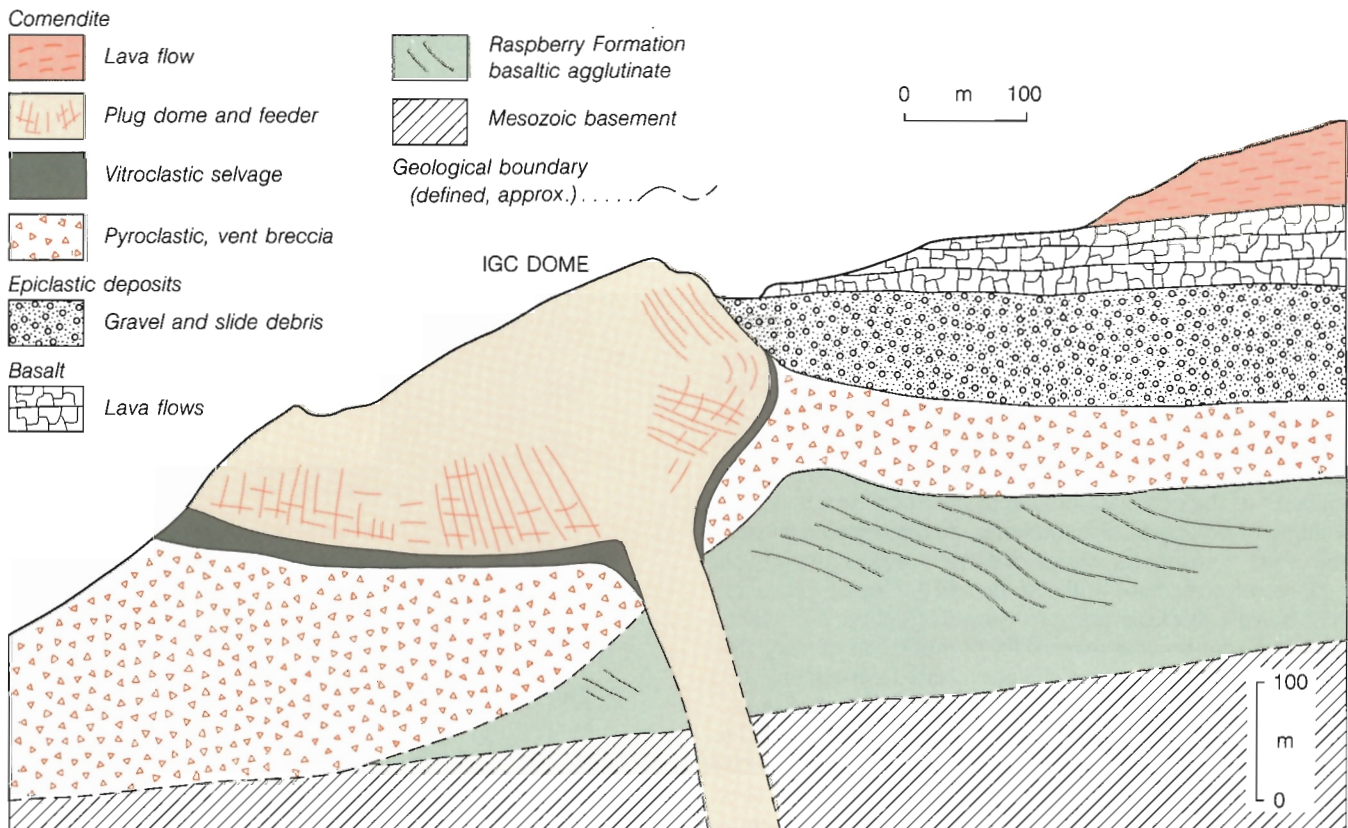


Figure 50. Cross-section of the IGC eruptive centre, the most westerly of the Armadillo satellitic vents.



Figure 51. Looking north at the dissected plug dome and breccia filling the IGC vent. (photo by R.L. Armstrong). GSC 204627.



Figure 52. Fan of long, slender columns in the central part of IGC plug dome. GSC 202468-P.

the other. Farther west where the structure flattens the obsidian is both overlain and underlain by a thin, welded layer of green, to greenish-blue pyroclastic rock with prominent eutaxitic texture (Fig. 53). The faint outlines of similar fiamme, up to 10 cm long, are visible on weathered surfaces of the obsidian indicating that it too originated by welding of hot, particulate material. At the extreme western end of the exposure the wedge of densely welded pyroclastic rock between the base of the dome and the top of the coarse vent breccia thickens to more than 20 m (Fig. 54). There the basal vent breccia is overlain by only 2 m of very fine white porcelain-like, unwelded but lithified ash cemented by secondary silica. This is overlain by a succession of eutaxitic rocks comprising at least four separate cooling units. Green to bluish-green welded lenticulite with perfectly formed fiamme up to 25 cm long and 2 cm across is the most common variant, but in one 1.5 m layer the green fiamme

are enclosed by a reddish-brown oxidized matrix. The persistent obsidian layer along the base of the dome is here more than 7 m thick and, although freshly broken surfaces appear to be structureless, granular to conchoidal black, lustrous glass, the outlines of lenticular fiamme up to 20 cm long are faintly visible on weathered joint faces. The obsidian grades upward into a layer about 12 m thick of greenish-blue, subvitreous lenticulite which, in turn, grades upward into flow banded comendite of the overlying lava dome.

The main body of the dome is green, fine grained, non-porphyrific comendite. Only the lower 15-30 m display flow layering. Above that the rock is either uniformly fine

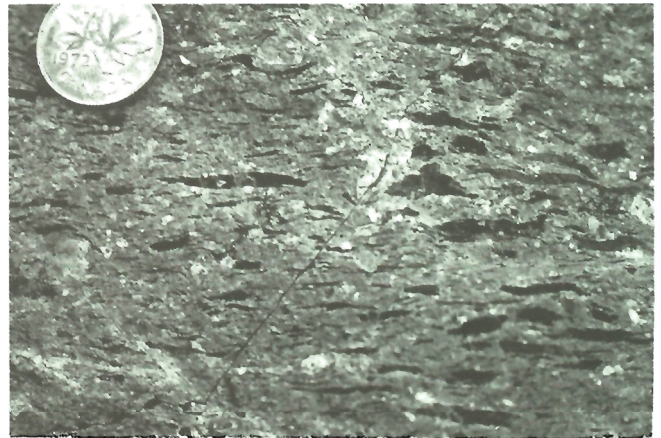


Figure 53. Prominent eutaxitic texture in welded pyroclastic layer within the western part of the IGC conduit, under the plug-dome (photo by Ulrich Kretschmar). GSC 202468-Q.

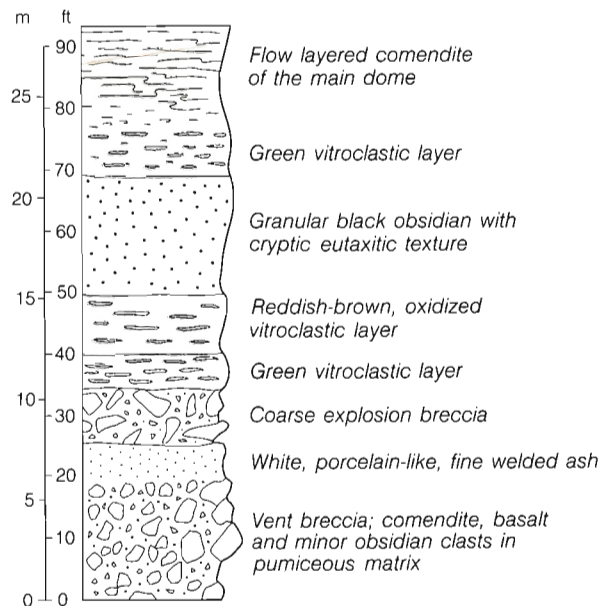


Figure 54. Schematic cross-section showing the sequence of pyroclastic deposits at the western end of IGC dome.

grained or contains ovoid, white alteration patches 1-2 cm across. Near the top of the ridge the rock contains irregular, roughly aligned voids 1-10 mm across with smooth, botryoidal interiors lined with a thin coating of native sulphur.

The lava dome and welded deposits along its lower contact show little evidence of vapour phase alteration. Except for sulphur lining the voids and the presence, locally, of white alteration spots, the comendite and associated glass are extremely fresh. This is in sharp contrast with the underlying vent breccia which is riddled with anastomosing channelways along which the matrix and fragments of the breccia have been transformed to soft ochre and yellow clay by the upward streaming of hot, fumarolic gases.

A substantial amount of time must have elapsed between the first explosive discharge of gas and coarse debris that formed the IGC vent breccia and distal ash flows and subsequent extrusion of the dome. During this time solfataric activity produced the alteration pipes in the breccia and deposited the thin, white, porcelain-like layer of siliceous sinter on the nearly flat crater floor. The period of quiet degassing was broken by several successive bursts of pumice and particulate material from the main vent. The discharge was directed westward depositing showers of molten particles that form the vitreous eutaxitic deposits that underlie the western part of the dome. Extrusion of lava followed shortly thereafter, welling out in a great bulbous, steep-sided dome. As it grew larger cascades of semimolten scale were shed from its surface and overridden by the expanding mass where the flattened particles fused together to form the basal, vitroclastic layer of obsidian.

The timing of the IGC eruption relative to other centres in the central lava complex is not known for certain, but it is thought to be intermediate in age between the initial eruption of Cartoona Ridge and the massive effusion of felsic lavas from Armadillo caldera. The presence of otherwise rare, euhedral aenigmatite phenocrysts in the comendite and associated glass of IGC dome and also in welded ash flows and air-fall pumice in Mess Creek Escarpment suggests a correlation. If this is valid then the IGC dome and the ash flows 6 km farther west, are proximal and distal deposits produced by the same event. This interpretation is in agreement with the local stratigraphy. In Mess Creek Escarpment the aenigmatite-bearing ash flows and tephra are underlain by primary air-fall pumice and trachyte-cobble fluvial gravel probably derived respectively, from the initial eruption and subsequent erosion of the Cartoona Ridge pile. Also, the ash flows are both overlain and underlain by several thin basalt flows. The dome is overlapped by felsic, fluvial gravels and pumiceous sand derived partly from IGC dome itself but mainly from domes and piles of flows growing farther east, in the vicinity of Armadillo and Tadedá. These fluvial beds are overlain by a few thin basalt flows from an unknown intra-Armadillo source, and immediately east of IGC dome the basalts are overlain by a 150-210 m thick succession of comendite flows that extend eastward toward a source in the vicinity of Armadillo or Tadedá.

Distal facies

The apron of sediment and ash that surrounds the central Armadillo felsic lava complex is exposed almost continuously along the Mess Creek Escarpment as far north as Kadeya Creek and as far south as Nagha Creek. Most of the eastern side of the pile was removed by erosion but small lenticular units are preserved in sections on Artifact Creek and the south fork of Tennaya Creek. The basal beds are probably co-extensive with unconsolidated ash and sediment that underlie the Cartoona Ridge lavas, but most of the material in the distal part of the pile is fluvial, and postdates eruption of the Armadillo lavas.

A wedge of clastic debris extends north from Cartoona Ridge for about 10 km. The proximal edge includes an inter-layering of thin lava flows, blocky debris flows, welded ash flows, air-fall pumice and reworked rhyolitic, clastic deposits. Some of the redeposited material is fine, laminated tuff, whereas some is coarse subrounded material resembling landslide debris, talus and colluvium. The most northerly exposure is a thin crystal-rich, highly welded ash flow with black glassy fiamme up to 15 cm long and 1 cm thick. It forms a lenticular exposure about 0.8 km long on the south side of Idiji Ridge where it rests on one of the distal flows of Raspberry basalt which, like the ash flow itself, was channelled into an old bedrock valley.

Sediments derived from the Armadillo deposits were not observed on the southeast part of the pile, but a single, moderately welded crystal-rich ash flow extends about 3 km beyond the southern edge of the Armadillo lavas. It rests directly on Little Iskut flows and is neither underlain nor overlain by air-fall pumice or sediments.

Most of the clastic debris eroded from the growing pile of Armadillo lavas in the Highlands was transported west, and accumulated on top of Raspberry basalt that previously flooded the western lowlands (Fig. 55, sections 2AR-4AR). Rapid deposition of the sediment and periodic flooding by basalt along this western flank of the pile was responsible for the burial and preservation of primary showers of air-fall pumice that did not survive erosion in the adjacent Highlands. At the western end of Raspberry Pass, Armadillo clastic and pyroclastic rocks have a combined thickness of about 180 m. Thick layers of loose air-fall pumice form prominent white recessive units that contrast with inter-layered beds of more competent gravel, cliff-forming units of orange weathering welded ash flows and thin black, intra-Armadillo basalt flows (Fig. 21). The felsic pile thins rapidly northward. Remnants of welded ash flows persist only about 3 km north of Raspberry Pass and from there to the most northerly exposures the felsic Armadillo rocks comprise only very fine white ash, pebbly rhyolitic sand and a few lenticular gravel beds interlayered with much thicker sequences of Armadillo basalts. As on the eastern side of the pile, the most distal remnants preserved are in cross-sections of old valleys where fluvial deposits derived from the Armadillo pile rest on older flows of Raspberry basalt that partly filled those same valleys. On both Tahwa and Kadeya creeks these fluvial deposits contain fragments of wood and a few stumps up to 25 cm across.

MOUNT EDZIZA

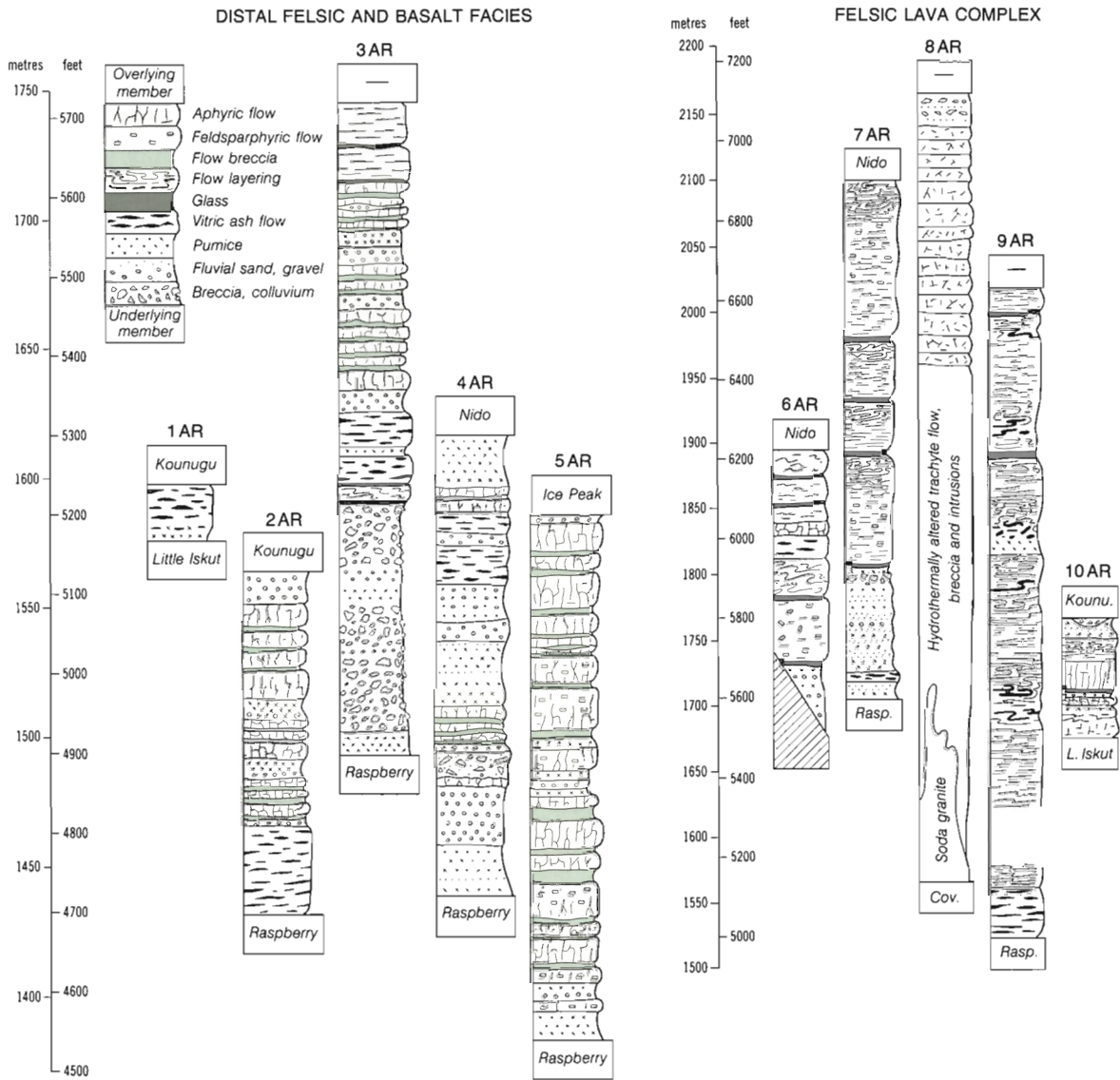


Figure 55. Typical stratigraphic sections of proximal and distal facies of the Armadillo Formation. Section numbers (1-10) refer to locations shown on the paleogeological map (Fig. 40). AR, Armadillo Formation; R, Raspberry Formation.

From Raspberry Pass south to Nagha Creek, Armadillo clastic and pyroclastic rocks are interlayered with a relatively thick succession of Armadillo basalt. Welded ash flows, which on the north side of Raspberry Pass are separated by only a thin layer of fluvial gravel, are here separated by up to 60 m of basalt.

A single prominent, highly welded ash flow about 30 m thick persists as far south as Kitsu Creek. Beyond that, ash, pebbly sand and gravel are found for another 10 km. The most southerly exposure on Yeda Creek comprises about 24 m of white pebbly ash and trachytic gravel resting on the most southerly exposure of Raspberry basalt.

The transition from the felsic lava complex to the peripheral wedge of clastics was locally very abrupt. Within 1.5 km a 460 m section of uninterrupted rhyolite flows near the summit of Raspberry Pass terminates against the 245 m section of clastic and pyroclastic rocks interlayered with intra-Armadillo basalt on Gnu Butte (Fig. 42). In the valley north of Gnu Butte, Armadillo lava is overlain and interbedded with thick lenses of coarse fluvial gravel. As discussed in a later section on drainage systems, this is believed to be the course through which much of the fluvial material was transported from the Armadillo highlands to the alluvial fans of the western lowlands.

Armadillo basalt

Eruption of Armadillo trachyte and rhyolite was accompanied by simultaneous eruptions of basalt from several separate sources. The thickest basaltic sections are exposed in Mess Creek Escarpment near the southwest end of Raspberry Pass and farther north, in the canyons of Sezill and Kedeya creeks. They include up to 180 m of basalt flows, interlayered with trachyte and rhyolite clastic and pyroclastic beds. Individual basalt flows are relatively thin (usually less than 3 m) and extremely persistent, suggesting a very fluid, mobile lava (Fig. 21).

The source of the southern pile is believed to be near the summit of Little Iskut volcano. On Artifact Ridge, Little Iskut trachybasalt is overlain at an elevation of about 6000 ft. (1800 m) by a thin layer of rhyolitic ash above which is a lenticular 90 m thick pile of thin, aphyric basalt flows, which are overlapped by a later flow of Armadillo trachyte. These basalts are clearly intra-Armadillo and, at such a high elevation, are probably near their source. The surface of a 120 m section of intra-Armadillo basalt farther west, at the summit of Raspberry Pass, is 5700 ft. (1737 m) in elevation and that of the uppermost intra-Armadillo basalt flow in Mess Creek Escarpment south of Raspberry Pass is 5300 ft. (1615 m). These three localities are believed to be part of a continuous basaltic lava field that spread westward down the gentle slope of Little Iskut shield to the western lowlands.

The source of Armadillo basalt now exposed at the north end of Mess Creek Escarpment has been buried by the younger edifice of Ice Peak. However, the trace of paleoslopes in the east-west canyons of Sezill and Kedeya creeks, as well as paleoflow directions from deformed pipe vesicles, indicate that they came from a source to the east, probably from a cluster of vents in the northwestern Central Highlands, identified schematically on Figure 40 as Sezill volcano. Flows from this centre are assigned to the Armadillo Formation on the basis of interlayered felsic deposits (Fig. 55, section 5AR) and K-Ar dates. However, they are moderately porphyritic and, lithologically, they more closely resemble the underlying Raspberry flows than the aphyric, Armadillo basalt farther south. It seems likely that Sezill volcano was active in pre-Armadillo time and that it continued to erupt similar basalt after the onset of Armadillo felsic volcanism.

Periodic eruption of basalt from these and other unidentified sources occurred regularly throughout much of early Armadillo time. Successive flows were covered by pyroclastic deposits and colluvial outwash from the felsic lava complex, and the course of the basalt must have been diverted several times by intervening thick piles of rhyolite.

STRATIGRAPHY

The Armadillo Formation is a bimodal time-stratigraphic map unit that embraces a variety of dissimilar facies. Basalt, rhyolite and trachyte flows, pyroclastic

rocks, subvolcanic intrusions and derived sediments are juxtaposed within a small area and so intimately mixed that no single stratigraphic section can be taken as typical (Fig. 55). The base of the formation is defined by the first appearance of felsic ejecta in the volcanic succession. It rests conformably on Little Iskut trachybasalt and both conformably and disconformably on Raspberry basalt, from which it is separated locally by an erosion surface with pockets of fluvial gravel. In areas such as the Armadillo basement high (Fig. 40) that were not previously flooded by either Raspberry or Little Iskut flows, the Armadillo rests unconformably on pre-Tertiary basement rocks. The top of the Armadillo Formation is defined by an erosion surface that separates it from the overlying Nido and Kounugu basalt successions neither of which include felsic members.

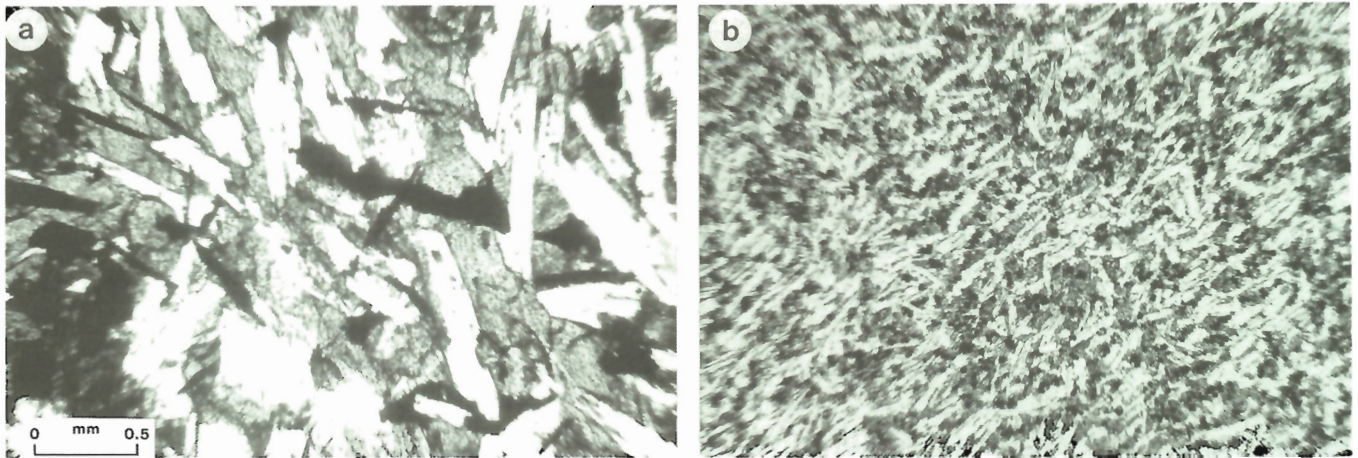
Included in the formation are all the products erupted during the episode of Armadillo felsic volcanism. These include flows, pyroclastic deposits, domes and subvolcanic intrusions of the felsic rocks themselves as well as basaltic rocks erupted during the same time interval. The latter are recognized by the presence of interlayered, or at least bracketing beds of felsic ash or ash flows. Insofar as scale permits, the basaltic and felsic facies are shown separately on the map.

PETROGRAPHY

Basalts

The Armadillo hawaiites and alkali olivine basalts are petrographically similar except for a slightly higher proportion of opaques and the presence of sparse feldspar phenocrysts in some of the hawaiites (Fig. 56). The feldsparphyric hawaiites are confined to the thick pile of flows that outcrop along the northern end of the Mess Creek Escarpment, in Sezill and Elwin Creek valleys, which issued from Sezill volcano (Fig. 40). They include up to 10% plagioclase (An_{55-65}) in an intergranular or subophitic groundmass of titanite, opaques and devitrified glass (Fig. 56a). Olivine is either absent or present only in trace amounts as tiny, widely dispersed grains in the groundmass. The proximal Sezill basalts are indistinguishable from those in the underlying Raspberry Formation except for carbonate alteration which is commonly more widespread and pervasive in the older flows.

Elsewhere, in the central and southern parts of Mess Creek Escarpment, and around the periphery of the felsic lava complex the Armadillo basalts are aphyric and very fine grained (Fig. 56b). They are mainly alkali olivine basalts which contain about equal amounts of well oriented plagioclase laths and moderately pigmented titanite either as intergranular or subophitic crystals, plus interstitial grains of opaque oxides and a trace of olivine (about Fe_{80}). They are commonly nonvesicular and free of carbonate alteration.



a — Medium grained subophitic hawaiite. Laths of plagioclase (white) and opaque oxide (black) are partly enclosed by titanite (grey), (plane light).

b — Fine grained, aphyric alkali olivine basalt comprising well oriented plagioclase laths and small intergranular crystals of olivine, titanite, and opaque oxides (plane light).

Figure 56. Photomicrographs of Armadillo basalt; scale bar 0.5 mm.

Felsic rocks

The subtle differences in chemistry which form the basis for subdividing this suite of rocks into trachytes, with agpaite indices (A.I.) less than one and comendites (A.I. > 1) have not resulted in significant or consistent differences in texture or mineralogy. Thus petrographic study can provide only a qualitative approximation of the chemical classification and even this is limited to the extreme end members of the series. The best mineralogical criteria are aenigmatite and ilmenite which exhibit an antipathetic relationship. Phenocrystic aenigmatite is present only in the most peralkaline comendites, whereas phenocrysts and microphenocrysts of ilmenite are found only in trachytes with relatively low agpaite indices. Although both minerals may be found in the groundmass of rocks throughout the series, aenigmatite (as well as arfvedsonite and kataphorite) is much more abundant toward the comenditic end and opaque oxides toward the trachytic end. Quartz phenocrysts are confined mainly to the comendites but some of the trachytes also contain partly resorbed quartz phenocrysts. A less consistent, purely empirical discriminant is provided by the phenocrystic feldspar which tends toward anorthoclase in the trachytes and towards sanidine in the comendites. However, both feldspars are present throughout the series and probe analysis (Fig. 57) show that their compositions overlap within a fairly narrow range (Or_{30-50}).

Holocrystalline rocks

Except for the minor differences noted above the Armadillo trachytes and comendites exhibit the same range of textures (Fig. 58) and mineralogy (Table 5). Nearly all of them are porphyritic, with from 2 to 20% feldspar phenocrysts ranging in size from less than 1 mm in glassy

phases to 1 to 3 mm in flows, and up to 1.5 cm in ponded lavas and subvolcanic bodies. The crystals, which occur both singly and in clusters, are commonly euhedral or slightly rounded but have consistently sharp boundaries against the enclosing groundmass. Rounded boundaries are commonly mimicked by a thin, well defined zone of tiny green euhedral crystals (acmite or sodic hedenbergite) that are enclosed within the outermost edge of the feldspar crystal. Most of the feldspars exhibit simple carlsbad twinning and have the optical properties of sanidine. However, very fine two directional polysynthetic twinning, suggesting anorthoclase, is present in some crystals, particularly in the trachytes. Quartz phenocrysts as euhedral hexagonal prisms and as rounded embayed crystals are second to feldspar in abundance. Commonly both euhedral and embayed types are present in the same section. Although phenocrystic quartz is most abundant in the comendites it is also present in some rocks that are chemically classified as trachytes. Phenocrysts of green, strongly pleochroic hedenbergite as tabular crystals up to 2 mm long and smaller prisms of acmite are widely but sparsely distributed as are small phenocrysts of ilmenite. A clear colourless pyroxene (salite?) and pale yellow fayalite (FeO_3) occur as rare microphenocrysts in some of the trachytes.

The groundmass consists mainly of small laths (0.05-0.1 mm) of alkali feldspar having about the same composition as the phenocrysts (Fig. 58a). In some rocks these occur as ragged, interlocking crystals that are crudely aligned and impart on the rock a fluidal, trachytic texture having layers that wrap around the phenocrysts. In others the groundmass feldspar is arranged in radiating spherulitic clusters. The feldspar in both types is surrounded and partly enclosed by clear "pools" of micropoikilitic quartz. These are crowded with tiny, nearly square euhedra of alkali feldspar as well as the perfectly terminated prisms of larger

Table 5. Representative microprobe analyses and structural data for the principal mineral phases in the Armadillo, felsic rocks.

	Feldspar			Pyroxene					Amphibole		Aenigmatite	
	Groundmass			Phenocryst					Groundmass		Phenocryst	
	AF1	AF2	AF3	AP1	AP2	AP3	AP4	AP5	AAM1	AAM2	AAE1	
SiO ₂	66.75	68.37	66.35	47.77	47.67	52.59	50.43	51.92	50.47	50.70	40.88	
Al ₂ O ₃	18.56	18.18	18.02	0.62	0.09	0.34	0.19	0.34	0.12	0.12	0.47	
TiO ₂	0.0	0.0	0.0	0.56	0.27	1.55	1.74	0.39	0.33	0.10	9.10	
Cr ₂ O ₃	0.0	0.01	0.0	0.0	0.01	0.0	0.01	0.02	0.0	0.0	0.01	
Fe ₂ O ₃	0.62	0.54	1.18	2.57	7.12	31.41	20.76	30.79	1.74	3.54	0.62	
FeO	0.0	0.0	0.0	28.25	23.46	0.85	9.49	2.51	32.56	32.11	40.84	
MnO	0.0	0.01	0.0	1.23	0.82	0.17	0.36	0.17	0.85	0.79	0.74	
MgO	0.0	0.01	0.0	0.02	0.13	0.0	0.0	0.01	0.14	0.01	0.05	
NiO	0.0	0.0	0.0	0.0	0.0	0.0	0.0	0.0	0.0	0.0	0.0	
CaO	0.10	0.02	0.10	19.75	16.89	0.41	7.33	3.15	1.08	0.59	0.42	
K ₂ O	7.53	11.32	6.50	0.60	2.37	13.52	9.19	12.01	8.57	9.12	7.28	
K ₂ O	6.11	0.16	7.63	0.0	0.03	0.01	0.0	0.0	1.39	1.18	0.0	
H ₂ O	0.0	0.0	0.0	0.0	0.0	0.0	0.0	0.0	0.0	0.0	0.0	
F	0.0	0.0	0.0	0.0	0.0	0.0	0.0	0.0	0.0	0.0	0.0	
Total	99.67	98.62	99.78	101.37	98.86	100.85	99.50	101.31	97.25	98.26	100.41	
	Number of ions on basis of 8(O)			Number of ions on basis of 6 (O)					Number of ions on basis of 23 (O)			
Si	2.9947	3.0282	2.9961	1.9523	1.9742	1.9975	1.9872	1.9831	8.1675	8.1247	11.7342	
Al	0.9813	0.9490	0.9590	0.0299	0.0044	0.0025	0.0098	0.0153	0.0	0.0	0.1590	
Cr	0.0	0.0	0.0	0.0172	0.0084	0.0	0.0039	0.0016	0.0	0.0	0.0023	
Fe ³⁺	0.0209	0.0180	0.0401	0.0007	0.0130	0.0	0.0	0.0	0.0	0.0	0.1045	
Al	0.0	0.0	0.0	0.0	0.0	0.0127	0.0	0.0	0.0229	0.0227	0.0	
Cr	0.0	0.0004	0.0	0.0	0.0	0.0443	0.0476	0.0096	0.0	0.0	0.0	
Ti	0.0	0.0	0.0	0.0783	0.2090	0.8976	0.6156	0.8851	0.0402	0.0121	1.9643	
Fe ³⁺	0.0	0.0	0.0	0.0	0.0003	0.0	0.0003	0.0006	0.2118	0.4268	0.0287	
Ni	0.0	0.0	0.0	0.0	0.0	0.0	0.0	0.0	0.0	0.0	0.0	
Fe ²⁺	0.0	0.0	0.0	0.9655	0.8125	0.0270	0.3127	0.0802	4.4072	4.3039	9.6048	
Mn	0.0	0.0004	0.0	0.0426	0.0288	0.0055	0.0120	0.0055	0.1165	0.1072	0.1799	
Mg	0.0	0.0007	0.0	0.0012	0.0080	0.0	0.0006	0.0006	0.0338	0.0024	0.0214	
				0.8648	0.7495	0.0167	0.3095	0.1289				
				0.0475	0.1903	0.9957	0.7021	0.8894				
				0.0	0.0016	0.0005	0.0	0.0				
Ca	0.0048	0.0009	0.0048						0.1873	0.1013	0.1292	
Na	0.6550	0.9721	0.5691						2.6890	2.8336	4.0516	
K	0.3497	0.0090	0.4395						0.2869	0.2412	0.0	

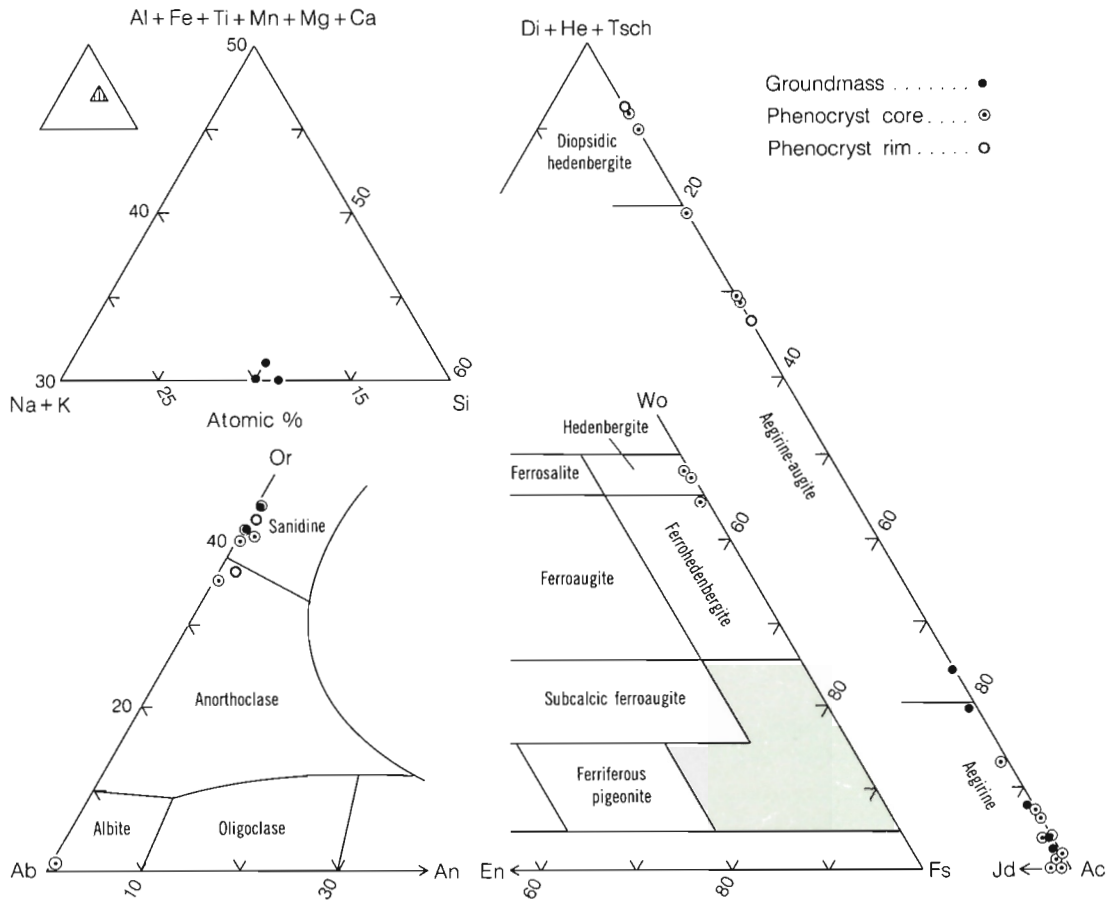


Figure 57. Plot of microprobe analyses of the principal mineral phases in the Armadillo trachytes, comendites, and soda granite.

groundmass feldspars that project into them. Femic minerals in the groundmass include variable amounts of aenigmatite, kataphorite(?), and acmite. These commonly occur as mossy clumps resembling aggregates of tiny bladed crystals, too small to analyze either optically or chemically. However, the widely scattered parts of any one clump are often in optical continuity indicating that they are, in fact, parts of relatively large (up to 1 mm) skeletal, highly poikilitic single crystals. The presence of kataphorite is assumed only on the basis of its association, habit, and strong yellow to yellowish-brown pleochroism. Aenigmatite, arfvedsonite and acmite are locally present in discrete crystals of sufficient size to probe (Fig. 58e) and their distinctive pleochroism and crystal habit provide confidence in identifying even the smallest grains. Where discrete grains of these minerals are present aenigmatite commonly displays euhedral crystal boundaries against both aegirine and arfvedsonite, and arfvedsonite commonly mantles the other two.

Fine grained comendites commonly exhibit distinct banding, either in the form of planar, very regular or highly contorted layers ranging from less than 1 mm to a few centimetres in width. It is caused by the parallel arrangement of several different features including microscopic voids,

lithophysae, spherulites or commonly by the partial segregation of felsic and mafic minerals into discrete layers. The voids are commonly lined or partly lined with quartz and a fringe of small, euhedral potassium feldspar crystals that project into them. Late, vapour phase minerals in both voids and lithophysae commonly include slender euhedral prisms of arfvedsonite or acmite and rarely analcime and/or fluorite.

Large (1-10 mm) irregular voids such as those in the comendite of IGC dome contain relatively large (about 1 mm) euhedra of aenigmatite and acmite and subordinate patches of arfvedsonite. The aenigmatite is commonly mantled by a rim of aegirine and both aenigmatite and aegirine crystals are partly enclosed by patches of anhedral arfvedsonite.

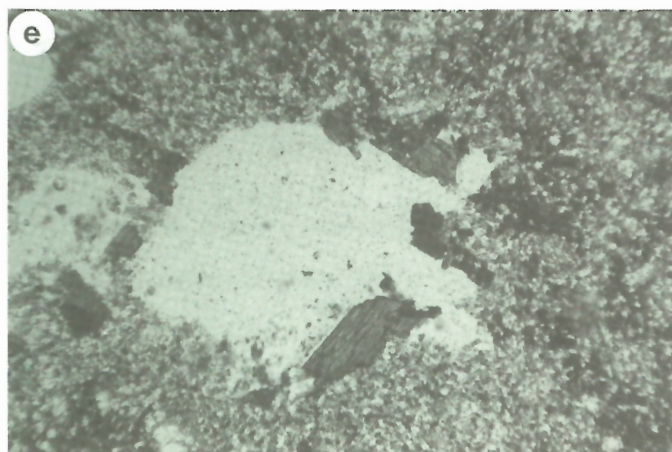
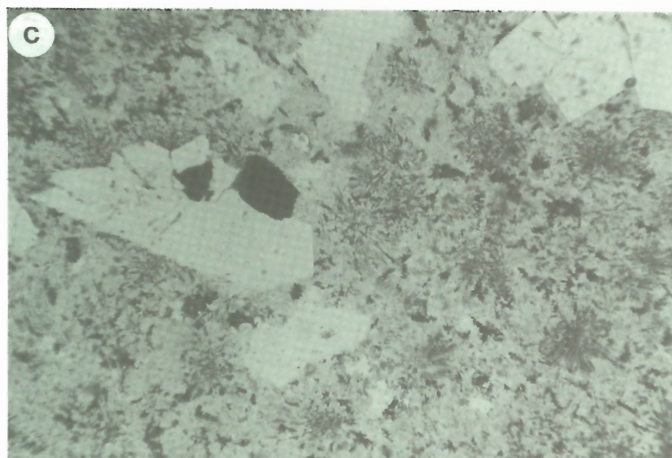
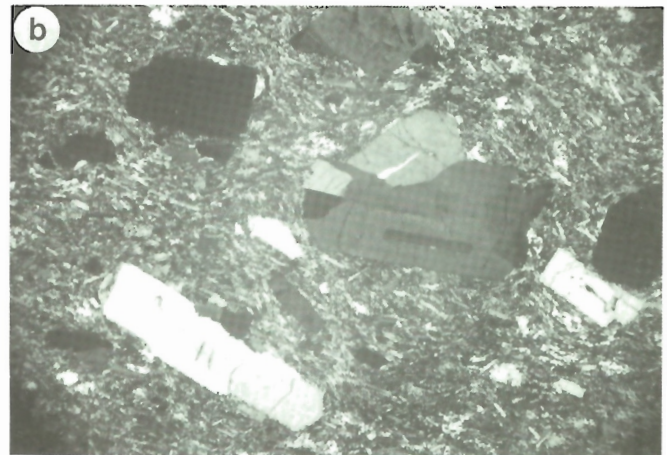
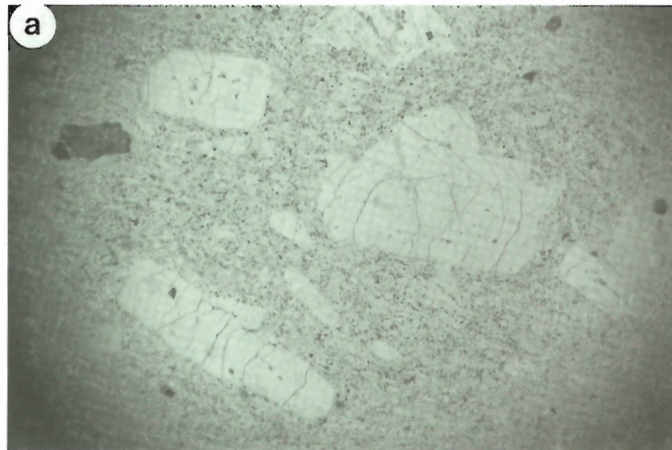
Vitreous rocks

Vitreous and subvitreous rocks comprise a very small proportion of the Armadillo felsic suite but they provide valuable insights into the nature of the magma during extrusion and its subsequent crystallization history. The

Armadillo obsidians are rarely aphyric, but few of them contain more than about 5% phenocrysts. Small elongated crystallites of alkali feldspar are the most abundant and they, along with subordinate acicular pyroxene and aenigmatite prisms are invariably aligned to give the glassy groundmass a pronounced fluidal texture. The flow layers wrap around larger phenocrysts (about 0.5 mm) which may include alkali feldspars, hedenbergite, acmite and aenigmatite. The feldspar phenocrysts, in contrast to the crystallites, form stout, almost equidimensional, rhombic crystals that are randomly

oriented with respect to the flow layering. The other phenocrystic phases tend to form elongate prisms that conform to the plane of flow layering.

Most of the vitreous comendites contain spherulitic structures. Some of these are very fine radiating clusters of secondary minerals which truncate the fluidal texture of the glassy groundmass and were clearly formed by late stage devitrification processes after flowage had ceased (Fig. 59a). However, a more common type of spherulite comprises radiating clumps of potassium feldspar prisms and



a,b — Feldsparphyric trachyte (a, plane light; b, crossed polarizers).

c,d — Feldsparphyric comendite (c, plane light; d, crossed polarizers).

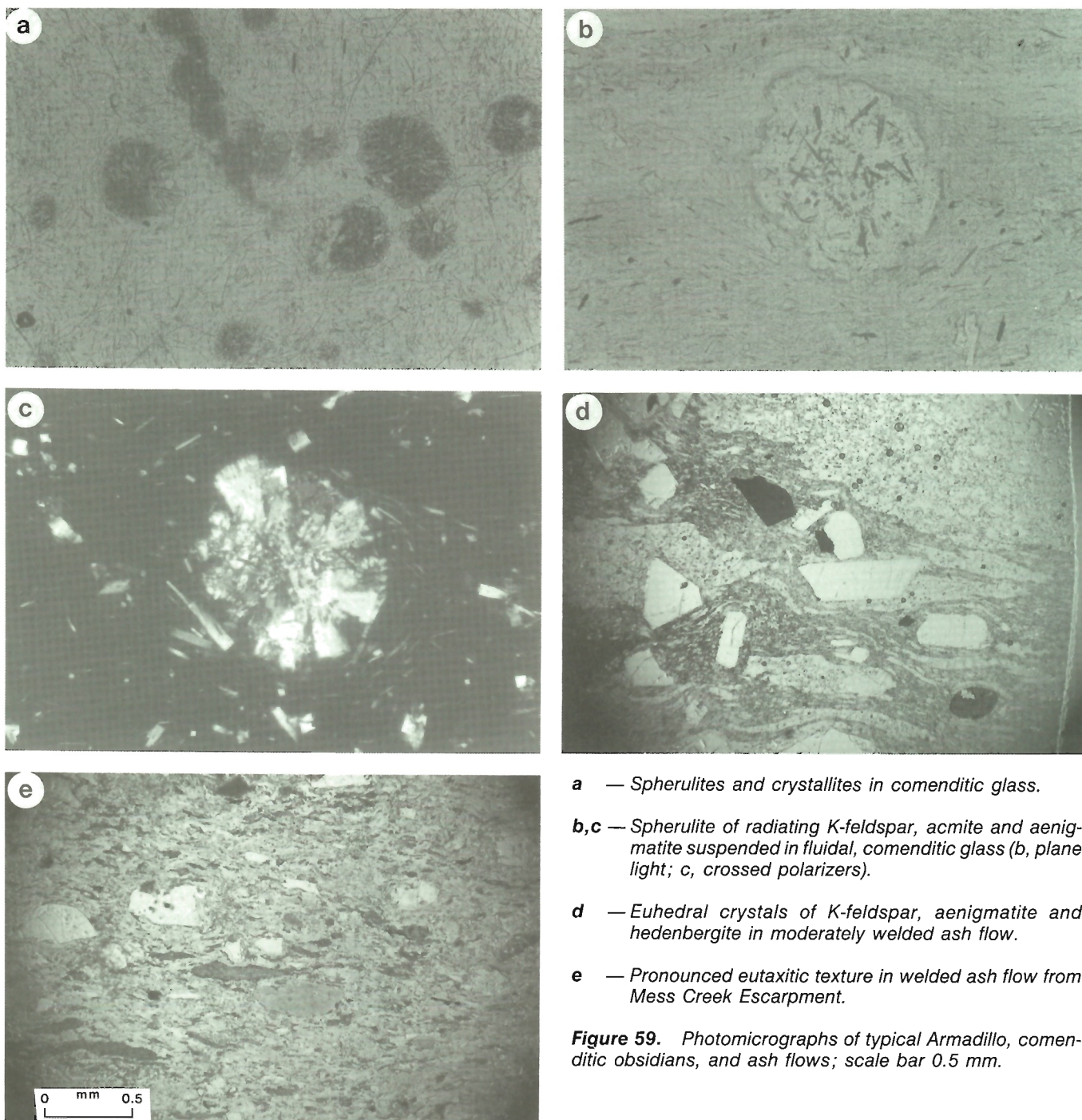
e — Small crystals of aegirine, aenigmatite and arvedsonite in comendite.

Figure 58. Photomicrographs of typical holocrystalline Armadillo trachyte and comendite; scale bar 0.5 mm.

MOUNT EDZIZA

tiny blades of amphibole, pyroxene and/or aenigmatite (Fig. 59b). The alignment of microlites in the fluidal glassy groundmass is deflected around these spherulitic clusters in the same manner as it is around discrete phenocrysts. It is apparent that this type of spherulite nucleated in the molten magma before or during eruption and continued to crystallize during flow. The close similarity between these “free floating” spherulites in comenditic glass and the close packed spherulites of many holocrystalline comendites suggests that the latter also nucleated while the groundmass was still fluid. The spherulitic clusters probably continued to

grow, along with single crystal phenocrysts, until the crystal-spherulite-liquid mush became too viscous to flow. At this point the siliceous, highly peralkaline residual liquid crystallized between the spherulitic clusters to form the pools of poikilitic quartz with its enclosed euhedra of potassium feldspar and mossy aggregates of alkali amphiboles and pyroxenes. Such a process would explain the apparent contradiction between the highly fluid, mobility of the comendite lava flows and the common absence of any orientation or flow structure in the holocrystalline groundmass.



a — Spherulites and crystallites in comenditic glass.
b,c — Spherulite of radiating K-feldspar, acmite and aenigmatite suspended in fluidal, comenditic glass (b, plane light; c, crossed polarizers).
d — Euhedral crystals of K-feldspar, aenigmatite and hedenbergite in moderately welded ash flow.
e — Pronounced eutaxitic texture in welded ash flow from Mess Creek Escarpment.

Figure 59. Photomicrographs of typical Armadillo, comenditic obsidians, and ash flows; scale bar 0.5 mm.

Ash flows

All of the Armadillo ash flows are of comenditic or pantelleritic composition. They are commonly crystal-rich, and include the same mineral species that occur as phenocrysts in the lavas (Fig. 59d). Broken or euhedral crystals of potassium feldspar and quartz are abundant. Hedenbergite and aenigmatite are lesser but widely distributed crystal components and small aegirine euhedra are rarely present. The crystals, along with cognate and accidental lithic inclusions, are enclosed in a eutaxitic, vitreous matrix. The degree of welding varies from one ash flow to another and from the base upward in most individual cooling units. Typically the dense basal part has been compressed and welded to such an extent that individual shards are no longer visible in thin section; instead they are drawn out into contorted, highly attenuated streaks that resemble flow layering in glassy lava. In the central, moderately welded, portion the lenticular outline of partly collapsed pumice fragments and the cusped form of smaller shards is clearly visible (Fig. 59e). The upper part of some Armadillo ash flows exhibits little or no welding or deformation of the pumice fragments. The clasts are, however, commonly cemented by a matrix of vapour phase minerals, principally silica and iron oxides.

Intrusive rocks

Subvolcanic intrusions of soda granite associated with the Armadillo cauldron complex are medium to coarse equigranular rocks comprising about 45% clouded alkali feldspar with extremely fine polysynthetic (albite) twinning, 45% quartz, 10% bright green to pale yellowish brown, pleochroic pyroxene and less than 1% opaque oxides. In the medium grained phases (2-5 mm) the feldspar and pyroxene are euhedral and exhibit sharp crystal boundaries against the enclosing, anhedral quartz (Fig. 60). In coarser phases (5-10 mm) the feldspar is commonly embayed. Myrmekitic intergrowths of quartz and sodic feldspar are extensively developed around the larger feldspar boundaries and pyroxene has been partly or wholly altered to granular iron

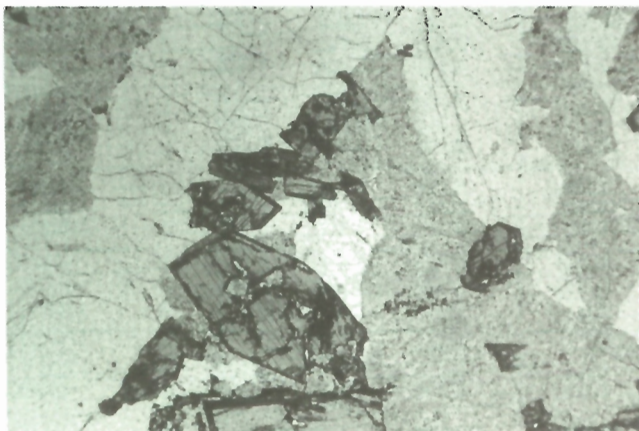


Figure 60. Photomicrograph of soda granite from Armadillo caldera.

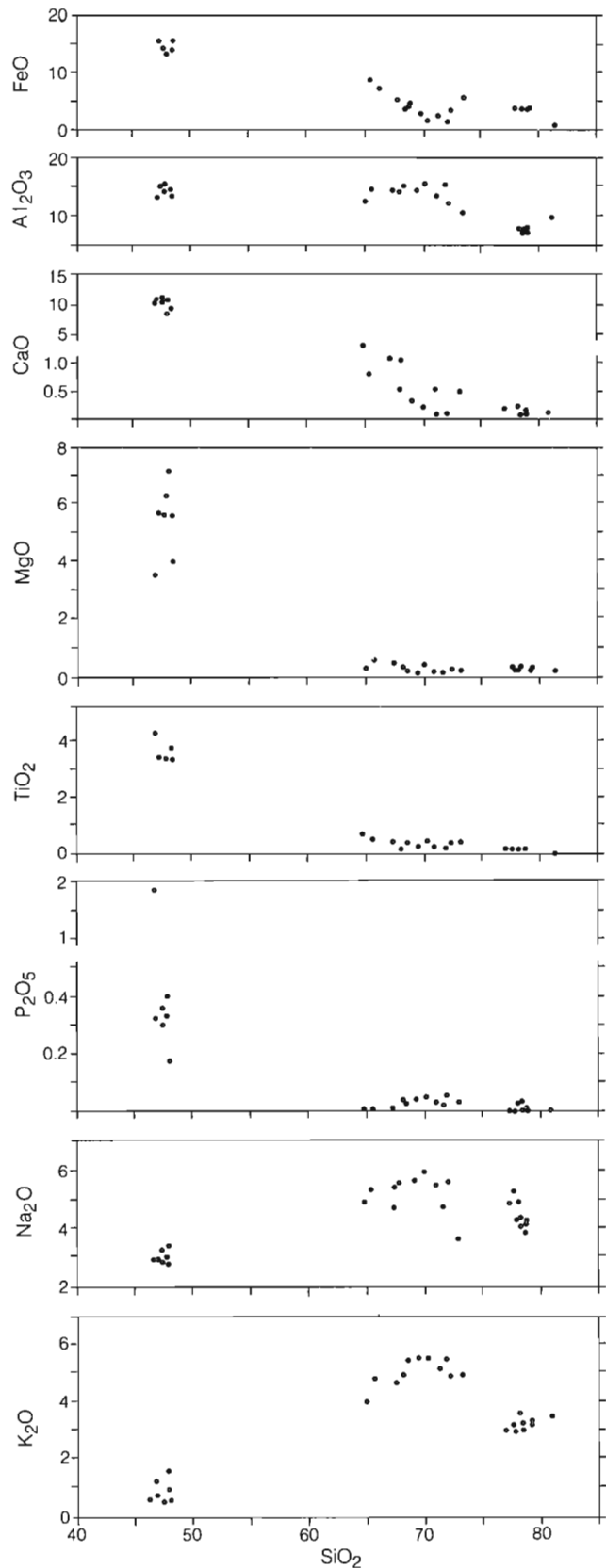


Figure 61. Harker diagram showing chemical variation in weight percent for 28 analyzed specimens from the Armadillo Formation.

oxides. Also, in the coarser grained phases, finely twinned feldspar has a patchy extinction suggestive of fine perthite. However, probe analysis of the feldspars (Fig. 57) indicates that they are almost pure albite (less than 2% Or). Similarly the pyroxene analyses all fall within a few percent of pure acmite (Fig. 57). Thus the mineralogy is consistent with major element chemistry in confirming the highly sodic nature of these rocks. Extrusive comendites in the upper part of the caldera complex are composed mainly of sanidine and anorthoclase (Or₄₅). Thus if the two rocks are comagmatic, as seems likely from their peralkaline affinity and close spatial association, it is necessary to appeal to some very efficient process of K₂O/Na₂O partitioning between intrusive and extrusive phases.

CHEMISTRY

Twenty-eight major element analyses of Armadillo rocks are plotted in Figures 61 to 64 and twelve superior analyses are listed in Table 6. Most of these plots emphasize the strongly bimodal nature of the formation. On the Harker diagrams (Fig. 61) and the total alkali vs. silica diagram (Fig. 62) the 7 analyzed basalts are seen to cluster between 45 and 49% silica, whereas the 21 analyses of felsic rocks all fall between 64 and 82% silica, leaving a gap between 49 and 64% that reflects the absence of intermediate rocks in the Armadillo Formation. The basalts, like those of the underlying Raspberry Formation, fall entirely within the sodic series (Fig. 63) and either within or close to the alkali basalt field of the Irvine-Baragar (1971) classification (Fig. 64).

The felsic rocks include alkali-rich trachytes with aegirite indices slightly less than one (Fig. 64) and peralkaline rocks (A.I. > 1) which fall outside the Irvine-Baragar classification. The latter plot almost entirely within the comendite field of Macdonald's (1974) Al₂O₃ vs. FeO diagram (Fig. 64). On the total alkali vs. silica diagram (Fig. 62) the felsic rocks exhibit a well defined alkali maximum at approximately 69% SiO₂. Higher silica values are nearly all from oversaturated peralkaline rocks with modal quartz, arfvedsonite and aegirine, whereas the lower silica values are from trachytes composed almost entirely of alkali feldspar. Although the drop in total alkalis with increasing silica is certainly influenced by the constant-sum effect, it is noteworthy that the position of the alkali maximum is very

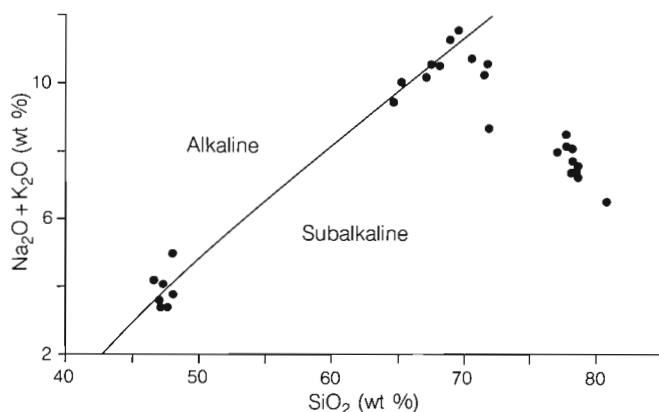


Figure 62. Plot of total alkalis vs. silica for 28 specimens from the Armadillo Formation.

Table 6. Representative chemical analyses of specimens from the Armadillo Formation.

Spec. no.	Basalt			Felsic							
	Alkali olivine basalt		Hawaiite	Trachyte			Peralkaline				
	71	2885	2656	2892	2894	2896	87	2879	2881	2882	2883
SiO ₂	46.400	46.100	44.400	63.600	66.600	66.800	72.100	77.800	78.000	77.100	76.700
Al ₂ O ₃	14.500	13.900	13.000	12.900	14.300	15.100	10.800	8.100	8.400	8.500	8.800
Fe ₂ O ₃	4.900	5.900	5.800	4.600	1.500	2.200	3.500	2.700	1.700	4.200	1.400
FeO	8.600	8.000	9.200	4.200	4.000	1.900	2.700	1.800	2.800	0.400	3.100
CaO	9.510	8.100	9.100	2.400	1.500	1.400	0.450	0.300	0.200	0.300	0.300
MgO	6.090	6.900	3.400	0.400	0.400	0.300	0.270	0.400	0.400	0.300	0.400
Na ₂ O	3.200	2.900	2.800	4.900	5.400	5.500	3.700	5.000	4.500	4.400	4.900
K ₂ O	0.790	0.800	1.200	4.400	4.700	4.900	4.910	3.100	3.200	3.700	3.200
TiO ₂	3.140	3.160	4.050	0.640	0.370	0.230	0.380	0.330	0.330	0.310	0.320
P ₂ O ₅	0.350	0.400	1.740	0.130	0.020	0.050	0.040	0.040	0.080	0.030	0.0
MnO	0.180	0.150	0.280	0.240	0.150	0.110	0.100	0.070	0.100	0.070	0.070
S	0.070	0.0	0.0	0.0	0.0	0.0	0.0	0.0	0.0	0.0	0.0
NiO	0.010	-	-	-	-	-	0.002	-	-	-	-
CO ₂	0.200	0.0	2.200	2.000	1.000	0.0	0.0	0.0	0.100	0.0	0.0
H ₂ O	2.000	3.500	2.700	0.700	0.500	0.900	0.700	0.700	0.600	0.800	1.000
Total	99.940	99.810	99.870	101.110	100.440	99.390	99.650	100.340	100.310	100.110	100.190

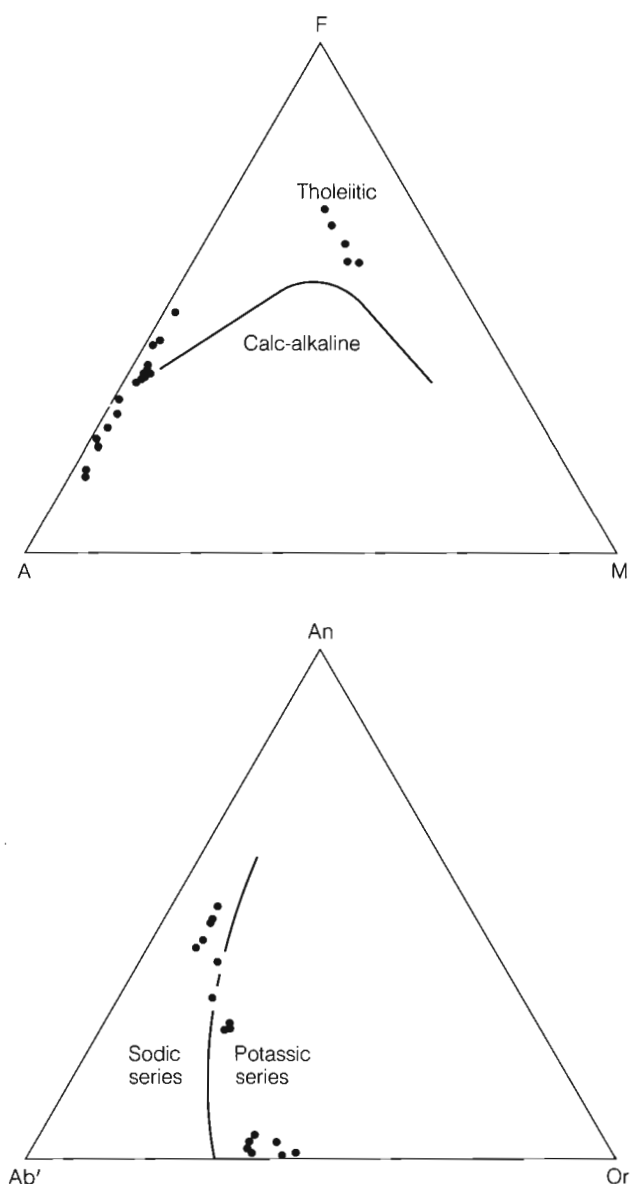


Figure 63. AFM and Ab'-An-Or plots of 28 analyses from the Armadillo Formation. (A = Na₂O + K₂O; F = FeO + 0.8998 Fe₂O₃; M = MgO; Ab' = Ab + 5/3Ne).

close to the theoretical SiO₂ content of alkali feldspar (68.75 for pure albite). Thus it appears that the alkali content of the rock is largely controlled by the amount of aluminum available to form feldspar, and that the maximum alkali content is present in rocks that approach a feldsparite composition (about 69.0% SiO₂). In the oversaturated, Q-bearing peralkaline rocks, which are deficient in Al relative to alkalis, the total alkali content drops sharply as silica increases beyond 69%, suggesting the partial removal of alkalis from these rocks in a volatile phase. The operation of such a system of alkali depletion is further supported by the occurrence of arfvedsonite, aegirine and aenigmatite as

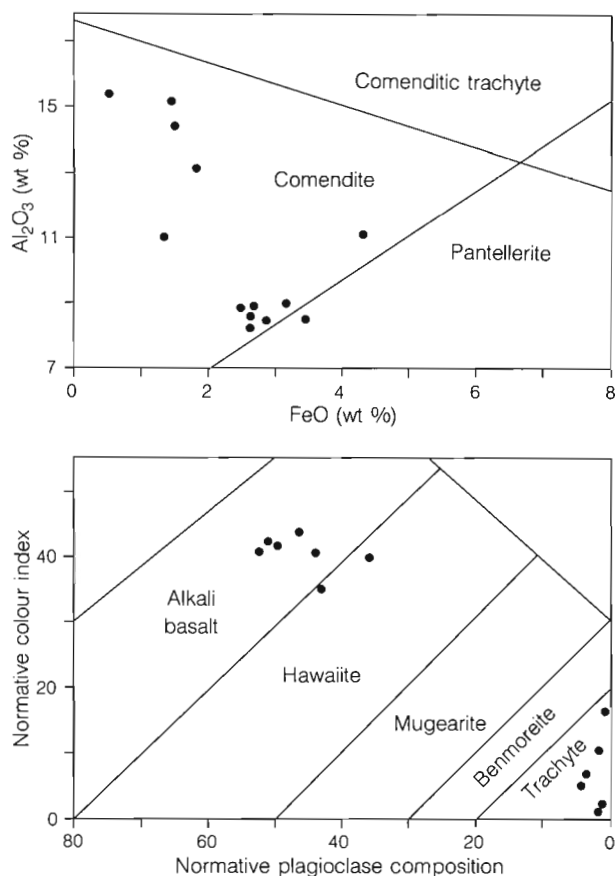


Figure 64. Plot of normative plagioclase vs. normative colour index for non-peralkaline rocks of the Armadillo Formation, and Al₂O₃ vs FeO for the peralkaline rocks.

vapour phase minerals lining open cavities in silica oversaturated comendites.

The bimodal character of the Armadillo is also apparent on the AFM diagram (Fig. 63) in which there is no apparent linkage between the two populations of points. The basalts display a fairly clear trend toward Fe-enrichment as compositions shift from alkali basalt to hawaiite. The apparent trend toward alkali enrichment within the felsic suite is, however, independent of silica variation, and supports the concept of alkali transfer in a late-stage, volatile phase.

NIDO FORMATION

GENERAL GEOLOGY

Introduction

Basalt erupted during the Nido stage of activity constitutes the most widespread formation in the map area (Fig. 65, Map 1623A, in pocket). It issued from several separate centres that lie mainly in a north-south zone along the eastern edge of the volcanic complex. North of the Armadillo Highlands overlapping flows from at least three major centres flooded an area of more than 350 km² that underlies most of the younger edifice of Mount Edziza. Similarly, coalescing flows from at least four centres covered most of the Spectrum Plateau and are now exposed around the periphery of the younger rhyolite complex which forms the Spectrum Range. The Armadillo Highlands acted as a topographic barrier between these two lava fields and were not themselves flooded by Nido basalt. Because they do not overlap, and because no single marker horizon extends completely across the area underlain by Nido rocks, the northern and southern domains are treated as separate members. The Tenchen Member embraces all the products of Nido volcanism that were erupted north of the Armadillo Highlands, and the Kounugu Member is restricted to the area south of Armadillo Highlands. However, the presence of glacial deposits containing Armadillo clasts under Nido flows in both domains suggests that volcanism in the two areas was more or less contemporaneous.

The three major centres north of Armadillo Highlands are deeply dissected and most of the eastern part of the pile has been stripped away by erosion, whereas the distal flows on the western edge are exposed beneath younger strata along Mess Creek Escarpment and in the upper canyon of Elwyn Creek. Most of the Tenchen basalt rests on the Armadillo Formation or on fluvial gravel carrying clasts of Armadillo rhyolite and trachyte. However, distal flows on the extreme northern edge of the pile extend beyond the apron of Armadillo colluvium and rest directly on pre-Tertiary basement. The upper contact is defined by the Pyramid rhyolite which overlies the Tenchen basalt along the eastern edge of Mount Edziza. This contact is commonly occupied by a layer of obsidian-bearing till or glacial fluvial gravel which extends beyond the limits of the Pyramid rhyolite and provides a fairly consistent marker above the distal flows of the Tenchen succession.

South of Armadillo Highlands at least two major centres of Kounugu volcanism have been completely destroyed by erosion, and their former locations can only be inferred from the distribution of flows, tephra and dyke swarms. Only those flows that lie close to the southern edge of the Armadillo Highlands are underlain by fluvial gravels and ash from the Armadillo Formation. Most of them rest

directly on pre-Tertiary basement or on gravel and colluvium derived from older rocks. The Nido basalt (Kounugu Member) south of Armadillo Highlands is overlain directly by rhyolite of the Spectrum Formation.

Except for minor porphyritic phases, found locally in the uppermost part of the pile, the Nido basalt is remarkably uniform, medium to dark grey, fine grained, with less than 5% small tabular plagioclase phenocrysts and sparse equant crystals of black pyroxene.

In contrast to its compositional uniformity, the Nido basalt exhibits a great variety of depositional facies. The thickness, vesicularity and jointing of flows, the relative proportions of lava to tephra, as well as the size and degree of welding of the tephra, all vary with distance from their source. In addition, some of the Nido basalt poured into bodies of water producing a quenched facies which bears no resemblance to its subaerial equivalents.

Tenchen Member

Flows and pyroclastic deposits of Tenchen basalt are exposed on both the east and west sides of Mount Edziza north of Raspberry Pass. On the east, steep-walled valleys cut across the principal areas of Tenchen volcanism, exposing the proximal flows and thick piles of tephra as well as feeder dykes, necks and subvolcanic intrusions in the source region (Fig. 66). Farther west, along Mess Creek Escarpment and in the canyon of Elwyn Creek the thin distal edge of the Tenchen pile is exposed in tiers of brown-weathering, columnar flows.

The western exposures include the eroded remnants of at least three major eruptive centres, Alpha peak, Beta peak and Gamma peak (Fig. 65), as well as isolated lenses of tephra and groups of flows from an unknown number of satellitic vents which have since been destroyed by erosion or buried beneath younger flows (Fig. 67).

Alpha peak

The actual vent and conduit system of Alpha peak are not exposed, but from the distribution of tephra and the slope of the upper contact the main source must have lain close to the present position of The Pyramid. Cliff sections on the south side of Pyramid Creek contain 50 to 60% coarse tephra, including bright red, spindle-shaped and 'cow-dung' bombs up to 0.6 m across, interlayered with irregular, highly vesicular, randomly jointed flows with rough hackly surfaces. On the opposite side of Pyramid Creek, the section contains less coarse tephra, but includes

MOUNT EDZIZA

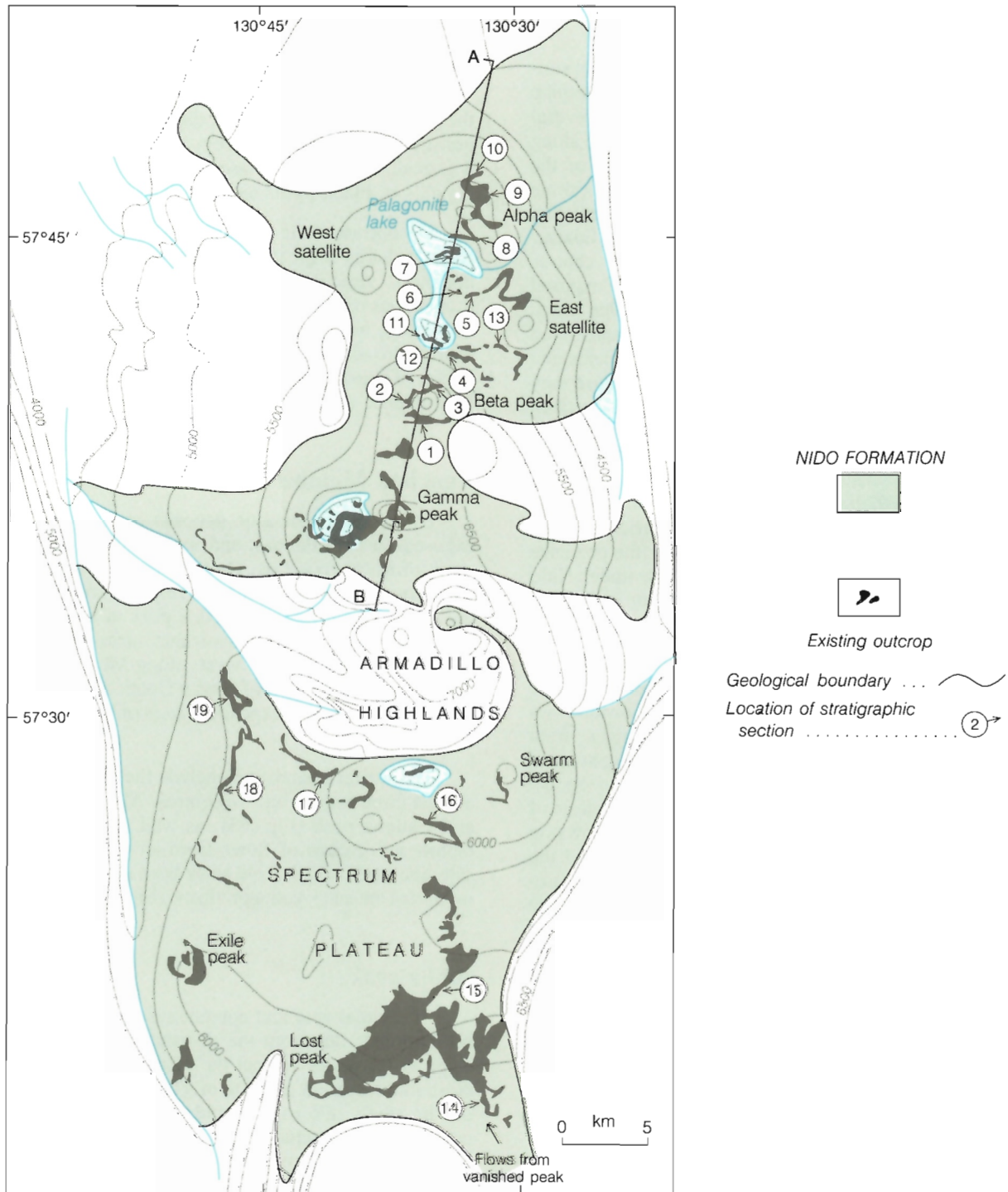
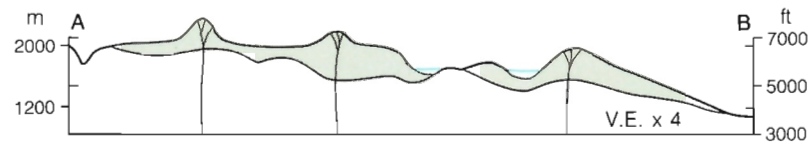


Figure 65. Paleogeological map showing the inferred maximum extent of Nido basalt at the end of Nido time, and schematic cross-section. Stratigraphic sections are shown in Figure 68.

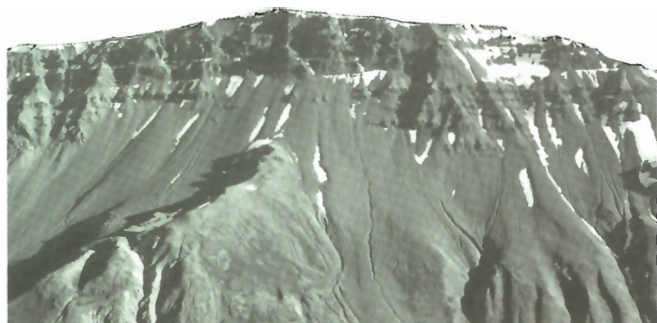


Figure 66. A typical section of Tenchen flows and tephra layers on the south side of Nido Creek. GSC 202468-R.

several prominent red layers of agglutinated, highly oxidized cinders which slope gently toward the northeast and must have been deposited directly from a fountaining vent. In contrast, the eastern and central exposures of the Alpha pile in creek canyons southeast of The Pyramid, are mainly uniform, rusty-weathering columnar flows separated by relatively thin, clinkery beds of flow breccia which were deposited by sloughing off the end of the advancing flows rather than by issuing directly from a vent.

Lenses of gravel, minor sand and silt are interbedded with the flows more or less at random throughout the Alpha pile (Fig. 68). The well-rounded, hematite-stained clasts are mainly basalt but fluvial beds below an elevation of about 5000 ft. (1525 m) include a significant proportion of chert-pebble conglomerate clasts from the Upper Jurassic,

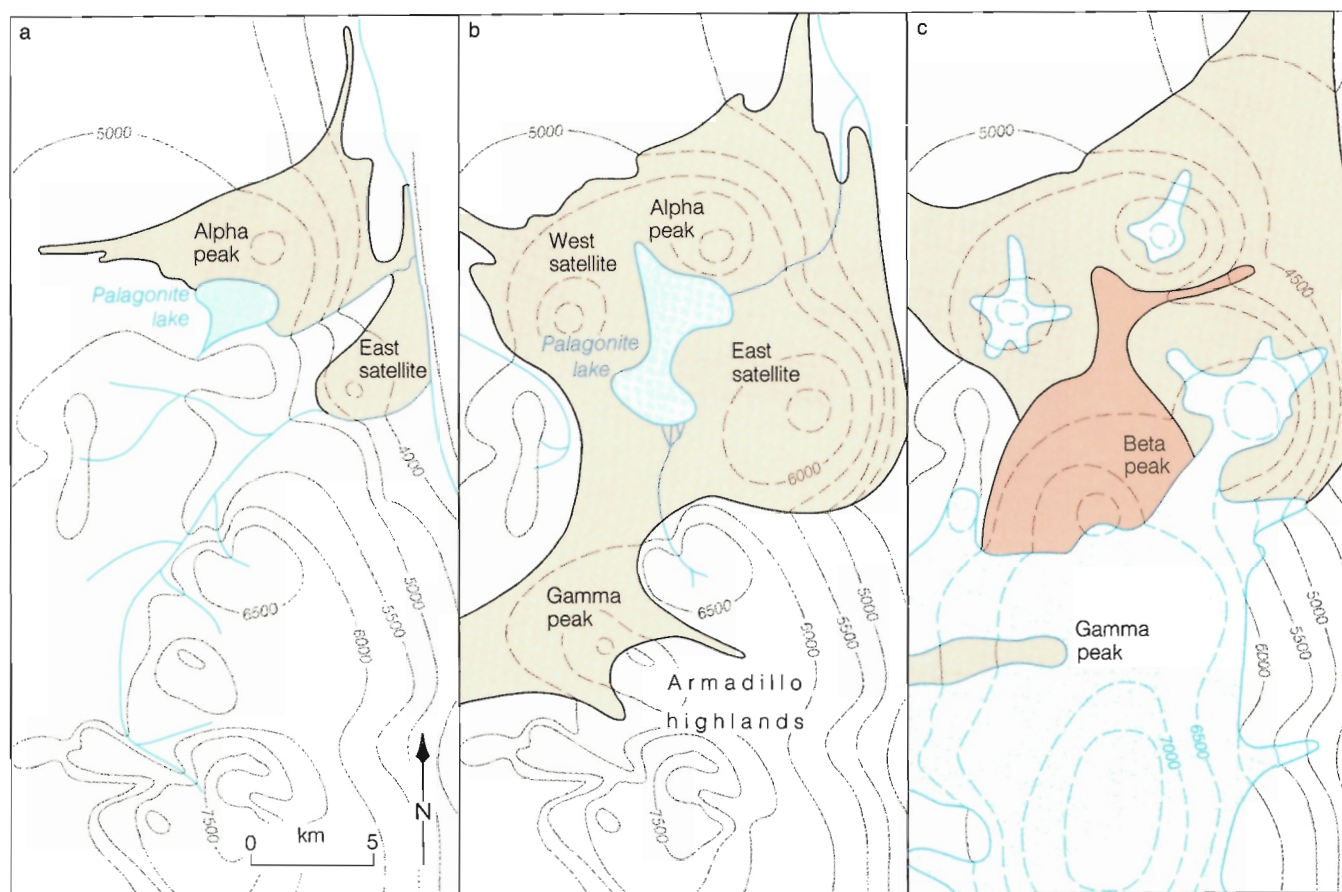


Figure 67. Three stages in the evolution of the Tenchen Member of the Nido Formation: (a) initial eruption of Alpha peak and East satellite resulting in the ponding of Palagonite lake, (b) maximum extent of Alpha peak and its satellites, initial eruption of Gamma peak and influx of fluvial sediments from the Armadillo highlands into Palagonite lake, (c) eruption of Beta peak and continued eruption of the Gamma peak vent (dark red) during a period of alpine glaciation (see Fig. 77)

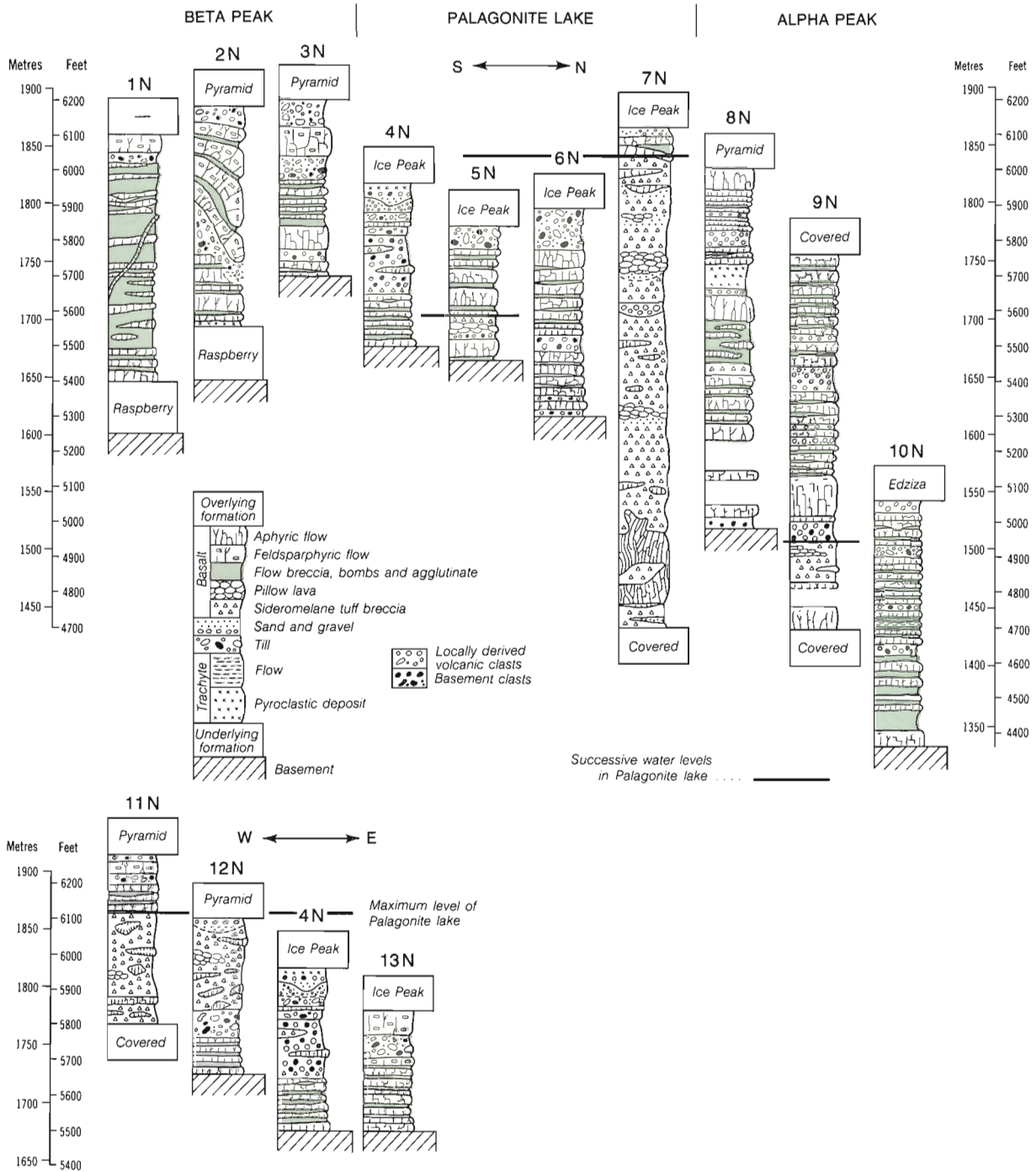


Figure 68. Stratigraphic sections of the Alpha peak and Beta peak piles along north-south and east-west profiles through the northern part of the Tenchen lava field. Successive levels of Palagonite lake are defined by the upper limit of hyaloclastite and pillow lava. Section numbers (1-14) refer to locations shown on the paleogeological map (Fig. 65). N, Nido Formation.

Bowser Formation and clasts of rhyolite, trachyte and obsidian from the Armadillo. Shingled boulders and crossbedded sandy layers indicate a northerly direction of transport, and suggest that the foreign clasts were derived from the Armadillo Highlands where streams had already cut through the mantle of Armadillo rhyolite into the underlying Bowser Formation. Where early flows from Alpha peak entered this northerly flowing drainage system, the gradient was disrupted; aggrading gravel bars formed behind the obstruction and were covered by later flows. As each successive flow of basalt entered the valley, it forced the streams out of their normal channels to ever higher spillways across the lava until the entire drainage system was eventually re-routed. Fluvial layers above an elevation of about 5000 ft. (1525 m) in the Alpha pile contain locally derived basalt clasts only, indicating that streams from the Armadillo Highlands had either been forced into some alternate route or that gradients were so reduced that gravel could no longer be transported as far north as Alpha peak.

In addition to buried lag gravels the edifice of Alpha peak also contains a few thin lacustrine deposits of fine sand and laminated silt, as well as piles of sideromelane tuff-breccia which accumulated in transient lakes ponded behind lava dams (Fig. 69). Lenses of tuff-breccia associated with quenched flows are found throughout the Alpha pile but their number and thickness increase toward the south and culminate in a nearly continuous waterlain pile on the southern flank of the volcano. On the north side of the pile, in Pyramid Creek Valley, a 30 m layer of sideromelane tuff-breccia and pillow lava occurs at the base of the section and is overlain by 15 m of lag gravel. Farther south similar

layers of tuff-breccia interbedded with normal subaerial flows appear at progressively higher levels, and south of The Pyramid, near the centre of the Alpha edifice, water-quenched lava toes, pillows and tuff-breccia make up more than half the section. There the coarse tuff-breccia is associated with up to 15 m of fine brown tuff comprising highly altered, fine basaltic ash with lapilli of frothy brown sideromelane and a few larger chunks of pale brown, altered basalt. These tuffs are believed to have formed by the fountaining of hot ash and lapilli from a nearby vent directly into a body of water.

A pile of sideromelane tuff-breccia and quenched lava tongues more than 365 m thick forms the southern flank of Alpha peak. It is exposed in structureless, yellow-brown cliffs which form most of the steep-sided ridge between The Pyramid and Tenchen Creek (Fig. 70). The tuff-breccia is made up of angular and subangular blocks and irregular globules of medium grey basalt up to 0.3 m across suspended in a completely unsorted matrix of subvitreous pale brown, hydrated fragments of basalt cemented by lapilli and ash-sized shards of yellow-brown basaltic glass (Fig. 71). Many of the small globules have an onion-skinned texture in which an outer rind of thin laminated glass surrounds a roughly spherical core of subvitreous basalt. Similar rinds, many with a lustrous yellow-brown sheen, coat pillows and quenched lava toes within the tuff-breccia.

Large irregular bodies of dark brown weathering basalt with small diameter curved and radiating columns form sill-like and bulb-like masses within the tuff-breccia. One such body near the base of the pile is roughly tabular and nearly 30 m thick. Locally, it rests on tuff-breccia like a flow while

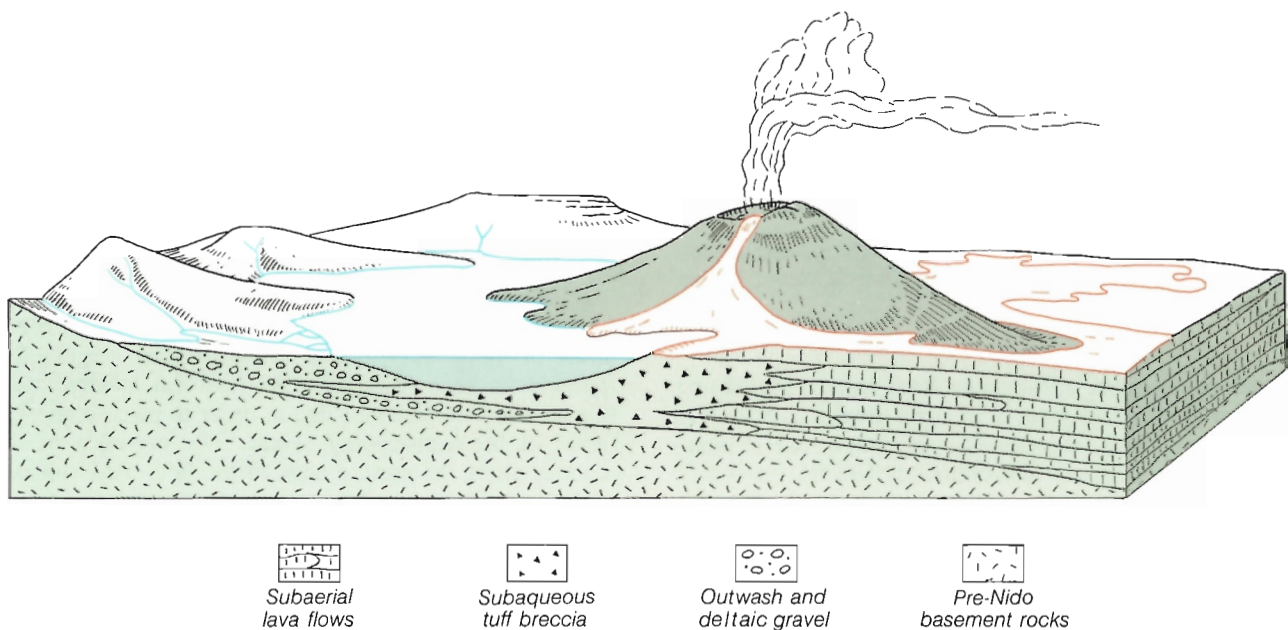


Figure 69. Schematic block diagram showing the relationship of Alpha peak to Palagonite lake and deposits of fluvial gravel from the south. View looking west toward an erosional remnant of Sezill volcano in background.

MOUNT EDZIZA

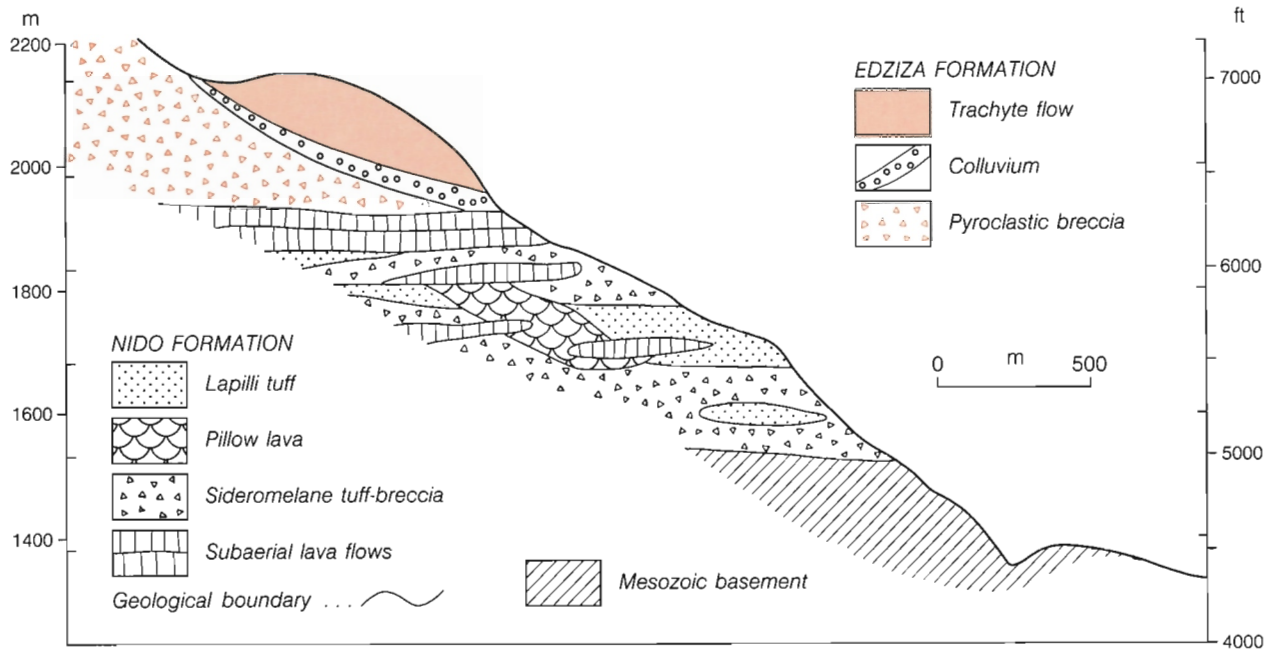


Figure 70. Sketch showing the relationship between Nido hyaloclastite and lava flows on the ridge between The Pyramid and Tenchen Creek.



Figure 71. Cliffs of Nido sideromelane tuff-breccia on the north side of Tenchen Creek. Summit area of Mount Edziza in background. GSC 202468-S.

at other places parts of the same mass have intruded and interfingered the tuff-breccia to form irregular dyke-like and neck-like forms. It passes laterally into a zone of inter-layered tuff-breccia and discontinuous lensoid masses of basalt.

In the upper third of the tuff-breccia pile, the proportion of tabular and lensoid bodies of basalt increases and imparts a crude stratification to the otherwise chaotic deposit. Lenses of well stratified, locally-derived, pebbly sand up to 1.5 m thick also increase in the upper part of the section. Many of these clearly occupy small basins eroded into the tuff-breccia and in several places, the sediment layers are

overlain by pods of pillow lava that later occupied the same small basins.

Beta peak

Prominent step-like outcrops of Tenchen basalt are exposed around the spurs and interflues on the east side of Mount Edziza between Tenchen and Sorcery creeks. The alternating cliffs of flat-lying, brown weathering columnar basalt and recessive ledges of interlayered scoria are the remains of a small composite shield that lay south of Alpha peak. It was formed from thin mobile flows that coalesced from several separate vents. Of these, only part of the central pyroclastic cone remains, and it has been deeply dissected. A section through it is exposed on the ridge north of Sorcery Creek where loosely agglutinated lapilli and red, oxidized spatter, enclosing larger blocks and bombs, has a crude stratification which dips gently south, away from the crest of the ridge (Fig. 72). The original height of this pyroclastic cone must have been several hundred metres higher than the present ridge in order to place it above the level of the surrounding shield. The presence of other centres along the eastern edge of the Beta peak shield can only be inferred from easterly thickening lenses of coarse tephra and bombs that are interlayered with the flows in the most easterly exposures, above Nuttlude Lake.

The bulk of the Beta peak pile is fine grained, aphyric or microphyric brownish-grey basalt. It is commonly vesicular, with voids wholly or partly filled with aragonite. However, the uppermost flows are highly porphyritic, containing up to 50% phenocrysts of clear white to amber

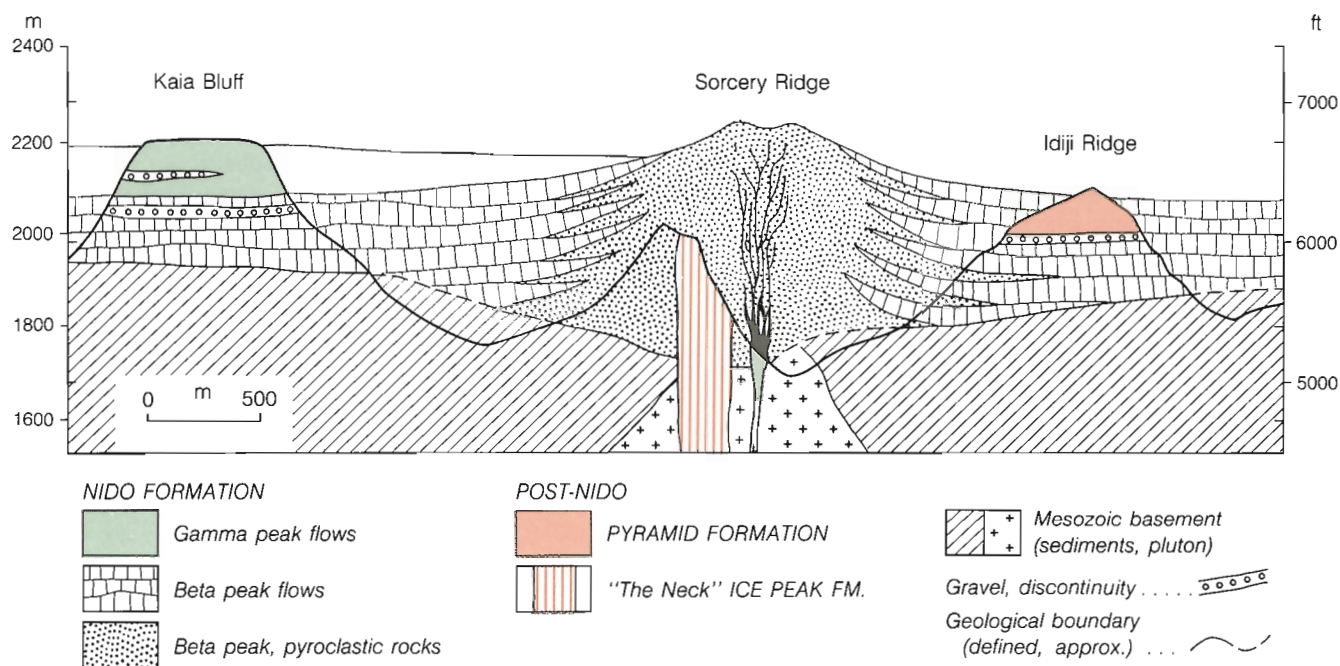


Figure 72. Restored cross-section through Beta peak showing the relationship of the existing remnants to its inferred maximum extent.

feldspar 1-3 cm across. These flows are consistently associated with layers of gravel from a few metres up to 27 m thick. The clasts are mainly basalt but a few boulders and cobbles of chert-pebble conglomerate, diorite and Armadillo rhyolite are everywhere present. Some of the gravel layers are crudely stratified and include lenses of coarse, pebbly sand which fill small channels scoured into the surface of poorly sorted, coarser gravel. More commonly, the deposits are totally unsorted. Boulders and cobbles of all sizes, some of them faceted and striated, are suspended in a fine silty to sandy matrix which shows no evidence of water sorting. These layers are clearly tills, associated with glacial fluvial outwash and channel deposits. The glacial deposits both overlie and underlie the coarsely porphyritic basalt at the top of the Beta peak section. Boulders of porphyritic basalt from Beta peak are present in some of the glacial fluvial deposits, as are layers and lenses of clear feldspar crystals, winnowed out of the tephra and redeposited in glacial fluvial channels and outwash.

Despite widespread glacial deposits interbedded with flows in the top of the Beta peak shield there is little evidence of contemporaneous volcanism and glaciation. On Idiji Ridge, about 30 m of crystal-rich, sideromelane tuff-breccia at the top of the Beta peak section suggests that some of the porphyritic basalt may have been erupted into ice-ponded bodies of water but elsewhere, the porphyritic flows are clearly subaerial. Even those that lie within the glacial-fluvial deposits are uniform sheets of columnar-jointed basalt, underlain by a mat of red oxidized scoriaceous flow breccia which extends for several kilometres. During the final stages of its development Beta peak must have been

near the margin of a fluctuating ice field from which lobes of ice periodically advanced onto the shield and receded, leaving successive layers of till and outwash gravels. Evidence that the earlier edifice of aphyric basalt was modified by erosion prior to eruption of the porphyritic flows is found on Idiji Ridge where coarsely porphyritic flows, underlain by a layer of crystal-rich tephra and subrounded colluvium, cuts steeply across the truncated flows of nonporphyritic basalt in the lower part of the pile. It seems probable that this erosion surface was formed, at least in part, by a minor glacial advance that preceded the final outpouring of porphyritic lava from Beta peak.

Palagonite lake

The thick pile of sideromelane tuff-breccia, pillow lava and subaqueous slide-debris on the south buttress of Alpha peak is only one of several features that indicate the presence of a large lake ponded between Alpha and Beta peaks during most of their active life. A similar pile of tuff-breccia forms prominent yellow-brown, structureless cliffs at the head of Nido Creek, about midway between Alpha and Beta peaks. Like the Alpha pile, the tuff-breccia on Nido Creek grades upward into subaerial flows at an elevation of about 6100 ft. (1860 m). Both piles are believed to have formed in an irregular, but at least temporarily interconnected body of water which will be called Palagonite lake (Fig. 67,69).

The southern edge of Alpha peak tuff-breccia has been eroded away and no trace of it remains on the south side of Tenchen Creek. The basement surface rises sharply towards

MOUNT EDZIZA

the south and, at least the lower half of the tuff-breccia pile, up to an elevation of about 5600 ft. (1710 m) could have been formed in a lake ponded against this surface. However, the top of the tuff-breccia stands at nearly 6100 ft. (1860 m) and, in order to reach this elevation, Palagonite lake must have been contained by barriers along its eastern and western margins that were higher than either the basement surface or the present upper level of Nido basalt on the south side of Tenchen Creek. The possibility of an ice dam is unlikely since the tuff-breccia pile is confined to one corner of the Alpha peak edifice and it is flanked on both the north and east by coeval subaerial flows at the same elevation. It seems more likely that Palagonite lake was contained by flows from one or more satellitic cones that developed southeast and southwest of Alpha peak and have since been eroded away. The presence of at least one such centre, along the eastern edge of Beta peak shield, is indicated by easterly thickening pyroclastic wedges containing high proportions of bombs interbedded with flows in the most easterly exposures on Nido Ridge.

As noted earlier, the Alpha peak tuff-breccia contains only minor lenses of fluvial gravel and slide debris except in the uppermost part where locally derived basaltic clasts have been deposited in small channels scoured into the tuff-breccia. In contrast, the Nido Creek tuff-breccia includes lenses and pods of polymict gravel and, along its eastern edge, it interdigitates with several hundred metres of crudely sorted gravel and pebbly sand which includes clasts of basement rock as well as basalt and Armadillo rhyolite.

On the east, this same gravel deposit interdigitates with normal subaerial flows of the Beta peak shield (Fig. 73). The gravel is believed to have been deposited in bars where northerly flowing rivers from the Armadillo Highlands entered the south end of Palagonite lake. Hence their occurrence between the subaerial and subaqueous facies of the Beta peak pile and the absence of foreign clasts in the Alpha Peak tuff-breccia which accumulated in the northern end of the lake, many kilometres from the inlet.

Between the Alpha peak and Nido Creek tuff-breccia piles, the Tenchen succession thins to almost 60 m and includes a random mixture of thin subaerial flows, pillow lavas, fluvial gravel and slide debris (Fig. 68). The latter are best developed around the southern flank of the Alpha peak pile where chaotic breccias containing angular to subrounded clasts of basalt, fragments of pillows and blocks of basalt up to several metres across are jumbled together in discontinuous piles up to 15 m thick. They are believed to be the product of subaqueous slides that slumped off the oversteepened south slope of the Alpha peak tuff-breccia and were swept into the centre of the lake. Large blocks are found only in outcrops as far south as Tenchen Creek. Farther south, the clastic beds are lapilli to ash sized brown tuff, similar to the matrix of the slide breccia. They were probably deposited from clouds of suspended particles that accompanied the subaqueous debris slides. Pillow lavas, basaltic gravel and thin subaerial flows in the central part of Palagonite lake must have been deposited during the early stages of its development, when the water level was low,

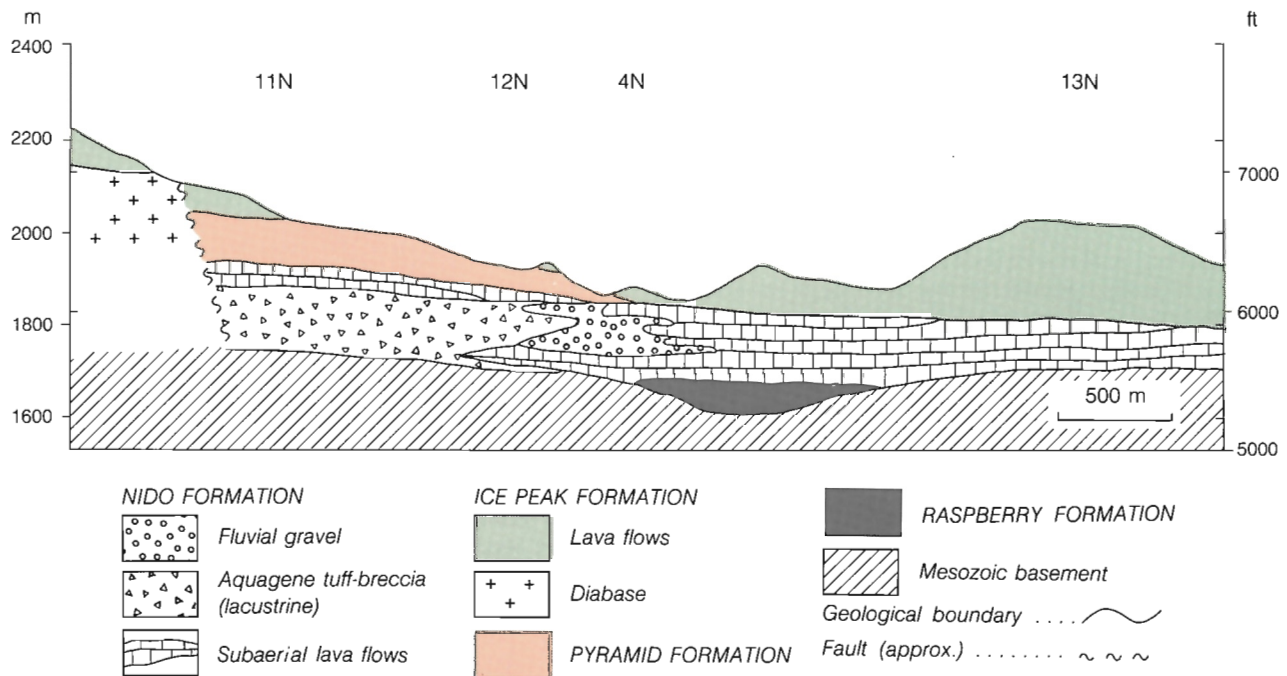


Figure 73. East-west cross-section along the axis of Nido Ridge, showing the relationship of subaerial and subaqueous flows to fluvial gravel deposited in the southern end of Palagonite lake. Numbers at top show the relative positions of stratigraphic sections in Figure 68.

and during the final stages of Tenchen volcanism when streams had cut through the eastern barriers, draining the lake and allowing the last few flows of basalt to spread out across its dry bed.

Gamma peak

The dissected central edifice of Gamma peak forms a prominent black spire, Cartoona Peak, and remnants of its western flank outcrop as far west as Mess Creek Escarpment



Figure 74. Cartoona Peak, an erosional remnant of Gamma peak volcano. GSC 125 604.

(Fig. 74). The pre-Nido surface on which it was built slopes steeply westward so it is unlikely that the eastern part of the pile was ever well developed and, what did exist, has since been removed by erosion. The eastern side of the central spire rests on Armadillo trachyte at an elevation of 7600 ft. (2315 m), at least 1000 ft. (300 m) higher than the summits of Alpha and Beta peaks. West of the summit the elevation of the basal contact drops below 6500 ft. (1980 m) within 1.5 km and, at their distal ends, Gamma flows rest on Armadillo ash at an elevation of 5000 ft. (1525 m). It is a composite pile; the lower unit consists mainly of aphyric basalt but includes a small volume of highly feldsparphyric basalt. The upper unit is olivine-rich basalt which grades locally into picrite. Both subaerial and subaqueous facies are present in each of these two main lithological units (Fig. 75).

Lower unit. The porphyritic flows of the lower, subaerial facies, are confined mainly to the northern edge of the pile, where coarsely and abundantly feldsparphyric basalt forms thick cooling units at or near the base of the Gamma pile. The rock, with clear feldspar phenocrysts up to 3 cm across, is similar to the uppermost flows which overlie glacial-fluvial deposits resting on Beta peak flows and pyroclastic deposits farther north.

Most of the lower part of Gamma peak comprises thin irregular, aphyric, brown-weathering flows interbedded with ropy, bright red, orange or chocolate-brown scoria.

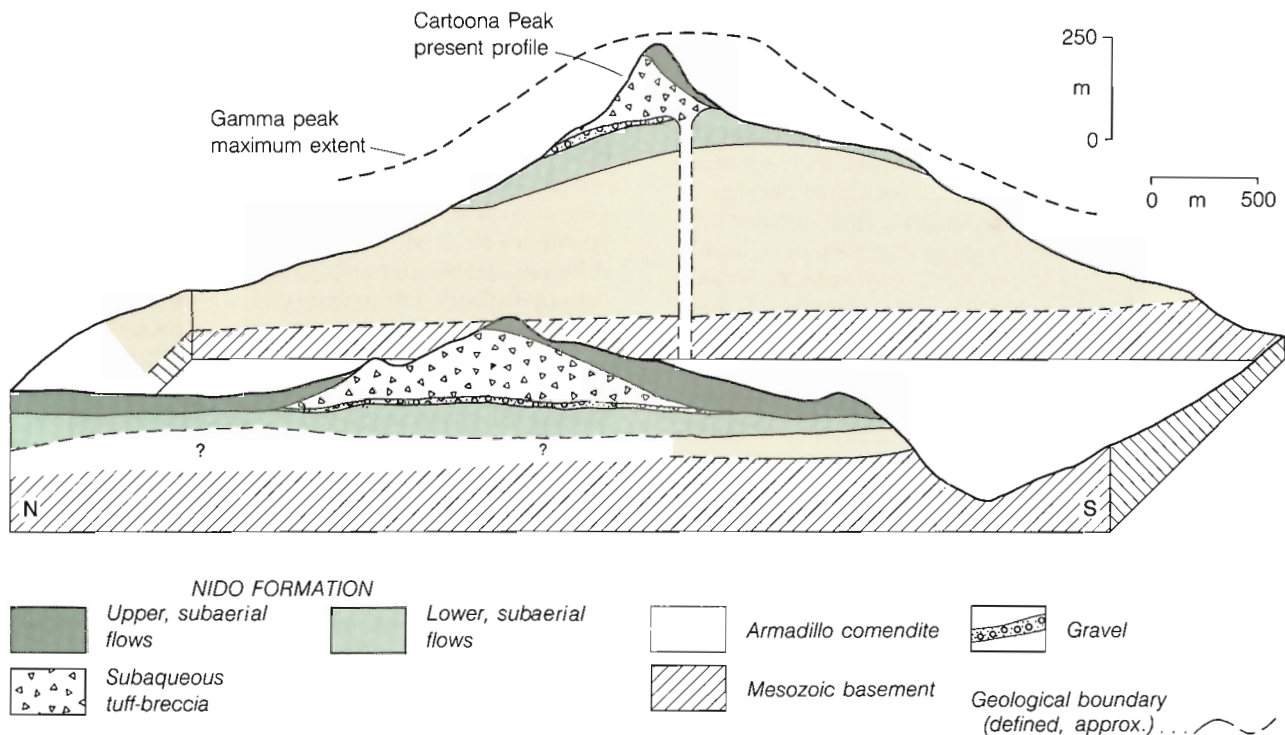


Figure 75. Schematic cross-sections through Gamma peak showing the subaerial and subaqueous facies, and the relationship of the present edifice of Cartoona Peak to the original form of Gamma peak.

MOUNT EDZIZA

The fresh rock is dark grey, very fine grained nonporphyritic or slightly porphyritic basalt containing small sparse phenocrysts of feldspar and pyroxene. The upper part of most flows is highly vesicular, containing irregular cavities, up to 2 cm across, lined with opal, aragonite and zeolites. Along the northern flank of the Gamma pile, these flows form sections up to 120 m thick. Locally, as on the south side of Shaman Creek, the flows grade into thick piles of agglomerate, tephra and discontinuous lava lenses—the eroded remnants of one of several subaerial pyroclastic cones that formed the Gamma peak complex. This particular pyroclastic pile is overlapped at an elevation of 6000 ft. (1830 m) by a succession of flows from some other much higher vent. Although it has not been identified, flat-lying subaerial flows that issued from it are exposed up to an elevation of 7000 ft. (2135 m). Lenses and pockets of fluvial gravel containing clasts of both basalt and Armadillo rhyolite are interbedded with the flows and indicate that construction of the lower, subaerial portion of the Gamma peak pile was interrupted by periods of quiescence, accompanied by erosion and the establishment of streams transporting a base load of small rounded gravel and boulders from the adjacent Armadillo Highlands. There is evidence too that some of the early Gamma flows came in contact with small glaciers or flowed into ice ponded lakes. Along the extreme northern edge of the pile, highly feldsparphyric flows are overlain by a thin layer of nonporphyritic, sideromelane tuff-breccia containing pillow fragments. This is overlain by nearly 90 m of quenched basalt that is lithologically similar to sparsely porphyritic feldspar, pyroxene basalt forming thin subaerial flows farther south. The quenched basalt is characterized by small-diameter radiating, sheathlike or curvilinear columns, or by small three-dimensional polygonal jointing. The surfaces of pillow-like forms and lava tongues have a pronounced selvage of dense black subvitreous basalt which contrasts with the fine grained grey vesicular rock in their interior. Individual flow units in the quenched sequence have no lateral continuity. Unlike their subaerial counterparts, the flow units have no associated partings of oxidized flow breccia or scoria. Instead, small tubular flow tongues are stacked randomly one against another or locally separated by isolated pockets of fine glassy particles, spalled from the quenched lava surface. The location of these deposits, midway between Beta peak and the growing edifice of Gamma peak, suggests that they were formed where northward flowing Gamma lava entered a meltwater lake or impinged on a small glacier between the two peaks.

Upper unit. The olivine-rich basalt that forms the upper part of Gamma peak includes two distinct subunits: (1) a lower subaqueous pile, and (2) an upper blanket of subaerial flows (Fig. 75).

Subaqueous subunit. The subaqueous pile can be further subdivided into a proximal or vent facies, and a distal, tuff-breccia facies. The vent facies is well exposed on 150 m cliffs on the northwest side of Cartoona Peak where a complex of tuff-breccia, pods of pillow lava and quenched flow

tongues are cut by subvertical irregular, dyke-like masses of vesicular basalt with small radiating clusters of columns. The tuff-breccia in this facies is a chaotic mixture of large and small clasts having no stratification or sorting. Large irregular masses of vesicular basalt, up to several metres across, partly surround or actually enclose pockets of matrix. Many smaller globules of lava are also irregular and tend to be molded around clumps of matrix, in some cases appearing to have been deformed after deposition. The matrix itself is a porous, but cohesive, aggregate of quenched basalt fragments which range in size from a few centimetres down to fine lapilli. Fragments of more than about 2 cm across have cores of black, subvitreous basalt surrounded by rims of yellowish-brown sideromelane, whereas smaller fragments consist entirely of glass. Discontinuous flow fragments and pockets of tubular pillow lava within the pile of tuff-breccia commonly have steep initial dips and, like the matrix fragments, they have a surface rind of yellow-brown to black sideromelane. Feeder dykes, sills and irregular intrusive masses up to a few metres across cut all the rocks in the vent facies, forming a random network of resistant ribs and ledges on the less resistant outcrops of tuff-breccia. A quenched selvage from a few millimetres to about 2 cm thick of black subvitreous basalt is present along contacts between many of these intrusive bodies and the tuff-breccia, but no sideromelane rind is present. Small spherical vesicles, mostly less than 2 mm in diameter, are aligned in successive planes parallel to their contacts and a few centimetres apart. Small diameter columns, commonly less than 0.3 m across are well developed normal to most contacts.

The distal tuff-breccia facies is defined by a relatively narrow lobe of low rounded hills which extend westward, across the surface of the Mess Creek plateau for about 5 km from the central vent of Gamma peak. Unlike the chaotic, structureless pile in the vicinity of the vent, the distal tuff-breccia exhibits some degree of layering and sorting (Fig. 76). In most exposures the matrix consists of fairly well sorted, loosely cemented, lapilli to coarse sand-sized granules of yellowish brown sideromelane and small, angular pebbles of black basalt. Crude bedding, due mainly to slight differences in the size and colour of granules, give most outcrops a distinctly layered aspect. Large blocks of grey vesicular basalt suspended in the fine brownish matrix are commonly concentrated in fairly well defined beds and in places coarse blocks 0.3 m or more across grade through smaller clasts into sandy layers. Large blocks at the base of such sets have deformed the layering in underlying strata whereas the overlying beds are undisturbed or lap against the upper part of the blocks. Unlike the highly irregular globules in the tuff-breccia near the vent, large blocks in the distal facies are angular, mostly wedge-shaped or bounded by polygonal fracture surfaces, suggesting that they were derived from broken pillows and quenched flow lobes. Although most of the distal tuff-breccia is more or less bedded, its internal structure is highly disorganized. Initial dips up to 40° vary from outcrop to outcrop. Slump structures, scoured channels and large scale crossbedding are common and locally, the well bedded sequences are interrupted by thick units of structureless slide debris.



Figure 76. Outcrop of crudely bedded tuff-breccia in the distal facies of the Gamma peak pile. GSC 202468-T.

The tuff-breccia facies of Gamma peak olivine basalt is clearly of subglacial origin. Tills and glacial fluvial gravel associated with the uppermost porphyritic flows from Beta peak provide evidence of earlier glaciations in the region. The extent of this ice must have fluctuated widely during the period of Gamma activity. Ice cover during the waning stages of Beta activity was followed by a recession during which the lower, mainly subaerial, pile of feldspar pyroxene basalt was built. At that time only small remnants of ice were present. One of these, between Beta and the developing edifice of Gamma peak provided the only ice contact features noted in the lower pile. By the time Gamma peak entered its second stage of activity and began to erupt olivine basalt, the glaciers had again expanded into a broad ice cap that covered the lower, subaerial shield of Gamma peak and extended several kilometres westward onto the flanking plateau (Fig. 77). The chaotic breccias of the vent facies accumulated in a meltwater lake thawed into the ice and churned by repeated phreatic explosions. Most of the material in the distal facies was probably initially deposited on the ice and later slumped or was carried by streams into a long linear trough, cut by thawing, on the surface of the ice down-slope from the vent lake.

Subaerial subunit. The subaqueous vent breccias on the present summit of Cartoona Peak are overlain by remnants of subaerial flows. Despite the steep slope on which they rest (initial dips up to 40°), most of the flows are more than 3 m thick and locally, single cooling units up to 60 m thick rest on slopes of 10-15°. The ability of this lava to cling so tenaciously to the slopes of the old edifice suggests that it

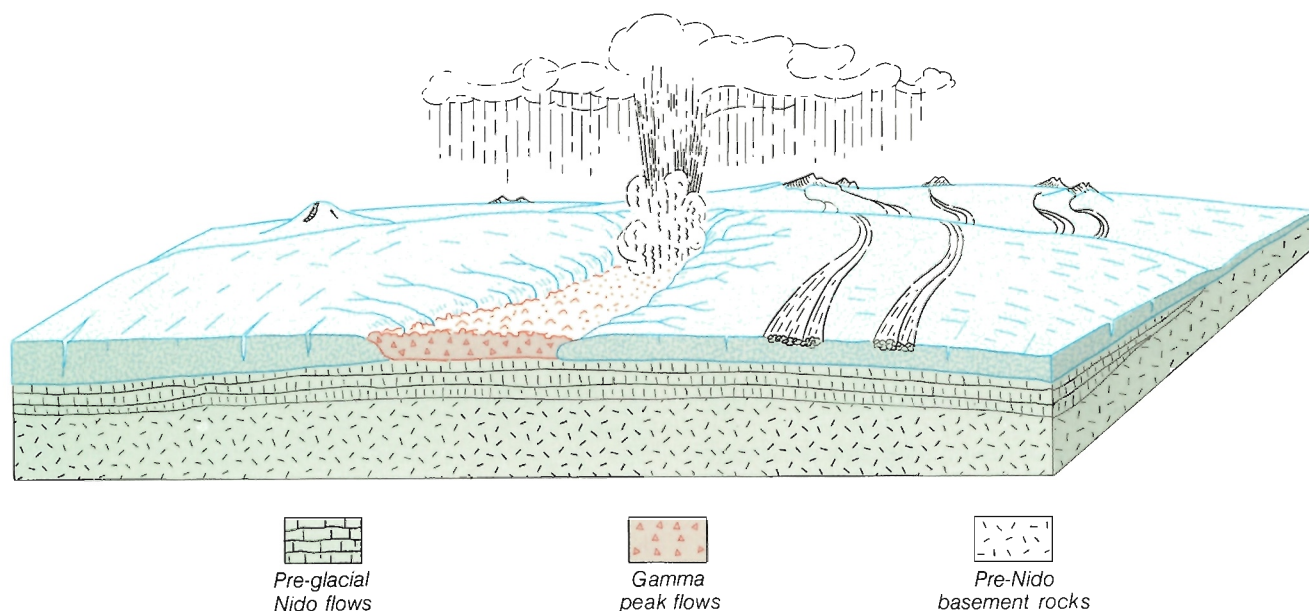


Figure 77. Schematic block-diagram showing late stage eruption of the Gamma peak vent during a period of extensive ice cover. View looking east shows Beta peak in the left background and nunataks in the Armadillo Highlands in the right background.

was highly viscous, yet remnants of lithologically similar flows occur several kilometres farther west where they form prominent rimrocks 3-6 m thick along the edge of the plateau, facing Walkout Creek. Columnar or blocky rectangular jointing and horizontal flow cleavage are well developed. These distal lobes of lava must have been diverted by, and flowed around, the old piles of subaqueous tuff-breccia. They are commonly underlain by a thin veneer of colluvium which includes clasts and pockets of the sideromelane breccia, but except on the central edifice itself, these are rarely more than a few metres thick.

Most of the lava in the upper subaerial unit appears to have issued rapidly from a vent near the summit of Gamma peak. No more than two or three cooling units are found in any section and, more commonly, only one flow is present. In the distal lobes, the rock is medium to light grey, light-grey-weathering, fine grained basalt with rare 1-3 mm phenocrysts of pale yellowish-green olivine. At two localities the basal flows of this distal lava contain clusters of olivine nodules.

The rimrock along the north fork of Walkout Creek, 5 km west of Gamma peak, contains about 5% olivine phenocrysts, sparse 2-4 mm phenocrysts of clear glassy plagioclase in stout prismatic crystals, and rare phenocrysts of black pyroxene in crystals usually less than 1 mm across. The percentage of phenocrysts increases in the more easterly exposures and the thick, proximal flow-remnants on the upper slopes of Gamma peak are highly porphyritic, containing up to 30% phenocrysts of olivine, plagioclase and pyroxene in about equal proportions. An analogous change is present in some of the single thick flows on the upper flanks of the peak. These are commonly sparsely porphyritic at the base and become increasingly porphyritic upward. Except for pyroxene, which is coarser grained (up to 1 cm) in the highly porphyritic phases, the phenocrysts vary little in size either within a single cooling unit, or in distal compared with proximal flows.

The systematic increase in phenocryst content with time provides a rational explanation for the observed difference in mobility of the distal and proximal flows. The first, aphyric or slightly porphyritic magma was highly mobile. It streamed down the slope of the main edifice around the piles of tuff-breccia at the base of the old cone and flowed to the outer edge of the pile, leaving little record on the steep slopes surrounding the vent. In contrast, the crystal-rich magma erupted near the end of the event was more viscous and consequently piled up in thick flows near its source.

There is no evidence of ice or water contact features within the subaerial subunit. The ice field that formerly covered Gamma peak and the surrounding plateau must have receded beyond the outer limits of the pile prior to eruption of the final pulse of olivine basalt from the central vent.

Kounugu Member

South of Raspberry Pass, sections of Nido basalt outcrop around the periphery of the Spectrum Range (Fig. 65). They are treated as a separate member, the Kounugu, because they are physically separated from the Tenchen by the broad east-west valley of Raspberry Pass, and because this southern part of the Nido pile extends beyond the limit of pre-Nido formations which define the base of the Tenchen Member farther north. Along the northern edge of this terrane, the Kounugu flows rest on the distal edge of Armadillo lavas, ash flows and pumice deposits, but farther south they form the basal unit of the pile, resting either directly on basement or on a layer of colluvium, gravel or slide debris which covers the old basement surface (Fig. 78). Deep erosion and extensive cover by younger rocks have obliterated the vents from which this lava issued, but indirect evidence points to at least four separate centres: 1. Swarm peak, 2. Vanished peak, 3. Lost peak, and 4. Exile hill.

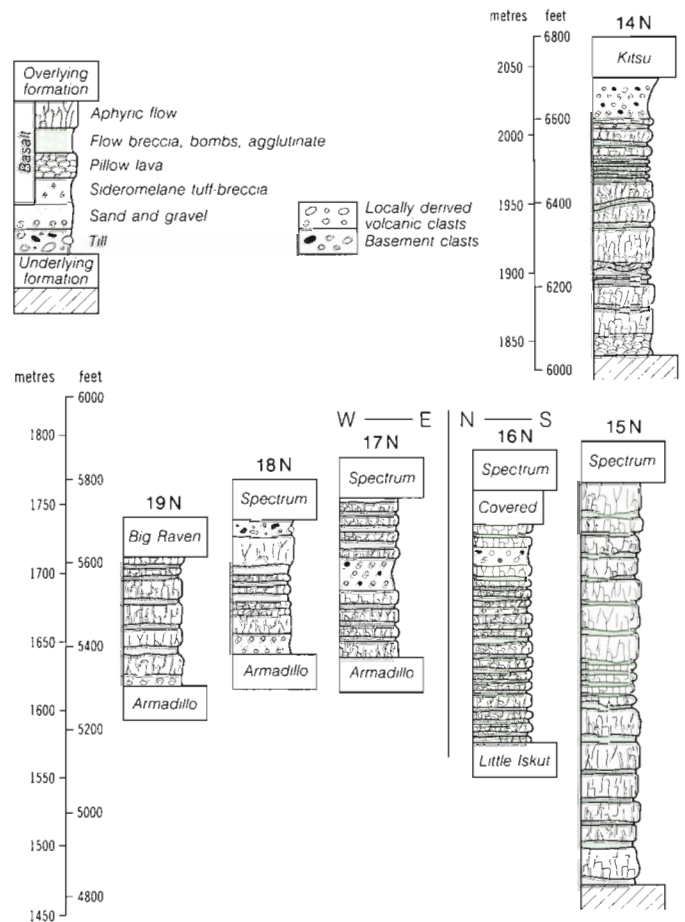


Figure 78. Stratigraphic sections of the Kounugu Member of the Nido Formation. Section numbers refer to locations shown on Figure 65, N, Nido Formation.

Swarm peak

Flows believed to have originated from Swarm peak are exposed around the southern end of the Spectrum Range where they form prominent cliffs in the escarpment facing Raspberry Pass and Mess Creek on the west, and Little Iskut River and Artifact Creek on the east. The northern edge of the pile laps against the steep southern slope of the Armadillo Highlands and the southern edge is almost completely covered by younger flows and domes of the Spectrum Range. The pile slopes gently westward and is more than 16 km long. On the east side, along Little Iskut River, the basal flows rest on Armadillo trachyte at an elevation of nearly 6000 ft. (1800 m). The elevation of this contact becomes progressively lower toward the west and along Mess Creek Escarpment, the basal flows rest on Armadillo-bearing tills and glacial fluvial gravel deposited at an elevation of 5100 ft. (1556 m).

The total thickness of the pile is rarely more than 90 m. An exception is found on Stewbomb Ridge where the thin, Swarm peak basalt flows and interlayered gravel beds have a combined thickness of more than 180 m. The Swarm peak flows are relatively thin, commonly from 1.5-6 m, with thick columns. They weather to a dark lustrous brown, nearly black surface and the ropy, highly vesicular layers of interbedded scoria are black with streaks and patches of red and bright orange. The basalt is commonly a dense black or very dark grey, nonporphyritic rock, though small sparse phenocrysts of feldspar are present in some flows. Many flows, particularly in the western source area are highly vesicular. Large irregular voids, as well as small spherical or elliptical vesicles, are lined with botryoidal goethite and partly or wholly filled with radiating crystals of white or amber aragonite. Although small crystals of aragonite are ubiquitous in the older basalts of the Mount Edziza Complex, they are particularly well developed and abundant in the Swarm peak lavas. In some of the more porous flows, aragonite forms up to 20% of the rock volume, mostly in amygdules less than 2 cm across, but in some places, forming radiating crystal clusters up to 25 cm across. In these larger voids, individual aragonite crystals are up to 1 cm thick and 15 cm long.

The source of the Swarm peak basalt must have been at the extreme eastern edge of the pile. It probably consisted of a group of several vents, none of which developed a large composite cone. The great lateral extent of the thin Swarm peak flows indicates a very mobile lava. Most of it must have flowed westward down the existing slope and accumulated in distal lobes leaving only a thin veneer of flows and a few cinder cones in the source area. Lenses of red, oxidized scoria containing spindle-shaped bombs are present in the section facing Little Iskut River and a 30 m layer of similar pyroclastic debris is present in the upper part of the section near the centre of Artifact Ridge. These few fire fountain deposits are all that remain of small pyroclastic cones that formerly clustered along the eastern edge of the Swarm peak pile. North of the scoria lenses in Little Iskut escarpment, the entire Kounugu basalt succession has been

removed by erosion, revealing a swarm of vertical, north-trending dykes (Fig. 79) that cut obliquely across the pre-Kounugu strata forming Swarm Ridge at the southeast end of Raspberry Pass. The 0.5-2 m wide dykes form prominent black ribs which stand out in bold relief against the poorly consolidated, light coloured layers of Little Iskut and Armadillo pyroclastic deposits which they cut. The dyke rock is fine grained, nonporphyritic basalt, similar to, and probably genetically related to the Swarm peak flows.

The north-south orientation of the dykes is roughly parallel with the regional distribution of the Nido volcanoes along the eastern edge of the Edziza pile. It seems probable that the dyke swarm exposed on Swarm Ridge is only one small part of a regional fracture system through which much of the Nido basalt reached the surface.

Nearly all of the Swarm peak flows are subaerial, but a single 45 m thick lens of palagonite tuff-breccia, near the base of the section on Artifact Ridge is clearly waterlain. There are no ice contact features elsewhere in the Swarm peak pile, so it is unlikely that the tuff-breccia is of subglacial origin. A more probable explanation is the ponding of



Figure 79. North-south dykes on Swarm Ridge, near the eastern end of Raspberry Pass, believed to be part of the feeder system through which the Swarm peak basalt was erupted. GSC 202468-U.

a small lake behind early Swarm peak flows followed by quenching and brecciation of subsequent flows that entered the body of water. The tuff-breccia is underlain by a few subaerial flows, or lenses of scoria, and these in turn are underlain by fluvial gravel deposits up to 12 m thick which rest directly on Armadillo trachyte. This gravel, which includes both trachyte and basalt cobbles and boulders, must have been deposited by streams flowing southward, out of the Armadillo Highlands. Channels cut into the upper surface of the gravel are exposed at several places along Artifact Ridge. They vary from 2-7 m in depth and are filled with basalt flows erupted during the initial stage of Swarm peak activity. Radial or fan-shaped clusters of columns, perpendicular to the cross-section of the old channels, are well developed in these flows. The basal, channel-filling flows are commonly overlain by a thin veneer of gravel on which the subaqueous tuff-breccia rests and similar gravels are interlayered with subglacial flows along the edge of the lens of tuff-breccia. The latter are believed to be lag gravels deposited by streams that bypassed the original obstruction after the lake had been displaced by lava.

Streams carrying gravel southward off the trachyte piles of Armadillo Highlands were diverted westward and merged with streams flowing northward off the high granitic terrane farther south. Thus, gravels interbedded with and overlying the distal end of Swarm peak flows exposed along Mess Creek Escarpment consist mainly of Swarm peak and older basalt, but also include small cobbles of Armadillo trachyte plus boulders and cobbles of granitic and other basement rocks (Fig. 80).

Vanished peak

The Vanished peak flows outcrop around the southeastern margin of the Spectrum Range where sections up to 365 m thick rest on the pre-Edziza basement surface. The northwestern edge of the pile is buried beneath younger rhyolite and trachyte of the Spectrum Range, whereas the southern edge laps against the steeply rising basement surface. At its thickest part, south of Kounugu Lake, the section rests directly on basement rocks at an elevation of 4850 ft. (1480 m). From the lake, the basal contact can be traced southward for 10 km to an elevation of 6200 ft. (1890 m). There, at the south end of the map area, only a few small remnants, none more than 90 m thick, form buttes on the deeply dissected basement terrane. South of the map area no evidence of their source is preserved among the rugged, ice encrusted ridges of Mesozoic sedimentary and plutonic rocks that comprise the Hankin Peak Massif.

At the head of Ball Creek, where erosion has stripped away the overlying Spectrum rocks, the Vanished peak flows form a series of low black terraces that contrast sharply with the brightly coloured Spectrum rhyolite and trachyte (Fig. 81). Elsewhere, the Vanished peak flows form prominent dark cliffs at the base of the Spectrum pile. Most of the flows are from 6-15 m thick with stout, well-formed columns which weather to a dark lustrous brown

surface. Interbedded layers of scoria are relatively thin, usually 0.5-1.5 m, and consist entirely of blocks, cinders and clinkers sloughed off the toe of the advancing flow. No primary pyroclastic deposits were found interlayered with the Vanished peak flows.

With a few exceptions, the Vanished peak basalt is a fine grained, dark grey, nonporphyritic rock. A single 2 m thick flow of picritic basalt in the upper part of the section north of Kounugu Lake, contains up to 30% clear, yellowish-green olivine phenocrysts, and proximal flows at the extreme southeast corner of the pile are moderately feldsparphyric. Vesicles, abundant in the upper part of most flows, are commonly lined with goethite, opal, quartz and rarely with calcite and aragonite. The quartz forms encrustations of tiny, perfectly terminated, prismatic crystals.

The Vanished peak flows clearly originated from a source that lay in the higher mountains south of the map area. The fluid basaltic lava must have been channelled northward through a relatively narrow valley and discharged onto the broad, upland surface of Spectrum Plateau where it spread out in thin, flat-lying lobes. The entire Vanished peak pile must have been erupted during a period of glacial recession. The only evidence of water-quenched flows is confined to the extreme southeast part of the pile where about 12 m of pillow lava and palagonite tuff-breccia form the basal member of the pile. These deposits rest directly on basement near what must have been the bottom of the distributary valley through which the flows were channelled, and they probably formed in a lake that was rapidly filled by the first surge of lava. The rapidity with which the Vanished peak flows accumulated is reflected in the scarcity of interlayered fluvial deposits. Only a few thin lenses of gravel were observed, and all of these are in the proximal, valley-filling succession where streams continued to flow northwest out of the Hankin Peak highlands during Vanished peak activity (Fig. 78). The clasts are almost entirely of basement rocks, suggesting only little erosion of the volcanic edifice itself during the period of its activity.

Lost peak

Lost peak (Fig. 65) rises to a prominent black pyramid-shaped cone near the southwestern edge of Spectrum Plateau. The upper part of the edifice and most of the western buttress consist of quenched lava toes, pillows and sideromelane tuff-breccia, whereas the eastern flank consists mainly of thin subaerial flows interlayered with thick scoria beds. The edifice is underlain by a few subaerial flows at the distal end of the Vanished peak pile, and a thick layer of coarse fluvial gravel is commonly present along the contact. The cobbles and boulders in these deposits are mainly fine grained, nonporphyritic basalt of Vanished peak type indicating a significant lapse of time between the end of Vanished peak volcanism and the onset of Lost peak activity. This is consistent with the change from subaerial to subaqueous conditions during the period between Vanished

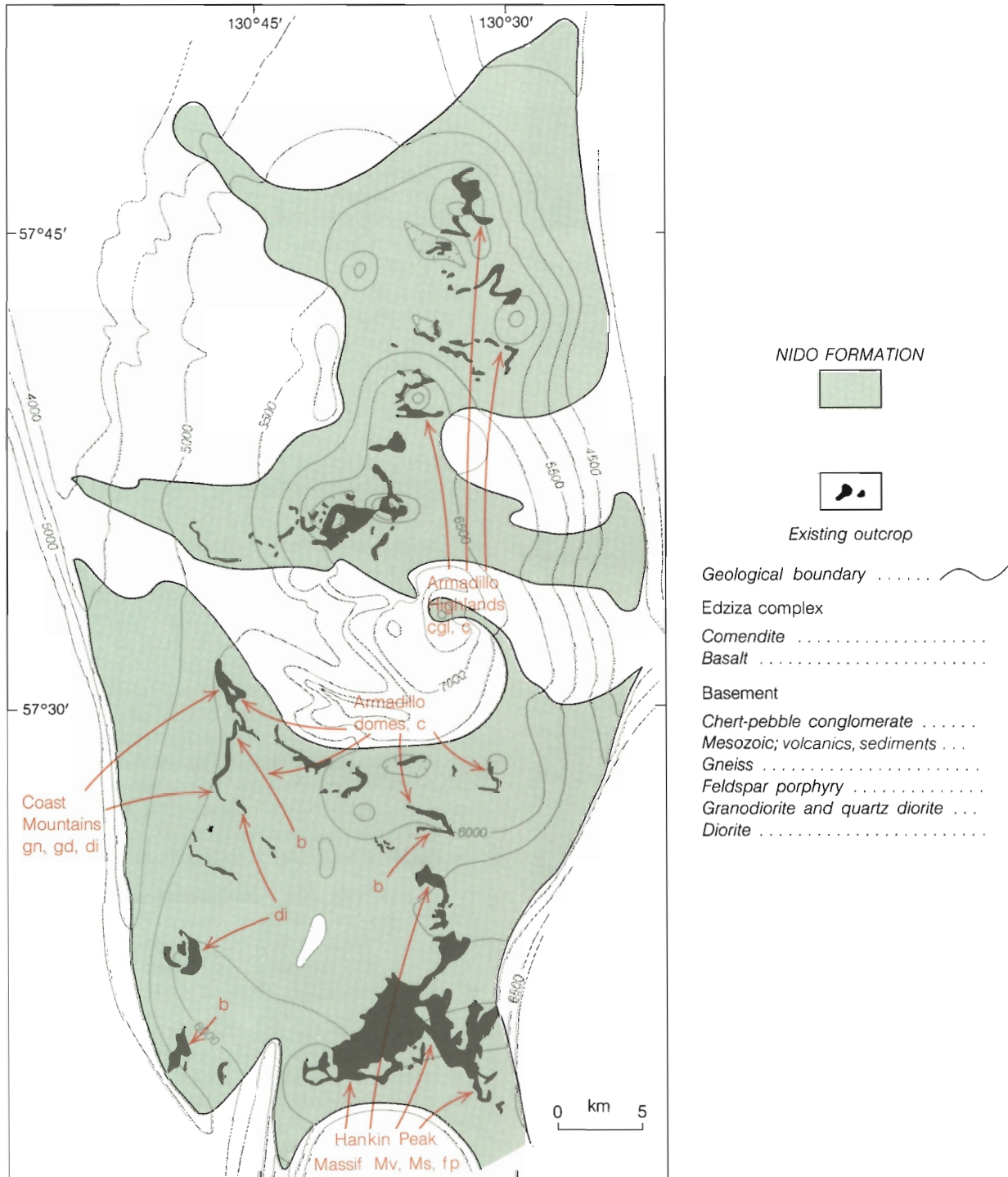


Figure 80. Map showing provenance and depositional areas of cobbles and boulders in fluvial deposits under and interbedded with Nido basalt flows.



Figure 81. Looking northwest across Kounugu Lake and Spectrum Plateau. Basalt flows of the Nido Formation form the dark coloured terraces on the plateau and the section at the base of Kounugu Mountain (background) where Nido flows are overlain by rhyolite of the Spectrum Formation. GSC 204627-A.

peak and Lost peak activity. No glacial ice could have been present during the emplacement of the underlying Vanished peak flows and their subsequent burial by fluvial gravel, whereas the western side of the Lost peak pile must have been ponded against a thick lobe of ice encroaching on the Spectrum Plateau from icefields in the Coast Mountains to the southwest.

Exile hill

Remnants of the Exile hill pile are preserved on Arctic Plateau where up to 180 m of basalt flows are exposed in isolated buttes and in cliffs along upper Mess Creek valley. Their source is believed to have been a centre near Exile hill, which is topographically higher than any of the other remnants. Also, thin flows on the north end of Exile hill grade southward into a thick wedge of mainly pyroclastic debris that forms its southeastern flank. These deposits, which include bombs and agglutinated spatter, are probably a small remnant of one of the pyroclastic cones that was built around the Exile hill vent. No primary pyroclastic material is interlayered with the more distal flows that form the cliffs along Mess Creek Escarpment.

The Exile hill flows are more varied in both morphology and composition than those in the Swarm peak or Vanished peak piles. Individual flows range in thickness from more than 30 m near the base to discontinuous rubble flows only a few metres thick at the top. The basal flows commonly have long curving columns in sheath-like clusters, whereas the upper flows are characterized by stout, spheroidally weathered columns or random, blocky jointing. The rock varies from dark grey aphanitic, aphyric

basalt which is most common in the distal flows, to fine grained basalt with up to 15% phenocrysts of feldspar, pyroxene and olivine in proximal flows on the upper part of Exile hill.

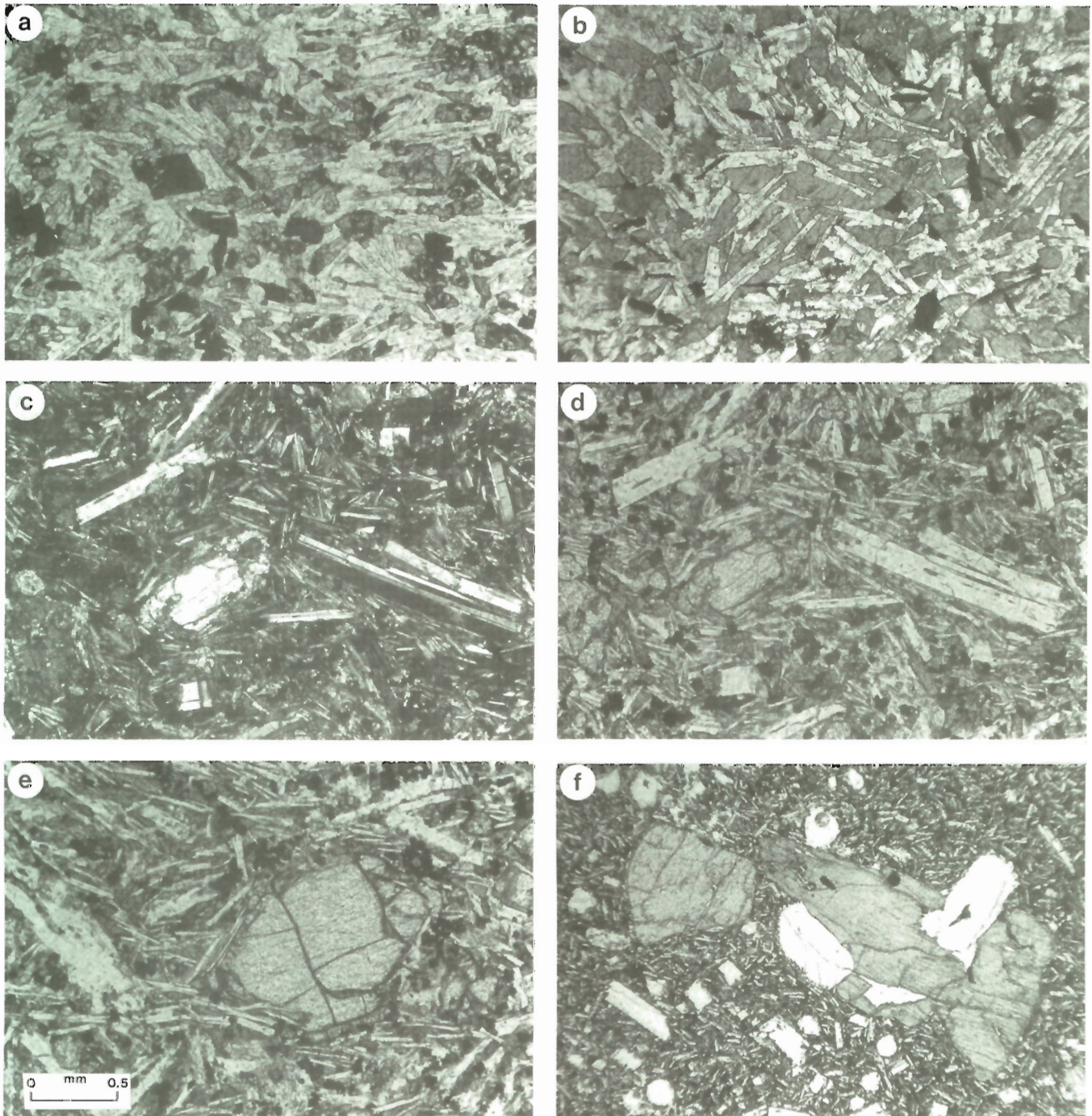
PETROGRAPHY

The mineralogy and texture of the Nido basalts are surprisingly uniform (Fig. 82) considering the long period over which they evolved and the many separate centres from which they issued. Plagioclase (An_{45-70}), titaniferous, calcic augite (salite), olivine (Fa_{20-50}) and opaque oxides (mainly ilmenite) are the essential mineral constituents (Table 7). Observed differences in lithology are due mainly to grain size and phenocryst content, neither of which provide a basis for subdividing the Nido into petrographically distinct units. Grain size, which varies from microcrystalline or subvitreous in quenched basalts to medium grained (± 1 mm) in thick or ponded lava flows, is a function of local cooling history. In closely related sequences of flows there is commonly a systematic upward increase in phenocryst content but this too is a local phenomenon, related to the evolution of a single magma batch. The most abundant phenocryst is plagioclase, followed by olivine and clinopyroxene. Opaque oxides rarely form phenocrysts in the Nido basalt.

Plagioclase phenocrysts are mostly euhedral, complexly twinned, tabular laths 2-5 mm long. They rarely form more than 5% of the Nido basalt but extremely porphyritic varieties, such as the upper Beta peak flows, contain up to 50% plagioclase phenocrysts as long as 2 cm. This high feldspar content tends to shift the rock toward hawaiite in the chemical classification (Fig. 83) but the feldspar composition is largely independent of total phenocryst content or size. Most of them have sharp boundaries against the enclosing groundmass but an older generation of slightly more calcic, embayed and rounded plagioclase is present in some sections. Twenty probe analyses (Fig. 84) indicate a range of phenocryst compositions from An_{44-68} and a normal zoning range of 5-6% An in individual crystals.

Phenocrysts and microphenocrysts of olivine form euhedral prisms with sharp crystal boundaries showing no evidence of reaction with the groundmass. Nine probe analyses (Fig. 84) showed a range from Fa_{22-45} , but no measurable zoning within single crystals.

Purplish-brown titaniferous augite is present as phenocrysts and microphenocrysts in about half of the Nido thin sections examined. The larger crystals (up to 3 mm) are commonly rounded, with embayed or fretted boundaries and many exhibit sector zoning. Microphenocrysts (< 1 mm) occur as fusiform, strongly zoned prisms with pigmented cores and clear rims. Nine probe analyses, of pyroxene, cluster in or near the salite field (Fig. 84). The aphyric Nido basalts are petrographically similar to the groundmass



a —Aphyric alkali olivine basalt, comprising euhedral laths of plagioclase, intergranular subhedral grains of clinopyroxene, minor olivine and opaque oxides (plane light).

b —Aphyric alkali olivine basalt with subophitic texture. Subhedral laths of plagioclase and opaque oxides are partly enclosed by clinopyroxene.

c,d—Microporphyritic hawaiite with euhedral microphenocrysts of plagioclase and olivine in a fine grained groundmass of

plagioclase, olivine, opaque oxides and intergranular clinopyroxene (c, crossed polarizers; d, plane light).

e —Euhedral olivine microphenocryst in a subophitic groundmass of randomly oriented plagioclase laths, clinopyroxene, olivine and opaques (alkali olivine basalt, plane light).

f —Cluster of olivine, clinopyroxene and plagioclase in alkali olivine basalt. Note reaction of plagioclase with fine grained groundmass.

Figure 82. Photomicrographs of typical Nido basalts; scale bar 0.5 mm.

Table 7. Representative microprobe analyses and structural data for the principal mineral phases in the Nido basalt. (NF, Nido feldspar; NP, Nido pyroxene; NO, Nido olivine).

	Feldspar				Pyroxene		Olivine			
	Phenocryst			Groundmass	Groundmass		Phenocryst	Groundmass		
	NF1	NF2	NF3	NF4	NP1	NP2	NO1	NO2		
SiO ₂	50.48	53.23	54.73	52.11	46.57	49.87	37.88	36.51		
Al ₂ O ₃	30.18	28.95	29.17	29.74	5.02	2.96	0.07	0.0		
TiO ₂	0.0	0.0	0.0	0.0	3.71	1.99	0.03	0.06		
Cr ₂ O ₃	0.0	0.0	0.0	0.0	0.0	0.0	0.0	0.0		
Fe ₂ O ₃	0.52	0.41	0.28	0.57	1.91	1.92	0.0	0.0		
FeO	0.0	0.0	0.0	0.0	8.88	8.06	23.89	33.48		
MnO	0.0	0.0	0.0	0.0	0.21	0.21	0.25	0.59		
MgO	0.0	0.0	0.0	0.0	11.25	12.90	37.06	29.60		
NiO	0.0	0.0	0.0	0.0	0.0	0.0	0.10	0.0		
CaO	13.59	11.23	11.16	12.81	21.34	21.80	0.21	0.44		
Na ₂ O	3.69	4.98	5.25	4.23	0.54	0.48	0.0	0.0		
K ₂ O	0.12	0.33	0.24	0.16	0.01	0.0	0.0	0.0		
H ₂ O	0.0	0.0	0.0	0.0	0.0	0.0	0.0	0.0		
F	0.0	0.0	0.0	0.0	0.0	0.0	0.0	0.0		
Total	98.58	99.13	100.83	99.62	99.44	100.19	99.49	100.68		
	No. of ions on basis of 8 (0)				Number of ions on basis of 6 (0)					
Si	2.3327	2.4309	2.4522	2.3771	Si	1.7739	1.8689	Si	0.9991	0.9989
Al	1.6437	1.5582	1.5403	1.5989	Al	0.2254	0.1307	Al	0.0	0.0
Cr	0.0	0.0	0.0	0.0	Ti	0.0008	0.0004	Cr	0.0	0.0
Fe ³⁺	0.0181	0.0141	0.0094	0.0196	Fe	0.0	0.0	Fe ³⁺	0.0	0.0
					Cr	0.0	0.0			
Al	0.0	0.0	0.0	0.0	Al	0.0	0.0	Al	0.0022	0.0
Cr	0.0	0.0	0.0	0.0	Ti	0.1055	0.0557	Cr	0.0	0.0
Ti	0.0	0.0	0.0	0.0	Fe ³⁺	0.0548	0.0542	Ti	0.0006	0.0012
Fe ³⁺	0.0	0.0	0.0	0.0	Cr	0.0	0.0	Fe ³⁺	0.0	0.0
Ni	0.0	0.0	0.0	0.0	Ni	0.0	0.0	Ni	0.0021	0.0
Fe ²⁺	0.0	0.0	0.0	0.0	Fe ²⁺	0.2829	0.2526	Fe ²⁺	0.5269	0.7660
Mn	0.0	0.0	0.0	0.0	Mn	0.0068	0.0067	Mn	0.0056	0.0137
Mg	0.0	0.0	0.0	0.0	Mg	0.6387	0.7206	Mg	1.4569	1.2071
					Ca	0.8709	0.8753			
					Na	0.0399	0.0349			
					K	0.0005	0.0			
Ca	0.6729	0.5495	0.5358	0.6261				Ca	0.0059	0.0129
Na	0.3306	0.4410	0.4561	0.3741				Na	0.0	0.0
K	0.0071	0.0192	0.0137	0.0093				K	0.0	0.0

Table 8. Five representative chemical analyses of specimens from the Nido Formation.

Sample	Alkali olivine basalt			Hawaiite	
	2655	43	91	2674	46
SiO ₂	46.300	46.600	47.400	45.100	48.700
Al ₂ O ₃	14.400	15.600	16.200	15.800	16.400
Fe ₂ O ₃	4.800	3.800	1.400	3.000	4.100
FeO	9.000	10.000	10.400	10.800	7.600
CaO	9.400	9.750	9.770	7.800	8.440
MgO	6.000	5.240	7.010	4.300	4.670
Na ₂ O	2.500	3.300	3.200	3.700	3.500
K ₂ O	0.700	1.100	0.960	1.500	1.430
TiO ₂	3.090	3.080	2.400	3.320	2.730
P ₂ O ₅	0.260	0.610	0.370	0.480	0.570
MnO	0.180	0.190	0.180	0.190	0.180
S	0.0	0.070	0.060	0.0	0.070
NiO	0.0	0.0	0.010	0.0	0.010
CO ₂	0.300	0.0	0.0	2.500	0.500
H ₂ O	2.500	0.400	0.100	1.800	1.600
Total	99.430	99.740	99.460	100.290	100.500

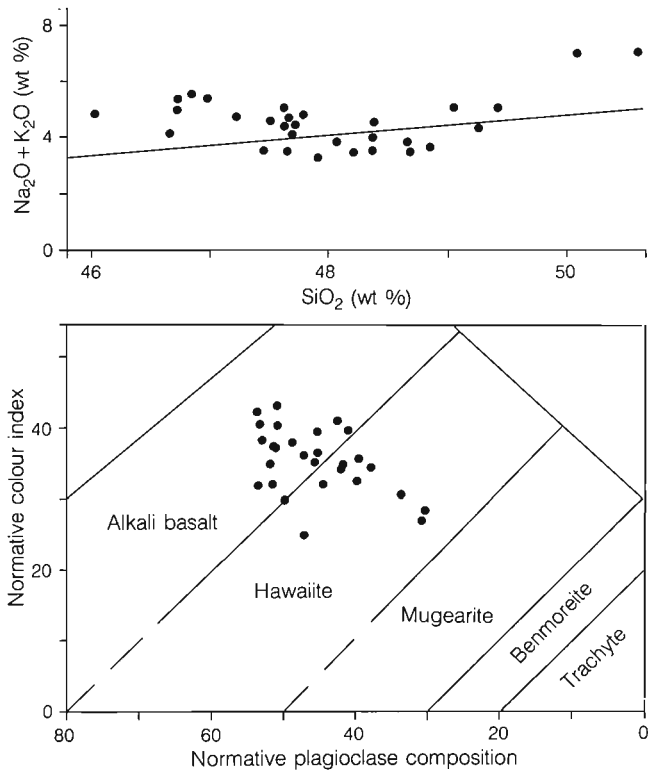


Figure 83. Plot of Nido basalt analyses on the total alkalis vs. silica, and normative colour index vs. normative plagioclase composition diagrams of Irvine and Baragar (1971).

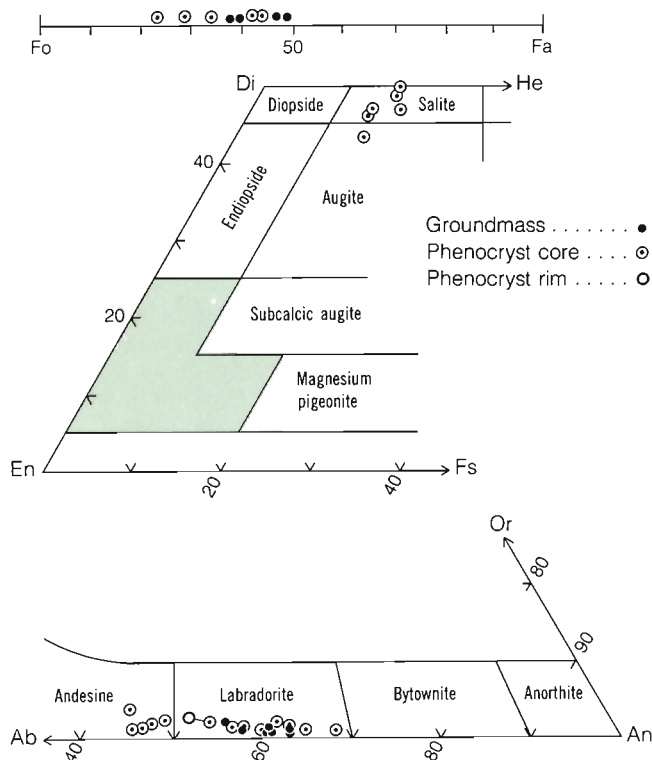


Figure 84. End member plots showing compositions of feldspar, pyroxene and olivine in Nido basalt, based on 20 microprobe analyses.

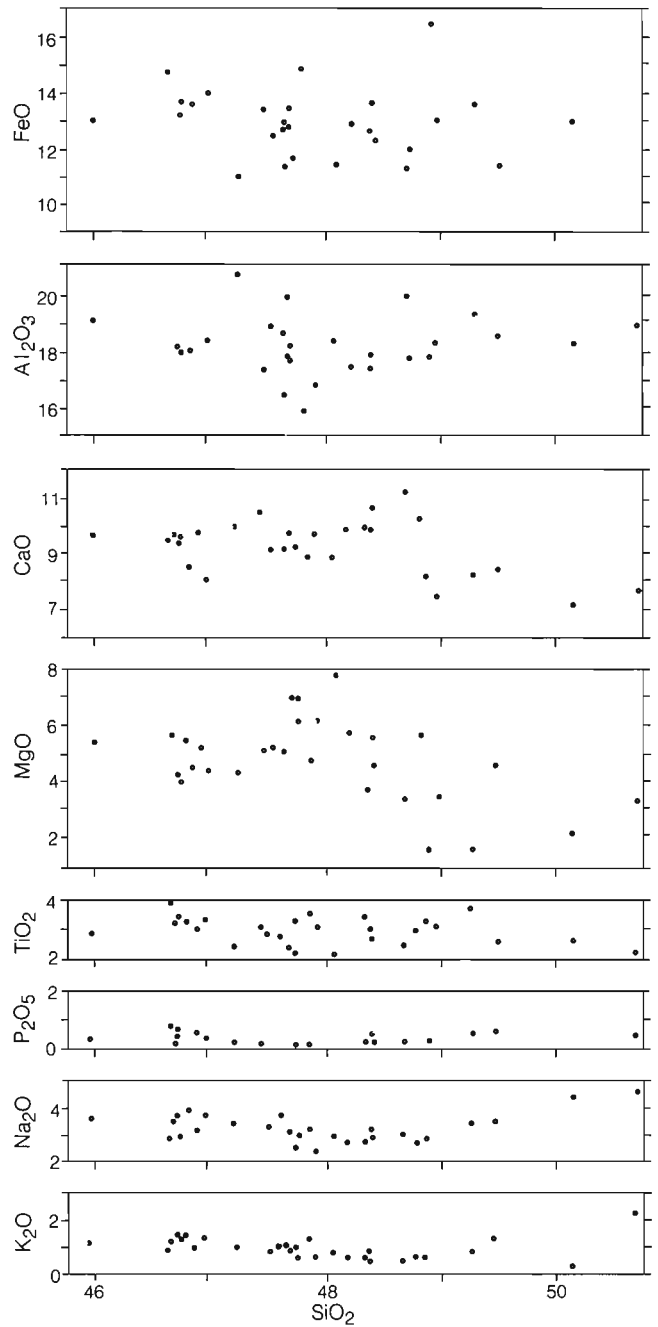


Figure 85. Harker diagram showing chemical variation in weight per cent for 25 analyzed specimens of Nido basalt.

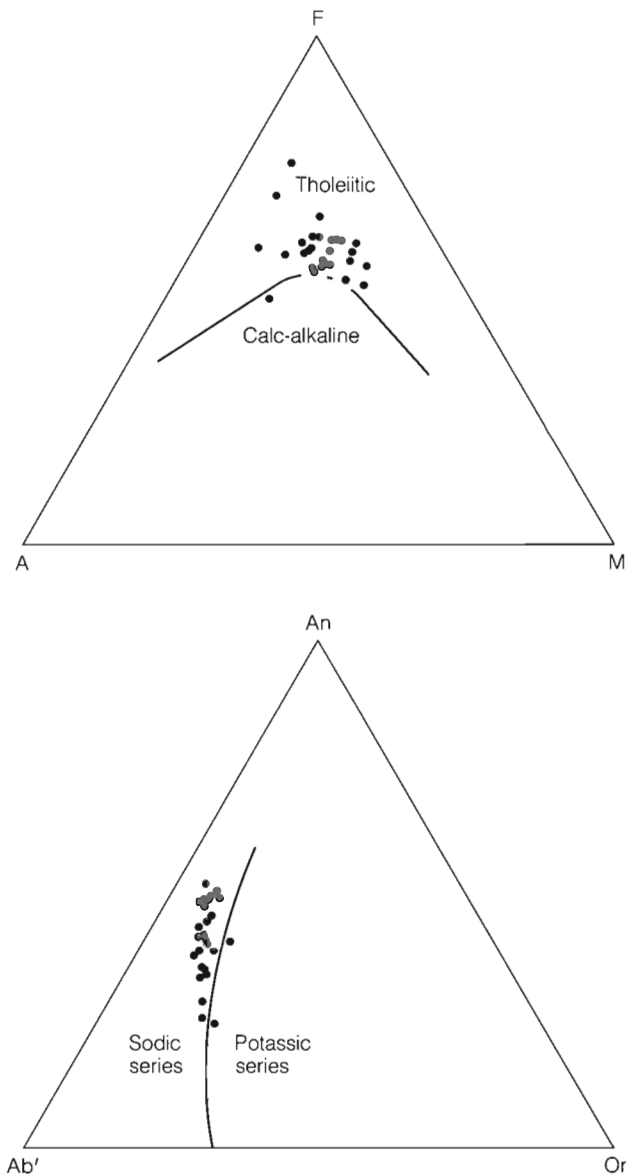


Figure 86. AFM and Ab'-An-Or plots of 25 analyses from the Nido Formation. ($A = Na_2O = K_2O$; $F = FeO = 0.8998 Fe_2O_3$; $M = MgO$; $Ab' = Ab = 5/3Ne$).

of those bearing phenocrysts. Ragged, strongly zoned laths of plagioclase (An_{55-65}) are crudely aligned to give the rock a pilotaxitic texture. Intersertal and poikilitic textures are common in which the feldspars are partly or wholly enclosed by purplish-brown, groundmass titanite. However, the groundmass pyroxene of some Nido basalts forms clusters of tiny, intergranular prisms between the plagioclase laths. Groundmass olivine, as tiny, equant grains (< 0.25 mm) is interstitial to the feldspars and commonly enclosed by the groundmass pyroxene. Their compositional range (Fa_{38-50}) is slightly higher in iron than the associated phenocrystic olivine (Fig. 84). Uniformly disseminated opaque oxides form 3-5% of most Nido basalts. They are interstitial to the groundmass feldspar and exhibit euhedral to subhedral crystal boundaries against the groundmass pyroxene. Partial probe analyses indicate an Fe/Ti ratio of about 1:1, suggesting ilmenite.

CHEMISTRY

Twenty-five major element analyses of Nido basalt are plotted in Figures 83 to 86 and five superior analyses are listed in Table 8. With two exceptions they plot in the field of Irvine and Baragar's (1971) sodic series on the Ab'-An-Or diagram (Fig. 86) and form a fairly tight cluster straddling the alkali basalt-hawaiite fields of the normative colour index vs. normative Pc diagram (Fig. 83). As noted in the previous section the shift toward hawaiite appears to result from higher than average contents of plagioclase phenocrysts. All of the aphyric rocks plot in the alkali olivine basalt field.

The Harker diagrams (Fig. 85) and alkali vs. silica diagram (Fig. 83) show no systematic variations with respect to silica. However, this is not surprising considering the very small range of silica (46 to 49.5%) in the Nido rocks. On the AFM diagram (Fig. 86) the Nido analyses also form a fairly compact population of points in the region of moderate to strong iron enrichment. In general the chemistry of the Nido basalt falls within the same narrow limits as the underlying Raspberry basalt. This suggests that both are primitive magmas that have erupted without undergoing significant modification either internally or as a result of changes in the source area during the four million year interval that separated Raspberry from Nido activity.

SPECTRUM FORMATION

GENERAL GEOLOGY

The Spectrum Range is a nearly circular cluster of long, narrow-crested ridges and pyramid-shaped peaks of rhyolite and trachyte at the southern end of the Mount Edziza Volcanic Complex (Fig. 87, Map 1623A, in pocket). The light grey, white, pale green and purple rocks weather to bright hues of red, yellow and orange which give the range its name. The Spectrum pile, once much larger, is now about 19 km across. Peaks, nearly 2500 m high at the centre of the range, are surrounded by a crudely radial system of ridges and lesser peaks that decrease in elevation toward the outer margins of the range (Fig. 88). The original surface was a broad dome, but erosion has reduced all but a few of the interfluvial areas to sharp-crested ridges. Only on a few small interfluves where the Spectrum rhyolite and trachyte were protected by younger basalt flows of the Kitsu member, is it possible to see part of the unmodified upper surface of the original edifice. The rock is closely jointed and commonly has a platy or flaggy flow layering that makes it highly susceptible to frost wedging. As a consequence, most ridges are covered with a thick mantle of felsenmeer and their steep, unbroken, slopes lie close to the angle of repose of free-running flaggy talus. Thus, while the Spectrum Range is almost totally free of vegetation, the rock is not well exposed. Continuous outcrops, where detailed relationships can be observed, are found only on the steep upper ribs of the highest peaks and ridges and on glacially oversteepened walls of cirques. Elsewhere, only small isolated buttresses of rock project through the pervasive mantle of loose, broken slabs.

Almost the entire Spectrum pile is underlain by Nido basalt. The only exceptions are found along its northern edge where the basalt wedges out against the southern edge of the Armadillo Highlands and overlying Spectrum trachyte rests on Armadillo rhyolite. Also, at the extreme southwestern corner of the pile, Spectrum rhyolite extends beyond the outer limits of the Nido basalt and overlies the old basement surface. At the few places where the basal contact is exposed in the central part of the pile, Spectrum rhyolite rests directly on glacially scoured flows of Nido basalt, whereas around the outer margins of the pile, a layer of gravel is commonly present at the base of the Spectrum sections. These include gravels derived from the underlying basement and Nido terranes, as well as gravels derived wholly, or in part, from earlier phases of the Spectrum Formation itself. The latter are most abundant along the western and southern part of the pile where trachyte and rhyolite clasts are the dominant lithology in the basal gravels. Clastic layers within the Spectrum pile are uncommon and, like the basal gravel, they are confined to its outer margins, particularly along the western side.

Main lava dome

Nearly all of the Spectrum rocks appear to have been erupted from a vent or cluster of vents that lay close to the high peaks at the centre of the range (Fig. 88). However, the existing peaks and ridges are merely remnants of a once continuous dome that extended far beyond the present limits of the range (Fig. 89). Truncated remnants of thick, gently dipping trachyte flows at the summit of Kitsu Peak, the highest peak in the range, indicate that the summit of the original dome was more than 8000 ft. (2400 m) above sea level. Its distal edge has been almost entirely removed by erosion, but a few remnants around the southwestern edge and along the northern edge, where it laps against the old Armadillo Highlands, indicate that the main dome was originally more than 25 km across. The most distal remnant, on Kitsu Plateau, northwest of Raspberry Pass, is about 11 km from the summit of the main dome. However, these relatively thin trachyte flows may have originated from a nearby satellitic vent.

Despite widespread development of talus and felsenmeer, the internal geometry of the main dome is locally well exposed. On Kitsu Peak and the high ridges radiating from Yeda Peak, the flows are nearly flat-lying, whereas those in the peripheral part of the range dip gently toward the edge of the pile. On the glacially oversteepened south face of Yagi Ridge, individual cooling units can be traced for several kilometres. These flows, which vary from 15 to 150 m thick, dip northwesterly away from the centre of the range (Fig. 90). The average gradient is about 300 m per kilometre, but initial dips up to 15° were observed where the lava has flowed over irregularities on the old surface.

More than 730 m of rhyolite and trachyte are exposed between the summit of Kitsu Peak and the head of Nagha Creek, where the base of the Spectrum pile rests directly on Nido basalt. Around the periphery of the range, sections of similar rock from 300 to more than 500 m thick are exposed along the truncated edge of the original pile. Calculations based on a restoration of the original surface (Fig. 87) suggest that the volume of the main Spectrum dome was about 101 km³. Nearly all of this immense volume was erupted as lava. Pyroclastic rocks, including air-fall pumice and ash flows, form only a small percentage of the total, and occur mainly along the northern edge of the range. Light coloured flaggy rhyolite is the dominant rock type in the lower two-thirds of the pile, whereas the upper part is mainly green, olive-green, brown to nearly black pantelleritic trachyte which outcrops in relatively massive, cliff-forming units on the crests of many of the higher mountains. However, there are exceptions to this general rule where rhyolite occurs in the upper part of the section or alternates with trachyte (Fig. 91).

MOUNT EDZIZA

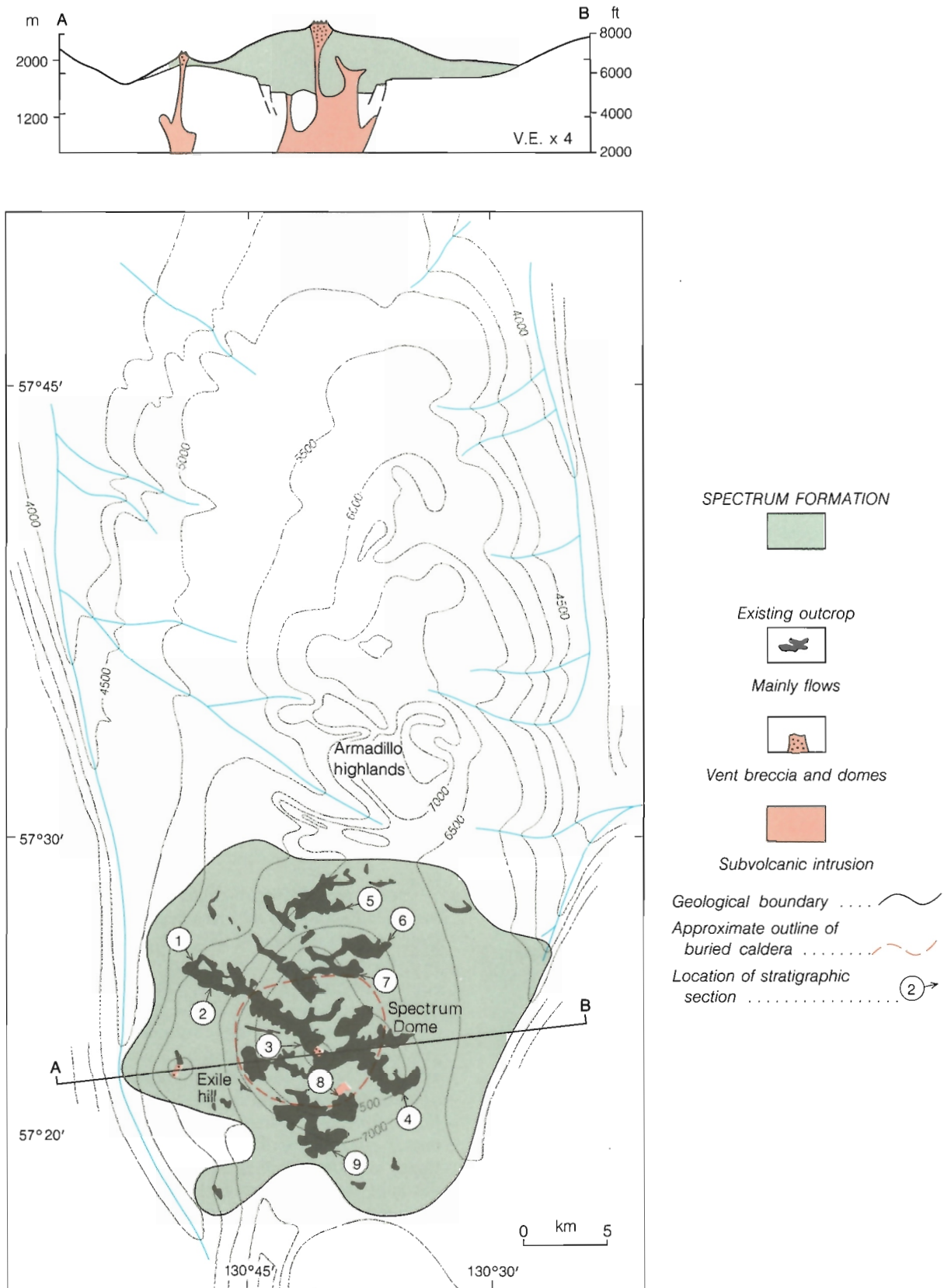


Figure 87. Paleogeological map and cross-section showing the inferred maximum extent of the Spectrum Formation at the end of Spectrum time, and the inferred position of the buried caldera. Stratigraphic sections are shown in Figure 91.



Figure 88. Looking west at Yeda Peak and dissected rhyolite domes of the central Spectrum Range. GSC 202468-V.

Flow morphology

Individual lava flows commonly display four distinct zones: (1) a basal quenched zone which includes glass, (2) a lower zone of flow layering, (3) a massive central core, and (4) an upper breccia zone. The nature and relative proportion of these four zones varies with the thickness and composition of the flow and with its proximity to the vent (Fig. 92). Most of the rhyolites have a relatively thick zone of flow layering and a relatively thin massive core as compared with trachyte flows of the same thickness. In very thick flows of either composition, the central core forms most of the mass. Proximal flows tend to have a relatively thick vitreous basal zone and a relatively thin upper breccia zone compared with distal flows.

Soda rhyolite and comendite

Proximal flows. Rhyolite at the eastern end of Yagi Ridge, is fairly typical of proximal rhyolite flows in the central part of the dome. The basal quenched zone is a layer of lightly welded pumiceous breccia from 1-3 m thick in which partly flattened fragments of pale green to yellowish white clasts of pumice, granular black obsidian, and angular lithic fragments are suspended in a fine grained, highly oxidized yellow to brown matrix. In some places the pumice has been deformed to lenticules and a crude flow structure is visible in the matrix. Pumice and obsidian clasts are commonly less than 3 cm across, whereas many lithic clasts are larger and may be up to 1 m across. The percentage of glass fragments increases upward until they coalesce to form a layer of granular obsidian which may contain a few lithic clasts. In some places, the outline of original vitric clasts can only be seen on weathered surfaces. Most are only a few centimetres across, but the shape varies from nearly equidimensional globules in some flows to flattened lenticules which impart a pronounced eutaxitic texture to others. No evidence of the clastic texture of these rocks is

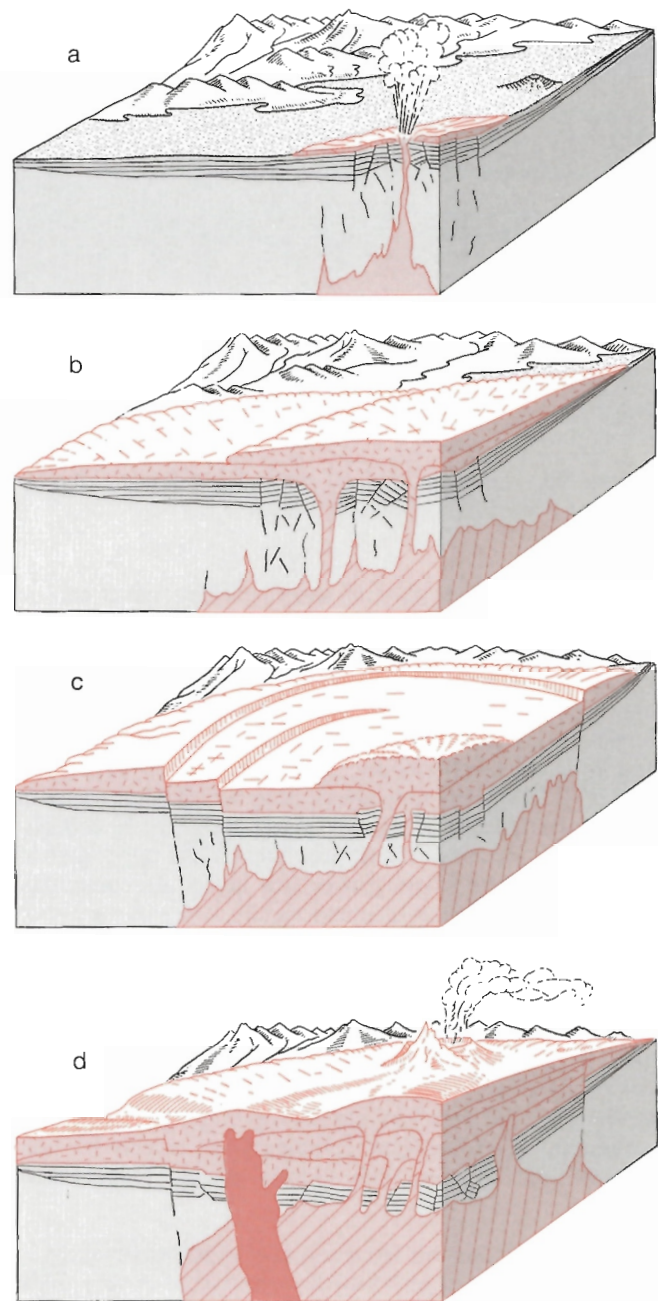


Figure 89. Schematic block diagrams showing four stages in the evolution of the Spectrum Range caldera and composite lava dome. (a) Explosive eruption of comenditic ash and lava onto the surface of Nido basalt flows covering the Spectrum Plateau. (b) Effusion of thick, platter-shaped flows and domes of comendite. (c) Collapse of caldera over magma chamber and eruption of the first of many resurgent domes within the depression. (d) Eruption of Yeda Peak near the centre of the composite lava dome and intrusion of soda granite along the southern margin of the buried caldera.



Figure 90. Looking north at thick, west-dipping rhyolite flows on Yagi Ridge. GSC 202468-W.

visible on freshly broken or sawn surfaces, but it can be enhanced by etching with hydrofluoric acid. In some flows the layer of granular obsidian grades upward into layers of massive unfractured glass which, even within a single flow, may vary from jet black to light greenish or bluish grey. Some are mottled, stippled, or intricately marbled with light and dark contorted streaks. Most zones of massive glass contain at least some flow layers along which devitrification and crystallization of vapour phase minerals is concentrated. This layering is most prominent in the upper part of the vitreous zone where planar flow layers are commonly associated with spherulites and patchy, irregular areas of white, pink or green devitrification. In some flows this zone is characterized by extensive development of lithophysae in which pea-sized, closely packed spherulites are surrounded by a matrix of pale green or grey glass. The transition from glass to flow layered rhyolite is commonly a mixed zone a few centimetres to 2 m thick in which thin layers of obsidian are interlayered with fine grained rhyolite. The layers are commonly contorted into complex folds which die out upward into rhyolite with closely spaced planar flow layering.

The lower one-third to one-half of most proximal rhyolite flows is prominently flow layered except in very thick flows (more than 60 m) in which the flow layered zone may be only a few metres thick. The layering may manifest itself as subtle differences in texture or colour which are visible only on weathered surfaces, or it may impart a bold, varicoloured banding with alternate layers in different shades and hues of white, yellow, green, brown and purple. The thickness of individual layers varies from less than a millimetre to several centimetres. Commonly, layers of dense, dark coloured aphanitic or subvitreous rhyolite alternate with porous, light coloured, relatively coarse grained layers along which lenticular open voids are present. The phenocrystic minerals such as feldspar are, if present, concentrated in the dense layers, whereas late stage, vapour phase minerals are concentrated in the porous layers and

cavity linings. The latter include tiny, pyramidal, clear or amethyst quartz, analcime, fluorite and acicular crystals of sodic hedenbergite and arfvedsonite. Some of the layered rhyolite is extremely porous with numerous small lenticular cavities forming 1-5% of the rock. The flow layering is deformed around these openings which were clearly formed by expansion of a vapour phase during flowage.

The transition from flow layered rhyolite to the massive central core of most proximal flows is gradational over an interval of several metres. The layering becomes less distinct upward and more widely spaced. Toward the centre of the transition zone individual flow layers lose their continuity, but discontinuous, varicoloured lenses still impart a distinct planar fabric to the rock. This, too, is lost in the upper part of the transition zone where the alignment of small nodes of vapour phase alteration give way to a patchy or mottled rock with only an indistinct fabric due to a crude orientation of phenocrysts and alignment of open cavities. The light patches in the mottled rhyolite commonly contain the same vapour phase minerals as those in the underlying flow layered rhyolite. In the upper part of the central core of some flows, cryptic, vapour phase mottling grades upward into prominent, varicoloured lithophysae. Individual lithophysae from a few millimetres to 3 cm across are commonly filled with a delicate filigree of vapour-phase minerals and devitrified glass in the form of thin concentric spheres. Some flows, particularly those 30 m or more thick, show no mottling, but rather a pervasive vapour phase alteration of the entire central core. Such flows are commonly bleached to nearly white and the texture is dominantly spherulitic.

In the proximal rhyolite flows, the upper brecciated zone is rarely more than a few metres thick and it may be missing altogether. Where present, it comprises a chaotic jumble of subangular, porous rhyolitic blocks up to about 1 m across. The entire mass is loosely welded together with what appears to be aphanitic, relatively dark rhyolite or cemented with highly oxidized, rust-stained particles, iron oxides and scraps of devitrified glass.

Distal flows. Toward their distal ends, the internal structure of the flows changes. The amount of lithic clasts in the lower quench zone increases at the expense of glass. Layers of granular and massive obsidian are commonly absent, and at their extreme distal end, the basal breccia of most flows contains no pumice and only a relatively few isolated clasts and irregular globules of granular obsidian interspersed with lithic blocks. The lithic blocks themselves commonly display complexly contorted flow layering and have annealed internal fractures.

The proportion of flow layered rhyolite increases at the expense of the massive core toward the distal end of most rhyolite flows. Also, planar uniform layering gives way to highly deformed layering with irregular folds and complex zones of fracturing. The latter are, in some flows, confined

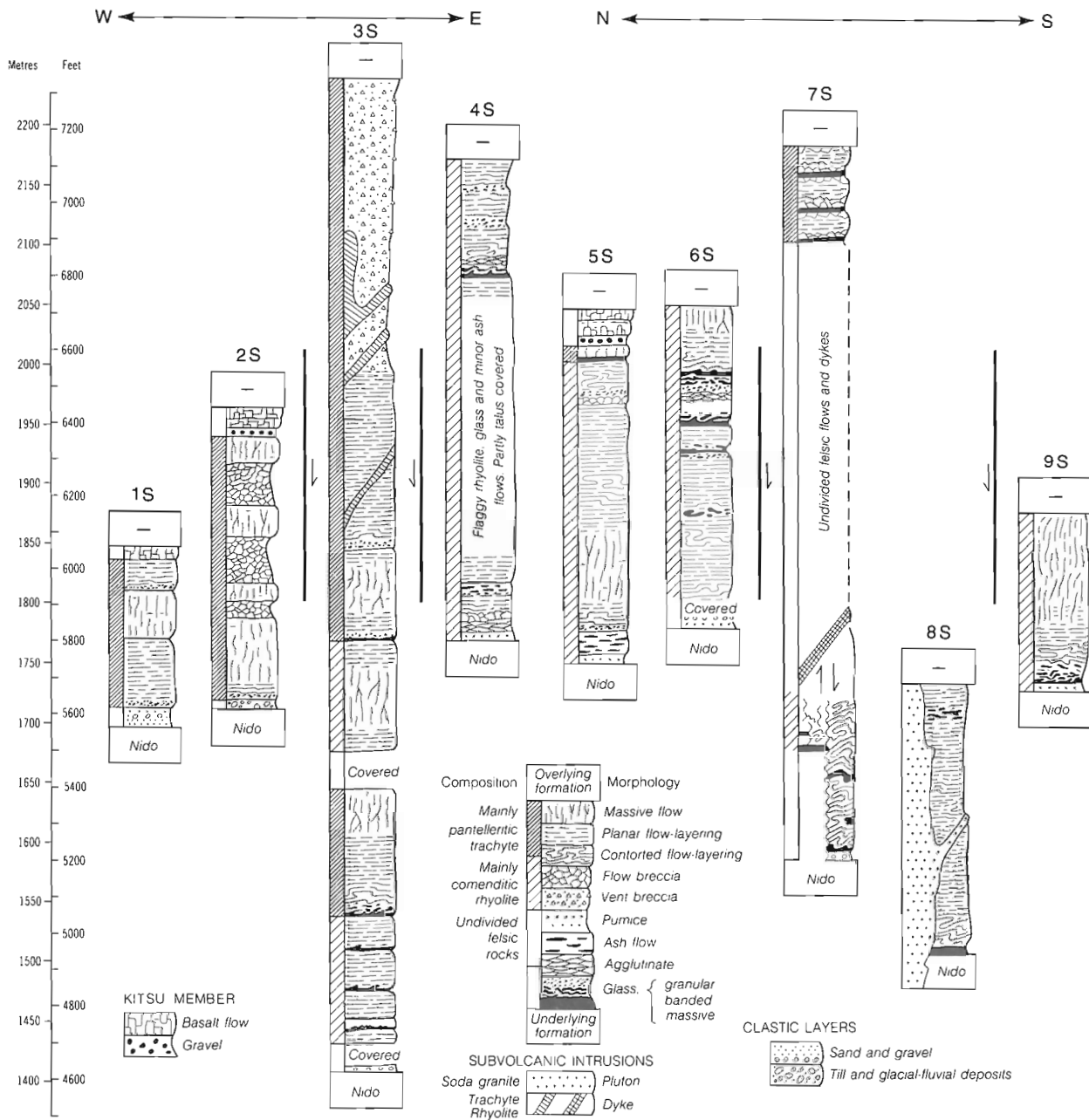


Figure 91. Typical stratigraphic sections of the Spectrum Formation. Heavy vertical lines show the relative position of the caldera margin to the stratigraphic columns. Section numbers (1-9) refer to locations shown on the paleogeological map (Fig. 87). S, Spectrum Formation.

to zones a few centimetres to several metres thick, bounded above and below by rhyolite with undeformed flow layering. Within the fractured zone, fragments of flow banded rhyolite have been rotated out of their original position to form a tightly stacked breccia of angular, mainly tabular blocks cemented by vapour phase minerals. In the distal and middle part of some flows, similar fractured zones cut up through the flow in the form of small thrust faults along which the advancing, semi-rigid flow was deflected upward. Above these fractures, the flow layering is commonly bent up into steep, nearly vertical attitudes.

Pantelleritic trachyte

Trachyte flows exhibit most of the same features observed in the Spectrum rhyolite, but the thickness of the different zones differs (Fig. 92). The basal quench zone is relatively thin and consists mainly of massive glass in the proximal part of most trachyte flows. Farther from their source, the glass is commonly absent, its place being taken by a relatively thick mat of basal flow breccia. Flow layering is less distinct than in the rhyolite flows, although the lower part of most trachyte flows has a well developed platy

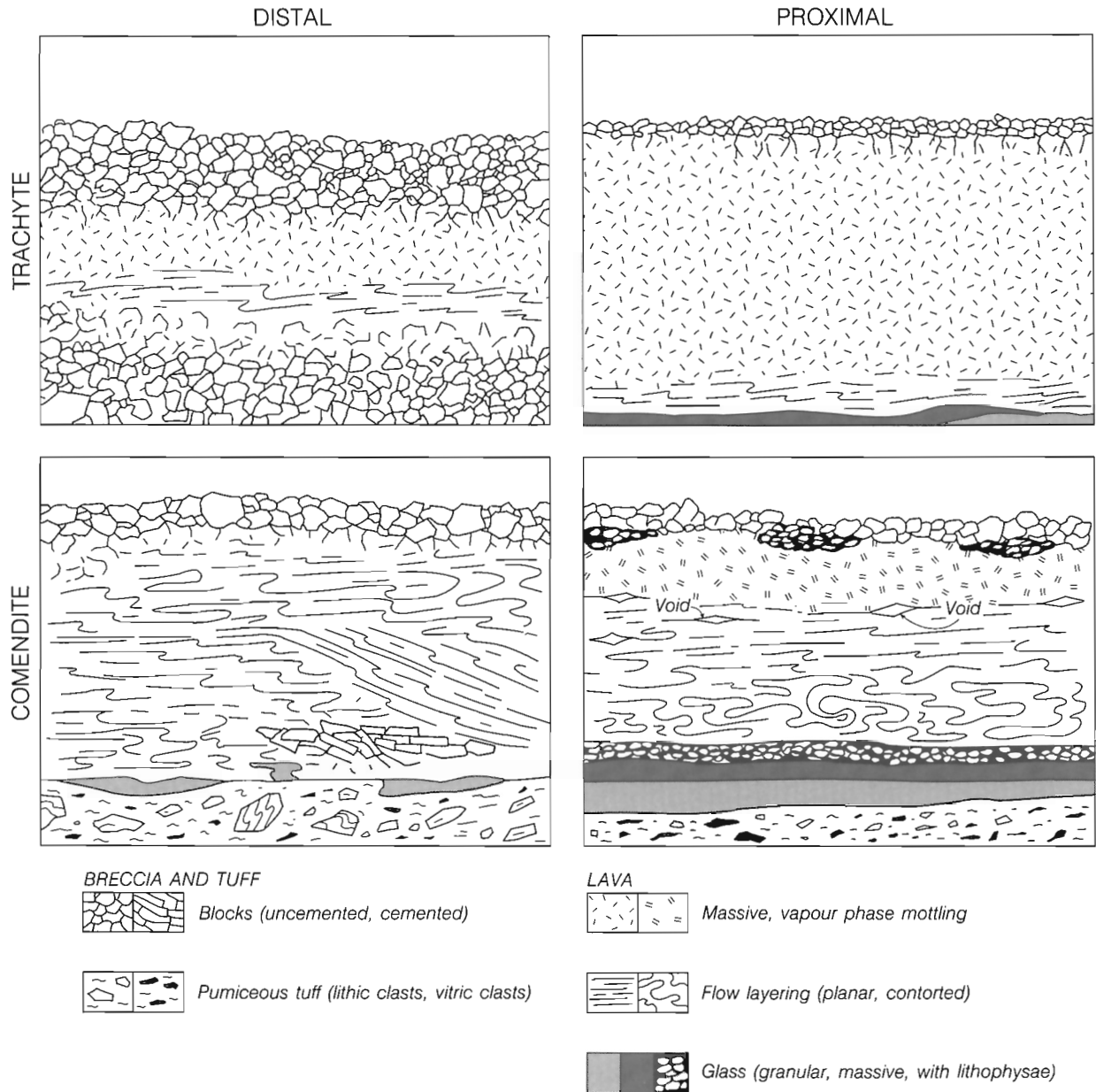


Figure 92. Schematic sketch showing the morphology of distal and proximal facies of Spectrum Formation comendite and trachyte flows.

or flaggy flow cleavage, and in a few places, mineral segregation along flow layers is well developed. In the distal trachyte flows at the east end of Artifact Ridge, for example, prominent flow layers are filled with a porous network of arfvedsonite crystals, and in the section facing Mess Lake, on the west side of the pile, similar flow layers are coated with clusters of aenigmatite and aegirine crystals. In the central part of the range, most trachyte flows consist mainly of medium to dark olive-green aphanitic rock with small (1-2 mm) randomly oriented feldspar phenocrysts. Vitreous and subvitreous phases are mainly black. In many thick trachyte sequences, the flows are separated by only a thin

glassy layer and 1-2 m of fine grained rock with indistinct flow banding. Contacts are commonly so subtle as, for example, on the upper part of Kounugu Mountain, that it is difficult to distinguish where one flow ends and the next begins. The middle and distal segments of such flows have developed thick basal and upper breccia zones which commonly exceed the thickness of the massive lava core. Excellent examples are exposed on the western end of Yagi Ridge where flow breccia of loosely or completely welded blocks of porous green trachyte forms recessive benches between nearly vertical cliffs of columnar jointed trachyte in the massive cores of successive flows. In the transition zone from

core to breccia, at both the top and bottom of the flow, the massive rock of the core is cut by a boxwork of healed fractures formed by autobrecciation of the nearly solid lava during the latter stages of movement.

Pyroclastic deposits

Primary pyroclastic deposits form a relatively small percentage of the main Spectrum dome. A layer of bluish-green breccia 1-10 m thick forms a widespread horizon at or near the base of the Spectrum pile, particularly in the central part of the complex. It comprises a mixture of pale green lenticular, subvitreous, welded fiamme and white, dark green and reddish-brown angular clasts of rhyolite. Maximum clast size is about 2 cm and the proportion of lenticular and angular material varies widely from place to place. Rocks containing mainly lenticular clasts have a pronounced fluidal or eutaxitic texture, whereas rocks in which angular clasts predominate are matrix-supported, unsorted breccias with no apparent internal fabric. In several places these green, basal breccias are associated with unwelded air-fall pumice. They are believed to have formed as blast deposits during the early stages of Spectrum activity when the effusion of small lava domes was accompanied by the explosive discharge of primary, gas-charged magma. The angular clasts are mainly rhyolite and were probably derived from the shattered remains of early-formed domes and flows that were deposited in and around the active vents.

Beds of unwelded, air-fall pumice from less than 1 m to about 2 m thick are present between a few of the rhyolite flows in the central part of the range, and more commonly, between distal flows along the northern edge of the pile. These vary from fine, white ash, through granular pumice deposits containing unflattened lapilli to extremely heterogeneous deposits of mixed pumice, crystals and lithic fragments. The air-fall deposits are commonly overlain and/or underlain by welded ash flows (Fig. 95c). The latter are nowhere more than about 5 m thick and are commonly much thinner. One densely welded 3 m ash flow comprising highly attenuated black vitreous fiamme and small, sparse lithic clasts outcrops near the base of the pile where it laps against the Armadillo Highlands. Elsewhere, the ash flows are only moderately to lightly welded and, like the air-fall pumice, their exposure is too random and fragmentary to permit correlation.

Flow mechanics

How was this great mass of rhyolite and trachyte erupted? Did it issue as enormous surges of lava from vents near the centre of the dome and flow outward to its periphery, or was each thick cooling unit deposited as incandescent particles which fused together to form a semimolten mass that later moved only enough to assume flow layering and other characteristics of a lava flow? There is evidence that both processes were operative, but the first was by far the most important. The slopes (up to 15%) on which most of

the units rest favours their emplacement as viscous lava flows rather than highly mobile incandescent clouds. Similarly, the great thickness of the main Spectrum dome compared to its relatively small diameter is consistent with the structure of a composite lava dome. If a significant amount of lava had been erupted as ash flows, their distal ends and associated air-fall deposits should have been preserved beneath younger basalts north of Raspberry Pass, but there is no evidence that Spectrum rocks were ever deposited that far north. The vitroclastic layer at the base of many flows, though it superficially resembles some primary pyroclastic rocks, was probably not deposited by a precursor ash fall or ash flow, but rather by incandescent showers of debris sloughing off the steep front of the advancing flow. Compaction and welding of this debris prior to quenching has locally imparted a eutaxitic texture similar to that of many welded ash flow deposits. Unlike ash flows, however, the basal quench breccias have a wide range of both vitric and lithic clast sizes, and often a random mixture of both pumice and obsidian fragments.

Although lava flows form most of the main Spectrum dome, at least some units originated from piles of semi-molten globules that accumulated around the fountaining vents and began to flow under their own weight. These rootless flows are found in the central part of the range where they occur as punky, pale green, structureless or crudely flow-layered units with numerous irregular voids. In some, the faint outline of the highly attenuated original globules is still visible. Although the transition zone between the proximal and distal ends of these flows was not observed, it is reasonable to assume that their fragmental character disappears with distance from the vent, and that their middle and distal segments are indistinguishable from other flow layered lavas in the pile.

Yeda Peak eruptive centre

Yeda Peak (7350 ft. ; 2240 m) forms a prominent spire at the intersection of three narrow ridges near the centre of the Spectrum Range (Fig. 88). Its northeastern face towers above the steep headwall of an active cirque in nearly vertical cliffs 300 m high. Breccia, which forms the central spire, is clearly visible in these cliffs, right down to the level of the ice and, although the cliffs themselves are inaccessible, the upper part of the spire can be reached from any of the three intersecting ridges. It consists of moderately well indurated explosion or vent breccia containing angular to subrounded clasts of mainly black, subvitreous porphyritic trachyte, some rhyolite, a few basement rocks, and basalt from the underlying Nido flows. There is no sorting or stratification. Clasts, mainly less than 30 cm across, but rarely as much as 2 m, are suspended at random in a matrix of loosely packed smaller particles cemented by brownish-yellow, hydrated glass and iron oxides.

The central spire of breccia is surrounded by an apron of talus that obscures its contact with the wall rocks, however, outcrops of trachyte and rhyolite on the ridges, beyond

the talus cover, are fractured and bleached. It is obvious that hydrothermal alteration affected the wall rock for several hundred m around the breccia pipe, as well as altering clasts and matrix within the pipe itself. The eruption that produced the Yeda Peak breccia pipe must have occurred late in the evolution of the main Spectrum dome. It was not, apparently, a long-lived vent from which many successive flows were erupted. No wedges of pyroclastic rock are inter-layered with the adjacent flows that form the wall rock. Instead, the Yeda Peak breccia pipe appears to cut steeply across the pre-existing stratigraphy, fracturing the wall rocks, and providing a conduit for the circulation of gases and hydrothermal solutions (Fig. 93). Its eruption was obviously an explosive event that blasted a crater through the central part of the dome and may have been the source of crystal-lithic welded ash flows in the upper part of the section on Artifact Ridge, 10 km to the north.

Fumarolic alteration

Fumarolic alteration is not restricted to the Yeda Peak breccia pipe and its peripheral zone of fracturing, although the hydrothermal system that followed its eruption was probably deeper, hotter and longer lived than elsewhere in the pile. The posteruptive fumarolic activity in the Yeda Peak crater may, in fact, have been due in part to degassing of the last remaining magma, trapped in chambers in and below the base of the dome. More commonly, hydrothermal alteration in the Spectrum composite dome can be related to small, relatively short-lived fumaroles, sustained by degassing of the lava flows themselves. Bright red, yellow and orange patches of altered rock throughout the Spectrum Range are commonly confined to fracture zones within a single flow. Overlying and underlying flows are seldom affected, indicating that most of these small, rootless fumaroles were active only during the cooling and degassing of the flow in which they occur. Beneath the brightly coloured surface of these altered zones, the rock is bleached white and veined with a stockwork of silica, iron oxide and, in a few places, peppered with finely disseminated pyrite and hematite.

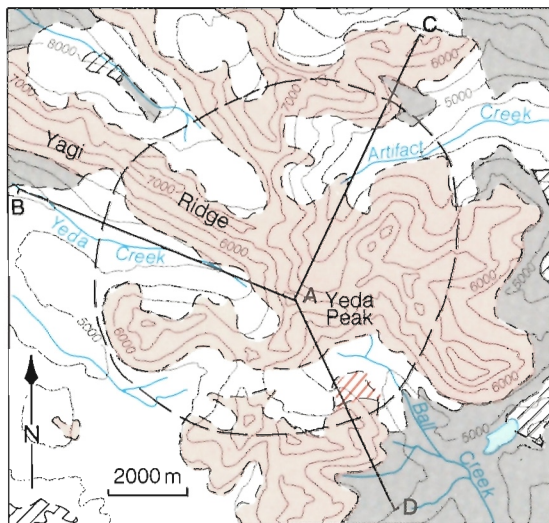
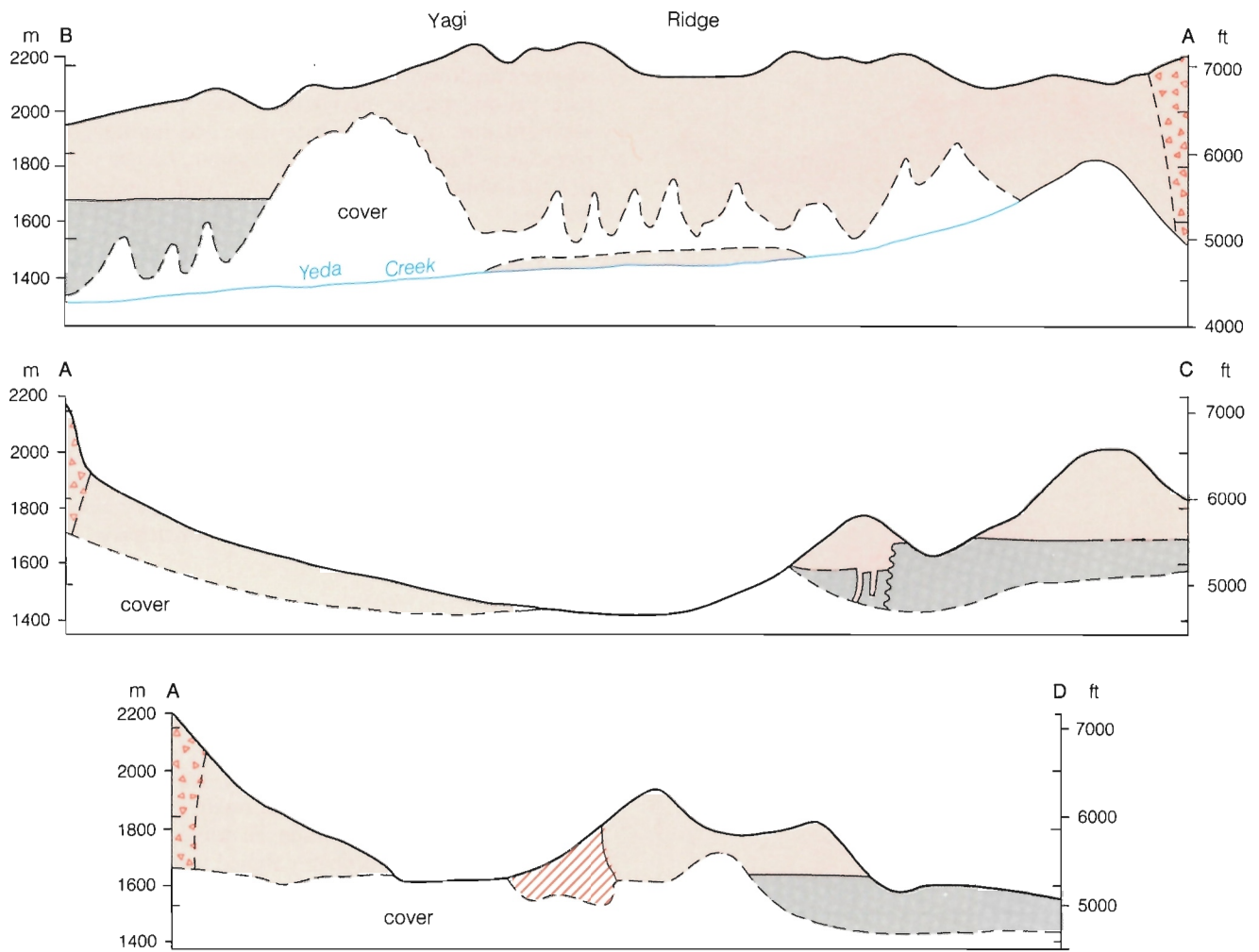
Subvolcanic intrusions and caldera collapse

A body of lustrous brown, medium- to coarse-grained soda granite outcrops at the head of Ball Creek Valley. It forms a group of low, glacially rounded rock bluffs along the southwestern side of the valley and extends up the eastern spur of the cirque of Yeda Glacier for at least 200 m above the floor of the valley. It is completely isolated from the surrounding rocks by snow and ice, but sharp, intrusive contacts between soda granite and altered Spectrum rhyolite were observed in talus blocks. The rock, which is almost entirely feldspar in stout, randomly oriented crystals locally coated with iron-manganese oxides, is unlike anything in the pre-Tertiary basement. There is little doubt that it originated

as a high level intrusion that invaded the lower part of the Spectrum pile in the late stages of its evolution, possibly during the explosive eruption of the Yeda Peak breccia pipe. The intrusion appears to lie along the edge of what may be a buried caldera or irregular collapse feature which underlies the central part of the Spectrum Range (Fig. 93). A short distance south of the granite intrusion, Spectrum rhyolite rests on the Nido basalt surface at an elevation of 5400 ft. (1646 m), whereas outcrops of highly altered Spectrum rhyolite are exposed below 5000 ft. (1524 m) in the valley bottom east of the granite. Similar, hydrothermally altered and locally pyritized rhyolite outcrops in Yeda Creek at least 213 m below the basal contact of the Spectrum rhyolite at the western end of Yagi Ridge. On Stewbomb Creek the difference is even greater. There, closely jointed, fresh, porous, green rhyolite outcrops down to the valley bottom (5000 ft. ; 1524 m), more than 366 m below the base of the Spectrum pile farther east on the adjacent ridge. On the north side of Stewbomb Creek, Spectrum rhyolite is in fault contact with Nido basalt. The nearly vertical fault trends northwesterly and its southwest side has dropped at least 90 m. Wall rocks along both sides are hydrothermally altered, and basalt on the downthrown side is cut by rhyolite dykes that parallel the fault. In each of the above cases, the base of the Spectrum pile under the central part of the range appears to be depressed relative to its outer margins (Fig. 93). Although the evidence is fragmentary because of poor exposure, it is reasonable to suppose that the central depression is a buried caldera that collapsed during withdrawal of the Spectrum lavas from a high level reservoir (Fig. 89). The depression lies within a roughly circular area about 9.6 km in diameter. If this was the diameter of the magma reservoir, then removal of the 101 km³ of lava that was erupted to form the main Spectrum dome could account for at least 1000 m of vertical caldera collapse.

Satellitic vents

The deeply dissected remnants of a small satellitic centre of Spectrum activity are exposed on Exile hill about 11 km west of Yeda Peak (Fig. 94). The hill itself is an erosional remnant of flat-lying Nido basalt flows with an aggregate thickness of about 244 m. On the west side, near its crest, a spire of platy green trachyte surrounded by breccia projects through the basalt. The central spire which has prominent vertical flow layering is about 213 m across and 60 m high. The surrounding breccia consists of rusty, highly altered trachyte clasts in a yellowish-brown microbreccia matrix. Clasts less than 10 cm across are completely altered, while larger ones retain a core of nearly black, vitreous trachyte. On the southwest side of the ridge, about 150 m below the top of the spire, the breccia is underlain by an irregular mass of porous green trachyte with platy, sub-horizontal flow layering. This is underlain by basalt and is considered to be part of a small tabular, subvolcanic intrusion injected laterally from the central conduit into the surrounding pile of basalt.



SPECTRUM FORMATION

Comendite and trachyte flows and domes

Subvolcanic intrusion

NIDO AND OLDER FORMATION

Basalt flows and pyroclastic rocks

BASEMENT

Mesozoic and Paleozoic rocks

Geological boundary

(defined, approximate)

Fault

Vent breccia

Inferred caldera margin

Figure 93. Map and projected cross-sections showing inferred position of the Spectrum caldera and its relationship to the Yeda Peak vent and subvolcanic intrusions.

MOUNT EDZIZA



Figure 94. Map and cross-section of the Exile Hill eruptive centre. Circles depict a gravel layer at the base of the Spectrum Formation.

North of the spire, the crest of Exile hill is capped by about 100 m of trachyte flows. They are separated from the underlying basalt by a thick layer of gravel composed almost entirely of well rounded pebbles and cobbles of Spectrum rhyolite and obsidian, presumably derived from the main dome to the east. The flows are mainly dark olive green, fine grained pantelleritic trachyte with stubby feldspar

phenocrysts 1-2 mm across. The central part of each flow is either massive or displays only a faint flow layering, whereas the lower part is strongly flow banded in shades of pale yellow, purple or white. Flows, particularly at the southern end of the trachyte cap, are interlayered with pyroclastic beds of agglutinated spatter, bombs and blocks of light coloured trachyte, commonly with contorted, fluidal banding.

The amount of lava erupted from the Exile hill centre is unknown, nor is it possible to estimate the number of other satellitic vents that were active during Spectrum time. Remnants of two trachyte flows on Wetalth Ridge and the ridge between Ball and Chachani creeks have all the characteristics of proximal flows, a thick layer of massive glass at the base, a thick massive core and little development of flow breccia on either the top or base. Their origin is unknown, but it is unlikely that they originated from the central dome, more than 11 km to the north. They more probably issued from nearby satellitic vents which have since been eroded away.

Kitsu Member

Erosional remnants of basalt overlie Spectrum rhyolite on Yagi and Artifact ridges and similar basalt rests disconformably on Kounugu basalt south of Kounugu Lake. Each of these remnants is underlain by fluvial gravel which includes clasts of rhyolite and/or trachyte, presumably derived from the Spectrum composite dome. The source of the basalt is unknown. It probably issued from several different vents during or shortly after the final stages of Spectrum, felsic volcanism. All the basaltic eruptive centres have been destroyed by later erosion and the widely scattered remnants of distal flows are assigned collectively to the Kitsu Member of the Spectrum Formation.

On the crest of Artifact Ridge four to six thin flows of sparsely feldsparphyric Kitsu basalt are interlayered with red scoria and may represent a proximal facies. Elsewhere the remnants include from one to three columnar flows up to 3 m thick, separated by thin layers of flow-top breccia. The rock is commonly pale grey, fine grained, slightly porphyritic basalt with sparse phenocrysts of plagioclase and olivine. Megacrysts of pyroxene, up to 2 cm across, and small cognate inclusions of coarse grained feldspar and pyroxene occur in several outcrops.

Gravel beneath the Kitsu Member varies greatly in thickness, clast size and composition. The remnants on Artifact Ridge are underlain by 0.5-1 m thick layers of locally derived rhyolite colluvium, whereas the remnants on Yagi Ridge rest on up to 8 m of coarse, well rounded rhyolite gravel. Gravel under the remnants south of Kounugu Lake consist mostly of basement clasts derived from the Hankin Massif to the south.

PETROGRAPHY

Felsic rocks

The Spectrum felsic rocks are mostly aphyric or microporphyritic with fewer than 10% phenocrysts greater than 2 mm across (Table 9). Porphyritic phases in which feldspar phenocrysts up to 5 mm long form 20-25% of the rock are volumetrically small, but are widely distributed throughout the pile. Vitreous and partly vitreous rocks (i.e. those showing varying degrees of devitrification), fluidal banding and lithophysae are also common (Fig. 95).

Comenditic glass is colourless to pale brown in thin section and relatively free of crystallites. It commonly contains sparse euhedral microlites (< 0.1 mm) of sanidine (Or₃₂₋₃₅) and bright green sodic hedenbergite (Fig. 95d). The pyroxene occurs as discrete crystals and also as tiny prisms that are partly or wholly enclosed by sanidine. Radiating clusters of bladed sanidine crystals (Fig. 95a), form spherulites in the same sections as discrete, euhedral microlites. They are commonly nucleated around an early-formed euhedral crystal of either sanidine or hedenbergite. Trachytic and pantelleritic glass differs from the comendite in having a higher proportion of crystallites and microlites and in the appearance of aenigmatite among the early-formed minerals.

The holocrystalline rocks, both comendites and pantellerites, commonly contain microphenocryst (< 1 mm) and rarely phenocrysts (> 1 mm) of sanidine and/or anorthoclase (Or₃₀₋₃₆) plus hedenbergite (Fig. 96). Where these occur together the pyroxene phenocrysts are euhedral and either partly or wholly enclosed by the feldspar. The larger feldspars have reacted strongly with the groundmass. Their boundaries are rounded and embayed and many are surrounded by reaction rims of arfvedsonite and acmitic pyroxene which project into the feldspar as slender, bladed crystals. Both euhedral and embayed hedenbergite phenocrysts may occur in the same rock. Those that show signs of resorption are commonly clouded with, or partly replaced by, fine granular or skeletal opaque oxides. Many of the hedenbergite phenocrysts exhibit prominent zoning, manifest in decreasing extinction angles and increasingly intense green pigmentation from the core outward, indicating a shift toward more acmitic compositions (Fig. 95b).

Phenocrystic aenigmatite is less abundant in the Spectrum rocks than in Armadillo rocks of similar composition. Where present it has reacted with the groundmass and been largely replaced by opaque oxides.

Arfvedsonite does not occur as a primary, independent phenocrystic phase but relatively large (± 0.5 mm) subhedral crystals are associated with clusters of sanidine microphenocrysts in both comendites and pantellerites. They commonly fill the space between adjacent feldspar phenocrysts and a few are partly or wholly enclosed by a single feldspar crystal. Many of these larger masses are associated with small aenigmatite crystals which are either enclosed by, or exhibit euhedral crystal boundaries against, the arfvedsonite.

The comendites and pantellerites differ in the proportion, rather than in the composition or paragenetic sequence, of the groundmass minerals—the comendites being relatively quartz-rich and the pantellerites having relatively more femic and opaque minerals. In both rock types the groundmass is a framework of ragged, crudely aligned sanidine laths. The density of this “framework” varies within a single section giving way to interstitial “pools” of poikilitic quartz crowded with tiny rhombs of sodic feldspar at least an order of magnitude smaller than the “framework” laths themselves. Aenigmatite, arfvedsonite, acmitic pyroxene, and kataphorite are also interstitial to the groundmass feldspar. They commonly form “mossy”, poikilitic clumps but in some pantellerites both arfvedsonite and sodic hedenbergite form relatively large, ophitic crystals which enclose the groundmass feldspars. The latter texture is common to the quartz-free pantelleritic trachytes (e.g. specimen 28 in Table 10) which are among the Spectrum rocks with the lowest silica and highest total alkali contents.

Vapour phase minerals include tridymite, arfvedsonite, bright green aegirine, and rarely analcime, fluorite and pyrite. Of these arfvedsonite is by far the most abundant and commonly the only mineral lining open voids. It also forms euhedral prisms up to 2 mm long in the porous flow layers of banded rocks. Such banding, which is very common in the Spectrum rocks, is caused by alternating dense, glassy layers with porous layers in which microscopic trains of voids are surrounded and penetrated by late, vapour phase minerals.

The plutonic phase of the Spectrum Formation is a medium grained (2-4 mm) soda granite comprising about 75% sanidine, 15% quartz and 10% soda-rich femics (aenigmatite, acmitic hedenbergite and arfvedsonite). The texture is hypidiomorphic granular with clear, unstrained quartz interstitial to subhedral crystals of feldspar. The feldspar (Or₄₀₋₄₅) is clouded by a “dust” of very fine opaque minerals. It is either untwinned or exhibits indistinct, extremely fine cross-hatched or patchy polysynthetic twinning. The femic minerals are interstitial to the feldspars and commonly enclosed by the quartz. Aenigmatite is the only femic mineral that occurs as subhedral and rarely as euhedral grains. Most of these are mantled by green, acmitic hedenbergite and blue pleochroic arfvedsonite. More commonly the three femic minerals form coarse poikilitic intergrowths with quartz. Probe analyses (Fig. 96; Table 9) indicate that the chemistry of the main constituent minerals of the soda granite is similar to that of fine grained equivalents in the extrusive comendites and pantellerites.

Kitsu basalt

Remnants of Kitsu basalt on Artifact and Yagi ridges are petrographically similar, very fine grained, alkali olivine basalt with 10% euhedral microphenocrysts (< 0.5 mm) of plagioclase and olivine. The groundmass is a holocrystalline, granular mosaic of very small clinopyroxene, plagioclase and opaque oxide crystals.

Table 9. Representative microprobe analyses and structural data for the principal mineral phases in the Spectrum felsic rocks.

	Feldspar				Pyroxene				Amphibole		Aenigmatite			
	Phenocryst		Groundmass		Phenocryst		Groundmass		Phenocryst		Phenocryst			
	SF1(int)	SF2	SF3	SF4	SP1(int)	SP2	SP3	SP4	SAM1(int)	SAM2	SAE1			
SiO ₂	66.73	67.18	67.52	67.00	49.81	48.49	47.83	48.55	50.49	49.08	40.58			
Al ₂ O ₃	17.38	18.43	18.69	18.27	0.12	0.12	0.20	0.22	0.36	0.06	0.39			
TiO ₂	0.0	0.0	0.0	0.0	0.35	0.42	0.46	0.86	0.0	0.13	7.66			
Cr ₂ O ₃	0.0	0.0	0.0	0.0	0.0	0.02	0.02	0.01	0.0	0.02	0.0			
Fe ₂ O ₃	1.40	0.39	0.49	1.31	9.99	3.20	1.86	5.35	11.24	2.30	1.74			
FeO	0.0	0.0	0.0	0.0	19.67	26.14	28.13	23.62	26.43	32.99	40.45			
MnO	0.0	0.0	0.0	0.0	1.06	1.10	1.01	1.14	0.90	1.15	0.74			
MgO	0.0	0.0	0.0	0.0	0.49	0.15	0.03	0.21	0.01	0.0	0.01			
NiO	0.0	0.0	0.0	0.0	0.0	0.0	0.0	0.0	0.0	0.0	0.0			
CaO	0.01	0.06	0.06	0.09	14.14	19.18	19.70	16.73	2.46	7.38	0.43			
Na ₂ O	6.30	7.03	7.50	7.58	4.33	1.35	0.68	2.62	5.57	1.32	7.60			
K ₂ O	7.41	6.49	5.90	5.61	0.02	0.0	0.0	0.03	0.34	0.0	0.0			
H ₂ O	0.0	0.0	0.0	0.0	0.0	0.0	0.0	0.0	0.0	0.0	0.0			
F	0.0	0.0	0.0	0.0	0.0	0.0	0.0	0.0	0.0	0.0	0.0			
Total	99.23	99.58	100.16	99.86	99.98	100.18	99.92	99.34	97.91	97.34	99.60			
	No. of ions on basis of 8 (0)				No. of ions on basis of 6 (0)				No. of ions on basis of 23 (0)				No. of ions on basis of 40 (0)	
Si	3.0227	3.0125	3.0053	2.9977	2.0048	1.9880	1.9790	1.9905	7.9791	8.0196	11.7932			
Al	0.9278	0.9740	0.9804	0.9634	0.0	0.0058	0.0098	0.0095	0.0209	0.0	0.1336			
Cr	0.0	0.0	0.0	0.0	0.0	0.0062	0.0113	0.0	0.0	0.0	0.0			
Fe ³⁺	0.0477	0.0132	0.0164	0.0441	0.0	0.0	0.0	0.0	0.0	0.0	0.0732			
Al	0.0	0.0	0.0	0.0	0.0057	0.0	0.0	0.0012	0.0462	0.0116	0.0			
Cr	0.0	0.0	0.0	0.0	0.0106	0.0068	0.0030	0.0265	0.0	0.0026	0.0			
Ti	0.0	0.0	0.0	0.0	0.3026	0.0987	0.0578	0.1649	0.0	0.0160	1.6741			
Fe ³⁺	0.0	0.0	0.0	0.0	0.0	0.0010	0.0007	0.0003	1.3368	0.2829	0.3084			
Ni	0.0	0.0	0.0	0.0	0.0	0.0	0.0	0.0	0.0	0.0	0.0			
Fe ²⁺	0.0	0.0	0.0	0.0	0.6621	0.8963	0.9733	0.8099	3.4937	4.5081	9.8310			
Mn	0.0	0.0	0.0	0.0	0.0361	0.0382	0.0354	0.0396	0.1205	0.1592	0.1822			
Mg	0.0	0.0	0.0	0.0	0.0294	0.0092	0.0019	0.0128	0.0024	0.0	0.0043			
					0.6098	0.8425	0.8733	0.7349						
					0.3379	0.1073	0.0546	0.2083						
					0.0010	0.0	0.0	0.0016						
Ca	0.0005	0.0029	0.0029	0.0043					0.4165	0.5095	0.1339			
Na	0.5533	0.6112	0.6472	0.6576					1.7373	2.3381	4.2824			
K	0.4282	0.3712	0.3350	0.3202					0.0685	0.2751	0.0			

The Kitsu remnants south of Kounugu Lake are medium grained aphyric basalt in which intergranular plagioclase and olivine euhedra are partly or wholly enclosed by subophitic plates of purplish-brown titanite.

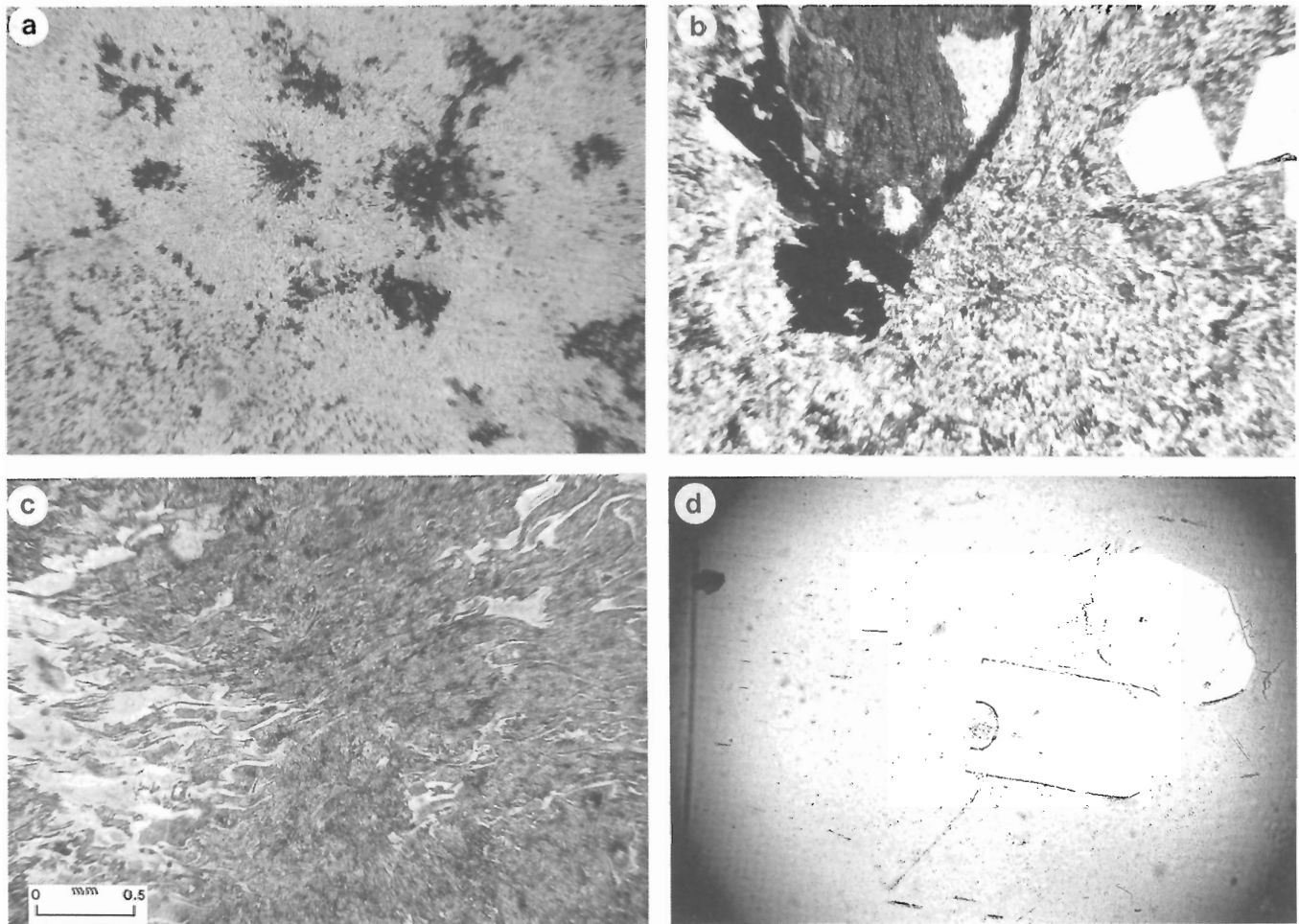
CHEMISTRY

Felsic rocks

Sixteen major element analyses of Spectrum felsic rocks are plotted on Figures 97 to 99 and five superior analyses are listed in Table 10. They range from 62 to 77% silica. The Harker diagrams (Fig. 97) show a systematic decrease in FeO, TiO₂ and Na₂O with increasing SiO₂ whereas the other oxides are scattered within fairly narrow

limits. All but three of the felsic samples are peralkaline, with an excess of total alkalis over alumina (A.I. > 1). They are further subdivided on the basis of Macdonald's (1974) Al₂O₃-FeO classification scheme. On this plot (Fig. 98) the Spectrum analyses are widely scattered over the fields of comendite, pantellerite and pantelleritic trachyte.

The three felsic samples with an excess of Al₂O₃ over total alkalis (A.I. < 1) are highly siliceous (SiO₂ 74 to 77%), leucocratic rocks that may have undergone late stage silicification. Relative to iron and magnesia they are among the rocks most highly enriched in alkalis as seen on the AFM diagram (Fig. 99). Although not strictly peralkaline, these highly alkaline (A.I. 0.7-0.9) rhyolites are chemically and mineralogically similar to the suite as a whole.



a — Spherulitic comendite. Radiating clusters of aegirite, arfvedsonite, acmitic pyroxene and sanidine are surrounded by clear areas of quartz.

b — Porphyritic pantellerite with euhedral microphenocrysts of sanidine, pyroxene, and aegirite. The pyroxene has a hedenbergite core mantled by a green, pleochroic rim of more acmitic composition.

c — Partly devitrified comenditic glass in a welded ash flow with distinct fluidal layering.

d — Sanidine microlites in clear glass from the base of a comendite flow.

Figure 95. Photomicrographs of Spectrum felsic rocks; scale bar 0.5 mm; plane light.

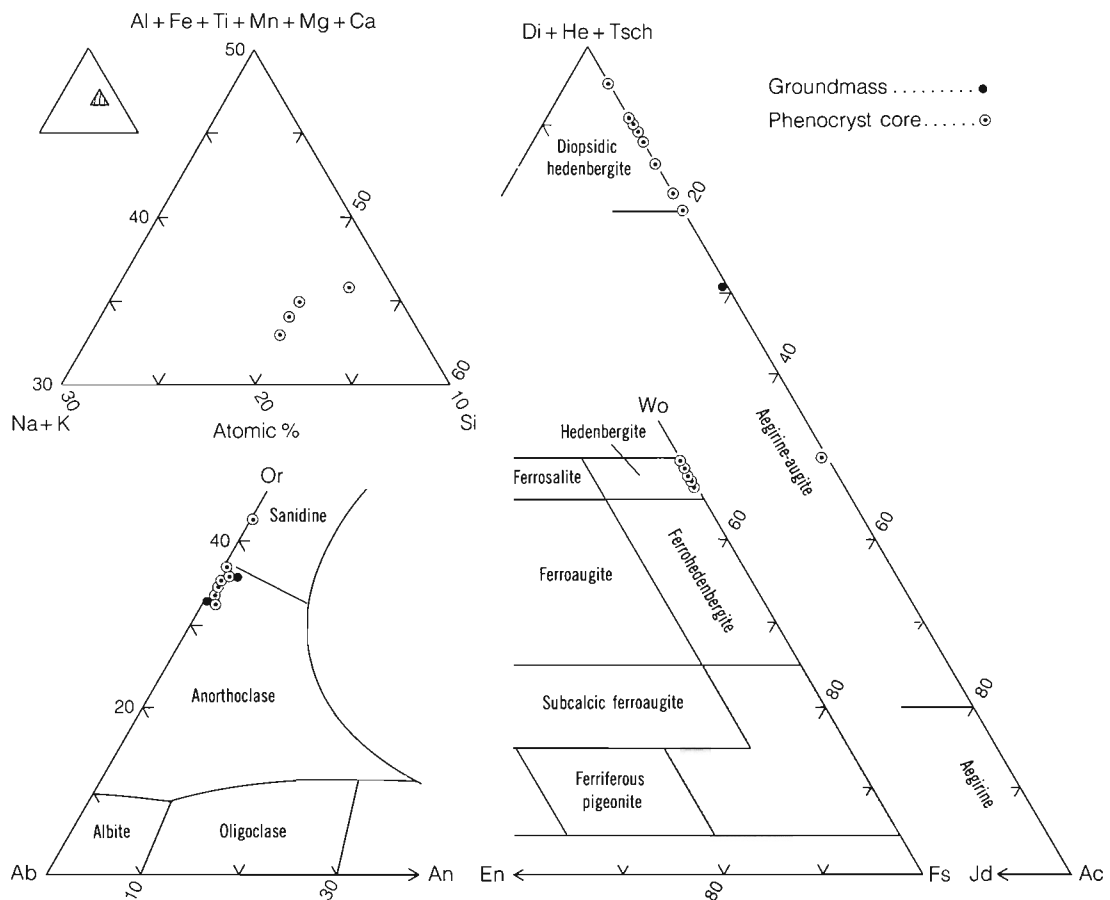


Figure 96. Plot of microprobe analyses of the principal mineral phases in the Spectrum rocks. (Amphibole classification after Ernst, 1962).

Table 10. Representative chemical analyses of specimens from the Spectrum Formation.

	Trachyte	Comendite			Pentelleritic trachyte	Pentellerite
Sample	29	26	2887	32	28	2872
SiO ₂	75.700	74.900	68.500	69.600	62.400	71.900
Al ₂ O ₃	12.100	11.700	13.500	13.400	14.400	8.600
Fe ₂ O ₃	1.700	0.600	4.100	2.200	4.700	4.200
FeO	0.0	2.000	2.200	2.400	3.700	3.200
CaO	0.230	0.280	1.000	0.620	1.360	0.700
MgO	0.270	0.170	0.400	0.230	0.320	0.600
Na ₂ O	3.000	4.700	6.100	6.100	7.100	5.000
K ₂ O	4.870	4.520	4.800	4.990	4.800	3.200
TiO ₂	0.180	0.170	0.500	0.370	0.640	0.500
P ₂ O ₅	0.040	0.040	0.020	0.050	0.100	0.050
MnO		0.050	0.140	0.110	0.200	0.110
S	0.070	0.070	0.0	0.080	0.080	0.0
NiO	0.0	0.0	0.0	0.0	0.010	0.0
H ₂ O	0.900	0.100	0.600	0.200	0.400	1.900
CO ₂	0.0	0.0	0.0	0.0	0.0	0.0
Total	99.060	99.300	101.860	100.350	100.210	99.960

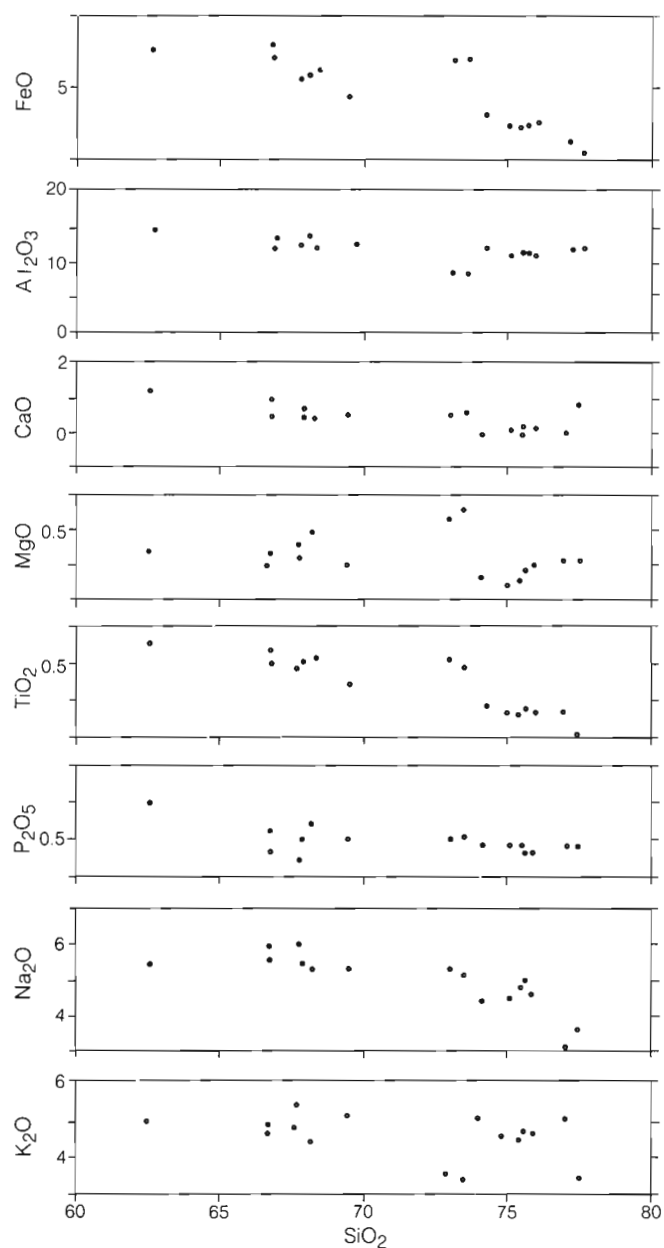


Figure 97. Harker variation diagram in weight per cent for 16 analyzed specimens from the Spectrum Formation.

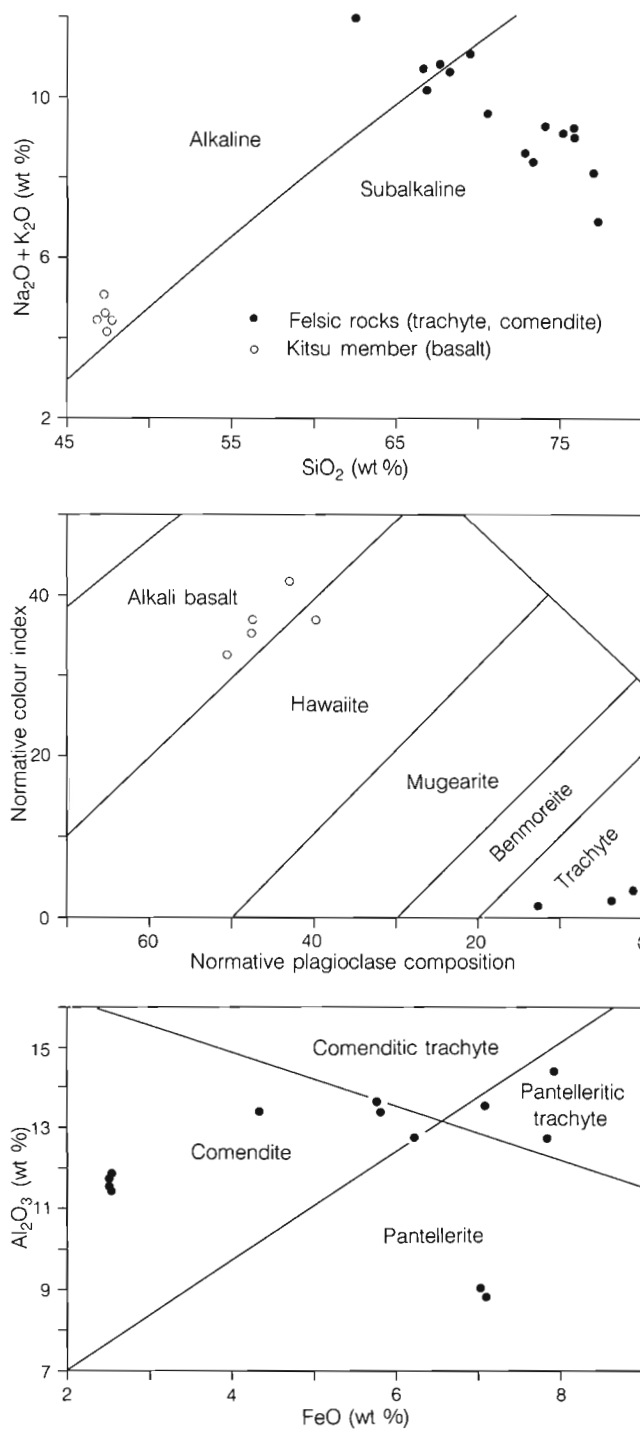


Figure 98. Plots of Spectrum Formation analyses. Alkaline rocks are plotted on the alkali vs. silica and normative colour index vs. normative plagioclase composition diagrams. Per-alkaline rocks are shown on the Al_2O_3 vs. FeO diagram.

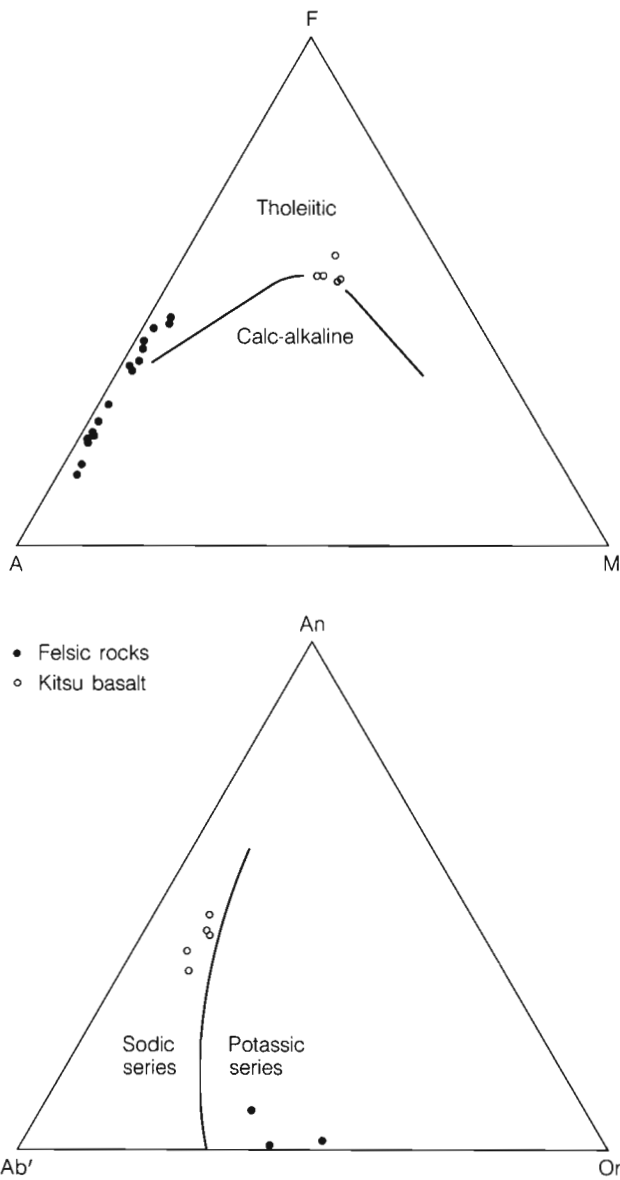


Figure 99. AFM and Ab'-An-Or plots of 16 analyzed specimens from the Spectrum Formation. ($A = Na_2O + K_2O$; $F = FeO + 0.8998 Fe_2O_3$; $M = MgO$; $Ab' = Ab + 5/3Ne$).

On the alkali-silica diagram (Fig. 98) the analyses of felsic, Spectrum rocks display the same abrupt decrease in total alkali content with increasing SiO_2 that characterizes the felsic members of the Armadillo Formation. In both suites the plot is fairly linear, it includes both alkaline and peralkaline rocks, and it intercepts the alkaline-subalkaline field boundary of Irvine and Baragar (1971) at about 68% silica. The slope of this line suggests that the apparent decrease in alkalis is not due entirely to a constant sum effect. More probably it is due to some process of alkali depletion, particularly Na depletion, in rocks with more than $\pm 68\%$ SiO_2 . The separation of a hydrous or vapour phase may have selectively removed Na with respect to SiO_2 in these siliceous end members. The operation of such a process during post-eruptive cooling has been suggested by Macdonald (1974, p. 514) to explain lower Na_2O in crystalline as compared to glassy rocks. However, the Na_2O content of three Spectrum obsidians (Fig. 98) is intermediate to the range covered by crystalline rocks, suggesting that pre-eruptive partitioning of Na_2O may also have been operative.

Kitsu basalt

Six analyses of Kitsu basalt plot in or near the alkali olivine basalt field of the Irvine and Baragar (1971) classification and are chemically indistinguishable from the underlying Kounugu basalts (Fig. 98).

PYRAMID FORMATION

GENERAL GEOLOGY

Introduction

Rhyolite and trachyte flows, domes and thick piles of primary pyroclastic breccia erupted during the Pyramid stage are exposed in prominent, light-coloured cliffs and narrow-crested ridges along the deeply dissected eastern flank of Mount Edziza. Basalt flows, believed to be coeval with the early stages of felsic activity, are included in the Pyramid Formation. They are defined by the presence of an underlying felsic pyroclastic member which has been recognized only in the immediate vicinity of the two northern felsic domes. The basalts are probably more widespread than shown on the map but, in the absence of a basal marker horizon, they could not be separated with confidence from the underlying Nido basalt.

Except for Pyramid dome itself, which was neither covered by younger lavas, nor greatly modified by erosion, the original form and extent of the Pyramid pile has been virtually obliterated. Pyramid dome and a few erosional remnants of flows and breccia are all that remain of the proximal facies. The distal facies, comprising air-fall pumice, lahars, and glacial fluvial gravels is preserved in thin discontinuous, usually recessive units interlayered with basalt flows in the canyons of Cook and Tenchen creeks. Both the proximal and distal units are underlain by Nido basalt and either overlain or surrounded by Ice Mountain flows. Those parts of the Pyramid pile that lay beyond, or projected above the level flooded by Ice Mountain lavas, have been mostly covered by younger flows of the Edziza or Big Raven formations.

Despite its limited preservation, the Pyramid pile displays sufficient internal variation to permit a reasonable reconstruction of its original form (Fig. 100). The source of the basal pyroclastic member and the basalt is not known but the main felsic flows and domes appear to have issued from three separate centres: The Pyramid, Sphinx dome and Pharaoh dome. The Pyramid is an endogenous dome, at the northern end of the area underlain by Pyramid Formation. It was emplaced and partly eroded before the eruption of Sphinx dome which overlaps its western flank. Pharaoh dome, at the south end of the Pyramid pile, is not in contact with The Pyramid. However, it is believed to be approximately coeval with, or slightly younger than, Sphinx and thus younger than The Pyramid. The Sphinx and Pharaoh piles are separated by an intervening region in which glacial, fluvial and lacustrine deposits accumulated. This material is derived mostly from the adjacent domes but it includes glacial deposits that originated beyond the region underlain by Pyramid Formation. Glacial-lacustrine

deposits on the north flank of the Pharaoh pile are believed to have accumulated in a transient body of water, Tut lake, which was ponded behind Sphinx dome.

Basal pyroclastic member

South and east of The Pyramid, in sections facing Cook Creek and Kakiddi Creek the uppermost, highly porphyritic basalt of the Nido Formation is overlain by up to 10 m of locally derived fluvial gravel and poorly sorted colluvium. This is overlain by a rusty-brown clast-supported pyroclastic unit up to 3 m thick containing trachytic pumice, lithic clasts and crystals of alkali feldspar and sodic pyroxene in a moderately indurated granular matrix (Fig. 101). Over 80% of the clasts are porous green trachytic pumice containing sparse euhedral pyroxene crystals. They are undeformed, subrounded and commonly less than 2 cm across. Lithic clasts are mostly vesicular basalt but include a small percentage of trachyte and dense, nonvesicular basalt. All of the lithic clasts exhibit some evidence of abrasion and the larger ones are subangular to subrounded. The matrix is a fine, sand-sized mixture of pumice, lithic grains and broken crystals cemented by iron oxides. There is no welding.

The deposit has a crude planar fabric defined by layers relatively rich and relatively poor in lithic clasts. There is no systematic grading or other evidence of water reworking, but the lower 2-3 m are slightly finer grained and contain fewer lithic clasts than the upper part. Most of the lithic clasts are only slightly larger than the pumice (1-5 cm) but a few blocks up to 30 cm across are present near the top.

The basal pyroclastic member is believed to be a surge deposit, formed during a precursor, vent-clearing eruption that preceded eruption of the main Pyramid domes.

Basalt member

The basal trachytic surge deposit is overlain by up to 65 m of basalt flows. The contact between the lower basalt and the top of the surge deposit is remarkably sharp (Fig. 102). There is no evidence of any modification of the surface by wind or water prior to burial, indicating that the explosive, surge event was followed almost immediately by the effusion of basalt. The basalt section (Fig. 103) includes from 6 to 10 cooling units each from 3-20 m thick. The thicker flows have well developed colonnades of stout reddish-brown weathering columns that extend through most of the flow and are overlain by a relatively thin blocky entablature and flow-top breccia. The upper 3 or 4 flows are

MOUNT EDZIZA

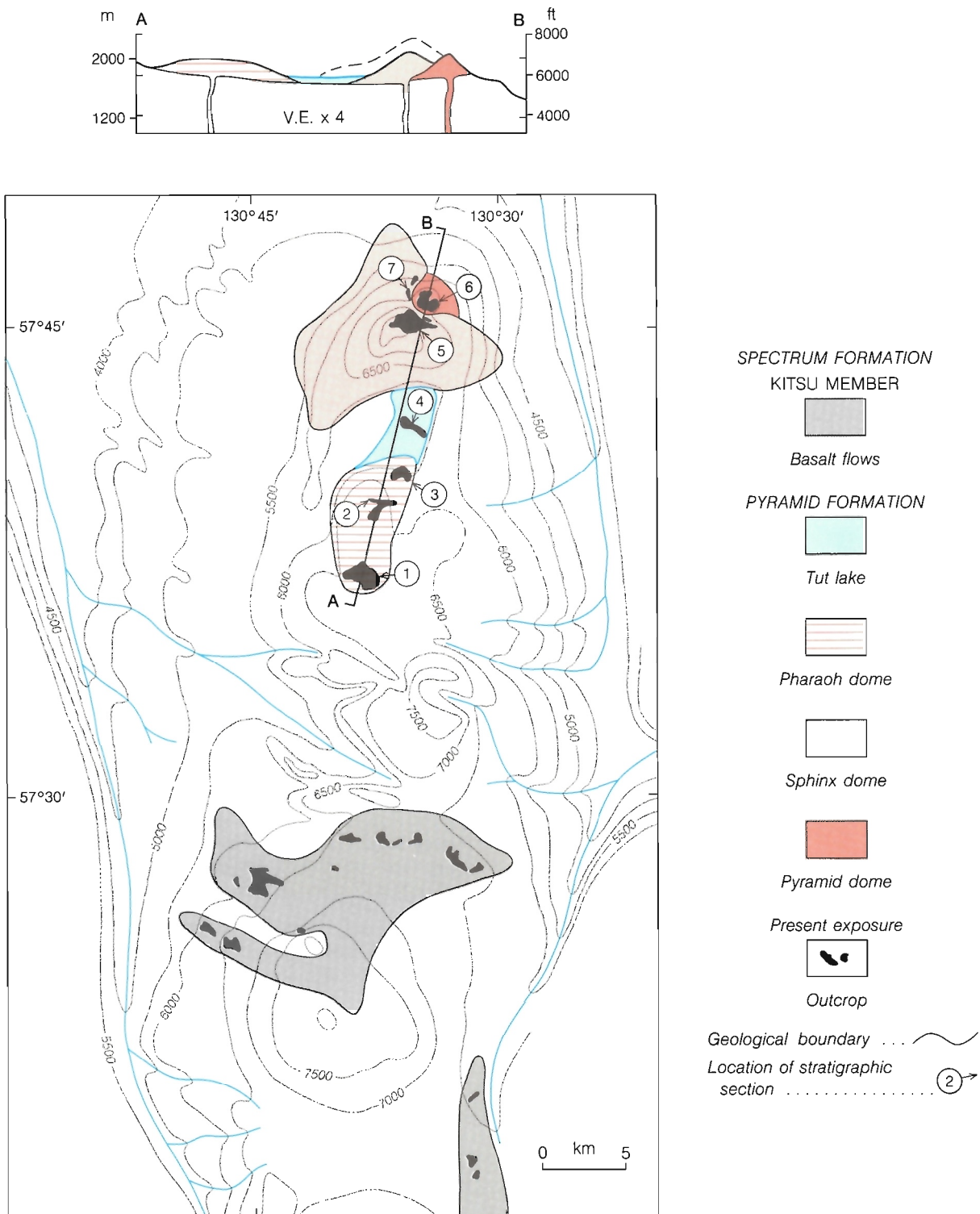


Figure 100. Paleogeological map and schematic cross-section showing the inferred maximum extent of the Kitsu Member of the Spectrum Formation and the maximum extent of the Pyramid Formation at the end of Pyramid time. Stratigraphic sections are shown in Figure 103.

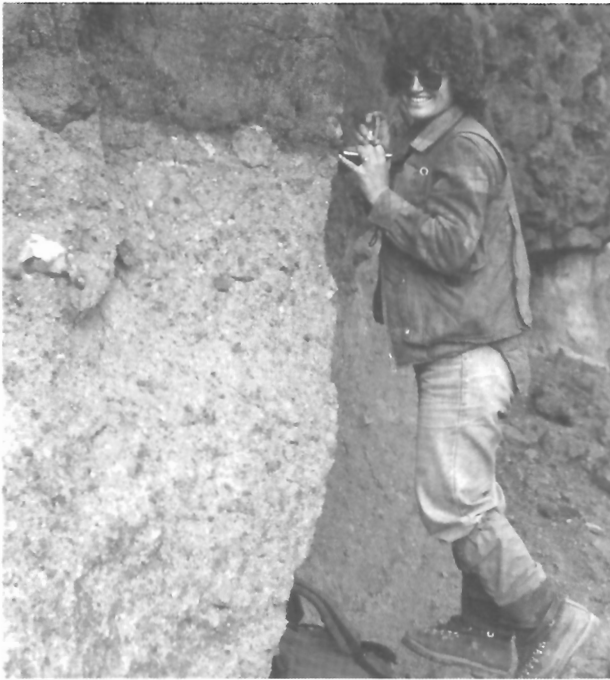


Figure 101. Surge deposit at the base of the Pyramid succession. GSC 125 605.



Figure 102. Contact between the top of the basal surge deposit and overlying basalt flows of the lower Pyramid Formation. GSC 125 606.

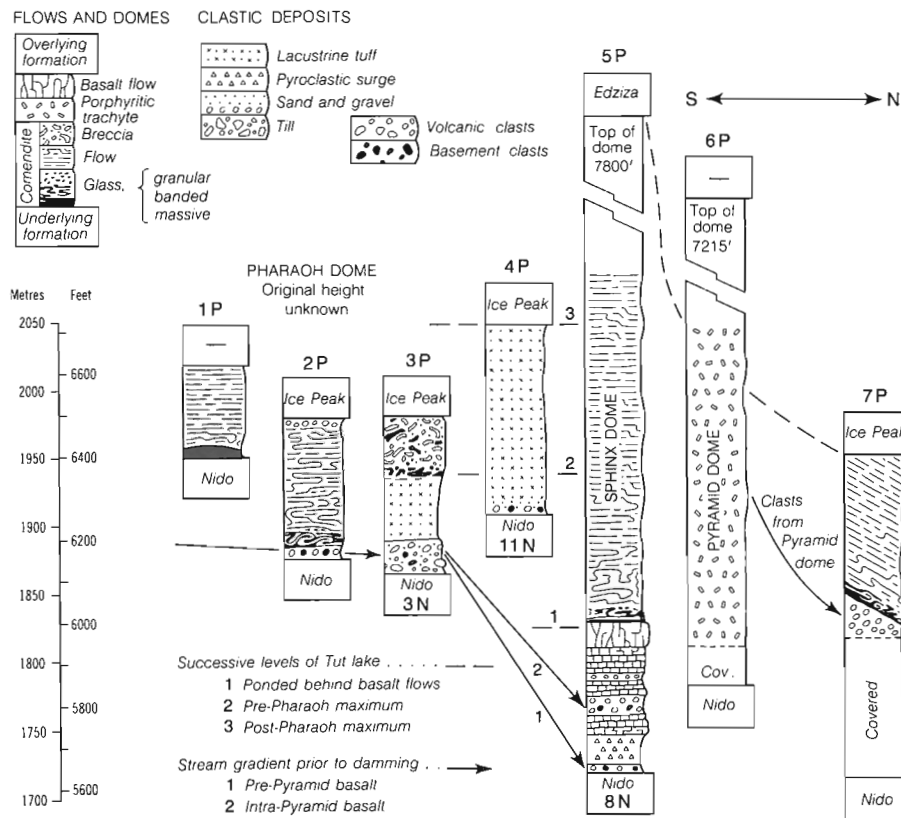


Figure 103. Stratigraphic sections from the Pyramid Formation, showing the relationship of the volcanic rocks to fluvial and epiclastic deposits and to changing stream gradients and lake levels during the evolution of the pile. Section numbers (1-7) refer to locations shown on the paleogeological map (Fig. 100). P, Pyramid Formation; N, Nido Formation.

MOUNT EDZIZA

aphyric whereas those in the lower part of the pile contain about 20%, randomly oriented phenocrysts of plagioclase 1-10 mm long and about 5% olivine and pyroxene in crystals up to 3 mm across.

The basalt section includes at least one layer of fluvial gravel from 2-3 m thick. Its position within the pile varies slightly from place to place but the morphology and composition is fairly uniform. Well rounded boulders up to 0.5 m across are randomly mixed with less mature, subangular boulders in a sparse pebbly or coarse sandy matrix (Fig. 104). Most of the clasts are locally derived basalt, but a few well rounded cobbles of Bowser, chert-pebble conglomerate (Upper Jurassic) and Mesozoic granitic rock are also present. The latter must have been transported at least 20 km from a source in the Armadillo Highlands.

The presence of channelling, the paucity of fines and the large size of the transported boulders are evidence of deposition in a high energy environment. It is probably a lag gravel deposited by a rapidly flowing alpine river that was repeatedly displaced from its course by successive basalt flows. The mixed load of rounded and subangular material suggests that it may be of glacial-fluvial origin. The presence of till at the base of the Pyramid succession farther south, on Idiji Ridge, is consistent with the continued presence of ice in and around the Armadillo Highlands at the onset of Pyramid activity.

The deposition of this gravel within the basalt succession does not imply a long period of erosion. In fact there is no evidence that the flows themselves were modified at all between successive eruptions. The entire episode of basaltic activity, including the deposition of lag gravel, could have been completed in a few tens of years.

The Pyramid

The Pyramid is a prominent conical dome that rises above the gently sloping interflue between Cook and Pyramid creeks (Fig. 105). It is about 366 m high and slightly more than 1 km across at its base. Except for well developed concentric and inward dipping joint sets, the dome exhibits no internal structure. The rock is an extremely uniform, coarsely and abundantly porphyritic trachyte with up to 50% stout, euhedral alkali feldspar phenocrysts from 0.5-2 cm across in a white, aphanitic matrix peppered with tiny clots of opaque oxides. The phenocrysts are randomly oriented and the matrix exhibits no layering or banding. In a few places a brown outer rind of rusty, altered, but texturally identical trachyte is plastered against the outer surface of the dome. These zones are from one to a few metres thick and have prominent, closely spaced joints parallel to the surface. They do not appear to be a weathering phenomenon and are believed to be remnants of the original outer, oxidized portion of the dome.

The Pyramid is completely isolated from adjacent rocks by a thick apron of active talus (Fig. 106). However, clasts derived from it appear in gravel lenses between the Nido and

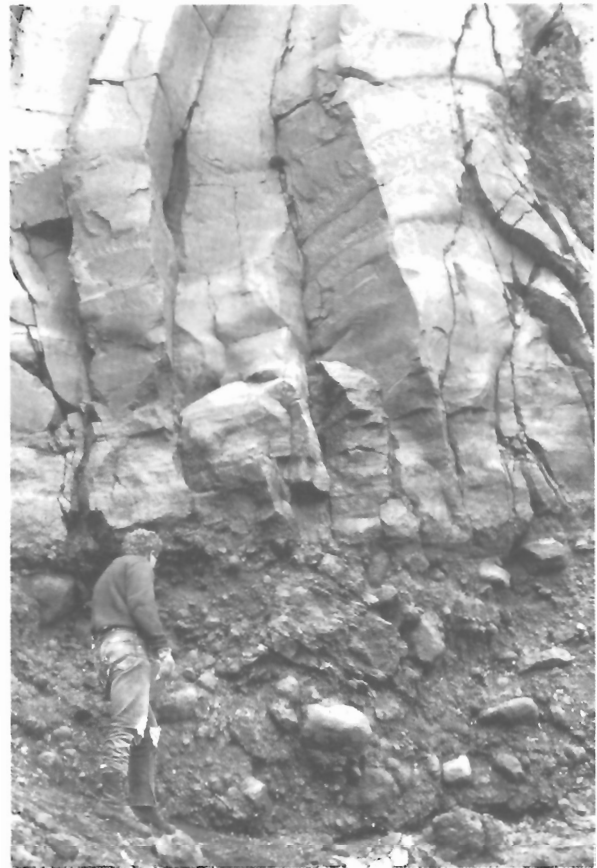


Figure 104. Pyramid basalt flow resting on coarse fluvial gravel deposit. GSC 202468-X.

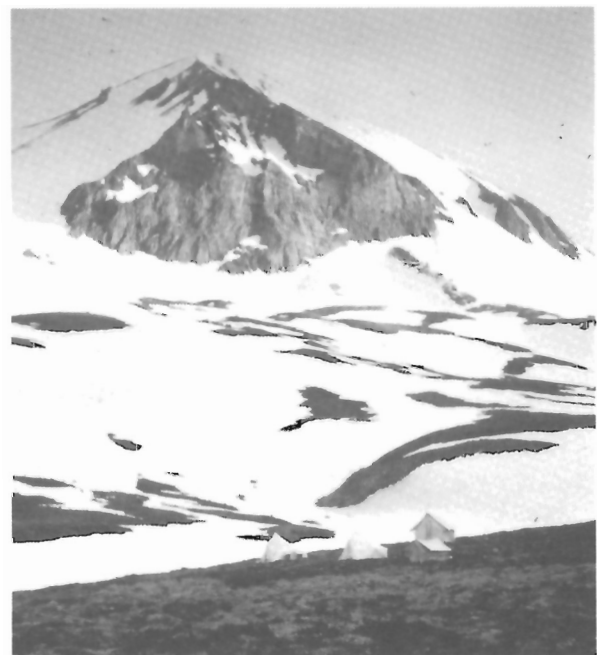


Figure 105. The Pyramid, an endogenous dome of coarsely porphyritic trachyte of the Pyramid Formation. GSC 202468-Y.

PYRAMID FORMATION

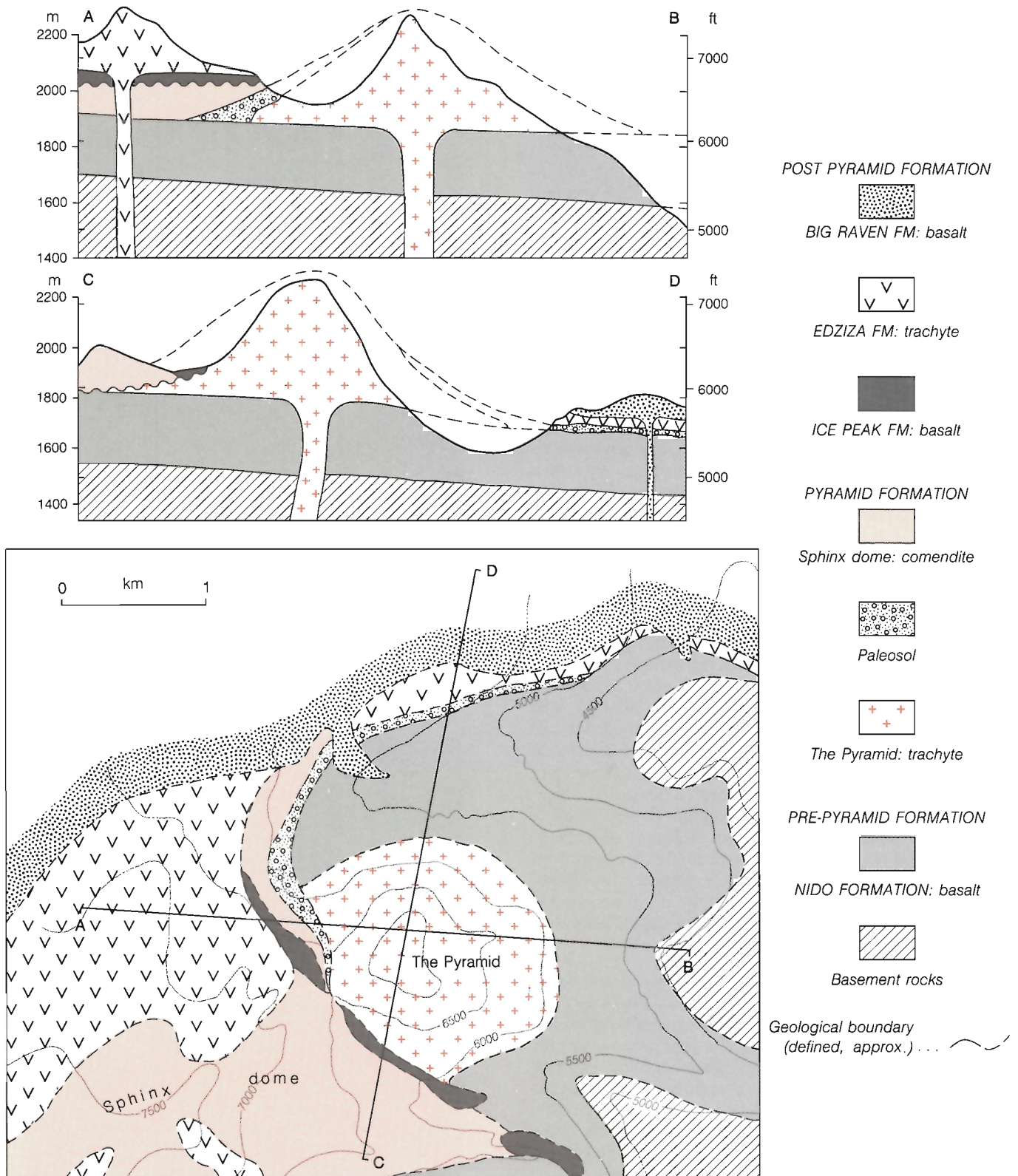


Figure 106. Map and cross-sections of The Pyramid, showing the relationship of Pyramid dome and its apron of epiclastic debris to Sphinx dome and younger flows of the Edziza Formation and Big Raven Formation.

MOUNT EDZIZA

Ice Peak basalts in Cook Creek valley, and also in thick gravel deposits beneath the prominent flow of Edziza Formation trachyte that caps the escarpment on the north side of Pyramid Creek. Similar, but less mature gravels, consisting wholly of subrounded clasts of coarsely porphyritic Pyramid trachyte, underlie the basal Sphinx dome rhyolite at the head of Pyramid Creek. These poorly rounded gravels are less than 1 km from the base of The Pyramid and do not imply that a long period of erosion separated eruption of The Pyramid and the onset of Sphinx activity. However, they clearly establish the relative age of the two piles.

Sphinx dome

The eastern side of Sphinx dome is exposed on the northeast flank of Mount Edziza, between Cook and Pyramid creeks. Its western half is buried beneath younger, Edziza trachyte and most of its southern edge has been removed by headward erosion of Cook Creek. The basal contact is exposed for about 1.5 km along the steep northern side of Cook Creek valley where the rhyolite rests on a nearly flat surface which dips a few degrees toward the east and is conformable with the underlying basalt. There, the basal surface is about 6000 ft. (1829 m) in elevation, whereas 3 km farther north, in the head of Pyramid Creek, the rhyolite, with steep northeast dipping flow layering, extends down to an elevation of 5600 ft. (1707 m), indicating that Sphinx dome was built on a moderately dissected surface cut into the underlying basalt. The thin eastern edge of Sphinx dome wedges out between this surface and overlying remnants of younger, Ice Peak basalt which covered the dome up to an elevation of about 6300 ft. (1920 m). The central part, which projected above the level flooded by Ice Mountain basalt, was slightly modified by erosion and then partly overridden by trachyte flows during the subsequent construction of the main edifice of Mount Edziza. The most westerly, and highest exposure of Sphinx dome rhyolite is overlain by Edziza trachyte at an elevation of 7500 ft. (2286 m) and two thick remnants of Edziza trachyte flows cling to its steep northern and southern slopes. These flows, which extend from above 7500 ft. (2286 m) down to about 6500 ft. (1980 m) must have occupied steep, radial valleys cut into the flanks of the Sphinx rhyolite dome.

The basal contact between Sphinx dome and underlying basalt is commonly obscured by an apron of talus shed from the closely jointed rhyolite. A layer of basaltic gravel is exposed at the base of the dome in a few places along the north side of Cook Creek, and at the head of Pyramid Creek the rhyolite rests on a thick mat of colluvium or fossil talus composed entirely of subrounded clasts of porphyritic trachyte derived from erosion of The Pyramid. The lower 3-9 m of Sphinx dome consist of glass which is commonly flow layered with prominent, ribbon-like layers of black obsidian separated by narrow trains of tiny white, pale pink and green spherulites. Well developed fractures parallel to the flow have given the outcrops a flaggy, bedded appearance. On flat surfaces, such as the contact along Cook

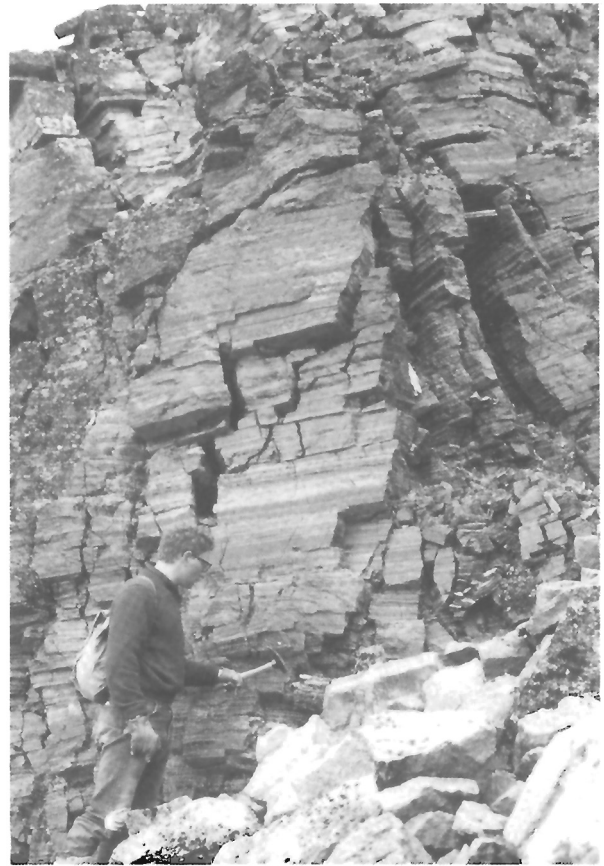


Figure 107. Planar flow layering in obsidian at the base of Sphinx dome comendite. GSC 202468-Z.

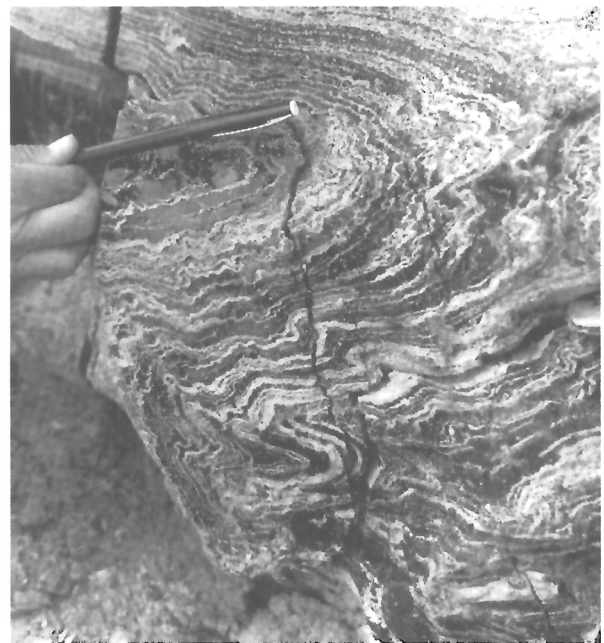


Figure 108. Complexly contorted flow folds in interlayered vitreous and crystalline comendite in the lower part of Sphinx dome. GSC 125 607.

Creek, the flow layering is almost planar, with individual layers having a continuity of several metres (Fig. 107). In contrast, the glass at the base of the steeply inclined rhyolite in Pyramid Creek is highly contorted, with intricate recumbent folds, overturned in the direction of flow. Near the top of the vitreous layer, thin bulbous and vitreous lenses of black or greenish-grey glass are folded into the adjacent rhyolite (Fig. 108). In this transition zone, the glass is commonly best developed in the crests of flow folds.

No coherent glass layers occur within the main body of the dome. The rhyolite for several tens of metres above the basal obsidian is prominently flow layered, with an intricate subparallel filigree of small interlocking spherulitic layers or fine laminar flow layering. Many of the flow layered rocks display flow folds overturned in the direction of flow. The crests of the folds and crenulations impart a prominent transverse lineation to the surface of individual flow layers, and small tensional gash fractures form a regular pattern of open "chattermarks" at an angle to the lineation. Individual gash fractures vary from less than 1 mm to about 1 cm across and are up to 3 cm long. They appear to have formed during the final stages of flow when the nearly solid magma responded to continued strain by incipient fracturing as well as plastic flow. In some of them the viscous lava has pulled away from enclosed phenocrysts, revealing small, transverse acicular crystals of arfvedsonite, aligned parallel with the lineation.

The main mass of Sphinx dome is a fine grained, intricately layered, light grey or green, nonporphyritic rhyolite, locally with patchy, vapour phase mottling. The upper 50-100 m of spheroidal rock have undergone intense vapour phase alteration which has bleached it white. In this zone lenticular voids lined with amethyst and other secondary minerals are aligned along prominently developed flow

layers. Locally the original outer surface of the dome has survived erosion. It comprises a zone of autobreccia several metres thick in which angular, cognate inclusions of flow layered rhyolite are surrounded by a granular aggregate of altered rhyolite and pumice particles and a fluidal-banded, devitrified glass.

At its centre Sphinx dome is at least 550 m thick, yet there is little evidence to indicate that it is a composite pile, formed by eruption of successive pulses of lava. On the contrary, the absence of internal glass or breccia layers, as well as the progressive, uninterrupted change in vapour phase alteration throughout its entire thickness, suggest that it was built in a single pulse of activity. It probably issued as an endogenous dome of relatively viscous magma which welled out into a bulbous mass above its vent, expanding laterally under its own weight. The absence of associated pyroclastic deposits suggests that the eruption was not accompanied by any significant explosive activity.

Pharaoh dome

Rocks believed to be remnants of Pharaoh dome are exposed in isolated remnants along the eastern flank of the Edziza Complex from Tennaya Creek south to Cartoona Ridge (Fig. 100). They are separated from Sphinx and Pyramid domes by an interval of almost 5 km in which Ice Mountain flows rest either directly on the underlying Nido basalt, or are separated from it by discontinuous lenses of glacial-fluvial gravel, some of which contain rhyolite and obsidian clasts derived from Sphinx dome.

Each of the four principal remnants of the Pharaoh pile is characterized by a unique set of stratigraphic and structural relationships (Fig. 103, 109). On Nido Ridge the entire

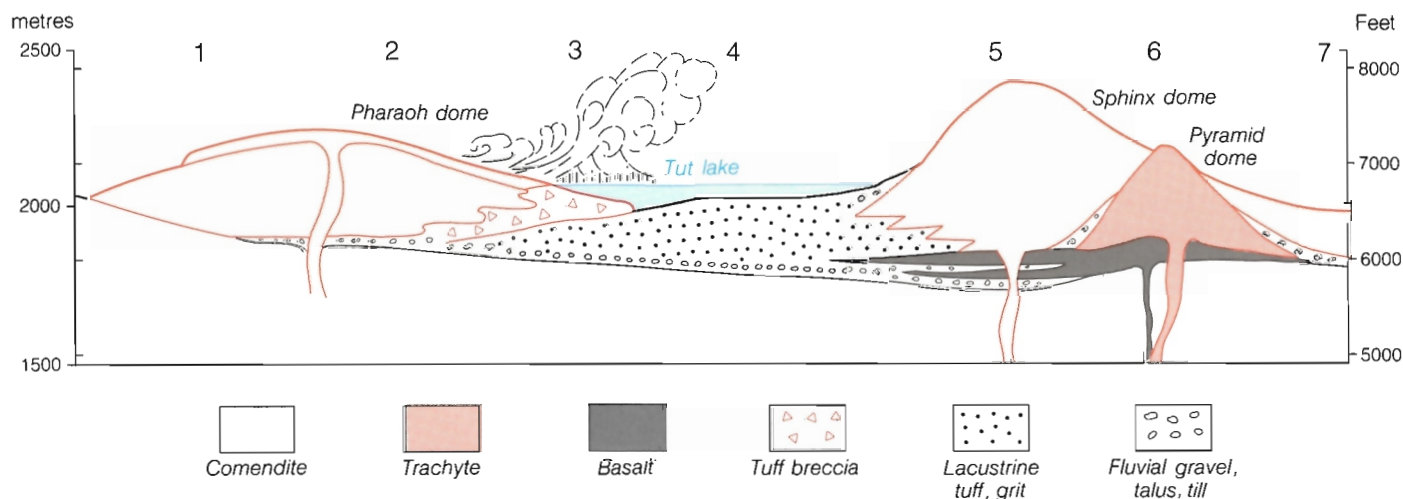


Figure 109. Schematic cross-section showing the relationship of the three Pyramid Formation domes to the Tut lake volcanoclastic sediments and to fluvial gravel. Numbers at top show the relative positions of stratigraphic sections (Fig. 100 and 103).

122 m section consists of bedded rhyolitic breccia, ash and volcanoclastic sediments deposited in Tut lake. Similar fragmental rocks on Idiji Ridge are overlain by nearly 60 m of rhyolite lava and, still farther south, on Sorcery Ridge, the clastic facies is missing and more than 150 m of rhyolite lava rests directly on the eroded surface of Nido basalt at an elevation of 6000 ft. (1829 m). At the extreme southern edge of the pile, at the head of Shaman Creek, a lobe of rhyolite, only 2-3 m thick at its distal end, rests on Nido basalt at an elevation of 6500 ft. (1981 m). The Pharaoh pile was thus deposited on an erosion surface of considerable relief.

The Pharaoh stratigraphy does not appear to extend to the western end of either Nido or Idiji ridges. The precise relationship is obscured by extensive talus cover in the upper part of these valleys, but isolated outcrops of basalt west of, and at the same elevation as flat-lying Pharaoh rhyolite on the eastern part of the ridges, indicate that the western edge of the Pharaoh pile is truncated by a steep north-trending contact. The possibility of a fault cannot be ruled out, but it seems more likely that this part of the Pharaoh pile was deposited in a deeply incised northerly-flowing river valley cut into the old basalt surface. The eastern side of this old valley has been stripped away, along with the main edifice of Pharaoh dome itself, but its eastern side is still partly preserved and forms the steep western edge of the Pharaoh dome pile.

Glass is extensively developed at the base of the Pharaoh dome lava flows. On Idiji Ridge where the rhyolite overlies related volcanoclastic deposits, a 1-3 m thick layer of massive, bright, clear, nonporphyritic obsidian has formed along the base. Similarly, a layer of massive, unfractured obsidian underlies the relatively thin distal lobe at the head of Shaman Creek. Unlike the glass on Idiji Ridge, it has a dull, resinous lustre and contains a few small (< 1%, ± 1 mm) feldspar crystals. In contrast, the glass which is 1-3 m thick at the base of the Sorcery Ridge section, is flow layered, having regular 1-10 cm vitreous layers separated by shear surfaces along which spherulites have formed. It is underlain by up to 0.3 m of fine, sand-size, poorly indurated, granular black glass, and overlain by a transition zone in which contorted layers of glass are infolded with spherulitic rhyolite.

A relatively small section of rhyolite, exposed by recent retreat of ice from the steep east-facing headwall of Tencho Glacier, is believed to be close to a vent. There, the base of the pile is a 3-4 m thick mat of highly welded pumice containing a few lithic clasts of rhyolite. It is overlain by 2-3 m of frothy, agglutinated spatter comprising a welded mass of pumice, lithic clasts and lenticules of glass. The latter is commonly brown, devitrified and highly oxidized in its lower part, but becomes less altered upward. Although this zone has a pronounced eutaxitic texture, it lacks many of the features characteristic of ash flows observed elsewhere in the Edziza Complex. It grades upward into a flow breccia, and was probably formed by spalling of incandescent

scale and oxidized debris from the front of the advancing flow. The flow breccia itself is up to 10 m thick and contains angular chunks of rhyolite with complexly contorted flow layers. Within this zone, grey, green and black obsidian form contorted layers and lenses, both within and between the breccia fragments.

The main mass of Pharaoh dome, like that of Sphinx, is fine grained to aphanitic, white, greenish-grey to purple flow layered rhyolite. Locally, it displays a prominent vapour phase mottling which imparts a characteristic "leopard skin" pattern to the surface. Near the top of the pile, the rock has been almost completely reconstituted to a pure white, spherulitic mosaic of secondary minerals. Lenticular, open spaces along the flow layers in this altered phase are lined with vapour phase minerals, including amethyst, fluorite, and hematite.

The upper surface of the Pharaoh dome lava is preserved beneath Ice Peak basalt on both Idiji and Sorcery ridges. It forms a 2-3 m thick layer of breccia containing bits of glass and clasts of rhyolite, commonly with red alteration rinds in a reddish-brown, frothy matrix of devitrified glass and pumiceous debris. On Sorcery Ridge, this breccia is overlain directly by Ice Mountain trachyte, whereas on Idiji Ridge, 2 m of unconsolidated pumice intervene between the breccia and the overlying basalt. A few thin lenses of gravel, containing small rhyolitic pebbles in a red earthy matrix, are present on top of the Pharaoh dome rhyolite. However, there is no evidence that the dome suffered extensive erosion prior to being covered by Ice Peak flows. Also, Pharaoh dome lava lacks any evidence of internal structures that might indicate successive eruptions of several flows. Like Sphinx and The Pyramid, it appears to be the product of a single rapid effusion of rhyolite, probably as an endogenous dome. But, unlike the other centres, the Pharaoh dome eruption was both preceded and followed by bursts of explosive activity that produced showers of air-fall pumice and minor ash flows.



Figure 110. Looking northeast at Nido Ridge. Bedded lacustrine tuff, deposited in Tut lake, forms the light coloured recessive unit resting on Nido basalt flows near the centre of the ridge. GSC 202469-A.

Tut lake volcanoclastic deposits

The northern edge of Pharaoh rhyolite dome is underlain by a wedge of poorly consolidated clastic material which thickens toward the north (Fig. 103). On Idiji Ridge the clastic member is about 60 m thick and is overlain by an equal thickness of rhyolite. Six kilometres farther north, on Nido Ridge, the rhyolite has wedged out and the clastic member is almost 122 m thick (Fig. 110). It forms smooth, recessive slopes which lie close to the angle of repose and are mostly covered by a thin veneer of loose debris. Where torrents have cut through these surficial deposits the underlying clastic rocks are seen to have fairly distinct horizontal bedding and a large range of clast sizes.

A basal layer of fine, bedded pumice is overlain by alternately coarse and fine textured beds. The coarse beds are felsic tuff-breccia with angular to subrounded blocks of flow layered vitreous and pisolitic rhyolite in a loosely aggregated matrix of small clasts and pumice. The blocks are mostly less than 5 cm across but a few much larger clasts, up to 30 cm across, are randomly distributed throughout the section. Some of the clasts, which have intensely contorted, concentric layers of glass and spherulitic rhyolite, appear to be quenched globules. The glass layers are consistently from 0.5-2 cm thick. They are uniformly segmented by curved transverse fracture surfaces which give them a crackled appearance, resembling broken safety glass. Disaggregation of this crackled glass has

Table 11. Representative microprobe analyses and structural data for the principal mineral phases in felsic rocks of the Pyramid Formation.

	Feldspar			Pyroxene		Olivine	
	Phenocryst			Phenocryst		Phenocryst	
	PF1	PF2	PF3	PP1		PO1	
SiO ₂	61.27	58.74	66.48	49.58		31.53	
Al ₂ O ₃	23.40	26.59	19.08	0.76		0.0	
TiO ₂	0.0	0.0	0.0	0.32		0.01	
Cr ₂ O ₃	0.0	0.0	0.0	0.0		0.0	
Fe ₂ O ₃	0.18	0.27	0.16	1.61		0.0	
FeO	0.0	0.0	0.0	21.36		59.85	
MnO	0.0	0.0	0.0	0.68		2.32	
MgO	0.0	0.0	0.0	5.56		6.44	
NiO	0.0	0.0	0.0	0.0		0.0	
CaO	5.27	8.51	0.61	20.19		0.21	
Na ₂ O	7.78	6.44	5.17	0.37		0.0	
K ₂ O	1.24	0.71	8.55	0.01		0.0	
H ₂ O	0.0	0.0	0.0	0.0		0.0	
F	0.0	0.0	0.0	0.0		0.0	
Total	99.14	101.26	100.05	100.44		100.36	
	No. of ions on basis of 8 (0)			No. of ions on basis of 6 (0)		No. of ions on basis of 4 (0)	
Si	2.7523	2.6019	2.9880	Si	1.9632	Si	1.0096
Al	1.2388	1.3881	1.0107	Al	0.0355	Al	0.0
Cr	0.0	0.0	0.0	Ti	0.0013	Cr	0.0
Fe ³⁺	0.0061	0.0090	0.0054	Fe	0.0	Fe ³⁺	0.0
				Cr	0.0		
Al	0.0	0.0	0.0	Al	0.0	Al	0.0
Cr	0.0	0.0	0.0	Ti	0.0082	Cr	0.0
Ti	0.0	0.0	0.0	Fe ³⁺	0.0480	Ti	0.0002
Fe ³⁺	0.0	0.0	0.0	Cr	0.0	Fe ³⁺	0.0
Ni	0.0	0.0	0.0	Ni	0.0	Ni	0.0
Fe ²⁺	0.0	0.0	0.0	Fe ²⁺	0.7073	Fe ²⁺	1.6027
Mn	0.0	0.0	0.0	Mn	0.0228	Mn	0.0629
Mg	0.0	0.0	0.0	Mg	0.3282	Mg	0.3074
				Ca	0.8566		
				Na	0.0284		
				K	0.0005		
Ca	0.2536	0.4039	0.0294			Ca	0.0072
Na	0.6776	0.5531	0.4505			Na	0.0
K	0.0711	0.0401	0.4902			K	0.0

MOUNT EDZIZA

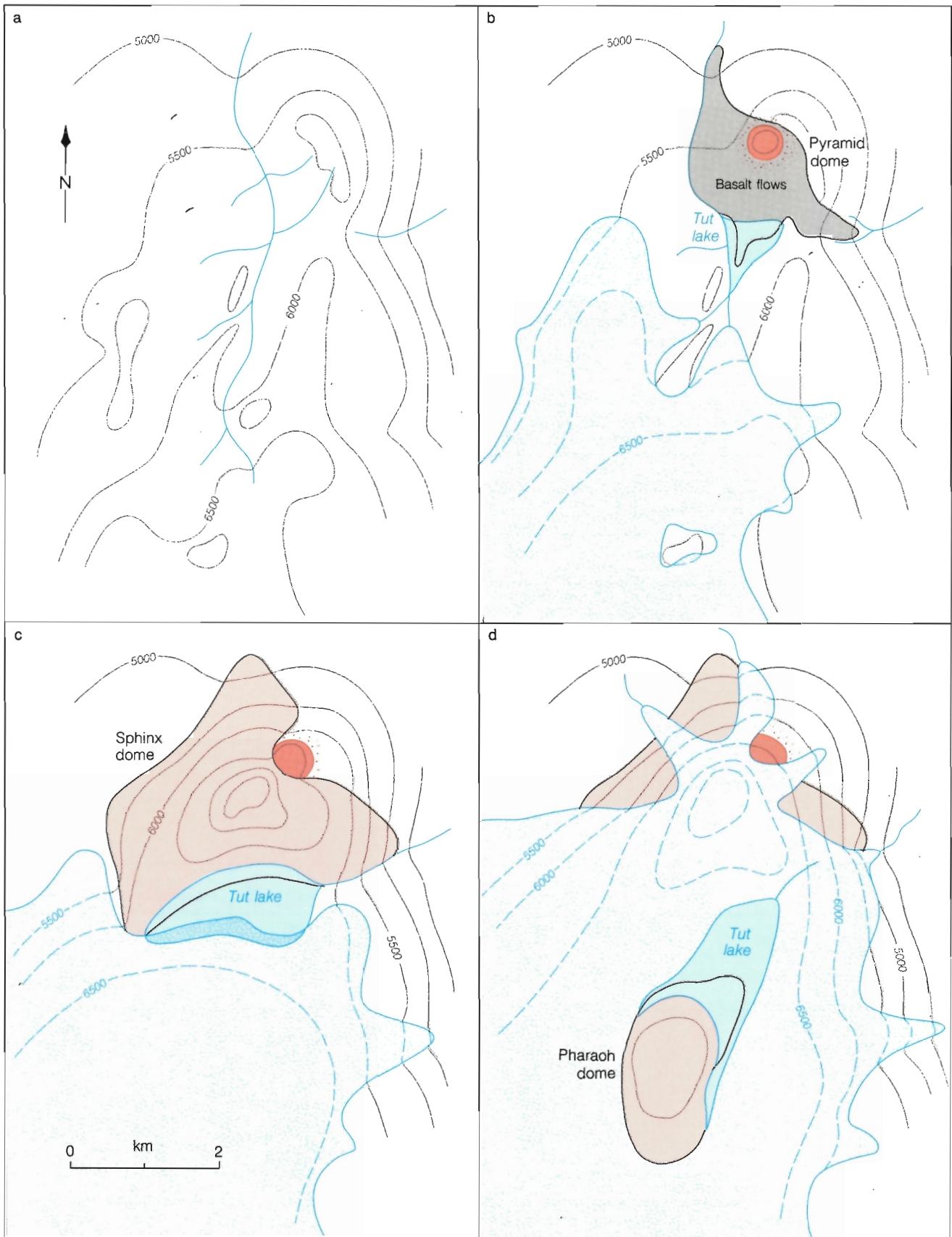
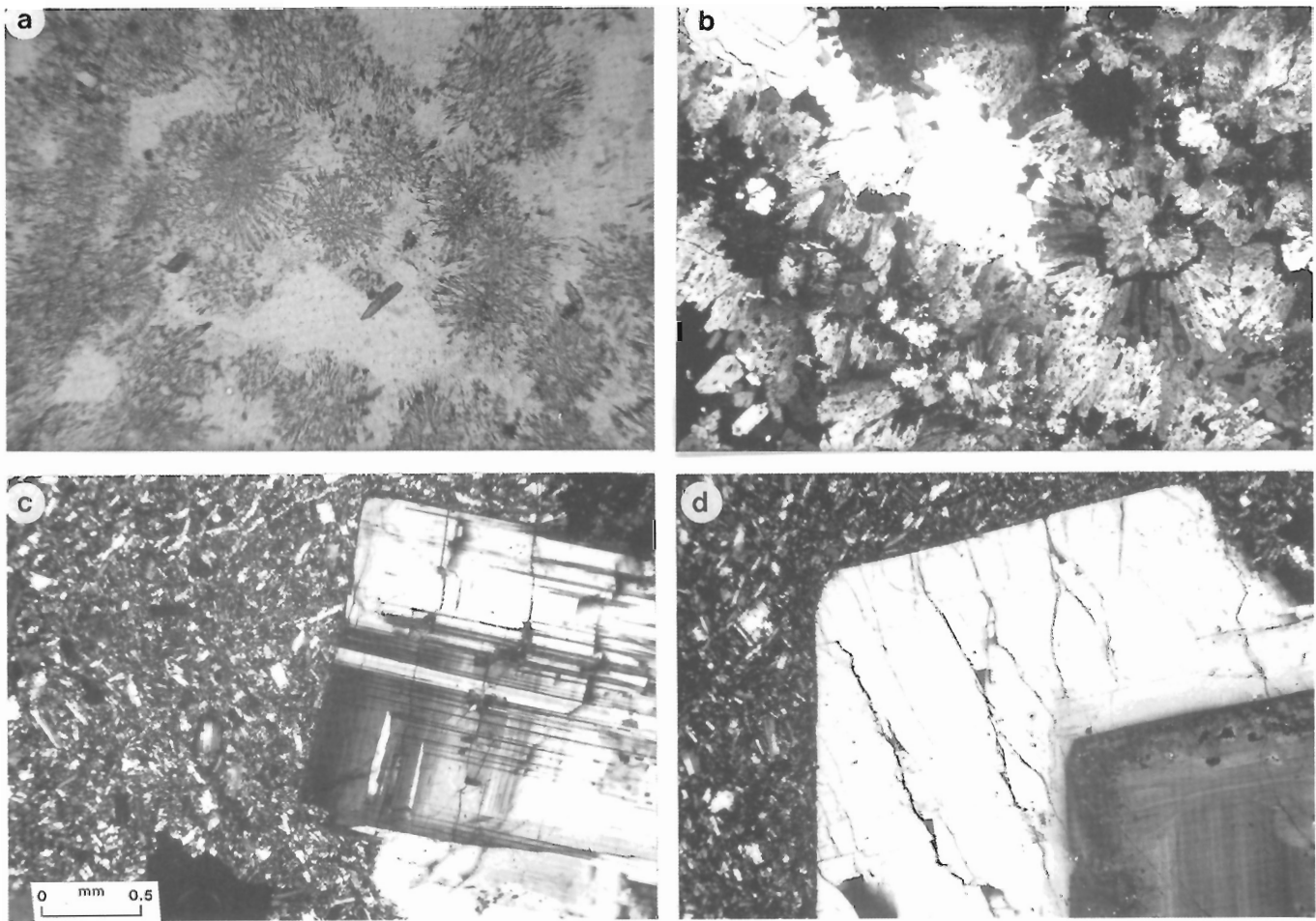


Figure 111. Sketch maps showing four stages in the evolution of the Pyramid pile. (a) Pre-Pyramid topography. (b) Onset of glaciation accompanied by eruption of basalt and pyroclastic surge deposits. Ponding of Tut lake and eruption of Pyramid dome on the basalt surface. (c) Advance of glacier ice accompanied by eruption of Sphinx dome. Accumulation of lacustrine tuff in Tut lake. (d) Continued glacial advance accompanied by subglacial eruption of Pharaoh dome. Accumulation of lacustrine tuff-breccia in Tut lake.

released small, faceted, black granules of obsidian which appear throughout the entire volcanoclastic section. Interbedded with the coarse tuff-breccia are sections up to several metres thick of fine grained bedded pumice, devitrified scale and white sandy layers containing tiny pebbles of rhyolite. These fine grained units commonly display size sorting and grading, and include thin beds composed wholly or partly of black faceted obsidian granules which have been redeposited in 1-10 cm thick beds.

On Nido and Idiji ridges the volcanoclastic unit is underlain by up to 15 m of unsorted polymict gravel consisting mainly of basaltic clasts, but including chert pebble conglomerate and gritstone from the underlying, Jurassic, Bowser Group and pebbles of obsidian similar to those in the overlying pyroclastic deposits. The clasts, most of which

are well rounded, are suspended in a clay-rich silty matrix, but locally exhibit crude stratification and are believed to be a mixture of tills, proximal glacial outwash, and glacial lacustrine deposits. They rest either directly on Nido basalt or on an older till that contains no obsidian but has numerous large feldspar crystals derived from the uppermost flows and tephra of the underlying Beta peak basalt (Fig. 103). The thick section of rhyolite on Sorcery Ridge is underlain by 2-2.5 m of fluvial, polymict gravel with comparatively well sorted basalt and basement clasts from which most of the fine matrix has been winnowed away. In contrast, the distal lobe of rhyolite, at the head of Shaman Creek, is underlain by an unreworked, residual deposit of basaltic tephra and coarse feldspar crystals, typical of the upper part of the Beta Peak pile.



a — Glassy comendite containing spherulitic clusters of feldspar, pyroxene and aenigmatite crystals and discrete microphenocrysts of ferrohedenbergite (plane light).
c — Comenditic trachyte. Euhedral phenocryst of anorthoclase in a groundmass of alkali feldspar, sodic pyroxene, arfvedsonite, and opaque oxides (crossed polarizers).

b — Holocrystalline comendite. Radiating clusters of alkali feldspar arfvedsonite and aenigmatite project into areas of clear quartz (crossed polarizers).
d — Alkali feldspar phenocryst in trachyte from Pyramid dome. Sodic andesine core is surrounded by a thick rim of sanidine. Groundmass of alkali feldspar, opaque oxides and ferrosalite (crossed polarizers).

Figure 112. Photomicrographs of Pyramid felsic rocks; scale bar 0.5 mm.

MOUNT EDZIZA

The volcanoclastic rocks of the Pyramid Formation are believed to be lacustrine. The body of water in which they accumulated, Tut lake (Fig. 100, 109, 111), may have been generated by the melting of glacier ice around the lava dome and the resulting lake contained by the surrounding ice itself. The presence of till and glacial-fluvial deposits beneath the lacustrine unit are evidence that ice was present shortly before, if not during, the volcanic activity. However, the absence of both lacustrine and glacial deposits either in or below the Sphinx dome pile suggests that the ice cover was not regional. A more probable explanation for the origin of Tut lake is the damming of a northerly flowing stream by Sphinx lava. Prior to Pyramid activity this stream

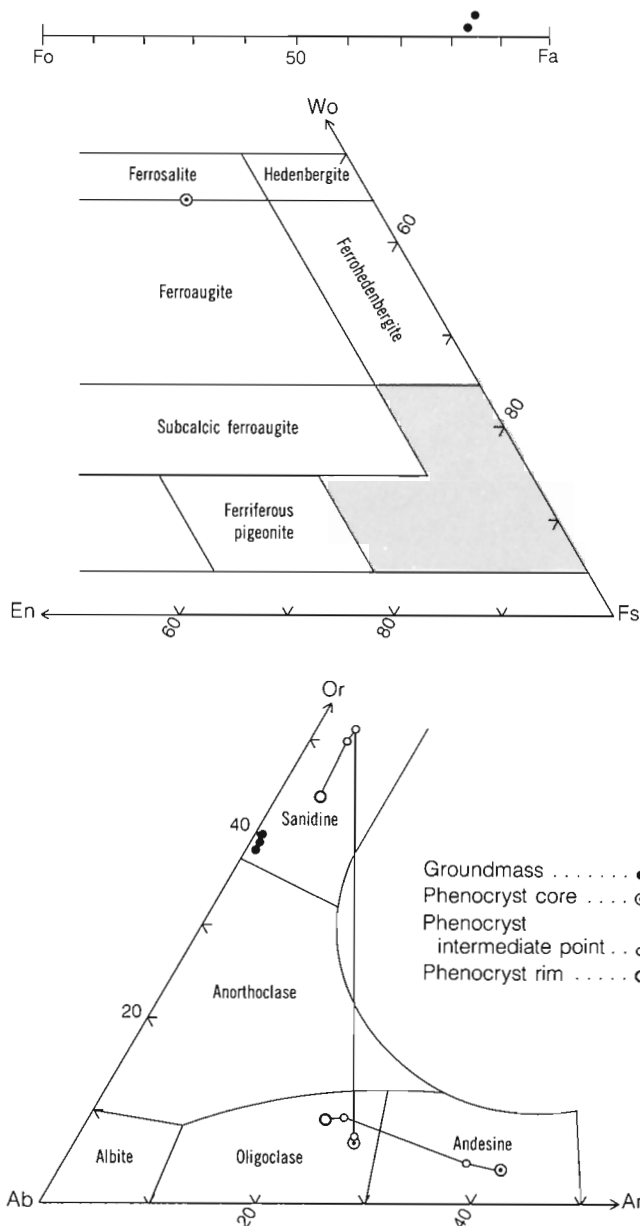


Figure 113. End-member plots showing compositions of feldspar, pyroxene and olivine in the Pyramid felsic rocks.

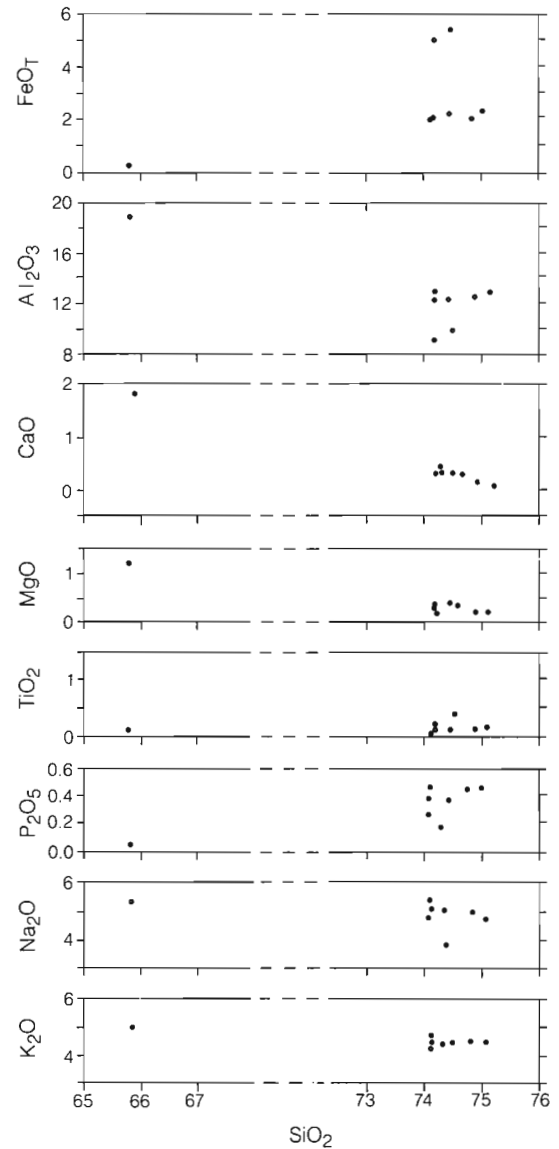


Figure 114. Harker diagram showing the the chemical variation in weight per cent of 8 analyzed specimens of Pyramid felsic rocks.

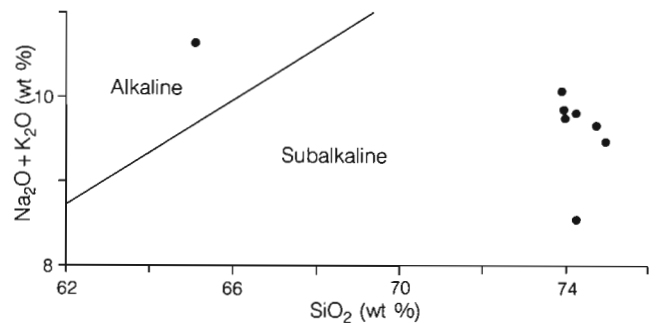


Figure 115. Plot of total alkalis vs. silica for 8 specimens from the Pyramid Formation.

occupied a deeply incised valley which headed in the ice-covered Armadillo Highlands. A distributary valley glacier may have occupied its upper reaches and generated the mixed glacial-fluvial deposits now exposed at the base of the Nido and Idiji Ridge sections. Farther north, a base load of mature river gravel was deposited on bars which were later covered by the precursor basaltic flows surrounding The Pyramid and now exposed in Cook Creek. The formation of a lava dam began with the basaltic flows and culminated with the eruption of Sphinx rhyolite, forming a barrier behind which Tut lake was ultimately raised to an elevation of at least 6500 ft. (1980 m). The lake was probably filled and water had begun to encroach on glacier ice in the head of the valley before the onset of Pharoah dome activity.

The eruption of Pharoah dome rhyolite near the southern end of Tut lake first produced the chaotic, proximal tuff-breccias exposed on Idiji Ridge and the distal, bedded tuffs which accumulated from finer grained debris that settled into deeper water in the central part of the lake, near what is now Nido Ridge. As the dome expanded, its northern edge overlapped the early-formed tuff-breccia, progressively raising the level of the lake and displacing its southern margin northward. The transport of debris into Tut lake was probably accomplished mainly through subaqueous slides, sloughed from unstable clastic wedges built out from the advancing lava front. Also, it seems likely that debris-covered glaciers surrounding parts of the lake may have calved into the rising water, releasing icebergs from which large drop-stones were added to the deep central part of the lake.

The absence of glacial or fluvial deposits beneath the rhyolite flow on the south side of Pharoah dome suggests that the surface on which it rests may still have been ice covered during the time that outwash and lacustrine deposits were accumulating farther north.

PETROGRAPHY

Basalt at the base of the Pyramid Formation is petrographically similar to that of the underlying Nido. Most of the flows are microporphyrific, containing from 10 to 20% small (<2 mm) plagioclase phenocrysts (An₅₀₋₇₀) and rare microphenocrysts of strongly zoned titanite in a matrix of anhedral plagioclase laths, granular olivine, titanite and opaque oxides. Interstitial glass, where present, has been devitrified and in part replaced by carbonate. Plagioclase microphenocrysts are mostly euhedral, with clear unzoned cores and sharply defined, strongly zoned margins. However, the Pyramid basalt also contains microphenocrysts and rare larger phenocrysts (2-5 mm) that have reacted with the groundmass and are characterized by embayed margins and fritted cores.

Coarsely porphyritic trachyte containing up to 50% (1-2 cm) alkali feldspar phenocrysts is unique to Pyramid dome. The smaller phenocrysts have cores of relatively unzoned anorthoclase with prominent crosshatched twinning and relatively thick outer rims of sanidine. Larger crystals have small cores of sodic andesine (Ab₅₈ An₃₇ Or₅) or oligoclase (Ab₆₈ An₂₅ Or₇) overgrown by thick mantles of

Table 12. Representative chemical analyses of specimens from the Pyramid Formation.

Sample	Comendite		Pantellerite	
	13	25	95	98
SiO ₂	73.700	74.200	73.600	73.200
Al ₂ O ₃	12.600	12.800	9.700	10.100
Fe ₂ O ₃	0.900	0.700	1.500	4.300
FeO	1.400	1.600	3.700	1.500
CaO	0.300	0.310	0.310	0.290
MgO	0.320	0.160	0.260	0.300
Na ₂ O	5.200	5.500	5.300	3.900
K ₂ O	4.520	4.600	4.420	4.520
TiO ₂	0.140	0.140	0.380	0.400
P ₂ O ₅	0.020	0.030	0.050	0.040
MnO	0.030	0.040	0.100	0.090
S	0.070	0.110	0.070	0.060
NiO	0.010			
CO ₂				
H ₂ O	0.100	0.200	0.500	1.300
Total	99.310	100.390	99.890	100.000

anorthoclase or sanidine ($Ab_{46} An_4 Or_{51}$) (Fig. 112d). The feldspars occur singly as euhedral crystals and in clusters of interpenetrating crystals. They show no evidence of reaction with the groundmass of small, randomly oriented alkali feldspars and finely disseminated opaque oxides (Fig. 112c). Mafic constituents include small (<0.5 mm) crystals of fayalite (Fa_{85}) and rare microphenocrysts of pale green ferrosalite ($Fs_{38} En_{17} Wo_{45}$). The latter are partly resorbed and surrounded by reaction rims of finely disseminated opaque oxides. Tiny clots (≤ 0.5 mm) of similar finely disseminated opaque oxide, which are scattered uniformly throughout the matrix, appear to be pseudomorphic after pyroxene, probably early-formed ferrosalite or ferroaugite that reacted completely with the residual melt.

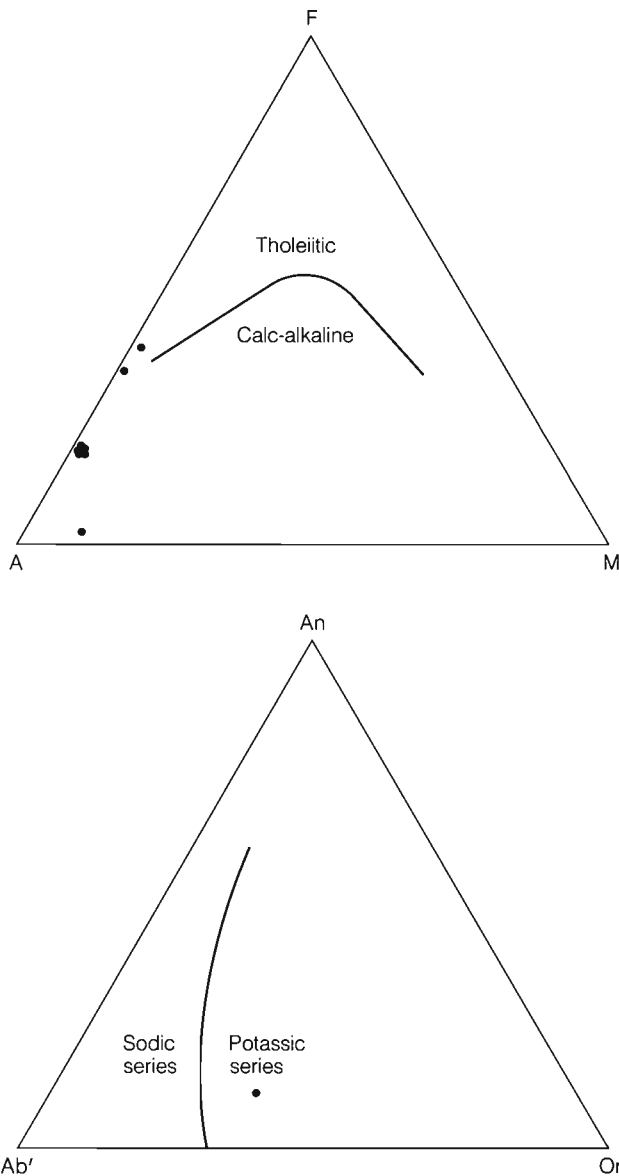


Figure 116. AFM and Ab'-An-Or plots of nine analyses from the Pyramid Formation. ($A = Na_2O + K_2O$; $F = FeO + 0.8998 Fe_2O_3$; $M = MgO$; $Ab' = Ab + 5/3Ne$).

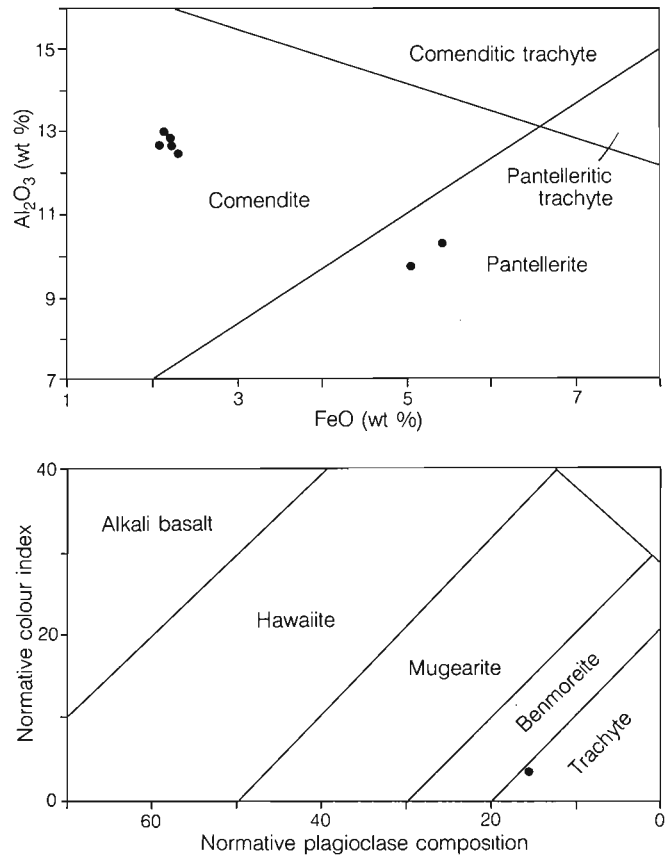


Figure 117. Plot of normative colour index vs normative plagioclase composition and Al_2O_3 vs FeO for alkaline and peralkaline rocks from the Pyramid Formation.

The comendite of Sphinx and Pharaoh domes and associated flows is similar petrographically to the Spectrum comendite. Glassy varieties commonly display complex fluidal folding on a scale of a few millimetres. Most of the comenditic obsidians contain tiny (± 0.5 mm) sparse crystals and crystal clusters of pale green euhedral hedenbergite which clearly crystallized prior to eruption. Posteruption nucleation of feldspar is manifest as tiny spherulitic clusters of radiating alkali feldspar crystals (Fig. 112a). These are commonly entrained along flow layers which are deflected around the spherulites. The holocrystalline comendites, like those of the Armadillo and Spectrum formations comprise closely packed spherulitic clusters of alkali feldspar, arfvedsonite and aenigmatite, and interstitial "pools" of clear quartz containing tiny euhedral rhombs of alkali feldspar (Fig. 112b). Microphenocrysts of arfvedsonite are locally abundant as 1-3 mm euhedral prisms, and sparse euhedra of sodic hedenbergite and sanidine are widely distributed. Vapour phase minerals lining open cavities, particularly in the Sphinx dome comendite, include amethyst quartz, fluorite, acmitic pyroxene, arfvedsonite and analcime.

Pantellerites from Pharoah dome are texturally and mineralogically similar to the comendites but have a higher modal proportion of femic minerals. Phenocrystic aenigmatite is present in some of the pantelleritic glass.

Microprobe analyses of representative minerals are listed in Table 11 and plotted on Figure 113.

CHEMISTRY

Major element analyses of Pyramid rocks are plotted on Figures 114 to 117 and four superior analyses are listed in Table 12. Porphyritic trachyte (A.I. 0.73) of The Pyramid is a nearly pure feldspar rock which plots near the alkali corner of the AFM diagram (Fig. 116) and slightly above

the alkaline-subalkaline boundary of the total alkalis vs. silica diagram (Fig. 115). The remaining rocks are peralkaline (A.I. 1.03 to 1.39) and include both comendites and pantellerites (Fig. 117). The two relatively iron-rich pantellerites, one glass and one crystalline rock, are from a distal flow lobe on the southern edge of the Pyramid pile. The five analyzed comendites, two obsidians and three crystalline rocks from the central part of the pile, plot within a very small field on both the AFM and Al_2O_3 vs. FeO diagrams (Figs. 116 and 117).

The Pyramid rocks do not display any systematic chemical variation between end members. Instead, plots of the trachytes, comendites and pantellerites form three chemically discrete populations on the variation diagrams and support the field evidence for several separate pulses of Pyramid activity.

ICE PEAK FORMATION

GENERAL GEOLOGY

Introduction

Most of the lava erupted during Ice Peak activity issued from vents near the summit of Ice volcano, a once symmetrical composite cone that lay about 5 km south of the peak of Mount Edziza (Fig. 118, Map 1623A, in pocket). The present broad, snow-covered ridge of Ice Peak is an erosional remnant etched from the eastern rim of the old summit crater. Its western flank is now completely covered by glaciers, but on the eastern side the internal structure of the volcano is exposed in the steep headwalls and narrow rock spurs of four active cirques at the head of Tennaya Creek (Fig. 119). Remnants of the eastern flank are preserved in pie-shaped, gently sloping interfluves between Tennaya, Nido and Tenchen creeks and distal flows on the western side form prominent escarpments around the upper rims of most of the canyons cut into the old plateau surface. The southern edge of the Ice Peak pile laps out against the Armadillo Formation and the slope of Gamma peak, whereas the northern flank is completely buried beneath the younger edifice of Mount Edziza.

The Ice Peak pile is divided into two principal assemblages, a lower assemblage of thin, very uniform basalt flows containing small, sparse phenocrysts of feldspar and pyroxene, and an upper, highly variable assemblage which includes trachyte, basalt and a variety of intermediate rocks. The lower basalt sequence forms most of the distal part of the pile, whereas the high, central edifice consists almost entirely of trachyte and intermediate rocks of the upper assemblage.

Two composite basaltic volcanoes, Cache Hill and Camp Hill rest on the old plateau surface southwest of the main Ice Peak pile (Fig. 118). Their moderately dissected central cones and small surrounding shields are believed to be approximately coeval with Ice volcano and they are included in the Ice Peak Formation.

Pre-Ice Peak surface

The central edifice of Ice volcano was superimposed on the southern part of the Pyramid pile. Pharoah dome and the clastic deposits of Tut lake were completely buried, whereas farther north, Sphinx dome and The Pyramid rose above the level flooded and northerly flowing streams of lava were diverted around them, covering only their lower flanks (Fig. 118). Flows descending the eastern and western sides of Ice volcano spread far beyond the limits of the Pyramid pile, across the old surface of Nido basalt and locally onto pre-Tertiary basement rocks beyond the edge of the eroded

shield. Wherever the base of the Ice Mountain succession is exposed, it is separated from the underlying rock by a layer of fluvial or glacial deposits. Beneath proximal flows, in the high source region, they are relatively thin, commonly consisting of only a few metres of slightly reworked Pyramid rhyolite. At the western end of Sorcery Ridge, for example, the basal Ice Peak flows rest on less than a 0.3 m of pebbly colluvium, derived entirely from the surrounding rhyolite flows. Similarly, a thin layer of redeposited pumice, locally containing lenses of rhyolite and basalt boulders and pebbles, separates Ice Peak flows from Pyramid rhyolite on the western end of Idiji and Nido ridges. Farther east, on each of these ridges, the Pyramid pile wedges out and the Ice Peak flows rest on either remnants of Nido basalt or directly on pre-Tertiary basement. They are underlain by relatively thick fluvial, and glacial-fluvial deposits comprising closely packed pebbles and boulders of basalt in a silty or sandy matrix. In some exposures, the basal deposits have a till-like aspect with unsorted, randomly oriented boulders suspended in a fine, silty matrix. In addition to basaltic clasts, derived from the underlying Nido basalt, both the fluvial and glacial deposits include a small percentage of chert-pebble conglomerate and banded rhyolite clasts, both from the Armadillo Highlands to the south, and obsidian granules and bits of pumice from the Pyramid pile to the west. At the extreme eastern end of Nanook Ridge, the Ice Peak flows appear to have entered a steep, easterly sloping valley cut into pre-Tertiary basement rocks. There, the basal flows are underlain by up to 120 m of old colluvium. Polymict fluvial gravels of basalt, chert pebble conglomerate, and a variety of pre-Tertiary crystalline rocks form the lower 15-18 m. They are overlain by a chaotic breccia of unsorted, angular to subangular basaltic blocks, scoria and a few rounded, fluvial boulders surrounded by a sparse matrix of silt and ash. It was probably deposited by a debris flow or lahar initiated by the early Ice Peak activity and channelled into the same valleys that were later occupied by the early Ice Peak flows.

Material beneath the distal flows on the western side of the Ice Peak pile appears to be almost wholly of glacial or glacial-fluvial origin. Most exposures are 1-3 m thick and the clasts are mainly basaltic, plus a small percentage of well rounded cobbles derived from crystalline basement rocks to the west, and a few granules of Pyramid obsidian. Some exposures are clearly tills, in which unsorted boulders up to 1 m across are randomly suspended in a silty clay matrix. Others show evidence of varying degrees of reworking, the fines have been winnowed away leaving a sparse sandy matrix. In some exposures, the gravel itself has been sorted, shingled or redistributed into clearly defined channel deposits. Faceted and striated boulders are present in both the tills and the glacial-fluvial gravels.

MOUNT EDZIZA

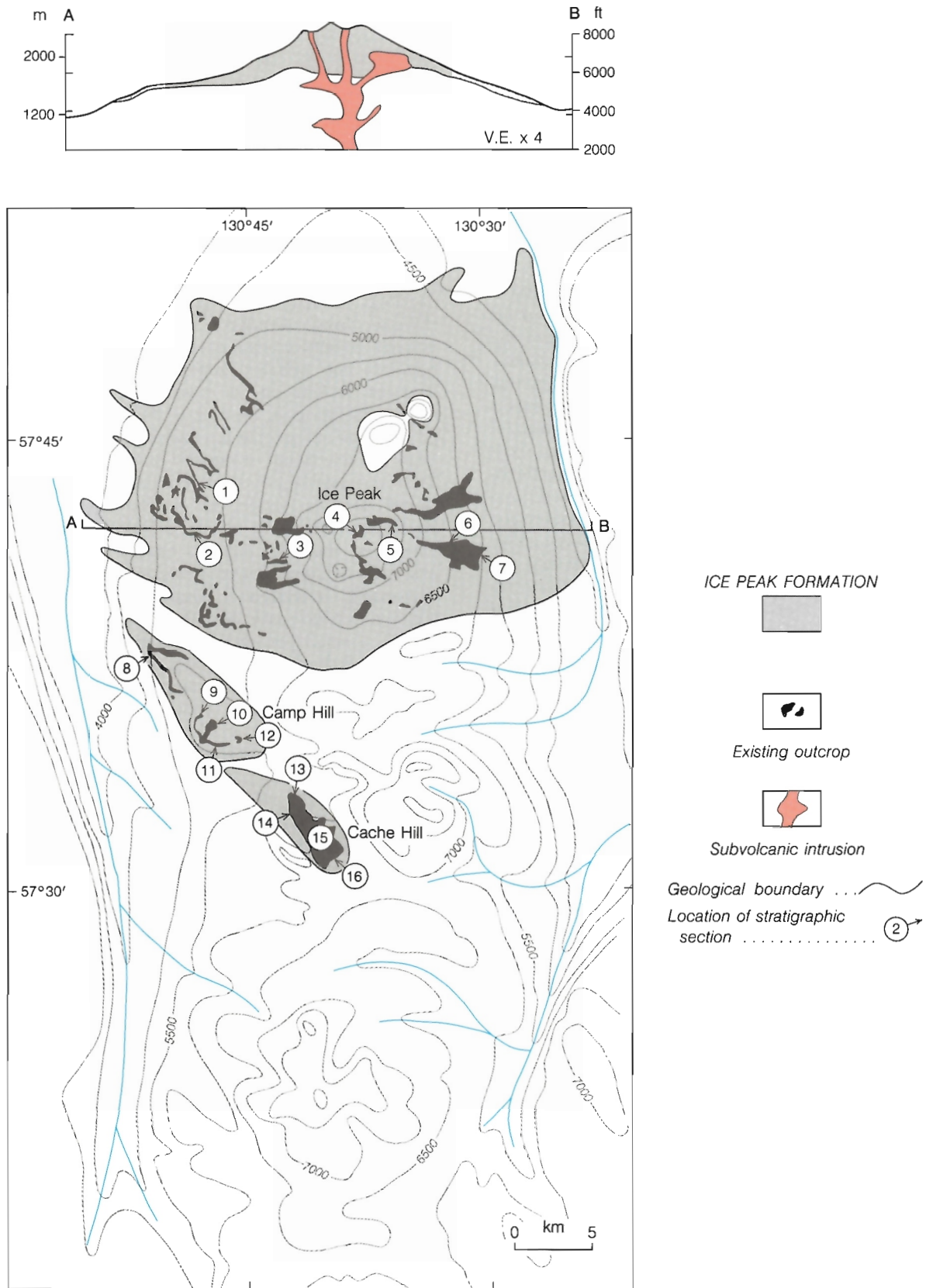


Figure 118. Paleogeological map and cross-section showing the inferred maximum extent of the Ice Peak Formation at the end of Ice Peak time. Stratigraphic sections are shown in Figure 120.

Lower assemblage

The lower Ice Peak assemblage (Fig. 120) includes two distinct lava types: feldspathic intermediate lava of very limited extent and plagioclase-pyroxene basalt, which forms most of the Ice Peak pile.

The intermediate lavas are mostly tristanite but include closely related trachybasalt and mugearite. They are confined to the eastern end of Nanook Ridge where they form a series of thick flows at the base of the Ice Peak succession. These overlap the edge of the underlying Nido basalt and occupy old, easterly-sloping valleys cut into the pre-Tertiary basement. Individual flows vary from 9 m to more than 45 m thick. They weather to a deep russet-brown surface and their widely spaced, rectangular joint sets are accentuated by mechanical weathering which has produced large spheroidal surfaces. The massive, cliff-forming flows are separated by thin, discontinuous layers of granular flow-top breccia. They have a composite thickness of about 150 m.

The distinction between tristanite, trachybasalt and mugearite is based on minor chemical differences that are not apparent in the field. Beneath a thick, brown, weathering-rind the fresh rock is medium grey and contains 50 to more than 80% plagioclase in stout, equant, randomly oriented crystals 5-10 mm across. The rock breaks along the cleavage and crystal boundaries of the closely packed feldspars to give it a distinctive, intricately faceted fracture surface.

Although intermediate lavas form the basal group of flows on the eastern end of Nanook Ridge, they may not have been the first material erupted. Similar flows were not recognized in sections farther west, and presumably closer to their source, but a few relatively thin flows of mugearite

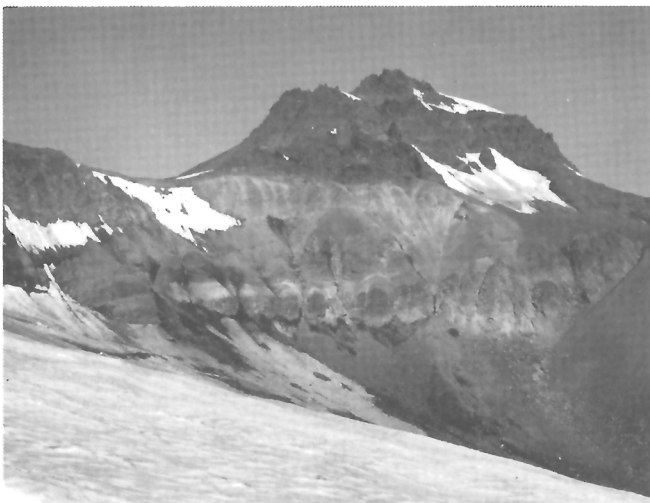


Figure 119. View looking west at the summit area of Ice Peak. Pyroclastic breccia and proximal flows of trachyte are exposed in the active cirques at the head of Tennaya Creek. GSC 125 608.

occur near the top of the lower assemblage on Nido Ridge. Thus, intermediate lavas may have been erupted at several times during the Ice Peak stage or alternatively, the Nido and Nanook Ridge mugearite may represent proximal and distal portions of the same flow system, the thick Nanook Ridge section having been ponded in depressions beyond the edge of the growing composite cone of Ice volcano.

Basalt, which forms most of the lower Ice Peak assemblage, is part of an asymmetrical shield which was built around the central vent area. Its southern edge lapped out against rising terrane about 5 km from the vent, but its gently sloping surface extended for at least 16 km in every other direction. Over this entire area the flows are extremely uniform except for minor variations in phenocryst content. Medium to dark lustrous grey aphyric basalt is present in a few places, particularly at or near the base of the proximal part of the pile. More commonly, the rock contains from 2 to 5% phenocrysts of plagioclase in tabular crystals up to 1 cm long and a scattering of black pyroxene in tiny euhedral crystals. The plagioclase phenocrysts are ubiquitous and help to distinguish Ice Peak basalt from the older, ophitic basalt of Nido and Raspberry formations. A few flows contain significantly more plagioclase phenocrysts but rarely show any increase in the content or size of pyroxene. These are commonly associated with a succession of related flows in which there is a progressive upward increase in plagioclase phenocryst content. The uppermost flow in each of these sequences is commonly thicker than those erupted earlier in the cycle and may contain up to 15% plagioclase crystals. Both plagioclase and pyroxene also occur locally as crystal aggregates as well as large isolated megacrysts. The aggregates occur as small rounded or elliptical inclusions from only a few grains up to clusters 5-10 cm across in which clear glassy plagioclase and black pyroxene and pale yellowish-green olivine form a mosaic of randomly oriented cumulate crystals. Megacrysts of clear glassy plagioclase in tabular crystals up to 3 cm long and black pyroxene in stout prismatic crystals up to 2 cm long are commonly present in the same flows that contain cumulate inclusions.

The basalt flows are relatively thin, usually less than 3 m. They have fairly well developed, thin columns which weather to a dark, chocolate-brown spheroidal surface. In the proximal parts of the pile the flows are separated by beds of loosely aggregated, ropy scoria and spatter from 1-2 m thick. In contrast to the uniform reddish brown of older scoria layers, the Ice Peak material is commonly jet black with streaks and patches of bright orange and yellow, or in some places, the entire scoria layer and adjacent joint surfaces are stained with a pale bluish-grey sublimate. Open vesicles, lined with iridescent iron-manganese oxides and opal, or partly filled with aragonite, are present in the upper one-half to one-third of most flows, and slender pipe vesicles are commonly developed perpendicular to the flow base. In some flows iron-manganese oxides occur as irregular fracture fillings, and locally colloform oxide masses occur as a cement in the porous scoria.

MOUNT EDZIZA

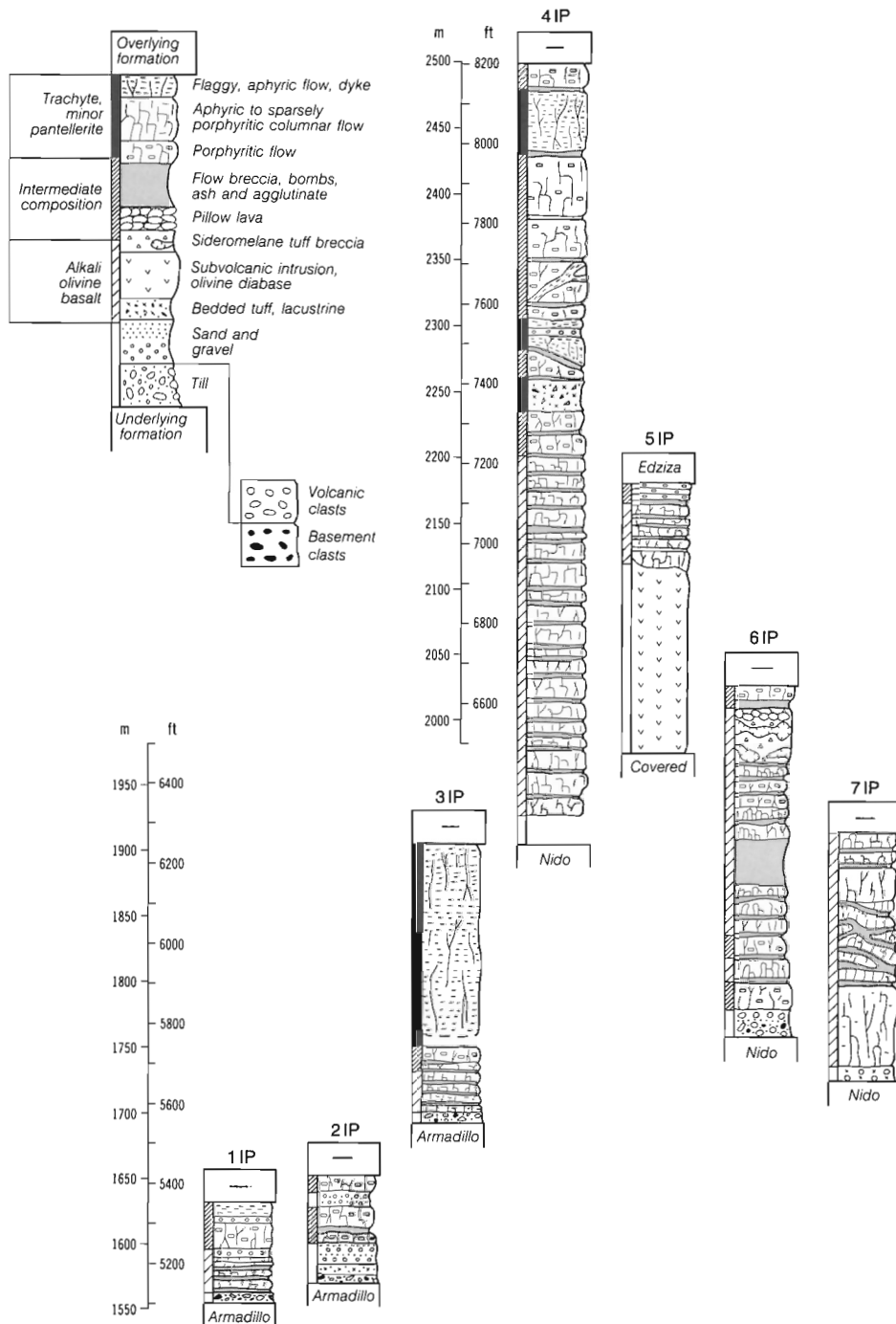


Figure 120. Typical stratigraphic sections of the Ice Peak Formation, showing the subdivision into Upper and Lower assemblages. Section numbers (1-7) refer to locations shown on the paleogeological map (Fig. 118). IP, Ice Peak.

The vents from which the lower Ice Peak basalt issued have not been identified, but the geometry of the pile, as well as the distribution of pyroclastic facies, suggest that the principal source lay near the head of Tennaya Creek. The elevation of both the top and bottom of the lower assemblage is greatest in that area and flows slope gradually away from it in all directions. Also, beds of fine tephra, some more than 30 m thick, are exposed in remnants close to the head of the valley and presumably near the eastern edge of a fountaining vent. These thin out and disappear about 1 km farther east, suggesting that fire fountaining was more or less confined to the vicinity of the central vent. Layers of tephra, including bombs and agglutinated spatter, are interbedded with the flows on Nanook Ridge and on the east end of Nido Ridge at the extreme northeast and east exposures of the pile. These are of limited extent and were probably deposited from small, short-lived satellitic vents. No similar deposits were found elsewhere in the distal parts of the shield.

Ice-contact deposits

Sideromelane tuff-breccia and pillow lava are extensively developed on the northeast flank of the Ice Peak pile. They are exposed on both Nido and Nanook ridges where up to 78 m of water-contact deposits lie within the lower Ice Peak basaltic assemblage. The zone dips east at a slightly lower angle than the pre-Ice Peak surface, thus the more westerly exposures rest directly on the pre-Ice Peak surface at elevations of about 6000 ft. (180 m), whereas the more easterly sections are underlain by older flows of subaerial Ice Peak basalt (Fig. 121). In both places the base of the waterlain succession is underlain by a gravel or till layer

containing clasts of rhyolite and chert pebble conglomerate derived from the Armadillo Highlands. The tuff-breccia comprises a chaotic mixture of large and small quenched basaltic clasts, flow tongues and detached globules of basalt with intricate splays, rosettes and sinuous sheaves of slender columns. The quenched rinds of clasts, as well as the entire fine, granular matrix surrounding them, consist of yellowish-brown sideromelane. Dense, black, unhydrated basaltic glass commonly forms a 2-10 mm thick layer between the sideromelane and dark grey basalt in the cores of the larger clasts and globules. Fragments of broken pillows are present in many of the tuff-breccias. They are characteristically wedge-shaped and have only one quenched surface. Also, stacks of unbroken, tubular pillows up to 30 m thick are locally interlayered with the tuff-breccia. Individual pillows are commonly several metres long and about 0.5 m across. They dip east at angles of 10-20°, much more steeply than the zone as a whole. In a few places well bedded tuff composed entirely of sideromelane granules exhibits crossbedding, channelling and slump structures.

The water-contact zones span an elevation difference of nearly 1000 ft. (300 m), from 6600 ft. (2015 m) in the west to less than 5700 ft. (1740 m) in the east, yet its thickness is everywhere close to 60 m. This precludes its origin in a large lake, nor does the shape of Ice volcano and the surrounding terrane provide any mechanism for ponding a single body of water 300 m deep on the upper slopes of the cone. More likely, the pillows and tuff-breccia formed where easterly advancing flows contacted glacial ice resting on the sloping flanks of the cone. Their development on the northeast slope of the cone is consistent with the preferential accumulation of ice and cirque formation on the relatively

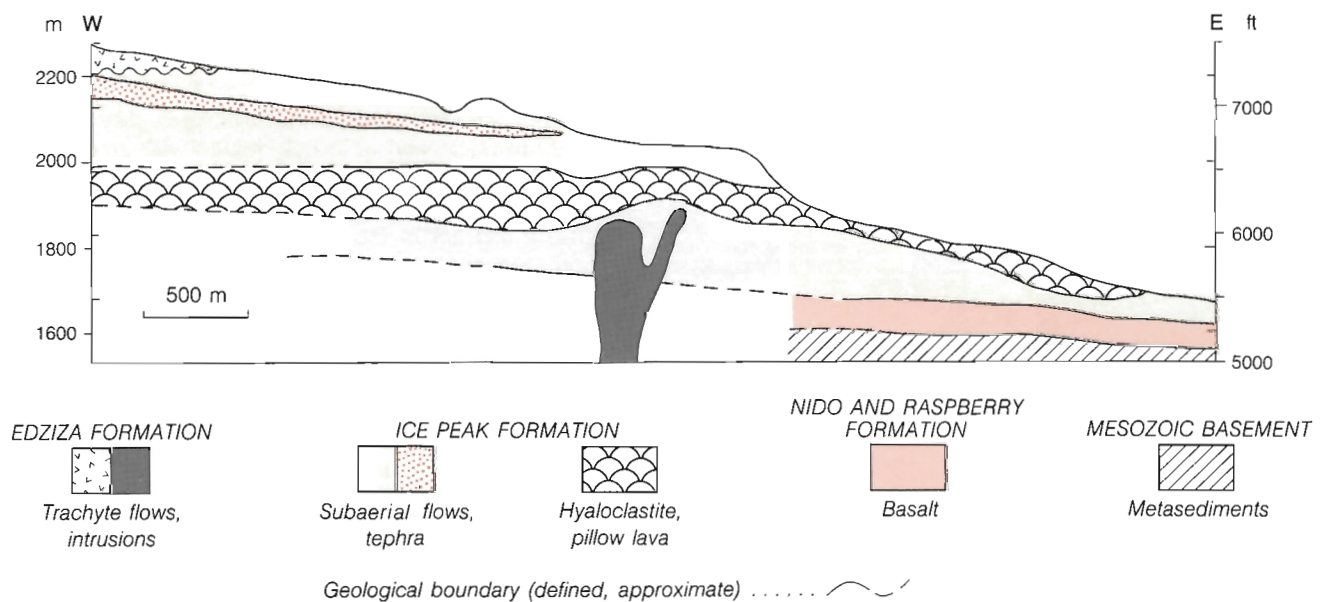


Figure 121. Cross-section showing the relationship of subaerial and subaqueous facies in the northeastern part of the Ice Peak pile. Section projected onto an east-west plane through Nanook Ridge.

MOUNT EDZIZA

shaded northeast slopes of present-day mountains. However, the presence of clasts derived from the Armadillo Highlands at the base of the subaqueous lava pile suggests that the ice originated beyond the limits of Ice Peak itself. Moreover, the subaqueous deposits are locally underlain by earlier subaerial flows that appear to be part of the Ice Peak succession. Thus, the advance of glacial ice onto the eastern flanks of the ancestral Ice Peak shield must have occurred during a fairly lengthy period of dormancy. When activity resumed, the northeast flank of Ice Peak was shrouded in ice and, as the central cone was enlarged, the lava encroached on the surrounding glacier ice. The subaqueous deposits probably formed in a relatively narrow trough of water thawed along the contact between the ice and the lava. With each successive flow, the ice front was displaced progressively farther down the slope (Fig. 122). Subaqueous deposits formed by the preceding flows were exposed above the level of the new meltwater lake and buried by the advancing lava. In this way a roughly tabular, moderately inclined deposit of subaqueous tuff-breccia was deposited in

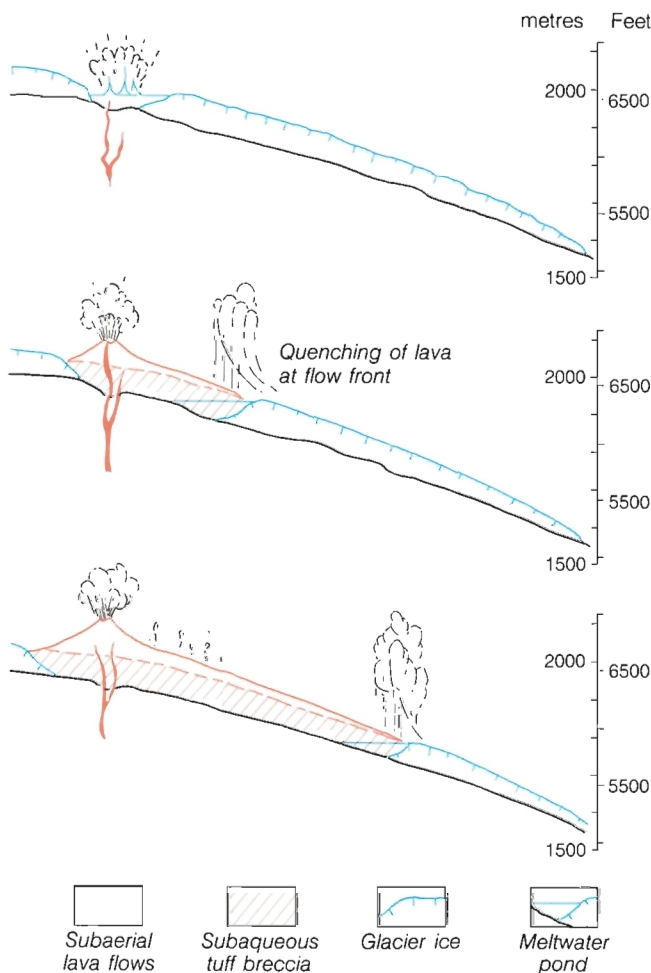


Figure 122. Series of schematic cross-sections showing the development of the subaqueous facies at the expense of alpine glaciers on the eastern side of Ice volcano.

successive increments along the easterly migrating contact between the growing edifice of Ice volcano and the retreating glacier ice on its eastern flank. The thickness of the subaqueous deposits was thus controlled by the thickness of ice behind which water was impounded, and they are uniformly about 60 m thick regardless of elevation. The subaqueous deposits have, in effect, replaced the space occupied by glacier ice prior to eruption of the final lavas of the lower Ice Peak assemblage.

Upper assemblage

The upper Ice Peak assemblage includes a highly varied succession of lavas and pyroclastic deposits which range from porphyritic, alkali-olivine basalt through trachybasalt, tristanite, mugearite, and benmoreite to trachyte. The different rock types do not exhibit any systematic, spatial or temporal relationships, instead each type occurs more or less at random throughout the pile; in many sections the extreme compositional end members form alternating flows (Fig. 120). The more highly evolved trachytes are most abundant in the proximal facies but all of the rock types occur in both the central composite cone and in thin distal flows that have spread many kilometres from their source.

Central cone and proximal deposits

The crescent-shaped summit ridge of Ice Peak (Fig. 119) is a remnant of the western rim of Ice volcano. It forms the margin of a great amphitheatre at the head of Tennaya Valley which mimics the original form of the western half of its summit crater and exposes the thick proximal flows and pyroclastic deposits of the composite cone in a series of steep, active cirques. The eastern half of the central cone has been completely removed by erosion, and Tennaya Creek has cut through the base of the pile and deeply into the underlying basement.

Flows exposed in the summit area are highly irregular, up to 90 m thick, and intimately mixed with equally thick deposits of pyroclastic breccia and epiclastic fill. The overall dips are gently away from the old crater, toward the west, southwest and northwest, but individual cooling units rest on initial slopes of up to 30°. Flows, several hundred metres thick, wedge out against piles of pyroclastic breccia and are overlapped by adjacent flows to form a series of en echelon lenses of lava surrounded by breccia (Fig. 123). These lenses are the cross-sections of proximal flows that spilled over the crater rim and occupied radial gullies on the surface of the original cone. The intermixed breccia contains bombs, blocks and fine tephra. Most of it is a completely random mixture that ranges from ash up to angular blocks 3 m across, but locally thick pockets of fine, white, green or yellow ash or beds of fine red cinders are preserved beneath the flows. The proximal flows include about equal volumes of highly porphyritic basalt, mugearite and slightly porphyritic trachybasalt, and a smaller volume of trachyte.



Figure 123. Thick trachyte flows and pyroclastic breccia in the summit area of Ice Peak. The lenticular, proximal flows were deposited in radial gullies on the surface of Ice volcano. GSC 125 609.



Figure 124. Looking west at the rock spur on the north side of Idiji Glacier. Prominent light coloured band is bedded, lacustrine tuff and epiclastic debris deposited in the summit crater of Ice volcano during an intermediate stage of its development. GSC 125 610.

The basalt is a medium to dark grey, massive, structureless rock which forms bold, spheroidal weathering cliffs. It has a characteristic knobby fractured surface and tends to break into small spherical chunks a few centimetres across. These litter the ledges of the steep upper slopes like loose marbles, making climbing extremely hazardous. The rock contains up to 25% plagioclase phenocrysts in thin, randomly oriented tabular crystals 1-2 cm across and up to 5% black pyroxene in stout prismatic crystals, most less than 1 cm long. Pale, yellowish-green olivine may or may not be present as a minor phenocrystic mineral. The trachybasalt and tristanite are characterized by a pale, greenish-grey colour and conspicuous flaggy cleavage caused by alignment of platy minerals, particularly feldspar, in well developed flow layers. As in the basalt, plagioclase, pyroxene and rarely olivine are present as phenocrysts, but they are much smaller and less abundant, rarely forming more than 5% of the rock. Trachyte occurs in the central edifice of Ice volcano as both extrusive and intrusive phases. It is either non-porphyrific or contains a small percentage of clear, tabular feldspar crystals less than 1 cm long. The flows are commonly thick, up to 90 m, pale green or greenish grey with long smooth columns and flaggy flow cleavage. Most are underlain by a light coloured pyroclastic breccia or ash layer. The flows themselves usually change from a dense, dark to medium greenish-grey flaggy aspect at the base to progressively lighter coloured and more porous rock toward the top. The upper 2-3 m of the very thick flows are punky and porous, without flow cleavage or any obvious orientation of feldspar plates.

In addition to flows and primary pyroclastic breccias, the proximal facies includes a variety of clastic deposits which are believed to have accumulated within the summit crater (Fig. 124). Well stratified deposits of ashy clay and silt containing poorly rounded to angular cobbles and pebbles of Ice Peak lava form prominent white recessive bands on several rock spurs at the head of Icefall Creek. They occur at several levels within the pile and are believed to be lacustrine deposits formed in a lake that periodically occupied the summit crater. In addition, some of the coarse breccias in the vent area contain large, loosely aggregated blocks of interlayered lava and tephra as well as lenses and chunks of fine, bedded material which shows evidence of reworking and redeposition in running water. It is probable that some of these breccias are epiclastic fill that slumped into the crater from its unstable, oversteepened inner walls. Small normal faults are also exposed in the summit area. Many of these bound slump blocks which slid on the glacially oversteepened slopes during erosion of the extinct cone, but others show evidence of intense hydrothermal alteration of rock adjacent to the fault plane. The latter must have formed while the volcano was still active and served as channelways for the escape of fumarolic gases or hot fluids. The largest of these faults is exposed on the rock spur bounding the south side of Tennaya glacier. Thick, flat-lying flows and interbedded lacustrine deposits on the eastern end of the spur have dropped about 60 m along a steep east-dipping normal fault.

Subvolcanic intrusions

Dykes, sills and irregular intrusions are prominently exposed in the dissected eastern face of the Ice Peak composite cone. They include all of the principal rock types found as lavas in the upper Ice Peak assemblage and range in size from dykes only a few centimetres across to tabular intrusive bodies more than 1.5 km long and 120-150 m thick.

Light green trachyte forms the most conspicuous intrusive bodies in the predominantly dark, rusty-weathering Ice Peak pile. The trachyte dykes are commonly large, usually more than 2 m thick, with sharp planar contacts. Several such dykes form prominent erosional ribs that can be traced for nearly 0.5 km. All of these are subvertical, nearly straight, and have a crudely radial distribution with respect to the central vent. Flow cleavage, which is so prominently developed in the trachyte flows, is present to a lesser degree in the dykes, particularly near the margins. Small tabular feldspars lie in the foliation planes, parallel with the dyke walls, and a layer of green fractured glass is invariably

developed along contacts. These chilled selvages vary from only a few centimetres to as much as 0.3 m thick, their size being apparently independent of the thickness of the dyke.

Sills and irregular intrusive masses of similar green trachyte are also abundant in the central part of the Ice Peak pile. On Nido Ridge an irregular sill-like body of green, flaggy trachyte nearly 0.5 km long and up to 60 m thick lies along the contact between Nido basalt and rhyolitic tuff-breccia of the Pyramid, Tut lake, succession (Fig. 125). At both its western and eastern ends, the trachyte body cuts up through the tuff-breccia and intersects the crest of the ridge. It appears to have been injected laterally into the weak, poorly indurated Tut lake tuff-breccia. Both the upper and lower contacts have 5-15 cm chilled selvages of green glass containing angular inclusions of rhyolite. Adjacent to this the tuff-breccia has been partly fused to a brown, subvitreous rock which retains its original fragmental texture.

A small neck or plug dome of similar green, strongly foliated trachyte is exposed in the northern headwall of Idiji Cirque. The main body of the dome is about 90 m across.

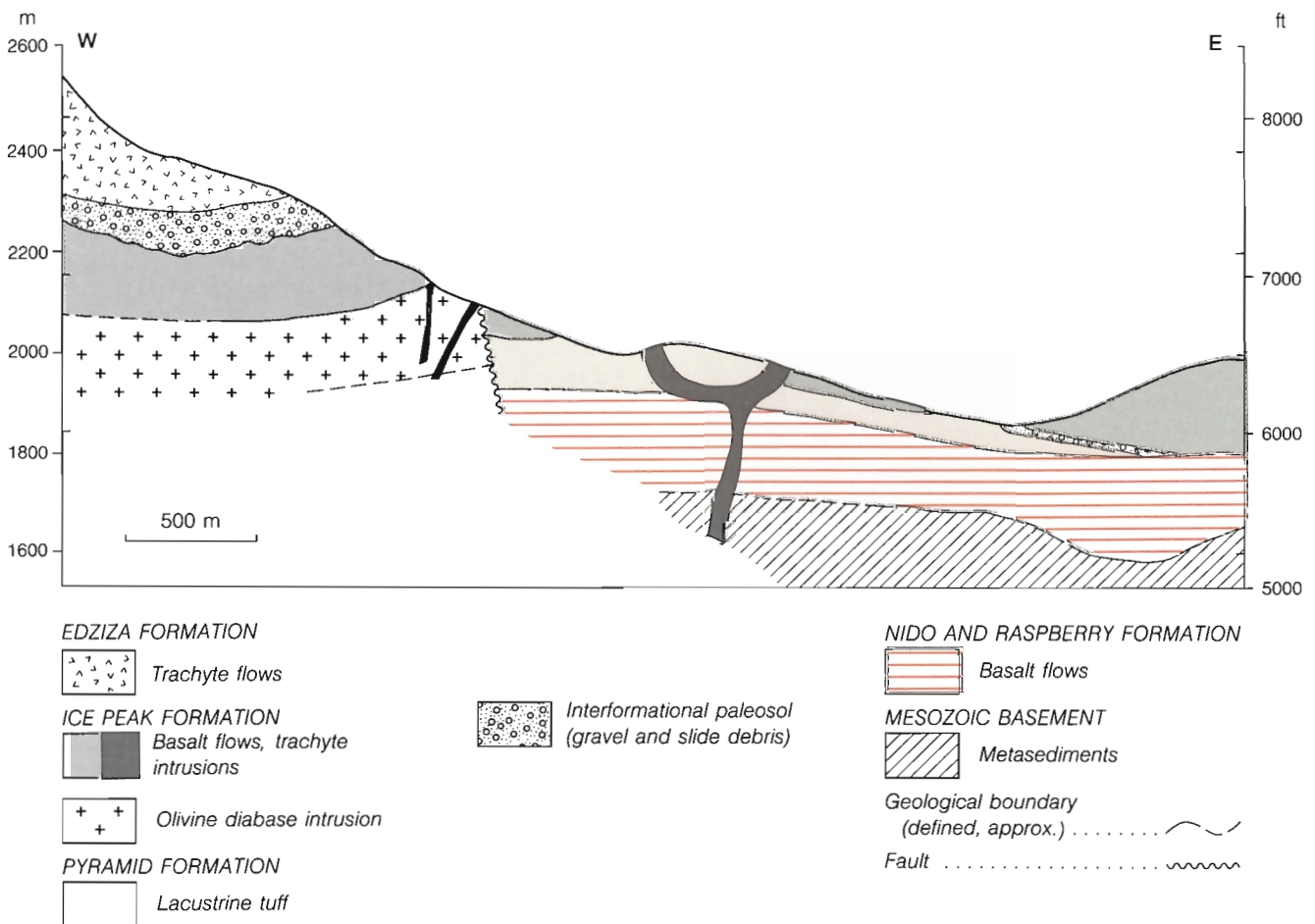


Figure 125. Cross-section through Nido Ridge showing the relationship of subvolcanic Ice Peak intrusions to older structures.

It cuts vertically through flat-lying porphyritic basalt flows, till, and pyroclastic rocks near the base of the upper Ice Peak succession and spreads out laterally in the form of a mushroom. The vertical contacts of the central plug, as well as the base of the upper dome, are quenched to a 0.5-1 m thick layer of banded and contorted black obsidian. Flow layers in the central plug are in the form of a steep concentric arch whereas those along its margins swing out horizontally to conform with the base of the upper dome (Fig. 126). A radial system of transverse fractures has formed normal to the lower contact where it flattens out at the junction between the central plug and the upper dome. The upper contact of the central plug is obscured by talus from several hundred metres of overlying vent breccia comprising angular randomly oriented blocks of both basalt and trachyte. This same horizon, believed to be an explosion breccia, appears to be intruded by the western edge of the upper dome which is itself brecciated around its outer margins. The explosion breccia was probably formed during a series of violent explosions from a small vent within the central Ice volcano crater. The plug dome itself formed by subsequent injection of viscous trachyte magma into the vent and laterally into the base of the overlying breccia.

A large mass of pale green trachyte with pronounced subvertical flow cleavage outcrops on the south side of Idiji Ridge, opposite the small plug dome described above. The similar lithology and vertical internal structure in both of these exposures suggest that they are part of the same large intrusive body. Unfortunately, the exposures on the south side of the ridge are isolated by talus and colluvium. Thus,

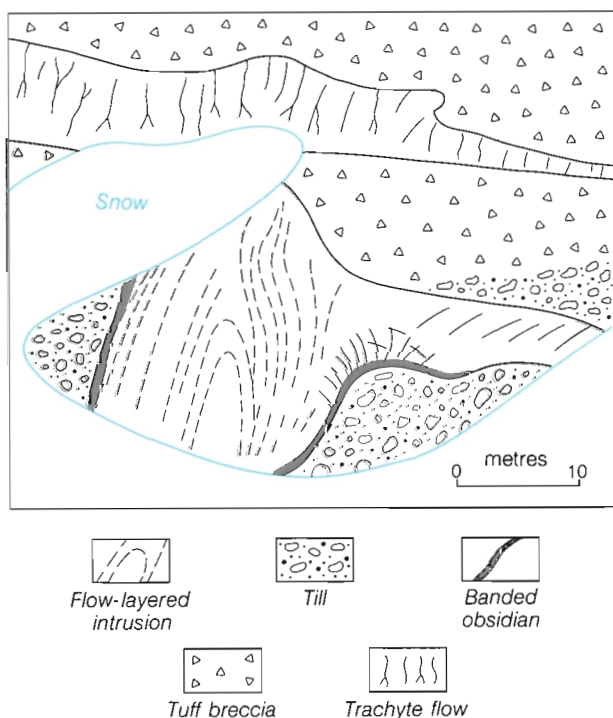


Figure 126. Sketch of subvolcanic intrusion of Ice Peak trachyte exposed in cross-section on the southern spur of Idiji Cirque.

no contacts were observed and the possibility remains that it may be younger than the Ice Peak rocks, either an oversteepened flow or a dissected neck related to Kakiddi trachyte which occurs as flow remnants farther down Sorcery Valley. Because the Edziza trachyte is commonly darker, coarser grained and has prominent subhorizontal flow-layering, the vertically layered trachyte is considered to be part of an Ice Peak subvolcanic intrusive body.

Dykes of trachybasalt and porphyritic basalt are grouped in randomly oriented swarms throughout the central Ice Peak edifice. They are smaller and more irregular than the trachyte dykes and do not have glassy selvages. In several exposures these dykes can be traced upward into thick flows that were fed by magma moving through the dyke system. Such dykes commonly flare out and merge with the base of the flow without any evidence of cutting it (Fig. 127).

The largest subvolcanic body related to Ice Peak volcano is a medium- to coarse-grained diabase (Fig. 125). It is crudely tabular, at least 120 m thick, and exposed for a distance of about 1.5 km along the northwestern headwall of Tennaya Valley. The lower few metres, exposed at only one place, have crude columnar jointing and rest on a layer of green altered tuff which could be part of either the Ice Peak or Pyramid succession. The upper contact is apparently conformable with overlying, gently east-dipping basalt flows of the lower Ice Peak succession. It is sharp and displays no clear evidence of either crosscutting relationships or an intervening erosion surface. The body is continuously exposed in steep cliffs throughout its entire thickness and shows no evidence of internal quench layers or breccia



Figure 127. Dyke of Ice Peak trachyte cutting lacustrine deposit on the east flank of Ice Peak. Dyke is a near surface feeder which flares out and merges with the overlying trachyte flow without cutting it. Note figure on snow for scale. GSC 202469-B.

zones. Instead, it appears to be a single cooling unit, either a thick lava lake, ponded in the central Ice Peak crater or, more probably, a tabular intrusive body.

The texture of the diabase varies systematically from top to bottom. The lower few metres, in which columnar jointing is developed, are fine- to medium-grained porphyritic basalt with sparse phenocrysts of feldspar, pyroxene and olivine. The clear, glassy feldspar phenocrysts are rarely more than 1 cm across, whereas stout prismatic phenocrysts of black pyroxene are commonly 2-3 cm long. Pale yellow olivine occurs as rare phenocrysts up to 5 mm across. In addition the lower part of the unit contains elliptical nodules of loosely aggregated feldspar, pyroxene and olivine crystals. The absence of either nodules or phenocrysts in the central part of the body suggests that they settled into the lower part while the magma was still fluid. The basalt becomes coarser grained upward, and within 50 m of the base it has a uniform, medium grained, nonporphyritic diabasic texture. The central part of the mass is a medium to coarse equigranular rock resembling gabbro (Fig. 133f). Locally it contains segregation veins and irregular masses, up to 2 m long, comprising a porous interlocking mosaic of clear feldspar crystals coated with and partly surrounded by iron oxides.

The diabase body is separated by talus from Pyramid, Tut lake rhyolite tuff-breccia on the eastern part of the Ridge, but both appear to occupy the same stratigraphic interval. If the green tuff underlying the diabase is part of the Tut lake rhyolite succession, then at least 90 m of the rhyolite has been displaced by the intrusion. Because the basaltic flows overlying both the diabase and the rhyolite lie along a fairly uniform east sloping gradient, space for the intrusion must have been provided by foundering of its floor. On this basis a fault is assumed to separate the eastern end of the intrusion from undisturbed Tut lake deposits farther east (Fig. 125).

Satellitic centres

The neck

A circular neck of trachyte about 300 m in diameter forms a prominent 215 m high buttress on Sorcery Ridge (Fig. 128). It consists of two parts: an outer cylinder made up of concentric shells from 2.5-3.5 m thick of fine grained foliated trachyte and an inner core of vertical, closely stacked planar or gently curved tabular bodies of similar, but coarse grained trachyte. A centripetal arrangement of horizontal columns, normal to the cylinder walls, is well developed in each of the outer shells, and similar, but larger and less regular, columns are developed normal to the vertical walls of tabular bodies within the core. It is surrounded by loosely agglutinated basaltic tephra, forming the lower part of the old Beta peak cone of Nido age.

The internal structure of the neck suggests that successive eruptions were separated by periods of time of sufficient duration to allow cooling of magma within the conduit.

Each of the outer shells and each of the tabular core bodies has developed its own distinct tier of columns, separated from the next tier by a 15 cm to 0.5 m zone of structureless, greenish-grey, porous rock. Columns in the outermost tier maintain their identity for up to 1.5 m into the altered and sintered pyroclastic deposits that enclose the neck. Thus the contact zone between lavas of the neck and pyroclastic deposits of the flanking cone can be observed in a single, horizontal column. At the centre of the outer lava shell, the rock is fine grained, dark grey trachyte with a few phenocrysts of clear tabular feldspar aligned in planes of pronounced vertical, flow-foliation. About 3 m from the outer contact the rock becomes streaked and banded, parallel with the foliation. Still closer to the contact the colour changes from dark grey to greenish grey and finally to silvery grey. The lighter the colour the more porous and platy the rock. In the contact zone itself this green platy rock is brecciated and the fragments welded into a matrix of similar green, altered trachyte. Also, within the contact zone clasts of normal, dark trachyte are surrounded by porous green reaction rims. Near the outer end of the columns the rock is a loosely welded mass of green and black fragments which grades outward into progressively less welded pyroclastic debris of the old cone.

The tabular, dyke-like bodies within the core are dark grey, lustrous, coarse grained trachyte. Unlike the distinctly flow-foliated trachyte of the outer shells, the core rocks exhibit no obvious fabric. Stout, prismatic and tabular crystals of plagioclase, which form most of the phenocrysts, are either random or show only slight vertical alignment.

A K-Ar date of 1.6 ± 0.2 Ma on trachyte from the neck compares with dates of 1.5 ± 0.4 and 1.5 ± 0.1 Ma on similar trachyte from massive flows in the upper part of the Ice

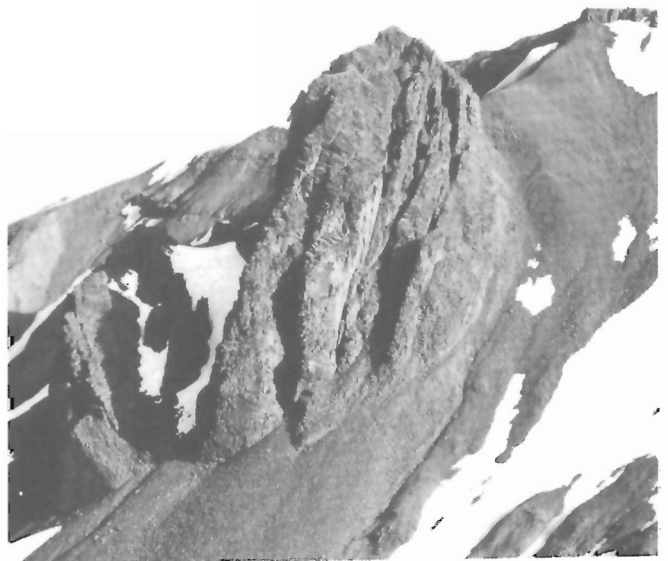


Figure 128. Looking south at Sorcery Ridge and the neck, a vertical cylinder of trachyte eroded from the conduit of a satellitic vent on the southeastern flank of Ice volcano. GSC 202469-C.

Peak edifice (Fig. 129). On the basis of this date the neck is believed to be a major conduit for lava that issued from a satellitic vent on the southeast flank of Ice volcano. However, the possibility that it was the source of much younger, Kakiddi, flows in Tennaya and Sorcery Creek valleys cannot be discounted until additional age determinations are done.

Ornostay and Koosick centres

Near the head of Sezill Creek, where the steep, western slope of Ice Peak merges with the surrounding shield, two thick lobes of trachyte project onto the plateau. Their source is concealed beneath the central ice cap but the flows form prominent westerly sloping bluffs bounded by cliffs that rise 60-90 m above the plateau surface. Koosick, the more southerly bluff, is nearly 2 km long and more than 1 km wide. Its nearly flat surface slopes west from an elevation of 6600 to 6200 ft. (2010 to 1890 m)—an average gradient of about 5%. The entire mass appears to be a single cooling unit of dense, flaggy, dark green, flow layered trachyte with large diameter columns extending through most of the entire 90 m high bounding escarpment. The uppermost 9 or 12 m are unjointed, pale green, porous trachyte which lacks the characteristic platy flow layering and may be either completely structureless, or display complex, fluidal banding. The base of the Koosick flow is concealed by talus and its source lies beneath the summit ice cap. A bulge in the ice surface 1 km east of the bluff, at the 7000 ft. (2135 m) level, may be a plug dome or cone in the vent area.

Ornostay Bluff is smaller than Koosick but it is similar in composition and morphology. Its source is also concealed under the summit ice cap but part of a tephra cone is exposed

in nearby nunataks and beneath the southern edge of the flow. It consists of fine, lapilli-sized pumice, glassy trachyte and rock fragments in a poorly indurated matrix of brown altered ash and iron oxide cement. The tephra is well bedded, with a westerly dip of only 8°. It is clearly waterlain, locally with good crossbedding and scouring. Also, some layers are polymictic, containing rounded cobbles and pebbles derived from older basaltic flows and basement rocks. The deposits are believed to be the distal edge of a tuff ring, built during the early stages of Ornostay activity when Ice volcano was covered by an ice field slightly larger than the present ice cap. The presence of 30 or 60 m of ice would account for the waterlain deposits of mixed primary tephra, old colluvium and glacially transported cobbles. Ice ponding would also account for the extremely thick, steep-sided morphology of the Ornostay and Koosick flow lobes. A K-Ar date of 1.5 ± 0.4 Ma on Ornostay trachyte suggests that it was one of the final Ice Peak eruptions. Thus, the glacial advance that culminated in later Pillow Ridge time may already have started before the Ornostay and Koosick eruptions.

Distal flows

With the exception of trachyte and pantellerite all of the lava types found in the central edifice of Ice Peak occur as thin cap flows in the most distal parts of the surrounding shield. On the northeast flank of the central cone many of the flows are interlayered with wedges of fine trachyte tephra or basaltic cinders. On Nanook Ridge, for example, a prominent 45 m thick recessive unit of trachyte pumice thins eastward and disappears about 5 km from the central crater. Beyond this distance none of the flows in the upper

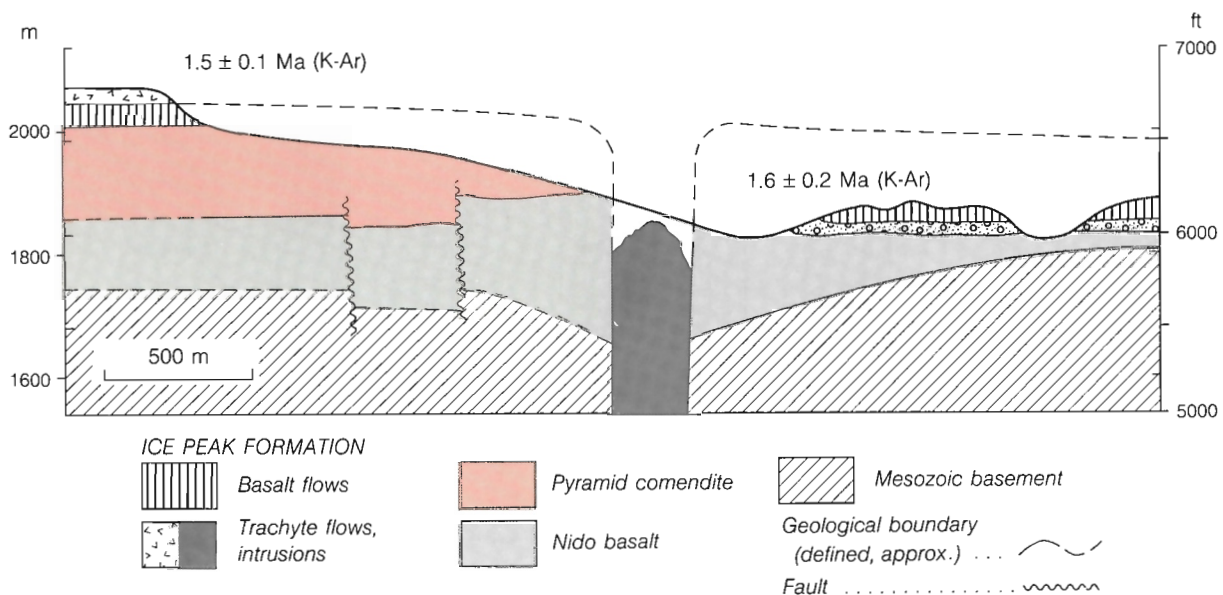


Figure 129. Cross-section through Sorcery Ridge showing the relationship of the neck to Ice Peak flows of similar age and composition.

MOUNT EDZIZA

Ice Peak assemblage are associated with an appreciable volume of primary tephra, suggesting that they travelled great distances from their source—probably from the central crater itself.

On the east flank of the pile the upper Ice Peak assemblage rests directly on basalt flows of the lower assemblage, but on the broad, nearly flat, distal shield to the west, the two assemblages are commonly separated by a layer of gravel, till, or redeposited, waterlain tephra. Boulders in both the tills and fluvial gravels are mostly of locally derived basalt, but from 1-10% are granitic, presumably from the high, crystalline terrane west of the shield. Locally the tills and fluvial gravels are interbedded with lenses of waterlain ash or basaltic tephra carried to the outer margins of the lower shield by west-flowing streams draining the upper slopes of the volcano.

This entire surface was subsequently flooded by a relatively thin veneer of lava flows during eruption of the upper Ice Peak assemblage. These flows are now exposed as prominent rimrocks along the Mess Creek Escarpment and tributary canyons between Elwyn and Walkout creeks. Commonly only 1 to 4 cooling units are present and these rarely have a composite thickness of more than 60 m. Individual cooling units of both porphyritic basalt and trachybasalt are commonly 6-24 m thick. The basalt forms

prominent dark brown to black cliffs of thick columns or widely spaced rectangular joint surfaces. It is similar to basalt in the vent area except that the feldspar phenocrysts are oriented in the plane of flowage. Trachybasalt and mugearite both have long smooth well formed, greenish-grey-weathering columns and pronounced flow layering. As in the proximal part of the pile, there is considerable interlayering of different rock types. In some exposures trachybasalt or mugearite overlie porphyritic basalt while at other exposures the sequence is reversed. The interlayering is most apparent immediately west of the vent whereas the more southerly exposures are predominantly trachybasalt and the more northerly exposures are predominantly porphyritic basalt. This suggests that the trachybasalt and basaltic lavas occur in separate, but overlapping lobes. The preferential accumulation of different lava types into northern and southern lobes suggests that they may have been discharged from different vents in the summit region of the volcano.

Subordinate centres

Two small intermontane shields occupy an old northwesterly-trending valley southwest of the main Ice Peak edifice (Fig. 118). The outer edges of the shields have been eroded back to low escarpments but their relatively

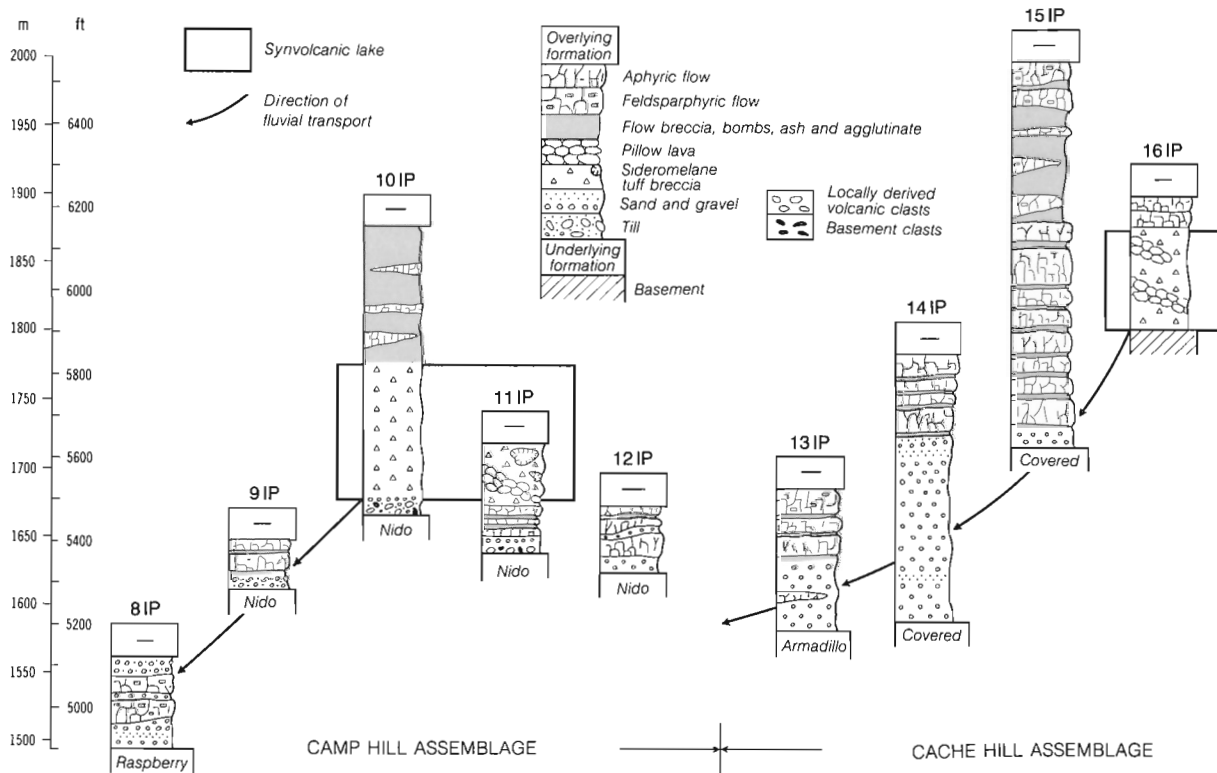


Figure 130. Stratigraphic sections of the Camp Hill (8-12) and Cache Hill (13-16) piles showing the relationship of subaerial and subaqueous facies to fluvial gravel deposits and synvolcanic lakes ponded behind the flows. Section numbers refer to locations shown on the paleogeological map (Fig. 118). IP, Ice Peak.

smooth, unbroken surfaces contrast with the complex topography of the older, surrounding ridges. The northwesterly elongation of the shields and the gentle northwesterly initial dip of the flows reflect the shape of the broad valley into which the lava flowed. The source of each shield is a small composite volcano near its southeastern extremity.

Camp Hill, the source of the more northerly shield, is a gently sloping conical hill that rises about 600 ft. (180 m) above the surrounding plateau. Its surface is mostly covered but exposures in moderately incised, radial meltwater channels and on the truncated southwest flank, reveal a composite structure. The lower half is brown, partly palagonitized sideromelane tuff-breccia, locally interbedded with pillow



Figure 131. Thin basalt flows interlayered with fluvial gravel near the distal, northwesterly, end of the Camp Hill pile. GSC 125 611.

lava, pillow-breccia and quenched pahoehoe toes. The upper half is a typical subaerial assemblage of basaltic tephra, bombs, irregular flows and red, oxidized scoria. Both the lower and upper parts of the hill are coarsely porphyritic basalt with abundant phenocrysts of plagioclase, olivine and clinopyroxene. The shield on which it rests comprises 4 to 6 flows with a composite thickness of up to 60 m (Fig. 130). The lower flows are aphyric to slightly feldsparphyric olivine basalt whereas the uppermost flows are abundantly feldsparphyric. The latter extend to the distal, northwestern end of the shield, where they are interlayered with fluvial gravel (Fig. 131). The base of the Camp Hill pile slopes from an elevation of 5500 ft. (1675 m) at its source to 4900 ft. (1495 m) at its northwestern edge. It is underlain by fluvial and glacial-fluvial gravels which include clasts of Mesozoic basement rocks as well as locally-derived basalt.

Cache Hill is a small composite volcano which rises about 120 m above the more southerly intermontane plateau. The symmetry of its cone is broken by a small, deeply incised cirque that exposes irregular flows and thick pyroclastic deposits on its eastern flank. The base of the surrounding shield slopes from an elevation of 5900 ft. (1800 m) at its southeastern end to 5400 ft. (1645 m) at its distal, northwestern extremity. The basal flow, which is sporadically exposed along the southwest side of the main pile, is a medium grey, coarsely porphyritic basalt with abundant clear to pale amber, tabular feldspar phenocrysts up to 1.5 cm long. It is overlain by six to eight relatively thin flows of dark grey, fine grained, aphyric, vesicular basalt flows which, throughout most of the pile, are clearly subaerial. They have uniform, well developed columnar joints and are separated by thin scoria beds that include oxidized red cinders, and bombs deposited from a fountaining vent.

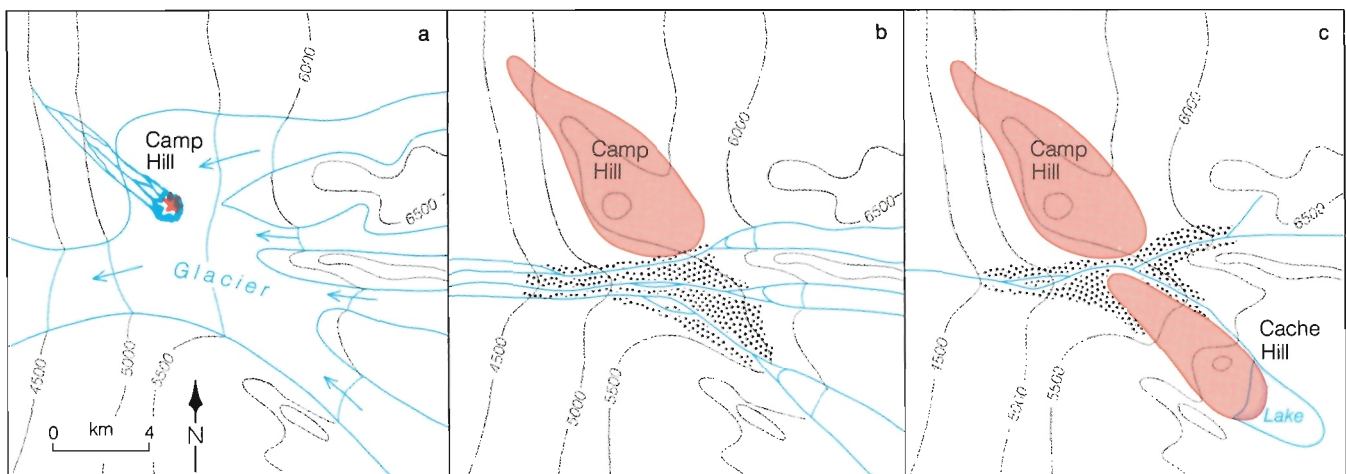
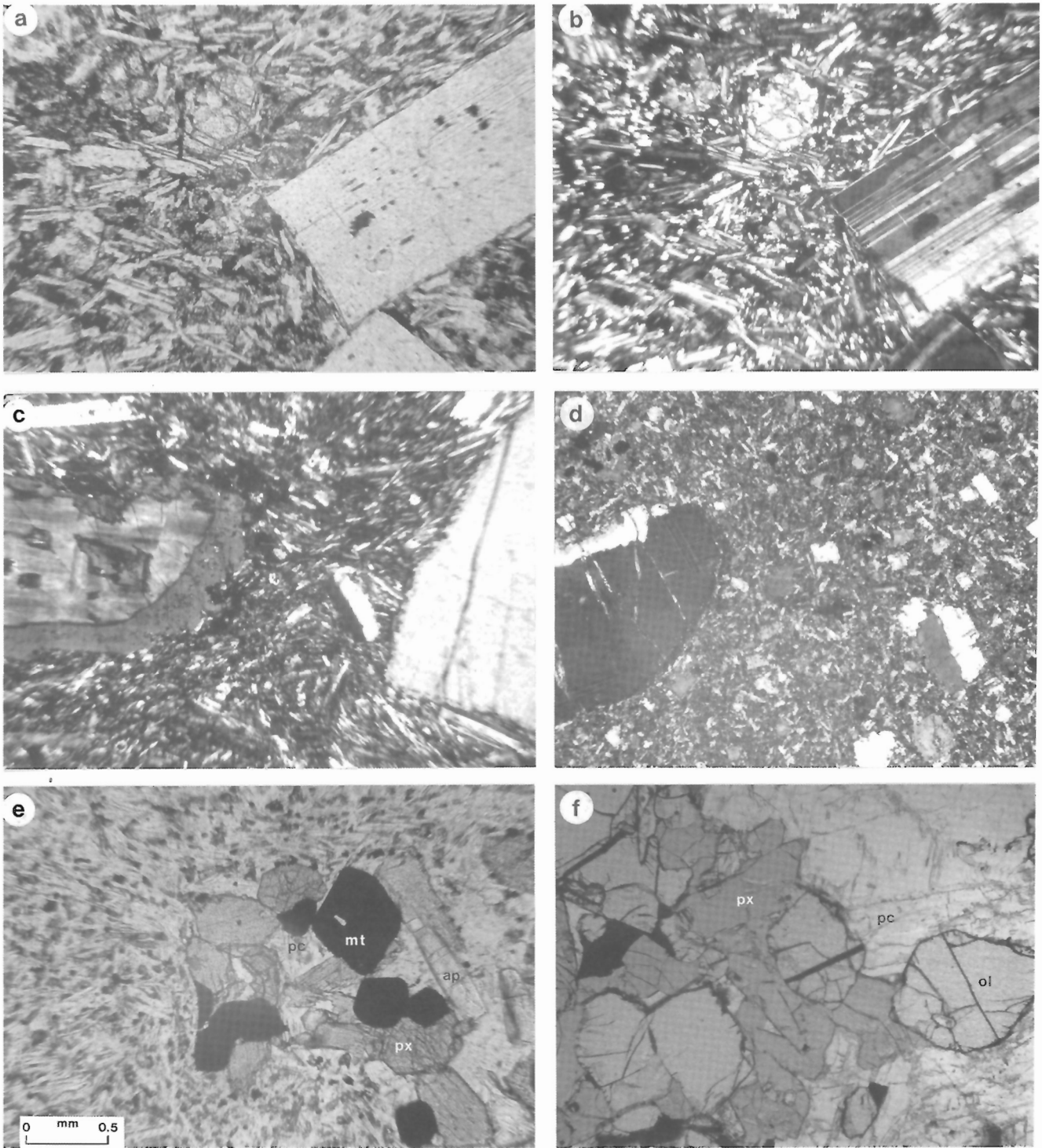


Figure 132. Three stages in the development of the Camp Hill and Cache Hill composite volcanoes. (a) Initial eruption of the Camp Hill vent, forming a tuff ring near the edge of a glacier on the plateau. (b) Eruption of the subaerial, upper part of Camp Hill during recession of the ice and accumulation of glacial-fluvial gravel in the upper part of the valley. (c) Eruption of the Camp Hill flows onto the gravel deposits and ponding of a temporary lake in the valley above the volcanic edifice.



- a,b** — Porphyritic alkali olivine basalt. Euhedral phenocrysts of unzoned plagioclase and olivine in a groundmass of plagioclase, salite, minor olivine and opaque oxides (a, plane light; b, crossed polarizers).
- c** — Mugearite with microphenocrysts of partly resorbed plagioclase mantled by less calcic feldspar. Groundmass of alkali plagioclase, salite, and opaque oxides (crossed polarizers).
- d** — Trachyte. Anorthoclase phenocryst in a groundmass of alkali feldspar and opaque oxides (crossed polarizers).
- e** — Small cumulate inclusion of plagioclase (pc), titanaugite (px), apatite (ap), and magnetite (mt) in fine grained trachyte (plane light).
- f** — Coarse grained, intrusive diabase comprising olivine (ol), plagioclase (pc), titanaugite (px) and interstitial opaque oxides (plane light).

Figure 133. Photomicrographs of Ice Peak rocks; scale bar 0.5 mm.

However, at the southeastern edge of the pile these same flows interdigitate with a 60-90 m thick pile of structureless sideromelane tuff-breccia and pillow lava. Locally this succession is overlain by a massive, cliff-forming flow of vesicular, bright red-weathering hawaiite which forms a prominent rimrock along much of the southwestern part of the shield. Above it, most of the plateau surface, as well as the low, conical edifice of Cache Hill, consists of medium grey, highly porphyritic basalt with randomly oriented phenocrysts of clear ragged feldspar up to 1 cm across, 1 to 2 mm grains of unaltered, yellowish-green olivine and small sparse grains of black pyroxene. This rock, unlike those in the lower part of the shield, breaks to a rough hackly surface and is filled with irregular, tear-shaped open cavities, apparently formed during viscous flow.

There are no apparent erosion surfaces or gravel layers between these flows but the basal flow is underlain by up to 135 m of gravel (Fig. 130). The gravel contains well rounded pebbles and boulders of mainly Armadillo rhyolite, a few chert pebbles and chips of shale from the underlying Bowser Lake Group and rare basaltic clasts, presumably from the Nido basalt.

The Cache Hill and Camp Hill composite volcanoes and surrounding intermontane shields are believed to have formed during the waning stages of glaciation, early in Ice Peak time. A thin lobe of ice must have remained on the plateau when Camp Hill activity began. The first lava was erupted into a shallow meltwater pond and formed the sideromelane tuff-breccia in the lower part of Camp Hill (Fig. 132). When the tuff ring grew above the level of the ponded water, fire fountaining and effusion of subaerial flows built the upper part of the composite cone. Camp Hill activity must have continued until much of the ice had receded and the final flows spread out across the surrounding deposits of glacial-fluvial gravel.

The absence of water-contact deposits in the lower part of the Cache Hill pile suggests that ice had already receded from that area prior to volcanic activity. Before the eruption of Cache Hill volcano the area now occupied by lava flows was part of a broad deglaciated valley fed by turbulent tributaries from the steep, deeply dissected Armadillo Highlands. Where these tributaries entered the main valley their load of sediment was dumped on alluvial fans, above which the main river began to aggrade its course. The eruption of Cache Hill volcano on the east flank of this valley formed a lava dam just above the aggrading gravel bars. A small, temporary lake formed on its upstream side and lava flowing into it formed the pillow lava and tuff-breccia preserved on the southeast side of the shield. Lava on the opposite side flowed northwest across the thick gravel deposits and successive flows spread out to build the shield. Eventually the lava-dammed lake overflowed toward the west and the outflow stream rapidly incised a new valley near what is now the western end of Raspberry Pass.

PETROGRAPHY

The broad spectrum of chemical compositions that characterizes the Ice Peak rocks is reflected in their varied textures and mineralogy (Fig. 133,134; Table 13), but it is rarely possible to discriminate, petrographically, between rocks of the sodic and potassic series.

Basalt

The alkali olivine basalts (of both Na and K series) include coarsely porphyritic, microporphyritic and aphyric varieties (Fig. 133a,b). Plagioclase, in euhedral to subhedral laths up to 1 cm long, is the most abundant phenocrystic phase (10-50%). Unzoned cores of labradorite (An_{50-70}) are commonly surrounded by narrow complexly zoned rims of andesine to oligoclase (An_{40-20}). Euhedral phenocrysts of olivine ($\sim Fo_{70}$) are present in all of the Ice Peak basalts. They are commonly less than 2 mm across and form 5-10% of the phenocrysts, but some picritic varieties contain 10 to 20% olivine as the dominant phenocryst. Phenocrysts of purplish-brown calcic titanite (salite) are present in most Ice Peak basalts as 1-3 mm euhedral or subhedral crystals. Titaniferous magnetite is a ubiquitous but

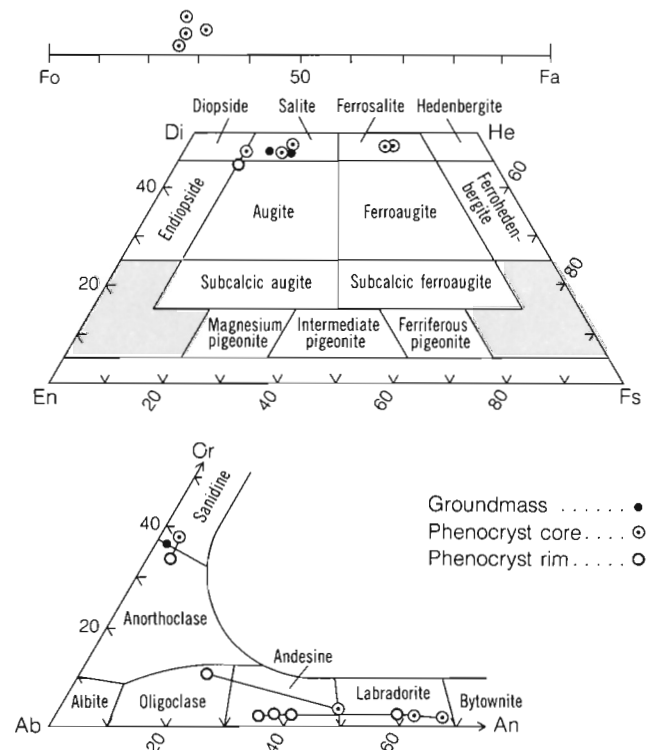


Figure 134. End-member plots showing the compositions of feldspar, pyroxene and olivine in Ice Peak rocks, based on 25 microprobe analyses.

Table 13. Selected microprobe analyses and structural data for feldspar, pyroxene and olivine from the Ice Peak Formation.

	Feldspar				Pyroxene			Olivine
	Phenocryst			Ground-mass	Phenocryst			Phenocryst
	core IF1	rim IF2	core IF3	rim IF4	IF5	IP1	IP2	IP3
SiO ₂	52.68	52.72	66.29	66.97	67.28	51.16	49.17	47.66
Al ₂ O ₃	29.77	29.64	19.61	19.73	19.21	2.68	1.03	4.84
TiO ₂	0.0	0.0	0.0	0.0	0.0	1.29	0.50	3.06
Cr ₂ O ₃	0.0	0.0	0.0	0.0	0.0	0.0	0.0	0.0
Fe ₂ O ₃	0.60	0.57	0.18	0.24	0.64	1.24	2.98	2.42
FeO	0.0	0.0	0.0	0.0	0.0	9.89	18.92	8.23
MnO	0.0	0.0	0.0	0.0	0.0	0.33	0.73	0.21
MgO	0.0	0.0	0.0	0.0	0.0	12.42	5.65	12.17
NiO	0.0	0.0	0.0	0.0	0.0	0.0	0.0	0.0
CaO	12.93	12.54	0.66	0.79	0.34	21.52	20.68	21.30
Na ₂ O	4.23	4.25	6.81	7.33	7.26	0.51	0.65	0.50
K ₂ O	0.23	0.25	6.57	5.89	6.39	0.01	0.0	0.0
H ₂ O	0.0	0.0	0.0	0.0	0.0	0.0	0.0	0.0
F	0.0	0.0	0.0	0.0	0.0	0.0	0.0	0.0
Total	100.44	99.97	100.12	100.95	100.12	101.05	100.31	100.39
			No. of ions on basis of 8 (0)				No. of ions on basis of 6 (0)	
Si	2.3841	2.3936	2.9635	2.9632	2.9783	1.9063	1.9419	1.7904
Al	1.5878	1.5860	1.0332	1.0289	1.0022	0.0937	0.0479	0.2096
Cr	0.0	0.0	0.0	0.0	0.0	0.0	0.0102	0.0
Fe ³⁺	0.0204	0.0195	0.0061	0.0080	0.0213	0.0	0.0	0.0
Al	0.0	0.0	0.0	0.0	0.0	0.0240	0.0	0.0047
Cr	0.0	0.0	0.0	0.0	0.0	0.0361	0.0047	0.0864
Ti	0.0	0.0	0.0	0.0	0.0	0.0349	0.0885	0.0685
Fe ³⁺	0.0	0.0	0.0	0.0	0.0	0.0	0.0	0.0
Ni	0.0	0.0	0.0	0.0	0.0	0.0	0.0	0.0
Fe ²⁺	0.0	0.0	0.0	0.0	0.0	0.3082	0.6249	0.2586
Mn	0.0	0.0	0.0	0.0	0.0	0.0104	0.0244	0.0067
Mg	0.0	0.0	0.0	0.0	0.0	0.6898	0.3326	0.6814
						0.8592	0.8751	0.8573
						0.0368	0.0498	0.0364
						0.0005	0.0	0.0
Ca	0.6270	0.6100	0.0316	0.0375	0.0161			
Na	0.3712	0.3741	0.5903	0.6288	0.6231			
K	0.0133	0.0145	0.3747	0.3325	0.3608			
						Ca		0.0084
						Na		0.0
						K		0.0

minor phenocrystic phase. There is no evidence of reaction between any of the phenocrysts and the groundmass. Sub-volcanic intrusions of Ice Peak basalt are commonly coarse grained, equigranular diabasic rocks consisting of olivine, pyroxene, plagioclase, and interstitial opaque oxides (Fig. 133f).

The groundmass of most Ice Peak basalts is either holocrystalline or includes only minor glass. It is commonly an intergranular mosaic of subhedral plagioclase laths

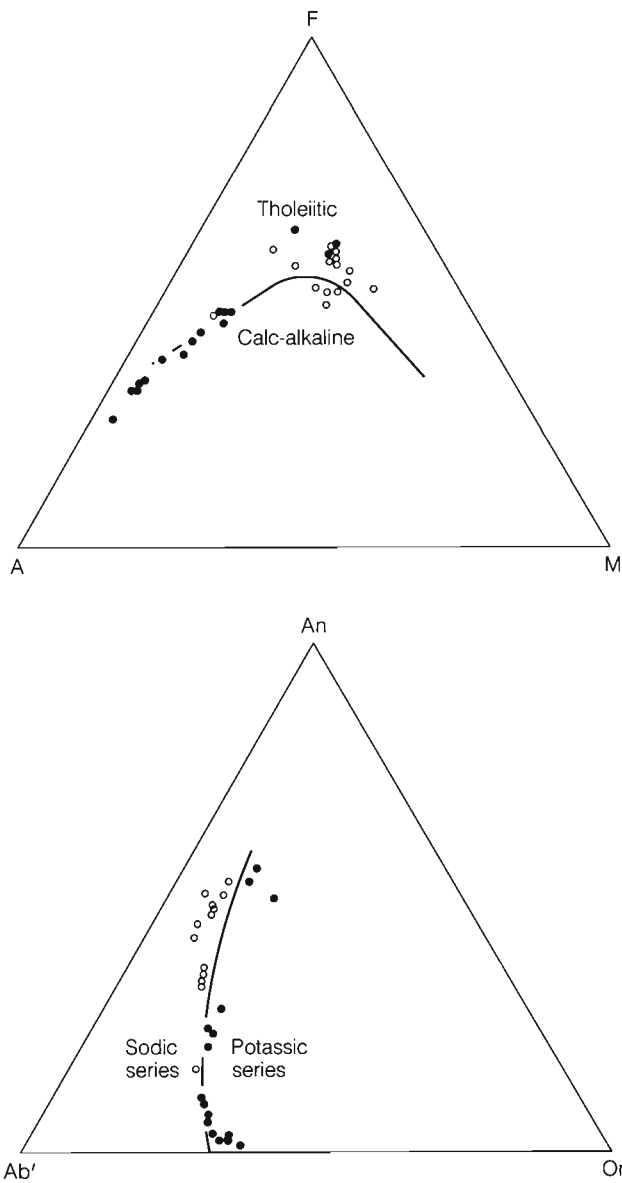


Figure 135. AFM and Ab'-An-Or plots of 29 analyses from the Ice Peak Formation. For explanation of symbols see Fig. 136. (A = Na₂O + K₂O; F = FeO + 0.8998 Fe₂O₃; M = MgO; Ab' = Ab + 5/3Ne).

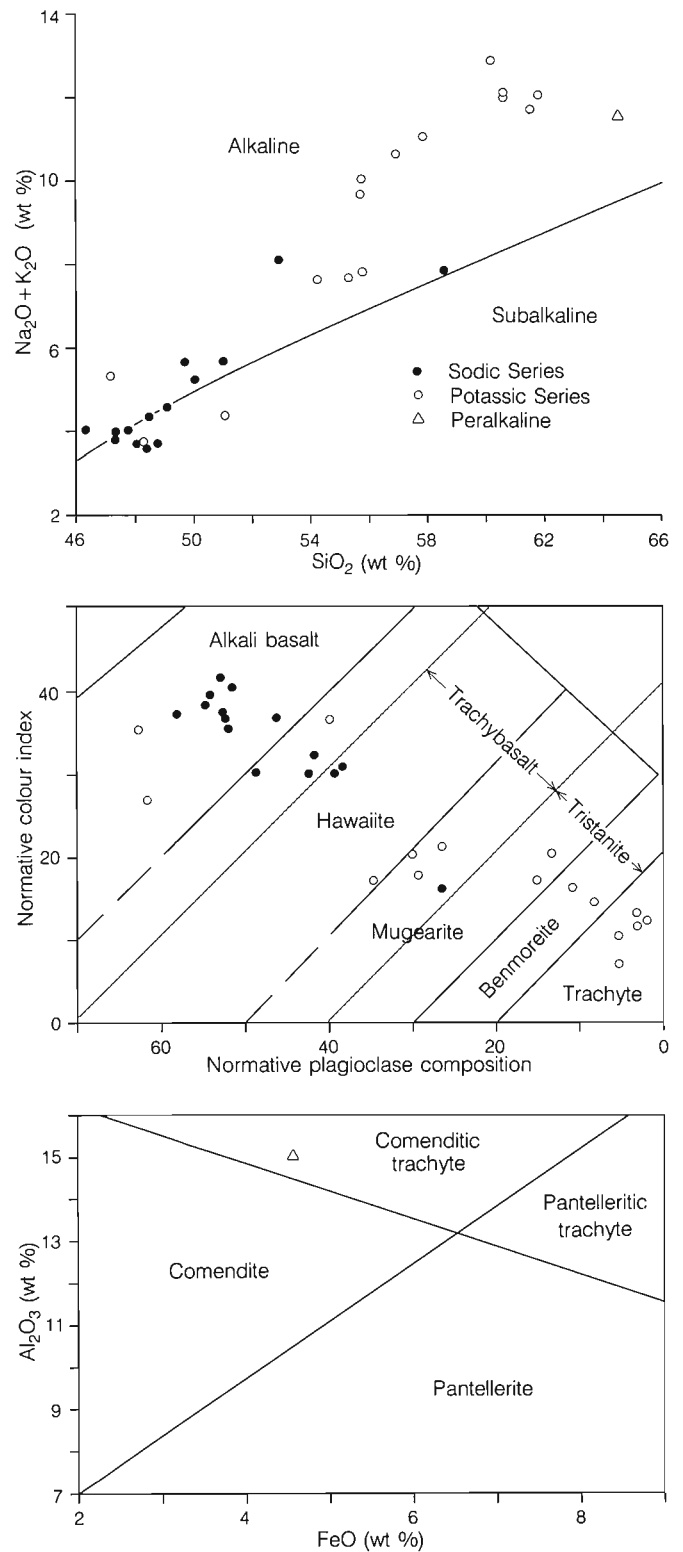


Figure 136. Plot of total alkalis vs. silica, normative colour index vs. normative plagioclase composition, and Al₂O₃ vs. FeO for 32 analyses of rocks from the Ice Peak Formation.

MOUNT EDZIZA

($\sim An_{50}$), tiny euhedra of augite and olivine plus finely disseminated opaque oxides. Less commonly the groundmass is micro-ophitic, with plagioclase laths and olivine grains partly or wholly enclosed by ophitic crystals of titanite. Carbonate alteration of the groundmass is present locally, but it is much less common than in the older basalts. In some basalts of the potassic series tiny euhedral crystals of alkali feldspar and biotite, crystallized from a vapour phase, are present in cavity linings. Most vesicles are void or lined with a thin rind of manganese-iron oxide.

The aphyric basalts include the same mineral species as the porphyritic varieties, but most have ophitic or subophitic textures.

Ice Peak hawaiite differs from the other basalts in having a higher content of opaque oxides and plagioclase phenocrysts.

Intermediate rocks

The Ice Peak mugearites, trachybasalts and tristanites are not readily distinguished from one another in thin section. The mugearite and trachybasalt are commonly microporphyritic with sparse phenocrysts of plagioclase, pyroxene and olivine, all of which have reacted strongly with the groundmass (Fig. 133c). Plagioclase phenocrysts ($\sim An_{50}$) have rounded, embayed margins mantled with an overgrowth of less calcic feldspar (An_{10-20}). Both olivine and pale green clinopyroxene are largely replaced by finely disseminated, opaque secondary minerals. Magnetite phenocrysts are embayed and surrounded by haloes of dispersed opaque oxide. The groundmass is a mosaic of interlocking feldspars, small euhedral clinopyroxene crystals and disseminated opaque oxides. The feldspar is characterized by stout, complexly zoned crystals which are intergrown along complex sutures. Pyroxene forms euhedral,

fusulinid-shaped crystals which are strongly zoned from purplish-brown titanite cores to colourless or pale green ferroaugite rims.

Tristanite is texturally similar to the mugearite and trachybasalt but phenocrysts display even greater evidence of reaction. The principal difference is in feldspar compositions. Overgrowths on resorbed phenocrysts and groundmass feldspars in the tristanites are mostly oligoclase with up to 10% orthoclase. Pale green ferrohedenbergite is commonly present in the groundmass as well as forming the outer rims on zoned titanite crystals. Pale yellow fayalitic olivine ($\sim Fo_5$) is also a sparse but widely distributed groundmass phase.

Trachyte

With increasing alkali feldspar content and decreasing feric constituents the tristanites grade into trachyte (Fig. 133d). Most Ice Peak trachytes are microporphyritic with two generations of feldspar phenocrysts. Euhedral laths of alkali feldspar with Carlsbad and fine, crosshatched twinning form up to 10% of the rock. Probe analyses plot near the anorthoclase-sanidine boundary on the Ab-An-Or plot (Fig. 134). A sparse, older generation of partly resorbed phenocrysts have deeply embayed cores of plagioclase mantled by anorthoclase. The groundmass is almost entirely alkali feldspar in ragged, interlocking laths aligned along planar or contorted flow layers. Interstitial to the groundmass feldspar are pale to medium green sodic ferrohedenbergite and fine granular opaque oxides. Bright green acmitic pyroxene, aenigmatite and arfvedsonite are minor constituents in the more alkaline trachytes and in the relatively rare peralkaline Ice Peak rocks, comenditic and pantelleritic trachyte.

Table 14. Selected chemical analyses showing the range of compositions found in the Ice Peak Formation.

	Alkali olivine basalt		Hawaiite	Mugearite	Tristanite	Trachyte		Peralkaline
Sample	75	2646	2684	2680	21	2	11	74
SiO ₂	46.800	47.100	49.300	56.300	56.500	59.400	61.500	62.500
Al ₂ O ₃	15.400	15.900	16.000	17.100	17.400	19.200	16.900	15.200
Fe ₂ O ₃	1.500	4.900	9.200	2.900	2.100	2.700	2.600	1.600
FeO	10.500	6.400	3.600	5.000	5.900	2.000	3.500	3.000
CaO	9.580	11.200	8.600	4.600	3.540	1.650	1.620	1.990
MgO	4.920	5.100	3.900	1.600	1.640	0.480	0.510	0.600
Na ₂ O	3.300	2.700	3.900	5.300	6.400	7.500	6.400	5.700
K ₂ O	0.870	0.900	1.600	2.100	4.180	5.170	5.610	5.460
TiO ₂	3.150	2.240	2.530	1.080	1.280	0.390	0.520	0.450
P ₂ O ₅	0.390	0.300	0.780	0.160	0.310	0.130	0.110	0.100
MnO	0.180	0.130	0.170	0.170	0.170	0.110	0.150	0.090
S	0.080	0.0	0.0	0.0	0.100	0.070	0.110	0.090
NiO	0.010	0.0	0.0	0.0	0.0	0.020	0.0	0.0
CO ₂	1.700	0.800	0.900	1.900	0.100	0.0	0.0	1.800
H ₂ O	1.700	1.400	0.500	0.800	0.500	0.400	0.500	0.600
Total	100.080	99.070	100.980	99.010	100.120	99.220	100.030	99.180

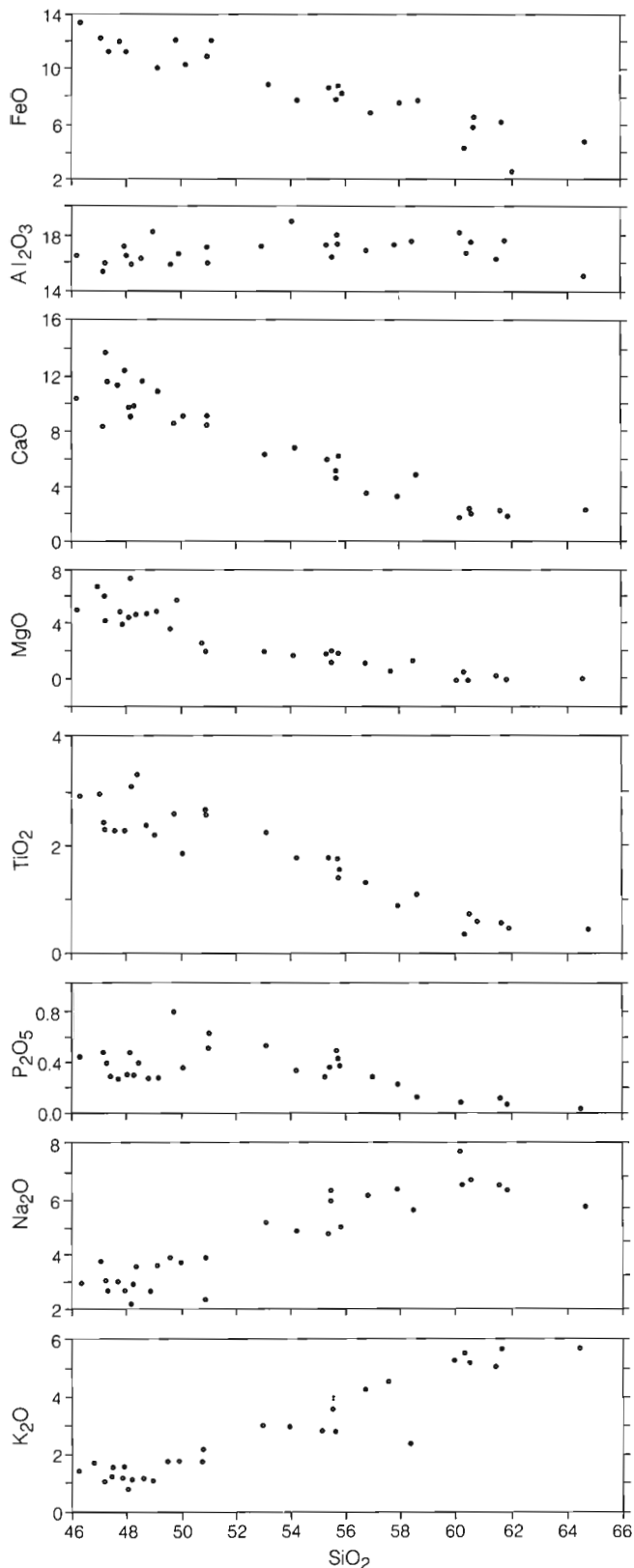


Figure 137. Harker diagram showing the chemical variation in weight per cent of analyzed specimens from the Ice Peak Formation.

Cumulate inclusions

Crystal clusters 1-10 mm across are sparsely scattered throughout most of the Ice Peak tristanites and trachytes (Fig. 133e). Rare, larger inclusions of similar texture and mineralogy (up to 10 cm) are found locally. They are loosely stacked, randomly oriented aggregates of euhedral unzoned plagioclase, titanite, magnetite and apatite crystals. Olivine may or may not be present. It forms up to 20% of most of the larger inclusions but may be absent in clusters of smaller size.

CHEMISTRY

The Ice Peak rocks have a wider range of compositions than those of any other formation in the Mount Edziza Volcanic Complex (Table 14). On the Ab'-Ab-An diagram (Fig. 135) the thirty analyzed specimens plot within a narrow field that crosses the boundary between the sodic and potassic series of Irvine and Baragar (1971). Most of the sodic rocks have normative plagioclase compositions greater than An₃₅ and are classified as alkali basalt or hawaiite (Fig. 136). The more highly fractionated rocks (normative plagioclase < An₃₅) belong mostly to the potassic series (Fig. 136) and plot within the fields of trachybasalt, tristanite and trachyte. Only one of the analyzed samples (comenditic trachyte, no. 74) is peralkaline, but a strong trend toward alkali-enrichment is apparent on both the alkali vs. silica and AFM diagrams (Fig. 135, 136). The regular variation of constituent oxides across the entire range of silica values (46 to 65% SiO₂) suggests a genetic lineage between the various rocks of the Ice Peak Formation (Fig. 137).

The Ice Peak assemblage appears to bridge the gap between basalt and trachyte that characterizes the Mount Edziza Volcanic Complex as a whole. As discussed in a later chapter, the entire range of chemical variation can be explained by crystal fractionation of an alkali basalt parent magma. Early separation of large amounts of plagioclase would result in the observed trend toward potash enrichment in the Ice Peak trachytes. But, unlike other formations in the complex, which are either bimodal or comprise only one end member, the Ice Peak includes a complete range of intermediate rocks. This implies that fractionating reservoirs were either repeatedly tapped during Ice Peak time or that older magma, residing in pre-Ice Peak reservoirs, was driven to the surface during Ice Peak activity. The underplating and remobilization of partly fractionated residual magma by primitive, Ice Peak basalt may account for the great diversity of lavas erupted during this relatively short period of time. Such a mechanism is consistent with local alternation of basalt and trachyte in the Ice Peak stratigraphy and with anomalous isotopic composition of the Ice Peak rocks (see Chapter on Isotope Chemistry).

PILLOW RIDGE FORMATION

GENERAL GEOLOGY

Introduction

The Pillow Ridge Formation is confined to two small areas, Pillow Ridge and Tsekone Ridge, high on the northwest side of Mount Edziza (Fig. 138, Map 1623A, in pocket). The narrow black crest of Pillow Ridge extends northwesterly from the north slope of Mount Edziza for nearly 4 km (Fig. 139). Its northeastern end, at an elevation of 8000 ft. (2400 m), is surrounded by the summit ice cap and it is bounded on either side by valley glaciers that descend almost to the level of the flanking plateau. The northwestern end of the ridge is buried beneath a thick layer of colluvium that covers the plateau surface and obscures the base of the Pillow Ridge pile. The ridge itself is a well exposed complex of basaltic aquagene tuff-breccia, pillow-breccia, pillow lava and dykes (Fig. 140). Tsekone Ridge is an isolated pile of basaltic tuff-breccia and pillow lava near the western end of Pillow Ridge (Fig. 138). It is elliptical in plan, with a length of nearly 2 km along its major, north-south axis. Its steep, rubble-covered slopes rise to a narrow-crested rocky ridge 600 ft. (180 m) above the plateau surface but its relationship to rocks on the surrounding plateau is completely obscured by talus.

Pillow Ridge

Crudely bedded, yellowish-brown, sideromelane tuff-breccia forms most of the central and lower part of the Pillow Ridge pile. On the high northeastern crest the bedding is nearly horizontal, but elsewhere it dips 10-30° outward, away from the ridge crest. The basal tuff-breccia is a chaotic mixture of brown, altered basaltic lapilli and glass, enclosing angular clasts from 1-10 cm across and irregular globules of dark grey, highly vesicular olivine basalt up to 1 m across. The surface of all fragments, both large and small, is coated with a pervasive rind of yellowish-orange palagonite. Higher in the pile the bedding is better developed, with conspicuous size sorting, particularly of the large, angular, clasts. The uppermost 30-60 m of tuff-breccia is well bedded, and in addition to small angular and irregular clasts, contains a significant number of pillow fragments (Fig. 141). These characteristically wedge-shaped chunks of basalt, with concentric layers of small spherical vesicles, are commonly bounded on four sides by converging joint surfaces, and on the other by a segment of the smooth, glassy, outer surface of the broken pillow. At the distal, northwestern end of the pile, pillow fragments are the only large clasts suspended in west-dipping deposits of glassy, brown basaltic lapilli.

The tuff-breccia is overlain by and locally interdigitates with an outer mantle of tubular pillow lava (Fig. 142). A small patch is preserved on the southwest crest of the ridge,

just below the ice cover, and includes both pillow lava and subaerial flows. A larger remnant, forming most of the northwestern nose of the ridge, is entirely pillow lava. Pillows in the upper remnant are poorly developed and have no consistent orientation but those in the lower remnant have a strong northwesterly alignment. Most are elongate bodies that form intertwined masses of long, sinuous or branching tubular forms which plunge 15-30° away from the ridge crest. In cross-section they are 0.3-1 m across and have the classical oval form of pillow lavas (Fig. 143). They are characterized by radial jointing, concentric layers of small spherical vesicles, which become larger and more numerous inward, and by a thin rind of lustrous black or brownish-orange altered glass. An open gas hole 5-20 cm across is present in the centre of most pillows. Spaces between adjacent pillows are also open, or partly filled with a finely laminated, silt-like deposit, thus, where the slope is parallel with the plunge of the lava, the original outer surfaces of tubular pillows can be observed. Individual bodies are exposed for up to 15 m. Most retain their elliptical form throughout, but bulbous protrusions and buds are common and in places a single tube branches into two or three distributary tubes all of about the same diameter.

The source of the Pillow Ridge basalt appears to be directly beneath the centre of the pile where the tuff-breccia is cut by numerous 0.3-1 m dykes. Most of these are vertical and more or less parallel with the ridge crest, but others trend east and north, cutting diagonally across the ridge. Several of the latter are continuously exposed from the ridge crest through cliffs to the glacier on the southwestern side. The dykes display many of the same structures as the pillows, including thin, glassy outer rinds, closely spaced 10-15 cm rectangular to crudely columnar transverse jointing, and trains of small spherical vesicles arranged in well defined planes parallel with the contacts. As in the pillows, the vesicles become larger and more numerous inward, and in many dykes they coalesce to form large voids within a highly porous central zone. Basalt in the dykes, pillows and larger breccia blocks is fine grained, highly vesicular and contains sparse, 1-3 mm phenocrysts of feldspar, olivine and rarely pyroxene.

Pillow Ridge tuff-breccia and pillow-breccia is sporadically exposed over a large area 2-3 km northeast of the ridge itself. It has been partly covered by younger lavas, slope wash and low vegetation. Outcrop is in the form of large isolated blocks 1-20 m across which project from the tundra surface as crumbling monoliths surrounded by spalled off debris. Bedding orientation within the blocks is completely random, suggesting that they are not in situ. They were probably carried to their present position as part of a landslide that sloughed off the north slope of the ridge.

MOUNT EDZIZA

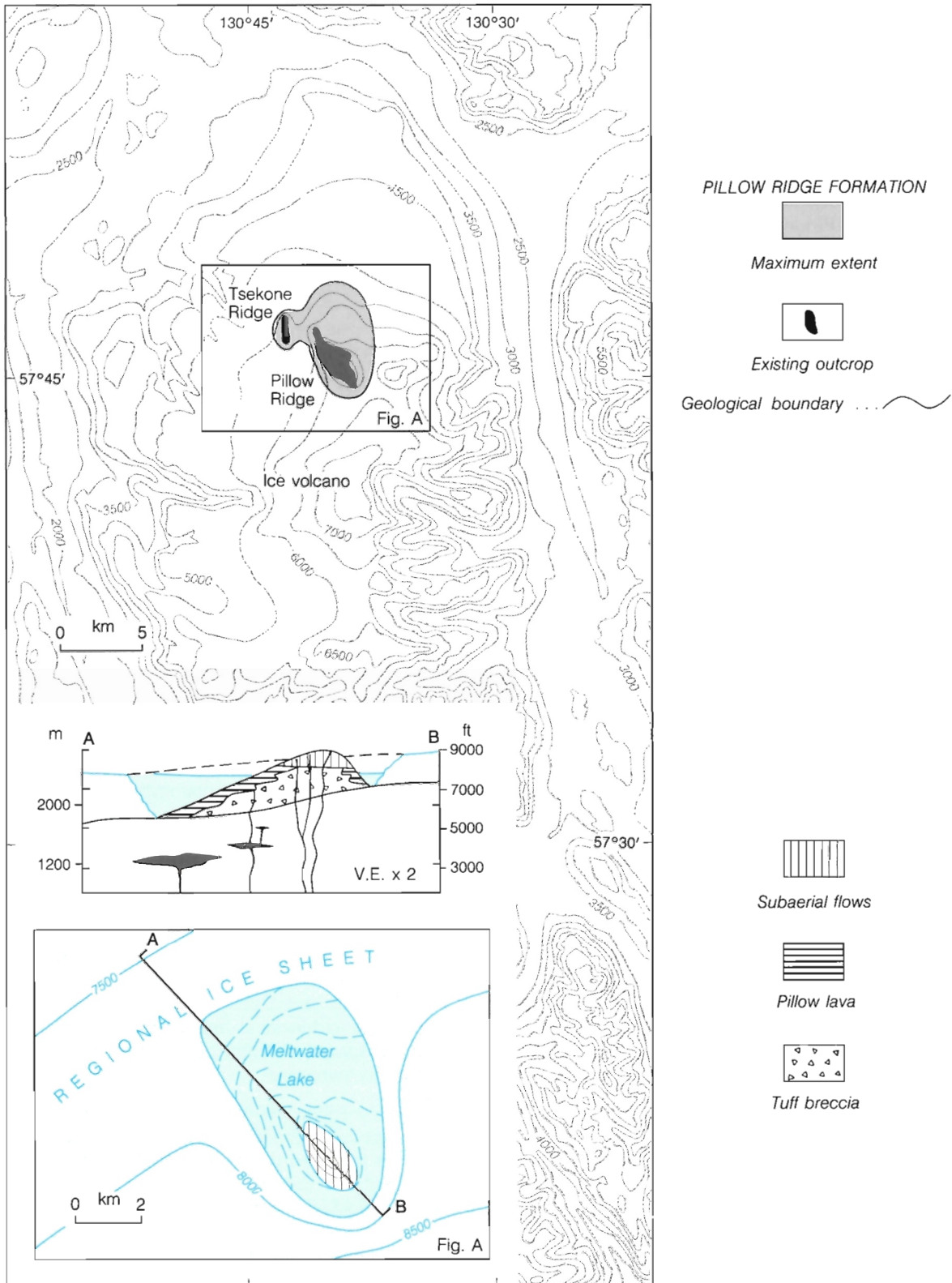


Figure 138. Paleogeological map showing the maximum extent of the Pillow Ridge Formation at the end of Pillow Ridge time. Figure A and cross-section show the relationship of the volcanic pile to glacier ice during the final stage of Pillow Ridge activity.

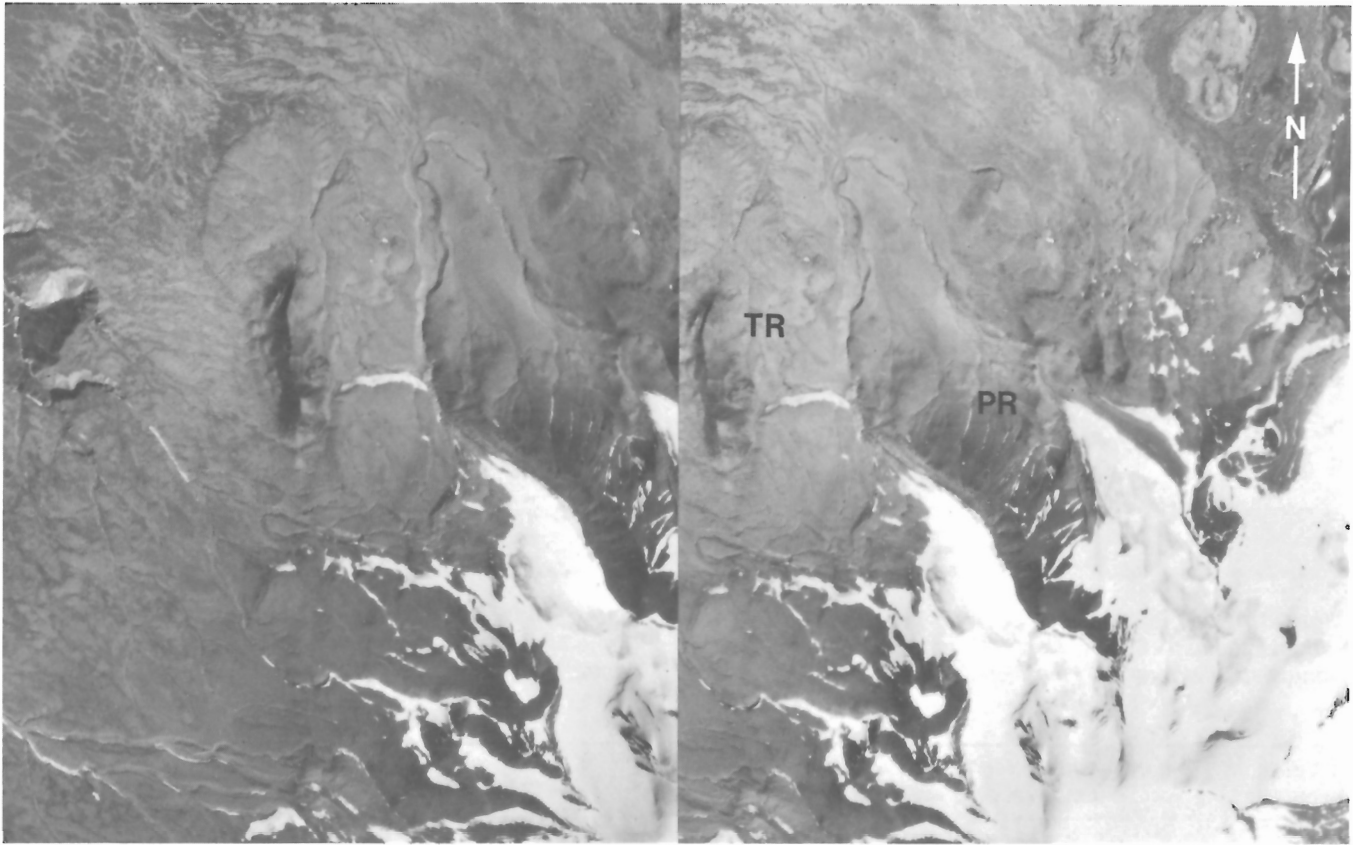


Figure 139. The northwest flank of Mount Edziza, showing the morphology of Pillow Ridge (PR) and Tsekone Ridge (TR). Stereoscopic pair. Province of British Columbia photos BC 5607-143, 144.



Figure 140. The southwest slope of Pillow Ridge showing the lower pile of aquagene tuff-breccia overlain by a mantle of pillow lava. Tsekone ridge in background. GSC 125 612.



Figure 141. Aquagene tuff-breccia near the top of Pillow Ridge. Fragments of broken pillows are suspended in a matrix of quenched basaltic lapilli and granular sideromelane. GSC 125 613.



Figure 142. Tubular pillow lava near the summit of Pillow Ridge. Initial dip of pillows is away from the ridge crest and approximately parallel to the slope. GSC 202469-D.

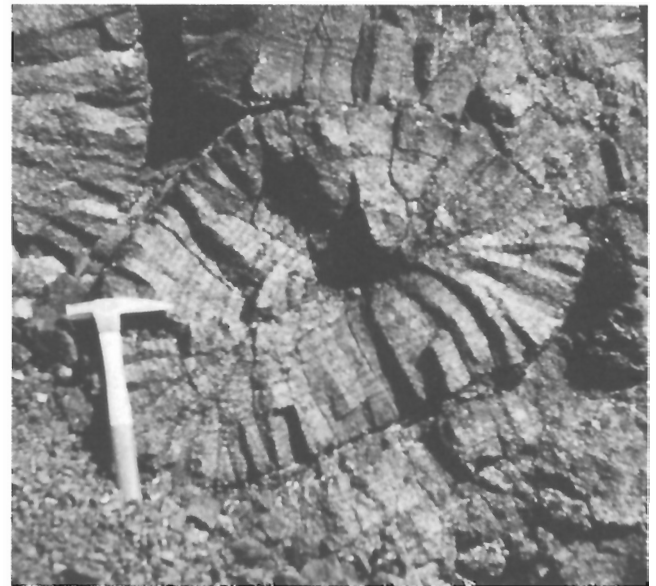


Figure 143. Cross-section of pillow structure on Pillow Ridge showing concentric vesicle trains, radial jointing and central gas cavity. GSC 202469-E.

Table 15. Representative microprobe analyses and structural data for the principal mineral phases in the Pillow Ridge rocks.

	Feldspar			Pyroxene		Olivine			
	Phenocryst			Phenocryst		Phenocryst			
	PRF-1	PRF-2	PRF-3	PRP-1	PRP-2	PRO-1	PRO-2		
SiO ₂	54.26	49.54	53.06	50.39	50.28	39.51	38.75		
Al ₂ O ₃	29.15	31.08	28.66	4.70	3.67	.10	0.03		
TiO ₂	.14	0.05	0.13	1.29	1.38	.01	0.03		
Cr ₂ O ₃	0.00	0.0	0.0	.58	.03	0.00	0.02		
Fe ₂ O ₃	.63	0.51	0.79	1.03	1.38	0.00	0.0		
FeO	0.00	0.0	0.0	6.29	8.22	16.75	20.29		
MnO	0.00	0.0	0.02	.17	.23	.22	0.26		
MgO	.06	0.06	0.11	14.46	12.72	42.70	40.32		
NiO	0.00	0.0	0.0	0.00	0.00	.25	0.0		
CaO	11.33	15.59	13.04	21.40	21.73	.24	0.24		
Na ₂ O	4.63	2.77	4.21	.38	.51	0.00	0.0		
K ₂ O	.42	0.15	0.28	0.00	.01	0.00	0.0		
H ₂ O	0.00	0.0	0.0	0.00	0.00	0.00	0.0		
F	0.00	0.0	0.0	0.00	0.00	0.00	0.0		
Total	100.62	99.75	100.30	100.69	100.16	99.78	99.94		
	No. of ions on basis of 8 (0)				No. of ions on basis of 6 (0)		No. of ions on basis of 4 (0)		
Si	2.4392	2.2744	2.4079	Si	1.8533	1.8793	Si	1.0034	0.9989
Al	1.5443	1.6817	1.5328	Al	.1467	.1207	Al	0.0000	0.0
Cr	0.0000	0.0	0.0	Ti	0.0000	0.0000	Cr	0.0000	0.0
Fe ³⁺	.0213	0.0176	0.0270	Fe	0.0000	0.0000	Fe ³⁺	0.0000	0.0
				Cr	0.0000	0.0000			
Al	0.0000	0.0	0.0	Al	.0570	.0410	Al	.0030	0.0009
Cr	0.0000	0.0	0.0	Ti	.0357	.0388	Cr	0.0000	0.0004
Ti	.0047	0.0017	0.0044	Fe ³⁺	.0286	.0388	Ti	.0002	0.0006
Fe ³⁺	0.0000	0.0	0.0	Cr	.0169	.0009	Fe ³⁺	0.0000	0.0
Ni	0.0000	0.0	0.0	Ni	0.0000	0.0000	Ni	.0051	0.0
Fe ²⁺	0.0000	0.0	0.0	Fe ²⁺	.1935	.2569	Fe ²⁺	.3557	0.4374
Mn	0.0000	0.0	0.0008	Mn	.0053	.0073	Mn	.0047	0.0057
Mg	.0040	0.0041	0.0074	Mg	.7927	.7086	Mg	1.6163	1.5492
				Ca	.8433	.8702			
				Na	.0271	.0370			
				K	0.0000	.0005			
Ca	.5457	0.7669	0.6340				Ca	.0065	0.0066
Na	.4035	0.2466	0.3704				Na	0.0000	0.0
K	.0241	0.0088	0.0162				K	0.0000	0.0

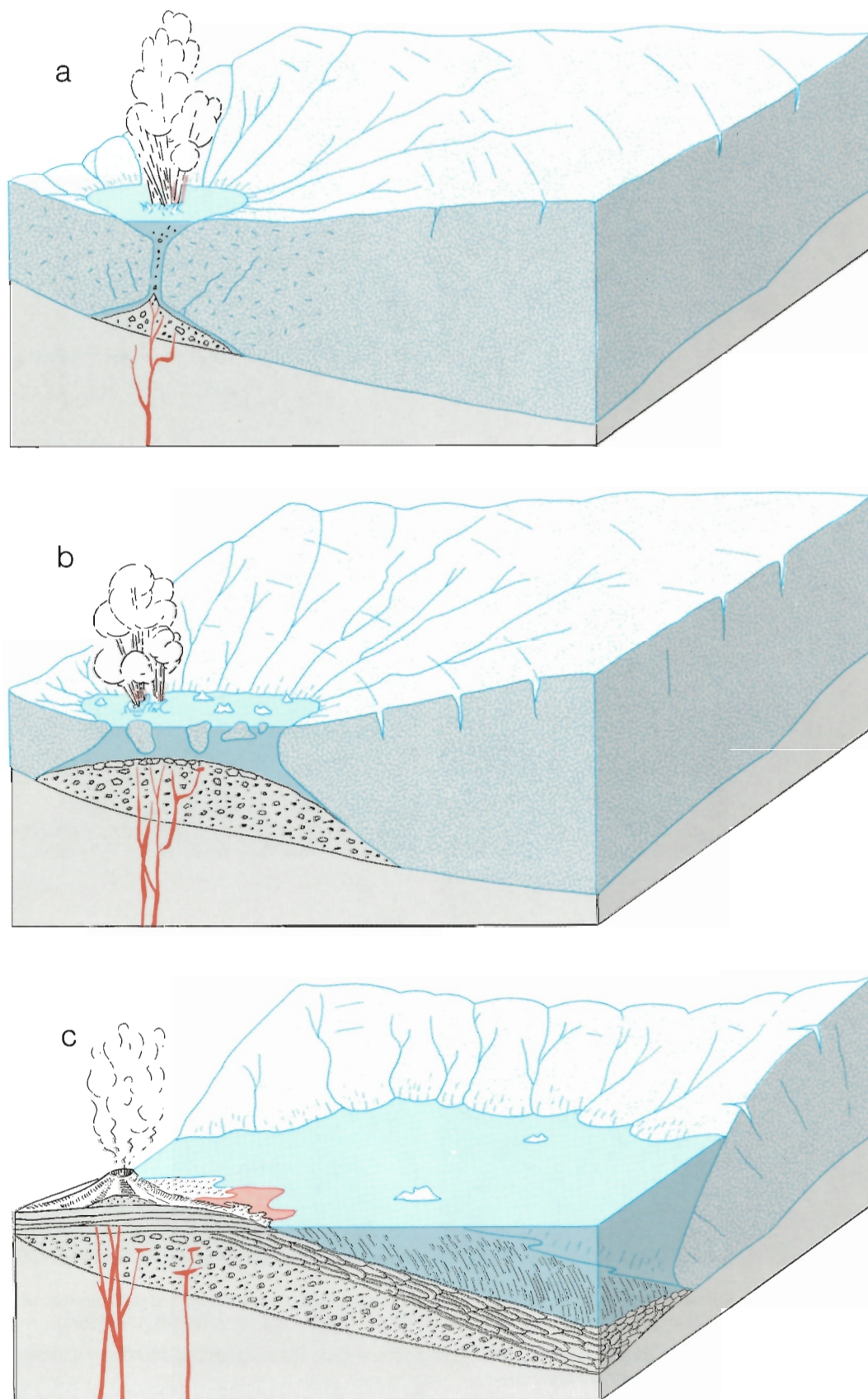
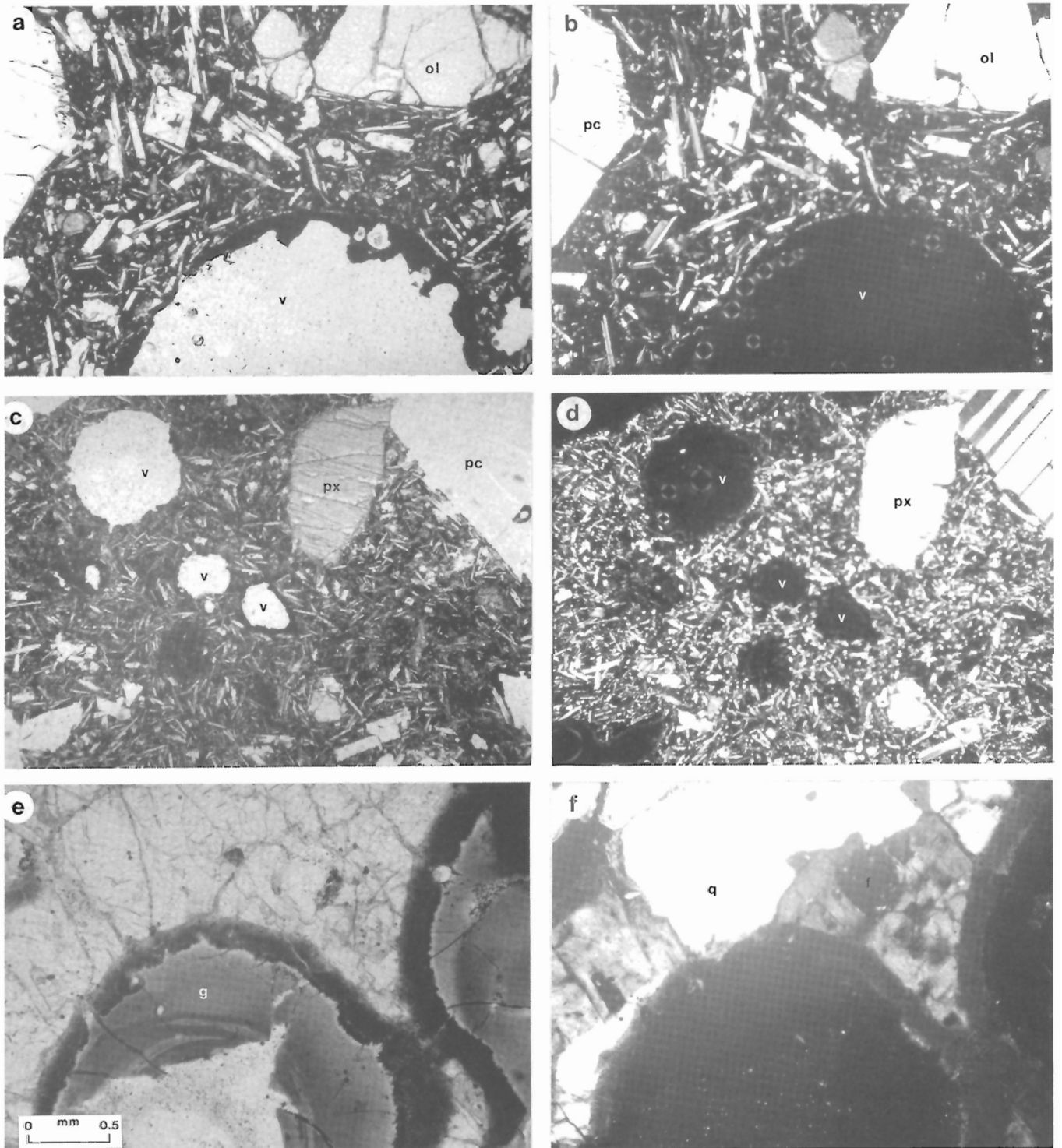


Figure 144. Block diagram showing three stages in the evolution of the Pillow Ridge pile. (a) Initial eruption of basalt beneath glacier resulting in a meltwater pond on the sagging surface of the ice. (b) Accumulation of the chaotic, basal breccia, formed from primary ejecta erupted into the meltwater pond, mixed with debris slumped in from its unstable margins. (c) Accumulation of bedded tuff-breccia in the upper part of the pile, after stabilization of the meltwater pond and construction of the mantle of pillow lava and subaerial flows on the relatively broad surface of the tuff-breccia pile.



a,b — Basalt from Pillow Ridge. Phenocrysts of plagioclase (pc) and olivine (ol) in fine grained basalt with open vesicles (v) lined with iron manganese oxide (a, plane light, b, crossed polarizers).
c,d — Basalt from Tsekone Ridge. Phenocrysts of plagioclase (pc), titanite (px) and open vesicles (v), (c, plane light; d, crossed polarizers).
e,f — Partly fused granitic inclusion of interlocking quartz (q) and feldspar (f) grains embayed by glass (g), (e, plane light; f, crossed polarizers).

Figure 145. Photomicrographs of Pillow Ridge basalt and granitic inclusion; scale bar 0.5 mm.

The lower contacts of the Pillow Ridge tuff-breccia are not exposed, but the pile is clearly older than the central cone of Mount Edziza. Patches of Edziza Formation trachyte rest on the upper surface of the ridge, and a large flow of trachyte overlaps the western edge of the pile. The latter is well exposed in a small box canyon between the edge of the flow and the northwestern end of Pillow Ridge. There, horizontally flow-banded trachyte is underlain by 1-2 m of porous flow breccia which rests directly on the truncated beds of steeply west-dipping pillow-breccia. Thus the Pillow Ridge pile must rest directly on the eroded surface of Ice volcano and must have formed during a period of major glaciation. A projection of the assumed profile of Ice volcano prior to the Pillow Ridge event suggests that the ice was at least 450 m thick (Fig. 144). Whereas the tuff-breccia could have accumulated in a narrow meltwater pond that migrated downslope as the pile grew, the mantle of pillow lava could only have formed in a body of meltwater that was ponded by ice up to an elevation of at least 7400 ft. (2250 m). The change from chaotic tuff-breccia at the base

upward through bedded tuff-breccia, pillow-breccia and finally to undisturbed pillow lava may be due in part to progressive enlargement of the meltwater pool thawed by the lava. The initial eruption may actually have broken through the ice to form a steep-sided pit crater in which the first ejecta accumulated as a pile of pyroclastic debris and scraps of lava mixed with blocks of ice and isolated pockets of water. As melting enlarged the crater this unstable mass progressively collapsed. Bombs, ash and lapilli thrown onto the surface of the glacier slumped back into the widening hole and were incorporated in the aquagene deposits to form the chaotic basal tuff-breccia. With continued melting the pond rapidly enlarged and filled with water. At that stage the first stratified deposits formed by size-sorting of primary ejecta thrown into the water and subaqueous slides spalling off the steep slopes of the growing pile. These settled out to form bedded tuff-breccia while unstable masses of pillow lava, formed around the central vent, repeatedly collapsed and were swept, along with other debris to the edge of the pile where they accumulated as foreset beds of pillow-breccia. As the pile grew laterally, its steep slopes became gentler and more stable, slumping ceased and the present veneer of pillow lava accumulated. The absence of tuff-breccia within the upper pillow lava succession suggests that the central vent may have grown above the surface of the meltwater lake during this final stage of activity. Thus the violent phreatic explosions which must have accompanied

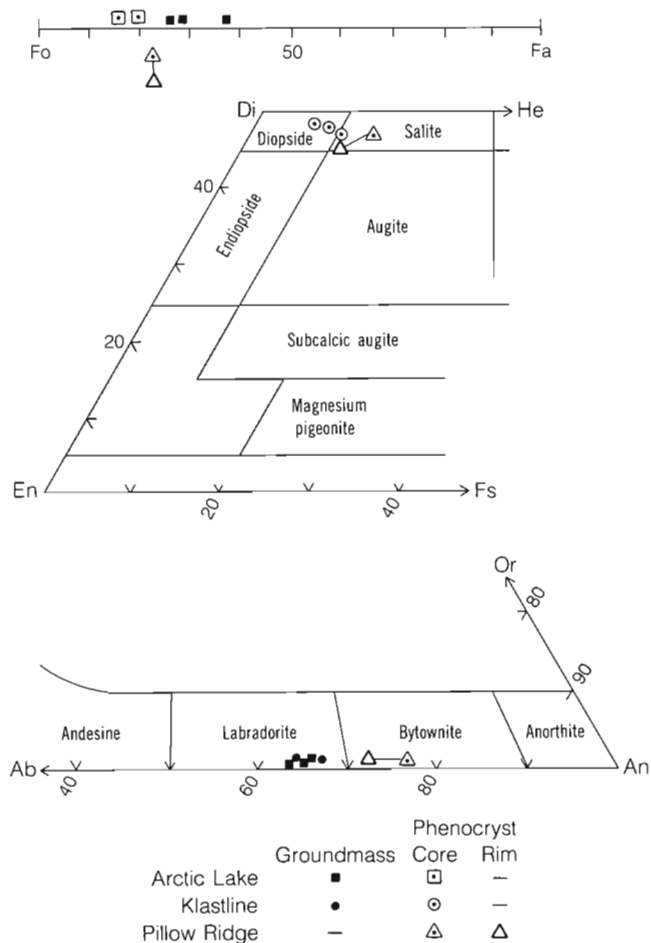


Figure 146. End-member plots of microprobe analyses, showing compositions of the principal mineral phases in rocks from the Pillow Ridge, Klastline and Arctic Lake formations.

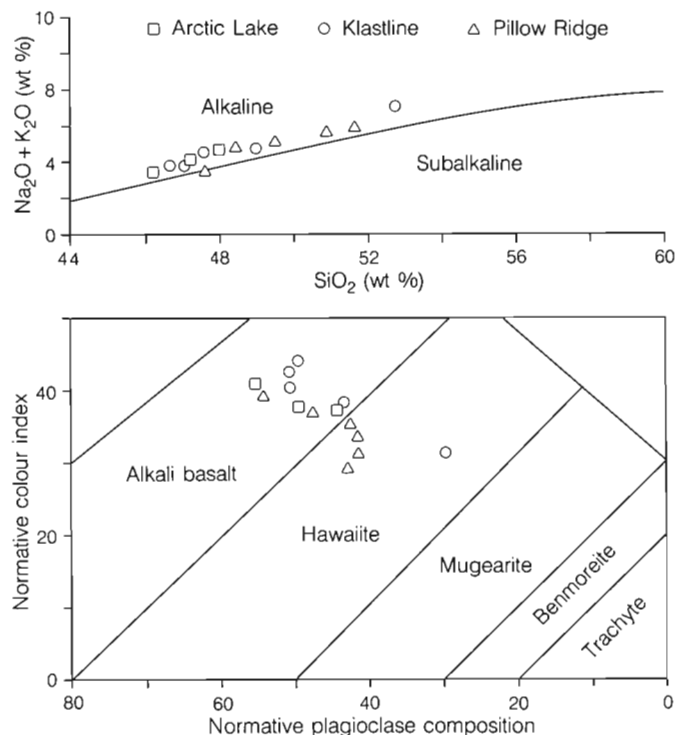


Figure 147. Plot of Pillow Ridge, Klastline and Arctic Lake chemical data on the total alkalis vs. silica, and normative colour index vs. normative plagioclase composition diagrams.

the subaqueous eruptions and generated masses of debris were succeeded by quiet outpouring of fluid streams of lava from a subaerial, island vent within the meltwater lake. Where these entered the water they were quenched to form the long tubular branching pillows that mantle the pile of tuff-breccia.

Tsekone Ridge

The lower and central part of the Tsekone pile is a loosely welded mass of black scoria and blocks of highly vesicular basalt. This is overlain by fractured, closely jointed pillows and lava tubes. Both the tuff-breccia and the pillow sequence are cut by vertical north-trending feeder dykes. Tsekone Ridge resembles the nearby Pillow Ridge pile but there are important differences. The Tsekone Ridge basalt, with up to 30% phenocrysts of clear, glassy feldspar, olivine and pyroxene, is distinctly more porphyritic than that of Pillow Ridge. Also in the Pillow Ridge pile most of the glass has been altered to palagonite and vesicles, though still open, are lined with an iron oxide coating. In contrast, the Tsekone Ridge pile is characterized by lustrous black, glassy surfaces of both pillows and scoria. Thin iridescent films of glass retain every detail of their original surface, including tiny unbroken bubbles. The hollow interior of many pillows is filled with a web-like filigree of iridescent glass strands, so thin that they are flexible, and there is no coating on the inner surfaces of vesicles.

Differences in glass alteration and vesicle lining suggest that the Pillow and Tsekone Ridge piles were erupted under slightly different conditions. Both are clearly subglacial, but the original mass of the Pillow Ridge pile was at least five

times that of Tsekone Ridge. Thus Pillow Ridge must have had a relatively long cooling history during which vigorous hydrothermal circulation through the porous tuff-breccia and loosely stacked pillows resulted in the observed hydration of glass and precipitation of hydrous iron oxide in fractures and vesicles. The absence of similar hydrothermal alteration in the Tsekone pile may be due to its small size and consequently short cooling history. Tsekone Ridge may also be somewhat younger than Pillow Ridge. Its higher phenocryst content and slightly more alkaline composition could result from modification of a portion of the primary batch of Pillow Ridge magma prior to its eruption at Tsekone Ridge. Partial crystallization, accompanied by removal of a small amount of olivine, could account for the observed chemical and petrographic differences.

Accidental inclusions

Xenoliths of partly fused granitic and gneissic rock are found throughout the Pillow Ridge pile, and less commonly on Tsekone Ridge. They vary in size from single crystals or crystal clusters to rounded masses over 0.3 m across, and in degree of melting from lenses of frothy, white felsic glass to subangular inclusions that have undergone only minor discolouration. Most of the inclusions exhibit a spongy texture in which the original framework of white quartz and feldspar crystals is permeated by a vermicular network of black, glass-lined voids.

Inclusions of coarse grained gabbro are smaller and less abundant than the granitic xenoliths. They form loosely stacked, dictytaxitic aggregates of clear, colourless feldspar and black clinopyroxene.

Table 16. Representative chemical analyses of specimens from the Pillow Ridge Formation.

Sample	Tsekone Ridge		Pillow Ridge	
	C-3	60	59	C-2
SiO ₂	49.49	47.60	47.20	50.62
Al ₂ O ₃	16.12	15.80	16.20	17.02
Fe ₂ O ₃	3.72	3.10	3.10	3.20
FeO	7.66	8.10	8.40	5.38
CaO	9.18	8.95	10.70	9.55
MgO	5.78	6.78	7.53	3.93
Na ₂ O ₃	3.65	3.50	2.80	3.73
K ₂ O	1.50	1.45	.66	1.76
TiO ₂	2.33	2.36	1.90	2.45
P ₂ O ₅	.44	.46	.24	.40
MnO	.01	.16	.18	.10
S		.08	.11	
NiO		.01	.01	
CO ₂		.50		
H ₂ O	1.04	.90	.20	2.52
Total	100.92	99.25	99.73	100.57

PETROGRAPHY

The Pillow Ridge alkali olivine basalt (Fig. 145a, b; 146; Table 15) contains sparse phenocrysts and microphenocrysts of plagioclase (An₇₅ zoned to rims of An₇₀), olivine (Fo₈₀), and clinopyroxene (titaniferous salite). The highly vesicular groundmass of nearly opaque glass contains ragged laths of plagioclase (An₆₀₋₆₅), dendritic crystals of titaniferous salite and disseminated iron titanium oxide grains and dendrites. The Tsekone Ridge hawaiite (Fig. 145c,d) includes the same mineral species but

it is distinctly more porphyritic. Microphenocrysts of clinopyroxene, plagioclase and olivine form up to 50% of the rock and strongly pigmented, purplish-brown titaniferous salite is commonly the most abundant phenocryst phase. The glassy, iron-rich groundmass is similar to that of the Pillow Ridge basalt.

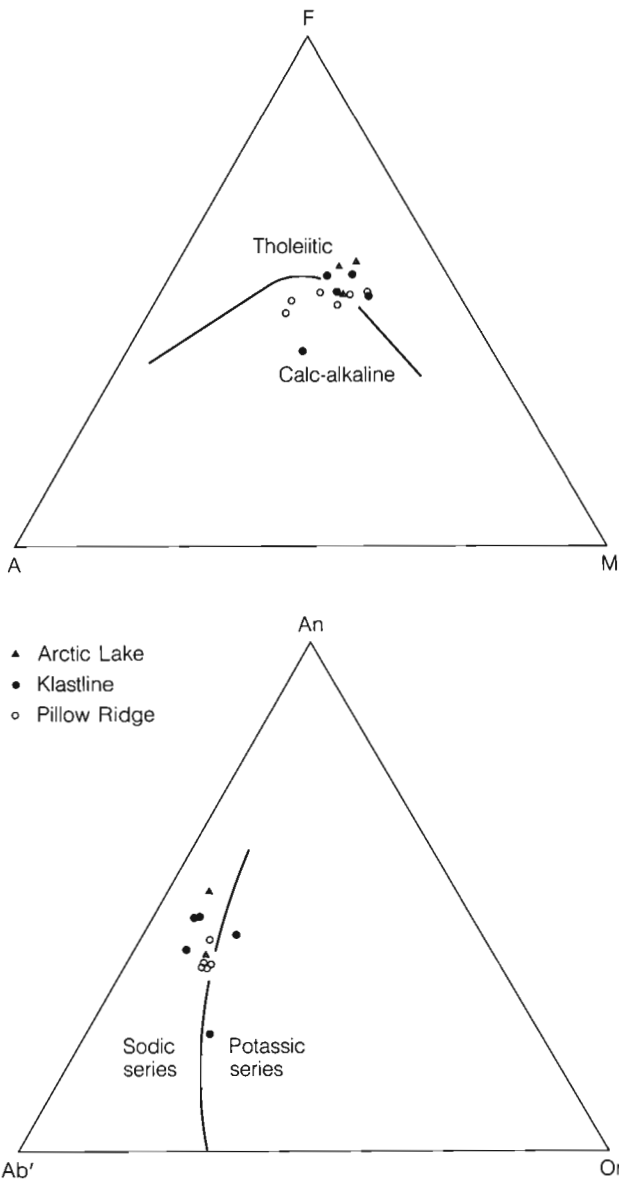


Figure 148. AFM and Ab'-An-Or plots of chemical data from the Pillow Ridge, Klastline and Arctic Lake formations. (A = Na₂O + K₂O; F = FeO + 0.8998 Fe₂O₃; M = MgO; Ab' = Ab + 5/3Ne).

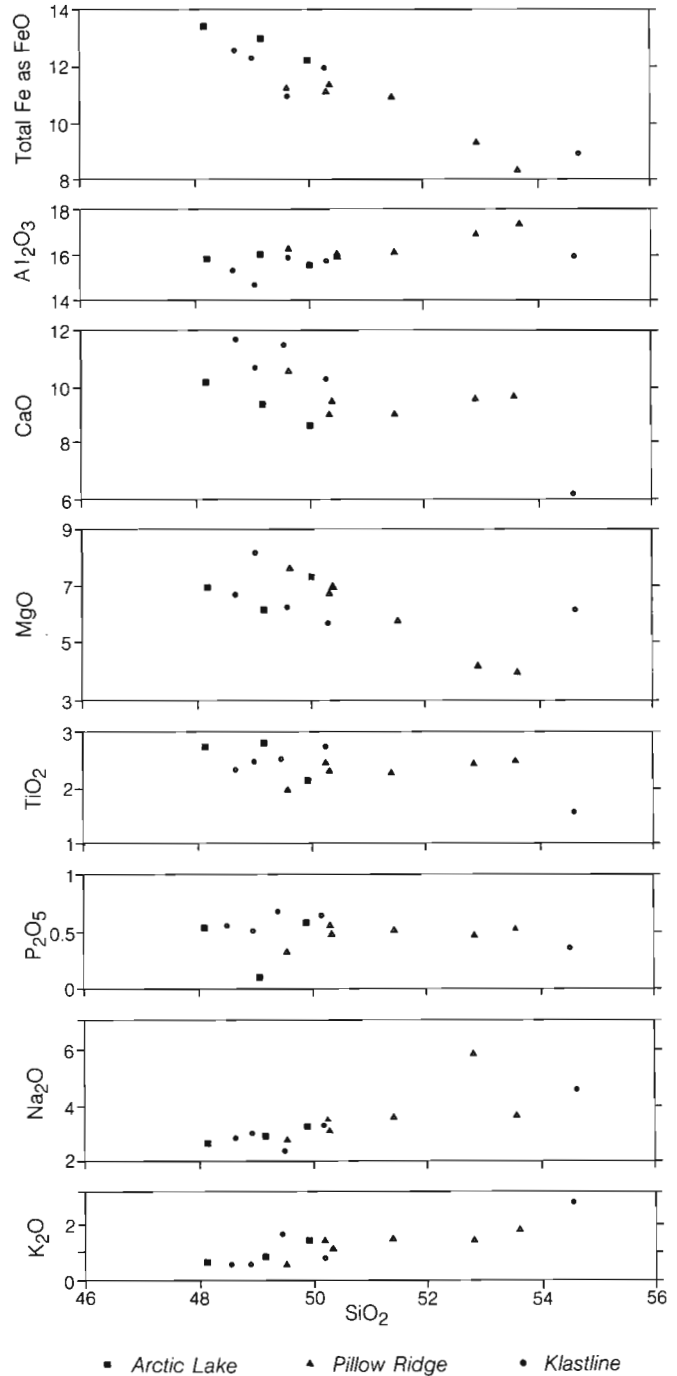


Figure 149. Harker diagram showing the range of chemical variation in weight per cent in the Pillow Ridge, Klastline and Arctic Lake formations.

Vesicles in the Tsekone hawaiite are mostly open, whereas those in the Pillow Ridge basalt are commonly lined with hydrous iron oxide, locally overgrown by fibrous carbonate.

Partly fused granitic inclusions are a mosaic of anhedral, interlocking grains of perthitic alkali feldspar, minor opaque oxides and varying amounts of glass (Fig. 145e,f). The light to dark brown, concentrically banded glass forms circular and amoeboid masses up to 5 mm across. These embay the feldspar and may contain a central void. Small, sparse crystals of euhedral feldspar and dendrites of Fe-Ti oxide have crystallized in some of the glass but most of it is completely vitreous. The granitic inclusions are probably of accidental origin, incorporated from basement rocks at relatively shallow depth.

The gabbro inclusions are holocrystalline, coarse grained (3-8 mm), dictytaxitic rocks that show no evidence of either partial melting or reaction with the enclosing basalt. They comprise about 45% unzoned labradorite (An_{60}), 45% titaniferous salite and 10% intergranular masses of opaque oxide. The mineralogy and cumulous texture of these inclusions suggests they are of cognate or parental origin.

CHEMISTRY

The six analyses of basalt from the Pillow Ridge Formation suggest a slight but consistent difference in the composition of rocks from Pillow Ridge, and those from Tsekone Ridge (Table 16). The suite from Pillow Ridge plots within the alkali olivine basalt field of the normative colour index vs. normative plagioclase diagram (Fig. 147) whereas the Tsekone Ridge samples plot in the field of hawaiite. The two suites also fall into separate groups on the AFM (Fig. 148) and alkali vs. silica diagrams (Fig. 147). The data set is too small and the differences too subtle to prove a separate origin. However, the chemical differences are in agreement with field and petrographic differences which, taken together, suggest that the two piles were erupted from different magma batches or magma in different stages of fractionation.

The range of chemical variation in the Pillow Ridge Formation is similar to that of the Klastline and Arctic Lake formations (Fig. 149).

EDZIZA FORMATION

GENERAL GEOLOGY

Introduction

The summit region of Mount Edziza is a nearly symmetrical composite trachyte volcano which was built on the dissected northern flank of Ice volcano during the Edziza stage of activity (Fig. 150, Map 1623A, in pocket). The central cone rises steeply to a summit crater nearly 9000 ft. (2700 m) in elevation and 2 km in diameter which is now filled with an almost flat field of stagnant ice (Fig. 151). Alpine glaciers flanked by morainal ridges mantle most of the upper edifice down to an elevation of 7000 ft. (2135 m). Only about half of the old crater rim is exposed in a series of spires and serrated nunataks that project above the glacier, but its nearly circular form is clearly preserved despite the ice cover. The northwestern and southern sides of the volcano have not been greatly modified by erosion and there, only the most recent flows are exposed beyond the terminal moraines of the alpine glaciers. The symmetry of the central cone is interrupted by several steep-sided lava domes.

On its east side the central crater has been breached by an active cirque at the head of Tenchen Creek and there, hydrothermally altered rocks of the central conduit and lava lakes that once filled the crater are exposed in nearly vertical, 300 m high cliffs of the headwall (Fig. 152). The adjacent, steep-sided spurs provide cross-sections through the eastern side of the main composite cone, exposing alternating flows and pyroclastic deposits, as well as feeder dykes and small subvolcanic intrusions (Fig. 153).

The total volume of material erupted during Edziza activity is estimated to be 18 km³. It consists entirely of trachyte with remarkably uniform composition, though the colour and fabric vary from dense, dark green, flow layered rock in the lower and central part of thick cooling units, to pale green frothy rock in the upper portion. Small tabular phenocrysts of honey-coloured alkali feldspar with conspicuous {010} cleavage are ubiquitous.

Pre-Edziza surface

Most of the major topographic features of the Edziza Complex were formed during an interval of erosion between the Ice Peak and Edziza eruptive stages (Fig. 138). Headward erosion by west-flowing tributaries of ancestral Mess Creek cut the valleys of Elwyn, Kadeya, Sezill and Walkout creeks into the gently sloping shield on the western flank of Ice volcano, but did not extend as far east as the central edifice. In contrast the relatively short streams, flowing east along steep gradients, from Ice volcano into Kakiddi Creek dissected the central edifice of the volcano, reducing the

eastern half of the shield to isolated remnants, preserved on interflaves between valleys cut deeply into the pre-Tertiary basement rocks. This early-formed topography was subsequently modified by ice during Pliocene glaciation. The asymmetrical form of the complex was further accentuated by active cirque and valley glaciers cutting rapidly into the east side of Ice volcano, in contrast to broad, relatively stagnant lobes of ice which spread out onto the western plateau surface. Eruption of the Pillow Ridge basalt during the climax of this glaciation produced the only volcanic edifice formed during this long period of fluvial and glacial erosion. Before the Edziza activity began the regional ice cap had receded, exposing the rugged topography that had been carved from the gently sloping surface of Ice volcano. Only the western rim of the central crater remained. Where the crater itself had been, a series of steep-walled cirques opened into the head of deep, U-shaped valleys that extended eastward to join the valley of Kakiddi Creek. The western side of Ice volcano still retained a semblance of its original form but its surface was covered by a thick mantle of glacial moraine deposited during retreat of the central ice cap. In contrast Pillow Ridge and Tsekone Ridge stood as rounded black prominences on its northwestern flank, their smooth, oversteepened slopes unmodified by erosion except for landslide scars.

Central composite cone

The composite cone of Mount Edziza rises to a circular summit crater almost 3 km in diameter. Its central depression is filled with permanent ice which flows through a breach in the east crater rim and discharges over shear, 300 m cliffs, onto the head of Tenchen Glacier (Fig. 152). The crater rim itself is defined by a discontinuous series of nunataks which include the precipitous 9143 ft. (2786 m) high spires of the summit ridge. These spires, on the south rim of the crater are uniform, greenish-grey, sparsely porphyritic trachyte with randomly oriented plates of feldspar 3-5 mm across. Perfectly formed, small diameter columns extend nearly vertically for more than 90 m from the ice to the top of the summit spire. Other, more subdued nunataks on the crater rim are glacially reworked trachytic pyroclastic debris.

A section through the central cone is well exposed in 850 m high cliffs along the north side of Tenchen Valley, which cuts through the eastern edge of the crater rim, exposing Edziza flows and breccias (Fig. 153, 154). Approximately the lower third of the pile is a chaotic explosion breccia, enclosing relatively small, discontinuous lenses and irregular masses of pale green, crudely-jointed trachyte lavas up to 120 m long and 15 m thick. The western, proximal breccias are extremely coarse, containing massive

MOUNT EDZIZA

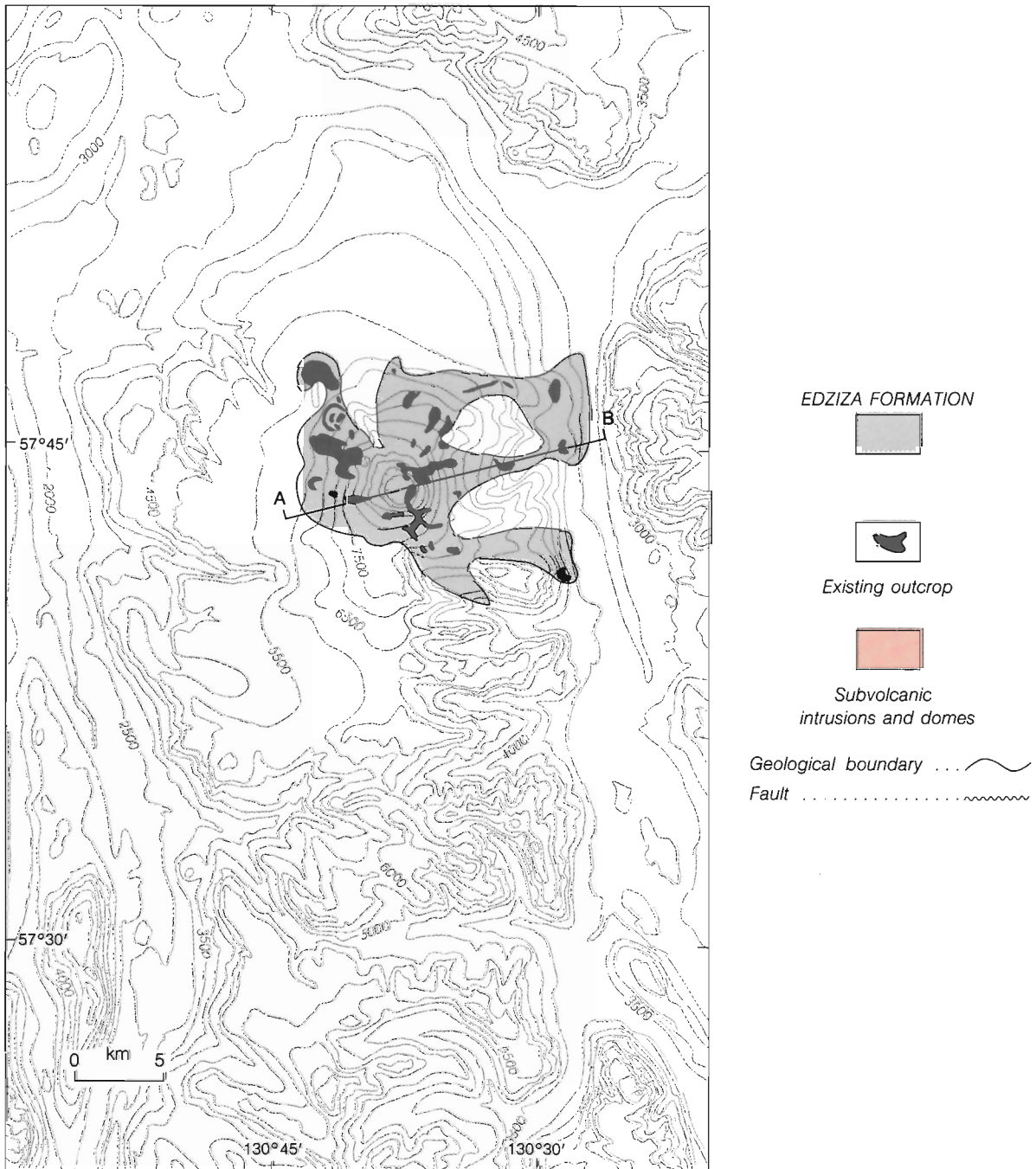
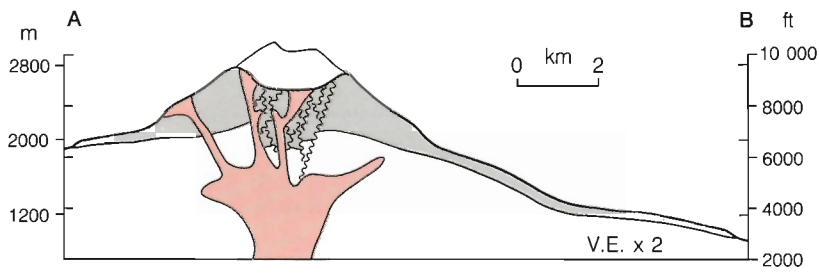


Figure 150. Paleogeological map and schematic cross-section showing the inferred maximum extent of the Edziza Formation at the end of Edziza time.

blocks up to 7.5 m across. All of the fragments are trachyte but their colour and density vary from dark green, dense, flow layered rock to pale, silvery green, very porous material almost as light as pumice. Fragments are commonly angular. In the proximal facies they are randomly stacked and the matrix of comminuted rock fragments, pumice and secondary silica and iron oxide cement is relatively sparse. They are probably primary breccias deposited directly from the active vent. The more distal breccias, at the eastern end of Tenchen Valley, rarely contain blocks more than 1.5 m across and locally rounding and stratification suggest landslide or lahar deposits. Distal breccias also contain a higher proportion of fine ashy or silty matrix. In some beds even the largest blocks are suspended in the fine, unstratified ashy matrix.



Figure 151. Looking southeast across the nearly flat, ice-filled summit crater of Mount Edziza. Nunataks are remnants of circular crater rim. GSC 202469-F.

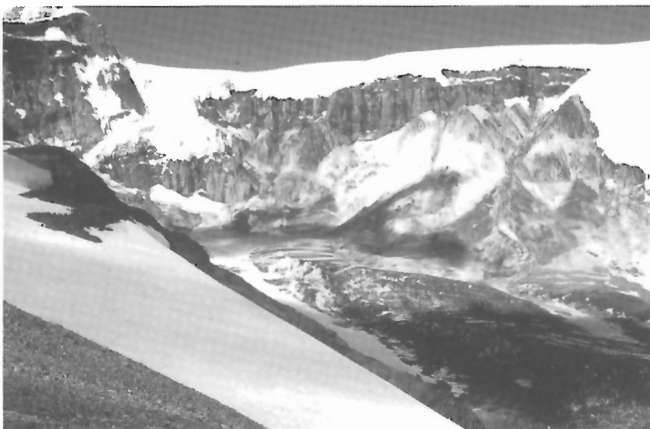


Figure 152. Headwall of Tenchen cirque which breaches the eastern side of the Mount Edziza summit crater. Flows and pyroclastic rocks of the main cone are exposed on the flanking spurs, and conduit breccia in the central part of the headwall is overlain by remnants of lava lakes that were ponded in the crater. GSC 202469-G.

In the upper part of the Tenchen section (Fig. 154) lava predominates over breccia. Individual cooling units are up to 150 m thick but are highly irregular or lenticular in cross-section. The body of each flow is a dark greenish-grey, dense trachyte with sparse, perfectly oriented tabular alkali feldspar phenocrysts 2-5 mm across. The rock commonly has a perfectly developed flow layering that imparts a platy or flaggy aspect to many outcrops, and a pronounced cleavage along which it splits to surfaces with a lustrous sheen. Long slender columns are developed normal to the flow cleavage. The upper half to one-third of most flows is lighter coloured, grading up into pale green, porous rock that lacks flow layering. A mat of similar pale green, loosely aggregated flow breccia underlies each flow, but there is rarely any colluvium or reworked material separating flows in the proximal part of the central cone.

Breccia within the central conduit is exposed in the steep headwall of Tenchen cirque, under the breach in the east crater rim (Fig. 155). Despite intense hydrothermal alteration the outline of both small breccia fragments and large rotated blocks, up to several metres across, is visible in most outcrops within the conduit. The brecciation is believed to have accompanied collapse and foundering of a once higher and narrower summit cone (Fig. 156). The broad, nearly flat summit of Mount Edziza, with its 3 km wide crater, is probably the truncated remnant of a cone that originally rose to a much smaller summit crater. As discussed in a later section, summit collapse may have accompanied the voluminous effusion of lava during the formation of satellitic domes or the Kakiddi lava flows.

Satellitic vents

A small, rounded mound with a shallow central depression projects from under the ice on the northwestern flank of Mount Edziza, south of Pillow Ridge. It comprises pale green, porous agglutinated trachyte bombs, spatter and pumice, and is believed to be a pyroclastic cone that erupted late in Edziza time. It was the source of at least two separate



Figure 153. Thick, irregular flows and coarse proximal breccia of Edziza trachyte on the north buttress of Tenchen cirque. GSC 125 614.

MOUNT EDZIZA

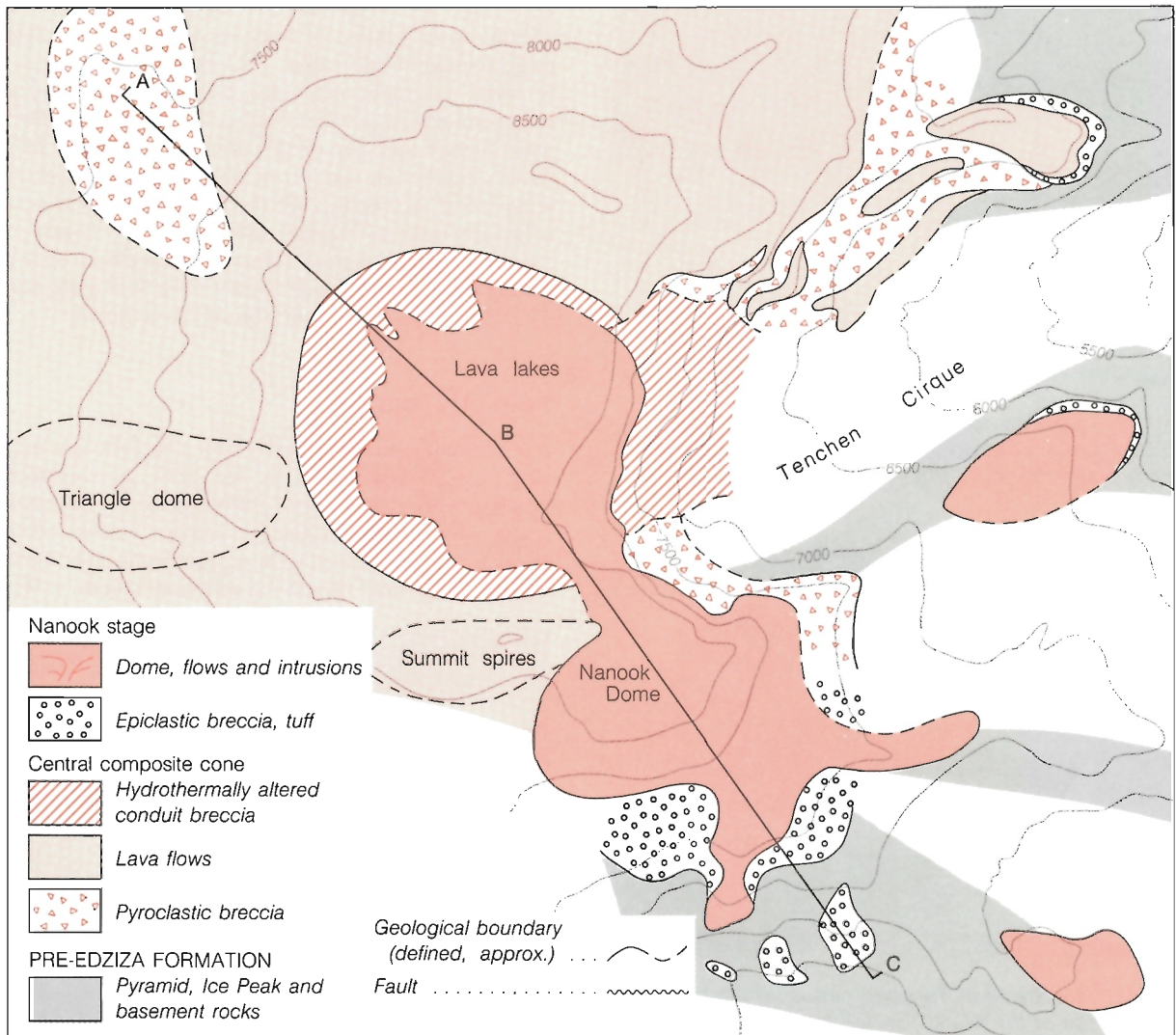
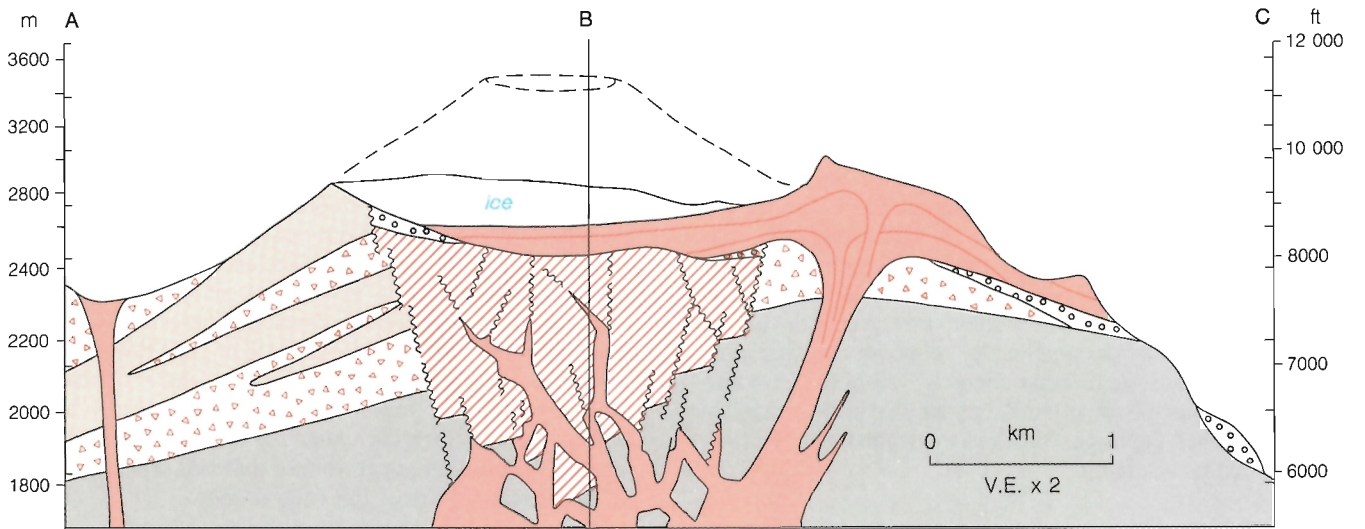


Figure 154. Map and schematic cross-section of the summit area of Mount Edziza, showing the relationship of proximal flows and pyroclastic breccia to the conduit breccia, Nanook Dome and lava lake exposed in Tenchen cirque.

lobes of lava, both of which are mostly covered with colluvium and ash. A northwesterly lobe abuts against, and overrides, Pillow Ridge breccia and partly surrounds Tsekone Ridge. The contact between the base of this trachyte flow and basaltic pillow-breccia is exposed in the canyon of upper Elwyn Creek. The two are separated by about 1 m of globular, porous, moderately agglutinated, pale green trachyte flow breccia which rests directly on the pillow-breccia. The absence of an intervening fluvial or glacial layer suggests that the ice did not reform over Pillow Ridge after its emplacement. A second lobe of lava, extending west from the cone, is isolated from both older and younger rocks by colluvium, but sections through the flow itself are well exposed in the upper tributaries of Elwyn Creek and in a series of ledges leading up to the cone. Platy flow layering is well developed in all parts of this flow lobe. In most outcrops it is planar and dips west at 10-15°, parallel to the flow surface, but locally the dips reverse and may sweep up to nearly vertical or display complex folds and fractures. In several exposures the gently west-dipping flow layers in the lower, distal portion of the flow are truncated by steeply east-dipping flow layers in the upper, proximal part of the flow. These structures are clearly formed in the later stages of flowage when the highly viscous, nearly crystalline but still moving mass was sufficiently rigid to fracture. When the distal part of the flow stagnated, it was overridden by the still moving upper portion along a series of curved, upward sweeping thrusts. Flow layers in the overriding slab were bent upward and commonly fractured. The ability of these lavas to fracture during the later stages of flow is clearly seen where they pass over small terraces on the basement surface. The flow responds to bending like a semi-rigid plastic. A regular set of tension fractures develop across the flow layers which are offset step-wise in a series of small slump blocks (Fig. 157). The bounding fractures curve downward and merge into the flow layers near the centre of the flow.

A short, thin flow on the northwest side of the cone is characterized by an abundance of partly resorbed cognate



Figure 155. Light coloured, hydrothermally altered vent breccia overlain by lava lakes in the headwall of Tenchen cirque. GSC 125 615.

inclusions. It lacks the well developed flow layering and jointing of the other flows and does not appear to extend more than a few thousand metres. It probably originated from a mass of glowing particulate debris that accumulated on the flanks of the cone, and slid off as a small, rootless flow of annealed bombs and spatter.

Lava domes

Three bulbous masses of trachyte form conspicuous protrusions on the flanks of the otherwise symmetrical central cone of Edziza. Each appears to be an exogenous dome formed by the rapid effusion of viscous trachytic lava from a central vent.

Nanook Dome (Fig. 158), the largest of the three, forms the southeast buttress of the central crater. It is nearly circular, about three-quarters of a kilometre in diameter and is bounded by steep, smooth convex margins 150-200 m high. Except for its northeastern corner, which is truncated by the headwall of Tenchen cirque, the present dome appears to be close to its original form. Prominent flow cleavage is nearly parallel to the existing surface and remnants of an outer rind of frothy, agglutinated trachyte scoria and blocks are preserved on its south and east slopes. South of the dome a small bluff on the ice-shrouded headwall of Tennaya Creek exposes about 15 m of spherulitic glass and pumice (Fig. 159). This is believed to be the quenched base beneath the southern edge of the dome. The dissected northeastern corner of Nanook Dome exposes tiers of short, perfectly formed columns which diverge outward in the form of a fan. The nearly vertical, 150 m high cliffs include three massive trachyte cooling units separated by thin recessive layers of less competent rock. The two lower units are truncated by a lobe of the upper unit that drapes across their steep northern edge and disappears beneath ice which fills the central crater. It is believed to be a source for one or more of the lava lakes ponded in the crater (Fig. 160).

The east side of Nanook Dome merges with relatively thin trachyte flows which cap the steep, east-dipping interfluvies between Tenchen and Tennaya creeks. A distal remnant of this same flow, preserved on the ridge south of Tennaya Creek, may have been ramped to its present position across pyroclastic fill that has since eroded away. Three large remnants of very coarse poorly consolidated breccia are plastered against the steep cliffs north of Tennaya Glacier (Fig. 161). They comprise a jumble of angular to subrounded blocks up to 2.5 m across, randomly suspended in a fine, yellow, ashy matrix. Most of the large clasts are green trachyte but the smaller clasts include basalt and gabbro from the underlying Ice Peak Formation. The abundance of large angular blocks of dense, flow-layered trachyte suggests that thick flows or domes were disrupted by explosive activity in the vent area, but most of this distal breccia was probably transported to its present position by landslides and debris flows. It is believed to be all that remains of a once extensive debris-fan, formed during the emplacement of Nanook Dome.

MOUNT EDZIZA

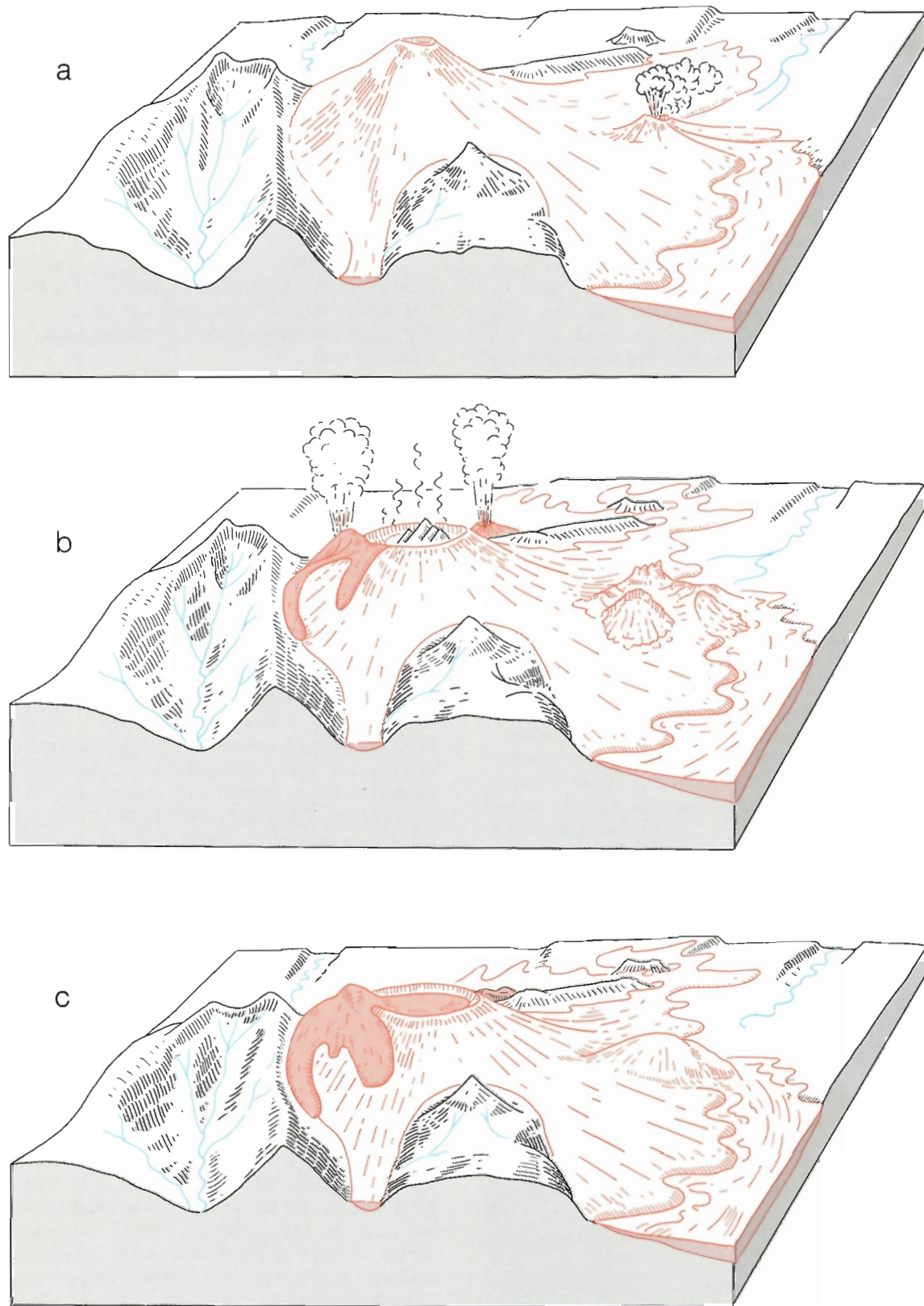


Figure 156. Block diagrams showing three stages in the construction and foundering of the summit cone of Mount Edziza. (a) Composite trachyte cone at its maximum development. (b) Effusion of lava from marginal domes and the beginning of summit collapse. (c) Final eruption of Nanook Dome and ponding of lava lakes in the summit crater.

The relationship of Nanook Dome to the Kakiddi valley flows and to the adjacent summit spires is not known. Truncation of the lower Nanook flows by the inner wall of the present crater and draping of the upper flow over them and into the crater suggest that summit collapse may have accompanied effusion of the Nanook trachyte (Fig. 156). The Nanook activity may have been coeval with the effusion of Kakiddi lava and a vent on or near the dome may actually have been one of the Kakiddi sources. Their lithological similarity and close spatial association suggest a genetic relationship between the valley flows, the dome and the summit spires. It is reasonable to suppose that the Nanook magma became increasingly viscous during the course of the activity. Early effusion of relatively fluid, volatile-rich trachyte may have formed the voluminous valley flows of the Kakiddi Formation. Removal of this enormous amount

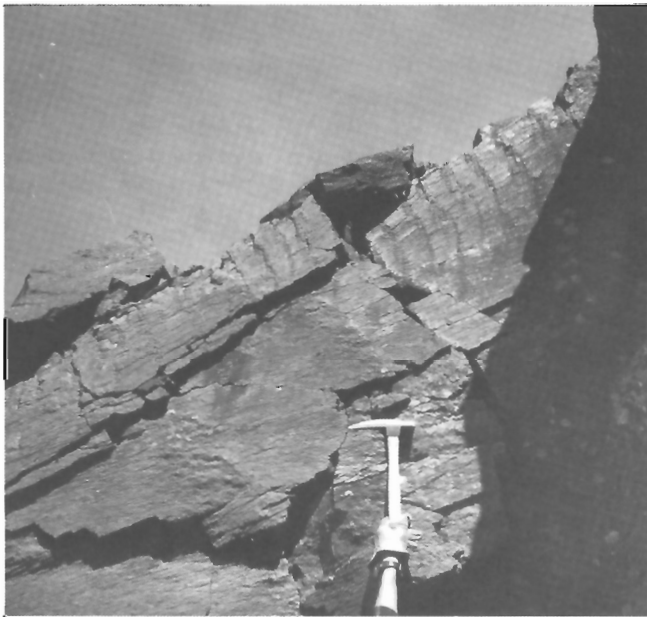


Figure 157. Flow layers and slump fractures formed in a viscous lava flow of Edziza trachyte where it passes over, and flexes above, a ledge in the underlying surface. GSC 125 616.



Figure 158. Nanook Dome, the largest of three endogenous domes in the Edziza pile, forms the southeastern buttress of the summit ridge. GSC 202469-H.

of material may have initiated the summit collapse. Later effusion of more viscous magma produced the thick flows of Nanook Dome and finally a spine of nearly solid trachyte was extruded to form the summit spires (Fig. 162).

Triangle Dome high on the west side of the central cone, and Glacier Dome far down on its northeastern flank, are elliptical masses of trachyte with concentric flow layers parallel with the present surface and long thin columns normal to it.

Glacier Dome (Fig. 163) which is built on a relatively flat surface stands about 700 ft. (210 m) high and flow layering around its margins dips from 45 to 60° outward. The rock in both domes is a light, silvery-green porphyritic trachyte with small, crudely aligned plates of clear alkali feldspar up to 1 cm across. Ragged, polygonal voids with rough, hackly inner surfaces are particularly abundant in Glacier Dome. They range from minute pore spaces less



Figure 159. Spherulitic glass at the base of Nanook Dome. GSC 202469-I.



Figure 160. The southeastern buttress of the summit ridge showing the uppermost Nanook flows which may be the source of lava lakes ponded in the summit crater. GSC 125 617.

MOUNT EDZIZA

than 1 mm across to cavities 3-5 cm across. Most are elongated, parallel to the flow layering which is clearly deformed around the larger cavities. They appear to have formed by gas expansion during the latter stages of emplacement, when the rock was sufficiently viscous to tear rather than deform plastically.



Figure 161. Remnants of very coarse pyroclastic, or epiclastic fill plastered against the steep northern and western sides of Tennaya valley. Large, angular clasts are mostly Edziza trachyte. GSC 125 618.



Figure 162. Summit spires of Mount Edziza may have been emplaced as a viscous plug-dome during the final stages of Nanook activity. GSC 125 619.

Lava flows

The Edziza trachyte displays a variety of forms which suggest extreme differences in mobility. The lava domes and thick, steeply-dipping flows which form the central cone were obviously emplaced as highly viscous lava. Similarly, remnants of late flows from the central vent, some more than 60 m thick, are perched on basement slopes of 15 to 25° on the northeast side of the mountain. Yet similar trachyte forms relatively thin flows that have spread onto slopes of less than 5°. As noted earlier, the bulbous 700 ft. (210 m) high mass of Nanook Dome trachyte merges on its eastern side with a relatively thin broad flow only 15-24 m thick. This suggests that the viscosity changed during a single episode of effusion, yet no differences in mineralogy, texture or percentage of phenocrysts is apparent. Presumably the first magma erupted during any given event was relatively rich in volatile components and may also have been at a higher temperature than magma erupted near the end of a cycle. The early phases were thus more mobile and tend to form relatively thin distal lobes and valley flows, whereas the later, partly degassed and consequently more viscous phases, piled up in domes above the vents or spread into thick flow lobes on the steep upper slopes of the mountain.

The prominent, light green rimrock on the north side of Pyramid Creek is one of the thinnest flows of Edziza trachyte even though it rests on a gently sloping surface. For most of its exposed length of 2 km it is 24 m thick but thins to about 15 m at the distal end where it passes from the plateau surface onto the steep valley wall. The rock is identical with that of Glacier Dome, and may have originated from that vent as an early, fluid phase (Fig. 164).



Figure 163. Glacier Dome, an endogenous mass of porous, columnar-jointed trachyte on the north flank of Mount Edziza. GSC 125 620.

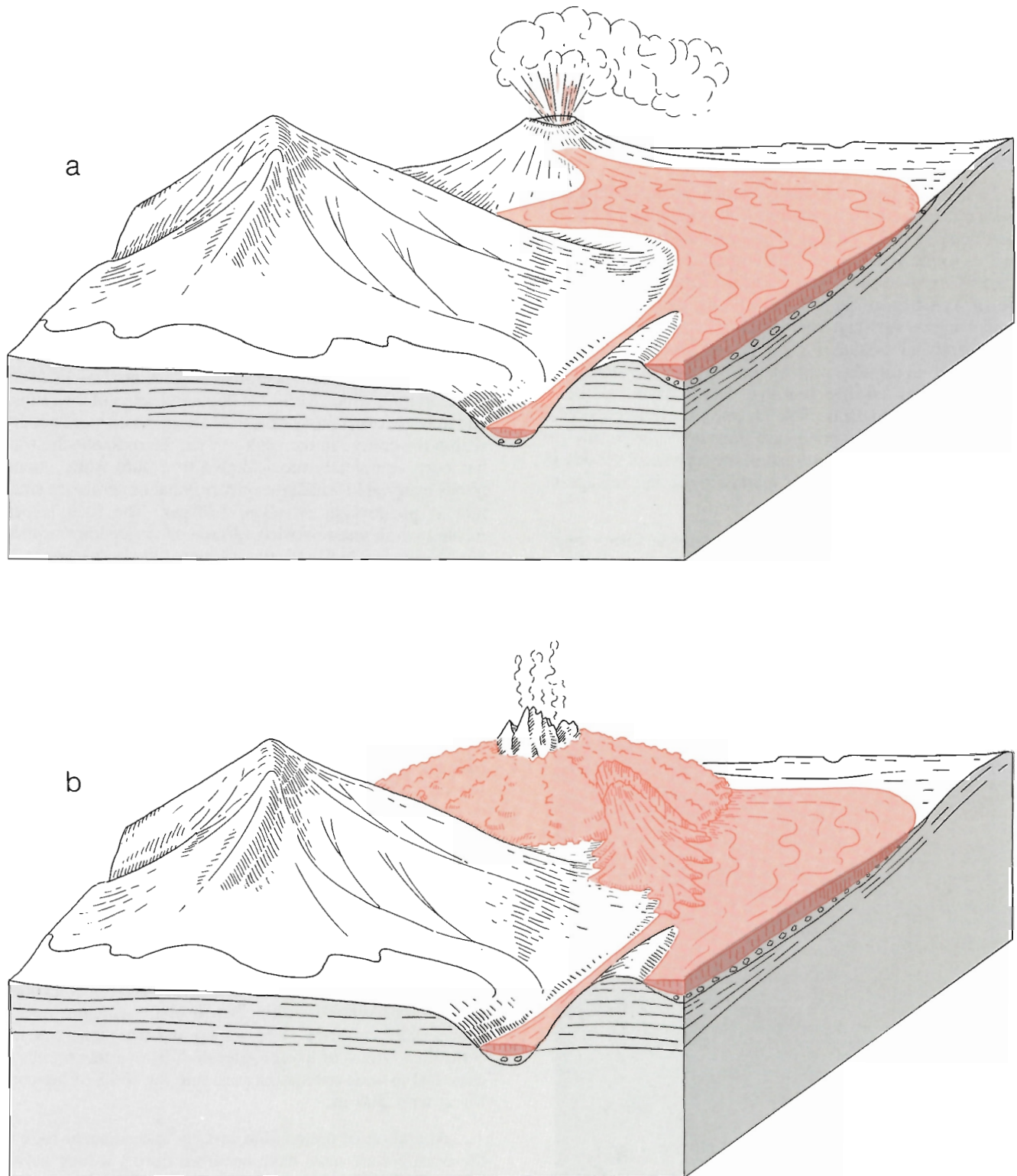


Figure 164. Block diagrams showing the possible relationship of Glacier Dome (centre background) to The Pyramid (left foreground) and to the trachyte rim rock along the north side of Pyramid Creek valley. Circles beneath the trachyte flow indicate gravel derived from erosion of The Pyramid. View is toward the west. (a) Effusion of trachyte lava during the initial stage of activity. (b) Emplacement of viscous trachyte during the final, dome-forming stage. (see Fig. 163)

Subvolcanic intrusions

Rapid erosion of its steep eastern side has stripped away large segments of the Edziza pile and cut sufficiently deep into the underlying basement to expose parts of the subvolcanic plumbing. Numerous dykes, sills, cupolas and irregular intrusive masses of green trachyte are believed to be part of the interconnecting conduit system.

Swarms of dykes are mostly vertical or subvertical and have a crudely radial distribution with respect to the crater. The thickness of individual dykes varies from a few centimetres to more than 6 m. The largest single dyke is continuously exposed for nearly 2 km in cliffs along the north side of Tenchen cirque. Dykes cutting pyroclastic rocks weather out as resistant ribs which pinch and swell along highly irregular boundaries; in places wedging out completely and in others welling into irregular, stock-like masses. Dykes cutting massive flows have relatively straight, planar contacts. The dykes are commonly pale green trachyte with pronounced flow layering parallel to their margins and a porous zone of tiny spherical vessels in the centre. Most contacts are marked by a thin selvage of pale green to black glass.

In addition to dykes the Edziza trachyte forms small cupolas both within the central edifice and in underlying rocks. At several places in Tenchen Valley masses of



Figure 165. Small irregular cupolas of trachyte, exposed by erosion of the enclosing pyroclastic deposit into which they were intruded. GSC 202469-J.

trachyte 3-9 m across project upward into thick pyroclastic deposits. Where the breccia has eroded away, these grotesquely shaped monoliths with bulbous projections and spires have been left standing like inverted sand castings up to 12 m high (Fig. 165). Their smooth outer surface is commonly covered by a rind of dark brown iron oxide stain and encrusted with a few remaining patches of breccia, cemented by iron oxide.

Hydrothermal alteration

The cirque at the head of Tenchen Valley cuts through the eastern rim of the main crater and exposes breccias, dykes and sills within the central conduit. These intensely altered, bright yellow and ochre-weathering rocks form most of the precipitous 300 m high cliffs of the headwall (Fig. 155). They grade laterally into unaltered rocks of the crater margin which forms the bounding spurs of the cirque, and they are overlain by unaltered flows which were ponded within the crater. In the centre of the altered zone the rock has been completely reconstituted to a pure white, amorphous material in which the only original minerals are small tabular phenocrysts of alkali feldspar. The rock is permeated by an anastomosing filigree of chalcedony veinlets less than 1 mm thick and cut by a more widely spaced stockwork of veins 1-5 cm across. Many of the larger veins contain tiny cubes of pyrite, and pyrite and marcasite are disseminated throughout the intervening rock. A few open cavities are lined with native sulphur.

Despite this pervasive alteration of the conduit breccia the faint outline of angular fragments can be seen on many surfaces. Large clasts, up to 1 m across, are surrounded by a jumble of smaller clasts, cemented by pyritiferous chalcedony. Local masses of rock within the conduit are less severely altered and stand out as relatively dark bluffs. In these zones the cores of the larger clasts retain their original greenish-grey colour, and in a few places remnants of unbrecciated dykes, sills and flows are preserved. Joints and fractures within these masses are bounded by alteration zones at least 10 cm wide in which the rock is bleached, silicified and pyritized. These partly altered zones become more numerous near the edges of the conduit and finally grade outward into green, unbrecciated trachyte flows and pyroclastic deposits of the conduit walls. Nearly every joint and fracture surface within 200 m of the conduit breccia shows some evidence of bleaching and irregular, fracture controlled, zones of intense alteration from a few metres to over 100 m wide extend outward into the walls of the cone for at least 500 m.

Alteration of the conduit breccia and adjacent rock of the central cone must have occurred during a long period of intense fumarolic activity from the central vent. Hot sulphurous gases and silica-saturated acid water streaming through the porous vent breccia and fractures in the adjacent cone reacted with the trachyte to produce an assemblage of chalcedony, secondary feldspars, clay minerals, pyrite and zeolites. Solfataric activity from the central vent may have



Figure 166. Detail of lava lakes, showing the irregular inner surface of the crater floor on which they were ponded. GSC 125 621.

ceased before the final effusion of trachyte lava because ponded flows within the crater and Nanook dome trachyte, which forms the southeast buttress of the cone, rest on the hydrothermally altered zone but are not altered themselves.

Lava lakes

The central crater of Mount Edziza is filled with approximately 60 m of glacial ice which discharges eastward into the cirque at the head of Tenchen Creek. Tongues of broken ice extend from the summit ice cap down to the valley glacier but the central part of the cirque is bare, its slopes swept by repeated avalanches from the ice cliffs that overhang its steep headwall. Just below the ice and resting on the altered vent breccia is a nearly vertical cliff through the eastern edge of a succession of lava lakes which were ponded within the crater (Fig. 166). At least four cooling units are exposed. The lower two are dark greenish-grey trachyte with well developed reddish brown-weathering columns. Each is about 30 m thick. They fill depressions on the hummocky surface of the crater floor and appear in cross-section as dark lenses which wedge out against the bright yellow vent breccia. The two upper flows are lighter green trachyte similar to that of Nanook Dome. The lower

of the two is nearly 90 m thick. It has well developed vertical, rectangular jointing along which the rock has broken to a shear cliff across the full width of the headwall. The uppermost flow is poorly exposed, and difficult to examine due to overhanging ice. It appears to be a mass of agglutinated blocks, particularly at the edge of the flow.

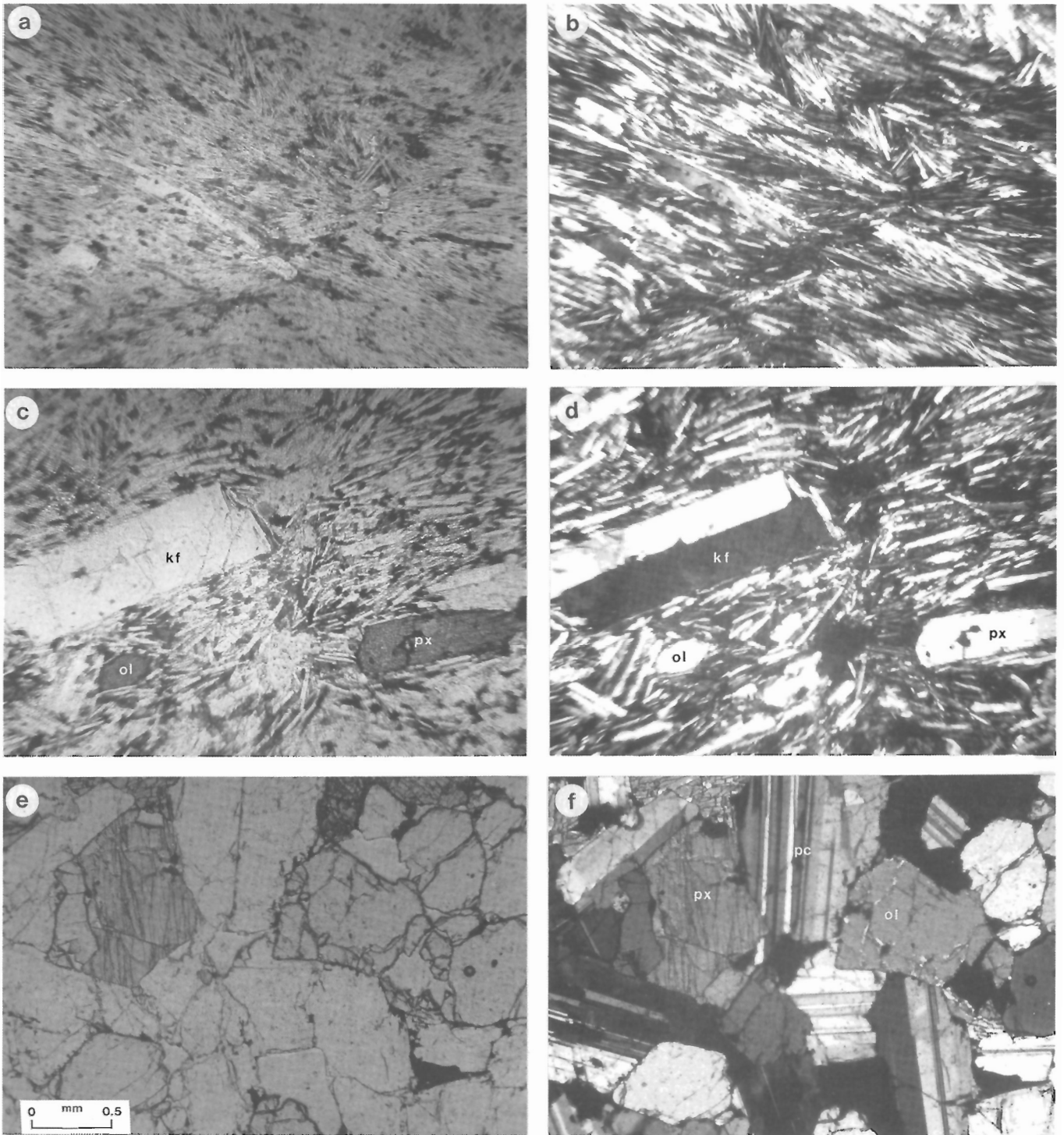
The absence of hydrothermal alteration along joint surfaces in either the lava lakes or the Nanook Dome trachyte suggests that degassing through the central conduit had virtually ceased before or shortly after the final effusion of lava. Moreover, the lithological similarity and spatial relationship of the lava lakes and Nanook Dome suggest that they were erupted from a common vent on the southeast margin of the crater rim. The uppermost flow of Nanook Dome forms the southeastern rim of the crater and is exposed in section on the south spur of Tenchen cirque. A relatively long southern lobe of this flow rests on gently south-sloping older flows of Nanook Dome, whereas the northern end bends abruptly down, truncating older flows and pyroclastic deposits along the steep inner walls of the summit crater (Fig. 160). At the point of flexure the flow is about 90 m thick and has a distinct sinusoidal cleavage and parting. This very thick remnant is believed to be part of a lava flow that spread southward onto the surface of Nanook Dome and northward into the crater where it was ponded to form the lava lakes.

PETROGRAPHY

Trachyte and comenditic trachyte

It is not possible to discriminate petrographically between the trachytes (Fig. 167a,b) and comenditic trachytes (Fig. 167c,d) of the Edziza Formation. Both are fine grained, aphyric to moderately porphyritic rocks with up to 10% microphenocrysts (<2 mm) and sparse, tabular phenocrysts (up to 1 cm) of alkali feldspar. Pyroxene and rarely pale yellow fayalitic olivine (Fo₃₋₂₅) also occur as microphenocrysts. The groundmass comprises alkali feldspar in felted clusters of slender laths or in stout, tabular crystals with interlocking, sutured boundaries. Deep green aegirine augite, pale to dark blue pleochroic arfvedsonite and dark red to black aenigmatite are interstitial to the groundmass feldspar and, together form less than 10% of most Edziza rocks. Opaque oxides occur both as finely disseminated granules and sparse microphenocrysts.

Feldspar phenocrysts are euhedral or have slightly rounded boundaries. Simple Carlsbad twins are common but very fine polysynthetic and crosshatched twinning are visible in some crystals. Small inclusions of aegirine augite and rarely of arfvedsonite form slender, euhedral prisms in the interior of feldspar phenocrysts and, more commonly in a narrow zone slightly inside and parallel with the crystal boundaries. Microprobe analyses (Fig. 168, Table 17) of both phenocrysts and groundmass feldspar deviate little from an average composition of Ab₆₅An₂Or₃₆ (potassic anorthoclase). A few phenocrysts exhibit a small range of normal and reverse zoning (Fig. 168).



a,b — Fine grained, aphyric trachyte comprising felted clusters of slender feldspar laths, interstitial arvedsonite, aegirine augite, aenigmatite and grains of opaque oxide (a, plane light; b, crossed polarizers).

c,d — Comenditic trachyte with microphenocrysts of alkali feldspar (kf), ferrohedenbergite (px) and fayalite (ol), (c, plane light; d, crossed polarizers).

e,f — Gabbro inclusion consisting of unzoned plagioclase (pc), clinopyroxene (px), olivine (ol) and opaque oxides (e, plane light; f, crossed polarizers).

Figure 167. Photomicrographs of rocks from the Edziza Formation; scale bar 0.5 mm.

Pyroxene microphenocrysts as stout euhedral or subhedral prisms are commonly zoned. Rare larger crystals may have a core of purplish-brown titaniferous salite surrounded by a rim of pale green ferrosalite or ferrohedenbergite. Many cores of ferrohedenbergite are rimmed with bright green aegirine augite, which is also the principal groundmass pyroxene.

Arfvedsonite occurs as interstitial grains in the groundmass, as an overgrowth on aegirine augite microphenocrysts and as small euhedra projecting into open cavities. Aenigmatite is found only as tiny crystal clusters in the groundmass.

Yellowish-orange, devitrified glass is a minor constituent of quenched phases, but no completely vitreous trachyte was found in the Edziza Formation.

Inclusions

Gabbroic and granitic inclusions up to 30 cm across occur in coarse trachyte tephra near the western summit of Mount Edziza. They are both subangular and rounded, and of two distinct petrographic types. The more common type, gabbro (Fig. 167e,f), contains about 50% clear, unzoned plagioclase (An₇₀), 20% olivine (Fo₇₇), 15% clinopyroxene (magnesian salite), and 15% opaque oxide. The constituent minerals form a randomly stacked aggregate in which both open, intergranular pore space and sutured crystal boundaries are present. Inclusions of this type are believed to be of cognate, cumulate origin, formed by crystal settling on floored chambers of crystallizing basaltic magma. In some of them the intergranular space is filled with a nearly opaque, vesicular, glassy residuum containing tiny euhedra of plagioclase, olivine and titaniferous clinopyroxene. The

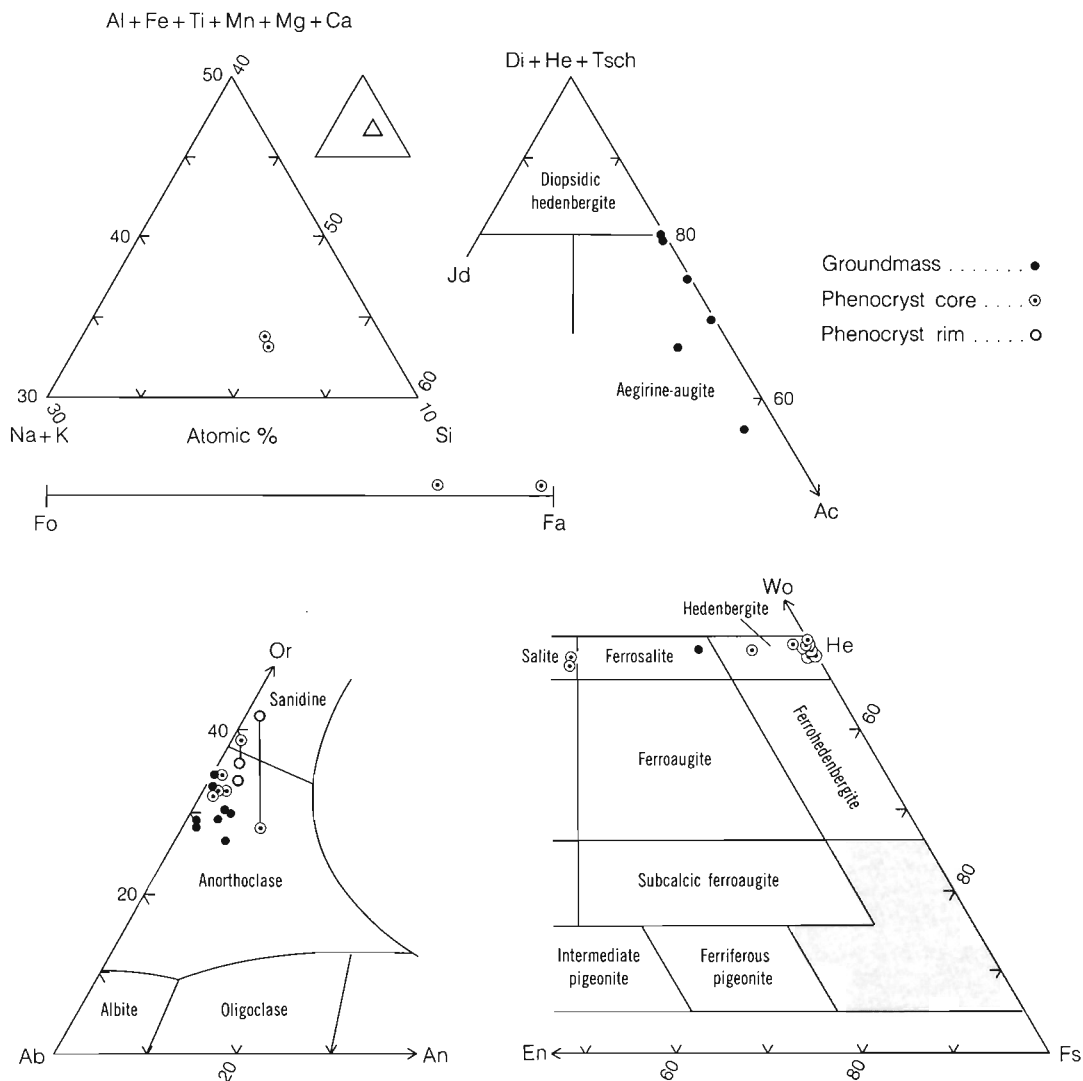


Figure 168. End-member plots of microprobe data showing the compositions of the principal mineral phases in rocks from the Edziza and Kakiddi formations.

MOUNT EDZIZA

residuum is clearly richer in Ti and Fe than the bulk composition of the inclusions, and may represent an early product of crystal fractionation.

The second type of inclusion comprises mostly alkali feldspar ($Ab_{60}An_6Or_{34}$), up to 10% hornblende, minor biotite, opaque oxides and glass. The feldspar is perthitic and

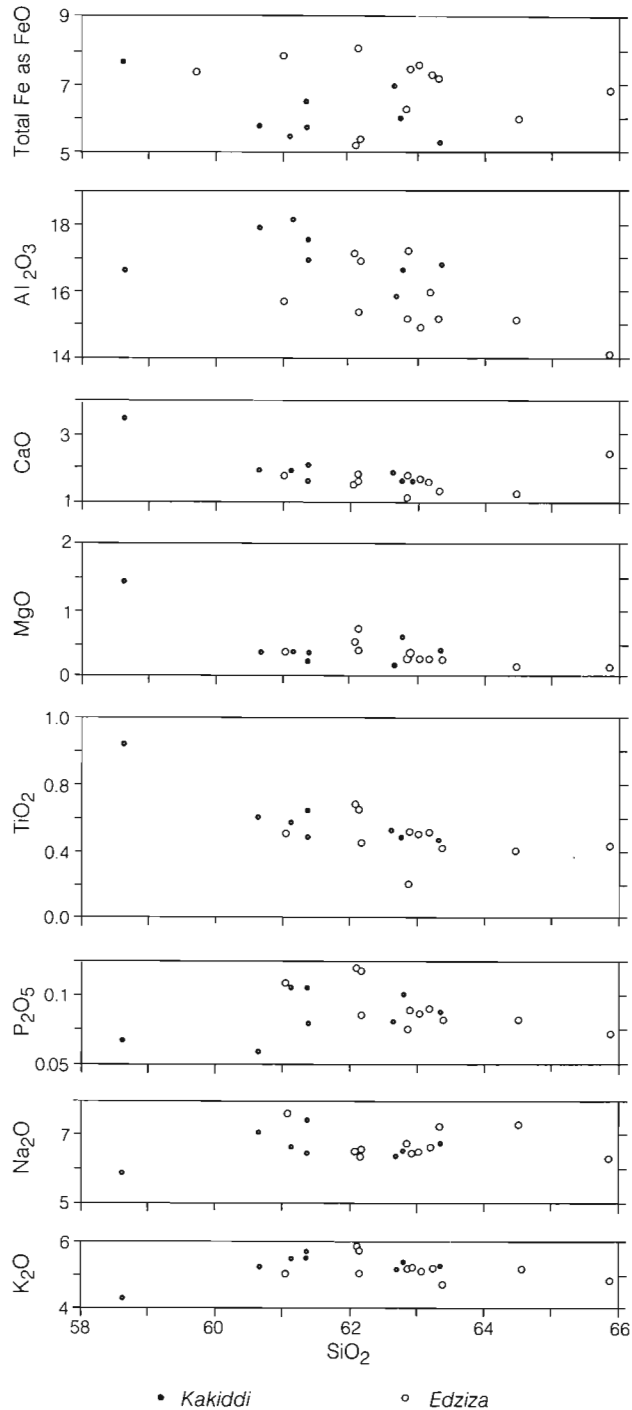


Figure 169. Harker diagram showing chemical variation in weight per cent of analyzed specimens from the Edziza and Kakiddi formations.

forms anhedral, interlocking grains. These inclusions are believed to be fragments of granitic, basement rock that were incorporated in and reacted with the Edziza trachyte magma. Preferential melting of hornblende has left areas of clear, pale brown glass around the embayed remnants of original crystals. Clusters of small, randomly oriented hornblende prisms in the glass are believed to have recrystallized from the melt during quenching. Glass has also formed around grains of opaque oxides and locally along feldspar boundaries. Biotite shows no evidence of fusion. However, it has been mostly replaced by granular, opaque oxides which form thick reaction rims around small, residual cores of dark reddish-brown, strongly pleochroic biotite.

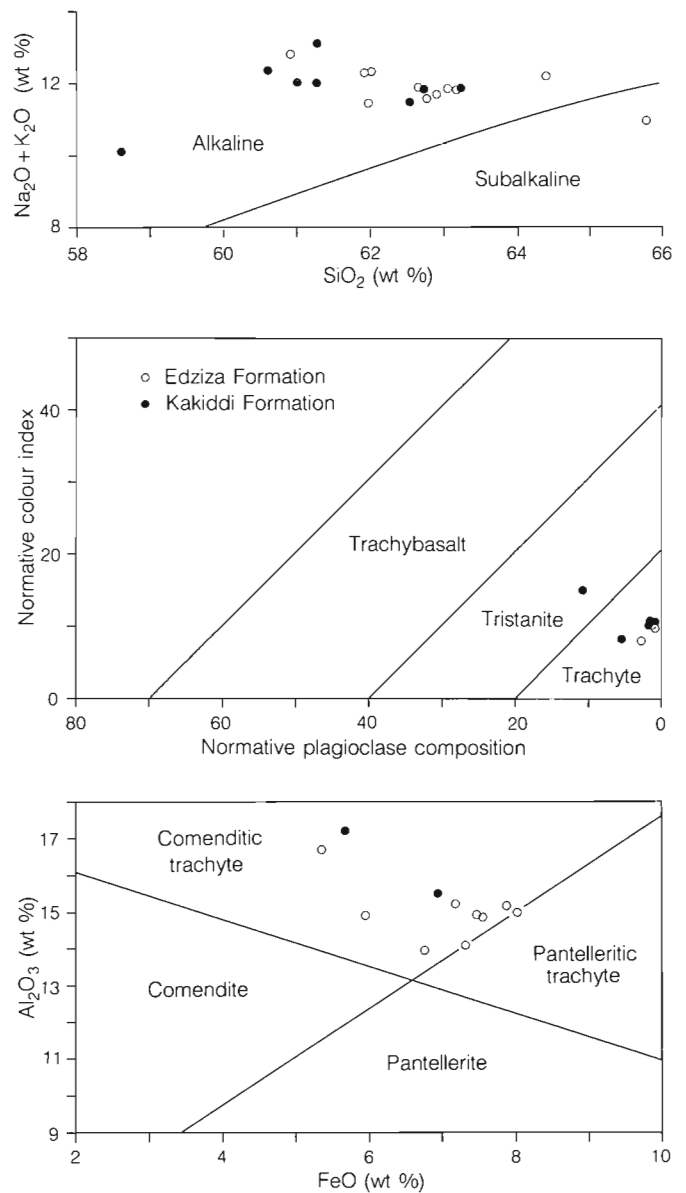


Figure 170. Plots of Edziza (open circles) and Kakiddi (solid dots) chemical data on the total alkalis vs. silica, normative colour index vs. normative plagioclase composition and Al_2O_3 vs. FeO diagrams.

Table 17. Representative microprobe analyses and structural data for the principal mineral phases in rocks of the Edziza (E) and Kakiddi (K) formations.

	Feldspar			Pyroxene						Olivine	Amphibole	Aenigmatite				
	Phenocryst		Groundmass	Phenocryst			Groundmass			Groundmass	Phenocryst	Groundmass				
	EF1	EF2	EF3	EP1	KP2	EP3	KP4	EP5	EO1	EAM1	EAE1					
SiO ₂	65.72	66.76	66.84	50.57	48.18	48.21	47.50	49.36	31.55	49.50	41.09					
Al ₂ O ₃	19.33	19.31	19.01	0.98	0.62	0.21	0.31	0.53	0.0	0.10	0.33					
TiO ₂	0.0	0.0	0.0	0.64	0.52	0.44	0.67	0.67	0.04	0.30	7.58					
Cr ₂ O ₃	0.0	0.0	0.0	0.0	0.0	0.01	0.01	0.0	0.0	0.01	0.0					
Fe ₂ O ₃	0.0	0.26	1.20	1.31	2.14	3.00	4.59	4.82	0.0	2.08	2.78					
FeO	0.0	0.0	0.0	15.15	24.53	26.78	26.14	21.22	55.51	33.06	39.62					
MnO	0.0	0.0	0.0	0.62	0.91	0.88	1.29	0.55	2.23	1.01	0.86					
MgO	0.0	0.0	0.0	9.11	1.99	0.06	0.69	1.72	9.49	0.06	0.03					
NiO	0.0	0.0	0.0	0.0	0.0	0.0	0.0	0.0	0.0	0.0	0.0					
CaO	0.48	0.64	0.75	21.01	20.56	19.49	15.19	16.23	0.56	2.71	0.40					
Na ₂ O	7.61	7.50	7.56	0.44	0.59	1.14	1.97	2.99	0.04	7.27	7.19					
K ₂ O	5.58	5.90	5.19	0.02	0.0	0.0	0.04	0.04	0.02	1.62	0.05					
H ₂ O	0.0	0.0	0.0	0.0	0.0	0.0	0.0	0.0	0.0	0.0	0.0					
F	0.0	0.0	0.0	0.0	0.0	0.0	0.0	0.0	0.0	0.0	0.0					
Total	99.04	100.37	100.55	99.85	100.04	100.22	98.40	98.13	99.44	97.73	99.94					
	No. of ions on basis of 8 (0)			No. of ions on basis of 6 (0)						No. of ions on basis of 4 (0)			No. of ions on basis of 23 (0)		No. of ions on basis of 40 (0)	
Si	2.9633	2.9725	2.9692	1.9571	1.9597	1.9803	1.9800	2.0120	0.9985	8.0417	11.8544					
Al	1.0272	1.0133	0.9953	0.0429	0.0297	0.102	0.0152	0.0	0.0	0.0	0.1122					
Cr	0.0	0.0	0.0	0.0	0.0106	0.0095	0.0048	0.0	0.0	0.0	0.0					
Fe ³⁺	0.0109	0.0087	0.0401	0.0	0.0	0.0	0.0	0.0	0.0	0.0	0.0334					
Al	0.0	0.0	0.0	0.0018	0.0	0.0	0.0	0.0255	0.0	0.0191	0.0					
Cr	0.0	0.0	0.0	0.0186	0.0053	0.0040	0.0162	0.0205	0.0	0.0013	0.0					
Ti	0.0	0.0	0.0	0.0382	0.0656	0.0927	0.1440	0.1479	0.0010	0.0367	1.6445					
Fe ³⁺	0.0	0.0	0.0	0.0	0.0	0.0003	0.0003	0.0	0.0	0.2547	0.5710					
Ni	0.0	0.0	0.0	0.0	0.0	0.0	0.0	0.0	0.0	0.0	0.0					
Fe ²⁺	0.0	0.0	0.0	0.4903	0.8344	0.9199	0.9112	0.7234	1.4706	4.4923	9.5603					
Mn	0.0	0.0	0.0	0.0203	0.0306	0.0306	0.0455	0.0190	0.0598	0.1390	0.2102					
Mg	0.0	0.0	0.0	0.5255	0.1206	0.0037	0.0429	0.1045	0.4481	0.0145	0.0129					
	0.0	0.0	0.0	0.8712	0.8960	0.8578	0.6784	0.7088								
				0.0330	0.0465	0.0908	0.1592	0.2363								
				0.0010	0.0	0.0	0.0021	0.0021								
Ca	0.0232	0.0305	0.0357						0.0190	0.4717	0.1236					
Na	0.6653	0.6475	0.6512						0.0025	2.2900	4.0218					
K	0.3209	0.3351	0.2941						0.0008	0.3357	0.0184					

MOUNT EDZIZA

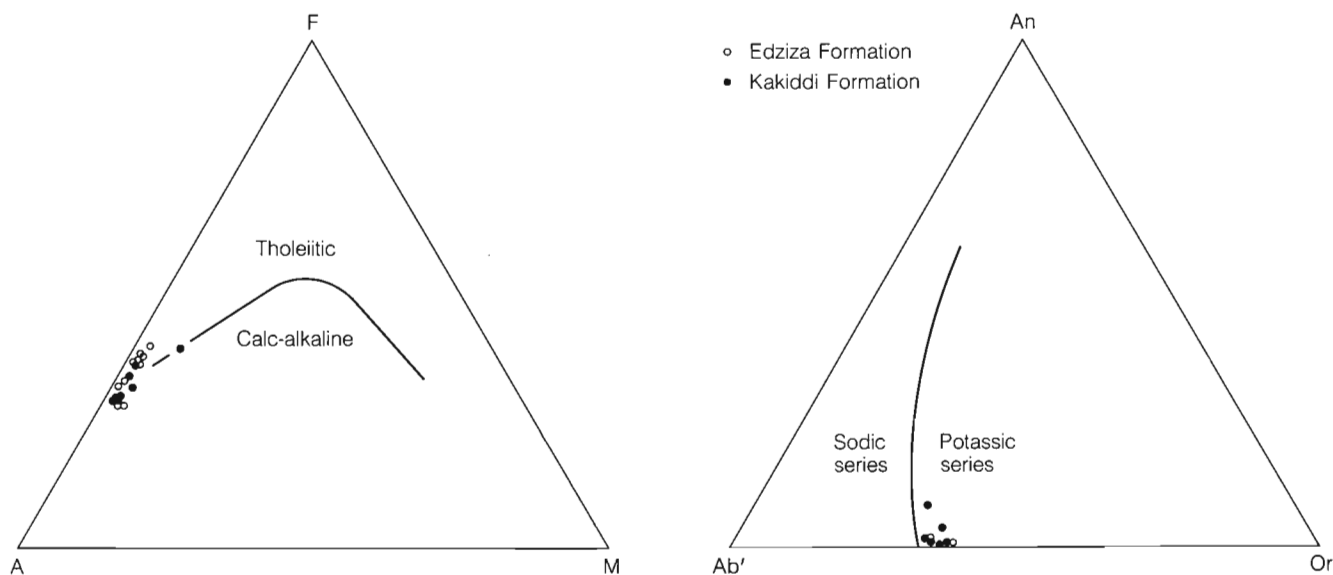


Figure 171. AFM and Ab'-An-Or plots of Edziza (open circles) and Kakiddi (solid dots) chemical data. (A=Na₂O+K₂O; F=FeO+0.8998 Fe₂O₃; M=MgO; Ab'=Ab+5/3Ne).

Table 18. Representative chemical analyses of specimens from the Edziza (E) and Kakiddi (K) formations.

	Tristanite	Trachyte			Peralkaline			
Sample	K19	K6	E5	E12	E68	K3	E16	
SiO ₂	57.700	61.900	61.500	60.700	63.000	61.600	65.700	
Al ₂ O ₃	16.400	16.400	16.900	15.300	15.300	15.600	14.000	
Fe ₂ O ₃	3.400	4.200	4.600	3.700	3.700	3.800	2.200	
FeO	4.500	2.000	1.900	4.400	3.800	3.400	4.700	
CaO	3.330	1.380	0.950	1.670	1.190	1.650	1.290	
MgO	1.450	0.580	0.250	0.370	0.250	0.360	0.180	
Na ₂ O ₃	5.800	6.400	6.600	7.700	7.100	6.200	6.200	
K ₂ O	4.190	5.310	5.080	5.030	4.680	5.090	4.830	
TiO ₂	1.130	0.440	0.190	0.450	0.430	0.500	0.460	
P ₂ O ₅	0.300	0.100	0.050	0.120	0.060	0.060	0.040	
MnO	0.190	0.150	0.150	0.210	0.180	0.210	0.200	
S	0.070	-	0.090	0.070	0.100	0.080	0.070	
NiO	-	-	0.010	0.010	0.0	-	0.010	
H ₂ O	0.300	0.300	2.000	0.200	0.700	2.000	0.700	
CO ₁	0.900	-	0.0	0.0	0.0	-	0.0	
Total	99.660	99.160	100.270	99.930	100.490	100.550	100.580	

CHEMISTRY

Eleven analyses of rocks from the Edziza Formation are plotted in Figures 169 to 171 and four representative analyses are listed in Table 18. All of the constituent oxides fall within very narrow limits and exhibit no systematic variation with respect to SiO₂ (Fig. 169). All but two of the analyzed specimens are peralkaline and plot in the comenditic

trachyte field of the Al₂O₃ vs. FeO diagram (Fig. 170). The remaining two are highly alkaline trachytes (A.I. > 0.95) of such similar composition that they are not discriminated by either the Na₂O+K₂O vs. SiO₂ or AFM plots (Fig. 170,171). The Edziza rocks are relatively Fe-rich (6-8% FeO). Thus, despite their high Na₂O+K₂O content the suite shows less apparent alkali enrichment on the AFM plot than the comenditic rocks of the Armadillo, Spectrum and Pyramid formations.

KLASTLINE FORMATION

GENERAL GEOLOGY

Remnants of thick basalt flows erupted during the Klastline time are preserved south of Buckley Lake, along the western side of Kakiddi Valley, and as small buttes and buttresses along Klastline Valley (Fig. 172, Map 1623A, in pocket). They occur as isolated, usually flat-topped erosional remnants bounded by low escarpments from 6-12 m high (Fig. 173). Flow cleavage is developed locally, particularly in the Buckley Lake lobe, but elsewhere the rock is extremely massive and nearly all cliffs are flanked by giant talus blocks which obscure the lower contact.

Most sections expose from one to three cooling units, each with a lower colonnade of stout 0.5-1 m diameter columns surmounted by an entablature of smaller, often curved or radiating columns. Flows are separated by a few metres of scoriaceous flow breccia but this has been completely stripped from the surface of the upper flow by fluvial and glacial erosion. Glacial grooves and stria are common and erratics of pre-Tertiary basement rocks were observed on all Klastline surfaces up to 5000 ft. (1525 m) elevation. The rock is a moderately porphyritic basalt with 10 to 30% phenocrysts of plagioclase, pyroxene, and olivine in a medium to light grey groundmass. The proportion and size of olivine and pyroxene phenocrysts is noticeably greater in the lower few metres of many of the thick flows, suggesting crystal settling. Vapour phase alteration, during the final stages of cooling, has produced a patchy brown mottling in the upper part of some flows.

The relative age of the Klastline and Edziza flows can only be inferred from indirect evidence because they were not observed in direct contact. The base of the large remnant near the mouth of Tenchen Creek is green, gently east-dipping, flow layered Edziza trachyte, whereas the top and east side are Klastline olivine basalt flows and tephra. Although the actual contact is obscured the persistent flow layering in the trachyte suggests that it forms a continuous slab beneath the basalt rather than a flow margin that has been diverted around an older obstruction. The basal contact of the Klastline pile was observed at only one place, a steep buttress on the west side of Klastline River, near the mouth of Buckley Creek. There the black, ropy base of the flow is underlain by a 1 m mat of brown, clinkery cinders and flow breccia which rest on river gravel containing rounded boulders up to 1.2 m across. The gravel layer itself is 6 m thick and rests directly on basement. The boulders include a mixture of both basement rocks and early phases of the Edziza Complex, and a few relatively small cobbles of green trachyte believed to have come from the Edziza Formation. Both the Edziza and Klastline Valley flows have undergone about the same degree of dissection and both have been

glaciated. It seems probable that the Klastline lavas were erupted near the end of the last interglacial, soon after the cessation of Edziza activity.

The Klastline basalt issued from at least three sources. Scattered outcrops of the Buckley Lake lobe can be traced eastward up to an elevation of 3500 ft. (1065 m), above which they are covered by colluvium and younger flows. About 2 km beyond the last outcrop the younger Big Raven flows have been diverted around a low grassy hill which rises to an elevation of 4000 ft. (1220 m). This is probably all that remains of the pyroclastic cone from which the Buckley Lake lobe originated.

The main source of the Klastline Valley flows is well exposed near the head of Pyramid Creek where Klastline cone forms a moderately dissected conical hill nearly 2 km across on the western side of Kakiddi Valley (Fig. 174). Its 4600 ft. (1400 m) summit is below the level of the plateau, thus most of the ejecta accumulated on the east side of the vent, forming a long wedge of tephra which extended down to the valley floor. Most of the pyroclastic pile is fine ash and lapilli (Fig. 175) containing random blocks and bombs up to 25 cm across and minor coarse agglutinated spatter and breccia. The deposits are characteristically well bedded with initial dips of 20 to 30°. Unlike the loosely agglutinated, oxidized tephra of the younger cinder cones this deposit is firmly indurated and unoxidized. Beds of ash and lapilli are cemented by secondary minerals and commonly form steep cutbanks along stream courses. The bedding is interrupted by small normal faults that bound slump blocks 1-5 m across. Displacement on individual slumps is up to 2 m. The slumped beds are not deformed but they are altered and more firmly cemented for a few centimetres adjacent to the bounding faults. This slumping appears to have taken place during construction of the cone, while the pile was still permeated with hot vapours. Several unique features of the cone suggest that it formed in a wet environment, possibly near the edge of an ice cap that had started to develop on the newly formed peak of Mount Edziza. The absence of pillows or palagonite tuff-breccia suggests that water was not ponded around the vent but that meltwater streams and groundwater flowing into the vent area generated repeated phreatic explosions and dense columns of steam. Fine ash and lapilli, saturated with rain from the condensing column of steam, clung in thin beds to the steep sides of the growing cone. Dehydration and compaction of this mass initiated the regular pattern of slump fractures through which hot water and steam were channelled, altering the adjacent rock and precipitating a siliceous cement. The absence of primary red oxidation of the tephra is probably also due to an abundance of steam which excluded oxygen and reduced burning of vent gases to a minimum.

MOUNT EDZIZA

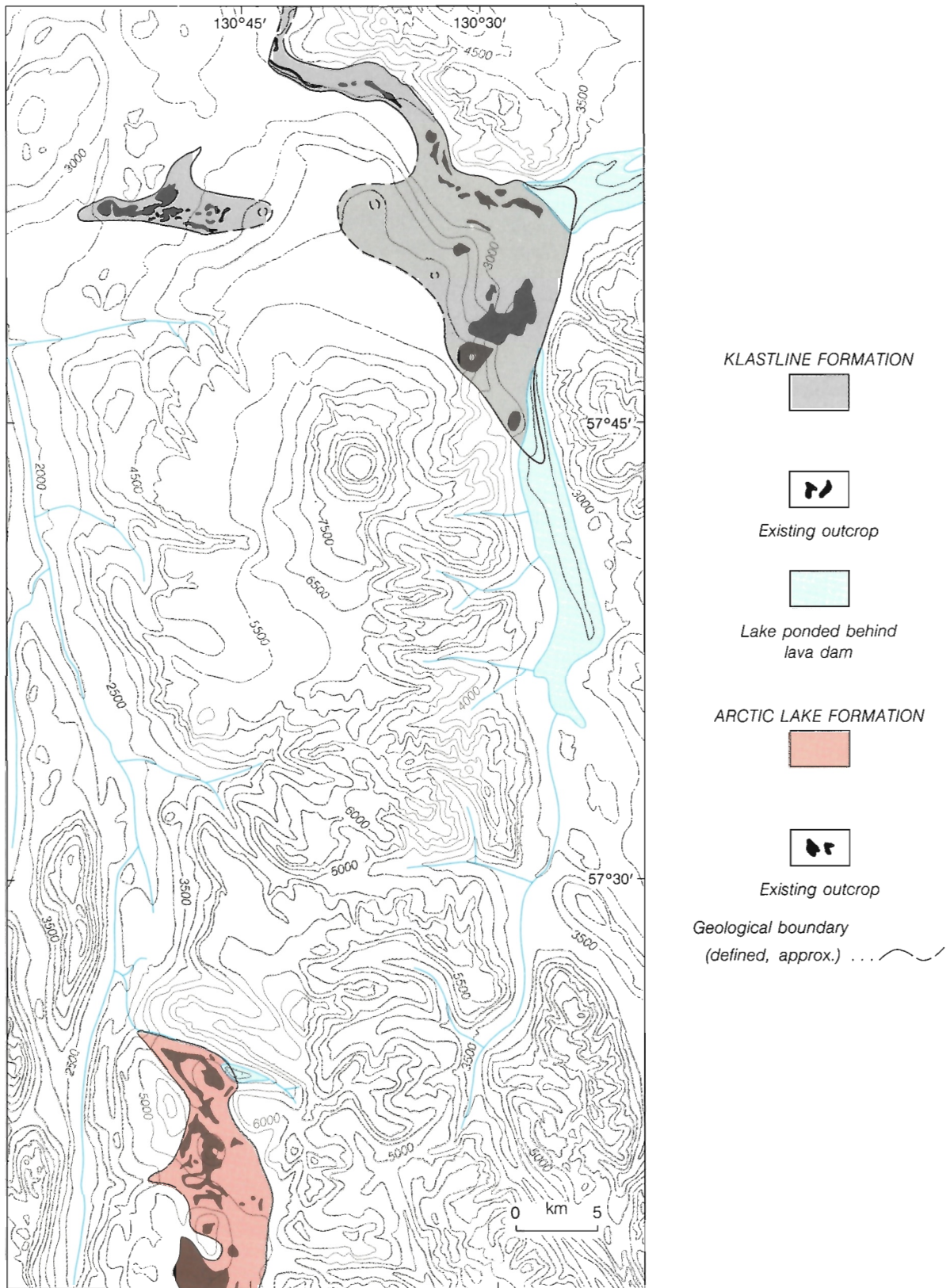


Figure 172. Paleogeological map showing the inferred maximum extent of the Klastline and Arctic Lake formations prior to the last major glaciation of the region.

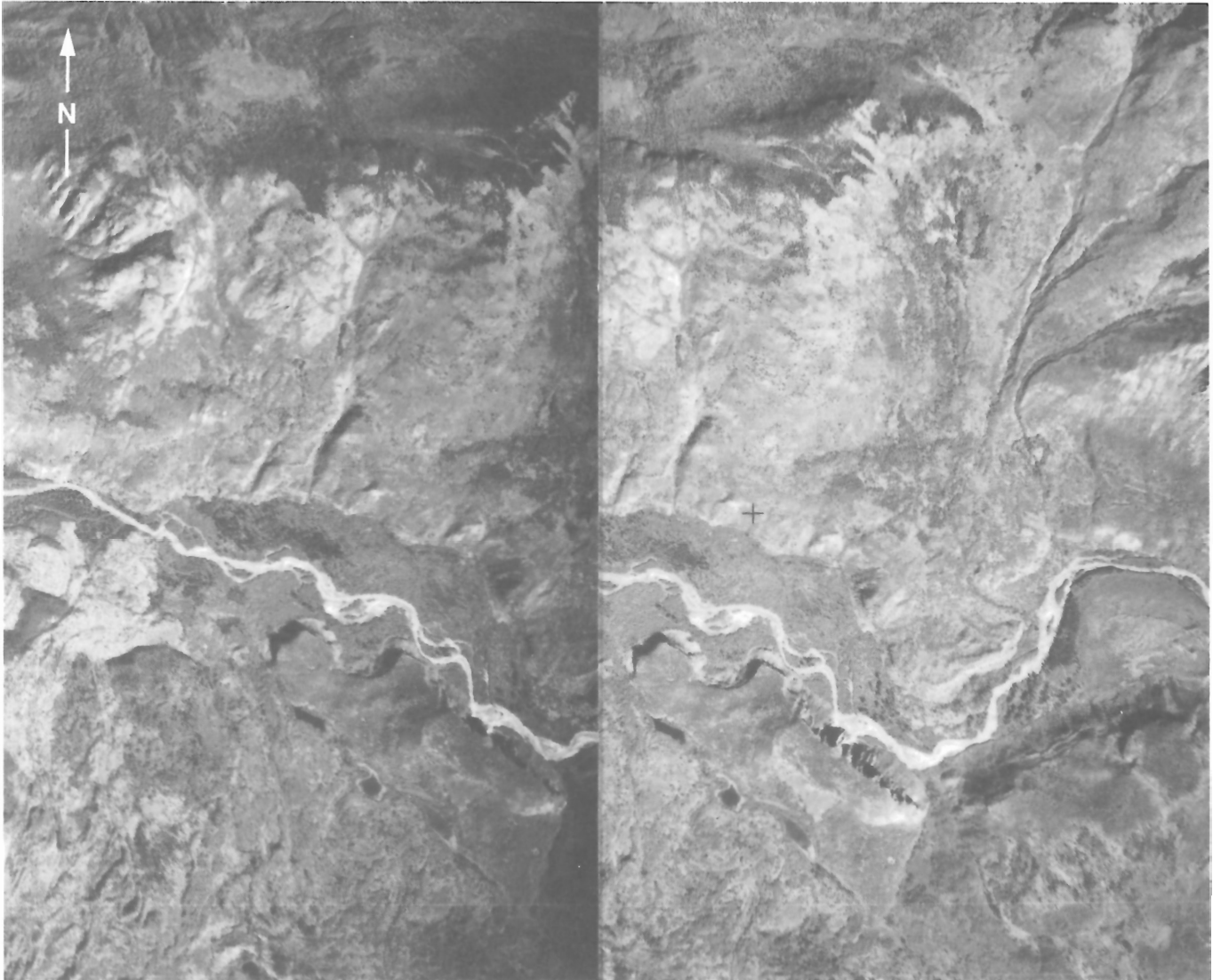


Figure 173. *Klastline valley, showing flat-topped remnants of Klastline basalt surrounded by fluvial deposits and younger flows of Big Raven basalt. Stereoscopic pair. NAPL A 12226-452, 453.*

MOUNT EDZIZA

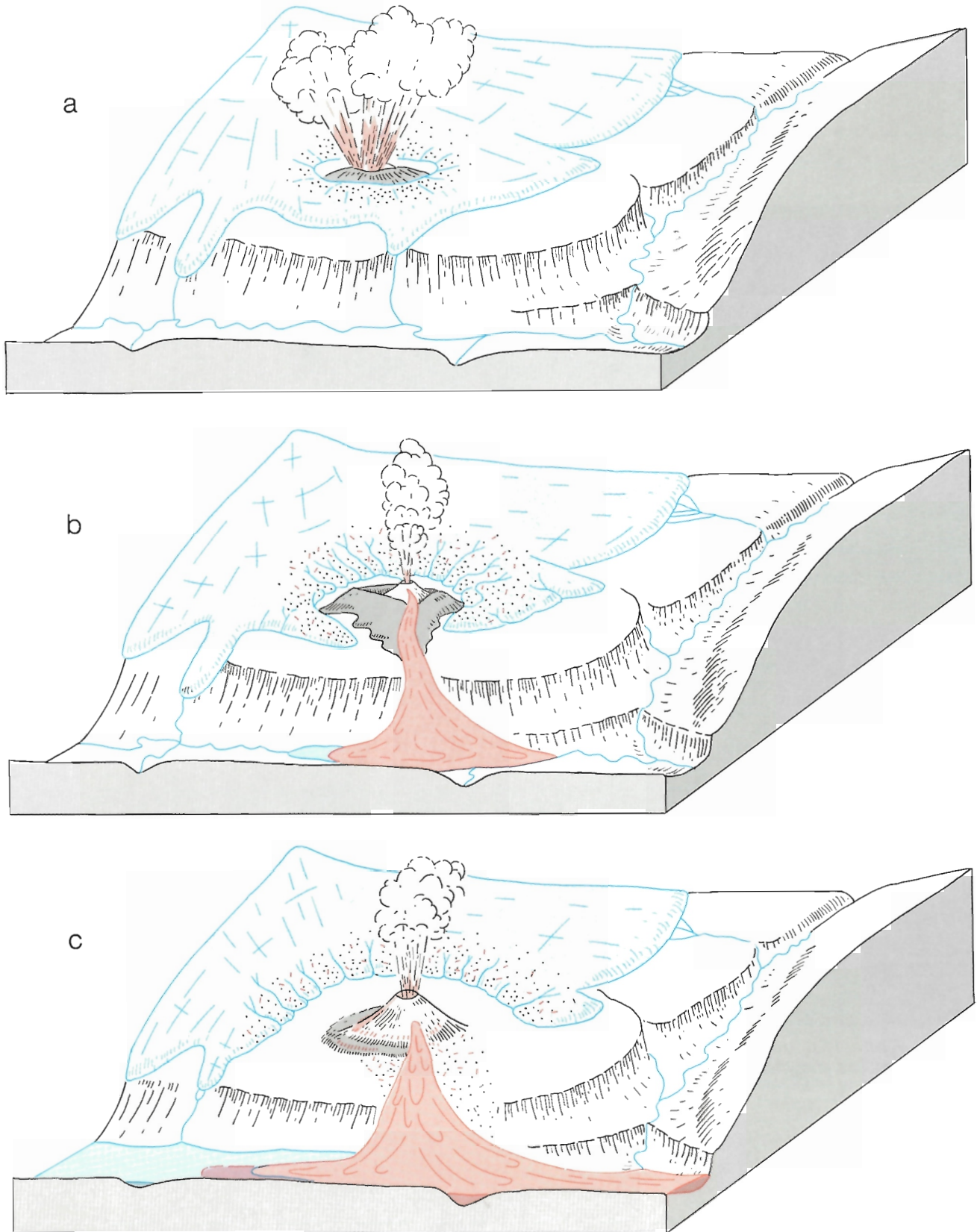


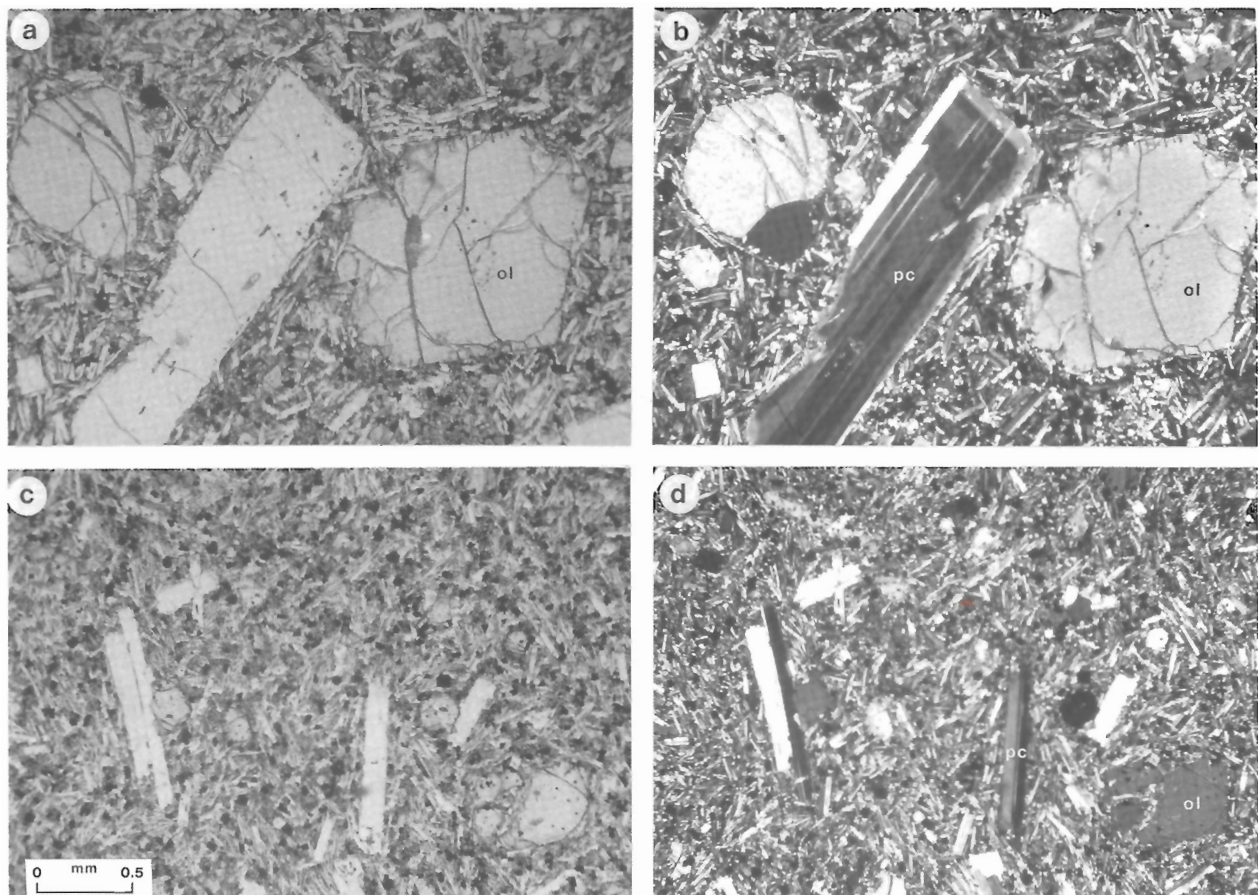
Figure 174. Block diagrams showing three stages in the evolution of Klastline Cone and disruption of the Kakiddi Creek and Klastline drainages by lava flows. (a) Flooding of the initial vent by meltwater from a nearby alpine glacier caused repeated phreatic explosions and the construction of a tuff ring. (b) Breaching of the ice dam and construction of a subaerial tephra cone accompanied by eruption of lava flows. (c) Massive effusion of lava into the valley and the formation of lava-dammed lakes in which pillow lava accumulated.



Figure 175. Thin-bedded, well indurated lapilli tuff on the flank of Klastline cone, a tuff ring formed by repeated phreatic eruptions during the early stages of Klastline activity. GSC 125 622.

Two glaciated cones farther north on the Big Raven Plateau (Fig. 172) may be remnants of other Klastline centres of eruption. These loosely aggregated subaerial piles of reddish-brown spatter and bombs were probably erupted beyond the edge of the Edziza ice cap.

Lava from Klastline cone flowed along the valley of Kakiddi Creek to its junction with Klastline River. There it merged with lava issuing from satellitic cones to form a series of thick valley flows which extend at least 20 km along Klastline Valley. Where the stream of lava entered Klastline Valley it formed a dam at least 120 m high, ponding water in the upper Klastline Valley up to approximately the 2500 ft. (760 m) contour. Pillow lavas, interbedded with gravel and coarse, pebbly, water-lain tuff are well exposed in flat-topped, flow-remnants in Klastline Valley downstream from the mouth of Kakiddi Creek. Clay, silt, gravel and ash deposited in the lake above the dam are exposed in terraces and cutbanks upstream from the dam.



a,b — Klastline basalt with phenocrysts of plagioclase (pc) and olivine (ol) in a groundmass of plagioclase, clinopyroxene, minor olivine and opaque oxides (a, plane light; b, crossed polarizers).
c,d — Arctic Lake basalt with microphenocrysts of plagioclase (pc) and olivine (ol) in a groundmass of plagioclase, clinopyroxene, minor olivine and opaque oxides (c, plane light; d, crossed polarizers).

Figure 176. Photomicrographs of Klastline and Arctic Lake basalts; scale bar 0.5 mm.

Table 19. Representative microprobe analyses and structural data for the principal mineral phases in the Klastline basalt.

	Feldspar			Pyroxene			Olivine		
	Phenocryst			Phenocryst			Phenocryst		
	KLF-1	KLF-2	KLF-3	KLP-1	KLP-2	KLO-1	KLO-2		
SiO ₂	48.37	53.67	56.68	47.85	49.55	36.93	39.56		
Al ₂ O ₃	33.48	29.10	27.35	5.97	3.95	.04	.06		
TiO ₂	.08	.16	.17	1.83	1.65	.05	.02		
Cr ₂ O ₃	0.00	.01	0.00	.20	0.00	0.00	0.00		
Fe ₂ O ₃	.60	.72	.58	3.17	1.13	0.00	0.00		
FeO	0.00	0.00	0.00	5.85	7.94	31.32	20.56		
MnO	.01	.01	.01	.19	.18	.51	.25		
MgO	.08	.09	.04	13.15	12.85	30.43	39.83		
NiO	0.00	0.00	0.00	0.00	0.00	.04	.13		
CaO	15.89	11.32	9.31	20.93	21.48	.35	.30		
Na ₂ O	2.30	4.62	5.22	.54	.47	0.00	0.00		
K ₂ O	.12	.39	.72	.02	0.00	0.00	0.00		
H ₂ O	0.00	0.00	0.00	0.00	0.00	0.00	0.00		
F	0.00	0.00	0.00	0.00	0.00	0.00	0.00		
Total	100.93	100.09	100.08	99.70	99.20	99.67	100.71		
	No. of ions on basis of 8 (0)			No. of ions on basis of 6 (0)			No. of ions on basis of 4 (0)		
Si	2.1963	2.4278	2.5448	1.7895	1.8668			1.0091	1.0114
Al	1.7916	1.5514	1.4472	.2105	.1332			0.0000	0.0000
Cr	0.0000	0.0000	0.0000	0.0000	0.0000			0.0000	0.0000
Fe ³⁺	.0205	.0245	.0196	0.0000	0.0000			0.0000	0.0000
Al	0.0000	0.0000	0.0000	.0527	.0421			.0013	.0018
Cr	0.0000	.0004	0.0000	.0515	.0467			0.0000	0.0000
Ti	.0027	.0054	.0057	.0891	.0321			.0010	.0004
Fe ³⁺	0.0000	0.0000	0.0000	0.0059	0.0000			0.0000	0.0000
Ni	0.0000	0.0000	0.0000	0.0000	0.0000			.0009	.0027
Fe ²⁺	0.0000	0.0000	0.0000	.1830	.2502			.7157	.4396
Mn	.0004	.0004	.0004	.0060	.0057			.0118	.0054
Mg	.0054	.0061	.0027	.7330	.7216			1.2393	1.5178
Ca	.7730	.5487	.4478	.8387	.8671			.0102	.0082
Na	.2025	.4052	.4544	.0392	.0343			0.0000	0.0000
K	.0070	.0225	.0412	.0010	0.0000			0.0000	0.0000

Table 20. Representative chemical analyses of Klastline basalt.

Sample	C-8	C-7	C-6	C-5
SiO ₂	47.350	46.600	47.790	46.630
Al ₂ O ₃	15.600	15.180	15.640	14.790
Fe ₂ O ₃	1.870	2.590	2.440	2.160
FeO	9.440	10.070	9.670	10.150
CaO	11.400	11.640	10.150	10.680
MgO	6.330	6.620	5.570	8.240
Na ₂ O	2.770	2.880	3.490	2.870
K ₂ O	1.670	.780	1.000	.730
TiO ₂	2.490	2.740	2.640	2.460
P ₂ O ₅	.580	.490	.550	.420
MnO	.010	.010	.010	.010
H ₂ O	.870	.490	.480	.590
Total	100.380	100.090	99.430	99.730

PETROGRAPHY

The Klastline basalt is moderately porphyritic, containing 10-30% phenocrysts of plagioclase, olivine and clinopyroxene (Fig. 176,146, Table 19). Plagioclase phenocrysts (calcic labradorite) are euhedral, unzoned and up to 5 mm long. Olivine (Fo₇₅) is present as both euhedral crystals with sharp boundaries and as larger (up to 5 mm) crystals that are deeply embayed by the groundmass. The latter are most abundant near flow bottoms and are probably of cumulous origin. Clinopyroxene phenocrysts (titaniferous salite) up to 3 mm long are also euhedral. They commonly display moderate zoning and contain a concentric layer of opaque inclusions between the core and a narrow, optically continuous overgrowth.

The groundmass is a holocrystalline mosaic of randomly oriented euhedral plagioclase laths (An₆₀Or₅), euhedral grains of Fe-Ti oxide and interstitial crystals of clinopyroxene and olivine. An intergranular residuum of alkali plagioclase commonly contains dendrites of an Fe-Ti opaque oxide and bladed clusters of purplish-brown clinopyroxene.

CHEMISTRY

Five analyses of Klastline rocks are plotted on Figures 147 to 149 and three superior analyses are listed in Table 20. Four of the samples, all from flow remnants in Klastline Valley, form a fairly tight cluster of points on the alkali vs. SiO₂ and AFM diagrams (Fig. 147,148) and plot within the alkali olivine basalt field of the normative colour index vs. normative plagioclase diagram (Fig. 147). The fifth sample, from the base of Klastline cone, is richer in SiO₂ and alkalis, and plots in the trachybasalt field. The low H₂O content (0.10) and Fe₂O₃/FeO ratio (0.11) suggest that its anomalous composition is not due to hydrothermal or vapour phase alteration. It is more likely a sample of the final residual liquid, produced by moderate fractionation of the Klastline alkali basalt, and erupted onto the cone near the end of Klastline activity.

ARCTIC LAKE FORMATION

GENERAL GEOLOGY

Introduction

Basalt flows and related pyroclastic rocks of the Arctic Lake Formation underlie most of the flat upland surface between Mess Creek and the southwestern edge of the Spectrum Range (Fig. 172). Because they are not in contact with either Ice Peak or Edziza rocks, their relative age can only be inferred from their state of erosion. They were clearly erupted after most of the present topography had developed, but before the end of the last major glaciation. They are probably, in part, coeval with the post-Edziza Klastline lavas, but they must have been erupted sporadically over a long period. Some phases are typical of subaerial flows and tephra cones, whereas others are characterized by water contact features that could only have formed during a period of extensive ice cover. Also, some phases are more thoroughly dissected than others.

The Arctic Lake basalt issued from at least seven separate, central vents, all on or adjacent to the Arctic Plateau. Their relative ages, based on degree of dissection and presence or absence of ice contact features, suggest that activity began with Outcast Hill, on the north end of the plateau and

progressed southward with time. Episodic activity appears to have occurred during an interval that spanned most of the last period of regional glaciation. Outcast Hill and Tadekho Hill are preglacial, Wetalth Ridge was built during the glacial maximum and Source hill, Thaw hill and Knobs 1 and 2 erupted during the waning stages of glaciation (Fig. 177).

Preglacial phase

The glacially modified cone of Outcast Hill rises about 800 ft. (245 m) above the surrounding plateau surface. It is flanked by a platform of gently west-dipping basalt flows which presumably issued from it, and now form the surface of a wedge-shaped interfluvium between Yeda and Tadekho creeks. Posteruptive erosion has removed the margins and distal end of the pile of flows and cut deeply into the underlying basement rocks. The resulting escarpment exposes from 2 to 5 flows of medium grey, brown-weathering basalt with a composite thickness of about 60 m (Fig. 178). The flows are clearly subaerial, with well developed, large-diameter transverse columns and partings of red, oxidized scoria containing no glass. The base of the pile is covered except at the extreme western edge where it rests directly

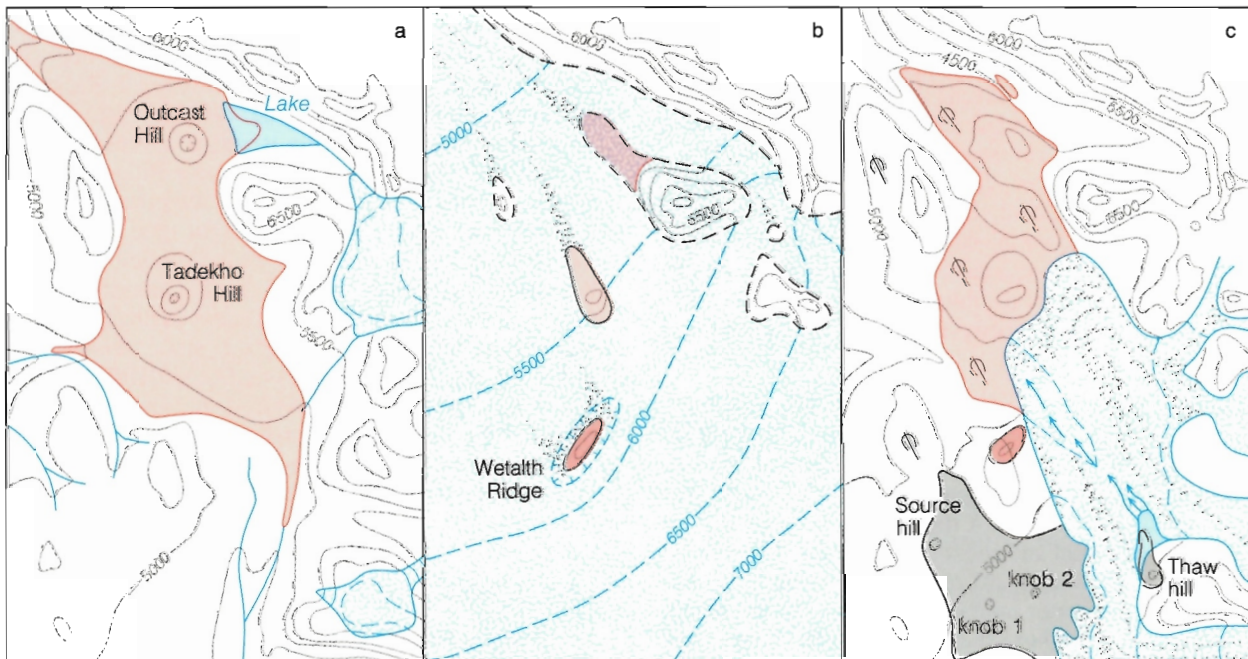


Figure 177. Series of sketch maps showing the relationship of the 7 Arctic Lake eruptive centres to glaciation. (a) Preglacial eruption of Outcast Hill and Tadekho Hill centres. (b) Eruption of the Wetalth Ridge centre during the glacial maximum. (c) Eruption of Thaw hill and the upland flows from Source Hill and knobs 1 and 2 during glacial retreat.

MOUNT EDZIZA

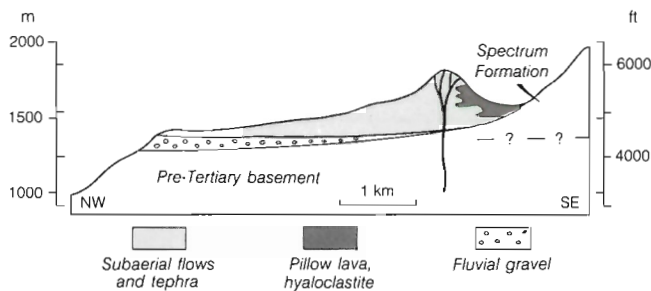


Figure 178. Cross-section through Outcast Hill showing its relationship to subaerial and subaqueous facies and pre-eruption fluvial gravel deposits.

on river gravels which are underlain by pre-Tertiary basement rocks. The gravel layer varies from 6 m to more than 60 m thick and contains mainly well rounded boulders and cobbles interlayered with minor lenses of coarse, pebbly sand. Both crossbedding and shingling indicate deposition by a fast, northwesterly-flowing stream. Most of the clasts are basalt, derived from the thick pile of Raspberry and Nido flows which were stripped from the area. Boulders and cobbles of Spectrum rhyolite and trachyte are present in smaller amounts.

The edifice of Outcast Hill itself is a complex of both subaerial and subaqueous flows and pyroclastic deposits. The subaqueous deposits, including pillow lava, pillow-breccia and sideromelane tuff-breccia, are confined mostly to its lower, northeastern side. Elsewhere, the steeply inclined layers of tephra, bombs and flows have all the characteristics of a subaerial, composite cone. It occupies a preglacial valley, near what was the confluence of two major streams flowing out of the Spectrum Range into Mess Creek (Fig. 172). Before Arctic Lake volcanism began, these streams had already eroded through the Raspberry and Nido basalt shields and cut deeply into the underlying basement rocks. Eruption of Outcast Hill into this valley produced a temporary dam, behind which the water was ponded. Lava that entered the lake produced the pillows and aquagene breccias now exposed on the northwestern side of the cone, whereas most of the lavas flowed westward downstream across dry gravel beds abandoned by the blocked river.

The nearly circular edifice of Tadekho Hill lies 4 km due south of Outcast Hill. It appears to have been built on a pre-existing hill of Spectrum trachyte which outcrops on the east side, almost up to the summit ridge of the cone, and forms a bench on the western flank. Like Outcast Hill, it includes both subaerial and subaqueous phases. Most of the basalt in the surrounding platform of flows is subaerial, but evidence of ice or water contact is seen at several places along Nahta Creek, where the relatively thick transverse columns give way to complex radiating or sheaf-like masses of slender columns. In places, these are nearly horizontal and the associated scoria contains a high proportion of brown, hydrated sideromelane. The lower part of the

Tadekho edifice is a dissected subaerial cone, but the summit ridge comprises almost 60 m of bombs and blocks suspended in a brown, glassy, limonitic matrix which appears to have been quenched. It seems likely that a small ice cap covered the pre-existing hill over which the Tadekho cone was built. Thus, only the initial ejecta was quenched. With continued activity, the ice was either melted or buried and the edifice developed into a normal subaerial composite cone. The quenched flows on its southwestern side may either have entered a body of ponded water or encroached on a lobe of ice in the old valley.

Outcast and Tadekho hills were overridden by northwesterly moving ice which scoured and grooved their surface and deposited erratics on both summits. Their relative age is not known, but both have undergone about the same amounts of erosion suggesting that they are approximately contemporaneous. They were probably erupted a short time before the last major glacial advance at a time when permanent ice was beginning to accumulate above an elevation of 5500 ft. (1675 m).

Intraglacial stage

Wetalth Ridge is an elongate pile of pillows and pillow fragments which rest partly on a remnant of flat-lying Nido basalt and partly on pre-Tertiary basement. Its 6100 ft. (1860 m) summit is only slightly below the glaciated top of Tadekho Hill which lies 4.5 km due north. Unlike the Outcast and Tadekho centres it is not surrounded by an apron of flows, nor is there any evidence of flows rooted within the cone itself. The entire mass comprises vesicular, quenched basalt with pillows, blocky pillow fragments and dykes predominating over finer pyroclastic deposits. Its external form is similar to that of Tsekone Ridge on the north flank of Mount Edziza and, like the latter, it may have an inner core of tuff-breccia which is covered by an outer envelope of pillows. Also, like Tsekone Ridge, it must have formed in a subglacial, meltwater cavity during a period of extensive ice cover. Although erratics are present on the Wetalth edifice, its relatively sharp summit ridge has not been modified as thoroughly as that of Outcast and Tadekho hills. It seems probable that it erupted during the last glacial maximum, when the ice surface stood above 6000 ft. (1800 m) and the older cones of Outcast Hill and Tadekho Hill were already being scoured and eroded beneath it. Much of the fine ash and possibly some of the lava erupted from Wetalth Ridge may have been deposited on the ice surface and carried some unknown distance to the northwest.

Late glacial stage

The southern end of the Arctic Lake plateau is covered by a veneer of basalt, the "upland flows", (Fig. 177) which issued from four or more small central vents or fissures. On the plateau itself, the flows include only one or two cooling units with a total thickness of 3-5 m, but at the southern end

of the plateau the lava from several centres was channelled into the head of More Creek and coalesced to form a composite valley flow up to 30 m thick that extends 4.5 km beyond the mapped area. The flows cover an area of about 100 km². Tributaries at the head of More Creek have cut several box canyons into the surface and along the margins of the flow, but the upland flows are not as thoroughly dissected as those from the Outcast and Tadekho centres.

The upland flows exhibit features that are characteristic of both subaerial and subaqueous lavas. Over most of the plateau they have stout, transverse columnar jointing, but locally this is distorted into radiating clusters of small diameter columns typical of ice-contact zones. Also, the basal flow breccia, unlike the red oxidized, clinkery scoria that underlies most subaerial basalt flows, is commonly a brown, sideromelane-rich quenched breccia. Post-eruptive glaciation has stripped most of the original surface from the upland flows, leaving a grooved and scoured pavement of truncated columns. Subsequent frost heaving has further disrupted the surface and, over wide areas reduced it to a jumble of joint-bounded blocks. This, in turn, is largely covered by glacial outwash deposits, drumlins, eskers and kettle lakes. Only on the extreme western edge of the pile, where the flows are above an elevation of 5000 ft. (1525 m), is their original surface preserved. There on the flanks of Source hill the scoured surface of the plateau grades up through a transition zone to a surface that still retains the sinuous outlines of lava levees and ridges, and on which the broken remains of slabs and scoriaceous blocks are still intact. Source hill itself consists of an elongate ridge of red oxidized spatter, bombs and ropy flow segments. It appears to have formed as a subaerial fissure eruption and it is obviously one of the main sources for the upland flows.

Thaw cone, a similar but smaller centre on the east side of the plateau, is a subaerial pyroclastic cone of red scoriaceous spatter and bombs. Its rounded, 5700 ft. (1740 m) summit is covered with slope wash, but its southern margin, truncated by a recent alpine glacier, reveals both west-dipping tephra beds and segments of blocky subaerial flows. Below, about 5100 ft. (1555 m), the flows are obviously quenched.

Two other eruptive centres, knob 1 and knob 2 (Fig. 177), are surrounded by flows on the glaciated surface of the plateau. They are below an elevation of 5000 ft. (1525 m) and both are piles of quenched lava toes and sideromelane tuff-breccia.

The above data suggest that the upland flows were erupted during the waning stages of regional glaciation, after most of the ice had receded westward into the high mountains of the Coast Range. Smaller ice caps still persisted in the lesser ranges, including Spectrum Range and the Hankin Peak Massif on the east side of the Arctic Plateau. When the Source hill eruption began, the plateau was covered by a lobe of stagnating ice fed by valley glaciers flowing out of the small ice cap to the east (Fig. 179). The Source hill fissure lay just beyond the western limit of ice, thus the pyroclastic cone and proximal flows have all the

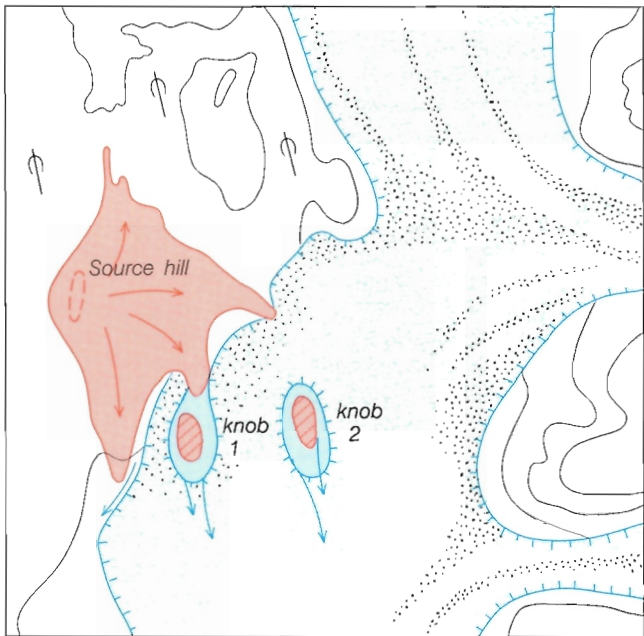
characteristics of a subaerial pile. Where the edge of the lava encroached on the ice, it was locally quenched, but along much of the interface an equilibrium appears to have been reached between advance of the lava and recession of the melting ice, such that there was minimal contact between the two. The key to maintaining this equilibrium was immediate removal of meltwater by a migrating stream that developed between the advancing lava and the receding ice. It discharged into the bed of More Creek without ever having been ponded against the lava front. Thus, only the sloughed off debris at the toe of the advancing flow was quenched in the marginal stream or against the receding ice to form the sideromelane-rich basal breccia, while the main body of the lava developed the characteristics of a subaerial flow. Pockets of quenched lava with small horizontal or radiating columns indicate that local rapid advances brought the lava into direct contact with the ice, but removal of the resulting meltwater quickly re-established an equilibrium distance between the flow and the ice. It is probable that most of the meltwater resulted from radiant heat and steam rising from the quenched toe of the advancing flow.

The subaqueous piles of knob 1 and knob 2 must have formed before the ice was melted since lava ridges and levees in the adjacent flows are deflected around them. They may be older than the Source hill centre or they may be approximately contemporaneous, but erupted within, rather than outside, the ice lobe. In any case, they must have accumulated within meltwater lakes that were ponded up to 5000 ft. (1525 m), the summit elevation of knob 1. This is 60 m below the elevation of Source hill and corresponds approximately with the upper level of glacial scouring on the Source hill flows.

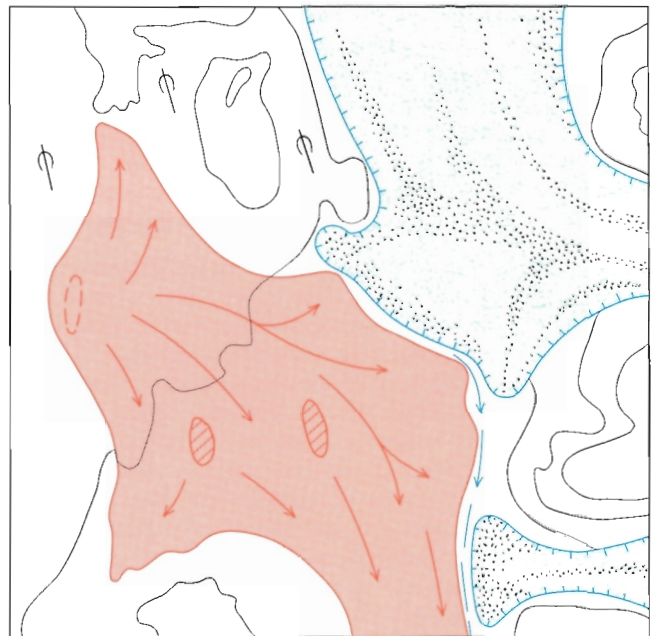
The presence of ice in approximately the same position before and after eruption of the Source hill flows is indicated respectively by the quenched basal breccia and by scouring of the flow surface. The pre-eruption lobe of ice on the plateau was probably in equilibrium with the supply of ice discharging from an accumulation area in the Spectrum Range. Following the Source hill eruptions and associated melting, the ice quickly re-advanced to its previous equilibrium front, overriding and stripping the rough scoriaceous surface from the newly formed flows. It must have stagnated in this position, and as the supply of new ice from the east gradually diminished, the distributary lobe on the plateau began to melt. Its wasted, rock-strewn surface became a jumble of rock cones and ridges and stagnant meltwater ponds which gradually filled with rock debris. Ultimately, this entire load of transported debris was deposited on the scoured surface of the plateau as a thin veneer of recessional moraine, dotted with small irregular drumlins and kettle lakes.

The characteristic topography of the drumlinoid plain defines the approximate limits of the wasting ice. It is crossed, from southeast to northwest, by a prominent swarm of eskers formed mostly of coarse sand, pebbles and rounded cobbles of basement rock and a few subrounded waterworn pebbles of vesicular basalt. Many of the cobbles are derived from a unique, very coarse orthoclase porphyry

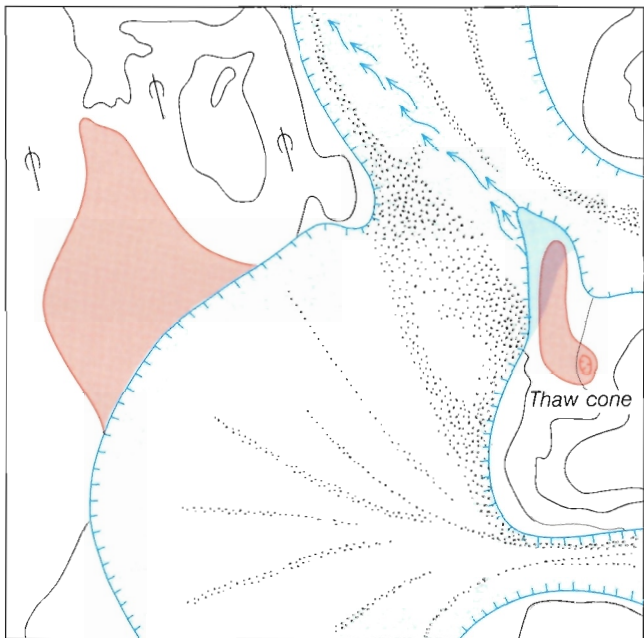
MOUNT EDZIZA



Lava flows from the Source hill, knob 1 and knob 2 centres encroaching on the distal lobe of a stagnating ice sheet



Maximum extent of the upland flows at the end of Source hill activity



Re-establishment of ice to its former, equilibrium position and eruption of Thaw hill, causing a meltwater channel to form across the ice



Present relationship of volcanic and glacial deposits

Glacial striae ↗

Meltwater channel ... →

Figure 179. Series of sketch maps showing the accumulation of the "upland flows" during the final stages of Arctic Lake activity.

which forms a local dyke swarm in the mountains east of More Creek. At its southeastern end, the esker swarm forms a complex network of tributaries (Fig. 180). These converge northwesterly into a relatively narrow zone of subparallel eskers which extends across the plateau to Little Arctic Lake at the edge of the drumlinoid plain. This was obviously a major drainage channel during the waning stages of glaciation. Its location may have been controlled simply by the configuration of the ice surface, but the proximity of the

tributary channels to Thaw cone suggests that the esker system may have been initiated by meltwater resulting from its eruption. As noted earlier, the 5700 ft. (1740 m) summit of Thaw cone is a pile of subaerial tephra, whereas associated flows below 5200 ft. (1585 m) exhibit quench features. Both the cone and the associated flows have suffered more erosion than eskers on the adjacent plateau. Thus the cone must have been modified by erosion before final wasting of the ice.

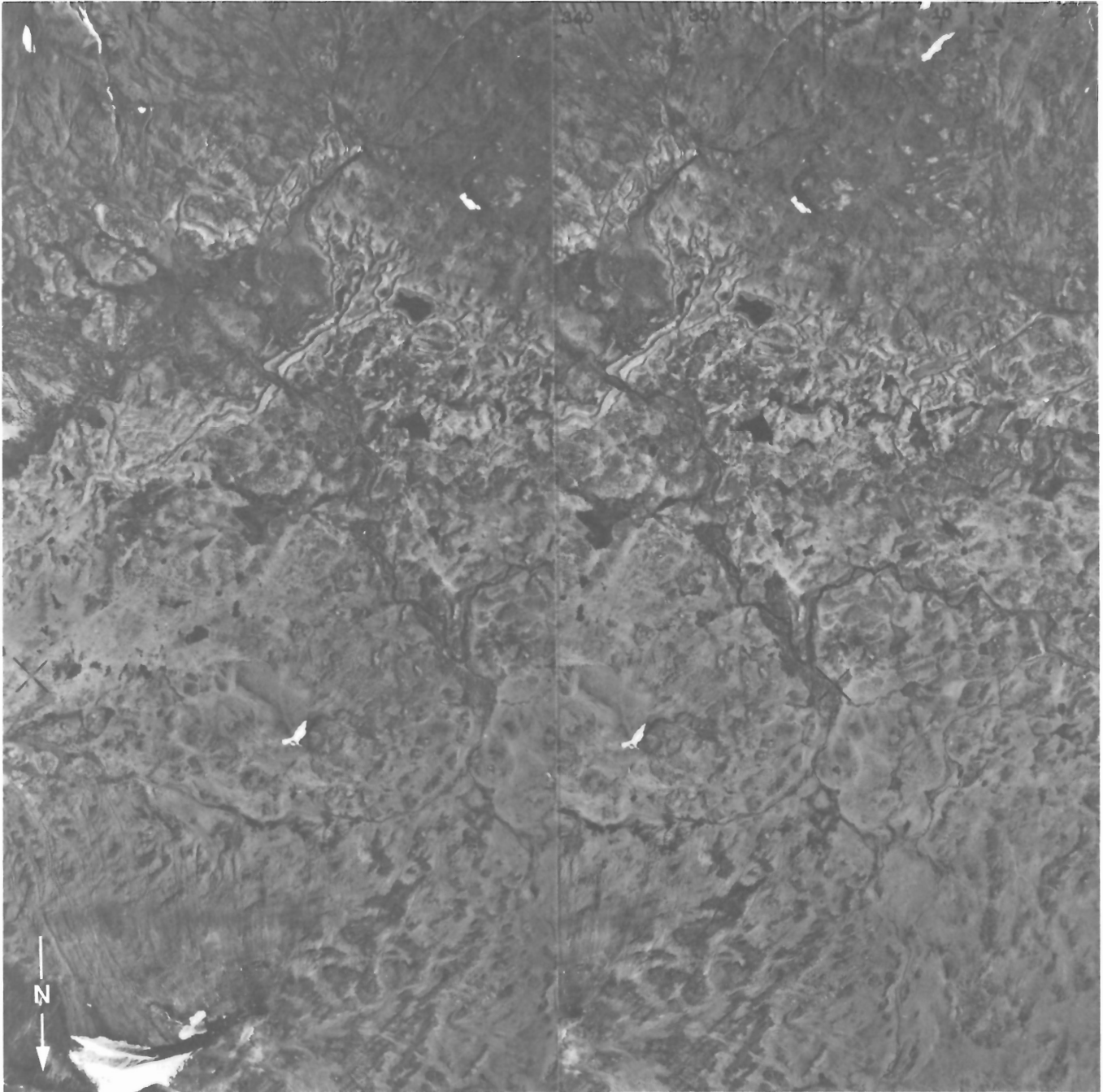


Figure 180. Thaw hill and the adjacent esker system. Note that main, northwesterly trending esker is cut by younger, south-flowing drainage into More Creek. Stereoscopic pair. Province of British Columbia photos BC 1213-19, 20.

Table 21. Representative microprobe analyses and structural data for the principal mineral phases in basalts of the Arctic Lake Formation.

	Feldspar			Pyroxene	Olivine
	Phenocryst		Groundmass	Groundmass	Phenocryst
	ALF-1	ALF-2	ALF-3	ALP-1	ALO-1 ALO-2
SiO ₂	54.14	50.52	52.10	48.28	40.17 36.18
Al ₂ O ₃	29.14	31.99	29.56	3.69	0.02 .01
TiO ₂	.01	.06	0.10	2.34	0.01 0.00
Cr ₂ O ₃	0.00	0.00	0.01	0.00	0.03 0.00
Fe ₂ O ₃	.32	.68	0.52	2.13	0.0 0.00
FeO	0.00	0.00	0.0	8.78	14.89 32.30
MnO	.01	0.00	0.01	.26	0.18 .51
MgO	.03	.03	0.10	12.03	44.60 30.62
NiO	0.00	0.00	0.0	0.00	0.0 .05
CaO	11.40	13.95	13.33	20.58	0.23 .29
Na ₂ O	4.95	3.39	3.98	.61	0.02 0.00
K ₂ O	.37	.25	0.25	.05	0.01 0.00
H ₂ O	0.00	0.00	0.0	0.00	0.0 0.00
F	0.00	0.00	0.0	0.00	0.0 0.00
Total	100.37	100.87	99.96	98.75	100.16 99.96
	No. of ions on basis of 8 (0)			No. of ions on basis of 6 (0)	No. of ions on basis of 4 (0)
Si	2.4404	2.2848	2.3727	Si 1.8430	Si 1.0056 .9925
Al	1.5480	1.7051	1.5865	Al .1570	Al 0.0 0.0000
Cr	0.0000	0.0000	0.0	Ti 0.0000	Cr 0.0 0.0000
Fe ³⁺	.0109	.0231	0.0178	Fe 0.0000	Fe ³⁺ 0.0 0.0000
				Cr 0.0000	
Al	0.0000	0.0000	0.0	Al .0090	Al 0.0006 .0003
Cr	0.0000	0.0000	0.0004	Ti .0672	Cr 0.0006 0.0000
Ti	.0003	.0020	0.0034	Fe ³⁺ .0613	Ti 0.0002 0.0000
Fe ³⁺	0.0000	0.0000	0.0	Cr 0.0000	Fe ³⁺ 0.0 0.0000
Ni	0.0000	0.0000	0.0	Ni 0.0000	Ni 0.0 .0011
Fe ²⁺	0.0000	0.0000	0.0	Fe ²⁺ .2803	Fe ²⁺ 0.3117 .7410
Mn	.0004	0.0000	0.0004	Mn .0084	Mn 0.0038 .0119
Mg	.0020	.0020	0.0068	Mg .6845	Mg 1.6642 1.2520
				Ca .8417	
				Na .0451	
				K .0024	
Ca	.5506	.6760	0.6504		Ca 0.0062 .0085
Na	.4326	.2973	0.3514		Na 0.0010 0.0000
K	.0213	.0144	0.0145		K 0.0003 0.0000

Table 22. Representative chemical analyses of Arctic Lake basalts.

Sample	C-9	C-10	C-11
SiO ₂	45.600	46.850	47.880
Al ₂ O ₃	15.680	15.900	15.660
Fe ₂ O ₃	4.260	3.780	2.750
FeO	9.550	9.590	9.780
CaO	10.040	9.580	8.720
MgO	6.830	6.230	7.410
Na ₂ O	2.620	3.030	3.350
K ₂ O	.770	.990	1.410
TiO ₂	2.690	2.850	2.190
P ₂ O ₅	.470	.440	.500
MnO	.010	.010	.010
H ₂ O	1.270	1.380	.660
Total	99.790	100.630	100.320

The proximity of the esker system to Thaw cone may be only a coincidence, but the following explanation is also possible. Lava from Thaw cone may have encroached on the edge of the ice and produced a torrent of meltwater that spilled out across the ice surface in numerous small streams (Fig. 179). These converged into a central channel, and as the drainage system became entrenched, it carried an ever increasing load of morainal debris sloughed off the rock-covered surface of the waning ice. Once established, this same drainage system may have persisted long after cessation of the Thaw cone activity, continuing to transport large volumes of meltwater, sand and gravel northwesterly across the ice surface while the cone itself was being eroded in the final stages of wasting. Gravel and sand in the meltwater channels were deposited on the plateau surface as esker ridges that were quickly cut by the present streams flowing south into More Creek (Fig. 180).

PETROGRAPHY

The Arctic Lake basalts display little variation in texture or mineralogy (Fig. 176,146, Table 21). They contain 5-15% microphenocrysts of euhedral olivine (FO_{80-85}) and plagioclase. The holocrystalline groundmass is an intergranular mosaic of euhedral to subhedral plagioclase laths (An_{65}), olivine (FO_{63-74}) and clinopyroxene. Opaque oxides occur as rare microphenocrysts and as a dispersed groundmass phase. Vesicles are uncommon but, where present, they are unfilled. A small amount of secondary carbonate was noted in sections of Outcast Hill basalt but elsewhere the Arctic Lake rocks are unaltered.

CHEMISTRY

Three analyzed samples from the Arctic Lake Formation (Table 22) are basic alkali olivine basalts with less than 48% SiO_2 (Fig. 149). They are chemically similar to alkali olivine basalts from the Klastline Formation and analyses from both formations plot within the same small areas of the alkali vs. SiO_2 , AFM, and normative colour index vs. normative plagioclase diagrams (Fig. 147,148).

KAKIDDI FORMATION

GENERAL GEOLOGY

Introduction

Remnants of thick trachyte flows and associated pyroclastic rocks occupy deeply incised valleys on the east side of Ice Peak (Fig. 181, Map 1623A, in pocket) and, higher on the mountain, they form east-dipping caps which truncate Ice Peak stratigraphy (Fig. 182). Similar trachyte, which forms a relatively thin flow lobe on the plateau west of Ice Peak, is associated with trachyte pyroclastic deposits of Punch cone. These scattered remnants are assigned collectively to the Kakiddi Formation. It is similar to the Edziza Formation in both lithology and morphology but the Kakiddi trachyte must have issued from vents south of the Mount Edziza composite cone (Fig. 181) and radiometric dates suggest that it is younger. The Kakiddi activity produced the last major effusion of intermediate lava in the Mount Edziza Volcanic Complex but its source is not known. Some of the trachyte remnants assigned to the Kakiddi Formation may be coeval or even coextensive with the youngest Edziza flows.

Flows and pyroclastic deposits

A single, massive trachyte flow forms the flat interfluvium between the lower reaches of Sorcery and Tennaya creeks. It is almost 1 km wide, from 60-120 m thick, and is continuously exposed for 7 km (Fig. 183). Its lower end extends into Kakiddi Valley and large, isolated areas of trachyte near Kakiddi and Nuttlunde lakes are believed to be remnants of a once continuous, terminal flow-lobe at least 5 km across which welled out into the valley. The flat upper surface of the flow, strewn with blocks of porous pale green trachyte, is only slightly modified by erosion. However, undercutting by the marginal streams has produced steep bounding cliffs, exposing columns 1-2 m across which extend the full thickness of the flow (Fig. 184). Beneath the upper rind of pale green flow-top breccia the dark greenish-grey rock weathers to a rusty ochre surface. It is characterized by prominent flow cleavage along which it splits to form flaggy, slate-like talus. Perfectly aligned thin tabular feldspars and acicular crystals of sodic amphibole and pyroxene impart a lustrous sheen to cleavage surfaces.

Upstream the flow divides into two tributary branches, one extending up Sorcery Valley and the other up Tennaya Valley. A short distance above the junction the flow is either buried by colluvium or eroded away, but additional remnants appear farther upstream in both main valleys and in their tributaries (Fig. 181). The remnants in upper Tennaya Valley can be traced almost continuously up to an elevation of 7200 ft. (2195 m) on the narrow spur between Tennaya and Idiji glaciers (Fig. 182). These upper remnants are underlain by beds of black, southeast-dipping trachyte

pumice that rest on a steep erosion surface cut into the underlying Ice Peak flows. A wedge of similar pumice is preserved on the steep southern spur of Tennaya cirque (Fig. 185). It is plastered against, and truncates, nearly flat-lying flows that form the cliffs on the east face of Ice Peak. The wedge is about 60 m thick and consists of well bedded black, loosely agglutinated pumice fragments up to 15 cm across. Bedding is due primarily to size sorting, with individual layers of coarse or fine tephra varying from a few centimetres to 1 m. Both the pumice wedge and beds of similar pumice under the upper flow remnants were probably once part of the same pyroclastic pile that buried the old topography on the east side of Ice Peak, filling the upper reaches of Tennaya and adjacent valleys during the early stages of Kakiddi activity and providing a ramp across which the lava subsequently flowed.

The pumice wedge is one of several remnants of poorly consolidated pyroclastic material preserved in upper Tennaya Valley. Three large remnants of very coarse Edziza breccia (Fig. 161) are plastered against the steep cliffs below Nanook Dome. They are believed to be remnants of a once continuous debris fan built during construction of the dome. This fan and the early pyroclastic ejecta provided a surface across which lava, possibly from the Nanook vent, was ramped to its present position on the south side of the valley. Subsequent erosion has almost completely removed both the poorly consolidated debris fan and the pumice deposits, along with any flows that may have remained on them (Fig. 186).

No pyroclastic deposits are associated with the flow remnants in Sorcery Creek or the south fork of Tennaya Creek.

A broad lobe of trachyte, resembling other Kakiddi flows, is partially exposed on the plateau west of Ice Peak. It is mostly covered by younger flows and tephra from Coffee Crater and by drifts of Sheep Track pumice. Its base is not exposed and its felsenmeer covered surface has been glaciated.

Eruptive centres

The source of the Kakiddi Formation valley flows is not known. The main flow that enters Kakiddi Valley appears to have been fed by at least two, and possibly three, tributaries (Fig. 181). The most northerly tributary may have been an extension of flow remnants that descend the east face of Ice Peak (Fig. 186) but a gap of 6 km now separates the most easterly exposure of the upper flows from the main valley flow. The upper flows and associated pumice are clearly from a vent near the present summit of Ice Peak and, as discussed previously, Nanook Dome may have been a major source.

MOUNT EDZIZA

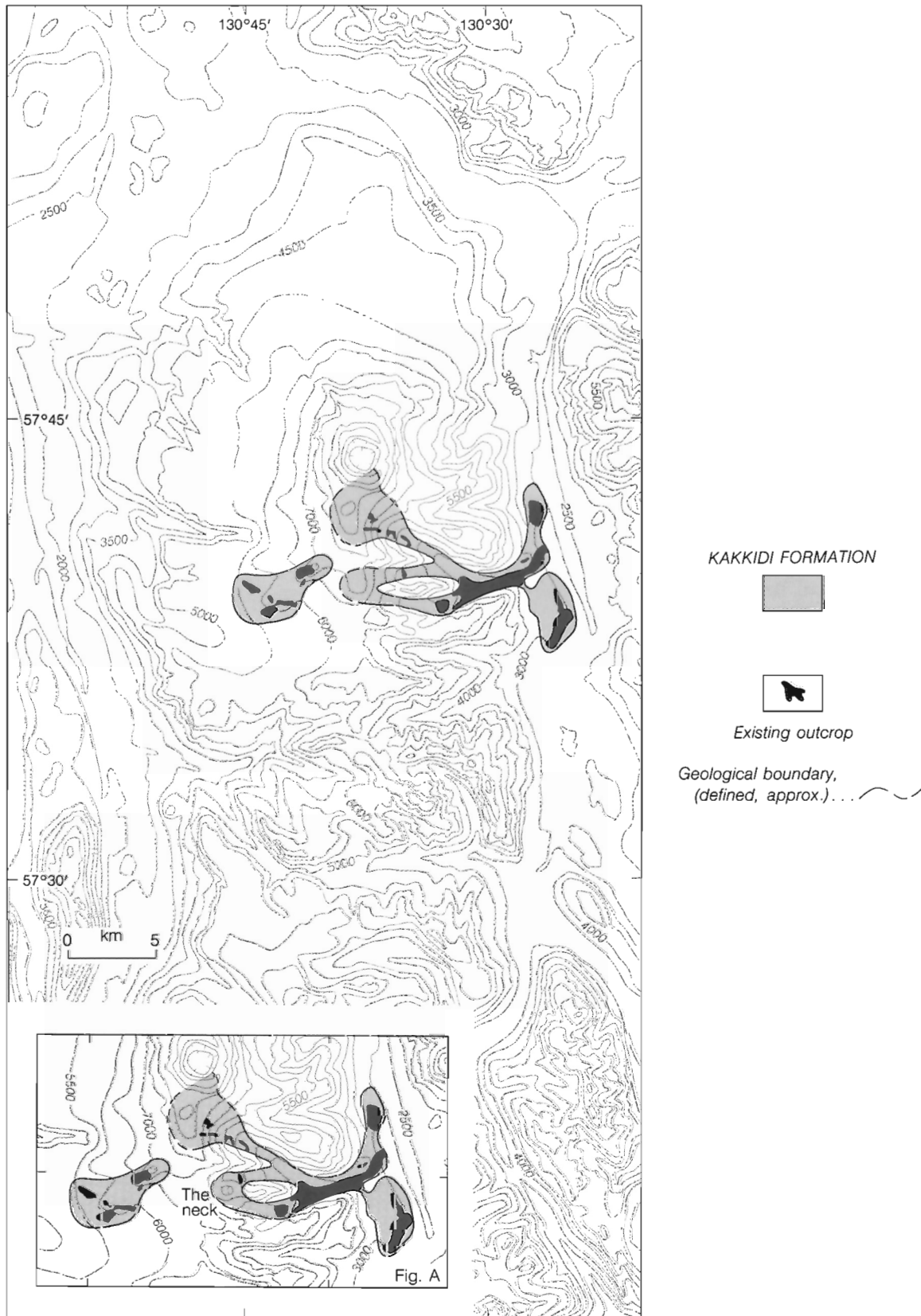


Figure 181. Paleogeological map showing the present distribution and inferred maximum extent of the Kakiddi intravalley trachyte flows. Their source may have been from vents, now ice-covered, on the summit ridge of Ice Peak, or some of the Kakiddi lava may have issued from The Neck (Fig. A).



Figure 182. Looking northwest at a thick remnant of Kakiddi trachyte capping the rock spur between Idiji and Tennaya cirques. The Kakiddi flow rests on a thick mat of trachyte tephra and cuts steeply across truncated Ice Peak flows. GSC 125 623, 125 624.

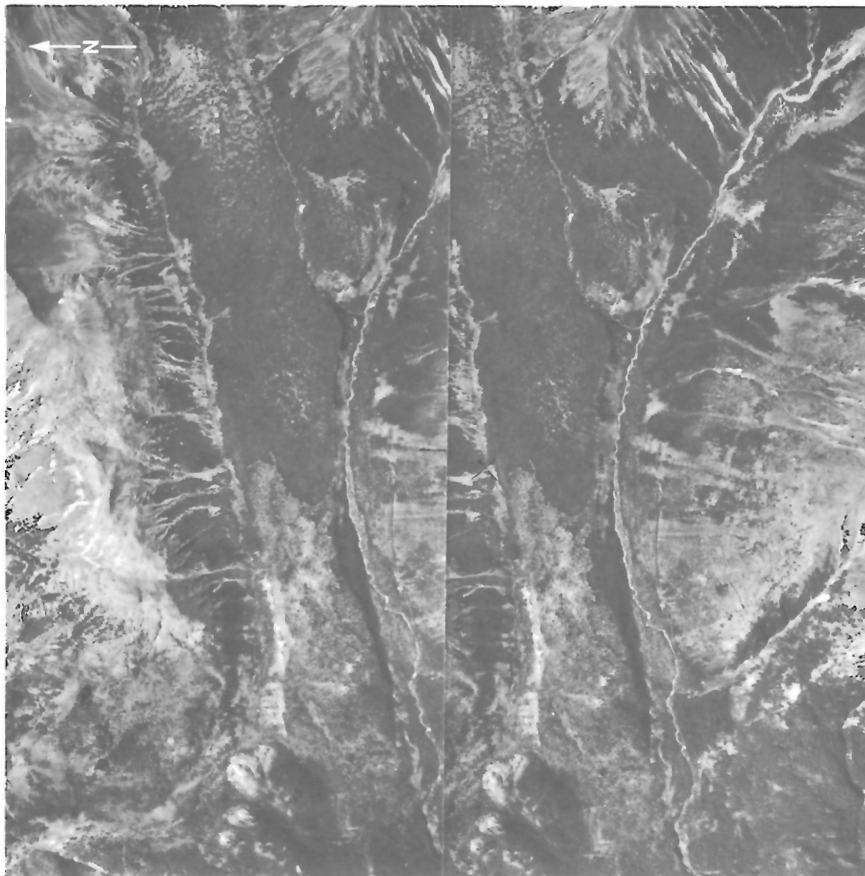


Figure 183. The valley occupied by Sorcery and Tennaya creeks. The flat interfluvium between the two creeks is a single, massive flow of Kakiddi trachyte. Stereoscopic pair. Province of British Columbia photos BC 1367-1, 2.



Figure 184. Massive columns extending the full thickness of Kakiddi intravalley flow. GSC 202469-K.

The other two tributaries are inferred from thick remnants of similar flow-layered trachyte in the two south forks of Tennaya Creek. Neither of these tributary streams of lava could have originated from the Nanook vent or from any other vent on the central cone of Mount Edziza because of the intervening ridge of Ice Peak. Thus, they must have issued from vents, now covered by ice on the south flank of Ice Peak, or from vents within the valleys themselves. The absence of Kakiddi trachyte on the rim of the plateau at the head of either valley favours the latter. No pyroclastic deposits related to the Kakiddi flows are preserved in either of these tributary valleys. However, this is not surprising since large sections of the flows have been eroded away and cones, formed within the pre-existing valleys, would be even more susceptible to erosion. An elliptical area of flaggy green trachyte about 0.5 km across at the head of the south fork of Tennaya Valley is mapped as an exhumed subvolcanic intrusion of Ice Peak age (see Ice Peak, Subvolcanic intrusions). However, it may be much younger and could be part of a conduit system related to the Kakiddi flows. Unlike the flows, which have consistently sub-horizontal flow layering, the layering in this area is vertical. In every other respect it resembles the Kakiddi trachyte in the flow remnants. The main body is isolated from adjacent rocks by a fringe of colluvium and talus, but small, irregular dyke-like masses of similar trachyte cut Ice Peak basalt in the adjacent cliffs.

The source of Kakiddi lava flows in the two south forks of Tennaya Creek was originally thought to be The Neck, a circular pillar of trachyte that outcrops on the ridge between the two valleys (Fig. 181, inset). However, a radiometric date of 1.5 Ma on trachyte from The Neck suggests that it is of Ice Peak age. The possibility that it may be a source of Kakiddi flows is nevertheless an appealing hypothesis which is supported by similar petrography, chemistry and morphology of The Neck and adjacent valley flows. The possibility cannot be dismissed until the age of The Neck is confirmed by additional dates.

The lobe of trachyte that underlies Coffee Crater, on the southwest side of Ice Peak is believed to have issued from Punch cone (Fig. 187), an elliptical, steep-sided ridge, about 1 km long, which projects from under the central ice cap. Its lower slopes are completely covered with younger, Sheep Track pumice but isolated outcrops on the felsenmeer-covered upper slopes reveal a competent mass of agglutinated, green, frothy trachyte scoria and pumice enclosing angular, cognate blocks of darker trachyte up to a few centimetres across. The tephra is cut by dykes of similar green, porous trachyte, and an irregular mass at the western end of the summit ridge appears to be part of a small neck about 300 m across.

PETROGRAPHY

It is not possible to discriminate petrographically between the Kakiddi tristanites, trachytes and comenditic trachytes (Fig. 188). All are moderately microporphyritic rocks with up to 10% phenocrystic feldspar ($An_5 Or_{25}$) as 1-2 mm euhedral laths. Sparse, euhedral microphenocrysts of clinopyroxene (< 1 mm) are also present in most Kakiddi thin sections. The pyroxenes are commonly zoned from cores of clear, colourless ferrohedenbergite to rims of deep green, slightly pleochroic, sodic hedenbergite. The groundmass is a holocrystalline mosaic of euhedral feldspar laths ($An_5 Or_{25}$) surrounded by interlocking overgrowths of untwinned alkali feldspar. Green sodic ferrohedenbergite,

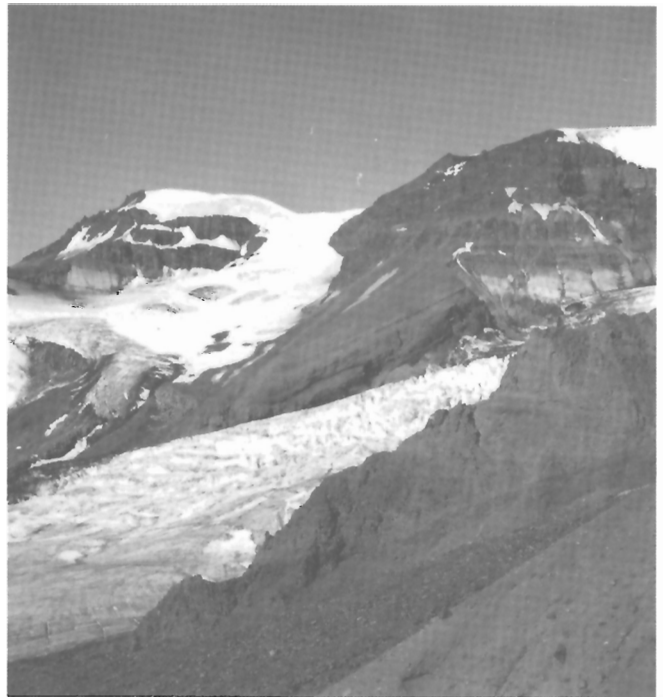


Figure 185. View west into Tennaya cirque. A steeply east-dipping wedge of Kakiddi trachyte pumice is plastered against the truncated remnants of Ice Peak flows that form the headwall. GSC 125 625.

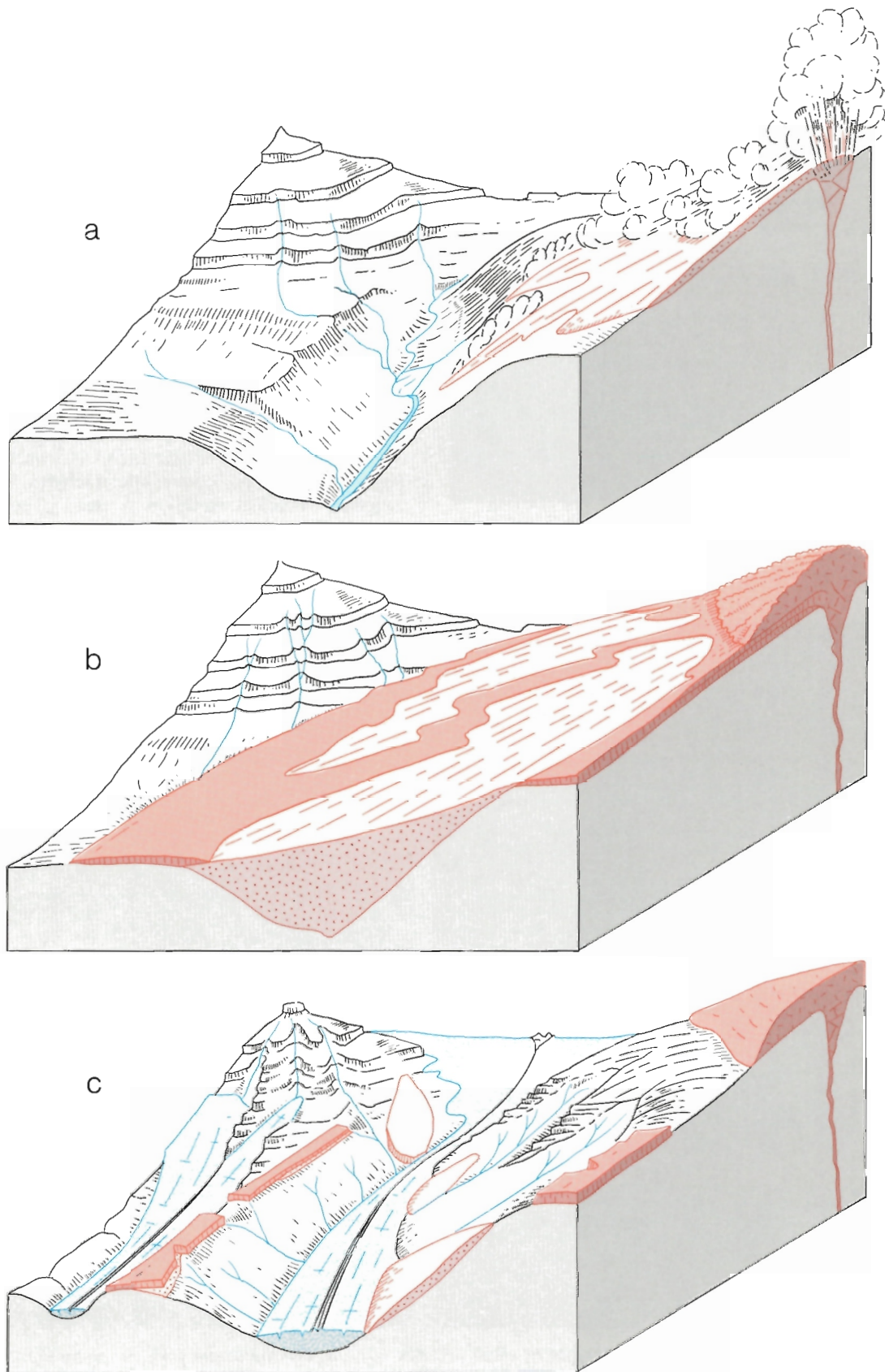


Figure 186. Schematic block diagrams showing the relationship of clastic and pyroclastic deposits in Tennaya Valley to Edziza and Kakiddi flow remnants. (a) Initial eruption in the vicinity of Nanook Dome produces pyroclastic and debris flows that sweep down into upper Tennaya Valley. (b) Trachyte lava flows across the surface of the pyroclastic cone, and the upper part of Nanook Dome is emplaced during the final stages of activity. (c) Present relationship of pyroclastic and flow remnants following post-Kakiddi erosion and alpine glaciation.



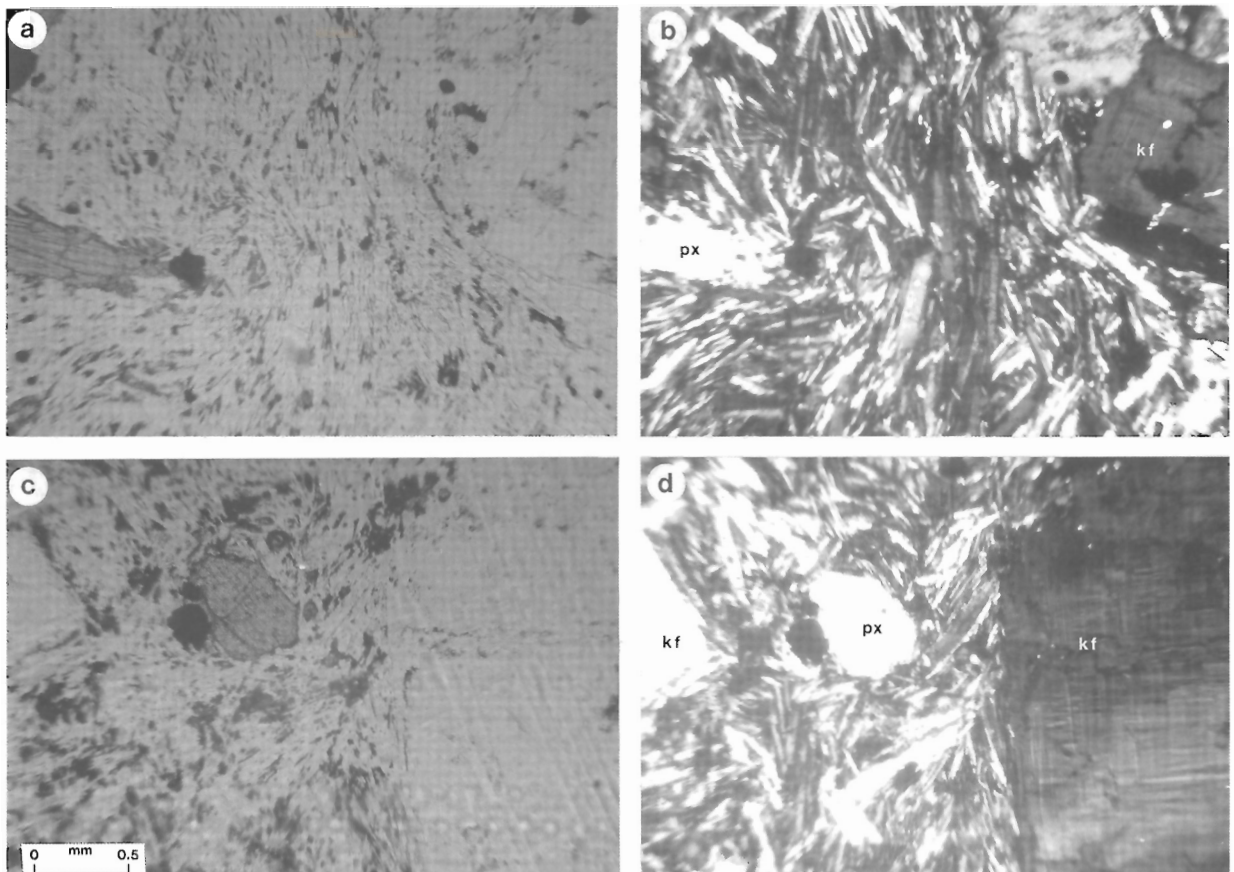
Figure 187. Looking east from Koosick Bluff at Punch cone, a pyroclastic pile of Kakiddi trachyte partly covered by drifts of Sheep Track pumice. GSC 125 626.

aenigmatite and rarely blue, pleochroic arfvedsonite occur only in the groundmass. They are interstitial to the groundmass feldspar and commonly form less than 5% of the rock. Opaque oxides occur as tiny euhedra disseminated in the groundmass and rarely as embayed microphenocrysts.

Probe analyses of representative minerals are reported in Table 17 and plotted on Figure 168.

CHEMISTRY

Eight analyses of specimens from the Kakiddi Formation are plotted on Figures 169 to 171 and three representative analyses are listed in Table 18. All specimens plot within the potassic field of the Ab'-Ab-An diagram and show little scatter on the alkali vs. SiO₂ and AFM plots. The suite includes one tristanite, five trachytes and two slightly peralkaline, comenditic trachytes, but the actual range of chemical variation is small. The rocks of the Kakiddi Formation are chemically indistinguishable from those of the Edziza Formation.



a,b — Trachyte with microphenocrysts of alkali feldspar (kf) and clinopyroxene (px), (a, plane light; b, crossed polarizers).

c,d — Comenditic trachyte with phenocrysts of ferrohedenbergite (px) and anorthoclase (kf), (c, plane light; d, crossed polarizers).

Figure 188. Photomicrographs of Kakiddi rocks; scale bar 0.5 mm.

BIG RAVEN FORMATION

GENERAL GEOLOGY

Introduction

The Big Raven Formation postdates the last episode of regional glaciation. It consists almost entirely of alkali olivine basalt and hawaiite plus a small volume of comenditic trachyte pumice that is assigned to the Sheep Track Member. The basalt issued from at least 30 satellitic vents that lie in a north-south zone extending from the north slope of Mount Edziza, south to Arctic Plateau (Fig. 189). Although some centres produced a single, isolated pyroclastic cone and lava flow, most occur as clusters of related vents from which many separate flows have coalesced into a composite lava field. The sequence of eruptions in each field can be established from the superposition of flows, but the relative ages of flows and cones in different lava fields can only be approximated from their state of erosion.

Weathering and vegetation cover vary with both age and elevation. On the lower slopes and in the valleys even the youngest flows have a sparse cover of stunted trees and shrubs, rooted in pockets of soil among the blocks of lava. Forest cover on the older flows is nearly as dense as that growing on basement rocks. Tree ring studies indicate that this vegetation, including poorly developed trees on the youngest flows, is at least as old as mature trees in the surrounding forest. Thus, lack of vegetation cover on the younger flows is not due to destruction of the forest by the lava, but rather to the slow rate of reforestation on the soilless flow-surface (Fig. 190). Because even the oldest trees of the region are much younger than the youngest flows, it seems probable that the forest was completely destroyed by fire long after the last volcanic activity, and that sparse pioneer vegetation on the flows is at least as old as that in the mature forest. It may, in fact, be older, because sparse, isolated pockets of vegetation on the flow surfaces would be more likely to survive a forest fire than the relatively dense, continuous mature forest.

At higher elevations where growth rates are slower, the difference in plant populations on flows of different ages is even more pronounced than in the valleys. The surface of the oldest flows is partly covered by a thin layer of transported soil that fills all depressions and supports a lush growth of alpine plants identical to that in the adjacent upland tundra. Only the larger features of the flows, the levees, tilted slabs and terminal ridges, form outcrops and the delicate outer rind of scoriaceous basalt and most of the small textural features have already been stripped from their lichen-covered surfaces. Flows of intermediate age support only isolated pockets of pioneer vegetation, and although they retain most of their original surface features, they are

more or less covered by lichen and caribou moss. In contrast, the youngest flows are completely devoid of vegetation, except for sparse patches of lichen. Their rough, blocky surfaces, strewn with precariously balanced slabs and spiny pinnacles of scoriaceous basalt, have remained virtually unchanged since the lava cooled (Fig. 191). Every detail of the original cooling surface, including fragile, paper-thin films and hairlike spines of glass, can still be found in protected depressions and on the underside of slabs.

Like the flows, the associated pyroclastic cones have undergone varying degrees of erosion. The older cones are deeply dissected or reduced to formless mounds of red, scoriaceous rubble. Those of intermediate age retain their original form, but the fine tephra has been washed away, leaving only the larger bombs and agglutinated spatter. A few of the youngest cones retain their mantle of fine cinders, but intermittent meltwater streams have already cut rills and small meandering channels into its surface and carried away the thin outer edge of the surrounding tephra fields.

In addition to differences in erosion and vegetation cover, the flows display minor differences in their original morphology. Blocky surfaces, formed of broken slabs up to several metres across, are the most common. They are characterized by very high surface relief. Levees, piles of upthrust slabs and steep terminal ridges are commonly from 3-12 m high (Fig. 192). These contrast with the relatively smooth uniform surface of other flows, whose surface is a clinkery aggregate of subrounded scoriaceous chunks, rarely more than 0.5 m across (Fig. 193). This latter type tends to have poorly developed levees and gently inclined flow fronts, suggesting a more fluid behavior. Least common are ropy surfaces. They are locally developed near vents, but were not observed in the distal or middle portions of flows.

All of the basalt erupted during Big Raven time is porphyritic with from 15 to less than 1% phenocrysts of plagioclase, olivine and clinopyroxene. The relative proportions of the three phenocrystic minerals, particularly olivine, also varies sufficiently to permit recognition of overlapping flows from different sources.

Desolation Lava Field

The Desolation Lava Field with an area of more than 150 km² is the largest and most conspicuous of the young volcanic features on Mount Edziza (Fig. 194). It covers most of the north slope of the mountain with blocky basalt flows, tephra cones and wind-sculptured ash beds that

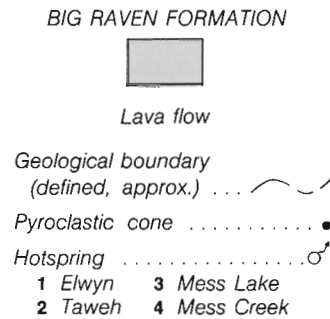
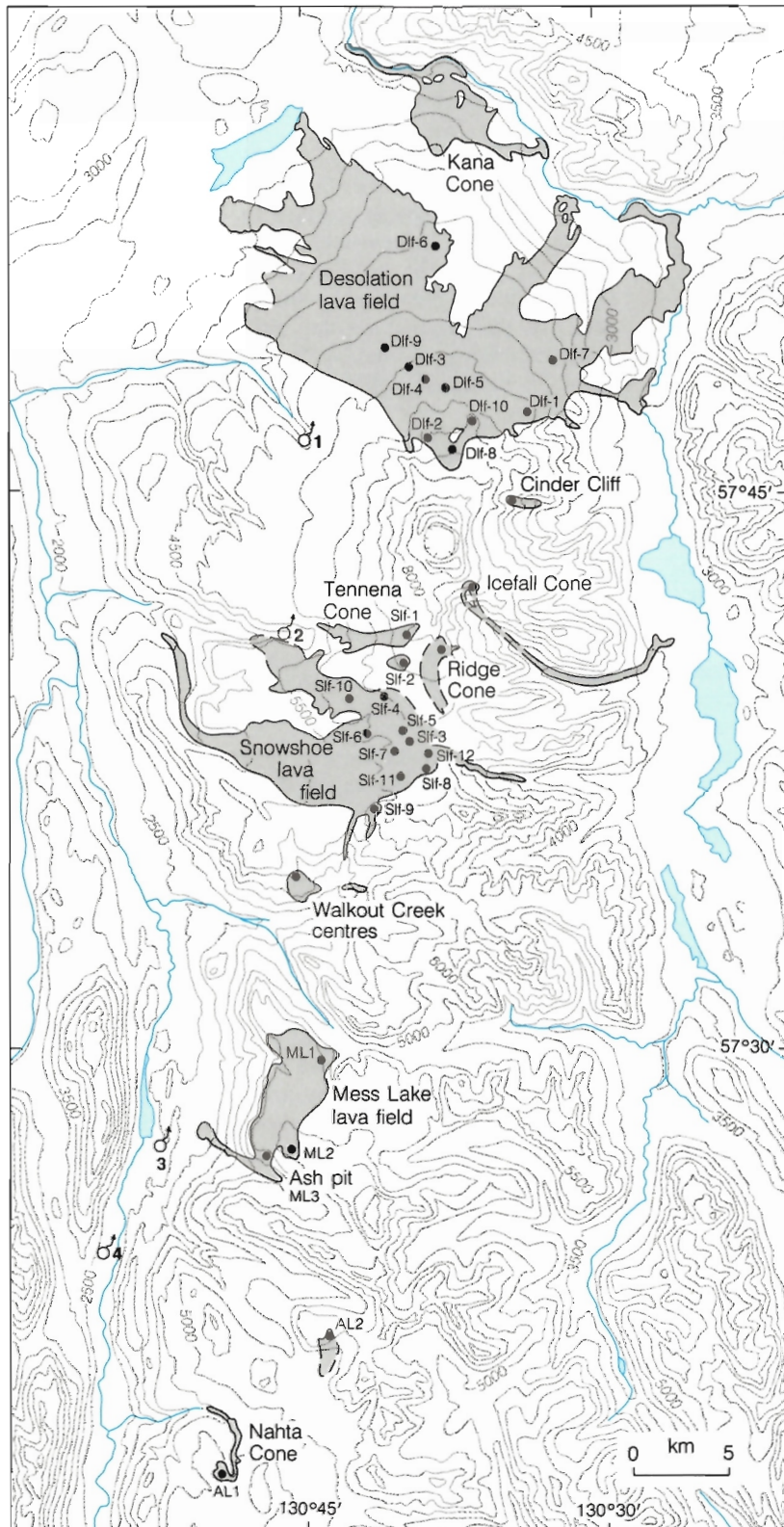


Figure 189. Geological map showing the present distribution of Big Raven basalt flows and pyroclastic cones.

Cones on Desolation Lava Field are: Dlf-1 (Sleet Cone), Dlf-2 (Storm Cone), Dlf-3 to Dlf-5 (Triplex Cones), Dlf-6 (Sidas Cone), Dlf-7 (Twin Cone), Dlf-8 (Moraine Cone), Dlf-9 (Eve Cone) and Dlf-10 (Williams Cone).

Kana Cone is an isolated composite cone on the extreme north slope of the complex. East Slope centres are Cinder Cliff, Icefall Cone and Ridge Cone.

Snowshoe Lava Field contains subglacial centres, Sif-1 (Tennena Cone), Sif-2 and Sif-3; transitional centres Sif-4 to Sif-6, Sif-7 (Coffee Crater), Sif-8; subaerial centres, Sif-9, Sif-10 (Cocoa Crater), Sif-11 and Sif-12 (The Saucer). Walkout Creek centres comprise two small cones.

Mess Lake Lava Field contains ML-1, ML-2 and ML-3 (Ash Pit).

Arctic Plateau is the site of two isolated cones AL-1 (Nahta Cone) and AL-2.

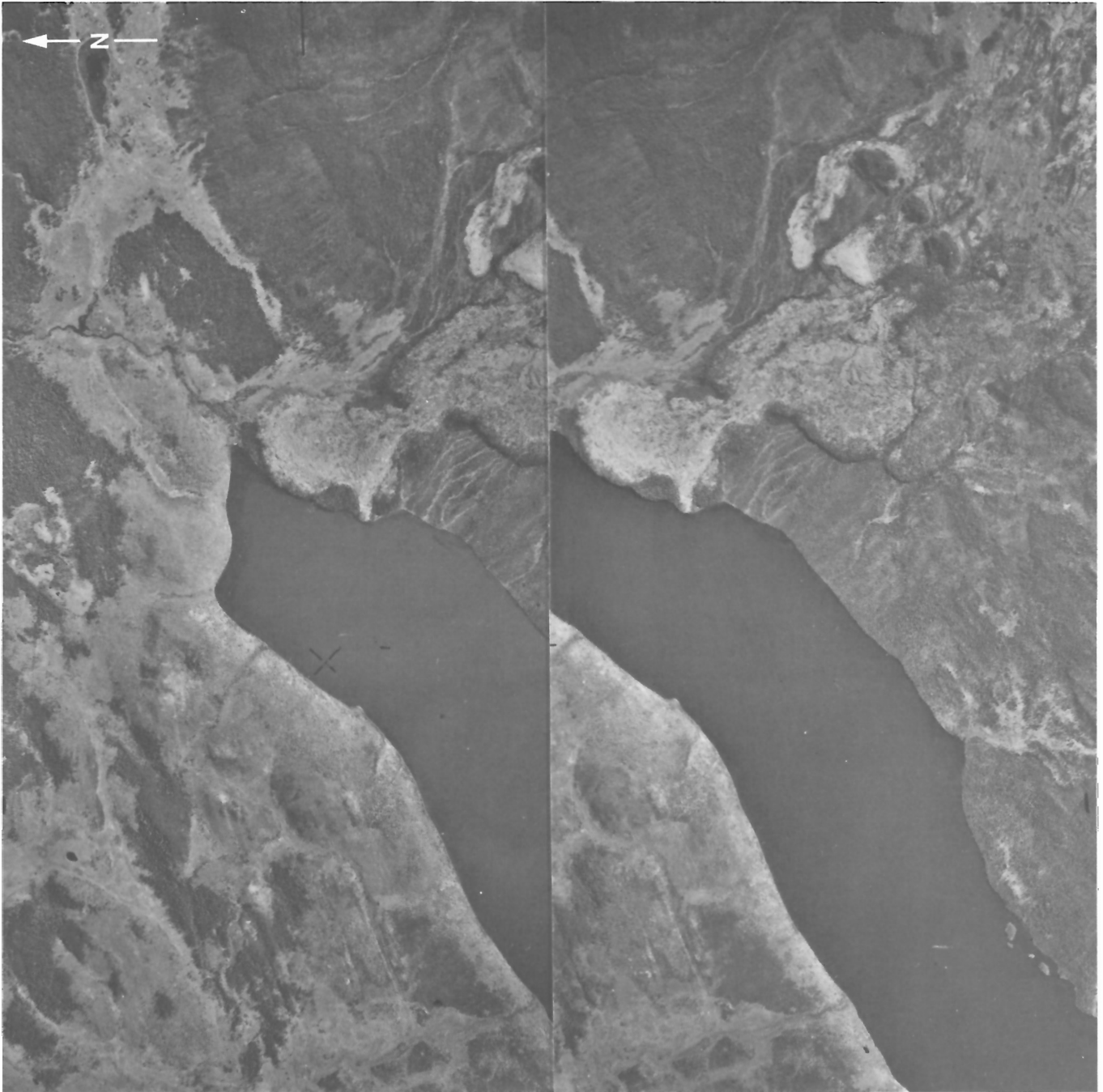


Figure 190. *Big Raven basalt at Buckley Lake. Sparse, stunted trees growing on the blocky flow surface are as old, or older, than trees in the adjacent, mature forest. Note sinuous levees and lava troughs left by flows descending the slope above the terminal flow lobes. Stereoscopic pair. Province of British Columbia photos BC 1373-64, 65.*

MOUNT EDZIZA

issued from at least ten separate postglacial centres. The vents are clustered near the base of the main composite cone of Mount Edziza, at elevations above 4500 ft. (1370 m), but the flows extend down into Klastline Valley (elevation 2200 ft. (670 m)) and to the shore of Buckley Lake (elevation 2700 ft. (820 m)).



Figure 191. Slabs of scoriaceous basalt thrust up onto a levee bounding a young Big Raven flow from Williams Cone in the Desolation Lava Field. GSC 125 627.



Figure 192. Margin of a blocky hawaiite flow from Williams Cone. Levees and terminal ridges formed of broken slabs give such flows a surface relief of up to 12m. GSC 125 628.

The sequence of eruptions (Fig. 194) based on superposition of overlapping flows and, where no overlap occurs, on the degree of erosion and vegetation cover, shows no systematic relationship to the location of the vents. Successive eruptions occurred more or less at random within a circular area about 6 km in diameter on the north slope. In addition to the ten Big Raven vents, the area includes a cluster of four preglacial or intraglacial cones assigned to the Klastline Formation. The morphology and composition of these cones is similar to that of the older Big Raven cones and all are probably part of the same volcanic cycle. However, the Klastline cones are covered by a layer of till which includes clasts of basement rock and must, therefore, be a recessional moraine deposited by retreating ice of the last regional glaciation. This till, which underlies all of the younger cones and flows, is taken arbitrarily as the stratigraphic boundary between Klastline and Big Raven lavas.

Each of the ten pyroclastic cones and associated flow sequences which comprise the Desolation Lava Field display minor differences that reflect both evolution of the magma and changing surface conditions during the period of activity. Informal names and numerical designations used in the following descriptions are keyed to Figure 194.

Sleet Cone (DLF-1) and Storm Cone (DLF-2)

Sleet and Storm cones, the two oldest in the Desolation Field, have been reduced to rounded, mostly soil-covered, conical mounds which retain only the gross features of their



Figure 193. Clinkery surface of an alkali-olivine-basalt flow from Sidas cone. The total relief on such flows is relatively small and levees are either absent or poorly developed. Large mass in centre of picture is a rafted block of agglutinated spatter from the collapsed pyroclastic cone. GSC 125 629.

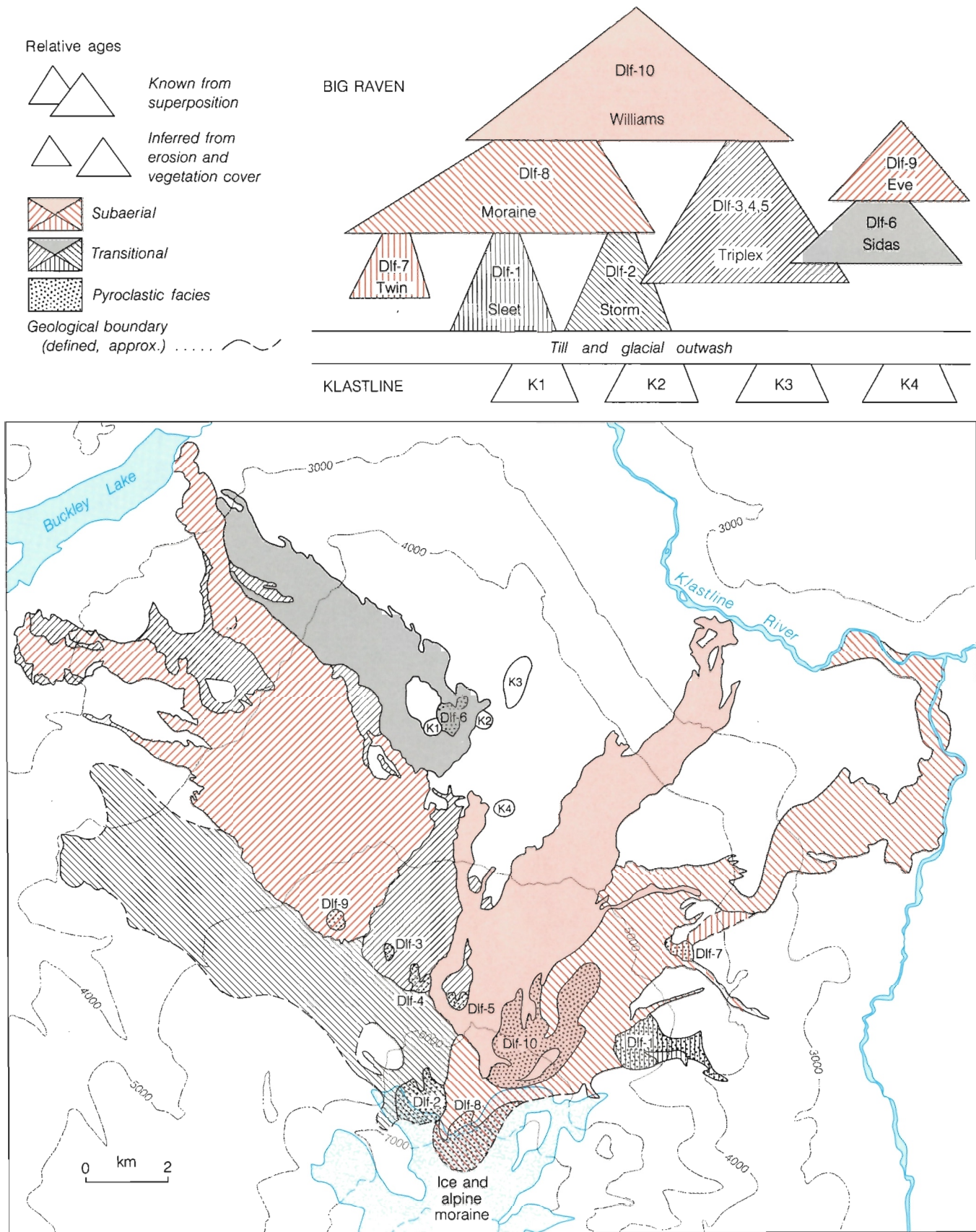


Figure 194. Lava flows and pyroclastic cones of the Desolation Lava Field on the north slope of Mount Edziza. The schematic diagram shows the relative ages of 10 pyroclastic cones in the Desolation Lava Field as inferred from superposition of flows and degree of erosion. Four glacially modified Klastline cones within the area of the Desolation Lava Field are separated from the Big Raven deposits by a layer of till.

MOUNT EDZIZA

original form (Fig. 195). Flows from both rest directly on till and are overlain by a thick wedge of outwash, sand and gravel. Locally, this covering layer is up to 9 m thick and it contains lenses of basaltic ash that originated from the cones themselves and were subsequently added to the load of fluvial sediments. Sleet Cone, with a summit elevation of 5844 ft. (1783 m), appears to consist entirely of red, oxidized subaerial tephra, bombs and spatter. Although it lies

almost on the rim of precipitous cliffs forming the north side of Pyramid Valley, surprisingly little lava spilled into the valley itself. Except for two narrow tongues of basalt, one draped precariously over cliffs of older strata which form the valley wall, the entire mass of Sleet lava was diverted by prominent levees around the north side of the older edifice of Klastline cone where it spread onto the broad, gentle western slope of Klastline Valley.

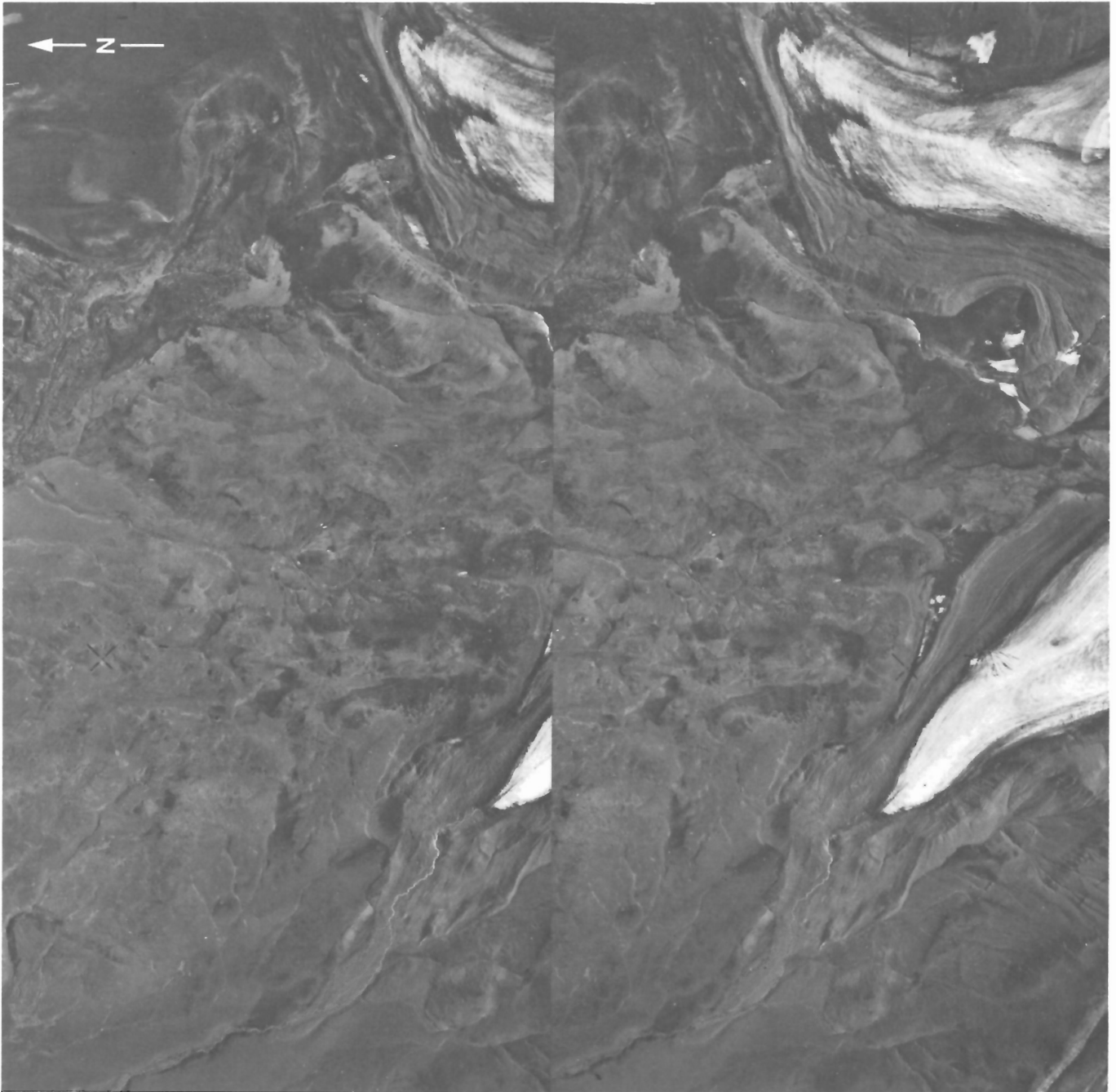


Figure 195. The glacially modified edifice of Storm Cone (lower right) is partly covered by alpine moraine above the trimline of the summit ice cap. The younger edifice of Williams Cone (upper left) is unglaciated and tephra from it covers part of the adjacent moraine. Stereoscopic pair. Province of British Columbia photos BC 1374-26, 27.

Storm Cone, whose 7000 ft. (2135 m) summit is more than 1200 ft. (365 m) higher than Sleet Cone, may have erupted when the receding ice front was at an elevation of about 5500 ft. (1675 m). The subaerial tephra cone and associated flows rest on a pile of tuff-breccia and minor pillow lava. Part of this is probably slide debris from the older tuff-breccia of nearby Pillow Ridge, but much of it contains appreciably more olivine than the Pillow Ridge basalt and is believed to be an early phase of the olivine-rich Storm Cone assemblage. The tuff-breccia consists mostly of lapilli, cinders and small blocks of dark grey, frothy basalt in a brown matrix of sideromelane and crystals. It is commonly well bedded, but attitudes are completely random from one outcrop to another, suggesting that it is a pile of rotated slump blocks. The tuff-breccia was probably deposited in meltwater temporarily ponded around the vent during the initial phase of Storm Cone activity. Much of it must have been deposited on relatively thin ice which, on melting, allowed the bedded tuff-breccia to collapse into a disorganized pile of slump blocks. Ultimately, the meltwater lake drained through a breach in the enclosing ice and exposed the jumbled blocks of tuff-breccia on which subsequent eruptions from the Storm Cone centre built the present, subaerial, tephra cone. During this latter phase, subaerial lava flows streamed across the irregular surface of the tuff-breccia and spread onto the plateau surface for more than 10 km beyond the breached ice front. Paraglacial streams pouring out of the receding ice cap continued to deposit fans of gravel and sand after the Storm Cone eruptions had ceased, and ash thrown onto the ice cap during the eruption was rapidly flushed off and added to the sediment load. The edifice of the pyroclastic cone and lava ridges down to an elevation of about 5500 ft. (1675 m) project above the outwash plane, but flows at lower elevations were covered by up to 10 m of outwash deposits before the next major eruption of Desolation basalt.



Figure 196. The deeply eroded remnants of Triplex Cones form the three low, circular mounds in the middle distance. Flows from Williams Cone have been diverted around one of them and the other two are surrounded by the soil-covered surface of Triplex flows. The symmetrical cone in the background is Eve Cone. GSC 202469-L.

Triplex Cones (DLF-3 to DLF-5)

Lava from a group of three closely related centres 3 km north of Storm Cone rests on ash-bearing outwash gravel deposited after the Storm Cone eruption. The coalescing lava forms a clinkery, partly soil- and lichen-covered surface which extends northwesterly from the cones at 5800 ft. (1770 m) for more than 12 km, almost to the south shore of Buckley Lake. The three pyroclastic cones at their source have been reduced to circular mounds on which the only remnants of their original structure are low concentric ridges of agglutinated spatter and bombs of red, oxidized basalt (Fig. 196). A tongue of frothy black basalt occupies a breach on the north side of the two highest cones (DLF-4, DLF-5), whereas the vent area of the third cone has been completely buried by lava flows.

Sidas Cone (DLF-6) and Twin Cone (DLF-7)

Lava flows from Sidas Cone and Twin Cone, situated respectively on the extreme north and west margins of the cluster of Desolation vents, do not overlap, but similar erosion and vegetation cover suggest they are approximately the same age. The Sidas Cone flows overlie those from Triplex Cones, whereas the Twin Cone flows are isolated from older Desolation lava flows and rest directly on post-Storm Cone, glacial-fluvial gravel. Both Twin and Sidas are complex cones formed by simultaneous fountaining from more than one vent and both produced relatively thin mobile flows of sparsely porphyritic, feldspar-olivine-pyroxene basalt characterized by clinkery surfaces having relatively low relief.

The edifice of Twin Cone (Fig. 197) is a breached pyroclastic cone of which only the northwestern half remains, the southeastern side having slumped away. In its place is a steep-sided lava dome comprising overlapping festoons of smooth, ropy basalt which dip radially outward at 25-30°. The lava pile is pockmarked with pit craters about 100 m across and up to 12 m deep. These, like much of the outer part of the dome, are lined with smooth overlapping lobes of lava draped toward the centre of the depression. These structures are believed to have formed by withdrawal of lava from the central conduit through lava tubes lower in the pile during collapse of the enclosing pyroclastic cone. Superimposed on the lava dome are two pairs of small spatter cones, each about 15 m high, with symmetrical summit craters 6-9 m deep. These mark the final stage of Twin Cone activity and all four conelets appear to have formed during the same fountaining event.

Sidas Cone (Fig. 198) is a composite of two overlapping cones which have merged into a single, elliptical mound of tephra containing two conical summit craters. These are separated by a narrow septum of agglutinated spatter, and each has breached the opposite rim of the cone, thus effectively splitting it longitudinally (north-south) into two, nearly symmetrical halves. The fact that both craters are still intact indicates that they were formed by simultaneous fire

MOUNT EDZIZA

fountaining during the latter stages of eruption. The Sidas Cone lava also issued from two separate vents on opposite sides of the tephra cone. That issuing from the northern vent was channelled by prominent levees into a well-defined stream which flowed northwest directly downslope. Lava from the south vent was initially ponded behind the edifice of Sidas Cone itself, and an adjacent, older cone (K1) of Klastline age. It welled out to form a low dome of overlapping lobes before streaming southwestwardly around the obstructions and merging with the northern lobe.

The combined discharge from the two Sidas Cone vents formed a lava field about 1.5 km wide which extends more than 8 km from its source, almost to Buckley Lake. Except for levees near its source, the lava surface has relatively low

relief. Its surface is a jumble of clinkery rubble in which the rough, nearly spherical blocks are rarely more than 0.6 m across. The lava, throughout the entire field, is extremely uniform medium grey, sparsely porphyritic basalt with small phenocrysts of clear plagioclase in ragged, crudely aligned crystals up to 0.5 cm long, and tiny, rare crystals of olivine and clinopyroxene.

Sparse but widely distributed accretionary lava balls are characteristic of the Sidas Cone lava field (Fig. 193). These giant blocks up to 10 m across have cores of bright red, well-bedded agglutinated spatter, bombs and lapilli more or less covered by an outer rind of lava. They clearly originated as blocks torn from the pyroclastic cone and were rafted to their present positions on the flow surface. The outer rind

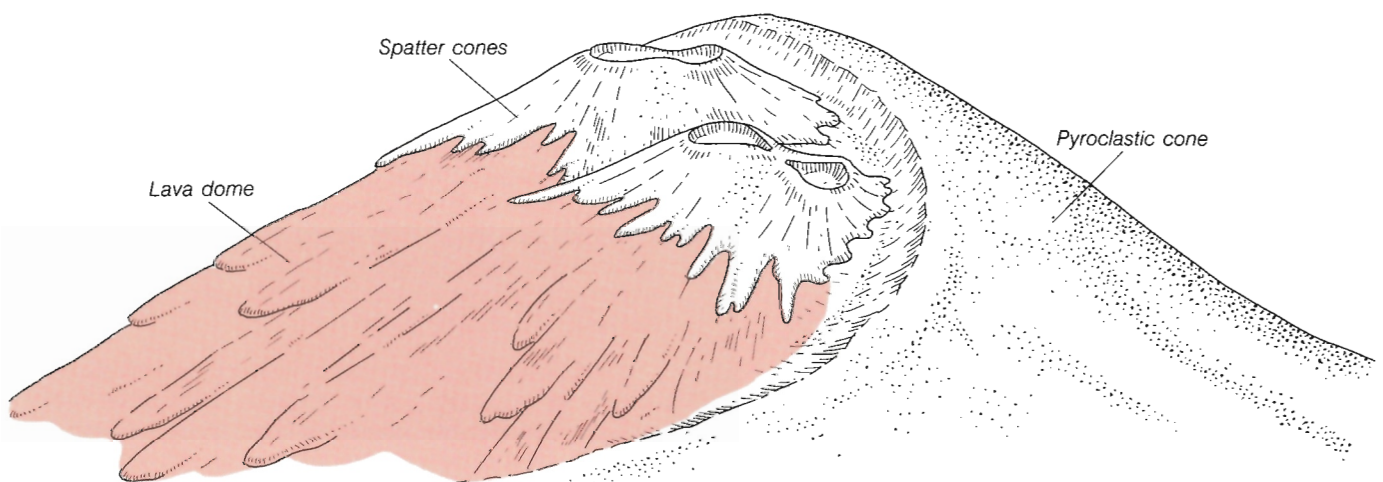
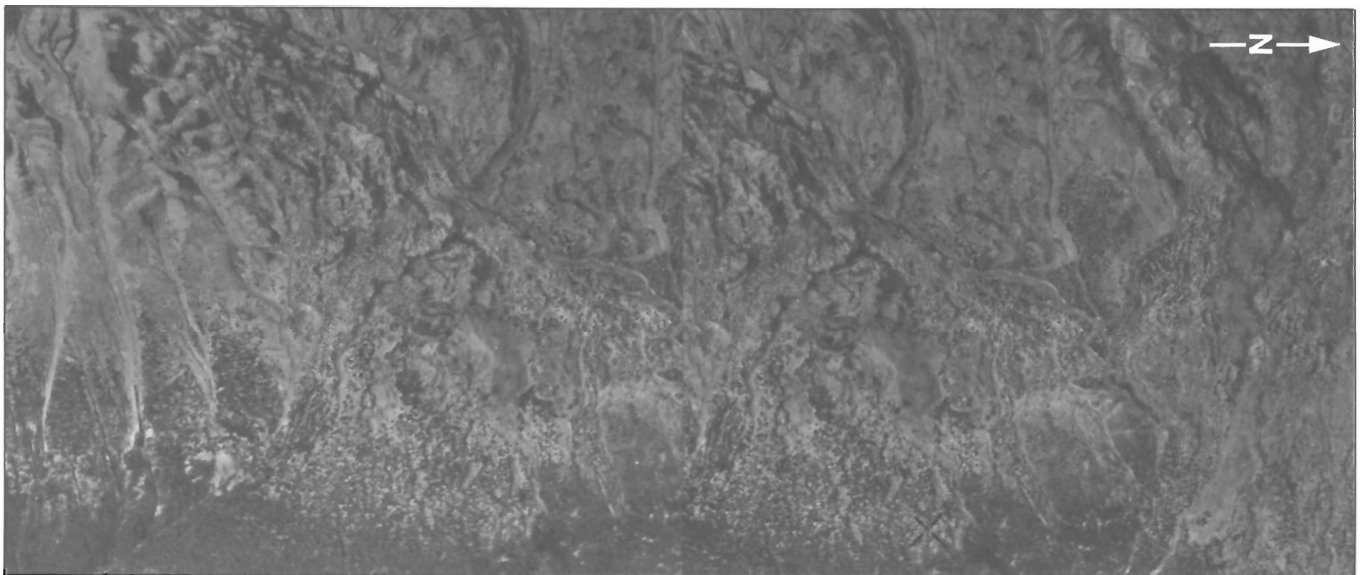


Figure 197. Stereoscopic pair and sketch map of Twin Cone showing the relationship between the truncated pyroclastic cone, the lava dome, and the two pairs of younger spatter cones. Province of British Columbia photos BC 1367-9, 10.

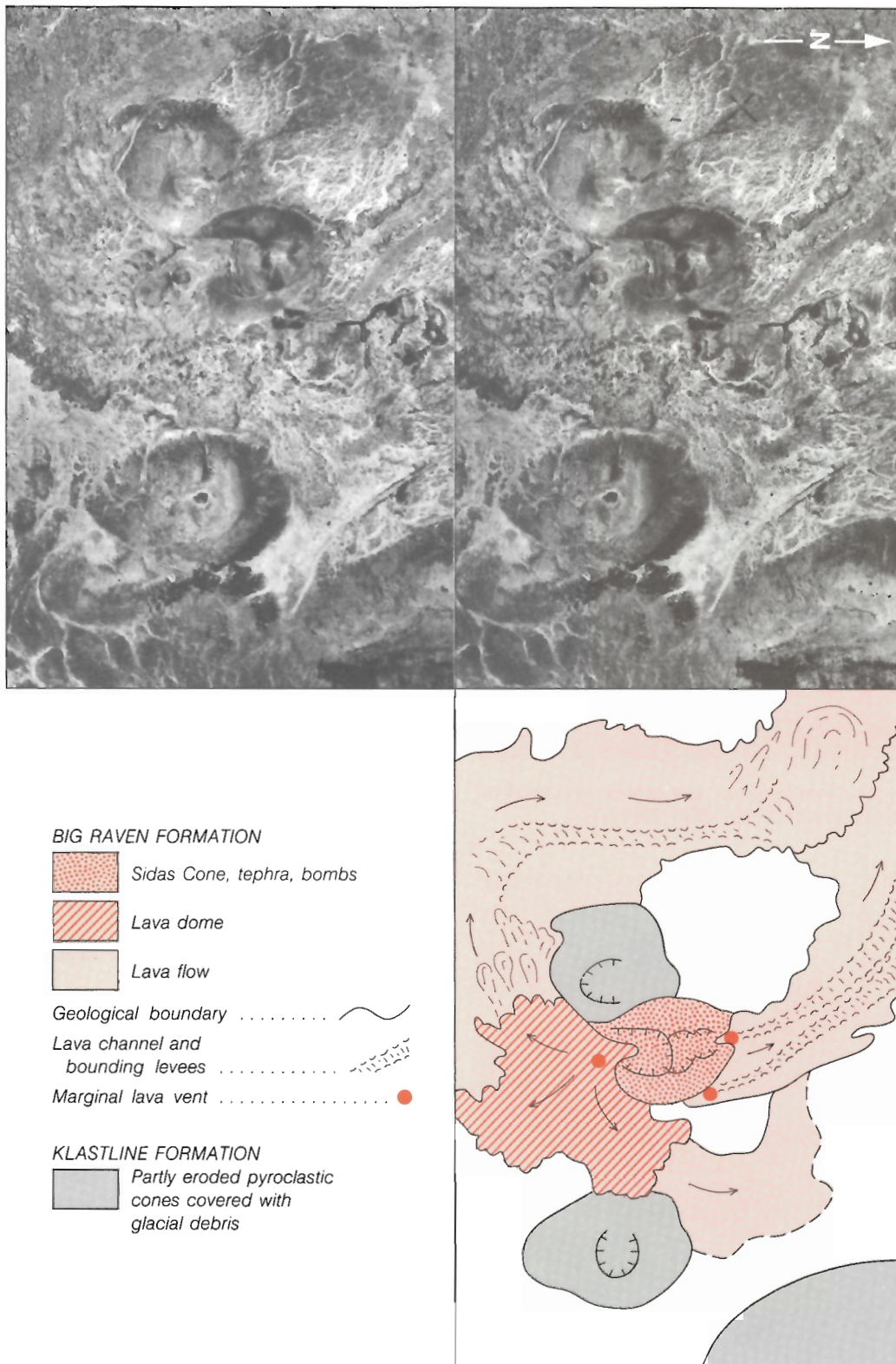


Figure 198. Stereoscopic pair and sketch map of Sidas cone. The pyroclastic cone contains two craters which must have formed by simultaneous fountaining from two adjacent vents. Sidas cone, and lava that issued from its north and south flanks, have partly overridden two nearby cones of late Klastline age. Province of British Columbia photos BC 1374-30, 31.

MOUNT EDZIZA

of lava must have adhered to them after the blocks slumped from the collapsing cone into molten streams of lava issuing from the vent. There is no evidence that they were further modified during as much as 4 km of transport on the clinkery flow surface. The presence of these blocks, scattered across the length and breadth of the Sidas Cone lava field, suggests that the partial collapse of the pyroclastic cone occurred several times during the course of the eruption. Breaching of the two present craters by upwelling lava or phreatic explosions was probably only the most recent in a succession of events that periodically destroyed parts of the growing cone, and added blocks of pyroclastic debris to the outpouring streams of lava.



Figure 199. Agglutinated spatter and cow-dung bombs in the central part of Moraine Cone. GSC 202469-M.



Figure 200. Steeply inclined, overthrust slabs of vesicular basalt and rafted block of agglutinated spatter on the surface of the most recent flow from Williams Cone. GSC 125 630.

Moraine Cone (DLF-8)

Moraine Cone is the most southerly and, at nearly 7000 ft (2135 m), the highest of the Desolation vents. Its edifice has been almost completely destroyed by alpine glaciation and most of the remainder is covered by marginal moraine flanking tongues of ice projecting from the central ice cap. Only the northwestern margin of the pyroclastic cone and its breached northern side project beyond the recent glacial cover. The cone consists almost entirely of coarse bright red agglutinated spatter and large globular and cow-dung bombs (Fig. 199). A breach in the north side exposes the ropy, unglaciated surface of the last lava to issue from the vent. Similar ropy surfaces are present on most of the slabs that characterize the blocky lava field which spreads northeast from Moraine Cone onto the northeastern slope of the mountain. Although the cone has been largely overridden by recent alpine glaciers, it does not exhibit any ice contact deposits such as those associated with Storm Cone. Thus, between Storm Cone and Moraine Cone activity, the central ice cap must have receded above its present limits. A pocket of pillow lava at the base of the Moraine Cone flow, where it spreads out onto the plateau surface (elevation 5200 ft. : 1585 m), probably formed where the lava entered a small lake and not as an ice-contact deposit. The proximal part of the Moraine Cone lava field rests on glacial-fluvial gravel and is partly covered by outwash deposits of fine gravel and sand which separate it from younger lavas and ashbeds of Williams Cone. The more distal portions rest directly on older colluvium or bedrock, and no younger deposits have accumulated on its blocky, unglaciated surface. The main lava stream enters the valley of Kakiddi Creek, 3 km above its junction with Klastline River and extends along the valley into Klastline Valley itself. Thus, both Kakiddi Creek and Klastline River were temporarily ponded behind dams of Moraine Cone lava. Both streams have subsequently etched new channels around or through the barriers, exposing beds of lacustrine silt in small terraces upstream from the lava.

Eve Cone (DLF-9) and Williams Cone (DLF-10)

Eve Cone and Williams Cone are the two youngest eruptive centres in the Desolation Lava Field. Both have produced about the same volume of porphyritic basalt (hawaiite) with abundant plagioclase and sparse phenocrysts of olivine and pyroxene. Flow surfaces have extremely high relief characterized by intertwined lava troughs flanked by sharp-crested levees up to 6 m high. The surface is a jumbled mass of large, precariously balanced blocks and tabular chunks of the original lava crust. The latter are commonly thrust one over another to produce stacks of warped, steeply inclined slabs of vesicular basalt (Fig. 200). Lava has completely drained from many of the troughs in the proximal part of the flows leaving only thin broken remnants of the scoriaceous crust which collapsed between the levees that contained the flow.

Eve Cone (Fig. 201) is a perfectly symmetrical pyroclastic cone that rises 150 m above the plateau surface to a circular, sharp-edged summit crater about 45 m deep. Its outer surface is a loose aggregate of bombs, cinders and ash which lie at the angle of repose (about 35°). Along the rim and steep inner face of the crater, the bombs and bright red agglutinated spatter are lightly welded into a porous but cohesive mass with crude outward dipping bedding (Fig.



Figure 201. *Eve Cone, a symmetrical pyroclastic cone that rises 500 ft. (150m) above the surface of the Desolation Lava Field. GSC 125 631.*



Figure 202. *Crudely bedded, agglutinated spatter and bombs exposed in the crater wall of Eve Cone. GSC 202469-N.*

202). A sharply defined colour difference, clearly visible on air photos separates the northern and southern halves of the cone. The northern half is covered with relatively fine, dark grey cinders and bombs, whereas the southern half is predominantly red, oxidized bombs and coarser clinkery spatter similar to that forming the steep inner walls of the crater. This may be due in part to deposition of a greater thickness of fine relatively cool tephra on the north side of the cone during the waning stages of activity. However, the south side has clearly been more deeply eroded. The dark tephra beds are truncated at the colour boundary and appear to have been stripped from the south face of the cone. Preferential wasting of the south slope is probably due to more extreme and more frequent temperature changes, and hence to accelerated frost wedging and solifluction.

Most of the Eve Cone lava appears to have issued from vents around the base of the cone, particularly on the south-east side where overlapping tiers of lava lobes form a broad buttress that stands almost 30 m above the general level of the surrounding lava field. Except for the mixed tephra of the cone itself, ash from the Eve Cone eruption has been completely stripped from the surrounding plateau. The proximal flows and the base of the cone support a sparse cover of pioneer vegetation and lichen.

Williams Cone (Fig. 203), over 900 ft. (275 m) high and 1.2 km across at the base, is the largest and youngest pyroclastic cone in the Desolation Lava Field. Its western side has slumped away leaving a large, steep-sided amphitheatre, within which a smaller cinder cone and several lava vents formed during the final stages of activity. Part of the debris from the main collapsed cone has piled up in mounds of rubble west of the breach, but much of it must have been rafted away on the lava flows. One such block, about 9 m across, is lodged in the narrow cleft between the inner rim of the main breached crater and the secondary, nested cone. It is half submerged in the steeply inclined stream of solidified lava and its core of bedded, agglutinated spatter and bombs, is encased in a 0.5 m rind



Figure 203. *Looking east into the breached crater on the western side of Williams Cone. GSC 202469-O.*

MOUNT EDZIZA

of similar lava (Fig. 204). The block, obviously broken from the walls of the adjacent cone, was being rolled along by the stream of lava when the eruption ceased and it came to rest in its present position.

Lava from several vents on the north and east base of Williams Cone merged with that from the breached central crater to form a broad stream of lava about 1.5 km wide and 13 km long. Unlike Eve Cone, much of the fine ash that settled on the lee side of Williams Cone is still present, indicating that it is the younger. The original tephra plume must have blanketed most of the plateau surface northeast of the cone but the fine, distal portion has been almost completely washed away. A few small patches of unconsolidated tephra comprising 1-3 mm particles of black frothy scoria occur up to 9.5 km northeast of the vent. Both grain size and thickness increase toward the source, and proximal beds of iridescent black frothy cinders 5-20 mm across are up to 4.5 m thick at the base of the cone. The base of the tephra is exposed in the banks of small streams northeast of the cone where it rests in a mature paleosol (Fig. 205). The charred, but still flexible stalks of alpine willow project into the lower few centimetres of tephra and a dense mat of roots is still preserved in the underlying paleosol. A ^{14}C date of 1340 ± 130 BP was obtained on willow twigs preserved within the tephra.

Kana Cone

Kana Cone is the most northerly vent of the Mount Edziza Volcanic Complex (Fig. 189). It is mainly covered with vegetation but its original circular form is well



Figure 204. Accretionary lava ball partly submerged in a solidified stream of lava on the breached, western flank of Williams Cone. Agglutinated spatter and bombs, forming the core of the lava ball, are part of the pyroclastic cone which collapsed into the stream of lava and became coated with a rind of molten basalt. GSC 202469-P.



Figure 205. Paleosol with roots and charred twigs of alpine willow beneath basaltic tephra on the lee side of Williams Cone. GSC 125 632.

preserved, and outcrops of brick red agglutinated spatter and bombs are exposed along its crest and within the central crater. The edifice is about 200 ft. (60 m) high with a conical summit crater about 20 m deep which is breached on the north. Red, highly scoriaceous lava within the breach is continuous with flows that fan out onto the slope below the cone and extend down into Klastline River valley. The lava appears to have issued in several pulses, each giving rise to a new set of marginal levees and terminal ridges (Fig. 206). The latter are 4.5-7.5 m high and form a series of terrace-like steps on the slope below the cone. Fresh lava was diverted around the terminal ridges of preceding flows, forcing the field to grow wider with each successive eruption. One lobe, diverted eastward around the growing pile and contained by high levees, flows almost normal to the original slope and enters Klastline Valley more than 5 km upstream from the main western lobe.

Both the eastern and western lobes of lava from Kana Cone flowed around flat-topped, erosional remnants of Klastline lava, which previously flooded the old valley, and advanced into the new channel, forcing the river tight against the northern valley wall. Above each of these obstructions, the river began to aggrade its course, forming a broad floodplain of gravel bars across which the present river meanders. On and below these dams the displaced river rapidly incised a new channel around or through the lava. On the narrow tongue of lava that extends down Klastline Valley from the western lobe, the river was initially confined by the lava levees themselves and began to etch its new course into the centre of the flow. The resulting box-canyon exposes up to 20 m of columnar basalt in cross-section, yet the scoriaceous blocky surface of the flows and levees bounding the canyon walls are scarcely modified by erosion.

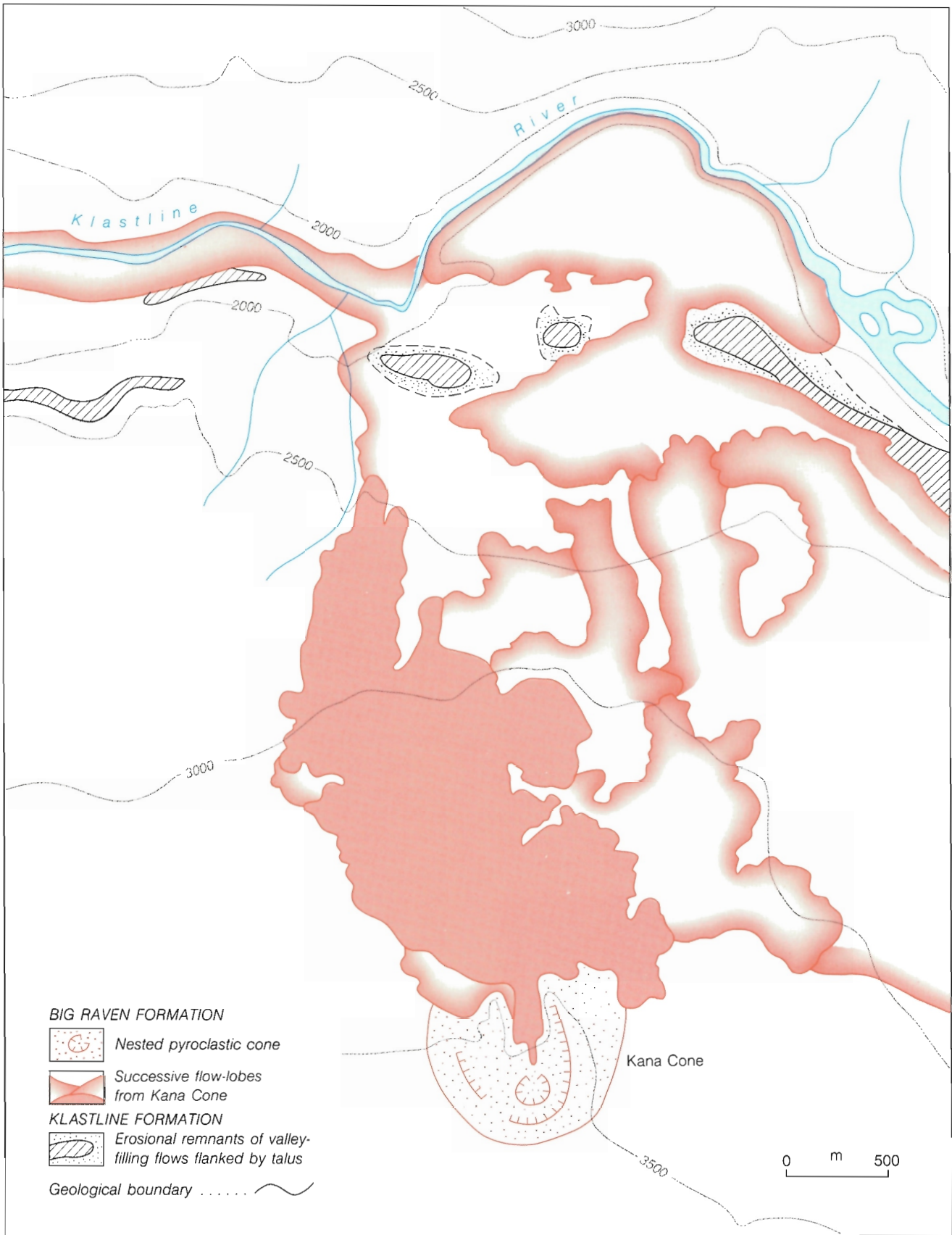


Figure 206. Detailed map of Kana Cone showing lobes and levees formed by successive pulses of lava that issued from the central vent and temporarily dammed Klastline River. Flows from this vent may have extended along Klastline Valley as far west as Stikine River.

No mineralogical variation was observed within the Kana Cone pile. It is uniform porphyritic basalt with 10 to 15% phenocrysts of clear feldspar (3-5 mm), black pyroxene (2-3 mm) and olivine (1-2 mm) in a medium grey, fine grained groundmass. Open vesicles are present in all of the flows examined, including the lower part of those exposed in cross-section.

East slope centres

At least three satellitic centres on the deeply dissected eastern slope of Mount Edziza postdate the present topography (Fig. 189). They are isolated from one another and from the large lava fields of the north and south slopes, but their lithology, feldsparphyric olivine basalt with many open vesicles, is typical of Big Raven basalt. Because of their location on the eastern face of the mountain with its active alpine glaciers and unstable, oversteepened slopes, both the cones and flows have been relatively deeply eroded and extensively covered by glacial, fluvial and landslide deposits.

The Cinder Cliff (Fig. 207) is a 700 ft. (210 m) high barrier of thin, slaggy olivine basalt flows, scoria and tuff-breccia in the north fork of Tenchen Creek. The pile fills the narrow western part of the valley to a depth of about 150 m. It is truncated on the east by steep rubbly cliffs and no remnants of more distal flows appear farther downstream, suggesting that the lava was ponded in the upper part of the valley behind an ice dam. The base of the pile includes mixed deposits of ash, tuff-breccia and glacial-fluvial gravel. Pockets of gravel as well as isolated stream boulders are present in the tuff-breccia, probably dumped in from the ice surface during the initial stages of eruption and melting. Quench features, including pillows and splays of small diameter columns are present, along with sideromelane tuff-breccia, in the lower 15-30 m of the pile. Above that, the Cinder Cliff consists entirely of rubbly subaerial flows and scoria. Thus, the initial body of meltwater must have



Figure 207. The Cinder cliff, a 700 ft. (210 m) high barrier of thin, slaggy basalt flows ponded in the north fork of Tenchen Creek valley. Ridge in background is Nido subaqueous tuff breccia. GSC 202469-Q.

drained away down the valley fairly soon after the onset of activity. Subsequent lava, protected from the ice by an insulating layer of ash and rock debris, must have partly overridden the upper edge of the ice dam (Fig. 208). Quenching must have occurred at the distal end of these supraglacial flows where the lava streams passed onto the ice surface, but in the proximal part of the pile that is now exposed, the upper part of the section has no water contact features. The present escarpment of Cinder Cliff is probably not the location of the ice barrier but rather the point at which the lava overrode the glacier and subsequently collapsed into rubble when the ice core melted.

Above the Cinder Cliff, the lava along with any cinder cone that may have been developed there, is completely covered by recent alpine moraine and active talus, but above the talus the white slopes of Pyramid rhyolite are cut by feeder dykes of olivine basalt. These stand out as prominent spiny ribs of black scoriaceous basalt up to 2 m wide and 3 m high (Fig. 209). The dyke rock contains numerous inclusions of angular to subrounded rhyolite up to 0.3 m across. These exhibit varying degrees of partial melting and are completely surrounded by a red reaction rim. Similar, but much less abundant inclusions, are also present in most of the Cinder Cliff flows. They are probably of surficial rather than deep-seated origin, having slid into the lava from the steep talus-covered valley walls. Inclusions in the dykes are also believed to be from talus or moraine through which the dykes cut. This also explains why the relatively fragile, easily eroded scoriaceous basalt of the dykes now stands in high relief on the relatively competent rhyolite of the wall rock. The exposed portion of the dykes must originally have been contained by a layer of rocky colluvium which has since eroded away.

The valley glacier that formed the Cinder Cliff ice dam was tributary to a much larger valley glacier which extended down Tenchen valley and spread out into a broad terminal lobe in Kakiddi Creek valley. Moraines and other features associated with this lobe of ice have been almost completely buried by epiglacial outwash which forms a huge, kettled alluvial fan that has forced Kakiddi Creek against the opposite valley wall. However, a small kame field north of the fan, on the east side of Kakiddi Creek, has escaped subsequent erosion and burial. It is a nearly flat, elliptical area


- 
- a — Initial eruption from vents on the valley wall and deposition of tephra on the glacier.
 - b — Advance of lava flows across the tephra and melting of underlying ice.
 - c — Collapse of lava, ash, and residual ice in lower part of valley.
 - d — Advance of glacier in upper part of valley and deposition of alpine moraine on top of the Cinder cliff.

Figure 208. Series of schematic cross-sections showing the inferred relationship of the Cinder cliff to residual ice in the north fork of Tenchen Creek valley.

BIG RAVEN FORMATION

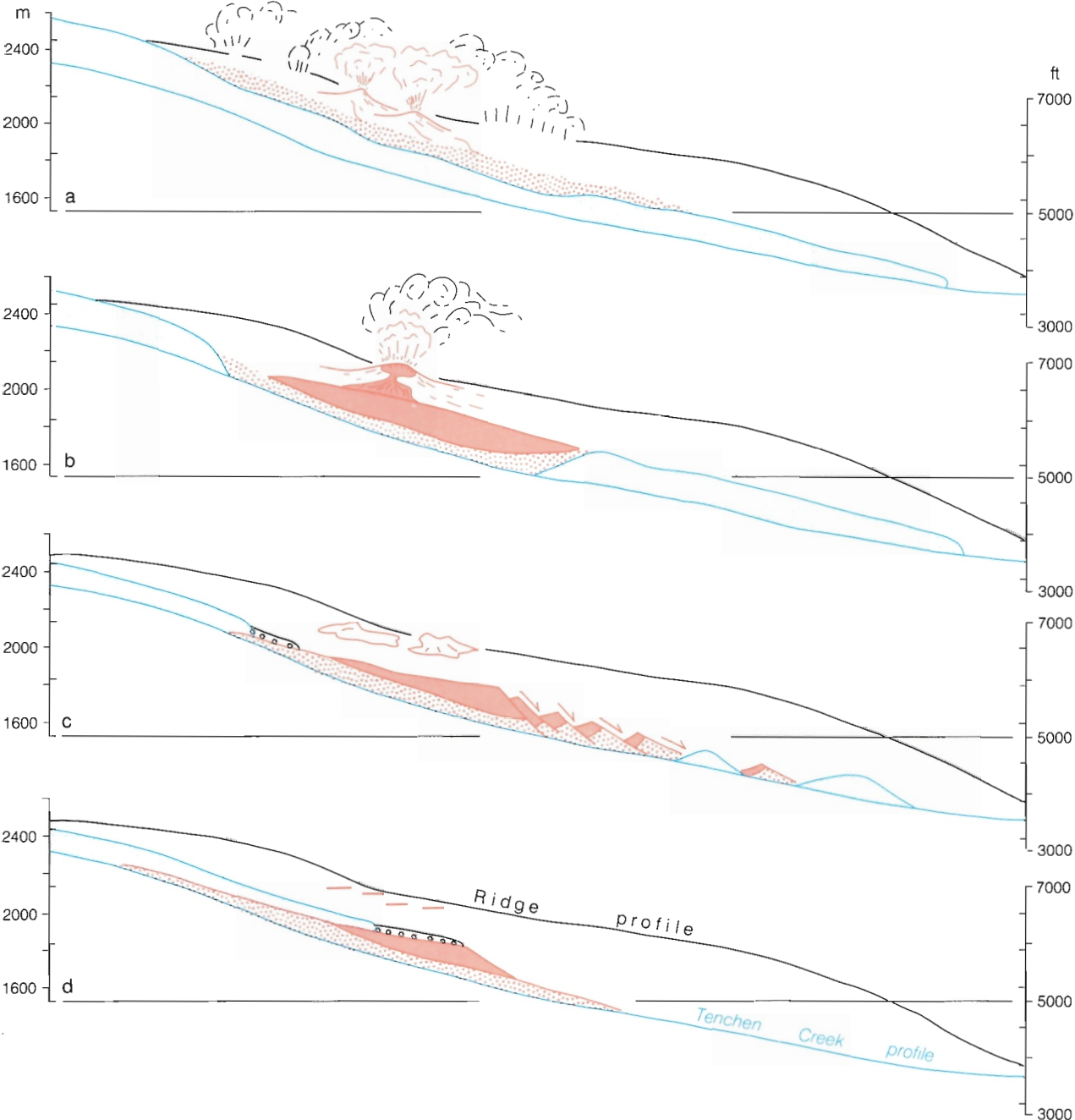




Figure 209. Feeder dyke of scoriaceous basalt cutting Pyramid rhyolite on the slopes above the Cinder cliff. GSC 202469-R.

of about 1.3 km² dotted with clusters of circular mounds from 15-30 m across and up to 9 m high. Material in the mounds is mainly fine ash and cinders, probably thrown onto the ice from the Cinder Cliff vent, carried to their present location as pockets on the ice surface, and deposited as kames when the glacier stagnated and finally melted. If this was the source, then the valley glacier must have persisted long enough after the Cinder Cliff eruption to transport their load of superincumbent ash for at least 6.5 km.

The remains of two additional young, satellitic centres are preserved high on the eastern rim of Ice Peak. Both are at an elevation of about 7500 ft. (2285 m), near the steep headwalls of active cirques and consequently they have been greatly modified by recent alpine glaciation, rockfalls and slumping. Icefall Cone (Fig. 189), on the northeast spur of Tennaya Cirque, has been completely overridden by glacier ice and its surface covered by moraine. Gullies on the south side expose red, loosely agglutinated spatter and bombs, associated with thin, slaggy flows of olivine basalt. Ridge Cone (Fig. 189), on the western rim of Idiji Cirque, has also been glaciated and is now almost completely covered by permanent snow. A section through its eastern edge, along the crest of the headwall, exposes beds of agglutinated spatter, bombs and cinders alternating with slaggy flows of vesicular basalt, in which the olivine, like that near other Big Raven vents, has been altered to dull red iddingsite.

Flows originating from these two centres have been almost completely covered by glacier ice, moraine, talus and fluvial gravel. Two small tongues of vesicular olivine basalt which project from beneath Tenchen Glacier onto the flat surface at the western end of Sorcery Ridge, are believed to be part of a lobe which spreads south from Ridge Cone. However, most of the lava from both Ridge and Icefall must have cascaded down the steep east-facing headwalls into Tennaya Valley. The only exposure of these proximal flows is a small bluff below Icefall Cone where three thin flows of scoriaceous olivine basalt appear to rest on, and are completely surrounded by, moraine. Similar basalt

appears 4 km farther downstream where a blocky, scoriaceous flow surface first projects through the thick layer of colluvium filling the upper part of the valley. From there it is intermittently exposed for another 6.5 km, almost to Kakiddi Lake. It occupies a narrow, wedge-shaped notch eroded along the north edge of the older, and much thicker flow of Kakiddi trachyte which previously flooded the valley (Fig. 210). The lower 2 km of the basalt flow are well exposed, revealing prominent, sharp-crested levees up to 7.5 m high and a blocky to slaggy unglaciated surface. The source of this flow is unknown. It could be from the Ridge or Icefall centres but it is more likely from some undiscovered source within the valley itself. A rounded hill now completely covered with surficial deposits occupies the valley bottom a short distance below the trimline of Tennaya Glacier. It may be the remains of a cinder cone and the source of the flow.

Snowshoe Lava Field

Blocky basalt flows, scoria and tephra cones of the Snowshoe Lava Field cover an area of about 40 km² on the southwestern flank of Ice Peak (Fig. 211). Although approximately the same age as the Desolation Lava Field, much of the surficial detail of the Snowshoe Lava Field is obscured by air-fall pumice of the Sheep Track Member which blankets the cones and most of the upper flows. The lava issued from a cluster of vents, mostly above 6000 ft. (1800 m), which lie near the lower edge of broad, platter-shaped glaciers projecting radially from the central ice cap. The glaciers have receded from well defined trimlines which lie up to 0.5 km beyond the present ice front and suggest that the ice surface during its maximum advance was 90-150 m above its present level. Snowshoe volcanic activity began during the climax of this glacial period, and so the early eruptions produced mainly subaqueous, ice-contact deposits. Volcanism continued during retreat of the ice, producing a group of transitional piles with both subaqueous

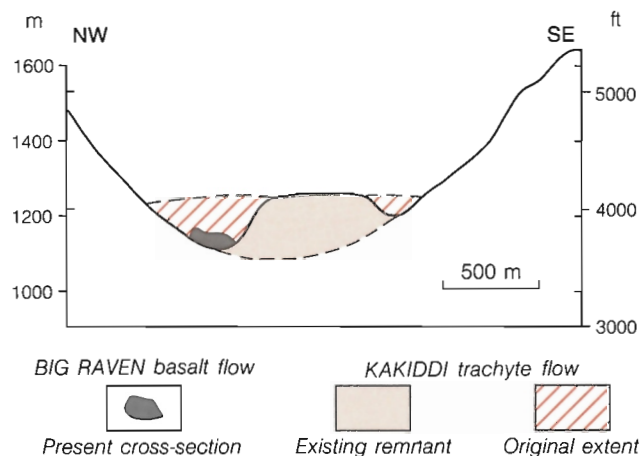


Figure 210. Cross-section of lower Tennaya Valley showing the relationship of Big Raven basalt flows to an older trachyte flow of Kakiddi age.

Relative ages of cones, from superposition

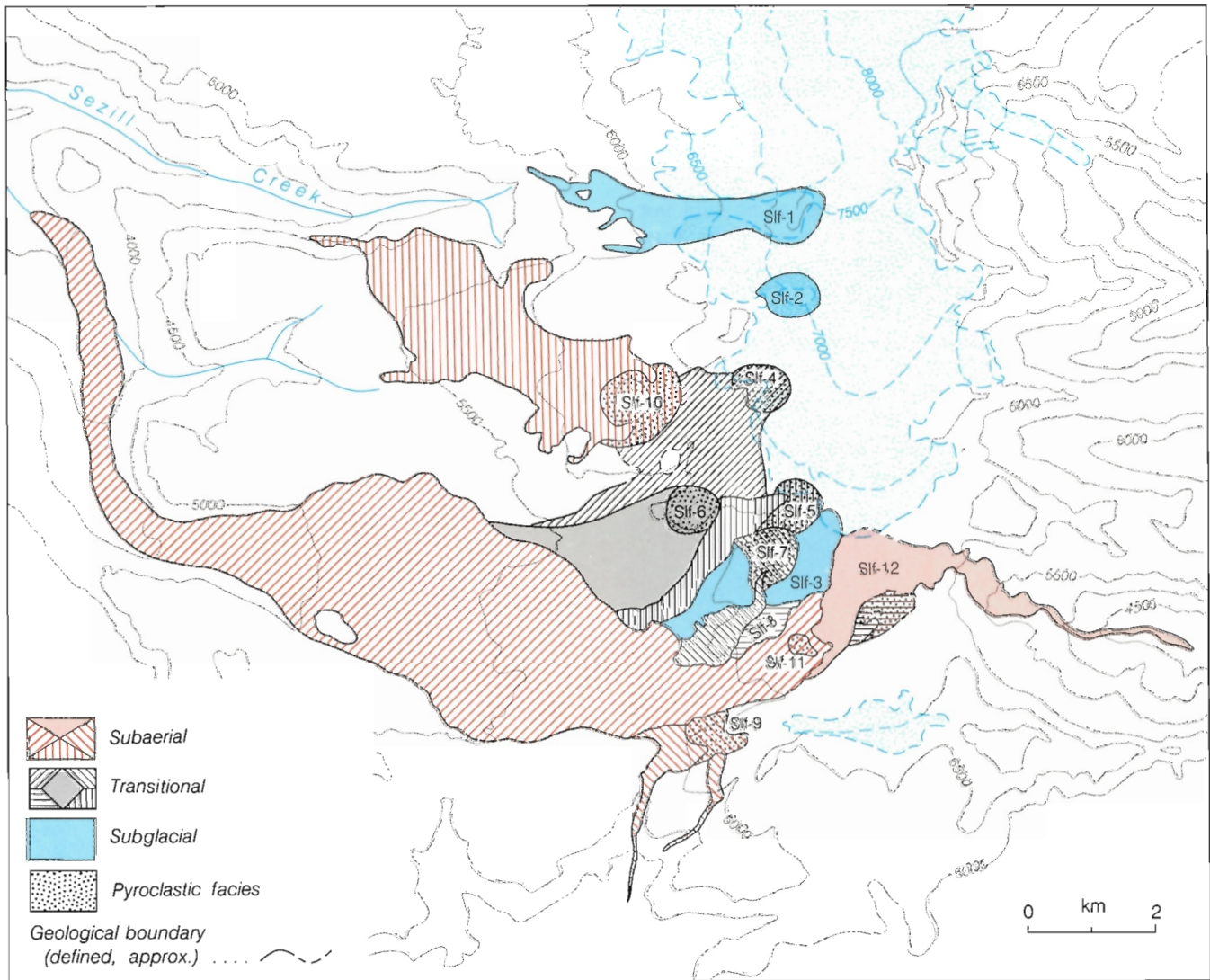
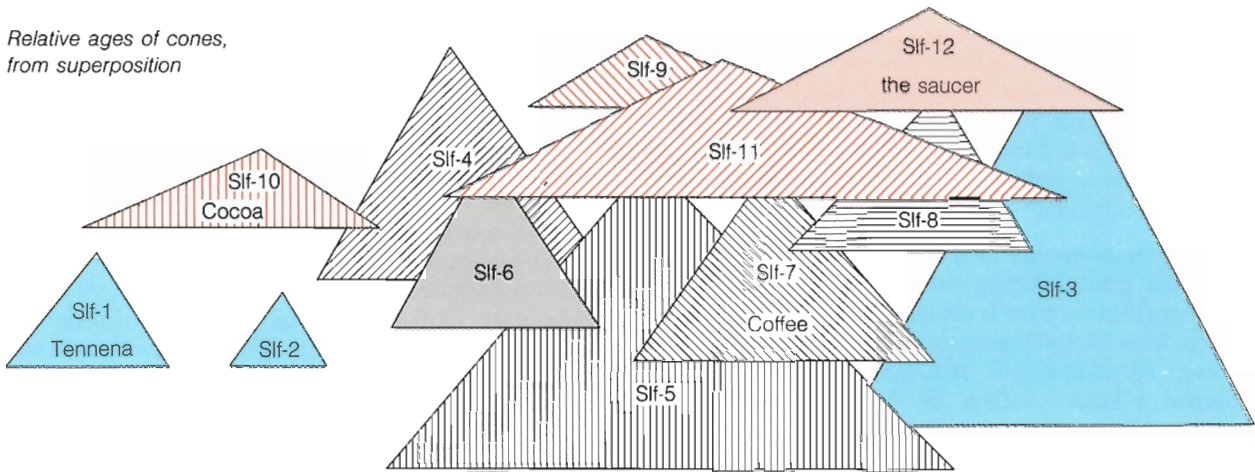


Figure 211. Lava flows and pyroclastic cones of the Snowshoe Lava field on the southwestern flank of Mount Edziza. Fluvial deposits and Sheep Track pumice have been omitted for clarity. The schematic diagram shows the age relationships of 12 eruptive centres in the Snowshoe Lava Field as inferred from superposition of flows, vegetation cover and degree of erosion. Subglacial cones consist entirely of pillow lava and sideromelane tuff-breccia; transitional cones have quench features only at their bases; and subaerial cones have no associated quench features.

and subaerial facies, and culminated with subaerial eruption of the most recent pyroclastic cones and flows. Twelve eruptive centres have been identified of which all but one are associated with a pyroclastic cone (Fig. 211). The exception (SLF-12) is a low circular dome of basalt where lava appears to have welled to the surface without accompanying fire fountaining.

Much of the Snowshoe lava was ponded in broad, thick sheets on the gently sloping surface of the surrounding plateau where the lava front is commonly bounded by levees up to 12 m high. A small amount spilled over into valleys on the east and north slopes, sending thin streams of lava into narrow tributary valleys of Walkout and Shaman creeks. The main body of the lava field converged into the head of Taweh Creek, to form a single thick tongue of lava which formerly extended beyond the junction with Sezill Creek, almost to Mess Creek, a distance of more than 15 km and a vertical drop of 3000 ft. (914 m). A second major flow over 2 km wide, spread from Cocoa Crater northwesterly across the plateau and spilled into the steep-sided upper canyon of Sezill Creek.

All of the Snowshoe lava is porphyritic basalt with varying proportions of plagioclase, olivine and clinopyroxene phenocrysts. The oldest phases tend to be least porphyritic, with about equal proportions of the three phenocrystic minerals. Transitional phases are commonly picritic with up to 15% large (± 4 mm) olivine crystals forming the dominant phenocryst mineral, whereas the youngest phases are feldsparphyric with only minor olivine and clinopyroxene. In addition small spherical clots of loosely aggregated plagioclase, olivine and pyroxene are present in all the transitional and young phases, and basalt from one of the centres contains numerous, partly fused inclusions of coarse grained felsic rock.



Figure 212. Tennena Cone, a subglacial pile of pillow basalt and sideromelane tuff-breccia high on the western flank of Ice Peak. GSC 125 633.

Subglacial centres (SLF-1 to SLF-3)

The main edifice of Tennena Cone (SLF-1) is a nearly symmetrical, black pyramid that rises about 500 ft. (150 m) above the present ice surface (Fig. 212). A smaller crescent-shaped nunatak (SLF-2) 1.5 km farther south, is either an extension of the main Tennena pile or part of a closely related satellitic cone. Both consist entirely of highly vesicular quenched basalt, occurring either as pillows or bulbous lava toes with concentric trains of small spherical vesicles, central gas cavities, and thin outer rinds of resinous black glass. Large slabs of similar, porous, quenched basalt form linear ridges on the associated lava flows, and frothy cinders of glass occur in pockets between the pillows and slabs. A narrow septum of moraine and isolated outcrops of pillow lava extend west from the base of Tennena Cone to the outermost, terminal moraine of the western trimline. The central rib of this medial moraine consists entirely of small slabs, blocks and cinders from the pile of pillow lavas, whereas the lower part, like the terminal moraine, includes a mixed assemblage of older Ice Peak rocks. A thin recessional moraine between the trimline and the present ice is also a mixed assemblage which rests on a polished and striated pavement of pillow basalt. Unglaciaded pillow lava forms thin flow tongues that extend about 1 km beyond the terminal moraine into the upper part of Sezill Creek canyon. Although their surface is partly covered with colluvium and alpine vegetation, the pillowed structure of these flows is still clearly visible. Despite the presence of quenched structures throughout their entire length, the flows are relatively thin (2-4 m) and they follow small depressions in the existing terrain, suggesting a relatively high mobility.

The base of the pillow-flow is exposed in several stream cuts near the terminal moraine (Fig. 213) and also, in upper Sezill Creek which has cut a narrow, 6 m deep, box canyon across the distal end of the flow. The flow is commonly



Figure 213. Pillow-flow from Tennena Cone. The bulbous, pillow-like structures rest on steeply west-dipping tuff-breccia and debris-flow deposits west of the trimline that marks the edge of the ice during eruption of Tennena Cone. GSC 125 634.

underlain by west-dipping, brown, well-bedded, waterlain tuff-breccia comprising blocks and irregular globules of vesicular basalt in a granular, sideromelane matrix. In many places the tuff-breccia contains stream-rounded cobbles and pebbles of older rock, and locally it is interlayered with glacial-fluvial gravels and mudflow deposits.

The initial eruption must have produced a relatively small volume of tuff-breccia and also thawed a spillway through which subsequent lava and meltwater were channelled beyond the western edge of the ice. The mobility of the Tennena flows was due in part to the steepness of this spillway, which drops from a summit elevation of 7700 ft. (2345 m) to 5000 ft. (1525 m) in 4 km. Despite the presence of copious amounts of meltwater, streams of molten basalt were obviously capable of flowing this entire distance without being quenched. It seems likely that the lava was channelled through thin-walled lava tubes which provided sufficient insulation to keep large, rapidly-moving lava streams from cooling and becoming too viscous to flow. Only those lava streams above some critical size, and hence some minimum thermal mass, were able to sustain flowage. Thus, the smaller buds that grew from the advancing flow front were quenched to form tubular pillows, while those more than a 1-2 m across continued to serve as conduits for the lava moving toward the advancing front. These trunk streams appear to have continued to flow and divide into small terminal lobes until the entire mass was made up of tubular pillows of about the same size. The only direct evidence of large distributary lava streams are ridges of quenched, porous basalt slabs believed to be the collapsed outer rinds of lava tubes.

Partly fused inclusions of felsic rock are locally abundant in the Tennena pile. They range from a few millimetres to 20 cm across, and in shape from diffuse, schlieren-like lenticles to subrounded or angular clasts with sharp, well defined margins. Fine- and coarse-grained inclusions may occur in the same outcrop and grain size is independent of the size of the inclusion. Both types have a white matrix of interlocking quartz and feldspar grains enclosing irregular, open cavities lined with resinous black glass. The diameter of the cavities ranges from less than 1 mm in the fine grained inclusions to more than 1 cm in the coarse grained inclusions. The remarkable similarity between these inclusions and those in the Pillow Ridge pile, 10 km farther north, suggests a similar origin, yet Pillow Ridge predates the Edziza trachyte, whereas the Tennena pillow lava is clearly younger than the adjacent flows of Kakiddi trachyte.

The crescent-shaped ridge of SLF-3 is exposed at the southern terminus of Tencho Glacier. The entire pile has been overridden by alpine glaciers and its northern part is buried by ice and alpine moraine. It consists entirely of crudely bedded sideromelane tuff-breccia and quenched flow-fragments, and it has no clearly defined crater or central edifice. The pile is believed to be a glacially modified tuff-ring which formed in a meltwater lake when Tencho Glacier extended onto the plateau, beyond its present trimlines. The different morphology of the Tennena and SLF-3

piles is probably due to differences in the slope of the underlying surface. Both lava and meltwater were channelled down the steep slope away from the Tennena vent, whereas the flat plateau surface at SLF-3 permitted the ponding of a meltwater lake in which the tuff-ring formed.

Transitional centres (SLF-4 to SLF-8)

Five pyroclastic cones in the Snowshoe complex include both subaqueous and subaerial ejecta and are considered to be transitional between the completely quenched piles and the younger, subaerial cones and flows which form the present surface of the field. Two of these, SLF-4 and SLF-5, lie inside the alpine trimlines, on the southwestern edge of the central ice field. They have been overridden by the ice, and reduced to low, drumlin-like ridges. The other three, SLF-6, SLF-7 and SLF-8, lie a short distance beyond the terminal alpine moraine. They are unglaciated and, although they retain their original conical form and their central craters are still intact, they have been sufficiently dissected to expose part of the inner structure. The basal part of each of the five cones is brown, sideromelane tuff-breccia. This is conformable with, and overlain by, concentric, outward-dipping beds of red, highly oxidized, subaerial cinders, agglutinated spatter and bombs which form the upper, subaerial, part of the cones.

Flows from these centres are largely covered by younger basalt and thick beds of unconsolidated Sheep Track pumice, making the correlation of isolated outcrops difficult. However, numerous small watercourses have removed the younger cover and locally cut through the underlying flows. In most exposures the lava from this group rests on either tuff-breccia, till, glacial fluvial gravel, or lahar deposits, all of which include a high proportion of reworked ash and cinders from the basalt itself. Also, clastic and pyroclastic deposits commonly occur as irregular layers and lenses between successive flows (Fig. 214).

The tongue of lava which extends southwestward from Coffee Crater (SLF-7) is bounded by a prominent, 18 m high escarpment along the northern edge of its terminal lobe. The upper part exposes a single, 15 m thick flow which, toward the edge of the escarpment, divides into several lava toes, each with radial jointing. Projecting from the escarpment at right angles, are three short 3-6 m high

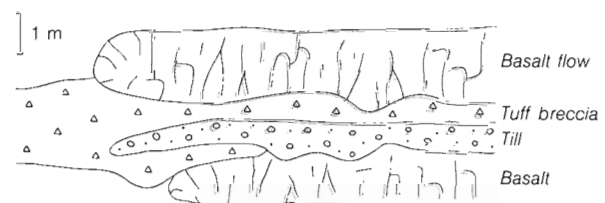


Figure 214. Sketch showing interdigitation of alpine till and tuff-breccia with quenched flows from SLF-5 near the trimline of Tencho Glacier.

transverse ridges of similar basalt forming fractured lava toes, pillows and minor tuff-breccia. The main escarpment appears to be an ice contact against which the flow was ponded, thus accounting for its great thickness. The small transverse ridges probably originated as tongues of lava that projected onto the glacier surface and collapsed to their present position as the ice melted (Fig. 215).

The relative ages of the five transitional cones and flows have been estimated from their morphology, lichen cover and degree of glaciation (Fig. 211), but extensive ash cover has obscured all but a few flow contacts. Also, all of the lava is similar olivine-rich basalt with large (3-5 mm) crystals of olivine forming up to 15% of the rock volume. Smaller amounts of clear plagioclase and black clinopyroxene are ubiquitous.

The presence, in this group, of flows and cones with ice-contact features up to 2.5 km beyond the terminal moraines of existing glaciers suggests that the present, conspicuous trimlines do not define the maximum limits of recent alpine glaciation, but rather an equilibrium position at which the ice stagnated for a prolonged period before the onset of the present recession. The absence of an older set of terminal moraines does not rule out the former presence of extensive ice beyond the present alpine trimlines. The initial buildup of ice during the last glacial advance may have been temporarily far more extensive than the equilibrium position but, because of rapid advance and retreat, left no conspicuous morainal ridges. Also, the climatic conditions that led to the last glacial advance must have led to the accumulation of smaller bodies of more or less stagnant ice

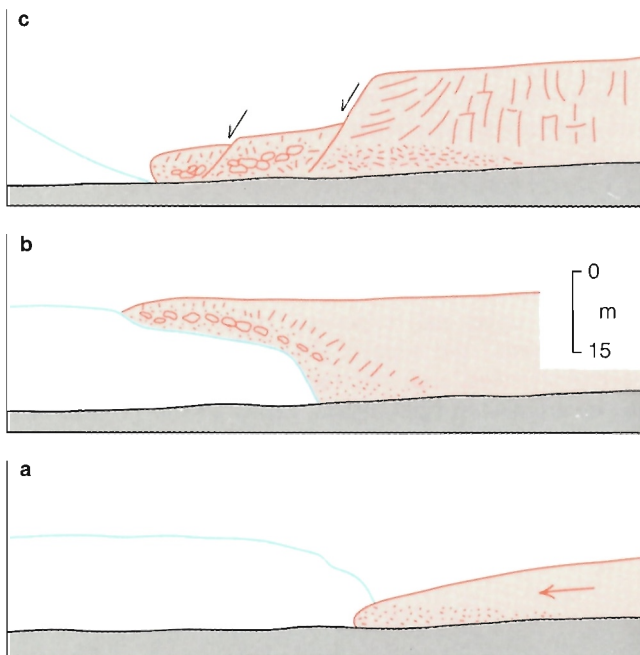


Figure 215. Sketch showing the inferred origin of a thick flow lobe southwest of Coffee Crater. The flow appears to have been ponded against, and partly overridden, a body of stagnant ice on the plateau.

as well as permanent snow on the plateau surface. It seems likely that the quenched tuff-breccia, pillows and ponded lava which characterized this group of transitional centres resulted from contact with thick snowfields and lobes of stagnant ice that lay beyond the edge of the active ice cap.

Subaerial centres (SLF-9 to SLF-12)

Most of the present surface of the Snowshoe Lava Field is covered with blocky basalt flows which issued from three subaerial centres, each associated with a pyroclastic cone. These cones consist entirely of red, highly oxidized agglutinated spatter, bombs and lapilli which, like the flows, show no evidence of quench features. Cocoa Crater (SLF-10), the largest cone in the group, is the source of a 2 km wide flow that curves around the western end of Koosick Bluff and spills over into the steep-walled, upper canyon of Sezill Creek. There the broad flow front ends abruptly, 600 ft. (180 m) above the valley floor. Water, flowing through channels under the lava, emerges at the base of the flow to form a group of moderate-sized streams which cascade down the lower cliffs and across the bouldery fill of the valley bottom (Fig. 216). The valley itself is mainly drift-filled but outcrops along the stream bank are of older basalt, suggesting that little if any of the Cocoa lava ever extended much beyond its present position. The flow front is truncated in a series of terraced cliffs, revealing a succession of three to six cooling units. The oldest flows occupy small depressions in the pre-Cocoa surface, and may in fact pre-date the Cocoa event. They are overlain by 6-9 m of highly irregular, scoriaceous flow-breccia above and around which the tongues of Cocoa basalt are stacked in irregular, levee-bounded lobes, each 1.5-6 m thick. The present lava front slopes diagonally along the valley wall descending from about 5000 ft. (1525 m) on the east to 4800 ft. (1464 m) on the western side of the flow. There a narrow tongue of lava, plastered against the valley wall, extends west for another 0.3 km and drops to 4400 ft. (1340 m). It seems



Figure 216. Subterranean streams emerging from beneath lava flows from Cocoa Crater. The flows end abruptly at this point, 600 ft. (180m) above the valley of Sezill Creek. GSC 202469-S.

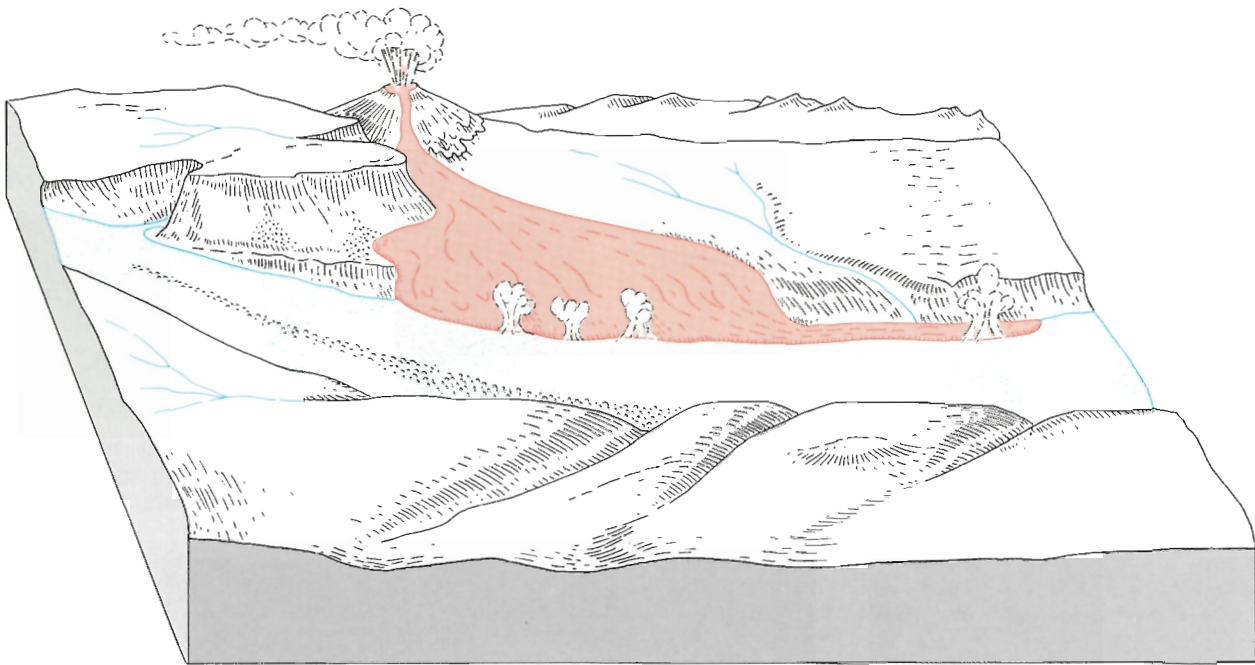


Figure 217. Block-diagram, showing the diversion of lava from Cocoa Crater along the margin of a stagnant mass of ice in upper Sezill valley.

likely that the trace of this westerly-sloping line of lava outcrops corresponds to the surface of a stagnant valley glacier which diverted the northerly flowing Cocoa lava westward into a narrow stream between the marginal moraines of the glacier and the valley wall (Fig. 217). It is unlikely that extensive quenching ever occurred in this environment because the stagnating ice was undoubtedly covered with a thick mantle of porous rock moraine which not only insulated the lava from the ice but also provided an outflow channel for the escape of meltwater, thus preventing the formation of a meltwater lake. Also, the northern edge of the flow, where quench features may have developed along the original lava front, has since broken away in landslides and slumps that accompanied and followed melting of the ice.

The largest volume of lava in the Snowshoe Field issued from vents near SLF-9 and SLF-11, both of which are well preserved subaerial, pyroclastic cones. The lava spread westward onto the gently sloping plateau surface, covering an area more than 3 km wide and 8 km long before converging into the upper part of Taweh Valley, to form a relatively narrow tongue of lava that formerly extended for at least another 12 km, almost to Mess Creek. The lower 3 km of this lava has been eroded away, except for small remnants along the banks of the fast-flowing main streams. But above a well defined nickpoint at 3300 ft. (1000 m) on Taweh Creek, the drainage is still dispersed into many small rivulets that have etched tiny box canyons along the flanks of the flow and locally, scoured smooth rock channels or spread a thin veneer of gravel across the blocky, scoriaceous surface. At the nickpoint itself, the flow is exposed in a

towering central rib of columnar basalt 42 m high around which the streams bounding the upper part of the flow converge into a single channel. Farther downstream, at 2400 ft. (730 m) on Taweh Creek, a remnant of the same flow forms the lip of a 18 m waterfall. There, the lava rests directly on unconsolidated river gravel which has eroded back, leaving a cavernous plunge-pool under the overhanging ledge of columnar basalt.

The youngest flow in the Snowshoe Field issued from a vent (SLF-12) near the southern edge of the central ice cap, on the crest of the divide between east and west-flowing drainage. Part of the lava spilled over into the head of Shaman Creek to form a narrow tongue of lava about 5 km long. The remainder spread westward as relatively thick, broad lobes on the nearly flat plateau surface. Unlike the other centres, it is not associated with a pyroclastic cone. Instead the sinuous ridges and levees of the flows diverge from "The Saucer", a low, nearly circular mound of scoriaceous lava about 0.5 km in diameter. A slight depression in the centre of "The Saucer" is surrounded by crudely concentric ridges of clinkery blocks that contrast with the relatively smooth, slabby surface of the adjacent flows. The lava appears to have welled quietly from a vent near the centre of the mound without any accompanying fire fountaining.

Sheep Track pumice, which forms thick drifts and pockets on the adjacent flows from Coffee Crater, is relatively sparse and much finer grained on "The Saucer" and its related flows. Although the evidence is not conclusive, eruption of "The Saucer" appears to postdate eruption of

MOUNT EDZIZA

the Sheep Track pumice. The sparse very fine pumice on its surface could easily be wind-blown material, carried in from adjacent pumice beds long after the actual pumice eruption.

Lava from "The Saucer", like that from the other three young subaerial centres, is medium grey, porphyritic basalt with up to 20% phenocrysts of plagioclase, olivine and clinopyroxene. Compared with the other lavas in the Snowshoe Field, the subaerial basalt is richer in plagioclase and poorer in olivine.

Walkout Creek centres

Remnants of two young subaerial, basaltic cinder cones and associated flows are preserved in Walkout Creek valley. Both are deeply dissected and poorly exposed but the larger



Figure 218. The Ash Pit, the youngest pyroclastic cone in the Mess Lake Lava Field, erupted on the steep, south-facing slope of Nagha Creek valley. GSC 202469-T.

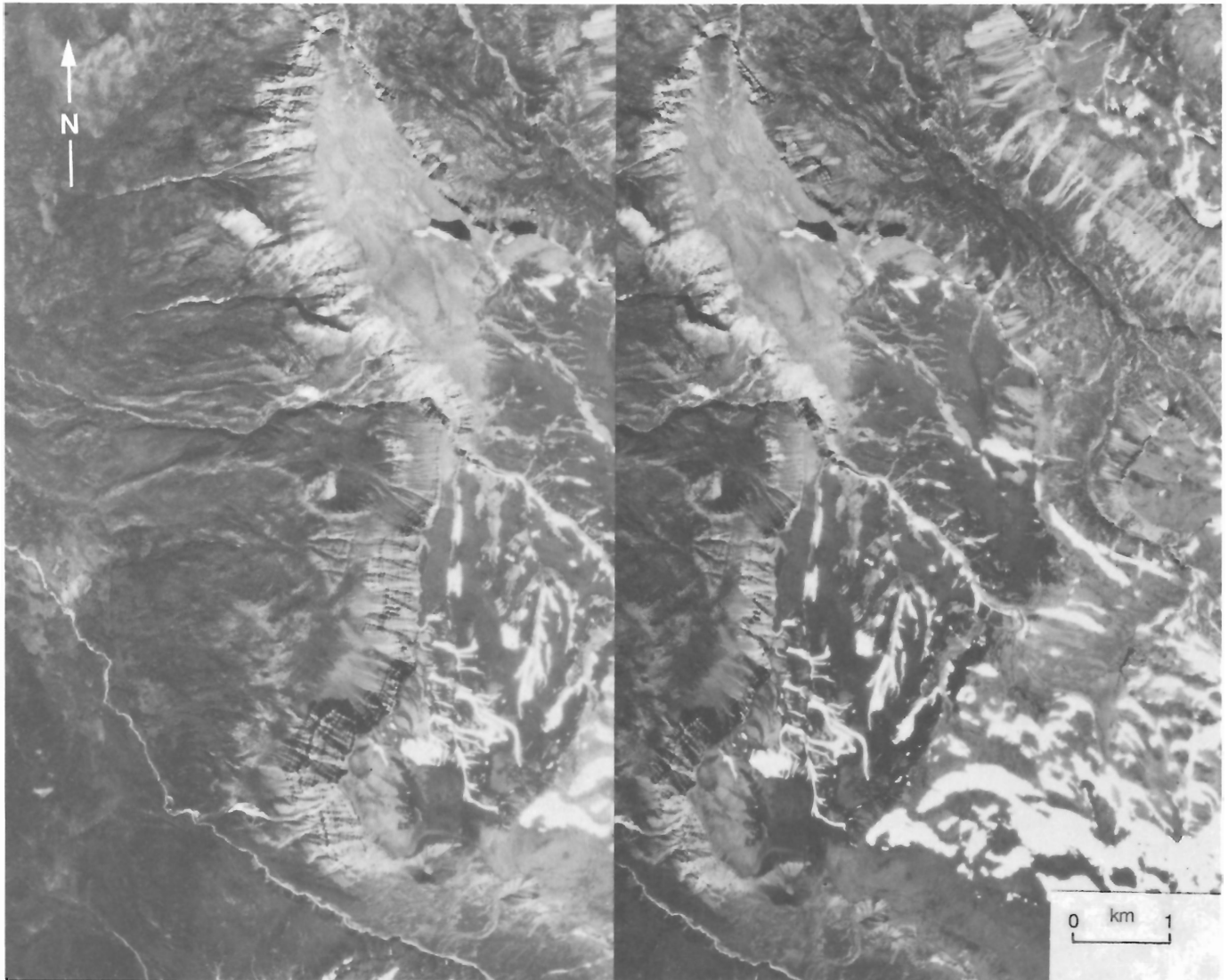


Figure 219. Aerial view of the tephra plume deposited on Kitsu Plateau during eruption of the Ash Pit (crater is in lower centre). Stereoscopic pair. Province of British Columbia photos BC 5607-204, 205.

of the two is of interest because of its relationship to an active landslide on the north side of the valley. The pyroclastic cone of agglutinated spatter and bombs is about 400 ft. (120 m) high. It was built on the upper part of one of several large, slow moving landslides which came off the escarpment into Walkout Creek. The typical hummocky, ridge and trough topography of the slide clearly controlled the deposition of the flows, some of which have been channelled into depressions along the base of small slide scarps. Thus the landslide predates the volcanic event, but continued movement of the slide has resulted in segmentation of the cinder cone itself into arcuate, step-like slices bounded by rotational slumps.

Mess Lake Lava Field

The plateau surface east of Mess Lake is covered by a field of young, clinkery basalt flows and tephra which extends from Raspberry to Nagha creeks and covers an area of about 18 km² (Fig. 189). The lava and ash issued from three separate vents, each marked by a pyroclastic cone. ML-1 and ML-2, the two oldest cones, have been slightly rounded by erosion and covered by tundra vegetation. However, their conical form and crater depressions are still apparent. Both are on the edge of steep escarpments where recent slumping has exposed irregular pale grey olivine basalt flows and red, agglutinated spatter which form the flanks of the cones. The base of both cones is a coarse flow breccia which, at ML-1 cone, rests directly on a pavement of Armadillo trachyte and, at ML-2 cone, rests on a thick layer of fluvial gravel. Lava from both of these centres flowed westward and is now exposed as crudely columnar rimrocks along the top of Mess Creek Escarpment. Much of the lava must have cascaded over the escarpment into Mess Creek valley, but no trace remains either on the precipitous cliffs or on the densely wooded surface of the landslide masses below the cliffs.

The Ash Pit (ML-3), at the south end of the field is the youngest of the three Mess Lake centres and may be the youngest centre in the entire Mount Edziza Volcanic Complex. It is a conical depression about 60 m deep and 0.4 km in diameter (Fig. 218) on the steep, south-facing side of Nagha Creek. The low south rim of the cone is a mixture of ash and bombs, whereas older rocks of the escarpment form most of the inner wall on the north side of the crater. A crescent-shaped ridge of fine black cinders rises an additional 90 m above the plateau surface and forms the northern rim of the asymmetrical cone. Blocky flows of pale grey, porphyritic olivine basalt, bounded by sharp-crested, 6 m high levees, extend down from the base of the cone into Nagha Creek where they are channelled into a single, narrow flow which follows the creek bed for about 3 km before welling out into a small lobe where Nagha Creek canyon opens into the broad valley of Mess Creek. The volume of lava from the Ash Pit is small compared with the amount of pyroclastic ejecta, most of which was thrown out as lapilli-sized cinders and ash. This material, in addition to

forming the north side of the cone, is preserved in an elliptical plume of air-fall tephra 2.5 km wide and 6.5 km long (Fig. 219). The plume is perfectly symmetrical around an axis trending N 20° E, indicating that a strong, uniform wind was blowing throughout the eruption. Because this is not the prevailing wind direction, it suggests that the event was very short-lived.

Ash thicknesses vary from about 30 m around the base of the cone to about 2 m near the centre of the plume to about 0.5 m at its northern end. Except for a few pockets of tephra the thin, distal edge of the plume has been eroded away and streams across its centre have cut channels which expose the barren surface of underlying flows from ML-1 cone and ML-2 cone. No material suitable for carbon dating was found at the base of the ash layer. However, pioneer vegetation on the surface of the Ash Pit tephra field is similar to that at the same elevation on the 1340 year old Williams Cone tephra, and the two are considered to be approximately coeval.

Arctic Plateau

Two eruptive centres of Big Raven age are located on or near Arctic Plateau (Fig. 189). Nahta Cone (AL1), near the northern edge of the plateau, is the most southerly post-glacial vent of Big Raven age in the map area. The edifice is a cluster of at least five tiny conelets, the largest of which rises about 60 m above the glacially scoured surface of the plateau. Its circular, sharp-crested, crater rim is breached on the east and filled with blocks of ropy lava at the source of a narrow flow that follows the drainage first northerly and then westerly for about 3 km into the head of Nahta Creek. Its blocky surface is unmodified by erosion and almost lichen-free but the displaced stream has already started to cut a new channel along its margins. Lapilli-sized tephra, like that of the Ash Pit, is concentrated on the north side

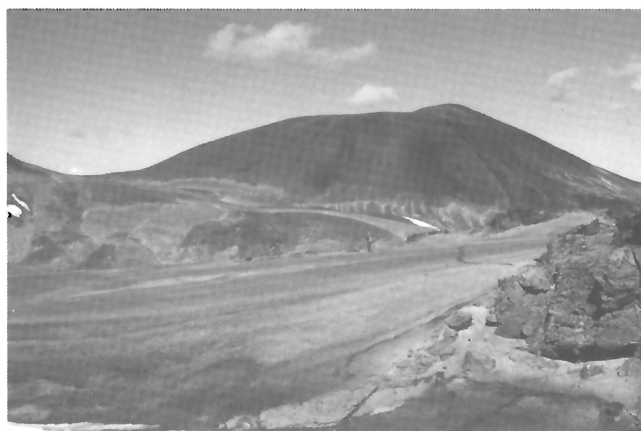


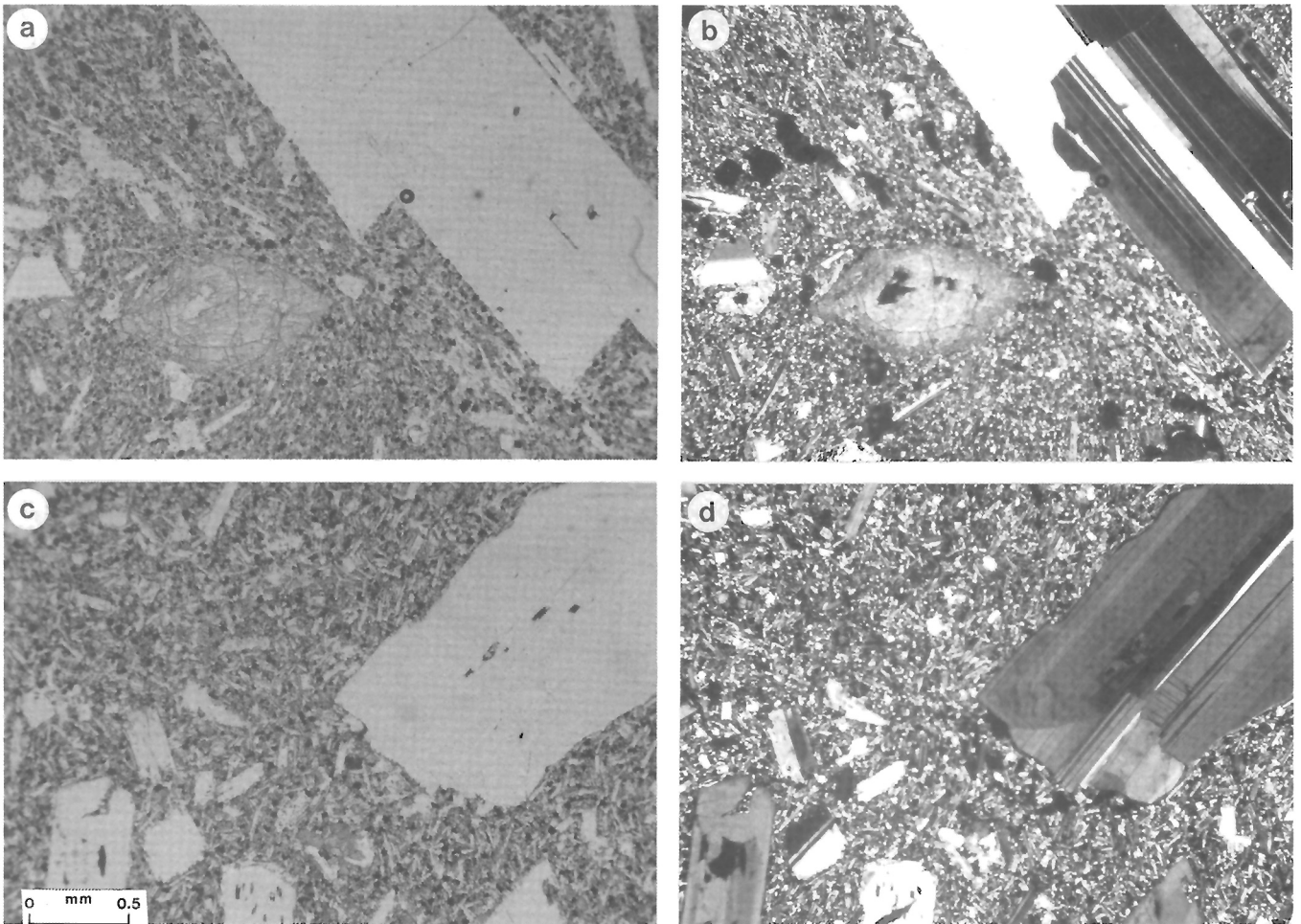
Figure 220. Air-fall pumice on Big Raven Plateau near the southwestern edge of Tencho Glacier. The unconsolidated pumice has washed from steep slopes, such as Cocoa Crater in the background, but covers most of the adjacent plateau to depths of a metre or more. GSC 202469-U.

of the vent, indicating a strong south wind at the time of the eruption. However, only the thickest parts of the Nahta tephra plume remain. All ash beyond about 300 m from the vent has been eroded away, suggesting that the Nahta eruption was somewhat earlier than that of the Ash Pit.

Steeply dipping scoriaceous, olivine basalt flows and coarse agglutinated pyroclastic beds, exposed on the south side of Kuno Peak, are believed to be remnants of a Big Raven pyroclastic cone (AL2). The basalt rests on a thick unconsolidated substrate of felsenmeer and talus which mantles the underlying Spectrum rhyolite. Repeated landslides and rapid solifluction on this unstable slope have carried away most of the original cone, leaving only a few remnants clinging precariously to the old talus. Flows which spread from this centre onto Arctic Plateau are completely covered by talus, and active alluvial fans.

Sheep Track Member

Unconsolidated, air-fall pumice of the Sheep Track Member of the Big Raven Formation blankets an area of about 40 km² on the southwest flank of Ice Peak and the adjacent plateau (Fig. 220). The maximum clast size occurs along the western margin of Tencho Glacier where fracture-bounded pumice fragments are up to 10 cm across. Clasts become more rounded and decrease rapidly in size to fine lapilli around the margins of the pile. The pumice has been largely removed from the drainage channels of small intermittent streams on the upper plateau but interfluvial areas are covered to depths of up to 2 m. It was deposited on all the Big Raven lava flows and cinder cones of the Snowshoe Lava Field except “The Saucer” which is covered by only thin drifts of wind-blown pumice. The Sheep Track pumice may also predate other areas of Big Raven basalt that lie



a,b — Alkali olivine basalt with phenocrysts of plagioclase and olivine in a fine grained matrix of plagioclase, clinopyroxene, minor olivine and opaque oxides (a, plane light; b, crossed polarizers).
c,d — Hawaiite with strongly zoned plagioclase phenocrysts in a matrix of plagioclase, clinopyroxene and opaque oxides (c, plane light; d, crossed polarizers).

Figure 221. Photomicrographs of Big Raven basalt; scale bar 0.5 mm.

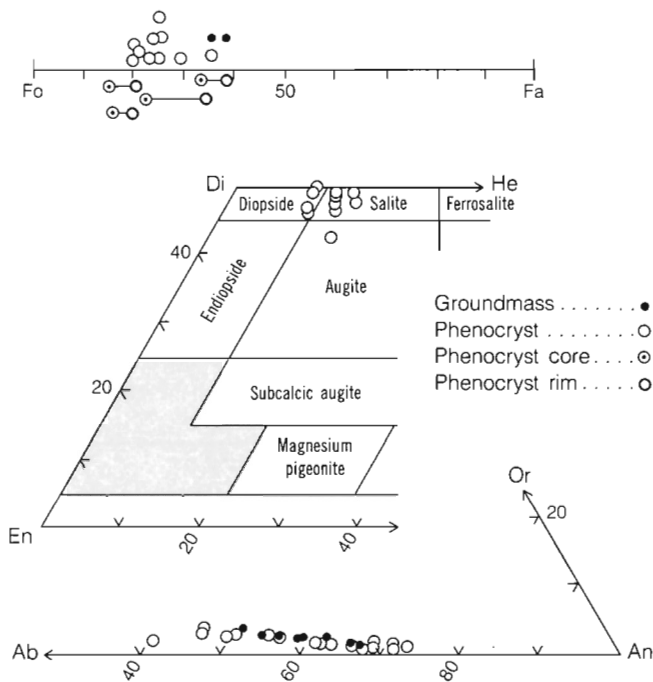


Figure 222. Plot of microprobe analyses of the principal mineral phases in Big Raven basalt.

beyond its area of deposition. The absence of pumice within the trimlines of the present alpine glaciers indicates that it was erupted during the last glacial advance, but its presence on subglacial Tennena Cone suggests that the glaciers had begun to recede prior to the Sheep Track eruption.

The Sheep Track pumice is a completely vitreous, aphyric froth of trachytic composition. Its source is unknown; probably hidden beneath Tencho Glacier. A deep, circular depression on the ice surface north of Coffee Crater may be an artifact of the Sheep Track eruption. The presence of thermal springs, fumaroles or elevated ground temperature around the vent could cause sufficient subglacial melting to sustain the surface depression.

PETROGRAPHY

Most of the Big Raven alkali olivine basalts are slightly porphyritic, with 2-5% phenocrysts of plagioclase, clinopyroxene, and olivine. Plagioclase phenocrysts, 1-3 mm long, are commonly euhedral or have slightly rounded margins. They have relatively large, unzoned cores of calcic labradorite surrounded by narrow rims, zoned to calcic andesine (Fig. 221a,b). Both olivine (Fa₁₀₋₄₀) and smaller amounts of titaniferous clinopyroxene (mostly salite) are also euhedral and show no evidence of reaction with the groundmass which is commonly a holocrystalline intergranular mosaic of labradorite laths, euhedral grains of olivine and clinopyroxene, and finely disseminated opaque oxides. The groundmass of basalt associated with the

hyaloclastites of the Snowshoe Lava Field contains interstitial glass charged with opaque dust and dendrites of clinopyroxene. The groundmass feldspar in these rocks exhibits swallowtail or hourglass forms, typical of quenched basalt.

Ankaramite is similar to the alkali olivine basalt in texture and mineralogy but it contains up to 30% of phenocrysts of olivine in euhedral crystals up to 5 mm across.

Big Raven hawaiites contain a higher proportion of feldspar and clinopyroxene phenocrysts than the alkali olivine basalts (Fig. 221c,d). Labradorite phenocrysts 1-10 mm long comprise 5-15% of most hawaiites. They include both euhedral, moderately to complexly zoned crystals and crystals that are rounded, embayed and have fritted cores. Salite phenocrysts are commonly larger and more abundant than olivine.

No consistent difference was detected in the compositional range of minerals in the Big Raven alkali olivine basalts and hawaiites (Fig. 222). Representative microprobe analyses are listed in Table 23.

The Sheep Track pumice contains rare microphenocrysts of alkali feldspar in a completely vitreous froth of clear trachytic glass containing tubular, open vesicles.

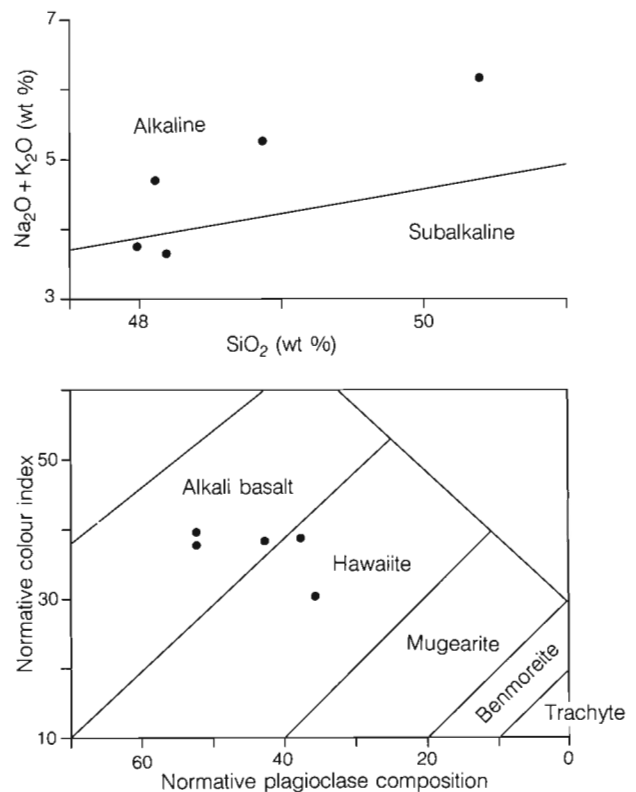


Figure 223. Plot of total alkalis vs. silica and normative colour index vs. normative plagioclase composition for 5 analyses of Big Raven basalt.

CHEMISTRY

Most of the Big Raven basalts are mildly alkaline, transitional rocks which plot close to the alkaline-subalkaline boundary on the alkali vs. silica diagram (Fig. 223), the alkali olivine basalt-hawaiite boundary on the normative colour index vs. normative plagioclase composition diagram, and the tholeiitic-calc-alkaline boundary of the AFM diagram (Fig. 224). An exception is the picritic basalt from Storm Cone (DLF 2) in the Desolation Lava Field which has an extremely high alkali (12%) and MgO (16%) content, and is classified as an ankaramite. It probably contains a high proportion of cumulus olivine in an alkaline residual

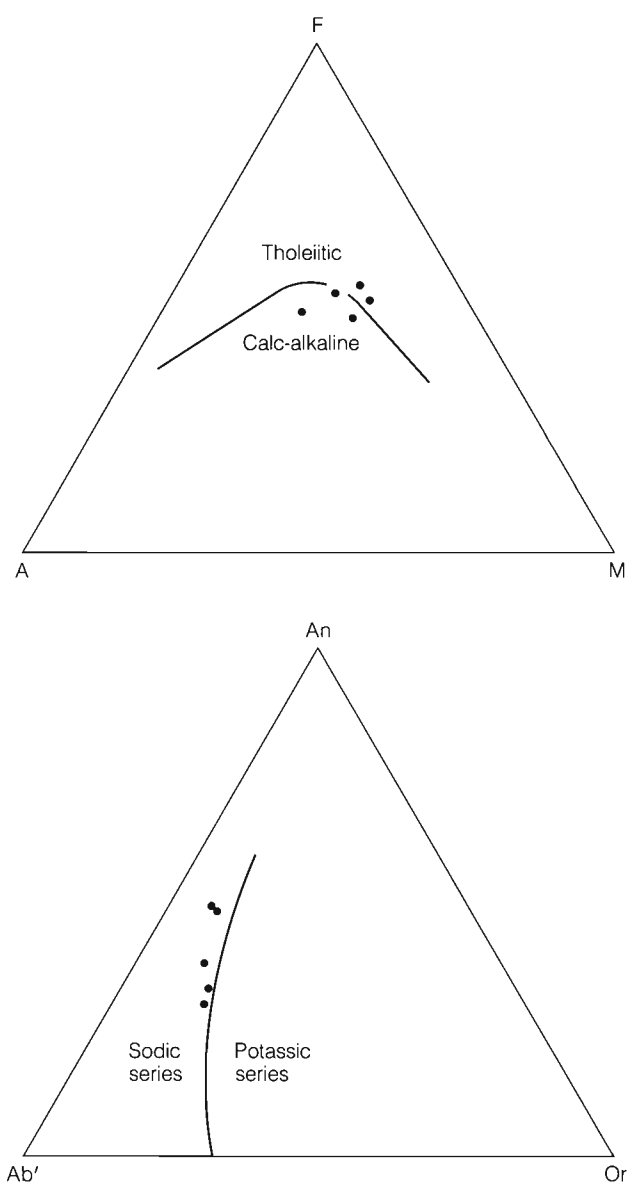


Figure 224. AFM and Ab'-An-Or plots of 5 analyses from the Big Raven Formation. (A = Na₂O + K₂O; F = FeO + 0.8998 Fe₂O₃; M = MgO; Ab' = Ab + 5/3Ne).

liquid. The anomalously low CaO content of this rock suggests the early fractionation of plagioclase.

The silica content of Big Raven basalt (Fig. 225) covers a fairly wide range (47.6 to 50.6%). There is a slight increase in total alkalis with increasing SiO₂ but the other oxides show no systematic variation.

A single analysis of pumice from the Sheep Track Member plots near the alkaline-peralkaline boundary (A.I. 1.07) and is classified as a comenditic trachyte.

Representative analyses of Big Raven basalt and the Sheep Track pumice are listed in Table 24.

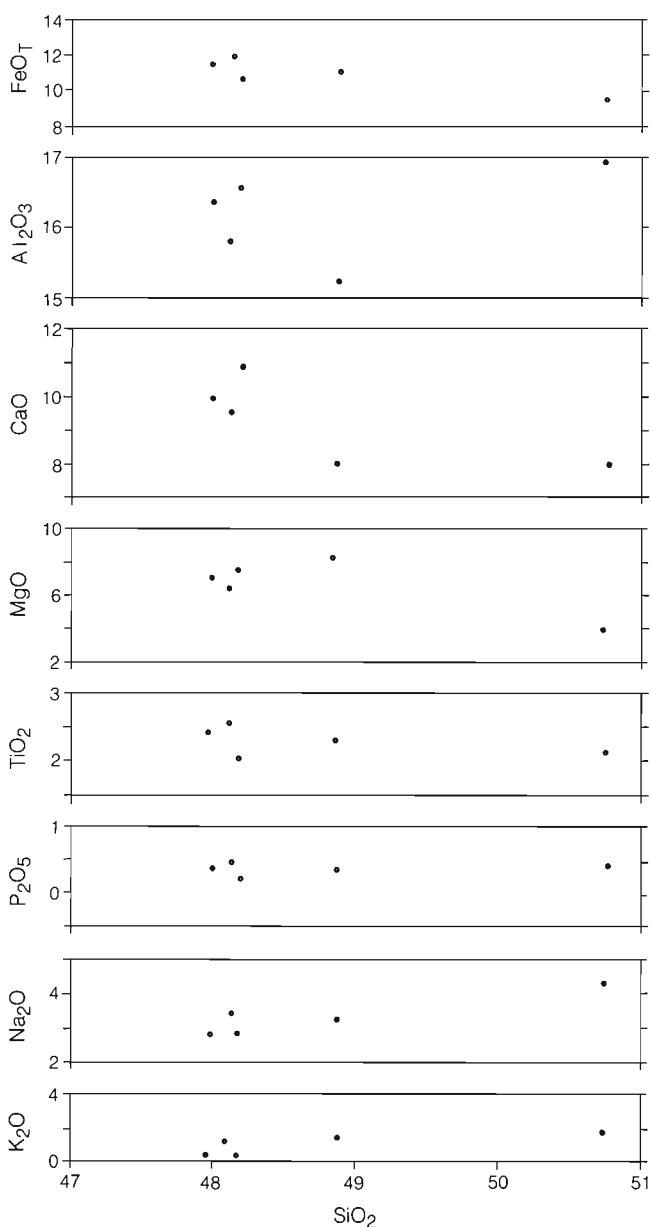


Figure 225. Harker diagram showing the chemical variation of 5 analyzed specimens of Big Raven basalt.

Table 23. Representative microprobe analyses and structural data for the principal mineral phases in the Big Raven basalt.

	Feldspar					Pyroxene				
	Phenocrysts				Groundmass	Phenocrysts				
	BF1 rim	BF2 core	BF3 rim	BF4 core		BF5	BP1 rim	BP2 core	BP3	BP4
SiO ₂	54.62	50.41	54.01	56.12	52.44	49.95	49.21	46.51	48.52	
Al ₂ O ₃	27.96	30.93	28.39	26.88	29.07	3.62	4.20	6.00	4.25	
TiO ₂	0.0	0.0	0.0	0.0	0.0	1.45	1.82	3.12	1.80	
Cr ₂ O ₃	0.0	0.0	0.0	0.0	0.0	0.0	0.01	0.10	0.0	
Fe ₂ O ₃	0.57	0.62	0.62	0.45	0.80	1.94	1.97	2.51	3.53	
FeO	0.0	0.0	0.0	0.0	0.0	7.21	7.00	8.43	5.08	
MnO	0.0	0.0	0.0	0.0	0.0	0.18	0.18	0.16	0.15	
MgO	0.0	0.0	0.0	0.0	0.0	13.44	13.22	11.74	13.47	
NiO	0.0	0.0	0.0	0.0	0.0	0.0	0.0	0.0	0.0	
CaO	10.80	14.45	11.50	9.58	12.33	21.50	21.43	20.75	21.94	
Na ₂ O	5.42	3.53	5.07	5.89	4.65	0.46	0.49	0.50	0.48	
K ₂ O	0.49	0.22	0.48	0.62	0.36	0.0	0.0	0.0	0.02	
H ₂ O	0.0	0.0	0.0	0.0	0.0	0.0	0.0	0.0	0.0	
F	0.0	0.0	0.0	0.0	0.0	0.0	0.0	0.0	0.0	
Total	99.86	100.16	100.07	99.54	99.65	99.75	99.53	99.82	99.24	
	No. of ions on basis of 8 (O)						No. of ions on basis of 6 (O)			
Si	2.4763	2.3012	2.4487	2.5417	2.3955	Si	1.8688	1.8458	1.7587	1.8231
Al	1.4940	1.6640	1.5169	1.4347	1.5651	Al	0.1312	0.1542	0.2413	0.1769
Cr	0.0	0.0	0.0	0.0	0.0	Ti	0.0	0.0	0.0	0.0
Fe ³⁺	0.0194	0.0213	0.0212	0.0153	0.0275	Fe	0.0	0.0	0.0	0.0
						Cr	0.0	0.0	0.0	0.0
Al	0.0	0.0	0.0	0.0	0.0	Al	0.0284	0.0315	0.0261	0.0113
Cr	0.0	0.0	0.0	0.0	0.0	Ti	0.0408	0.0513	0.0887	0.0509
Ti	0.0	0.0	0.0	0.0	0.0	Fe ³⁺	0.0548	0.0555	0.0715	0.0999
Fe ³⁺	0.0	0.0	0.0	0.0	0.0	Cr	0.0	0.0003	0.0030	0.0
Ni	0.0	0.0	0.0	0.0	0.0	Ni	0.0	0.0	0.0	0.0
Fe ²⁺	0.0	0.0	0.0	0.0	0.0	Fe ²⁺	0.2256	0.2196	0.2666	0.1596
Mn	0.0	0.0	0.0	0.0	0.0	Mn	0.0057	0.0057	0.0051	0.0048
Mg	0.0	0.0	0.0	0.0	0.0	Mg	0.7495	0.7391	0.6617	0.7544
						Ca	0.8618	0.8612	0.8407	0.8833
						Na	0.0334	0.0356	0.0367	0.0350
						K	0.0	0.0	0.0	0.0010
Ca	0.5246	0.7068	0.5586	0.4649	0.6035					
Na	0.4764	0.3124	0.4457	0.5172	0.4119					
K	0.0283	0.0128	0.0278	0.0358	0.0210					

	Olivine				
	Phenocrysts				
	BO1 rim	BO2 core	BO3	BO4 rim	BO5 core
SiO ₂	36.02	37.25	38.87	39.57	39.37
Al ₂ O ₃	0.0	0.01	0.01	0.04	0.03
TiO ₂	0.04	0.02	0.01	0.02	0.04
Cr ₂ O ₃	0.0	0.0	0.0	0.0	0.0
Fe ₂ O ₃	0.0	0.0	0.0	0.0	0.0
FeO	32.60	29.16	22.44	17.63	14.44
MnO	0.55	0.46	0.27	0.25	0.19
MgO	30.76	33.82	39.13	41.31	44.54
NiO	0.05	0.07	0.10	0.27	0.25
CaO	0.27	0.28	0.29	0.28	0.24
Na ₂ O	0.0	0.0	0.0	0.0	0.0
K ₂ O	0.0	0.0	0.0	0.0	0.0
H ₂ O	0.0	0.0	0.0	0.0	0.0
F	0.0	0.0	0.0	0.0	0.0
Total	100.29	101.07	101.12	99.37	99.10
	No. of ions on basis of 4 (O)				
Si	0.9868	0.9927	1.0000	1.0127	0.9971
Al	0.0	0.0	0.0	0.0	0.0
Cr	0.0	0.0	0.0	0.0	0.0
Fe ³⁺	0.0	0.0	0.0	0.0	0.0
Al	0.0	0.0003	0.0003	0.0012	0.0009
Cr	0.0	0.0	0.0	0.0	0.0
Ti	0.0008	0.0004	0.0002	0.0004	0.0008
Fe ³⁺	0.0	0.0	0.0	0.0	0.0
Ni	0.0011	0.0015	0.0021	0.0056	0.0051
Fe ²⁺	0.7469	0.6499	0.4828	0.3774	0.3058
Mn	0.0128	0.0104	0.0059	0.0054	0.0041
Mg	1.2561	1.3434	1.5005	1.5759	1.6814
Ca	0.0079	0.0080	0.0080	0.0077	0.0065
Na	0.0	0.0	0.0	0.0	0.0
K	0.0	0.0	0.0	0.0	0.0

Table 24. Representative chemical analyses of specimens from the Big Raven Formation.				
Sample	Alkali olivine basalt		Hawaiite	
	9	67	66	61
SiO ₂	47.900	48.400	48.700	50.600
Al ₂ O ₃	15.700	16.600	15.200	16.900
Fe ₂ O ₃	1.600	0.900	1.000	1.100
FeO	10.400	9.900	10.400	8.800
CaO	9.580	10.900	8.010	8.280
MgO	6.480	7.540	8.190	5.080
Na ₂ O	3.500	3.000	3.700	4.300
K ₂ O	1.200	0.690	1.580	1.910
TiO ₂	2.490	2.040	2.250	2.090
P ₂ O ₅	0.460	0.260	0.370	0.450
MnO	0.190	0.160	0.180	0.160
S	0.090	0.100	0.080	0.090
NiO	0.020	0.010	0.020	0.010
Cr ₂ O ₃	0.0	0.0	0.030	0.0
H ₂ O	0.100	0.0	0.100	0.300
CO ₂	0.0	0.0	0.0	0.0
Total	99.710	100.500	99.810	100.070

THERMAL SPRINGS

Four groups of thermal springs are located either within or adjacent to the Mount Edziza Volcanic Complex (Fig. 189). Three of them, Elwyn Hot Springs, Taweh Hot Springs, and Mess Lake Hot Springs are close to recent eruptive centres and may be discharging from shallow hydrothermal systems driven by residual magmatic heat. The fourth group (Mess Creek Hot Springs) which lie on the trace of a major fault bounding the west side of Mess Creek Valley, may be a deeply circulating hydraulic system. The springs were originally described by Souther (1975). More detailed chemical and physical data (Appendix 4) were collected in a later study by Piteau and Associates (1984) which is the source for much of the following description.

ELWYN HOTSPRINGS

The Elwyn thermal waters discharge from approximately ten vents near the base of the volcanic pile, where Nido basalt rests on Early Tertiary leucogranite. Discharge rates vary between 0.05 and 0.3 litres per second (L/s) and a maximum temperature of 36°C was recorded in August 1983. Precipitation of calcite and aragonite from fossil and active vents has created thick tufa deposits along the banks of Elwyn Creek between elevations of 4440 ft. (1350 m) and 4720 ft. (1440 m) asl. The cluster of cinder cones 6 km east of the springs, along the southern edge of the Desolation Lava Field, is a major centre of recent basaltic volcanism and may be the heat source.

TAWEH HOTSPRINGS

Extensive tufa deposits and numerous seeps of warm water are scattered for more than 0.5 km along Sezill Creek, about 7 km above its junction with Taweh Creek. The principal vent discharges 46°C water at a rate of about 0.5 L/s. A colourful, mushroom-shaped, tufa deposit on the north side of the creek rises from a narrow pedestal to a basin filled by a jet of 43°C water charged with CO₂ gas. The Taweh Hot Springs issue near the base of the volcanic pile where Armadillo basalt rests on basement rocks. They are only about 4 km from recently active cinder cones on the northwestern edge of the Snowshoe Volcanic Field. Residual heat from that activity is probably the heat source for a shallow hydrothermal system which is flowing along the basal unconformity and discharging at Taweh Hot Springs.

MESS LAKE HOTSPRINGS

Massive formations of spring deposited tufa cover an area of more than 120 hectares near the southeast corner of Mess Lake. A fossil vent, near the east side of the deposits and 80 m above lake level, stands approximately 10 m high and is surrounded by lesser vent deposits from 0.5 to 2 m high. Below these mounds a series of terraced tufa bluffs cascade between flat, playa-like areas covered with fine white powder. In 1965 a vigorous flow of warm water was issuing from a central, 20 cm diameter, conduit surrounded by concentric ring-shaped ridges of pure white tufa (Fig. 226). The symmetry of these deposits and the smooth vertical walls of the discharge pipe suggest that they were formed by geysering. When next visited in 1974 the discharge rate had diminished to a trickle and in August 1983 both the vent and adjacent terraced pools were dry. At that time the only remaining seep was discharging 14°C water at less than 0.01 L/s from a low tufa mound midway between the main vent area and the lake.

The Mess Lake Hot Springs issue from Triassic basement rocks about 560 m below the elevation of overlying Raspberry flows and only 2.5 km west of The Ash Pit, one of the youngest volcanic centres in the Mount Edziza Volcanic Complex. Residual heat from that eruption probably



Figure 226. Concentric tufa rings surrounding an extinct geyser vent at Mess Lake Hot Springs. (Photo by M.B. Lambert). GSC 20297.

resulted in a shallow, short-lived hydrothermal system which discharged through fractures in basement rock surrounding the conduit. Massive limestone is exposed in nearby Permian sections and may account for the relatively large volume of calcareous tufa deposited by the springs.

MESS CREEK HOTSPRINGS

Mess Creek thermal waters issue from two principal vents in fluvial gravel on the west side Mess Creek valley, about 7 km south of Mess Lake. The springs have a combined flow of about 1 L/s and discharge 42.5°C water directly into a 200 m² pool lined with limy mud. The pool contains numerous algal rafts and is dammed on one side by a terraced levee of vegetation but contains no tufa or

sinter deposits. Massive cliffs of Permian limestone, which bound the valley west of the springs, are bounded by faults which are part of a major, north-trending normal fault system. The springs are far removed from any centres of recent volcanic activity and are probably related to deep circulation of meteoric water along intersecting faults.

GEOCHEMISTRY OF THERMAL WATERS

The following interpretation of water chemistry and isotope hydrology is summarized from Piteau and Associates (1984) and analytical data from that report are reproduced in Appendix 4.

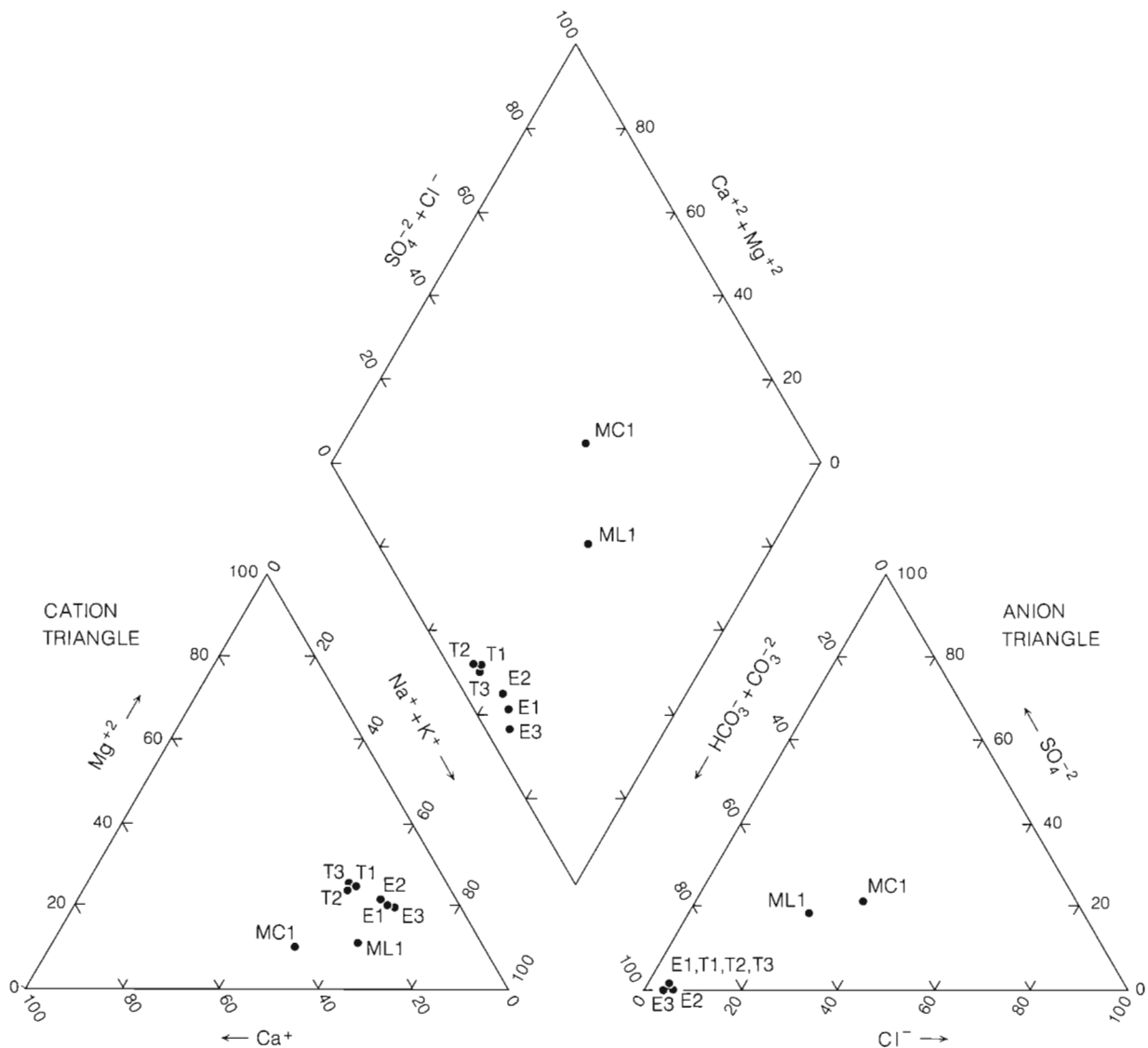


Figure 227. Piper diagram, showing the chemical nature of thermal waters from Elwyn (E), Taweh (T), Mess Lake (ML), and Mess Creek (MC) hotspots. Numbers following the letter code refer to different samples from a given spring. After Piteau and Associates (1984)

Table 25. Estimates of subsurface temperature from chemical geothermometers. From Piteau and Associates (1984).

HOTSPRINGS	TEMPERATURE (°C)							Mean Value
	Measured	Na-K-Ca-Mg	Mg-K	Na-Li	Qtz	Chalc	SO ₄ -H ₂ O	
E1 Elwyn Vent #1	19.5	< 50 ⁽¹⁾	56	78	-	-	-	61
E2 Elwyn Vent #2	29.0	< 50	57	79	-	-	-	62
E3 Elwyn Vent #3	36.0	< 50	60	77	114	81	23	68
T1 Taweh Main Vent	45.9	< 50	64	80	113	80	47	73
T2 Taweh Mushroom	43.0	< 50	64	81	-	-	-	65
T3 Taweh South	46.0	< 50	61	81	-	-	-	64
MC1 Mess Creek Vent #1	42.5	83	56	105	100	64	57	78
ML 1 Mess Lake Hotspring	13.0	< 50	58	85	105	71	-	74

1 High magnesium content indicates that subsurface temperatures are not significantly higher than discharge temperatures. Precise temperature estimate not possible.

Thermal waters discharging from the two hot springs associated with recent volcanic activity (Elwyn and Taweh) have total dissolved solids in excess of 3000 mg/L and are classified as sodium-bicarbonate waters with minor chloride and unusually low levels of sulphate (Appendix 4a, Fig. 227). Gas discharging from both springs is more than 90% CO₂ of probable volcanogenic origin (Appendix 4c). With the exception of barium, boron, iron, and strontium, trace metal concentrations are near or below detection limits. This chemistry is consistent with leaching and alteration reactions between meteoric waters at elevated temperatures and volcanic rocks along the flow path. Very low concentrations of oxygen-18 and deuterium (Appendix 4b) suggest that glacier ice was the principal source of recharge and low tritium values indicate that the spring water was recharged prior to 1952. A shift of less than 1‰ to the right of the meteoric water line indicates that very little oxygen-18 exchange has taken place with hot rock. This implies that temperatures were relatively low, in agreement with maximum temperatures of less than 100°C predicted by chemical geothermometry (Table 25). It is unlikely that water discharging from these low temperature hydrothermal systems ever penetrated much below the base of the volcanic pile.

Thermal waters from Mess Creek Hot Springs have lower total dissolved solids (1216 mg/L) than water from the other springs. They are classified as sodium/calcium bicarbonate waters with significant chloride and sulphate and the associated gas discharge is mainly nitrogen rather than carbon dioxide. The relatively high chloride and sulphate levels (209 and 150 mg/L respectively) probably result from deeper penetration and extensive rock leaching in an area less dominated by volcanogenic CO₂. Unlike the other springs, the Mess Creek thermal waters are undersaturated with respect to the major deposit-forming minerals, calcite and amorphous silica which accounts for the absence of tufa or sinter deposits. Mess Creek thermal waters have higher oxygen-18 and deuterium contents than water from Elwyn or Taweh hot springs and show no ¹⁸O shift from the meteoric water line. This suggests that they were recharged from a relatively low elevation and that they were not in prolonged contact with rock at high temperatures.

Water samples taken from seeps in the vicinity of the Mess Lake Hot Spring deposits are probably not representative of the thermal waters which deposited the massive tufa and sinter formations. The extremely low flow rates allow significant evaporation which could account for the high salinity of these samples (TDS 4858 mg/L) and for a positive ¹⁸O shift from the meteoric water line.

GEOCHRONOLOGY

The relative ages of formations within the Mount Edziza Volcanic Complex are apparent from their superposition in numerous undeformed, nearly flat-lying stratigraphic sections. But, in the absence of fossils, the stratigraphy of the rocks provides few clues to their absolute age. Without such information, correlation between distant sections within the complex is difficult where facies changes have resulted in loss of marker units, and where lithologically similar rocks occur in units of different age. Also, without an estimate of their absolute age, it is impossible to correlate rocks of the Edziza Complex with those in other volcanic piles.

The range of ages within the Mount Edziza Volcanic Complex spans the limits of resolution between the radiocarbon and potassium-argon methods, but by exercising extreme care in sampling and laboratory procedures a good fit has been achieved between radiometric dates and stratigraphy. The basic geochronology provided by potassium-argon (Souther et al., 1984) and radiocarbon dating (Lowdon et al., 1967) was supplemented with experimental work using fission-tracks (Aumento and Souther, 1973), and paleomagnetism (Souther and Symons, 1974; Fig. 228). Much of the geochronological data are published in the foregoing papers. Large sections of the original text are reproduced here for completeness but subsequent revisions in the stratigraphic correlation have resulted in changes in interpretation which are also included in the following summary.

POTASSIUM-ARGON

K-Ar dates were determined on samples from all of the formations in the Mount Edziza Volcanic Complex except the postglacial Big Raven Formation (Fig. 229). The 43 dates reported in Table 26 were determined over a period of 10 years in the laboratories of the Geological Survey of Canada and at the University of British Columbia. Ar extraction techniques and mass spectrometry procedures at both labs are similar and did not greatly change over that time interval. Where possible, feldspars at 40 to 80 mesh grain size were separated using density and magnetic methods. These usually gave lower atmospheric Ar yields and, especially if K-rich, the feldspars gave more precise dates. If feldspars were very fine grained, whole-rock samples were crushed to about 80 mesh and ultrasonically washed in deionized water containing a few percent hydrochloric acid. This removed dust and carbonate and yielded minimal trapped atmospheric argon.

Most of the dates fit the observed stratigraphic framework (Fig. 230). Significant anomalies probably result from excess radiogenic argon, present at the time of eruption, and

from isotopic fractionation during analysis. Excess argon has been observed in other young volcanic rocks (Dalrymple, 1969; Krummenacher, 1970; Fisher, 1971) and is especially prevalent in xenolith-rich or rapidly cooled basaltic magmas from ice-contact or subaqueous environments (Rutherford et al., 1972; Dalrymple and Moore, 1968; Armstrong, 1978). In the Mount Edziza Complex, the obvious examples of excess initial radiogenic argon involve the Ice Peak and Pillow Ridge lavas. The excess is made evident by large discordance of dates for overlying and underlying stratigraphic units, and is associated with unusual bulk chemistry and excess radiogenic Sr in the case of Ice Peak, and with partly fused granitic xenoliths and ice-contact features in the case of Pillow Ridge. Confirmation of excess argon in Pillow Ridge lavas is provided by fission-track dates (see below) that are much younger than the observed K-Ar date and are in accord with the stratigraphy.

Probable isotopic fractionation during analysis is illustrated by other anomalously old dates and may contribute to the Ice Peak and Pillow Ridge anomalies. In every case, the rocks are basaltic, relatively low in K, and unusually rich in atmospheric argon. This abundance of atmospheric argon shows up in Figure 230 as elongated error bars, because the calculated precision of the analysis is inversely proportional to the observed percentage of radiogenic argon. The correction for atmospheric argon assumes that the ratio of ^{36}Ar to ^{40}Ar is exactly atmospheric. This assumption fails for these samples because atmospheric argon is fractionated by diffusion during pumpdown (Baksi, 1974). In atmospherically clean samples this is not a serious problem, but where large amounts of atmospheric argon are trapped, as in partly altered rocks, the ^{36}Ar , which is removed by diffusion out of the sample during pumpdown, escapes more rapidly than ^{40}Ar . In extreme cases, this fractionation could exceed 5%. The atmospheric argon eventually analyzed may thus have several percent excess ^{40}Ar . Where the radiogenic argon is itself only a few percent of total argon extracted, the discrepancy in calculated date can exceed a factor of two. Two extreme, but instructive cases, not listed in Table 26, gave dates of 16 ± 6 Ma (2.3% radiogenic) and 22 ± 8 Ma (2.7% radiogenic) for rocks approximately 7 Ma old. In both cases the 95% confidence limits would include the correct age, but the errors are so large that the dates are not stratigraphically useful. Only about 2% isotopic fractionation by diffusion would explain this systematic overestimation of age.

FISSION-TRACK

Two fission-track dates were obtained on apatite from partly fused granitic inclusions and 17 dates from glasses.

MOUNT EDZIZA

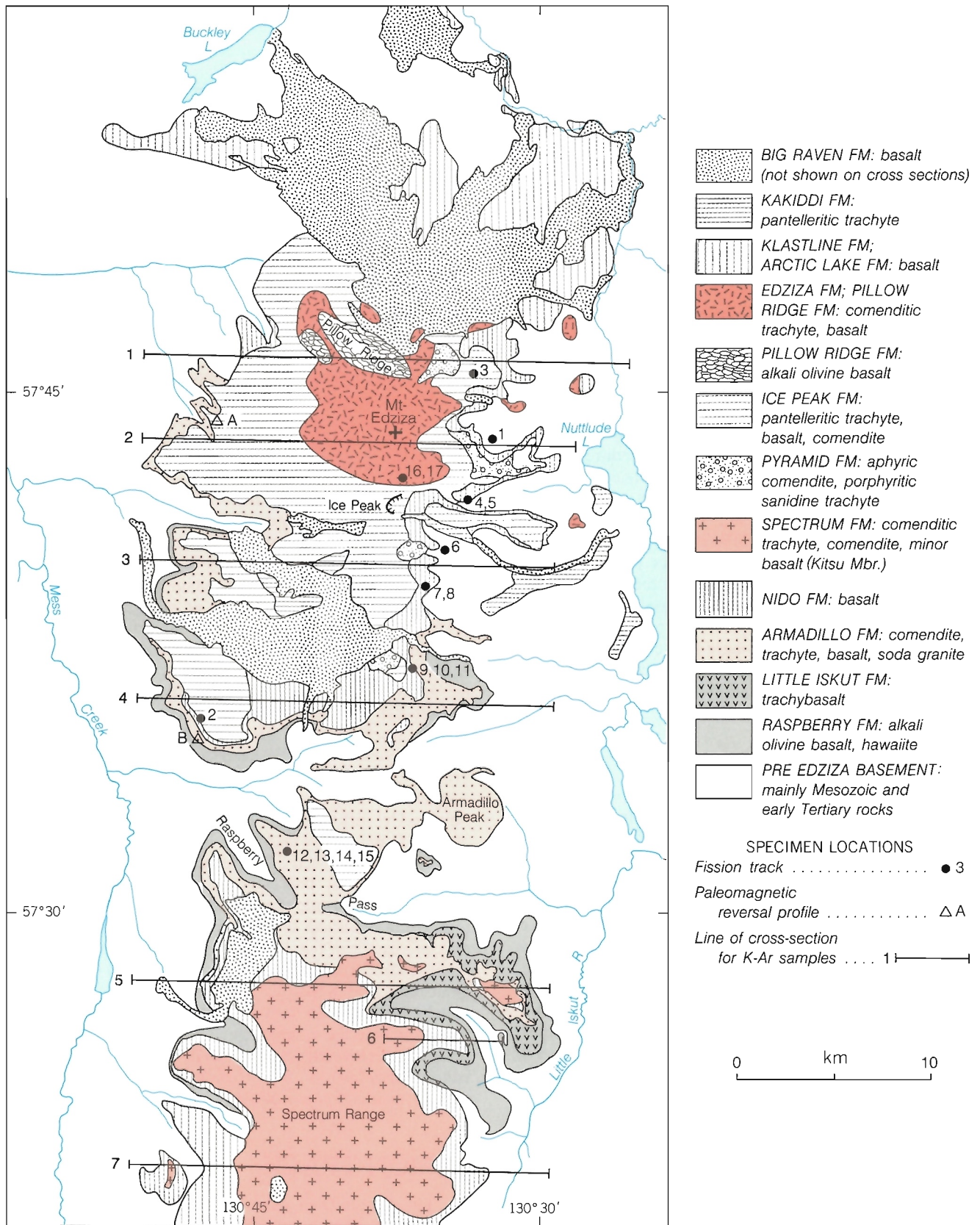


Figure 228. Map showing the location of fission track specimens (see Table 27), paleomagnetic polarity profiles (see Fig. 232), and cross-sections on which the K-Ar dates are plotted (see Fig. 229).

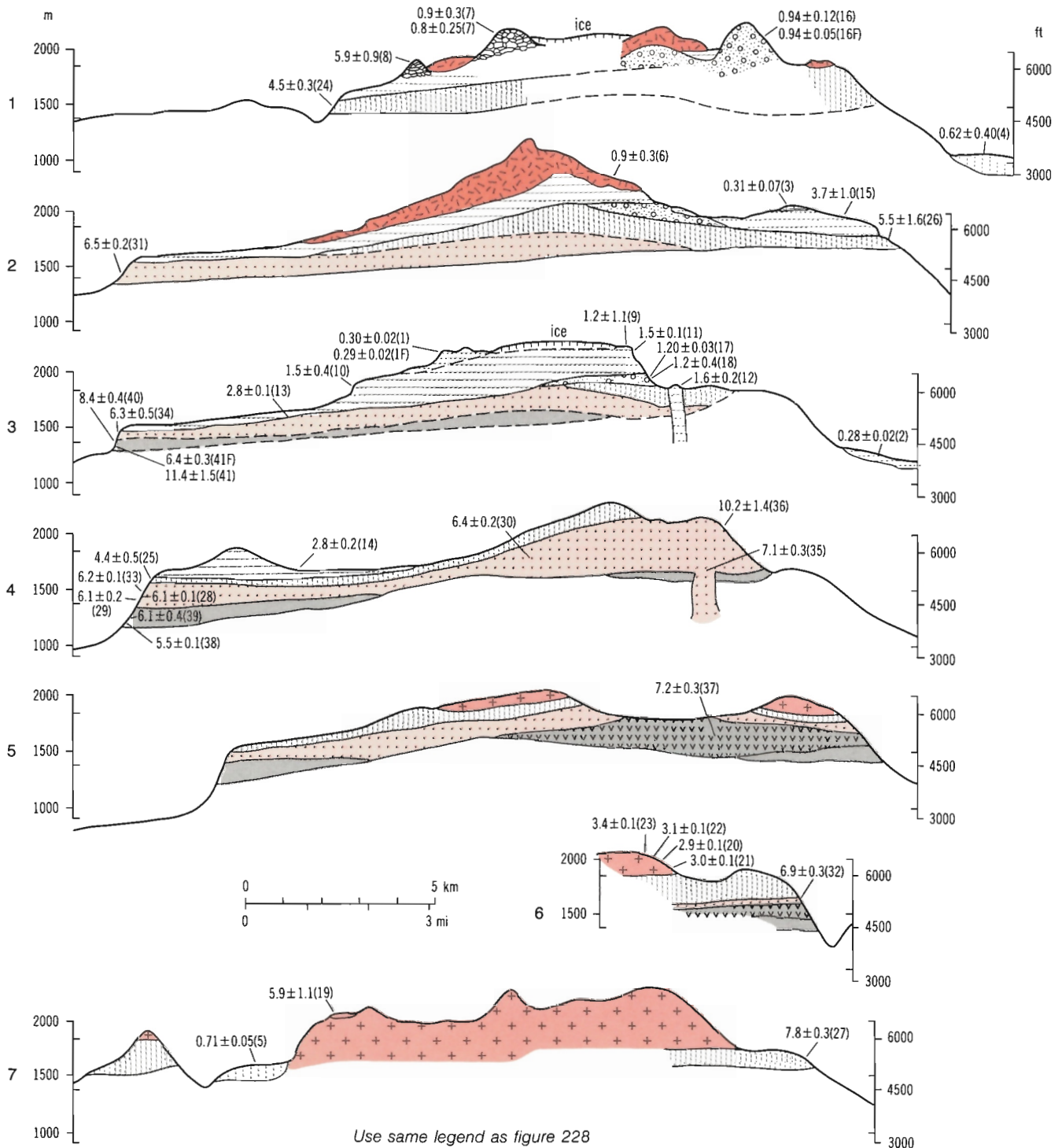


Figure 229. Schematic cross-sections (locations from Fig. 228) showing the locations of K-Ar samples relative to the stratigraphy. Sample numbers refer to those listed in Table 26.

MOUNT EDZIZA

Table 26. K-Ar and fission-track (apatite) dates from the Mount Edziza Volcanic Complex (from Souther et al., 1984).

Sample no.	Formation and lithology	Geographic co-ordinates	Laboratory	Method	% K	Ar 10 ⁻⁶ cc/g	%Σ ⁴⁰ Ar	Date Ma
1	Kakiddi Trachyte	57° 39.8' N 130° 41.2' W	UBC	K-Ar wr	4.36	0.0516	18.4	0.30 ± 0.02
1F	Kakiddi	57° 39.8' N	UBC	K-Ar Feldspar	5.68	0.0639	27.9	0.29 ± 0.02
2	Kakiddi Pantelleritic trachyte	57° 41.1' N 130° 34.7' W	UBC	K-Ar wr	4.12	0.0442	27.0	0.28 ± 0.2
3	Kakiddi Mugearite	57° 41.3' N 130° 32.0' W	UBC	K-Ar wr	1.066	0.0129	5.2	0.31 ± 0.07
4	Klastline Alkali olivine basalt	57° 56.1' N 130° 37.2' W	UBC	K-Ar wr	0.933	0.02236	17.3	0.62 ± 0.04
5	Arctic Lake Alkali olivine basalt	57° 21.5' N 130° 46.5' W	UBC	K-Ar wr	1.33	0.0365	16.4	0.71 ± 0.05
6	Edziza Pantelleritic trachyte	57° 44.5' N 130° 34.5' W	UBC	K-Ar wr	4.09	0.1376	2.8	0.9 ± 0.3
7	Granitic xenolith in Pillow Ridge Alkali olivine basalt	57° 46.1' N 130° 40.3' W	UBC	Fission tr. Apatite				0.9 ± 0.3
7	Granitic xenolith in Pillow Ridge Alkali olivine basalt	57° 46.1' N 130° 40.3' N	UBC	Fission tr. Apatite				0.8 ± 0.25
8	Pillow Ridge Alkali olivine basalt	57° 46.5' N 130° 42.0' W	UBC	K-Ar wr	1.185	0.2745	3.6	5.9 ± 0.9
9	Ice Peak Pantelleritic trachyte	57° 40.3' N 130° 36.0' W	UBC	K-Ar wr	4.94	0.2352	14.0	1.2 ± 0.1
10	Ice Peak Pantelleritic trachyte	57° 41.8' N 130° 43.3' W	UBC	K-Ar wr	3.54	0.2074	3.1	1.5 ± 0.4
11	Ice Peak Pantelleritic trachyte	57° 40.4' N 130° 36.5' W	UBC	K-Ar wr	3.69	0.2107	49.2	1.5 ± 0.1
12	Ice Peak Pantelleritic trachyte	57° 39.5' N 130° 35.5' W	UBC	K-Ar wr	1.32	0.0813	8.8	1.6 ± 0.2
13	Ice Peak Trachyte	57° 41.3' N 130° 43.9' W	UBC	K-Ar wr	0.840	0.0927	18.1	2.8 ± 0.1
14	Ice Peak Hawaiite	57° 32.3' N 130° 41.8' W	UBC	K-Ar wr	0.899	0.0999	14.0	2.8 ± 0.2
15	Ice Peak Hawaiite	57° 41.4' N 130° 32.1' W	UBC	K-Ar wr	2.55	0.3722	4.0	3.7 ± 1.0
16	Pyramid Trachyte	57° 45.7' N 130° 33.6' W	GSC	K-Ar wr	4.07	0.1487	14	0.94 ± 0.12
16F	Pyramid Trachyte	57° 45.7' N 130° 33.6' W	GSC	K-Ar Feldspar	5.66	0.2076	29	0.94 ± 0.05
17	Pyramid Comenditic glass	57° 40.4' N 130° 35.4' W	GSC	K-Ar wr	3.83	0.179	51	1.20 ± 0.03

Table 26 (cont.)

Sample no.	Formation and lithology	Geographic co-ordinates	Laboratory	Method	% K	Ar 10 ⁻⁶ cc/g	%Σ ⁴⁰ Ar	Date Ma
18	Pyramid Comenditic glass	57° 40.4' N 130° 35.4' W	UBC	K-Ar wr	3.76	0.1743	3.3	1.2 ± 0.4
19	Spectrum (Kitsu) Alkali olivine basalt	57° 25.5' N 130° 47.2' W	UBC	K-Ar wr	0.868	0.2009	3.8	5.9 ± 1.1
20	Spectrum Comenditic glass	57° 26.5' N 130° 36.4' W	GSC	K-Ar wr	3.98	0.4505	75	2.9 ± 0.1
21	Spectrum Comendite	57° 26.4' N 130° 36.0' W	UBC	K-Ar wr	4.00	0.4625	70.0	3.0 ± 0.1
22	Spectrum Comendite	57° 26.4' N 130° 37.7' W	GSC	K-Ar wr	3.87	0.4630	75	3.1 ± 0.1
23	Spectrum Comenditic glass	57° 26.0' N 130° 39.9' W	UBC	K-Ar wr	3.78	0.5047	76.3	3.4 ± 0.1
24	Nido Alkali olivine basalt	57° 46.1' N 130° 44.1' W	GSC	K-Ar wr	0.88	0.153	14	4.5 ± 0.3
25	Nido Alkali olivine basalt	57° 35.5' N 130° 48.3' W	GSC	K-Ar wr	0.55	0.095	5.8	4.4 ± 0.5
26	Nido Alkali olivine basalt	57° 41.5' N 130° 32.5' W	UBC	K-Ar wr	0.531	0.1149	3.4	5.5 ± 1.6
27	Nido (Kounugu) Alkali olivine basalt	57° 17.5' N 130° 32.6' W	UBC	K-Ar wr	0.625	0.1903	53.7	7.8 ± 0.3
28	Armadillo Comenditic ash flow	57° 35.3' N 130° 48.6' W	GSC	K-Ar wr	4.48	1.060	45	6.1 ± 0.1
29	Armadillo Hawaiiite	57° 35.4' N 130° 48.3' W	GSC	K-Ar wr	3.25	0.777	36	6.1 ± 0.2
30	Armadillo Comenditic glass	57° 32.3' N 130° 44.5' W	UBC	K-Ar wr	3.77	0.9469	51.7	6.4 ± 0.2
31	Armadillo Hawaiiite	57° 44.1' N 130° 48.1' W	UBC	K-Ar wr	0.574	0.1452	31.0	6.5 ± 0.2
32	Armadillo Comenditic ash flow	57° 26.2' N 130° 34.4' W	GSC	K-Ar wr	2.36	0.6344	42	6.9 ± 0.3
33	Armadillo Hawaiiite	57° 35.4' N 130° 48.3' W	GSC	K-Ar wr	1.0	0.2428	55.7	6.2 ± 0.1
34	Armadillo Hawaiiite	57° 40.8' N 130° 47.2' W	GSC	K-Ar wr	0.592	0.1462	5.0	6.3 ± 0.5
35	Armadillo Soda granite	57° 33.0' N 130° 32.7' W	UBC	K-Ar wr	3.70	1.024	26.1	7.1 ± 0.3
36	Armadillo Comendite	57° 35.8' N 130° 35.5' W	UBC	K-Ar wr	4.48	1.779	6.9	10.2 ± 1.4
37	Little Iskut Trachybasalt	57° 26.7' N 130° 31.4' W	UBC	K-Ar wr	3.58	1.009	79.4	7.2 ± 0.3
38	Raspberry Alkali olivine basalt	57° 35.3' N 130° 49.0' W	GSC	K-Ar wr	0.915	0.1958	49	5.5 ± 0.1
39	Raspberry Alkali olivine basalt	57° 35.4' N 130° 48.9' W	GSC	K-Ar wr	1.51	0.3603	30	6.1 ± 0.4
40	Raspberry Hawaiiite	57° 35.3' N 130° 48.6' W	UBC	K-Ar Feldspar	0.381	0.1251	19.6	8.4 ± 0.4
41F	Raspberry Hawaiiite	57° 38.9' N 130° 50.9' W	UBC	K-Ar Feldspar	0.489	0.1215	25.2	6.4 ± 0.3
41	Raspberry Hawaiiite	57° 38.9' N 130° 50.9' W	UBC	K-Ar wr	1.49	0.663	4.2	11.4 ± 1.5

MOUNT EDZIZA

The apatite dates (Table 26) were run to check a K-Ar date of 5.9 ± 0.9 Ma obtained on a sample from the Pillow Ridge Formation. This is obviously out of line with the age of underlying and overlying formations (Fig. 230). Contamination and introduction of excess argon from partly fused xenoliths of granitic and gneissic rock, which abound in the Pillow Ridge basalt, is believed to be responsible for the anomalously old age. An independent check was made by means of fission-track dating, using apatite from granitic clasts incorporated in the basalt. The partly fused clasts were obviously raised far above the blocking temperature for apatite (ca. 100°C). The resulting dates of 0.9 ± 0.3 and 0.8 ± 0.25 Ma are consistent with the stratigraphy.

Seventeen specimens of obsidian from the Mount Edziza Volcanic Complex were dated by the fission track method. When these dates were first reported (Aumento and Souther, 1973), the comendites and trachytes that lie above the basal, Raspberry basalts were lumped together as "stage 1 comendite". Subsequent mapping and stratigraphic work resulted in the subdivision of these felsic rocks into the Armadillo and Pyramid formations, of similar lithology but very different age. The original specimen numbers used by Aumento and Souther (1973) are retained in Table 27, but they have been regrouped according to the revised stratigraphy.

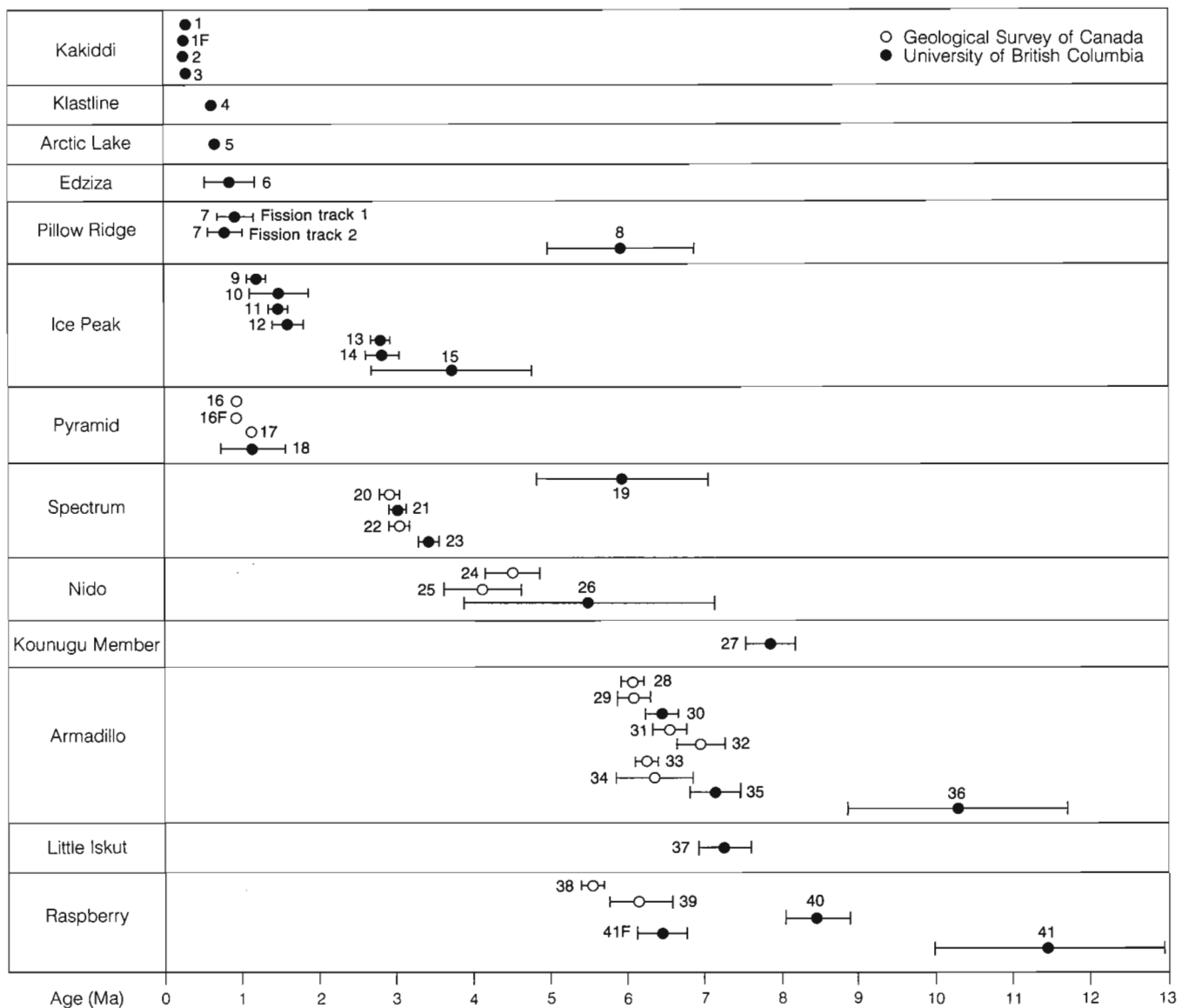


Figure 230. Plot of K-Ar and fission-track (from apatite) age dates versus stratigraphic position. Error bars are one standard deviation.

Table 27. Fission-track, thermal neutron flux, uranium content, and age data for obsidians from the Mount Edziza Volcanic Complex (from Aumento and Souther, 1973).

Formation	Specimen no.	Surface characteristics of glass	Spontaneous fission track density tracks/cm ²	Thermal neutron flux n.v.t. x 10 ¹⁵ ± 0.7%	Induced fission track density tracks/cm ²	Uranium content (p.p.m.) ± 3.5%	Age (ka)	
Sheep Track	16	Many microlites	0.1 ± 100%	4.91	812 000 ± 2.3%	17.2	10	
	17	Mediocre	0.01 ± 100%	6.87	1 268 000 ± 3.2%	19.2	1 ± 6	
Pyramid	3	Excellent	1564 ± 5.3%	7.06	1 576 100 ± 1.6%	23.2	429 ± 24	
	4	Slight imperfections	2587 ± 4.0%	4.91	795 000 ± 1.6%	16.9	980 ± 40	
	5	Good	184 ± 32%	6.75	1 278 000 ± 1.8%	19.8	59 ± 20	
	6	Excellent	4675 ± 2.1%	7.40	2 238 000 ± 1.0%	31.0	947 ± 33	
				4729 ± 3.0%	7.40	2 232 000 ± 2.1%	31.5	960 ± 40
	7	Very poor		6.68	270 690 ± 2.9%	4.2		
	8	Good	2635 ± 4.3%	7.49	1 235 000 ± 1.6%	17.2	976 ± 42	
	9	Good	1400 ± 3.0%	4.91	657 000 ± 1.6%	14.0	641 ± 22	
Armadillo	10	Many microlites	500 ± 7.0%	4.91	550 000 ± 7%	11.7	280	
	11	Excellent	1156 ± 10%	7.13	708 380 ± 2.1%	10.3	712 ± 75	
	1	Excellent	8100 ± 3.1%	7.32	1 169 400 ± 1.9%	16.6	3106 ± 115	
	2	Interstitial glass only	1200 ± 3.9%	4.91	215 000 ± 2.3%	3.3	990 ± 50	
	12	Interstitial glass only	617 ± 6%	4.91	357 000 ± 3.1%	7.6	519 ± 35	
	13	Very poor, patchy	400 ± 25%	7.55	294 880 ± 2.3%	4.1	560 ± 140	
	14	Poor	320 ± 9%	7.55	314 000 ± 2.0%	6.7	350 ± 32	
	15	Poor	18.4 ± 32%	6.80	275 460 ± 3.1%	4.2	28	

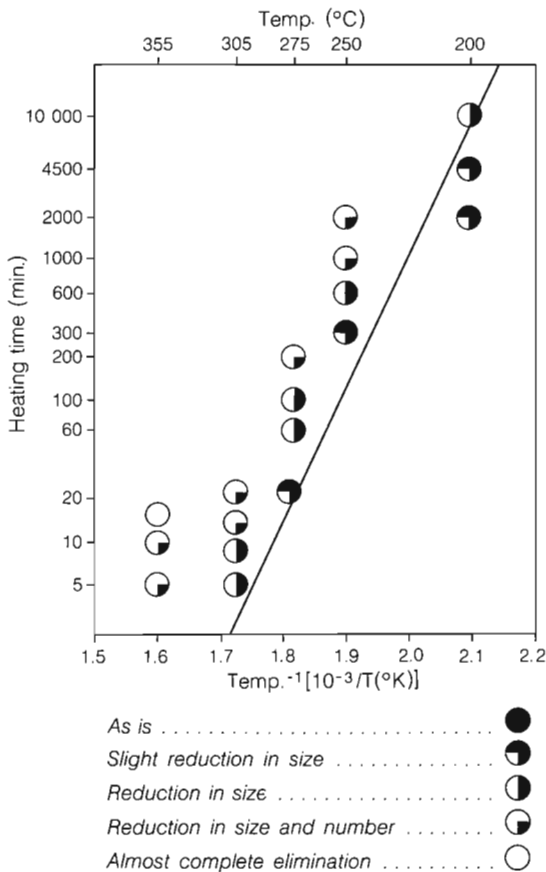


Figure 231. Annealing characteristics of specimen 6 (Table 27). The line separates the field between time/temperature conditions that would have no effect on the age determinations, and those which would produce erroneously low dates.

Age determinations based on the spontaneous fission of ²³⁸U (Fleischer and Price, 1964), are reliable only if the specimens have not been annealed by a combination of time and temperature since their solidification. The annealing characteristics of Edziza glasses were tested by heating small specimens at different temperatures and varying times, and observing the effects on the fission tracks. Heating for periods of up to 7 days at 200°C resulted in a noticeable reduction in the fission track size, but not number (Fig. 231). Extrapolation of this data suggests that specimens which were not heated above 200°C for more than a few days should provide reliable dates, but the effects of very slow annealing for millions of years is not known. Fission-track dates may also be affected by plastic flow and by migration of uranium. Plastic flow is not a problem in the undeformed Edziza rocks, but loss of uranium by diffusion may be important, particularly from noncrystalline glasses.

The precision of the fission-track dates appears to be greatly influenced by the uranium content and post-solidification history of the particular sample. Specimen number 6 (Table 27), a very clear Pyramid glass with 31 ppm uranium, was dated by two independent researchers, giving fission track dates of 947 ± 33 ka (Monroe, 1970) and 960 ± 40 ka (Aumento and Souther, 1973) which are in close agreement with one another and with K-Ar dates of 1.14 ± 0.14 Ma and 1.19 ± 0.13 Ma on the same material. Such ideal results are not always attainable. Some of the Mount Edziza obsidians contain very small microlites. When the polished surface of these glasses is etched, the microlites are destroyed preferentially, producing pits which are almost indistinguishable from those of fission tracks. This may account for some of the scatter in the data. In general, the most consistent fission-track dates were obtained on relatively young glasses with good surface

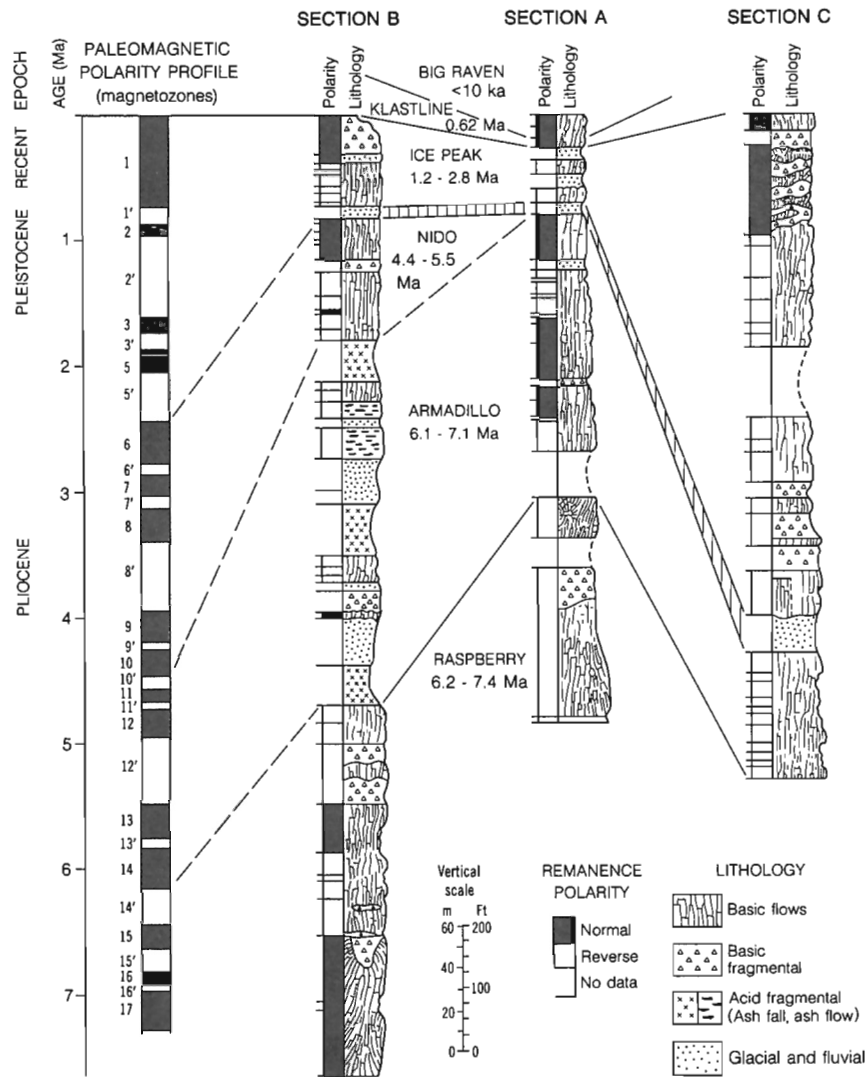


Figure 232. Correlation chart showing lithology and magnetic polarity profiles of three stratigraphic sections in the Mount Edziza Volcanic Complex, and their approximate relationship to the standard magnetozones of Cox (1969). The range of K-Ar dates for each of the sampled formations is shown below the formation name. Section locations are shown on Figure 228.

characteristics. Fission track dates on the Armadillo specimens are anomalously young, compared to the K-Ar data, suggesting that long-term annealing has resulted in a loss of tracks in the older glasses. Most of the Pyramid glasses give fission-track dates that are close to the ± 1 Ma K-Ar age for the Pyramid Formation. Those that deviate significantly from this average age commonly show signs of devitrification or contain numerous microlites. Despite poor surface characteristics on glass associated with the Sheep Track pumice, the fission track dates of 1000 to 10 000 years are in reasonable agreement with a 1340 ± 130 year ^{14}C date on closely associated Big Raven basaltic tephra.

PALEOMAGNETISM

Paleomagnetic polarity profiles were determined for three measured sections of lavas within the Mount Edziza Volcanic Complex (Fig. 232). For a description of sampling and laboratory procedures and details of stratigraphy, lithology and remanence data, the reader is referred to the original report on this work (Souther and Symons, 1974). Since the data were first published, additional K-Ar dating and mapping have resulted in a re-interpretation of both correlation between the three sections and between the sections and the standard polarity profile of Cox (1969). The revised correlation between the three stratigraphic sections is consistent

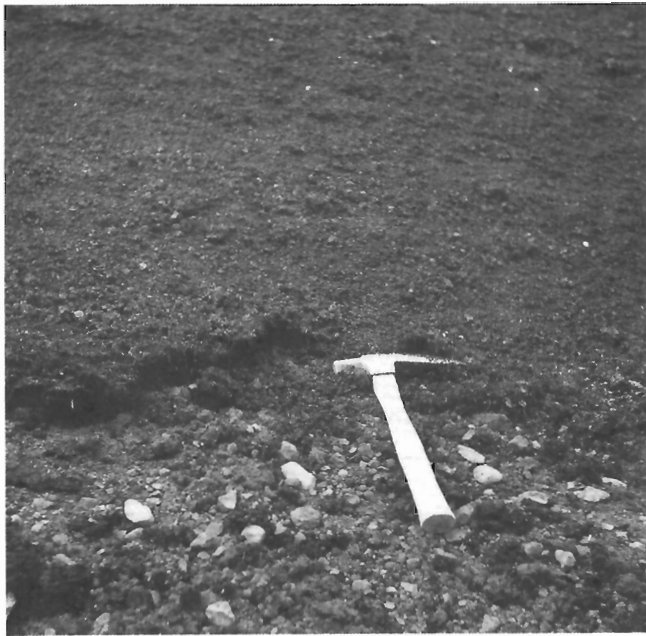


Figure 233. Basaltic tephra from Williams Cone resting on a paleosol in which the charred remnants of willow stems are still rooted. A ^{14}C date of $1340 \pm 130\text{a}$ was obtained on carbon collected from this site. GSC 125 635.

with both lithology and paleomagnetic polarity. The thickest section (section B, Fig. 232) records six reversals in the earth's magnetic field, but K-Ar dates indicate that the section spans approximately 7 Ma, a period during which the earth's magnetic polarity changed at least 31 times. Thus, there is no unique correlation between the observed reversal profiles and the standard magnetozones of Cox (1969).

RADIOCARBON

Carbonized wood is preserved beneath many of the flows and tephra layers of the Mount Edziza Volcanic Complex but, with the exception of that associated with the Big Raven Formation, it is too old to provide ^{14}C dates.

Charred willow twigs, preserved beneath a thick layer of unconsolidated Big Raven basaltic tephra from Williams Cone (Fig. 233) yielded a ^{14}C date of 1340 ± 130 BP (Lowdon et al., 1967).

Basalt flows, capping terraces in Klastline Valley, west of the map area, are believed to be correlative with older flows of the Big Raven Formation. Carbonized wood, collected by P.B. Read, from paleosols under these flow-remnants yielded ^{14}C dates of 8350 ± 80 , 8440 ± 80 , and 8610 ± 80 years BP (P.B. Read and J.F. Psutka, 1985; unpublished report to B.C. Hydro and Power Authority).

PETROCHEMISTRY

INTRODUCTION

The chemistry and petrography of representative rocks from each formation are described in the foregoing chapters on general geology. In this section the same data are examined in the broader context of the volcanic complex as a whole. Despite its long and varied history of activity, the range of mineralogical and chemical variation among rocks of the Mount Edziza Volcanic Complex remained relatively constant through time. Its most characteristic feature is a statistical separation of basaltic and felsic rocks into two populations, each with distinctive major- and trace-element chemistry and each having a distinctive suite of mineral species.

Alkali olivine basalt, either aphyric or with sparse plagioclase phenocrysts, is volumetrically the most abundant rock type in the Mount Edziza Volcanic Complex. It comprises euhedral to subhedral laths of plagioclase, titanite, small granular olivine crystals, opaque oxides and devitrified glass. The pyroxene occurs either as ophitic plates enclosing the other minerals or as zoned microphenocrysts.

Many basalt sequences become increasingly porphyritic upward, commonly culminating in a few highly feldsparphyric flows in which plagioclase phenocrysts up to 2 cm across form as much as 50% of the rock. This change in mineralogy is accompanied by a shift in bulk composition from alkali olivine basalt to hawaiite. The hawaiites also contain lesser amounts of pyroxene and olivine in a subophitic or interstitial groundmass of plagioclase laths, granular olivine, and opaques.

Transitional rocks between basalt and the felsic suite are relatively rare. Trachybasalt and tristanite, which are confined to the Little Iskut and Ice Peak formations, are the only volumetrically significant rocks in the complex that fall within the potassic series as defined by Irvine and Barager (1971). They are commonly aphyric or contain sparse microphenocrysts of alkali feldspar and ferrohedenbergite in a felted groundmass of subhedral, potassic anorthoclase, intergranular prisms of ferrohedenbergite, minor fayalite and finely disseminated opaque oxides. Transitional members of the sodic series, mugearite and benmoreite, are even less abundant than trachybasalt, and are confined mainly to the Ice Peak Formation.

Many of the older basalt flows (Raspberry and Armadillo) have a pervasive carbonate alteration in which the interstitial glass has been hydrated and partly replaced by calcite. Vesicles in these flows have been lined or filled with aragonite, calcite, silica and ankerite. However, the alteration does not appear to have affected the silicate minerals. The Nido, Kounugu basalts show no petrographic

evidence of alteration, but may contain extensive carbonate as vesicle fillings. Basalts younger than the Nido are both unaltered and have open vesicles.

The felsic suite includes both alkaline and peralkaline members which appear to grade from one to another without any obvious mineralogical or chemical gaps. The trachyte is a nearly pure feldspar rock comprising sparse microphenocrysts of alkali feldspar in a trachytic groundmass of ragged alkali feldspar laths, finely disseminated opaque oxides, minor interstitial sodic pyroxene and rarely a sodic amphibole. Sparse phenocrysts of more calcic feldspar and pyroxene are present in many of the trachytes. These have reacted with the groundmass, the feldspars having fritted cores and the pyroxenes being embayed, rounded and mantled by green sodic ferrohedenbergite. With the appearance of interstitial and phenocrystic quartz, the trachytes grade into sodic rhyolites composed mostly of quartz and alkali feldspar with only a trace of feldspar minerals (mainly sodic pyroxene) and opaque oxides. The transition to peralkaline rocks is manifest in the appearance of soda-rich feldspar minerals (aenigmatite, arfvedsonite, aegirine, and kataphorite) and by the disappearance of plagioclase, leaving sanidine and/or anorthoclase as the only feldspar phase. The same minerals are present in all of the peralkaline members, but the comendites are relatively rich in both phenocryst and groundmass quartz, and the pantelleritic rocks are relatively rich in feldspar minerals and opaque oxides.

The felsic rocks are mostly fine grained and holocrystalline, but unaltered obsidians are present as a quenched basal layer on trachyte and comendite flows. The holocrystalline felsic rocks are unaltered except for partial oxidation of opaque oxides. Voids in these rocks are commonly lined with an assemblage of euhedral, vapour-phase minerals including quartz, aegirine, arfvedsonite, aenigmatite, minor biotite, fluorite and analcime.

MINERAL CHEMISTRY

The compositions of the principal mineral phases in representative samples from each of the 13 formations in the complex, and from cumulate inclusions, were determined by microprobe (Appendix 1). Analyses were performed by L.C. Pigge on the University of British Columbia ARL SEMQ microprobe, using 10 2s counting periods for each element. Reduction of the silicate analyses to end member compositions was done by P.B. Read using programs from Australian National University modified by E.J. Essene and P.B. Read. Analyses of opaque oxides were recalculated according to the method described by Carmichael (1967).

Feldspar

Feldspar compositions from rocks of the Mount Edziza Volcanic Complex are concentrated in the labradorite and anorthoclase fields of the feldspar ternary (Fig. 234), reflecting the bimodal whole-rock chemistry of the suite. Plagioclase microphenocrysts in the basalts commonly have relatively large unzoned cores surrounded by narrow rims with up to 10 mol. percent normal zoning. Core compositions range from An₇₅ to An₅₄. Larger phenocrysts, particularly those in the hawaiites, display complex oscillatory and reverse zoning and range in core compositions from An₇₅ to An₄₂. Groundmass plagioclase is either unzoned or displays slight normal zoning of less than 2 mol. percent. Up to 2.9 mol. percent Or is present in the phenocrystic plagioclase of the alkali olivine basalts, whereas phenocrysts in the more highly evolved hawaiites contain as much as 4.4% Or.

Phenocrystic and groundmass feldspar in the less abundant intermediate rocks (trachybasalt, mugearite, benmoreite) ranges from An₁₀ to An₃₀ and may contain up to 18% Or. Andesine cores in the larger phenocrysts commonly grade to rims of anorthoclase and groundmass feldspars are zoned from oligoclase to anorthoclase.

Anorthoclase is the most abundant feldspar in the felsic rocks (trachytes, comendites) but sanidine is also present as

both a phenocryst and groundmass phase in many of the comendites. Feldspar in the trachytes contains up to 3% An compared to less than 1% in feldspar from most of the comendites.

Pyroxene

In the alkali olivine basalts, groundmass pyroxene occurs as purple to brown ophitic or subophitic grains that enclose the groundmass feldspar or, less commonly, as interstitial aggregates of small clear to pale green euhedral crystals. Analyses from both types plot near the augite-salite field boundary of the pyroxene quadrilateral (Fig. 235) but the strongly pigmented ophitic pyroxene has a significantly higher TiO₂ content (up to 5%). Calcic augite phenocrysts in the alkali basalts and hawaiites are commonly twinned and many are distinctly zoned. Both groundmass and phenocrystic clinopyroxenes in the intermediate rocks (hawaiite to trachybasalt) range from aluminous augite through ferroaugite to hedenbergite. The compositions of pyroxene phenocrysts from the felsic rocks range from ferroaugite and hedenbergite in trachybasalts and trachytes to sodic hedenbergite, aegirine augite or acmite in the comendites. Those analyses with more than 10% Ac have been recalculated to Jd — Ac + Tsch + Di + He and plotted on the sodic pyroxene ternary of Clark and Papike (1968) (Fig. 236). Groundmass pyroxenes in the comendites are

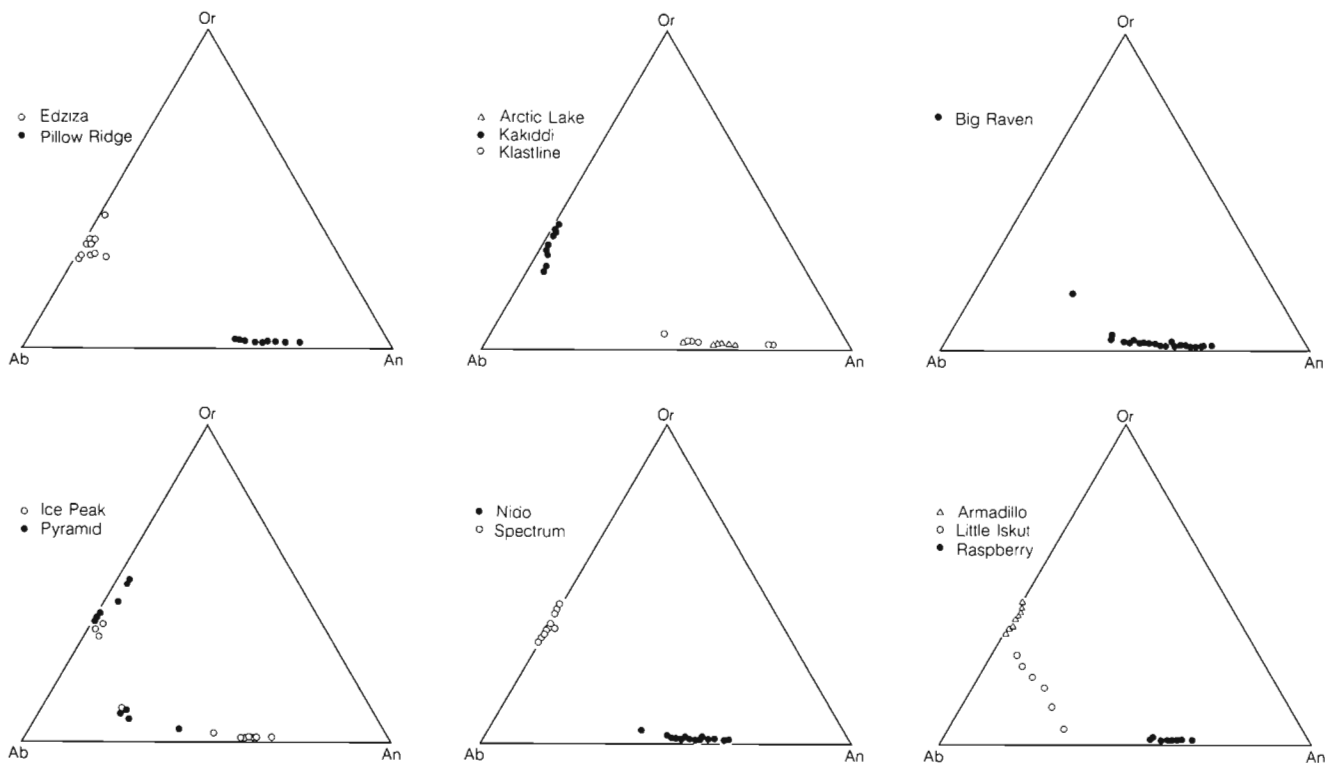


Figure 234. Ab-An-Or plots of feldspar compositions from the Mount Edziza Volcanic Complex, showing the distinct separation of feldspar compositions related to the basaltic, felsic, and chemically transitional formations.

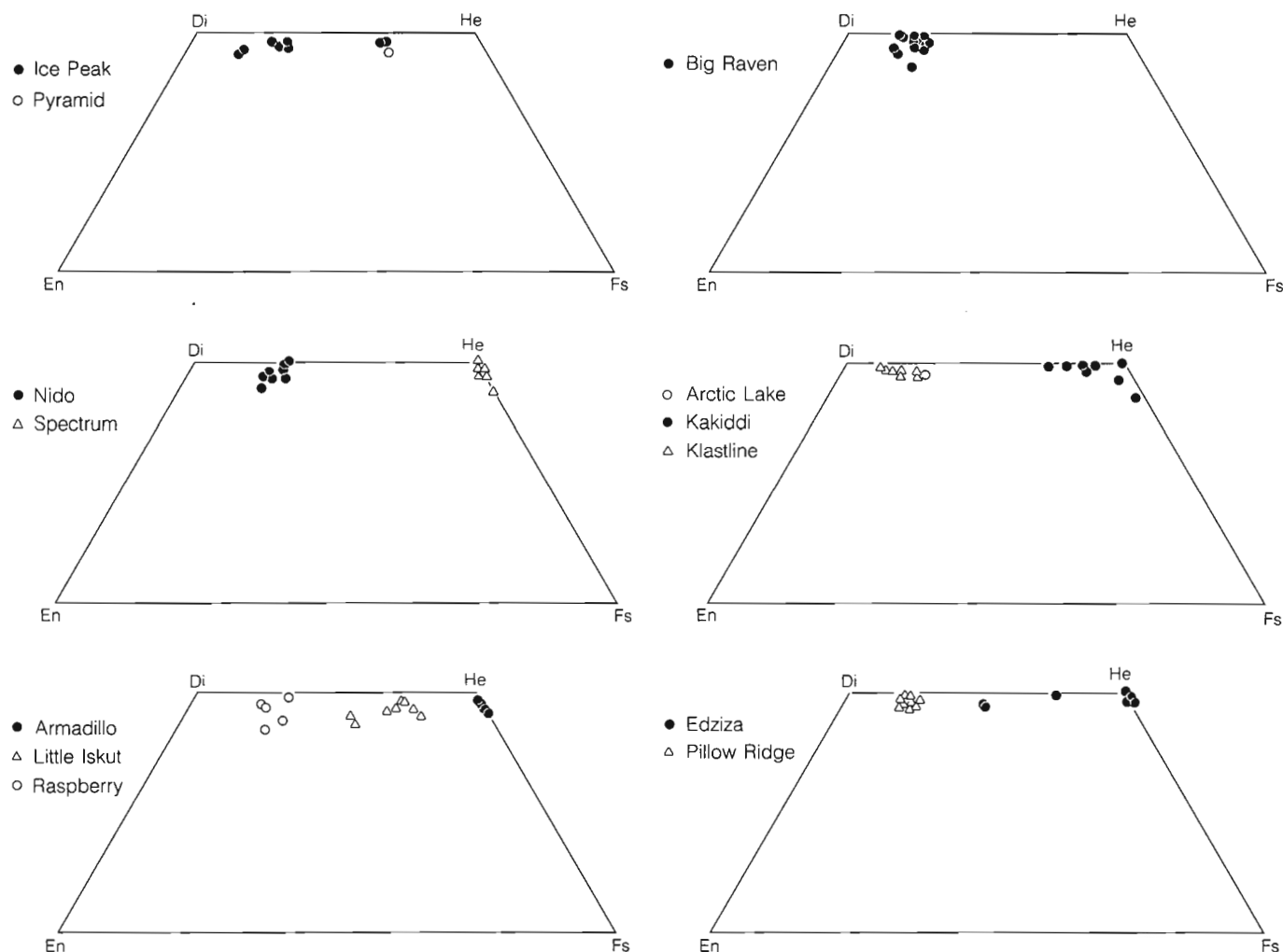


Figure 235. *En-Fs-Di-He plot of clinopyroxene compositions, showing the close relationship between pyroxene composition and rock type. Diopside augite is characteristic of basaltic formations whereas pyroxenes from felsic formations are mainly hedenbergite. Pyroxenes of intermediate composition are confined to rocks from formations such as the Little Iskut and Ice Peak which have intermediate whole-rock compositions.*

nearly pure end member acmite ($\text{NaFe} + ^3\text{Si}_2\text{O}_6$). The crystallization trend of clinopyroxenes in rocks of the Mount Edziza Volcanic Complex mimics that of the whole-rock chemistry, extreme Fe-enrichment followed by a sharp increase in Na_2O .

Olivine

Almost the entire range of olivine compositions is present in rocks of the Mount Edziza Volcanic Complex (Fig. 237). Forsteritic olivine is a major phenocrystic and groundmass phase of the alkali olivine basalts and a less abundant phase of the hawaiites. Phenocryst compositions range from Fo_{74} to Fo_{85} whereas groundmass olivines are between Fo_{65} and Fo_{50} . Zoning over a range of about 10% is common.

Pale yellow fayalitic olivine is present in minor amounts as microphenocrysts in the trachybasalts, trachytes and comendites. It is commonly too small to probe but a composition of $\text{Fo}_{2.7}$ from a relatively large phenocryst in Little Iskut trachybasalt suggests that fayalite in the more felsic rocks is approaching a pure, end member composition.

Amphibole

Amphibole (Fig. 238) is found only in the peralkaline felsic rocks of the Mount Edziza Volcanic Complex. It is widespread as a groundmass mineral where it is usually associated with aenigmatite and acmitic pyroxene. The groundmass amphibole is commonly poikilitic and too fine grained to analyze by microprobe. It includes blue to brown pleochroic arfvedsonite and a pale yellow to dark yellow

MOUNT EDZIZA

pleochroic amphibole of similar habit that is probably kataphorite. Arfvedsonite also forms subhedral microphenocrysts and mantles around fayalite and aenigmatite phenocrysts. All of the probe analyses were made on these coarser grains.

Aenigmatite

Aenigmatite ($\text{Na}_2\text{Fe}_5\text{TiSi}_6\text{O}_{20}$) is a common constituent of the comenditic trachytes and comendites of the Mount Edziza Volcanic Complex (Yagi and Souther, 1974). It

occurs in the groundmass as poikilitic grains and radiating acicular crystals associated with arfvedsonite, acmite and quartz in spherulites. It is also found as subhedral microphenocrysts in comendite lavas and tephra and as microlites in comenditic obsidian. Microprobe analyses show no significant differences in the composition of groundmass and phenocryst phases, or between the cores and rims of individual phenocrysts.

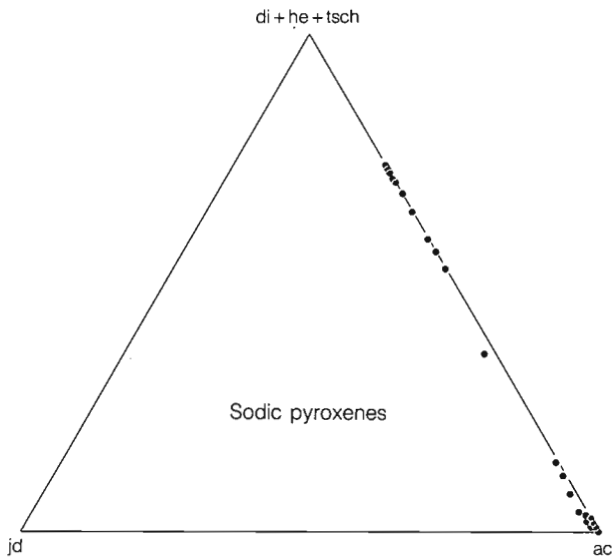


Figure 236. Jd-Ac-(Di + He + Tsch) plot of sodic pyroxenes (> 10% Na_2O) from the Mount Edziza Volcanic Complex. Diagram based on Clark and Papike (1968).

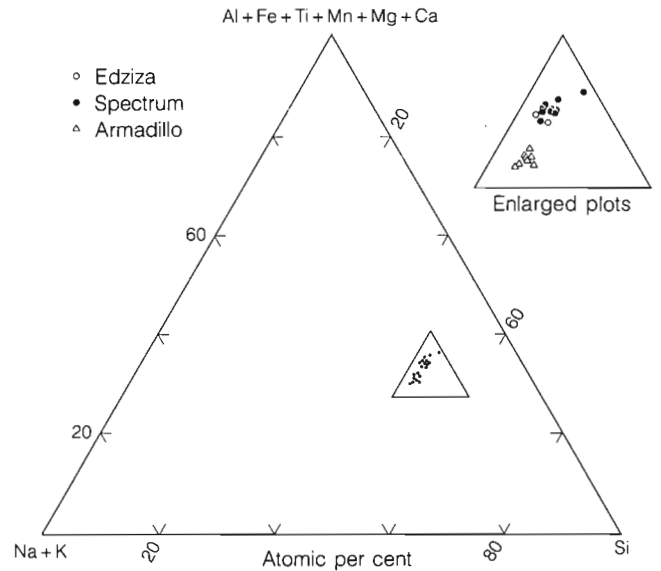


Figure 238. Si-(Na + K)-(Al + Fe + Ti + Mn + Mg + Ca) plot of sodic amphibole from felsic rocks of the Mount Edziza, Spectrum and Armadillo formations. Diagram based on Ernst (1962)

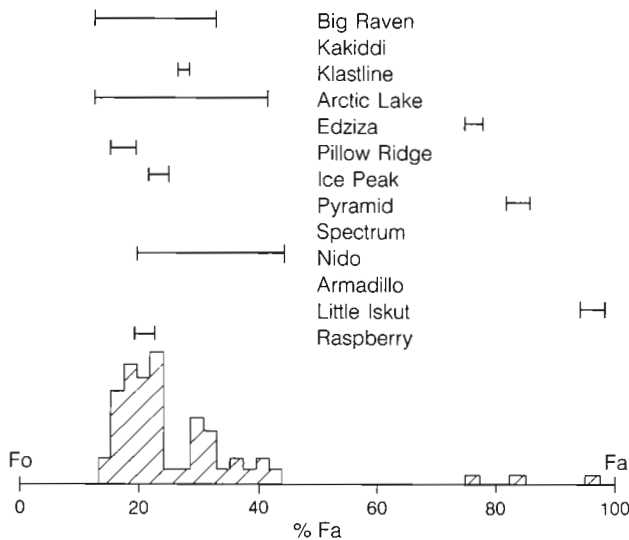


Figure 237. Frequency distribution of olivine compositions in rocks of the Mount Edziza Volcanic Complex, and the range of compositions found in each olivine-bearing formation.

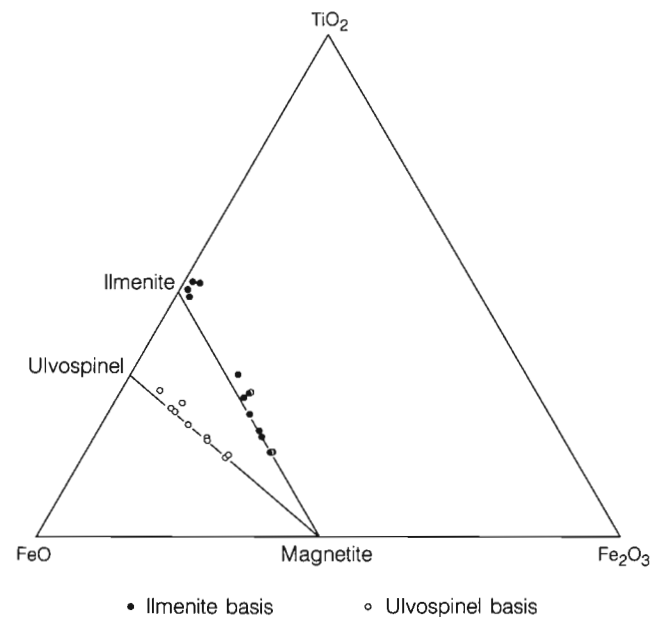


Figure 239. $\text{FeO-TiO}_2\text{-Fe}_2\text{O}_3$ plot of 16 microprobe analyses from the Mount Edziza Volcanic Complex. End members recalculated by the method of Carmichael (1967).

Iron-titanium oxides

Iron-titanium oxides are present in both the basic and felsic rocks of the Mount Edziza Volcanic Complex. In the basalts they are found as microphenocrysts, groundmass granules and as inclusions in both feldspar and ferromagnesian minerals. Most of the opaque oxide in the trachytes and comendites occurs as groundmass granules and inclusions.

Rare microphenocrysts are commonly surrounded by reaction rims that may include aenigmatite and/or amphibole.

The opaque oxides were not studied in polished section but probe analyses indicate a range of TiO_2 from pure ilmenite to titanomagnetite containing less than 50% ulvospinel. Analyses were recalculated using the method of Carmichael (1967) and plotted on the $\text{FeO-TiO}_2\text{-Fe}_2\text{O}_3$ ternary (Fig. 239).

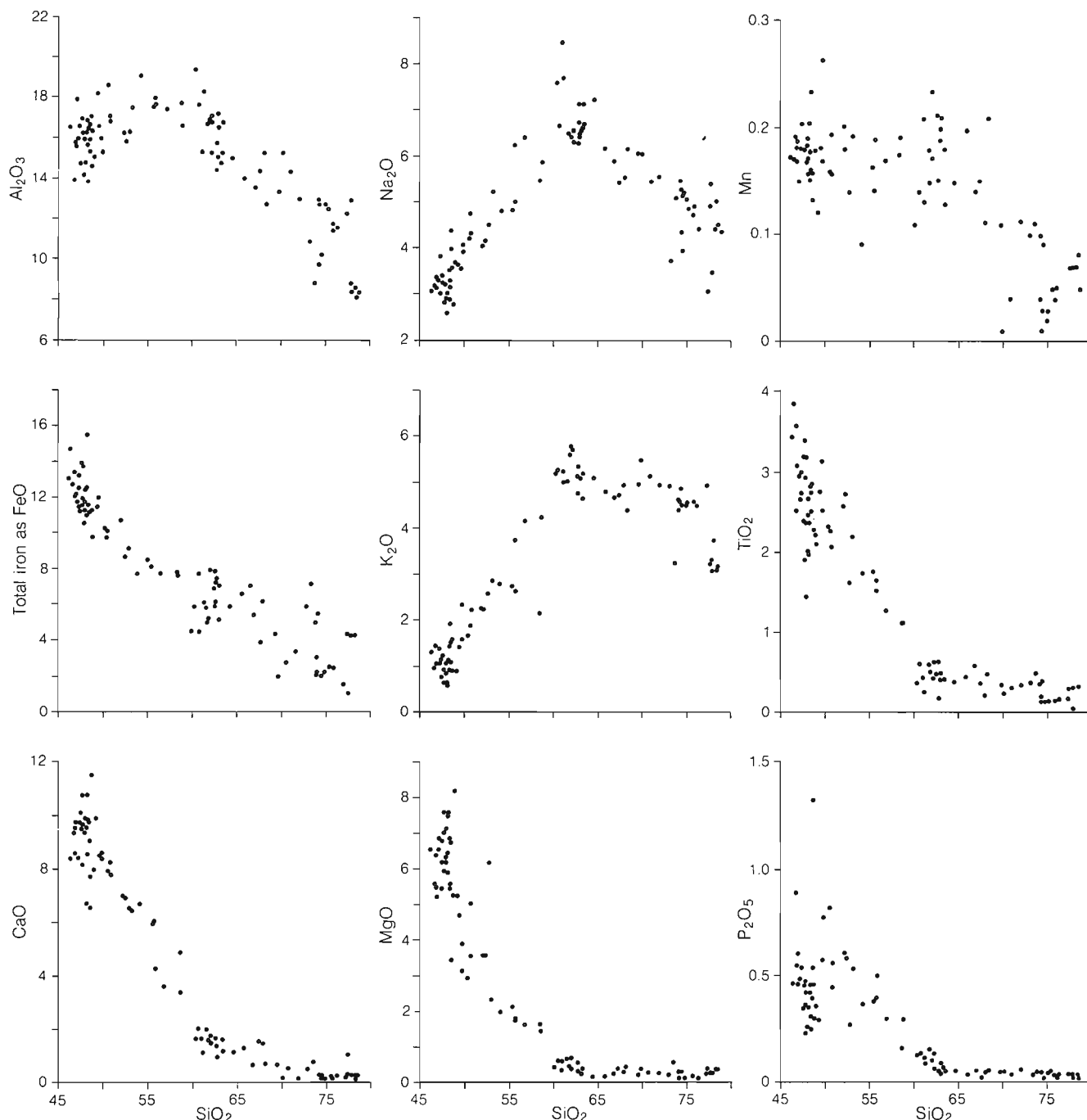


Figure 240. Harker diagram showing the variation in weight per cent in major element abundances vs. SiO_2 for 95 analyses of rocks from the Mount Edziza Volcanic Complex.

MgO is relatively enriched in oxide phases from basalts of the Raspberry and Big Raven formations and depleted in oxide phases from trachytes and comendites of the Ice Peak and Edziza formations. A similar relationship between MgO and MnO and rock types was noted by Bevier (1978) in basic and felsic peralkaline lavas of the Rainbow Range in central British Columbia.

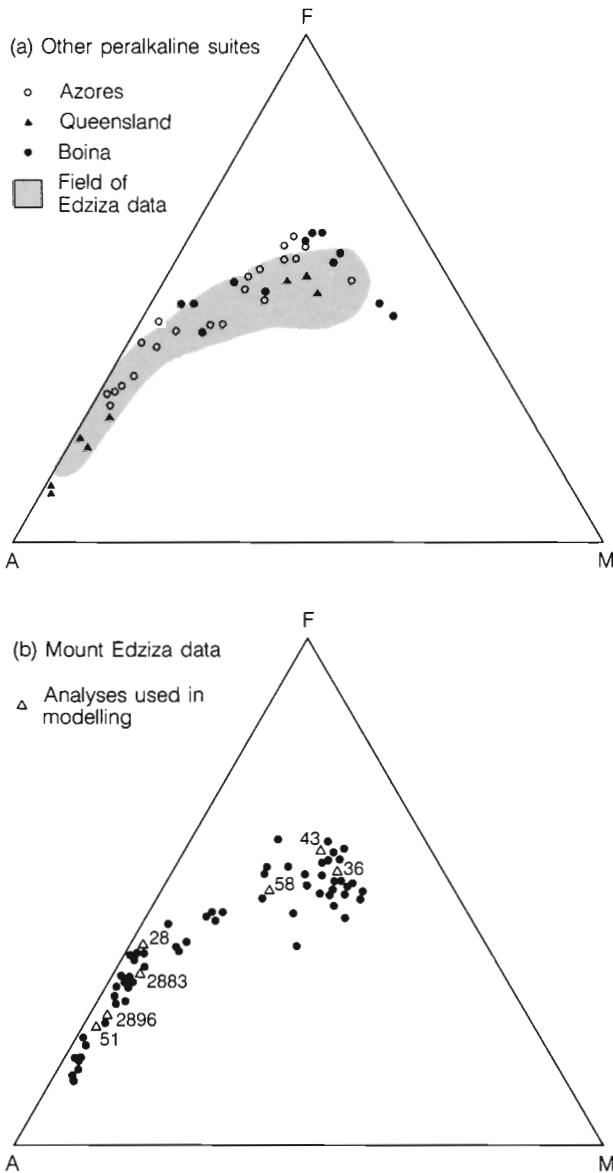


Figure 241. AFM diagrams. (a) A comparison of the Mount Edziza Volcanic Complex data with that from Boina (Barberi et al., 1975), SE Queensland (Ewart et al., 1968) and the Azores (Self and Gunn, 1976). (b) The distribution of the Mount Edziza Volcanic Complex data and the positions of analyses used in the petrological modelling.

WHOLE-ROCK CHEMISTRY

Major elements

Whole-rock chemical analyses were made by the Geological Survey of Canada, under the direction of S. Abbey and J.A. Maxwell. X-ray fluorescence (XRF) techniques were used for SiO₂, Al₂O₃, total Fe as Fe₂O₃, CaO, MgO, K₂O, TiO₂, MnO, NiO, and Cr₂O₃. Total H₂O, CO₂, P₂O₅, Na₂O, and FeO were measured by rapid chemical means. Sulphur was determined by conventional chemical methods and Fe₂O₃ by difference. The 95 superior analyses presented in this study (Appendix 2) were selected such that totals are within 1% of a hundred and the total of H₂O plus CO₂ is less than 3 wt%.

The suite of analyzed rocks includes representative specimens from each of the 13 formations. It covers a range of silica values from 46 to 80% but volumetrically there is

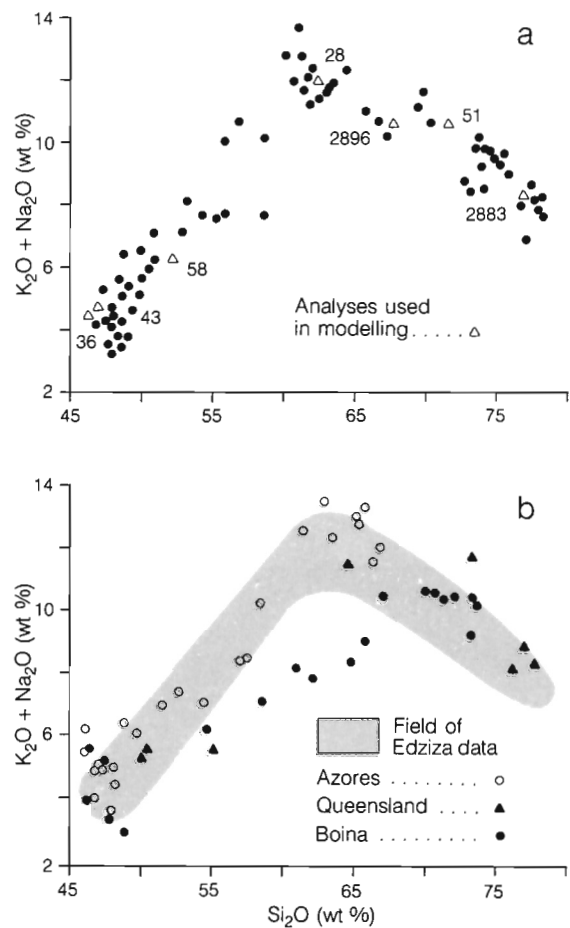


Figure 242. Plot of total alkalis vs. SiO₂. (a) The distribution of the Mount Edziza Volcanic Complex data and the positions of analyses used in the petrological modelling. (b) A comparison with other peralkaline suites (see Fig. 241).

a distinct compositional gap between 52 and 62% silica (Fig. 240). The gap appears to form a boundary zone across which there is a profound change in the proportions of most of the constituent oxides, particularly the alkalis, CaO, and MgO. It is partly bridged by a volumetrically small group of intermediate rocks, mostly from the Little Iskut and Ice Peak formations, that show a regular variation between the end-member groups.

The trends on the AFM and alkali vs. silica diagrams (Fig. 241,242) are similar to other peralkaline suites in British Columbia such as Level Mountain (Hamilton, 1981), Rainbow Range (Bevier, 1978) and the Ilgachuz Range (Souther, 1984), and to peralkaline suites from other regions such as the Afar Rift (Barberi et al., 1975), the

Azores (Self and Gunn, 1976), and Mayor Island (Ewart et al., 1968). There is a nearly linear increase in total alkalis between 46 and about 66% silica. The decline in total alkalis at higher silica values is certainly due in part to the constant sum effect but it could be accentuated by the separation of an alkaline vapour phase as proposed by Gibson (1972) to explain chemical differences between the pre- and post-caldera suites of Fantale, and by Lindsley et al. (1971) to account for the separation of a peralkaline residuum from the Picture Gorge basalt. It could also be influenced by extensive fractionation of alkali feldspar or a soda-rich mineral such as aenigmatite or acmitic pyroxene, all of which are present as phenocrysts in some of the Edziza comendites.

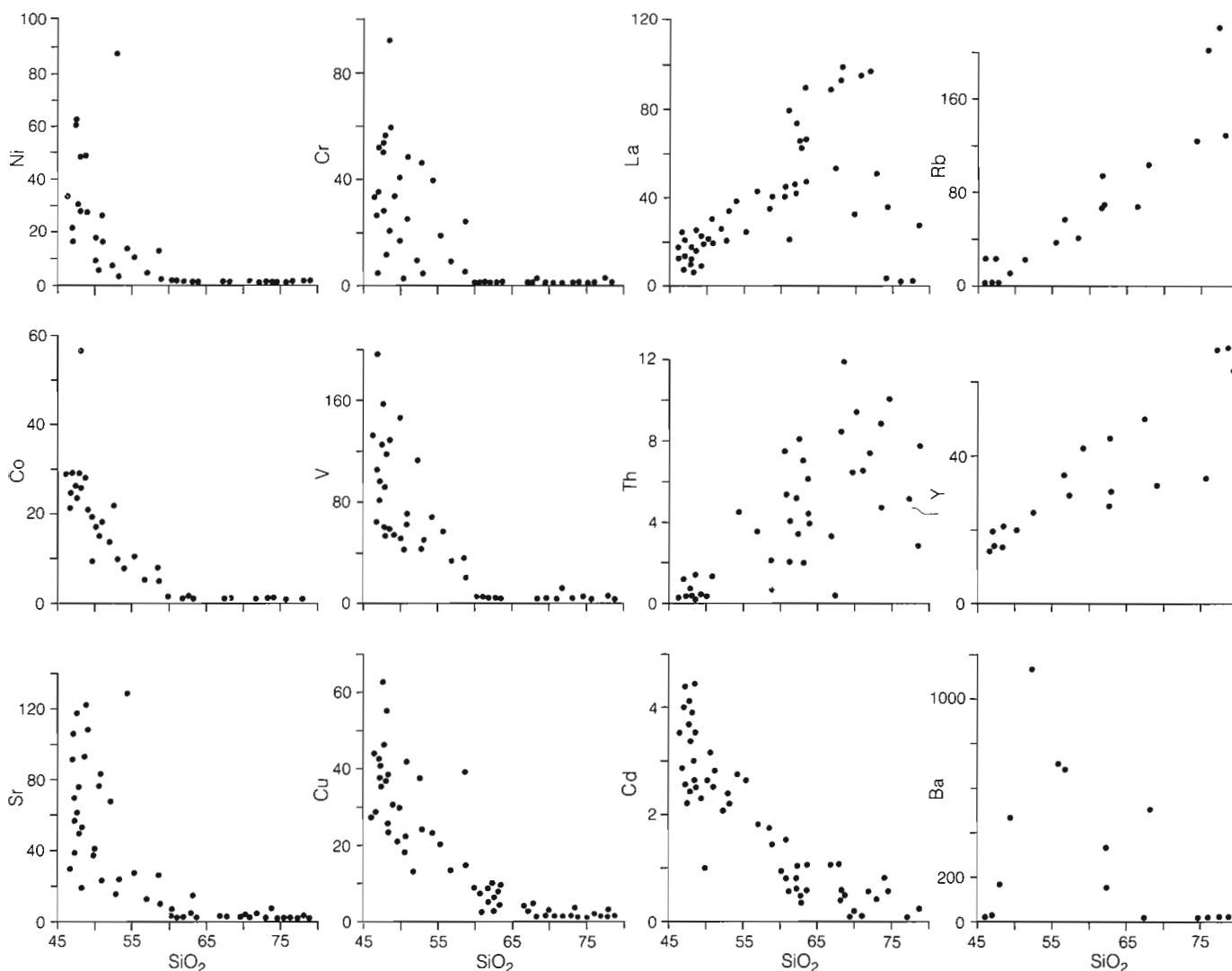


Figure 243. Plot of trace elements in weight per cent Ni, Co, Sr, Cr, V, Cu, La, Th, Cd, Rb, Y, Ba (ppm) vs. SiO₂.

Minor elements

Two groups of minor element analyses were run on the same powders prepared for the major element analyses (Appendix 2). The first group of 90 samples was analyzed by Acme Analytical Laboratories of Vancouver, for Sr, Cr, Ni, Co, Cu, Zn, V, Cd, La, and Th using an inductively coupled argon plasma (ICP) method. A second group of 19 samples was analyzed by C. Hickson for Ba, Rb, and Y, using XRF spectrometry.

Nova Track Analysts Limited of Vancouver analyzed ten samples by neutron activation for the rare-earth elements La, Ce, Nd, Sm, Eu, Tb, Yb, and Lu (Appendix 3).

Minor-element distribution

The variation in minor element abundances within a suite of genetically related rocks should ideally reflect the major-element chemistry in a predictable and systematic manner. In the case of a fractionation series the minor-element variation is controlled by the crystal/liquid partition coefficients (K_D) for each of the minor elements in the melt and by the order in which the different cumulate phases are removed by fractionation. However, the K_D values for any given element (Irving, 1978; Berman, 1981) may vary widely depending on bulk composition, temperature, pressure, and oxygen fugacity. Also, many trace elements are concentrated in minerals such as apatite and zircon which form small crystals and consequently have very slow settling rates. As a result, such elements may remain suspended in the melt long after they have been partitioned into a mineral phase. In view of these difficulties, a quantitative treatment of trace-element behaviour was not attempted but the affinity of certain trace elements for specific cumulate phases is so strong that their variation provides at least a qualitative test of fractionation processes.

The variation of 12 trace-elements with respect to increasing silica (Fig. 243) shows four types of trends: (1) abrupt depletion between 45 and 58% silica; (2) systematic depletion over the entire range of silica values; (3) systematic increase over the entire range of silica values; and (4) increase to a maximum at an intermediate silica value followed by depletion.

The first type is illustrated by Ni, Co, Cr, V and Sr, all of which decrease at least an order of magnitude between 45 and 58% silica and are near or below detection limits in the more siliceous end members. Major-element variations across this same silica range show a sharp decline in MgO, CaO, FeO, TiO₂ and P₂O₅ probably caused by the early fractionation of olivine, plagioclase, pyroxene, titaniferous magnetite and apatite. The affinity of olivine for Ni ($K_D \sim 20$) and Co ($K_D \sim 3$) would account for the sharp decline in nickel and the somewhat slower decline in cobalt with increasing silica. The decrease in Cr ($K_D > 100$) and V ($K_D \sim 40$) is probably due to removal of these elements in titanomagnetite (or other iron titanium oxide) during the

early stages of fractionation. The sharp decrease in strontium between 45 and 50% silica and somewhat slower decrease between 50 and 58% silica can be explained by strong initial fractionation of plagioclase ($K_D \sim 2-4$). The abrupt decrease in P₂O₅ between 45 and 50% silica suggests that apatite was one of the first mineral phases separated from the melt. Its occurrence as tiny prisms with extremely slow settling rates (Shaw, 1965) preclude its removal as an independent phase. Instead, an early formed suspension of apatite microlites may have been scavenged from the melt as inclusions in minerals such as olivine and plagioclase which form larger crystals with higher settling rates.

Elements which show a systematic decrease across the entire range of silica values (Cu, Cd) appear to correlate with FeO which displays a linear decrease across the entire suite. Depletion of these elements could be caused by the removal of pyroxene and opaque oxides which, from petrographic observations, continued to separate throughout the entire fractionation process.

The increase of 4 elements La, Th, Rb and Y with increasing silica is explained by the very low distribution coefficients ($K_D \ll 1$) with respect to any of the cumulate phases that are believed to have separated from the Edziza suite. They have behaved as incompatible elements, excluded by all of the crystalline phases, and thus concentrated in the residual liquid.

Barium shows considerable analytical scatter but it roughly parallels the variation of Na₂O and K₂O which increase up to a maximum at about 58% silica and then decline. The initial increase in both alkalis and Ba probably results from the fractionation of large quantities of plagioclase and mafic minerals. As the residual liquid became increasingly alkaline the proportion of K₂O and Ba entering the feldspar structure also increased. Because of the strong affinity of potassium feldspar for Ba ($K_D \sim 3-10$) a decrease of Ba would be expected soon after the appearance of an alkali feldspar on the liquidus. The subsequent separation of relatively large amounts of alkali feldspar would effectively scavenge any remaining barium from the melt, leaving the felsic end-members barium-depleted.

Rare-earth elements

Chondrite-normalized rare-earth patterns and trace-element variation for a group of ten representative samples (Fig. 244) are distinctly different for the basic and felsic rocks. The felsic rocks show a fifteen-fold increase in light REE abundances compared to a much smaller increase of two to five times in the heavy rare-earths.

The basic suite shows a progressive increase in ΣREE from alkali olivine basalt through hawaiite, mugearite and trachybasalt to benmoreite, but there is little change in the ratio of light to heavy REE. Europium is either undepleted or displays only a slight decrease relative to Sm and Tb. In

contrast the felsic rocks, trachyte, comenditic trachyte and comendite, show a large increase in both Σ REE and the ratio of light to heavy REE and europium shows a strong negative anomaly.

The relatively uniform light to heavy REE ratios in the basic suite support the other major- and trace-element evidence for early removal of olivine, for which the crystal/liquid partition coefficients are almost the same for both light and heavy rare-earths (Irving, 1978). This is further supported by the progressive depletion of Ni with increasing Σ REE (Fig. 244).

Because of its strong affinity for the REE, apatite ($K_D \sim 50$) may exert an overriding influence on the distribution of rare-earth and other incompatible elements such as Zr, Nb, Ce, U (Nagasawa, 1970; Zielinski, 1975). In the case of the Mount Edziza Volcanic Complex, P_2O_5 was effectively removed by early fractionation of apatite, before the incompatible elements had been concentrated in the melt. Thus, despite the high bulk distribution coefficients, the removal of incompatible elements by apatite was small, and their exclusion by subsequent cumulate phases led to the observed increase in the more highly fractionated rocks.

The increase in the ratio of light to heavy REE in the trachytes and comendites having high Σ REE abundances is probably due to extensive removal of an Fe-Ti oxide during the middle stages of fractionation. Ilmenite/liquid partition coefficients at 1140°C are an order of magnitude higher for Tm and Yb than for Ce (McKay and Weill, 1976). Thus separation of an oxide would leave the residual liquid relatively enriched in the light rare-earths. The fractionation of an Fe-Ti oxide phase is supported by the sharp decrease in both Fe and Ti abundances on the SiO_2 variation diagram (Fig. 240).

The pronounced negative Eu anomaly in the REE profiles of the trachytes and comendites confirms the importance of feldspar fractionation in the origin of these rocks. The effect of feldspar removal is also seen in the abundances of Sr and Ba (Fig. 244). These elements, which are concentrated in the feldspar structure, decrease in concentration from 5-70 ppm in the basic suite to less than 1 ppm in the trachytes and comendites. The distribution of K_2O with respect to Σ REE is also instructive (Fig. 240). The decline in Ni, due to olivine separation, was accompanied by systematic increase in K_2O in the residual magma up to a maximum of 5.6% in the most primitive trachyte (No. 11). The

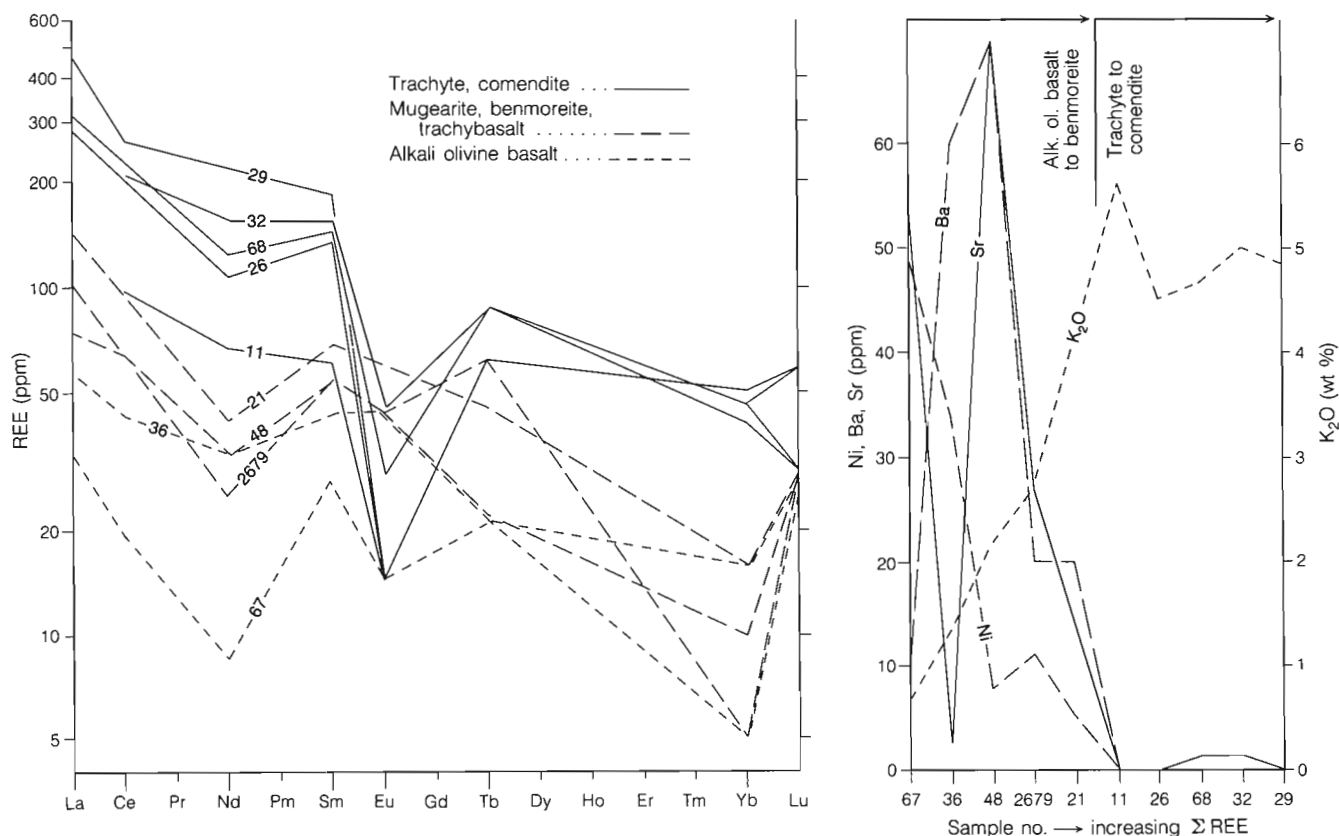


Figure 244. Chondrite normalized REE profiles, and variation of Ni, Ba, Sr, and K versus Σ REE (from Souther and Hickson, 1984).

subsequent fall in K_2O in the felsic rocks, having still higher ΣREE abundances, suggests that the late stage separation of alkali feldspar was an important factor in the evolution of the felsic suite.

Rb, Sr and Sr isotopes

Rb, Sr and Sr isotopic compositions of representative rocks from the Mount Edziza Volcanic Complex are reported in Souther et al. (1984) from which the following summary is taken. Eleven rocks and one feldspar

separate were analyzed for Rb, Sr and Sr isotopic composition (Table 28). The present-day isotopic $^{87}Sr/^{86}Sr$ ratios vary from 0.7026 to 0.720. The basalts, relatively rich in Sr and low in Rb/Sr ratio, are for the most part between 0.7026 and 0.7029 and are not subject to any correction for *in situ* decay. Much of the more radiogenic Sr in other samples is generated by Rb decay in rocks with very high Rb/Sr ratios and, because the ages of these rocks are known from K-Ar dating, initial ratios can be calculated (Table 28). The initial ratios are clearly variable, suggesting that the volcanic suites have erupted without isotopic homogenization or rapid, closed-system fractionation.

Table 28. Sr-isotope data and Rb/Sr ratios of lavas of the Mount Edziza Volcanic Complex (from Souther et al., 1984).

Sample no.	Formation and lithology	Geographic co-ordinates	ppm Sr	ppm Rb	$^{87}Rb/^{86}Sr$	$^{87}Sr/^{86}Sr$	Age	Initial $^{87}Sr/^{86}Sr$
ML270665	Big Raven basalt	57° 51.3' N 130° 38.4' W	468	32	0.197	0.7029	~0.01	0.7029
SE442065	Kakiddi Trachyte	57° 39.8' N 130° 41.2' W	5.4	103	54.7	0.7036	0.30 ± 0.02	0.7034
ML2902a65	Edziza Trachyte	57° 41.8' N 130° 42.5' W	145	103	2.06	0.7026	0.8	0.7026
SE281967	Ice Peak Trachyte	57° 40.4' N 130° 36.1' W	467	75.5	0.4666	0.7029	~1	0.7029
SE3815a67	Ice Peak Mugearite	57° 42.5' N 130° 32.0' W	13.5	82	17.6	0.7087	~1	0.7084
SE2902a66	Pyramid Comendite	57° 37.3' N 130° 37.1' W	0.8	119	408	0.7145	1.1	0.7081
SE130172	Spectrum Comendite	57° 26.4' N 130° 36.0' W	*1.64	185	327	0.720	3.0 ± 0.1	0.7060
SE140272	Spectrum Comendite glass	57° 26.0' N 130° 39.9' W	*2.10	190	265	0.718	3.4 ± 0.1	0.7053
SE190265	Armadillo Comenditic glass	57° 32.3' N 130° 44.5' W	5.2	136	76.4	0.7111	6.4 ± 0.2	0.7042
ML300765	Armadillo Basalt	57° 41.4' N 130° 45.2' W	431	18.5	0.124	0.7029	~6.5	0.7029
SE142166	Raspberry Hawaiiite	57° 38.9' N 130° 50.9' W	665	23.7	0.103	0.7033	6.4 ± 0.3	0.7033
SE142166	Raspberry (Feldspar)	57° 38.9' N 130° 50.9' W	1584	0.5	0.001	0.7027	11.4 ± 0.3	0.7027

*Sr concentration determined by isotope dilution

Rb and Sr concentrations were determined by replicate analysis of pressed powder pellets using X-ray fluorescence. U.S. Geological Survey rock standards were used for calibration; mass absorption coefficients were obtained from Mo $K\alpha$ Compton scattering measurements. For concentrations above 20 ppm Rb/Sr ratios have a precision of 2% (1 σ) and concentrations a precision of 5% (1 σ). At low concentrations the precision is ± 1 ppm. Sr isotopic composition was measured on unspiked samples prepared using standard ion exchange techniques. Two samples with very low Sr were spiked with nearly pure ^{84}Sr and the Sr concentrations thus determined by isotope dilution with a precision of 2% (1 σ). The mass spectrometer (60° sector, 30 cm radius, solid source) is of U.S. National Bureau of Standards design, modified by H. Faul. Data acquisition is digitized and automated using a NOVA computer. Experimental data have been normalized to a $^{86}Sr/^{88}Sr$ ratio of 0.1194 and adjusted so that the NBS standard $SrCO_3$ (SRM987) gives a $^{87}Sr/^{86}Sr$ ratio of $.71022 \pm 2$ and the Eimer and Amend Sr a ratio of 0.70800 ± 2 . The precision of a single $^{87}Sr/^{86}Sr$ ratio is 0.00013 (1 σ). Rb-Sr dates are based on a Rb decay constant of $1.42 \times 10^{-11} a^{-1}$.

The extremely low Sr contents of more fractionated rocks are evident in Figure 245, which compares Sr abundance and initial isotopic composition of the Edziza suite with volcanic arc and ocean-floor samples of a global compilation (Faure and Powell, 1972). The Edziza trend lies outside the arc field, either with lower $^{87}\text{Sr}/^{86}\text{Sr}$ ratio for samples rich in Sr or with much lower Sr content for samples enriched in radiogenic Sr. The observed pattern is like that of the Rainbow Range, another peralkaline central volcanic complex in British Columbia (Bevier, 1981).

Radiogenic Sr in low-Sr rocks at the time of eruption can be explained by contamination or by radiogenic accumulation during residence in a magma chamber prior to eruption. Both explanations may apply to Mount Edziza.

Two samples (Table 28, nos. SE142166, SE3815a67) show clear evidence of contamination with radiogenic, probably crustal, Sr. They are shown with distinctive symbols (Fig. 245,246,247) to distinguish them from samples for which contamination is less certain or unimportant. The Raspberry Formation basalt-feldspar pair is discordant (Table 28, no. SE142166); the matrix rock is more radiogenic, yet lower in Sr. The difference cannot be explained

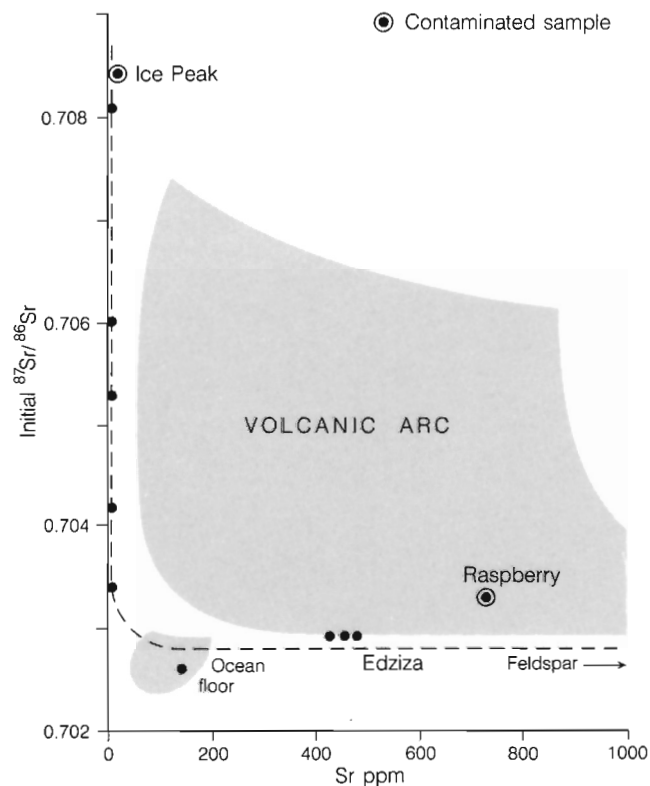


Figure 245. Plot of initial $^{87}\text{Sr}/^{86}\text{Sr}$ vs. Sr abundance, showing the trend of isotopic compositions of the Edziza suite (dotted line) compared to the fields (shaded) for volcanic arc and ocean floor samples. The feldspar sample (Table 28, no. SE412166) plots outside the diagram. The two anomalous samples, Raspberry (no. 1) and Ice Peak (no. 2), are attributed to crustal contamination (from Souther et al., 1984).

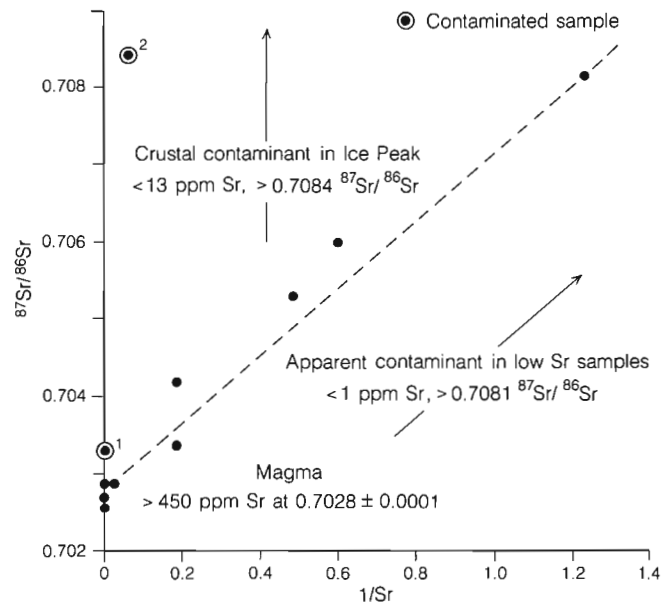


Figure 246. Plot of $^{87}\text{Sr}/^{86}\text{Sr}$ vs. $1/\text{Sr}$, showing the clustering of high-Sr, low-initial-ratio basalts around 0.7028, representative of the magma source. The high $^{87}\text{Sr}/^{86}\text{Sr}$ ratios of two samples, Raspberry (no. 1) and Ice Peak (no. 2), are attributed to contamination with radiogenic crustal Sr. The high $^{87}\text{Sr}/^{86}\text{Sr}$ and low Sr of the more differentiated end members are probably due to extreme feldspar fractionation and growth of ^{87}Sr during residence of the magma in crustal reservoirs, or to contamination with a low Sr and high $^{87}\text{Sr}/^{86}\text{Sr}$ magma that might be produced by extreme fractionation of a hybrid magma such as the Ice Peak (no. 2). In this diagram, mixing of two components produces a linear spread of points, with the pure components lying at or beyond the ends of the line defined by observed analyses. The nature of possible components involved in mixing processes that might produce the Mount Edziza Volcanic Complex magmas is indicated in the diagram (from Souther et al., 1984).

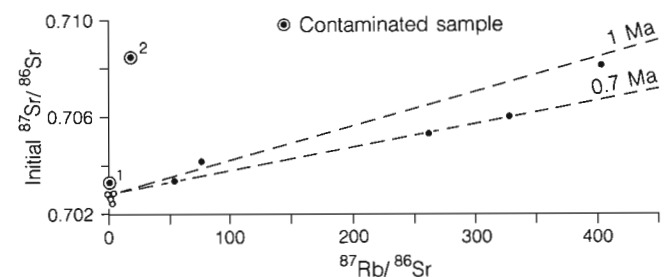


Figure 247. Rb-Sr isochron diagram for 11 whole-rocks and 1 feldspar from the Mount Edziza Volcanic Complex. The anomalously high $^{87}\text{Sr}/^{86}\text{Sr}$ ratios for two samples, Raspberry (no. 1) and Ice Peak (no. 2), are attributed to crustal contamination. The increasing $^{87}\text{Sr}/^{86}\text{Sr}$ ratios in more highly differentiated end members may be due to the growth of ^{87}Sr during residence of the magma in crustal reservoirs for periods of 0.7 to 1 Ma or to contamination with Sr-depleted but moderately radiogenic material (from Souther et al., 1984).

by age or error. The rock has acquired radiogenic Sr between the time of feldspar crystallization and eruption. Mugearite from the Ice Peak Formation (Table 28, no. SE3815a67) is likewise much too enriched in radiogenic Sr to be explained by any process other than contamination with crustal Sr. In the Ice Peak Formation, excess radiogenic Sr (Fig. 230,245) is associated with excess Ar, a problem that is most serious and virtually unique to the Ice Peak Formation. Whatever process supplied the radiogenic Ar may also have added radiogenic Sr and contributed to the distinctive chemical character of the Ice Peak rocks. Hybridization with fractionation, rather than close-system fractionation is indicated.

The high-Sr, low-initial-ratio basalts and the feldspar separate indicate a mafic magma source with 450 ppm Sr and $^{87}\text{Sr}/^{86}\text{Sr}$ approximately 0.7028 ± 0.0001 . These values are typical of mantle sources, in the range observed for ocean-ridge basalts, and somewhat lower than the values reported for plume-type sources (Hart and Brooks, 1981). Low Sr in more differentiated rocks is usually attributed to removal of large amounts of feldspar by fractional crystallization (Bevier, 1981). This is required to achieve the $^{87}\text{Rb}/^{86}\text{Sr}$ ratios that exceed 100.

In rocks with $^{87}\text{Rb}/^{86}\text{Sr}$ ratios greater than 50, the growth of ^{87}Sr is relatively rapid. The isochron diagram (Fig. 247) suggests that radiogenic Sr-enrichment in all samples, except the two already discussed, could be produced in time intervals of 0.7 to 1.0 Ma. If no contamination has occurred, these times would be effective pre-eruption residence times for the respective magmas. The actual residence times would be greater if the magma were undergoing progressive fractionation and increase in Rb/Sr

ratio while awaiting eruption. Comparable initial isochrons of 0.6 to 0.9 Ma have been observed for other young per-alkaline volcanoes in British Columbia (Hoodoo Mountain, unpublished data; Rainbow Range, Bevier, 1981) and elsewhere (Gibson, 1972). The similar results for volcanoes on different types of crust lends favour to the idea that a common process, residence of high Rb/Sr magmas in the crust prior to eruption, may be in effect.

The alternate view, that the radiogenic additions are simply contamination, is suggested in Figures 245 and 246. According to Faure (1977), simple end-member mixing should produce a hyperbola on $^{87}\text{Sr}/^{86}\text{Sr}$ versus Sr and a straight line on $^{87}\text{Sr}/^{86}\text{Sr}$ versus $1/\text{Sr}$. The low-Sr Edziza rocks follow the expected patterns but require an unusual contaminant, one that is fairly radiogenic ($^{87}\text{Sr}/^{86}\text{Sr} > 0.7081$) and very low in Sr (<1 ppm). No familiar crustal rock would qualify, but the crust-contaminated Ice Peak magma, after further extreme fractionation to give the low Sr content, would provide a possible contaminant for the rock series. It seems rather contrived to have such material repeatedly available or repeatedly created during the long history of the volcanic complex, but that possibility cannot be ruled out.

The radiogenic initial Sr enrichments observed in Edziza rocks are probably of complex origin, in part direct contamination, in part contamination during fractionation, in part the result of magma mixing, and in part the result of Rb decay in materials with high Rb/Sr ratio during residence in magma chambers for periods of as much as 1 Ma. Some of these complexities were recognized by Stettler and Allegre (1979) in their study of a slightly older alkaline volcano in France.

PETROGENESIS

MAJOR-ELEMENT MODEL

The cyclical repetition of basalt, trachyte, comendite eruption sequences (Table 29) and the relatively smooth compositional variation within and between the end member groups (Fig. 241,242) suggest a close genetic relationship between the basic and felsic members of the Mount Edziza Volcanic Complex. Moreover, the minor element abundances (Fig. 243), the distribution of the rare-earth elements (Fig. 244) and the anomalously low Sr in rocks with high $^{87}\text{Sr}/^{86}\text{Sr}$ ratios (Fig. 246) can be explained, at least qualitatively, by the early fractionation of olivine and pyroxene, followed by removal of feldspar.

Several authors have shown that fractional crystallization of alkaline basaltic magma can lead to an oversaturated, peralkaline residuum (Lindsley et al., 1971; Gibson, 1972; Barberi et al., 1975; Bryan, 1976; Self and Gunn, 1976). In order to test the ability of crystal fractionation to produce the range of compositions observed in the Mount Edziza Volcanic Complex solutions were sought to least-squares, mass balance equations using a program developed by Albarède and Provost (1977). The published results of this modelling are reproduced here from Souther and Hickson (1984). In all calculations the whole-rock and mineral analyses were assigned an error value of $\pm 2\%$ of the concentration of each element present. In the final solutions,

Table 29. Table of formations, listing the principal lithologies, estimated volumes and radiometric ages, and their possible relationship to 5 basalt-trachyte-comendite magmatic cycles.

Magmatic cycle	Formation	Lithology	Volume km ³	Age Ma
5	Sheep Track	Trachyte	< 1.0	< 0.002
	Big Raven	Alkali olivine basalt Hawaiite	1.7	0.002
4	Kakiddi	Trachyte	8.3	0.3
	Klastline	Alkali olivine basalt	5.4	0.62
	Arctic Lake	Alkali olivine basalt	2.0	0.71
3	Edziza	Trachyte Comenditic trachyte	18	0.9
	Pillow Ridge	Alkali olivine basalt	2.9	0.9
	Ice Peak	Alkali olivine basalt hawaiite, mugearite benmoreite, trachyte	76.7	~ 1
2	Pyramid	Trachyte comendite, pantellerite	11.4	1.1
	Spectrum	Trachyte, comendite and pantelleritic trachyte, rhyolite	118	3.1
	Nido	Alkali olivine basalt, hawaiite	127	4.4
1	Armadillo	Alkali olivine basalt comendite, trachyte	50 109	6.3
	Little Iskut	Trachybasalt	14.6	7.2
	Raspberry	Alkali olivine basalt hawaiite	119	7.4

reported residuals of less than 1.0 indicate that the calculated solution is within the assigned 2% analytical error value.

An attempt was made to choose aphanitic rocks for the mathematical modelling. Eight analyzed rocks listed in Table 31 were selected as end members for the fractionation models (no. 36, 43, 58, 78, 2896, 28, 2883, 51). Of these the alkali olivine basalt (no. 36) is the only truly aphyric rock. It has the lowest silica and alkali contents, the lowest apatitic index, and the lowest Σ REE, suggesting that it is the least fractionated member of the suite and probably most closely approaches the composition of the primary magma. Attempts to calculate the derivation of oversaturated rocks directly from alkali olivine basalt gave nonconverging solutions, but a good fit was achieved using a multistage model (Fig. 248, 249) in which the cumulate assemblage changes as fractionation progresses.

Both cumulate inclusions and phenocrysts are used in the fractionation models. Inclusions of olivine gabbro in trachytic tephra are believed to be representative of the cumulate assemblage separated during the initial stage of fractionation from basalt to trachyte (Table 31). Their mineralogy is similar to that of phenocrysts in the basalt, but minerals in the inclusions are more uniform in composition and exhibit less zoning and reaction than the phenocrysts. No inclusions of late stage cumulate rocks were found in the oversaturated end members, but incomplete separation of early formed minerals has left large, sparsely distributed, phenocrysts in the felsic rocks. These phenocrysts comprise minerals that were on the liquidus prior to eruption and their composition must approximate that of minerals separated in the late stages of fractionation.

With the exception of apatite, which is too finely disseminated to analyze, the mineral compositions were determined by microprobe analysis (Table 31). Six stages of fractionation were tested (Fig. 248): (1) alkali olivine basalt to hawaiite; (2) alkali olivine basalt to trachybasalt; (3) alkali olivine basalt to trachyte; (4) trachybasalt to comendite; (5) trachybasalt to trachyte; (6) trachyte to comendite. Each of the parent-daughter magma-pairs

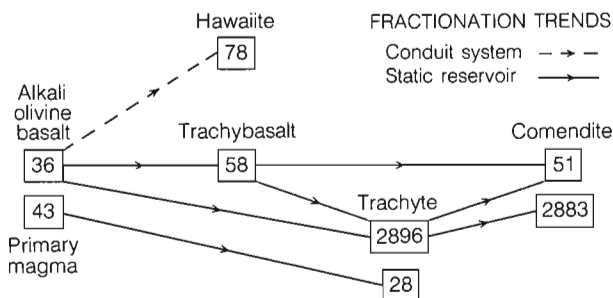


Figure 248. Flow chart showing the various lines of liquid descent modelled in Table 30 and summarized in Figure 249 (from Souther and Hickson, 1984). Chemical analyses of the end members are listed in Appendix 2.

listed above yielded solutions in which the adjusted mineral and whole-rock compositions are within the 2% analytical error. The results are listed in Table 30 and summarized in Figures 248, 249.

ALKALI OLIVINE BASALT-TRACHYBASALT-TRACHYTE-COMENDITE

The closest approach to the actual line of liquid descent is probably given by the sequence alkali olivine basalt-trachybasalt-trachyte-comendite (Fig. 249A). Early removal of olivine, titanite, magnetite and plagioclase in approximately the proportions observed in the cumulate nodules would account for the sharp decrease in MgO, TiO₂, and CaO seen on the silica variation diagrams (Fig. 240). Also the extensive fractionation of plagioclase, having a higher Na₂O to K₂O ratio than the alkali olivine basalt, would drive the residual liquid toward K₂O-enrichment with a composition analogous to the trachybasalt (plagioclase effect of Bowen, 1945). The derivation of up to 20% trachyte from trachybasalt is accomplished by continued fractionation of the nodule assemblage of minerals plus alkali feldspar having the composition of phenocrysts in the trachybasalt (Kf, Table 31). The removal of alkali feldspar with Na₂O/K₂O ratios lower than the trachybasalt would drive the residual toward a soda-rich liquid analogous to the trachyte.

Trachyte appears to be the most acceptable starting material from which to derive the oversaturated, peralkaline end members. The separation of alkali feldspar plus a small amount of olivine (Fo₁₆) and hedenbergite from trachyte is capable of producing at least 62% of residual liquid having the composition of comendite (Fig. 249A). The depletion of Al₂O₃ relative to the alkalis during this final stage of alkali feldspar fractionation drives the residual liquid toward a peralkaline composition.

The fractionation of large amounts of alkali feldspar relative to mafic phases suggested by this model is in close agreement with the process proposed by Gibson (1972) to explain the later stages of fractionation of the Fantale lavas.

ALKALI OLIVINE BASALT-TRACHYTE-COMENDITE

The use of trachybasalt as an intermediate stage in the foregoing model is justified by the stratigraphic position of Little Iskut trachybasalt between Raspberry alkali olivine basalt and Armadillo trachyte and comendite (Table 29). However, if trachybasalt was an essential stage on the liquid line of descent, it was not tapped and erupted in any significant amount during subsequent magmatic cycles which include both alkali olivine basalt and trachyte. The derivation of trachyte directly from alkali olivine basalt was tested in two models. The first (Fig. 249B) uses Raspberry alkali

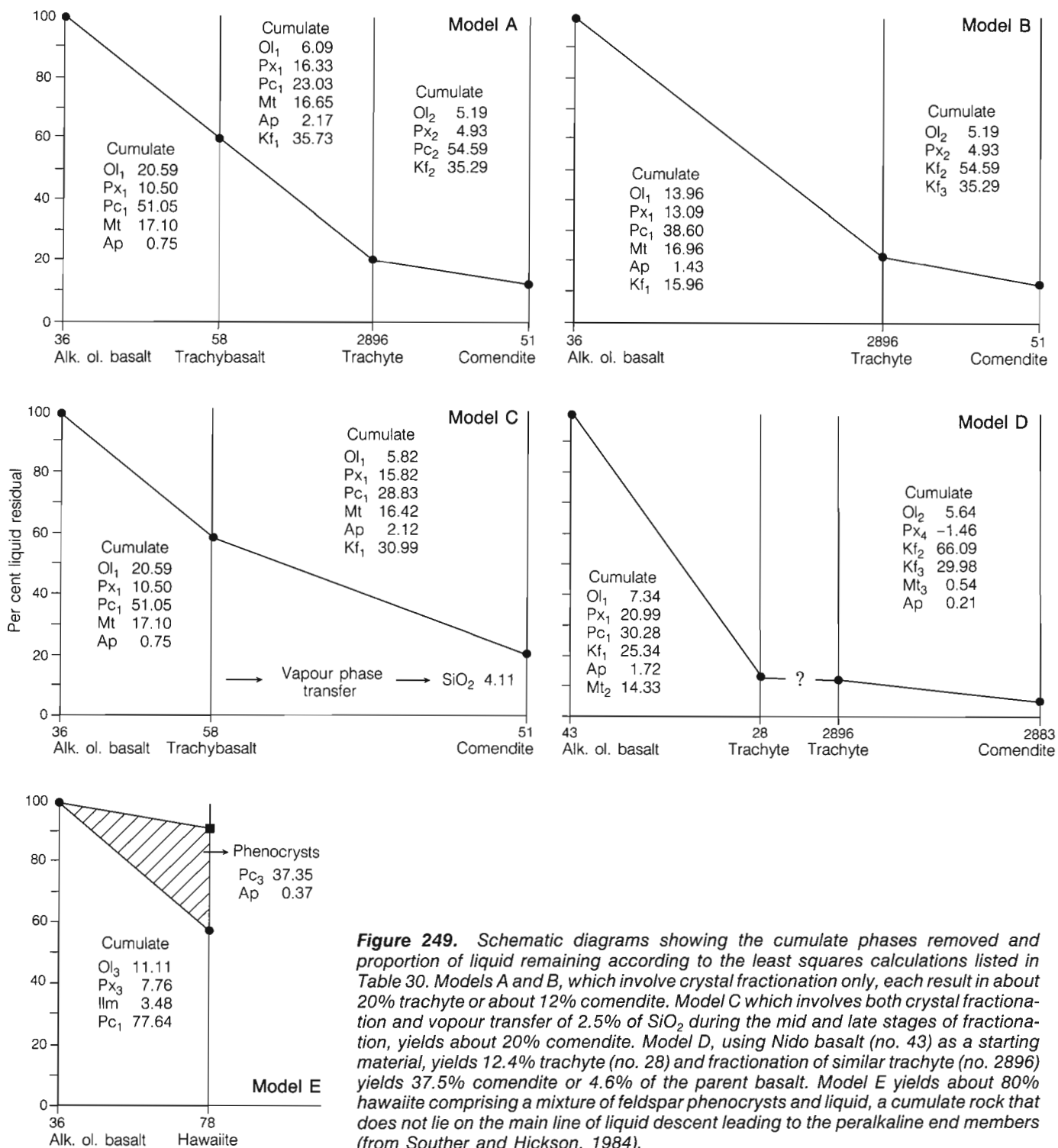


Figure 249. Schematic diagrams showing the cumulate phases removed and proportion of liquid remaining according to the least squares calculations listed in Table 30. Models A and B, which involve crystal fractionation only, each result in about 20% trachyte or about 12% comendite. Model C which involves both crystal fractionation and vapour transfer of 2.5% of SiO₂ during the mid and late stages of fractionation, yields about 20% comendite. Model D, using Nido basalt (no. 43) as a starting material, yields 12.4% trachyte (no. 28) and fractionation of similar trachyte (no. 2896) yields 37.5% comendite or 4.6% of the parent basalt. Model E yields about 80% hawaiiite comprising a mixture of feldspar phenocrysts and liquid, a cumulate rock that does not lie on the main line of liquid descent leading to the peralkaline end members (from Souther and Hickson, 1984).

olivine basalt (no. 36) as the parent magma and produces 20% of Armadillo trachyte (no. 2896) by fractionating the mineral constituents of the cumulate inclusions (olivine, pyroxene, plagioclase, titaniferous magnetite and apatite) plus alkali feldspar (Kf₁, Table 31). The second model (Fig. 249D) derives 12.4% of Spectrum trachyte (no. 28) from a slightly porphyritic Nido alkali olivine basalt (no. 43) by fractionating the same cumulate phases except that the magnetite from the Nido was used. Fractionation of mainly alkali feldspar from a similar trachyte (no. 2896) yields 37.5% liquid having the composition of comendite (no. 2883) for a net yield of only 4.6% comendite from the parent basalt (Fig. 249D). This is substantially less than the 12.1% yield of model A (Fig. 249A), and leads to a negative pyroxene value in the cumulate, suggesting incomplete separation. Both models provide good fits in which all residuals are within the limits of analytical error (Table 30).

ALKALI OLIVINE BASALT-TRACHYBASALT-COMENDITE

An alternative model in which trachybasalt, derived from an alkali olivine basalt parent, is fractionated directly to comendite is summarized in Figure 249C. This model has the advantage of producing a relatively large amount of comenditic liquid but it requires a departure from pure crystal fractionation in order to adjust the silica values. By including quartz with the cumulate phases a good fit is obtained between trachybasalt (no. 58) and comendite (no. 51) but the solution leads to a negative quartz value of 4.11% in the cumulate assemblage. Thus the model requires a net transfer of approximately 2.5% silica to the residual liquid. The occurrence of quartz as a late, cavity filling mineral in most of the comendites indicates that silica was redistributed by a vapour phase during final cooling. The

Table 30. Major-element models. All reduced residuals in all models are less than 1 (from Souther and Hickson, 1984). Initial rock compositions used in the calculations are listed in Appendix 2, and the compositions of minerals used as cumulate phases are listed in Appendix 1.

Alkali olivine basalt (#36) to Trachybasalt (#58)							
	Ol ₁	Px ₁	Pc ₁	Mt ₁	Ap		
Mineral (%)	20.59	10.50	51.05	17.10	0.75		
Std. deviation	1.85	3.50	4.62	0.92	0.25		
Percentage of trachybasalt remaining			= 57.6				
Standard deviation			= 3.65				
Initial compositions							
	Ol ₁	Px ₁	Pc ₁	Mt ₁	+ Ap	Trachybasalt	Alk. ol. basalt
SiO ₂	38.920	50.780	49.320	0.220	0.0	52.330	46.200
Al ₂ O ₃	0.020	4.090	31.370	2.730	0.0	15.930	16.630
TiO ₂	0.020	0.940	0.0	23.470	0.0	2.740	3.450
†FeO T	21.430	6.870	0.460	67.500	0.0	10.770	13.180
P ₂ O ₅	0.0	0.0	0.0	0.0	40.000	0.590	0.470
MgO	39.650	14.770	0.0	3.490	0.0	3.570	6.580
CaO	0.290	21.370	14.710	0.020	54.000	6.980	8.450
Na ₂ O	0.0	0.450	3.110	0.0	0.0	4.130	3.080
K ₂ O	0.0	0.020	0.100	0.0	0.0	2.240	1.340
Reduced residuals							
	Ol ₁	Px ₁	Pc ₁	Mt ₁	Ap	Trachybasalt	Alk. ol. basalt
SiO ₂	0.034	0.022	0.105	0.001	0.000	0.290	0.446
Al ₂ O ₃	-0.001	-0.003	-0.107	-0.004	-0.000	-0.147	0.265
TiO ₂	-0.015	-0.015	-0.036	-0.298	-0.001	-0.355	0.734
†FeO T	0.121	0.022	0.020	0.308	0.000	0.412	-0.862
P ₂ O ₅	0.000	0.000	0.001	0.000	0.001	0.004	-0.006
MgO	-0.151	-0.030	-0.009	-0.014	-0.000	-0.110	0.317
CaO	-0.000	-0.003	-0.011	-0.000	-0.001	-0.014	0.029
Na ₂ O	0.001	0.001	0.012	0.001	0.000	0.038	-0.052
K ₂ O	-0.013	-0.007	-0.035	-0.011	-0.000	-0.271	0.340
Trachybasalt (#58) to Trachyte (#2896)							
	Ol ₁	Px ₁	Pc ₁	Mt ₁	Ap	Kf ₁	
Mineral (%)	5.76	16.37	23.16	16.76	2.18	35.76	
Std. deviation	.91	2.27	4.11	0.46	0.16	6.54	
Percentage of trachybasalt remaining			= 34.4				
Standard deviation			= 8.4				

development of a silica-rich volatile phase during the latter stages of fractionation may also have played a subsidiary role leading to silica-enrichment of the residual liquid. The importance of a volatile phase in the evolution of oversaturated peralkaline rocks has been emphasized by Kogarko (1974). This model suggests that volatile transfer may have contributed to the evolution of the most highly fractionated, silica-rich members of the Mount Edziza suite.

ALKALI OLIVINE BASALT TO HAWAIIITE

Hawaiiite is intermediate in composition between alkali olivine basalt and trachyte and its component oxides plot on the trends displayed by the variation diagrams (Fig. 241,242). However, most of the Mount Edziza Volcanic Complex hawaiiites are highly porphyritic. Models using the

Table 30 (cont.)

Trachyte (#2896) to Comendite (#51)							
	01 ₂	Px ₂	Kf ₂	Kf ₃			
Mineral (%)	5.19	4.93	54.59	35.29			
Std. deviation	1.04	1.56	9.71	4.97			
Percentage of comendite remaining				= 62.0			
Standard deviation				= 4.6			
Alkali olivine basalt (#36) to Trachyte (#2896)							
	01 ₁	Px ₁	Pc ₁	Mt ₁	Ap	Kf ₁	
Mineral (%)	13.82	13.11	38.70	17.01	1.43	15.93	
Std. deviation	1.00	2.10	3.10	0.50	0.12	4.23	
Percentage of trachyte remaining				= 20.3			
Standard deviation				= 2.1			
Trachyte (#2896) to Comendite (#2883)							
	01 ₂	Px ₄	Kf ₂	Kf ₃	Mt ₃	Ap	
Mineral (%)	5.64	-1.46	66.09	28.98	0.54	0.21	
Std. deviation	0.78	0.97	4.11	3.17	0.18	0.21	
Percentage of comendite remaining				= 37.5			
Standard deviation				= 0.10			
Alkali olivine basalt (#43) to Trachyte (#28)							
	01 ₁	Px ₁	Pc ₁	Kf ₁	Ap	Mt ₁	
Mineral (%)	7.34	20.99	30.28	25.34	1.72	14.33	
Std. deviation	0.80	1.95	3.33	5.16	0.11	0.46	
Percentage of trachyte remaining				= 12.4			
Standard deviation				= 0.21			
Trachyte (#58) to Comendite (#51)							
	01 ₁	Px ₁	Pc ₁	Mt ₁	Ap	Kf ₁	Q
Mineral (%)	6.05	16.47	30.02	17.10	2.21	32.26	-4.11
Std. deviation	.93	2.49	4.51	0.47	0.16	7.13	2.37
Percentage of comendite remaining				= 35.6			
Standard deviation				= 3.1			
Alkali olivine basalt (#36) to Hawaiiite (#78)							
	01 ₃	Px ₃	Ilme	Pc ₁			
Mineral (%)	11.11	7.76	3.48	77.64	% Liquid remaining = 53.05		
Std. deviation	1.34	3.88	0.40	24.64	Std. deviation = 2.72		
					% Cumulate feldspar (Pc) = 37.53		
					Std. deviation = 12.11		
					% Cumulate apatite (Ap) = 0.37		
					Std. deviation = 0.06		
					% Hawaiiite remaining = 91.85		
					Std. deviation = 14.89		

Table 31. Major-element analyses of representative rocks and Microprobe analyses of representative mineral phases used in the petrological modelling. Notations in parentheses are identification codes, keyed to the models (Fig. 249, Table 30)

FORMATION	RASPBERRY		LITTLE ISKUT	ARMADILLO				
Oxides	Alk. 01. Basalt (# 36)	Hawaiite (# 78)	Trachybasalt (# 58)	Trachyte (# 2896)	Comendite (# 2883)	Comendite (# 51)		
SiO ₂	45.00	49.40	51.90	66.80	76.70	70.60		
Al ₂ O ₃	16.20	18.30	15.80	15.10	8.80	12.80		
Fe ₂ O ₃	3.60	4.00	5.20	2.20	1.40	3.80		
FeO	9.60	6.50	6.00	1.90	3.10	0.0		
CaO	8.23	7.83	6.92	1.40	0.30	0.16		
MgO	6.41	2.89	3.54	0.30	0.40	0.27		
Na ₂ O	3.00	4.10	4.10	5.50	4.90	5.50		
K ₂ O	1.31	1.67	2.22	4.90	3.20	4.90		
TiO ₂	3.36	2.30	2.72	0.23	0.07	0.34		
P ₂ O	0.46	0.81	0.59	0.05	0.0	0.60		
MnO	0.17	0.16	0.18	0.11	0.0	0.11		
S	0.06	0.06	0.10	0.0	0.0	0.0		
NiO	0.01	0.0	0.0	—	—	0.0		
Cr ₂ O ₃	0.0	0.0	0.0	0.0	0.0	0.0		
CO	0.0	1.20	1.20	0.0	0.0	0.0		
H ₂ O	2.6	1.00	1.00	0.90	1.00	0.60		
TOTAL	100.0	100.2	100.7	99.4	100.2	99.1		
FORMATION	NIDO	SPECTRUM						
Oxides	Alk. 01. Basalt (# 43)	Trachyte (# 28)						
SiO ₂	46.30	62.40						
Al ₂ O ₃	15.60	14.40						
Fe ₂ O ₃	3.80	4.70						
FeO	10.00	3.70						
CaO	9.75	1.36						
MgO	5.24	0.32						
Na ₂ O	3.30	7.10						
K ₂ O	1.10	4.80						
TiO ₂	3.08	0.64						
P ₂ O	0.61	0.10						
MnO	0.19	0.20						
S	0.07	0.08						
NiO	0.0	0.01						
Cr ₂ O ₃	0.0	0.0						
CO	0.0	0.0						
H ₂ O	0.40	0.40						
TOTAL	99.7	100.2						
FORMATION	CUMULATE INCLUSION				RASPBERRY			
Oxides	Olivine (O ₁)	Pyroxene (Px ₁)	Feldspar (Pc ₁)	Magnetite (Mt ₁)	Olivine (O ₁₃)	Pyroxene (Px ₃)	Feldspar (Pc ₂)	Ilmenite (Ilme)
SiO ₂	38.92	50.78	49.32	0.22	38.46	49.30	51.96	0.11
Al ₂ O ₃	0.02	4.09	31.37	2.73	0.0	2.96	29.88	0.04
Fe ₂ O ₃	0.0	1.51	0.51	47.73	0.0	2.06	0.51	—
FeO	21.43	5.57	0.0	21.97	22.20	10.83	0.0	46.58
CaO	0.29	21.37	14.71	0.02	0.29	19.69	12.93	0.05
MgO	39.65	14.77	0.0	3.49	39.44	12.57	0.0	2.00
Na ₂ O	0.0	0.45	3.11	0.0	0.0	0.44	4.07	0.0
K ₂ O	0.0	0.02	0.10	0.0	0.0	0.0	0.22	0.0
TiO ₂	0.02	0.94	0.0	23.47	0.01	2.00	0.0	51.16
MnO	0.27	0.13	9.0	0.55	0.25	0.24	0.0	0.51
NiO	0.07	0.0	0.0	—	0.13	0.0	0.0	—
Cr ₂ O ₃	0.0	0.39	0.0	0.02	0.0	0.0	0.0	0.04
TOTAL	100.7	100.0	99.1	100.2	100.8	100.1	99.6	100.5
FORMATION	LITTLE ISKUT	SPECTRUM	PYRAMID					
Oxides	Feldspar (Kf ₁)	Pyroxene (Px ₂)	Olivine (O ₁₂)	Feldspar (Kf ₂)rim	Feldspar (Kf ₂)core	Pyroxene (Px ₄)	Fe-Ti Oxide ≡(Mt ₄)	Fe-Ti Oxide ≡(Mt ₂)
SiO ₂	62.36	48.49	31.53	66.17	61.26	49.58	0.0	0.0
Al ₂ O ₃	21.98	0.12	0.0	19.13	24.20	0.76	0.0	0.0
Fe ₂ O ₃	1.11	3.20	0.0	0.15	0.23	1.61	—	—
FeO	0.0	26.14	59.85	0.0	0.0	21.36	65.45	77.50
CaO	4.90	19.18	0.21	0.69	6.03	20.19	0.0	0.0
MgO	0.0	0.15	6.44	0.0	0.0	5.56	0.0	0.0
Na ₂ O	7.11	1.35	0.0	5.36	7.38	0.37	0.0	0.0
K ₂ O	2.18	0.0	0.0	8.25	1.24	0.01	0.0	0.0
TiO ₂	0.05	0.42	0.01	0.0	0.0	0.32	34.55	22.50
MnO	0.03	1.12	2.32	0.0	0.0	0.68	0.0	0.0
NiO	0.0	0.0	0.0	0.0	0.0	0.0	0.0	0.0
Cr ₂ O ₃	0.0	0.03	0.0	0.0	0.0	0.0	0.0	0.0
TOTAL	99.7	100.2	100.4	99.7	100.3	100.4	100.0	100.0

hawaiite composition as either the daughter product of alkali olivine basalt or the parent magma of trachyte either failed to converge or gave unacceptably large residuals. In order to derive the Edziza Complex hawaiite from alkali olivine basalt mathematically it was necessary to use different cumulate phases than those used in the foregoing models. Complex normal and reverse zoning of both feldspar (An_{75-55}) and pyroxene (En_{30-55}) phases in the hawaiite, as well as a wide range of Fe-Ti ratios in the opaque oxides, makes the selection of cumulate phases difficult. A reasonable mathematical fit was achieved by using two feldspar compositions (Fig. 249E) which bracket the range of probe analyses. The solution yields 92% residual of hawaiite composition, comprising 59% liquid and 41% feldspar. The

model demonstrates that the porphyritic hawaiite can be derived from parental alkali olivine basalt with only slight fractionation. However, it also suggests that the Edziza hawaiites are accumulative rocks and do not represent intermediate compositions on the line of liquid descent leading from alkali olivine basalt to trachyte. The complex zoning of the phenocryst phases in the hawaiite compared with unzoned plagioclase in the cumulate nodules used in the alkali olivine basalt to trachybasalt model, suggests a very different environment of crystallization. The zoned crystals in the hawaiite must have formed in a dynamic environment, possibly a column of magma ascending more rapidly than the settling rate of the crystals, whereas the unzoned, cumulate feldspars and pyroxenes used in the previous models must have crystallized in a uniform, static environment.

CONCLUSIONS

The long history of the Mount Edziza Volcanic Complex began almost ten million years ago with the eruption of basaltic magma from a source in the rolling hinterland east of the ancestral Coast Mountains of north-western British Columbia. The initial flood of basalt was followed by the eruption of silicic magma from a central vent. Because of their different physical properties the basaltic and silicic magmas resulted in very different land forms. The fluid basalt spread in thin flows to build a broad shield, whereas the more viscous, silicic magma piled up around its vent to form a composite central cone. Throughout its subsequent history this same pattern of activity was repeated at least four times from different groups of vents. Successive basaltic shields coalesced to form a composite volcanic plateau, and above the plateau four steep-sided composite, felsic volcanoes lie along the north-south axis of the volcanic complex. Episodic activity continued through several periods of regional and local glaciation, resulting in the construction of subglacial as well as subaerial volcanic landforms. The older elements of the complex have been greatly modified by glacial and fluvial erosion but the youngest, postglacial, lavas and cinder cones have undergone little change since they were erupted a few thousand years ago.

The Mount Edziza Volcanic Complex is part of the Stikine Volcanic Belt which extends north across the central Coast Mountains and then swings northwest in a broad arc through central British Columbia into southern Yukon. The belt is defined by groups of post-Late Miocene alkaline volcanoes which are crudely aligned within the belt along a series of north-south, en echelon segments. The Mount Edziza Volcanic Complex occupies a central position in the southern and best defined segment of the Stikine Volcanic Belt. The alignment of eruptive centres within the complex and the trace of associated normal faults reflect the north-south orientation of the segment as a whole. Normal faults which cut the volcanic succession show progressively greater offset of the older flows, suggesting that they are growth faults which were coeval with, and probably genetically related to the volcanic activity.

The Stikine Volcanic Belt lies entirely within Stikinia, the largest block of a composite terrane which was accreted to the continental margin in the Jurassic (Monger, 1984). The tectonic setting during the life of the Mount Edziza Volcanic Complex was probably similar to that at present, with right-lateral movement of about 5.5 cm/a between the Pacific oceanic plate and the North American continent along northwesterly-trending faults of the Queen Charlotte system (Riddihough, 1977), coupled with weak convergent motion of about 1 to 2 cm/a (Hyndman and Ellis, 1981). The en echelon segments of the Stikine Volcanic Belt lie about 300 km inland from this margin. They are interpreted

to be gash fractures, zones of incipient east-west extension within the continental plate, possibly formed in response to shear along the plate margin (Souther, 1977).

The smaller centres of the Stikine Volcanic Belt are mostly monogenetic cones and small associated flows of alkali olivine basalt, many of which contain lherzolite nodules. In contrast, the Mount Edziza Volcanic Complex includes a significant volume of felsic as well as basaltic rocks in which lherzolite nodules are extremely rare and comparatively small. The basaltic rocks of the complex belong to the alkaline rock series. Ophitic to intergranular alkali olivine basalt, comprising calcic plagioclase, titaniferous augite, olivine and an iron-titanium oxide, is volumetrically the most abundant. Porphyritic hawaiite, containing large plagioclase phenocrysts, is commonly present in smaller amounts near the top of basaltic sequences. The felsic rocks are commonly peralkaline and include trachyte, comendite, and lesser amounts of pantellerite. The trachyte is a nearly pure K-feldspar rock, containing minor sodic amphibole, acmitic pyroxene, and an opaque oxide. With the appearance of interstitial quartz the trachyte grades into comendite, and with an increase in mafic constituents (arfvedsonite, aegirine, ferrowedenbergite, aenigmatite) the comendite grades into pantellerite. A relatively small volume of rocks having intermediate compositions; trachybasalt, tristanite and mugearite, is confined mainly to two formations, the Little Iskut and the Ice Peak, where they occupy stratigraphic positions between major basaltic and felsic successions. The Edziza suite of rocks is chemically and mineralogically similar to other bimodal suites such as the Azores (Self and Gunn, 1976), the Afar depression (Barberi et al., 1975), parts of the Great Basin of the western United States (Noble and Parker, 1974), and the Rainbow Range of central British Columbia (Bevier, 1981). A continental, extensional tectonic environment is common to these peralkaline volcanic terranes, adding support to the structural evidence that the en echelon segments of the Stikine Volcanic Belt are zones of incipient rifting, formed in response to east-west extension.

The entire range of intermediate and felsic rocks in the Mount Edziza Volcanic Complex can be derived by crystal fractionation of a common alkali olivine basalt parent. Major element modelling indicates that it is possible to derive 12-20% comenditic residual melt and even larger volumes of intermediate liquids by fractionating mineral assemblages observed in phenocrysts and cumulate nodules. The major element model is consistent with the observed variation in trace element abundances, including the rare-earth elements. A $^{87}\text{Sr}/^{86}\text{Sr}$ ratio of 0.7028 ± 0.0001 indicates a mantle source for the alkali basalt, whereas the low Sr, high $^{87}\text{Sr}/^{86}\text{Sr}$ values of the intermediate and felsic rocks are consistent with prolonged (± 1 Ma) feldspar fractionation in

high-level reservoirs (Souther et al., 1984). Also, the stratigraphic repetition of at least four magmatic cycles, each beginning with basalt followed by a lesser volume of felsic lava, is consistent with the repeated injection of primitive, mantle-derived alkali olivine basalt into crustal magma chambers.

The tectonic setting of the Mount Edziza Volcanic Complex, in a region of crustal extension, would favour the development of high-level reservoirs of sufficient size and thermal capacity to sustain prolonged fractionation. That such reservoirs did exist beneath the Mount Edziza Volcanic Complex is suggested by the paucity and small size of lherzolite inclusions in the compositionally diverse Mount Edziza Volcanic Complex, compared with the abundance of larger nodules in lava erupted from adjacent, monogenetic alkali olivine basalt cones. Assuming a common mantle origin for the alkali olivine basalt from both the central and peripheral vents, it is reasonable to suppose that lherzolite nodules were originally present in both. Conduits leading to the peripheral, monogenetic cinder cones, were narrow enough so that ascent velocities remained sufficiently high to transport the nodules to the surface. In contrast, much of the magma rising beneath the central, highly fractionated complex must have passed through large magma reservoirs. The resulting decrease in ascent velocity would allow any nodules to settle out and at the same time provide a favourable environment for crystal fractionation.

The initial fractionation of alkali olivine basalt magma to produce a trachytic residual liquid may have been accomplished by crystal settling of calcic plagioclase, olivine, titanite and opaque oxides. Such a process is suggested by the cumulus texture of olivine gabbro inclusions in trachyte tephra. Crystal settling cannot account for the separation of alkali feldspar from trachyte to yield a comenditic residual liquid. Both the viscosity of the melt and the small density difference between melt and crystals preclude such a process. Crystallization of feldspar on the walls of the chamber and separation of the residual liquid by buoyant upflow, as proposed by McBirney (1980), offer a possible mechanism. The present study suggests that late stage crystal fractionation was accompanied by volatile transfer of silica and alkalis.

The fractionation model presented here provides a mechanism that is capable of deriving the felsic end members from a parent alkali olivine basalt, but in so doing the evolving magma must pass through a continuum of intermediate compositions. Although a range of intermediate rocks with compositions close to the theoretical line of liquid descent is present in the Mount Edziza Volcanic Complex they are distinctly less abundant than the end members. An eruption mechanism in which buoyancy was the driving force could explain the bimodal character of the pile. Each magmatic cycle was initiated by a surge of alkali olivine basalt rising from the mantle. Because of its hydraulic continuity with a fluid, magma-column extending into dense rocks at the base of the crust and upper mantle the magma would rise to the surface despite its relatively high specific gravity. The highly porphyritic hawaiites that commonly

terminate this initial phase of the cycle are probably the product of crystallization within the upper part of the conduit system. They formed during the waning stages of basaltic effusion from the mantle, when ascent velocities had fallen to a point where cooling and crystallization could begin but were still high enough to carry the crystal-liquid mixture to the surface without appreciable fractionation.

Once the supply of new magma from the mantle ceased, any basaltic melt remaining in crustal reservoirs would no longer be driven to the surface by new material rising through a deep conduit system in high density, lower crustal rocks. Because of its high specific gravity (2.7) relative to the enclosing rocks the trapped magma would stagnate, undergoing prolonged crystal fractionation until a silicic residual melt evolved having sufficiently low density to rise out of its crustal environment. Liquids of intermediate composition, such as the trachybasalt, mugearite and benmoreite would thus tend to remain in the reservoirs, undergoing further fractionation until the density threshold was reached and the residual melt began its ascent to the surface.

Spera et al. (1982) have calculated that characteristic residence times for the development of compositional heterogeneity in fractionating magma reservoirs is in the order of 10^6 years. This is in good agreement with the length of magmatic cycles in the Mount Edziza Volcanic Complex as determined by stratigraphy and age dates (Table 29), and with pre-eruption residence times of 0.7-1.0 Ma suggested by Sr enrichment in felsic rocks of the complex (Fig. 247).

The chemical diversity of the Mount Edziza Volcanic Complex compared with the uniformity of flanking, monogenetic, alkali-olivine-basalt centres is explained by its position over a zone of extension. Such a zone would favour the formation of crustal reservoirs having sufficient size to sustain the long periods of crystal fractionation required to generate the peralkaline, silicic residual magmas.

There is no evidence that the geodynamic framework of the Stikine Volcanic Belt has changed significantly during the life of the Mount Edziza Volcanic Complex, nor is there any suggestion in the stratigraphy and petrochemistry of the volcanic pile that the recurring cycles of magmatic activity have come to an end. On the contrary, there is every reason to expect that the Mount Edziza Volcanic Complex and other centres in the Stikine Volcanic Belt will continue to erupt periodically as long as the present tectonic relationship between the North American and Pacific plates prevails. A few hundred years have lapsed since the effusion of Big Raven basalt and the explosive eruption of Sheep Track pumice, but the history of the Mount Edziza Volcanic Complex includes many such periods of dormancy. It may be another few hundred years before the next lava issues from a vent in the Stikine Volcanic Belt but sooner or later the next cycle will begin. When it does, some part of the present surface will be preserved beneath new lava, adding yet another layer of surficial deposits to the stratigraphic succession, and recording another chapter in the continuing history of the Mount Edziza Volcanic Complex.

REFERENCES

- Albarede, F. and Prevost, A.**
1977: Petrological and geochemical mass-balance equations: an algorithm for least square-fitting and general error analysis; *Computers and Geosciences*, v. 3, p. 309-326.
- Armstrong, R.L.**
1978: K-Ar dating: Late Cenozoic McMurdo Volcanic Group and dry valley glacial history, Victoria Land, Antarctica; *New Zealand Journal of Geology and Geophysics*, v. 21, p. 685-698.
- Aumento, F. and Souther, J.G.**
1973: Fission-track dating of Late Tertiary and Quaternary volcanic glass from the Mount Edziza Volcano, British Columbia; *Canadian Journal of Earth Sciences*, v. 10, no. 7, p. 1156-1163.
- Baksi, A.K.**
1974: Isotopic fractionation of a loosely held atmospheric argon component in the Picture Gorge Basalts; *Earth and Planetary Science Letters*, v. 21, p. 431-438.
- Barberi, F., Ferrara, G., Santacroce, R., Treuil, M., and Varet, J.**
1975: A transitional basalt-pantellerite sequence of fractional crystallization, the Boina Centre (Afar Rift, Ethiopia); *Journal of Petrology*, v. 16, p. 22-56.
- Berman, R.G.**
1981: Differentiation of calc-alkaline magmas: evidence from the Coquihalla Volcanic Complex, British Columbia; *Journal of Volcanology and Geothermal Research*, v. 9, p. 157-179.
- Bevier, M.L.**
1978: Field relations and petrology of the Rainbow Range Shield Volcano, west-central British Columbia; unpublished M.Sc. thesis, University of British Columbia, Vancouver, 100 p.
1981: The Rainbow Range, British Columbia: Miocene peralkaline shield volcano; *Journal of Volcanology and Geothermal Research*, v. 11, p. 225-251.
- Bowen, N.L.**
1945: Phase equilibria bearing on the origin and differentiation of the alkaline rocks; *American Journal of Science*, v. 243-A, p. 75-89.
- Bryan, W.B.**
1976: A basalt-pantellerite association from Isla Socorro, Islas Revillagigedo, Mexico; in *Volcanoes and Tectosphere*, Aoki, H. and Iizuka, S. (eds.), Tokai University Press, New York, N.Y., p. 75-91.
- Carmichael, I.S.E.**
1967: The iron-titanium oxides of salic volcanic rocks and their associated ferromagnesian silicates; *Contributions to Mineralogy and Petrology*, v. 14, no. 1, p. 36-64.
- Clark, J.R. and Papike, J.J.**
1968: Crystal-chemical characterization of omphacites; *American Mineralogist*, v. 53, no. 5 and 6, p. 840-868.
- Cox, A.**
1969: Geomagnetic reversals; *Science*, v. 163, p. 237-245.
- Dalrymple, G.B.**
1969: $^{40}\text{Ar}/^{36}\text{Ar}$ analyses of historic lava flows; *Earth and Planetary Science Letters*, v. 6, p. 47-55.
- Dalrymple, G.B. and Moore, J.G.**
1968: Argon 40 excess in submarine pillow basalts from Kilanea Volcano, Hawaii; *Science*, v. 161, p. 1132-1135.
- Ernst, G.W.**
1962: Synthesis, stability relations, and occurrence of riebeckite and riebeckite-arfvedsonite solid solution; *Journal of Geology*, v. 70, no. 6, p. 689-735.
- Ewart, A., Taylor, S.R., and Capp, A.C.**
1968: Geochemistry of the pantellerites of Mayor Island, New Zealand; *Contributions to Mineralogy and Petrology*, v. 17, p. 116-140.
- Faure, G.**
1977: *Principles of Isotope Geology*; Wiley, New York, 464 p.
- Faure, G. and Powell, J.L.**
1972: *Strontium Isotope Geology*; Springer, Berlin, Heidelberg, New York, 188 p.
- Fisher, D.E.**
1971: Excess rare gases in a subaerial basalt in Nigeria; *Nature, Physical Science*, v. 232, no. 29, p. 60-61.
- Fleischer, R.L. and Price, P.B.**
1964: Techniques for geological dating of minerals by chemical etching of fission fragment tracks; *Geochimica et Cosmochimica Acta*, v. 28, p. 1705-1714.
- Geological Survey of Canada**
1957: Stikine River area, Cassiar District, British Columbia; Geological Survey of Canada, Map 9-1957, scale 1 inch to 4 miles.
- Gibson, I.L.**
1972: The chemistry and petrogenesis of a suite of pantellerites from the Ethiopian Rift; *Journal of Petrology*, v. 13, p. 31-44.
- Hamilton, T.**
1981: Late Cenozoic alkaline volcanics of the Level Mountain Range, northwestern British Columbia: geology, petrology and paleomagnetism; unpublished Ph.D. thesis, The University of Alberta, Edmonton.
- Hart, S.R. and Brooks, C.**
1981: Sources of terrestrial basalts: isotopic characteristics; in *Basaltic Volcanism Study Project: Basaltic Volcanism on the Terrestrial Planets*, Pergamon Press, New York, p. 987-1014.
- Hyndman, R.D. and Ellis, R.M.**
1981: Queen Charlotte fault zone: microearthquakes from a temporary array of land stations and ocean bottom seismographs; *Canadian Journal of Earth Sciences*, v. 18, no. 4, p. 776-788.
- Irvine, T.N. and Baragar, W.R.A.**
1971: A guide to the chemical classification of the common volcanic rocks; *Canadian Journal of Earth Sciences*, v. 8, no. 7, p. 523-548.
- Irving, A.J.**
1978: A review of experimental studies of crystal-liquid trace element partitioning; in *Proceedings of the International Conference on Experimental Trace Element Geochemistry*, *Geochimica et Cosmochimica Acta*, v. 42, p. 743-770.

MOUNT EDZIZA

- Kerr, F.A.**
1948: Lower Stikine and western Iskut areas, British Columbia; Geological Survey of Canada, Memoir 246.
- Kogarko, L.N.**
1974: Role of volatiles; *in* The Alkaline Rocks, Sorenson, H. (ed.), John Wiley and Sons, New York, N.Y.
- Krummenacher, D.**
1970: Isotopic composition of argon in modern surface volcanic rocks; *Earth and Planetary Science Letters*, v. 8, p. 109-117.
- Lindsley, D.J., Smith, D., and Haggerty, S.E.**
1971: Petrography and mineral chemistry of a differentiated flow of Picture Gorge basalt near Spray, Oregon: geologic setting and mechanisms of differentiation; *Carnegie Institution of Washington, Yearbook*, no. 69, p. 264-285.
- Lowden, J.A., Fyles, J.G., and Blake, W., Jr.**
1967: Radiocarbon Dates VI: Geological Survey of Canada, Paper 67-2, Part B, 42 p.
- Macdonald, R.**
1974: Nomenclature and petrochemistry of the peralkaline oversaturated extrusive rocks; *Bulletin of Volcanology*, v. 38, p. 498-516.
- McBirney, A.R.**
1980: Mixing and unmixing of magmas; *Journal of Volcanology and Geothermal Research*, v. 7, p. 357-371.
- McKay, G.A. and Weill, D.F.**
1976: Petrogenesis of KREEP; *Proceedings of the 7th Lunar Science Conference*, p. 2427-2447.
- Monger, J.W.H.**
1984: Cordilleran tectonics: a Canadian perspective; *Société Géologique de France, Bulletin*, v. 2, p. 255-278.
- Monroe, R.L.**
1970: Quaternary geochronology and the fission track dating method; unpublished manuscript, Department of Geography, Carleton University, Ottawa, Ontario, 30 p.
- Nagasawa, H.**
1970: Rare earth elements in zircon and apatite in acidic volcanic and igneous rocks; *Earth and Planetary Science Letters*, v. 9, p. 359-364.
- Noble, D.C. and Parker, D.F.**
1974: Peralkaline silicic, volcanic rocks of the western United States; *Bulletin Volcanologique*, v. 38, no. 3, p. 803-827.
- Piteau and Associates**
1984: Geochemistry and isotope hydrology of the Mount Edziza and Mess Creek geothermal waters; Geological Survey of Canada, Open File 1732.
- Porter, S.P. and Denton, G.H.**
1967: Chronology of neoglaciation in the North American Cordillera; *American Journal of Science*, v. 265, p. 177-210.
- Riddihough, R.P.**
1977: A model for recent plate interactions off Canada's west coast; *Canadian Journal of Earth Sciences*, v. 14, p. 384-396.
- Rutherford, R.H., Craddock, C., Armstrong, R.L., and White, C.M.**
1972: Tertiary glaciation in the Jones Mountains; *in* Antarctic Geology and Geophysics, Adie, R.J. (ed.), Universitetsforlaget, Oslo, p. 239-243.
- Self, S. and Gunn, B.M.**
1976: Petrology, volume and age relations of alkaline and saturated peralkaline volcanics from Terceira, Azores; *Contributions to Mineralogy and Petrology*, v. 54, p. 293-313.
- Shaw, H.R.**
1965: Comments on viscosity, crystal settling, and convection in granitic magmas; *American Journal of Science*, v. 263, p. 120-152.
- Souther, J.G.**
1967: Acid volcanism and its relationship to the tectonic history of the Cordillera of British Columbia, Canada; *Bulletin Volcanologique*, v. 30, p. 161-167.
1968: Cordilleran volcanic study, 1967, British Columbia (104G/7, G/10, G/15, G/16); *in* Report of Activities, Part A, Geological Survey of Canada, Paper 68-1A, p. 42-43.
1969: Geology of Mount Edziza Volcano; 19th Alaskan Science Conference (abstract).
1971: Geology and mineral deposits of Tulsequah map-area, British Columbia; Geological Survey of Canada, Memoir 362.
1972a: Telegraph Creek map-area, British Columbia; Geological Survey of Canada, Paper 71-44, 38 p.
1972b: Mesozoic and Tertiary volcanism of the western Canadian Cordillera; *in* The Ancient Oceanic Lithosphere, Irving, E. (ed.), Department of Energy, Mines and Resources, Earth Physics Branch Publication, no. 42, p. 55-58.
1975: Geothermal potential of Western Canada; Second United Nations Symposium on Development and Use of Geothermal Resources, Proceedings, v. 1, p. 259-269.
1977: Volcanism and tectonic environments in the Canadian Cordillera — a second look; *in* Volcanic Regimes in Canada, Barager, W.R.A., Coleman, L.C., and Hall, J.M. (eds.), Geological Association of Canada, Special Paper, v. 16, p. 3-24.
1981a: Volcanic hazards in the Stikine region of northwestern British Columbia; Geological Survey of Canada, Open File 770, 2 p.
1981b: Quaternary volcanism in the Stikine region of northwestern British Columbia and potential hazards from future eruptions; Geological Association of Canada, Annual Meeting, 1981, Abstracts, A-52.
1984: The Igachuz Range, a peralkaline shield volcano in central British Columbia; *in* Current Research, Part A, Geological Survey of Canada, Paper 84-1A, p. 1-10.
- Souther, J.G. and Hickson, C.J.**
1984: Crystal fractionation of the basalt comendite series of the Mount Edziza Volcanic Complex, British Columbia: major and trace elements; *Journal of Volcanology and Geothermal Research*, v. 21, p. 79-106.
- Souther, J.G. and Symons, D.T.A.**
1974: Stratigraphy and paleomagnetism of Mount Edziza Volcanic Complex, northwestern British Columbia; Geological Survey of Canada, Paper 73-32, 48 p.
- Souther, J.G., Armstrong, R.L., and Harakal**
1984: Chronology of the peralkaline, late Cenozoic Mount Edziza Volcanic Complex, northern British Columbia, Canada; *Geological Society of America, Bulletin*, v. 95, p. 337-349.
- Spera, F.J., Yuen, D.A., and Kirschvink, S.J.**
1982: Thermal boundary layer convection in silicic magma chambers: effects of temperature-dependent rheology and implications for thermogravitational chemical fractionation; *Journal of Geophysical Research*, v. 87, no. B10, p. 8755-8767.
- Stettler, A. and Allegre, C.J.**
1979: $^{87}\text{Rb}/^{87}\text{Sr}$ constraints on the genesis and evolution of the Cantal continental volcanic system (France); *Earth and Planetary Science Letters*, v. 44, p. 269-278.

Sutherland Brown, A.

1969: Aiyansh lava flow, British Columbia; Canadian Journal of Earth Sciences, v. 6, p. 1461-1468.

Thompson, R.N., Esson, J., and Dunham, A.C.

1972: Major element chemical variation in the Eocene lavas of the Isle of Skye, Scotland; Journal of Petrology, v. 13, p. 219-253.

Thornton, C.P. and Tuttle, O.F.

1960: Chemistry of igneous rocks: I. Differentiation Index; American Journal of Science, v. 258, p. 644-684.

Wheeler, J.O.

1961: Whitehorse map-area, Yukon Territory; Geological Survey of Canada, Memoir 312.

Yagi, K. and Souther, J.G.

1974: Aenigmatite from Mt. Edziza, B.C., Canada; American Mineralogist, v. 59, p. 820-829.

Zielinski, R.A.

1975: Trace element evaluation of a suite of rocks from Reunion Island, Indian Ocean; Geochimica et Cosmochimica Acta, v. 39, p. 713-734.

APPENDIX 1

Mineral chemistry from microprobe analysis

CLINOPYROXENES

Sample: Formation: Type:	SE31-4-1 Raspberry GM		SE31-4-2 Raspberry GM		SE32-1-1 Raspberry GM		SE32-1-2 Raspberry GM		SE36-4-1 Raspberry GM		SE128-2-1 Little Iskut PHR		SE128-2-2 Little Iskut PHC		SE128-3-1 Little Iskut PHR		SE128-3-2 Little Iskut PHC		SE131-1-1 Little Iskut PHC		SE131-4-1 Little Iskut PHC		SE131-5-1 Little Iskut PHR		SE14-1-2 Armadillo PHR		SE14-1-3 Armadillo PHC									
	GM	GM	GM	GM	GM	GM	GM	GM	GM	GM	Little	Iskut	PHR	Little	Iskut	PHC	Little	Iskut	PHC	Little	Iskut	PHR	Little	Iskut	PHR	Little	Iskut	PHC	Little	Iskut	PHC					
SiO ₂	50.61	49.30	48.09	48.45	46.61	47.61	48.27	48.22	48.17	47.81	48.43	48.68	49.11	51.77	51.80																					
Al ₂ O ₃	1.86	2.96	4.19	3.93	4.74	1.83	2.67	2.05	3.01	1.35	1.49	1.31	1.32	0.13	0.13																					
Cr ₂ O ₃	0.04	0.00	0.02	0.03	0.03	0.00	0.00	0.01	0.00	0.00	0.00	0.00	0.00	0.00	0.00																					
TiO ₂	1.44	2.00	2.49	2.60	3.52	1.37	1.28	1.11	1.52	0.64	0.65	0.53	0.56	0.64	1.11																					
(Fe ₂) _{total} as FeO	(10.91)	(12.68)	(9.73)	(10.06)	(12.10)	(26.38)	(18.71)	(23.57)	(18.82)	(24.02)	(23.10)	(24.23)	(24.23)	(29.48)	(29.61)																					
Fe ₂ O ₃	1.24	2.06	2.62	1.98	2.67	2.27	2.19	3.61	2.86	2.86	2.21	2.26	2.00	24.60	28.67																					
FeO	9.79	10.83	7.37	8.28	9.70	24.34	16.74	20.32	18.30	21.45	21.11	22.07	24.23	7.34	3.81																					
MnO	0.23	0.24	0.22	0.20	0.21	0.99	0.67	0.90	0.67	0.93	0.87	0.92	0.87	0.29	0.30																					
MgO	14.39	12.57	12.96	12.91	10.79	3.71	7.97	5.29	7.88	4.16	4.76	4.16	4.21	0.02	0.02																					
CaO	19.29	19.69	20.91	20.83	20.98	19.00	19.55	19.79	18.99	20.50	20.42	20.71	20.64	5.39	4.60																					
Na ₂ O	0.30	0.44	0.48	0.45	0.60	0.38	0.42	0.49	0.34	0.36	0.40	0.36	0.00	10.33	11.40																					
K ₂ O	0.01	0.00	0.01	0.00	0.03	0.03	0.08	0.12	0.01	0.00	0.00	0.01	0.00	0.00	0.01																					
Total	99.20	100.09	99.36	99.66	99.88	101.53	99.84	101.91	99.47	100.06	100.34	101.02	100.94	100.51	101.85																					

Formula based on 6 oxygens

Si	1.911	1.864	1.816	1.827	1.777	1.898	1.887	1.888	1.890	1.920	1.928	1.934	1.954	2.008	1.976																						
Al	0.083	0.132	0.184	0.173	0.213	0.086	0.113	0.095	0.110	0.064	0.070	0.061	0.046	0.000	0.006																						
Fe ³⁺	0.006	0.004	0.000	0.000	0.010	0.016	0.000	0.017	0.000	0.016	0.002	0.004	0.000	0.000	0.019																						
Al	0.000	0.000	0.003	0.002	0.000	0.000	0.010	0.000	0.030	0.000	0.000	0.000	0.016	0.006	0.000																						
Cr	0.001	0.000	0.001	0.001	0.001	0.000	0.000	0.000	0.000	0.000	0.000	0.000	0.000	0.000	0.000																						
Ti	0.041	0.057	0.071	0.074	0.101	0.041	0.038	0.033	0.045	0.019	0.019	0.016	0.017	0.019	0.032																						
Fe ²⁺	0.029	0.054	0.074	0.056	0.066	0.052	0.064	0.089	0.017	0.070	0.064	0.063	0.000	0.718	0.804																						
Mg ²⁺	0.810	0.708	0.730	0.726	0.613	0.220	0.464	0.309	0.461	0.249	0.282	0.246	0.250	0.001	0.001																						
Fe ²⁺	0.309	0.342	0.233	0.261	0.309	0.811	0.547	0.666	0.601	0.720	0.703	0.733	0.806	0.238	0.122																						
Mn	0.007	0.008	0.007	0.006	0.007	0.033	0.022	0.030	0.022	0.032	0.029	0.031	0.029	0.010	0.010																						
Ca	0.780	0.798	0.846	0.842	0.857	0.811	0.819	0.830	0.798	0.882	0.871	0.882	0.880	0.224	0.188																						
Na	0.022	0.032	0.035	0.033	0.044	0.029	0.032	0.037	0.026	0.028	0.031	0.028	0.000	0.777	0.843																						
K	0.000	0.000	0.000	0.000	0.002	0.002	0.004	0.006	0.001	0.000	0.000	0.001	0.000	0.000	0.001																						
Z	2.000	2.000	2.000	2.000	2.000	2.000	2.000	2.000	2.000	2.000	2.000	2.000	2.000	2.000	2.000																						
XY	2.000	2.000	2.000	2.000	2.000	2.000	2.000	2.000	2.000	2.000	2.000	2.000	2.000	1.998	2.000																						
Jo ¹	0	0	0	0	0	0	0	0	0	0	0	0	0	1	0																						
Ac	3	4	3	3	6	4	4	6	2	5	3	4	0	73	80																						
Ti-Cats	4	6	7	7	10	4	4	3	4	2	2	2	2	0	0																						
TiSi ₂ O ₆	0	0	0	0	0	0	0	0	0	0	0	0	0	0	0																						
Fe-Cats	0	1	4	3	1	1	2	3	0	0	0	0	0	0	0																						
Cats	0	0	0	0	0	0	1	0	3	0	0	0	0	0	0																						
Wo	37	37	38	37	38	38	38	39	37	43	42	43	43	11	9																						
En	40	35	36	36	30	11	23	15	37	12	14	12	12	0	0																						
Fs	15	16	11	13	14	41	27	33	30	35	36	36	41	12	6																						
Bu	1	1	1	1	1	1	1	1	1	1	1	1	1	1	1																						
%-age calc.	(89)	(88)	(88)	(89)	(88)	(89)	(88)	(88)	(89)	(88)	(89)	(88)	(88)	(98)	(98)																						
"Wo"	41.1	43.2	46.8	46.0	48.2	44.0	44.7	46.0	42.9	47.6	46.9	47.4	45.5	2.008	2.000																						
"En"	42.6	38.3	40.3	39.7	34.5	12.0	25.4	17.1	24.8	13.4	15.2	13.2	12.9	0.000	0.000																						
"Fs"	16.3	18.5	17.4	14.3	17.4	44.0	29.9	36.9	32.3	38.9	37.9	39.4	41.6	2.008	2.000																						

* Calculated ferrous and ferric oxides based on XY + Z cations = 4. Total iron expressed as ferrous oxide is given in parentheses.
 † Normalized end member compositions in per cent. The percentage of the composition calculated into end members is placed in parentheses.
 " Molecular percentages of "En" = Mg/R x 100, "Fs" = Fe²⁺/R x 100, and "Wo" = Ca/R x 100 where R = Mg + Fe²⁺ + Ca
 PH :: phenocryst, GM = groundmass, C = core, R = rim

CLINOPYROXENES

Sample:	SE14-3-1	SE14-3-2	SE14-5-1	SE15-2-1	SE15-2-2	SE15-4-1	SE15-4-2	SE15-5-1	SE19-1-3	SE19-3-4	SE19-4-2	SE20-2-1	SE20-3-1	SE20-5-2	SE27-1-2
Formation:	Armadio	Armadio	Armadio	Armadio	Armadio	Armadio	Armadio	Armadio	Armadio	Armadio	Armadio	Armadio	Armadio	Armadio	Armadio
Type:	PHR	PHC	PH	PHC	PHR	PH	PH	PH	PHR	GM	GM	GM	PH	GM	PHR
SiO ₂	52.02	52.19	52.26	47.77	47.61	48.14	47.58	48.39	49.22	51.15	50.43	51.92	52.06	51.76	47.67
Al ₂ O ₃	0.23	0.31	0.17	0.62	0.39	0.20	0.59	0.40	0.12	0.15	0.19	0.34	0.30	0.38	0.09
Cr ₂ O ₃	0.00	0.00	0.00	0.00	0.02	0.01	0.00	0.00	0.00	0.00	0.01	0.02	0.02	0.00	0.01
TiO ₂	0.41	0.60	0.14	0.56	0.39	0.50	0.58	0.42	0.23	1.66	1.74	0.39	0.80	0.63	0.27
(Fe _{Tot} as FeO)	(30.74)	(30.05)	(31.21)	(30.56)	(29.96)	(30.66)	(30.48)	(30.20)	(30.35)	(28.55)	(28.17)	(30.22)	(29.66)	(29.07)	(29.87)
Fe ₂ O ₃ *	32.63	30.15	31.61	2.57	2.27	3.79	2.19	1.31	5.93	19.55	20.76	30.79	29.05	27.65	7.12
FeO*	1.38	2.92	2.77	28.25	27.92	27.25	28.51	29.02	25.01	10.96	9.49	2.51	3.52	4.19	23.46
MnO	0.23	0.16	0.28	1.23	1.16	1.18	1.27	1.19	0.84	0.41	0.36	0.17	0.18	0.25	0.82
MgO	0.01	0.01	0.03	0.02	0.04	0.01	0.04	0.01	0.03	0.02	0.00	0.01	0.02	0.03	0.13
CaO	2.44	2.42	2.52	19.75	20.06	17.50	19.41	20.00	17.63	8.30	7.33	3.15	3.33	4.10	15.89
Na ₂ O	12.46	12.23	12.13	0.60	0.52	1.53	0.57	0.51	2.27	8.75	9.19	12.01	11.84	11.36	2.37
K ₂ O	0.01	0.01	0.01	0.00	0.00	0.01	0.00	0.00	0.01	0.01	0.00	0.00	0.02	0.01	0.03
Total	101.82	101.01	101.92	101.37	100.38	100.12	100.75	101.25	101.29	100.96	99.50	101.31	101.14	100.36	98.86
Si	1.976	1.996	1.987	1.952	1.964	1.982	1.957	1.978	1.989	1.992	1.987	1.983	1.991	1.997	1.974
Al	0.010	0.004	0.008	0.030	0.019	0.010	0.029	0.019	0.006	0.007	0.009	0.015	0.009	0.003	0.004
Fe ⁺³	0.014	0.000	0.005	0.018	0.017	0.008	0.014	0.003	0.005	0.001	0.004	0.002	0.000	0.000	0.021
Al	0.000	0.010	0.000	0.000	0.000	0.000	0.000	0.000	0.000	0.000	0.000	0.000	0.005	0.014	0.000
Cr	0.000	0.000	0.000	0.000	0.001	0.000	0.000	0.000	0.000	0.000	0.000	0.001	0.001	0.000	0.000
Ti	0.012	0.017	0.004	0.017	0.012	0.016	0.018	0.013	0.007	0.049	0.052	0.011	0.023	0.018	0.008
Fe ⁺²	0.919	0.868	0.900	0.961	0.953	0.109	0.053	0.037	0.175	0.572	0.612	0.884	0.836	0.803	0.201
Mg	0.001	0.001	0.002	0.001	0.002	0.001	0.002	0.001	0.002	0.001	0.000	0.001	0.001	0.002	0.008
Fe ⁺²	0.044	0.093	0.088	0.966	0.963	0.938	0.981	0.992	0.845	0.357	0.313	0.080	0.113	0.135	0.812
Mn	0.007	0.005	0.009	0.043	0.040	0.041	0.044	0.041	0.029	0.014	0.012	0.006	0.006	0.008	0.029
Ca	0.099	0.099	0.103	0.865	0.886	0.772	0.855	0.876	0.763	0.346	0.310	0.129	0.136	0.170	0.750
Na	0.918	0.907	0.894	0.048	0.042	0.122	0.046	0.040	0.180	0.661	0.702	0.889	0.878	0.850	0.190
K	0.001	0.001	0.001	0.000	0.000	0.001	0.001	0.000	0.001	0.001	0.000	0.000	0.001	0.001	0.002
Z	2.000	2.000	2.000	2.000	2.000	2.000	2.000	2.000	2.000	2.000	2.000	2.000	2.000	2.000	2.000
XY	2.000	2.000	2.000	2.000	2.000	2.000	2.000	2.000	2.000	2.000	2.000	2.000	2.000	2.000	2.000
Jd [†]	0	1	0	0	0	0	0	0	0	0	0	0	0	1	0
Ac	91	88	90	6	5	10	5	4	17	58	63	88	85	81	20
Ti-Cats	0	0	0	1	1	0	1	1	0	0	0	1	0	0	0
TiSi ₂ O ₆	1	2	0	2	0	2	1	0	1	5	5	0	2	2	1
Fe-Cats	0	0	0	0	0	1	0	0	1	1	1	0	1	0	0
Cats	0	0	0	0	0	0	0	0	0	0	0	0	0	0	0
Wo	4	5	4	42	44	38	42	43	37	17	15	6	6	8	37
En	0	0	0	0	0	0	0	0	0	0	0	0	0	0	0
Fs	2	4	4	48	48	47	49	50	42	18	15	4	5	7	40
Bu	1	0	1	2	2	2	2	2	2	1	1	1	1	1	2
%age calc:	(99)	(99)	(98)	(98)	(99)	(99)	(98)	(99)	(99)	(97)	(96)	(99)	(97)	(98)	(97)
"Wo"				47.2	47.9	45.1	46.5	46.9	47.4						47.7
"En"				0.1	0.1	0.0	0.1	0.0	0.1						0.5
"Fs"				52.7	52.0	54.8	53.3	53.1	52.5						51.8

Formula based on 6 oxygens

* Calculated ferrous and ferric oxides based on XY + Z cations = 4. Total iron expressed as ferrous oxide is given in parentheses.
† Normalized end member compositions in per cent. The percentage of the composition calculated into end members is placed in parentheses.
" Molecular percentages of ⁵⁶En = Mg/R x 100, ⁵⁸En = Fe⁺²/R x 100, and ⁵⁶Wo = Ca/R x 100 where R = Mg + Fe⁺² + Ca
PH = phenocryst, GM = groundmass, C = core, R = rim

CLINOPYROXENES

Sample: SE27-1-3 SE126-1-1 SE126-1-2 SE126-1-3 SE126-2-1 SE126-2-2 SE126-2-3 SE126-2-4 SE126-4-1 SE126-4-2 SE107-1-3 SE115-1-1 SE115-1-2 SE120-2-1 SE123-3-1	Armadiillo PHC	Armadiillo PHR	Armadiillo PHC	Armadiillo PHR	Armadiillo PHC	Armadiillo PHR	Armadiillo PHC	Armadiillo PHR	Armadiillo PHC	Nido GM	Nido GM	Nido GM	Nido GM	Nido GM
Formation:														
Type:														
SiO ₂	47.56	52.42	52.51	52.39	52.82	52.01	52.71	52.56	53.17	46.93	51.26	49.87	50.71	46.57
Al ₂ O ₃	0.09	0.37	0.24	0.49	0.47	0.19	0.35	0.40	0.40	4.68	2.10	2.96	2.68	5.02
Cr ₂ O ₃	0.00	0.00	0.00	0.00	0.00	0.00	0.00	0.00	0.00	0.01	0.00	0.00	0.00	0.00
TiO ₂	0.28	0.00	0.03	0.04	1.33	0.04	2.00	0.85	0.03	3.44	1.51	1.99	1.13	3.71
(Fe ₉₀ as FeO)	(30.20)	(30.05)	(30.16)	(30.04)	(29.45)	(30.24)	(28.90)	(29.79)	(30.21)	(11.24)	(9.62)	(9.79)	(9.55)	(10.60)
Fe ₂ O ₃ *	6.61	33.39	33.52	33.38	31.33	31.41	30.07	32.63	33.57	2.66	1.10	1.92	1.21	1.91
FeO	24.25	0.00	0.00	0.00	1.26	0.00	1.84	0.43	0.00	8.85	8.63	8.06	8.46	8.88
MnO	0.80	0.65	0.24	0.29	0.17	0.19	0.19	0.14	0.54	0.18	0.26	0.21	0.21	0.21
MgO	0.10	0.03	0.00	0.02	0.00	0.00	0.01	0.01	0.00	11.12	13.10	12.90	14.16	11.25
CaO	17.00	0.10	0.03	0.04	0.65	0.03	0.69	0.46	0.02	21.52	21.92	21.80	20.50	21.34
Na ₂ O	2.17	14.00	13.77	13.56	13.39	13.71	13.34	13.45	13.81	0.60	0.50	0.48	0.31	0.54
K ₂ O	0.01	0.00	0.01	0.01	0.00	0.00	0.01	0.02	0.00	0.00	0.00	0.00	0.01	0.01
Total	98.87	100.98	100.35	100.22	101.42	99.78	101.21	100.95	101.54	99.99	100.38	100.19	99.74	99.44
Si	1.974	1.997	2.008	2.004	1.997	2.002	1.997	1.996	2.008	1.781	1.914	1.869	1.898	1.774
Al	0.004	0.003	0.000	0.000	0.003	0.000	0.003	0.004	0.000	0.209	0.086	0.131	0.102	0.225
Fe * 3	0.022	0.000	0.000	0.000	0.000	0.000	0.000	0.000	0.000	0.010	0.000	0.000	0.000	0.001
Al	0.000	0.014	0.011	0.022	0.018	0.009	0.012	0.014	0.018	0.000	0.006	0.000	0.016	0.000
Cr	0.000	0.001	0.000	0.000	0.000	0.000	0.000	0.000	0.000	0.000	0.000	0.000	0.011	0.000
Ti	0.009	0.000	0.001	0.001	0.038	0.001	0.044	0.024	0.001	0.098	0.042	0.056	0.032	0.106
Fe * 3	0.184	0.957	0.964	0.961	0.891	0.974	0.898	0.932	0.954	0.066	0.031	0.054	0.034	0.054
Mg * 2	0.006	0.002	0.000	0.001	0.000	0.000	0.001	0.001	0.000	0.629	0.729	0.721	0.790	0.639
Fe	0.842	0.000	0.000	0.000	0.040	0.000	0.058	0.014	0.000	0.281	0.270	0.253	0.265	0.283
Mn	0.028	0.021	0.008	0.009	0.005	0.006	0.006	0.005	0.017	0.006	0.008	0.007	0.007	0.007
Ca	0.756	0.004	0.001	0.002	0.026	0.001	0.017	0.019	0.001	0.875	0.877	0.875	0.822	0.871
Na	0.175	1.034	1.021	1.006	0.982	1.024	0.980	0.991	1.011	0.044	0.036	0.035	0.022	0.040
K	0.001	0.000	0.001	0.001	0.000	0.000	0.001	0.001	0.000	0.000	0.000	0.000	0.001	0.001
Z	2.000	2.000	2.008	2.004	2.000	2.002	2.000	2.000	2.008	2.000	2.000	2.000	2.000	2.000
XY	2.000	2.033	2.006	2.003	2.000	2.014	2.000	2.000	2.002	2.000	2.000	2.000	2.000	2.000
Jd [†]	0	1	1	2	2	1	1	1	2	0	0	0	0	0
Ac	18	98	98	97	90	98	88	96	97	6	3	4	1	4
Tr-Cals	0	0	0	0	0	0	0	0	0	10	4	6	3	11
TiSi ₂ O ₆	1	0	0	0	4	0	6	2	0	0	0	0	0	0
Fe-Cals	0	0	0	0	0	0	0	0	0	1	0	1	2	0
Cals	0	0	0	0	0	0	0	0	0	0	0	0	0	0
Wo	38	0	0	0	1	0	1	1	0	39	42	40	37	37
En	0	0	0	0	0	0	0	0	0	0	0	0	0	0
Fs	41	0	0	0	2	0	3	0	0	31	36	36	40	32
Bu	2	1	1	1	1	1	1	0	1	1	1	1	1	1
%age cal/c.	(98)	(98)	(97)	(98)	(98)	(97)	(97)	(97)	(98)	(98)	(98)	(99)	(98)	(99)
"Wo"	47.1									49.0	46.7	47.3	43.8	48.6
"En"	0.4									35.3	38.9	39.0	42.1	35.6
"Fs"	52.5									15.7	14.4	13.7	14.1	15.8

Formula based on 6 oxygens

* Calculated ferrous and ferric oxides based on XY + Z cations = 4 Total iron expressed as ferrous oxide is given in parentheses.
 † Normalized end member compositions in per cent. The percentage of the composition calculated into end members is placed in parentheses.
 "Wo" = Molecular percentages of "En" = Mg/R x 100, "Fs" = Fe + 2R x 100, and "Wo" = Ca/R x 100 where R = Mg + Fe + 2 + Ca
 PH = phenocryst, GM = groundmass, C = core, R = rim

CLINOPYROXENES

Sample Formation:	SE123-3-2 Nido	SE123-3-3 Nido	SE125-5-1 Nido	SE125-5-2 Nido	SE92-1-3	SE94-1-3	SE94-3-1	SE98-1-1	SE98-2-1	SE100-1-1	SE100-1-2	SE100-2-1	SE100-2-2	SE100-2-3	SE100-3-1
Type:	GM	GM	PHR	PHC	PH	PH	PHC	GM	PH	PH	PH	PH	PH	PH	PH
SiO ₂	45.03	48.96	49.78	49.92	49.81	48.60	48.49	48.55	47.63	47.01	47.74	48.02	47.38	54.51	47.83
Al ₂ O ₃	6.33	3.48	4.25	4.06	0.12	0.16	0.12	0.22	0.22	0.33	0.30	0.20	0.28	1.51	0.20
Cr ₂ O ₃	0.02	0.01	0.01	0.00	0.00	0.00	0.03	0.01	0.01	0.02	0.00	0.00	0.00	0.25	0.02
TiO ₂	4.53	2.49	1.64	1.68	0.35	0.48	0.42	0.86	0.72	0.61	0.56	0.42	0.58	0.14	0.46
(Fe ₂ O ₃ as FeO)	(10.87)	(11.27)	(9.02)	(9.25)	(28.66)	(29.25)	(29.02)	(28.43)	(29.44)	(29.76)	(29.27)	(29.46)	(29.56)	(12.90)	(29.80)
Fe ₂ O ₃ *	2.34	1.44	1.61	1.84	9.99	3.67	3.20	5.35	3.61	2.37	0.83	1.97	1.80	1.83	1.86
FeO*	8.76	9.97	7.57	7.59	19.67	25.95	26.14	23.62	26.19	27.63	28.52	27.69	27.94	11.25	28.13
MnO	0.19	0.24	0.23	0.22	1.06	1.33	1.10	1.14	1.30	1.07	1.03	0.97	1.03	0.34	1.01
MgO	10.66	11.85	12.70	13.06	0.49	0.13	0.15	0.21	0.29	0.03	0.02	0.01	0.03	29.25	0.03
CaO	21.17	20.88	21.68	21.33	14.14	18.41	19.18	16.73	18.63	20.08	19.79	20.12	20.04	1.17	19.70
N ₂ O	0.60	0.58	0.60	0.60	4.33	1.60	1.35	2.62	1.23	0.48	0.56	0.71	0.53	0.01	0.68
K ₂ O	0.02	0.00	0.00	0.00	0.00	0.00	0.00	0.03	0.00	0.01	0.01	0.01	0.00	0.01	0.00
Total	99.65	99.90	100.07	100.30	99.98	100.33	100.18	99.34	99.83	99.64	99.36	100.12	99.61	100.27	99.92
Formula based on 6 oxygens															
Si	1.717	1.852	1.859	1.860	2.005	1.988	1.988	1.990	1.965	1.955	1.985	1.980	1.968	1.937	1.979
Al	0.283	0.148	0.141	0.140	0.000	0.008	0.006	0.000	0.011	0.016	0.015	0.010	0.014	0.063	0.010
Fe ⁺³	0.000	0.000	0.000	0.000	0.000	0.004	0.006	0.000	0.024	0.029	0.000	0.010	0.018	0.000	0.011
Al	0.001	0.007	0.046	0.038	0.006	0.000	0.000	0.001	0.000	0.000	0.000	0.000	0.000	0.001	0.000
Cr	0.000	0.000	0.000	0.000	0.000	0.000	0.001	0.000	0.000	0.001	0.000	0.000	0.000	0.007	0.001
Ti	0.130	0.071	0.046	0.047	0.011	0.015	0.013	0.026	0.022	0.019	0.018	0.013	0.018	0.004	0.014
Fe ⁺³	0.067	0.041	0.045	0.052	0.303	0.109	0.093	0.165	0.088	0.046	0.026	0.051	0.038	0.049	0.046
Mg	0.606	0.668	0.707	0.725	0.029	0.008	0.013	0.018	0.018	0.002	0.001	0.001	0.002	1.549	0.002
Fe ⁺²	0.279	0.315	0.236	0.236	0.662	0.888	0.896	0.810	0.904	0.961	0.992	0.955	0.971	0.334	0.973
Mn	0.006	0.008	0.007	0.007	0.036	0.046	0.038	0.040	0.045	0.038	0.036	0.034	0.036	0.010	0.035
Ca	0.865	0.846	0.868	0.851	0.610	0.807	0.842	0.735	0.824	0.895	0.882	0.889	0.892	0.045	0.873
K	0.044	0.042	0.044	0.043	0.338	0.127	0.107	0.208	0.098	0.039	0.045	0.057	0.043	0.001	0.055
Na	0.001	0.000	0.000	0.000	0.001	0.000	0.000	0.002	0.000	0.001	0.001	0.001	0.000	0.001	0.000
Z	2.000	2.000	2.000	2.000	2.005	2.000	2.000	2.000	2.000	2.000	2.000	2.000	2.000	2.000	2.000
XY	2.000	2.000	2.000	2.000	1.995	2.000	2.000	2.000	2.000	2.000	2.000	2.000	2.000	2.000	2.000
Jd ¹	0	0	0	0	1	0	0	0	0	0	0	0	0	0	0
Ac	5	4	5	5	31	11	9	16	8	5	2	4	3	0	4
Tr-Cats	13	7	5	5	0	0	0	0	0	1	0	0	0	0	0
T ₂ Si ₂ O ₆	0	0	0	0	1	1	1	3	2	1	2	1	2	0	1
Fe-Cats	2	0	0	0	0	1	1	1	1	0	1	1	1	4	1
Cats	0	1	4	4	0	0	0	0	0	0	0	0	0	0	0
Wo	35	38	38	38	30	40	41	37	40	44	43	44	44	0	43
En	30	33	36	36	1	0	0	0	1	0	0	0	0	79	0
Fs	14	16	11	11	34	45	46	41	45	48	50	48	48	16	49
Bu	1	1	1	1	2	2	2	2	3	1	2	2	2	1	2
%age calc.	(99)	(99)	(98)	(99)	(98)	(98)	(98)	(97)	(98)	(99)	(99)	(98)	(98)	(97)	(99)
"Wo"	49.4	46.3	47.9	47.0	47.4	48.2	47.2	47.2	47.2	48.2	47.0	48.2	47.8	2.3	47.2
"En"	34.6	36.5	39.0	40.0	0.5	0.5	0.8	0.8	1.0	0.1	0.1	0.0	0.1	80.4	0.1
"Fs"	16.0	17.2	13.1	13.0	52.1	51.3	52.0	52.0	51.8	51.7	52.9	51.8	52.1	17.3	52.7

* Calculated ferrous and ferric oxides based on XY + Z cations = 4. Total iron expressed as ferrous oxide is given in parentheses.
 † Normalized end member compositions in per cent. The percentage of the composition calculated into end members is placed in parentheses.
 " Molecular percentages of "En" = Mg/R x 100, "Fs" = Fe²⁺/R x 100, and "Wo" = Ca/R x 100 where R = Mg + Fe²⁺ + Ca
 PH = phenocryst, GM = groundmass, C = core, R = rim

CLINOPYROXENES															
Sample:	SE100-4-1	SE100-4-4	SE100-5-2	SE100-5-3	SE100-6-2	SE102-2-1	SE103-2-2	SE84-2-1	SE41-3-2	SE44-3-1	SE44-3-2	SE46-2-1	SE46-2-2	SE46-4-1	SE46-4-2
Formation:	Spectrum	Spectrum	Spectrum	Spectrum	Spectrum	Spectrum	Spectrum	Pyramid	Ice/Peak	Ice Peak	Ice Peak	Ice Peak	Ice Peak	Ice Peak	Ice Peak
Type:	PH	PH	PH	PH	PH	PH	PHC	PHC	GM	PHR	PHC	PHR	PHC	GM	GM
SiO ₂	47.46	46.57	47.84	47.88	47.92	48.12	48.74	49.58	47.66	49.17	49.94	50.57	51.16	50.37	51.14
Al ₂ O ₃	0.30	0.20	0.19	0.25	0.16	0.18	0.10	0.76	2.68	1.03	0.87	2.59	2.68	2.69	1.96
Cr ₂ O ₃	0.00	0.00	0.02	0.00	0.00	0.00	0.00	0.00	0.00	0.00	0.01	0.03	0.00	0.02	0.01
TiO ₂	0.61	0.40	0.36	0.44	0.00	0.30	0.41	0.32	3.06	0.50	0.41	1.29	1.29	1.17	0.76
(Fe ₁₀₁ as FeO)	(29.74)	(29.62)	(30.04)	(29.99)	(29.83)	(30.50)	(28.36)	(22.81)	(10.41)	(21.60)	(21.66)	(12.44)	(11.01)	(11.74)	(12.72)
Fe ₂ O ₃	1.79	4.10	2.86	2.31	2.81	0.81	3.51	1.61	2.43	2.98	2.08	2.58	1.24	1.64	2.32
FeO*	28.13	25.93	27.47	27.91	27.55	29.77	25.20	21.36	8.22	18.92	19.79	10.12	9.89	10.26	10.63
MnO	1.10	1.06	0.99	1.05	0.90	1.05	1.07	0.68	0.21	0.73	0.71	0.38	0.33	0.40	0.40
MgO	0.02	0.02	0.00	0.04	0.02	0.12	0.20	5.56	12.17	5.65	5.48	11.63	12.42	11.49	11.79
CaO	20.02	20.15	19.49	19.80	19.18	18.24	18.84	20.19	21.30	20.68	21.09	21.63	21.52	21.60	21.59
Na ₂ O	0.51	0.68	0.88	0.69	0.91	0.73	1.69	0.37	0.50	0.65	0.60	0.53	0.51	0.53	0.45
K ₂ O	0.00	0.01	0.00	0.01	0.00	0.00	0.01	0.01	0.00	0.00	0.00	0.00	0.01	0.00	0.01
Total	99.94	99.12	100.10	100.38	99.45	99.32	99.77	100.44	100.39	100.31	100.98	101.10	101.05	100.17	101.06
Formula based on 6 oxygens															
Si	1.966	1.946	1.975	1.972	1.989	2.003	1.998	1.963	1.790	1.942	1.960	1.896	1.906	1.903	1.919
Al	0.015	0.010	0.009	0.012	0.008	0.000	0.002	0.036	0.210	0.048	0.040	0.104	0.094	0.097	0.081
Fe ³⁺	0.019	0.044	0.016	0.016	0.003	0.000	0.000	0.001	0.000	0.010	0.000	0.000	0.000	0.000	0.000
Al	0.000	0.000	0.000	0.000	0.000	0.009	0.003	0.000	0.005	0.000	0.000	0.010	0.024	0.022	0.006
Cr	0.000	0.000	0.001	0.000	0.000	0.000	0.000	0.000	0.000	0.000	0.000	0.001	0.000	0.001	0.000
Ti	0.019	0.013	0.011	0.014	0.000	0.009	0.013	0.010	0.086	0.015	0.036	0.029	0.036	0.033	0.021
Fe ²⁺	0.037	0.085	0.073	0.056	0.085	0.025	0.108	0.047	0.069	0.078	0.061	0.073	0.035	0.047	0.056
Mg	0.001	0.001	0.000	0.002	0.001	0.007	0.012	0.328	0.681	0.333	0.320	0.650	0.690	0.647	0.659
Fe ²⁺	0.975	0.906	0.948	0.962	0.956	1.036	0.864	0.707	0.258	0.625	0.650	0.317	0.308	0.324	0.334
Mn	0.039	0.038	0.035	0.037	0.032	0.037	0.037	0.023	0.007	0.024	0.024	0.012	0.010	0.013	0.013
Ca	0.869	0.902	0.862	0.874	0.853	0.814	0.828	0.857	0.857	0.875	0.887	0.869	0.859	0.874	0.868
Na	0.041	0.055	0.070	0.055	0.073	0.059	0.134	0.028	0.036	0.050	0.046	0.038	0.037	0.039	0.033
K	0.000	0.001	0.000	0.001	0.000	0.000	0.001	0.001	0.000	0.000	0.000	0.000	0.001	0.000	0.001
Z	2.000	2.000	2.000	2.000	2.000	2.003	2.000	2.000	2.000	2.000	2.000	2.000	2.000	2.000	2.000
XY	2.000	2.000	2.000	2.000	2.000	1.997	2.000	2.000	2.000	2.000	2.000	2.000	2.000	2.000	2.000
Jd [†]	0	0	0	0	0	1	0	0	0	0	0	0	0	0	0
Ac	3	7	6	5	7	3	11	3	4	5	4	4	3	3	4
Ti-Cats	0	0	0	0	0	0	0	1	9	1	1	3	4	3	2
TiSi ₂ O ₆	2	1	1	1	0	1	1	0	0	0	0	0	0	0	0
Fe-Cats	1	1	1	1	1	0	0	2	3	3	2	3	0	2	3
Cats	0	0	0	0	0	0	0	0	0	0	0	1	1	2	1
Wo	44	44	42	43	42	40	42	42	37	43	44	41	41	41	41
En	0	0	0	0	0	0	0	16	34	16	34	32	34	32	33
Fs	48	45	48	48	48	53	44	35	13	31	32	15	15	16	15
Bu	2	2	2	2	2	2	2	1	0	1	1	1	1	1	1
%age calc.	(98)	(97)	(98)	(99)	(99)	(99)	(98)	(98)	(100)	(99)	(99)	(98)	(98)	(98)	(98)
¹¹ W ₀ [‡]	47.6	49.9	47.6	47.6	47.1	43.8	48.6	45.3	47.7	47.7	47.7	47.3	46.3	47.4	46.7
¹¹ En [‡]	0.1	0.1	0.0	0.1	0.1	0.4	0.7	17.3	37.9	18.2	17.3	35.4	37.1	35.0	35.4
¹¹ Fs [‡]	52.3	50.1	52.4	52.3	52.8	55.8	50.7	37.4	14.4	34.1	35.0	17.3	16.6	17.6	17.9

* Calculated ferrous and ferric oxides based on XY + Z cations = 4. Total iron expressed as ferrous oxide is given in parentheses.

† Normalized end member compositions in per cent. The percentage of the composition calculated into end members is placed in parentheses.

‡ Molecular percentages of ¹¹En = Mg/R x 100, ¹¹Fs = Fe²⁺/R x 100, and ¹¹Wo = Ca/R x 100 where R = Mg + Fe²⁺ + Ca

PH = phenocryst, GM = groundmass, C = core, R = rim

CLINOPYROXENES

Sample:	SE51-3-1	SE135-1-1	SE135-1-2	SE135-3-1	SE135-3-2	SE135-3-3	SE135-4-1	SE135-4-2	SE136-2-1	SE136-2-2	SE137-3-1	SE137-3-3	SE137-4-1	SE137-4-2
Formation:	Ice Peak	Pillow Ridge Nodule	Pillow Ridge Nodule	Pillow Ridge Nodule	Pillow Ridge Nodule	Pillow Ridge Nodule	Pillow Ridge Nodule	Pillow Ridge Nodule	Pillow Ridge PHR	Pillow Ridge PHC	Pillow Ridge PHR	Pillow Ridge PHC	Pillow Ridge PHR	Pillow Ridge PHC
Type:	PHC													
SiO ₂	49.01	48.68	49.01	48.14	49.21	47.84	48.63	50.41	50.39	50.28	49.70	49.50	50.52	50.21
Al ₂ O ₃	6.00	4.29	4.18	5.67	5.19	4.96	4.98	4.13	4.70	3.67	4.56	4.83	3.46	3.56
Cr ₂ O ₃	0.28	0.39	0.02	0.00	0.00	0.00	0.01	0.01	0.58	0.03	0.12	0.26	0.02	0.04
TiO ₂	1.69	1.58	1.53	2.15	1.91	1.83	1.76	1.52	1.29	1.38	1.57	1.48	1.33	1.30
(Fe _{101.45} FeO)	(7.59)	(9.27)	(9.27)	(9.31)	(9.22)	(8.99)	(8.88)	(9.20)	(7.22)	(9.46)	(8.62)	(8.20)	(9.21)	(8.97)
Fe ₂ O ₃ *	1.71	2.44	3.59	1.69	1.26	3.50	2.63	1.19	1.03	1.38	0.79	1.89	2.03	2.11
FeO*	6.05	5.86	6.06	7.79	8.09	5.84	6.51	8.13	6.29	8.22	7.91	6.50	7.38	7.07
MnO	0.17	0.15	0.20	0.20	0.20	0.18	0.19	0.20	0.17	0.23	0.15	0.12	0.19	0.15
MgO	14.15	14.83	13.43	12.35	12.64	12.83	13.03	13.36	14.46	12.72	12.68	13.05	13.23	13.47
CaO	20.68	21.06	21.24	21.10	21.29	21.43	21.23	21.13	21.40	21.73	21.61	22.19	22.14	21.85
Na ₂ O	0.47	0.49	0.54	0.53	0.53	0.54	0.56	0.51	0.38	0.51	0.53	0.47	0.45	0.42
K ₂ O	0.00	0.01	0.02	0.00	0.00	0.00	0.00	0.02	0.00	0.01	0.01	0.01	0.00	0.01
Total	100.21	100.54	99.82	99.62	100.32	98.95	99.53	100.61	100.69	100.16	99.63	100.30	100.75	100.19

Formula based on 6 oxygens

Si	1.811	1.831	1.834	1.809	1.834	1.808	1.824	1.870	1.853	1.879	1.862	1.840	1.875	1.871
Al	0.189	0.169	0.166	0.191	0.166	0.192	0.176	0.130	0.147	0.121	0.138	0.160	0.125	0.129
Fe ⁺³	0.000	0.000	0.000	0.000	0.000	0.000	0.000	0.000	0.000	0.000	0.000	0.000	0.000	0.000
Al	0.073	0.047	0.018	0.060	0.062	0.028	0.044	0.050	0.057	0.041	0.063	0.051	0.026	0.027
Cr	0.008	0.011	0.001	0.000	0.000	0.000	0.000	0.000	0.017	0.001	0.004	0.008	0.001	0.001
Ti	0.047	0.036	0.043	0.061	0.054	0.052	0.042	0.042	0.036	0.041	0.044	0.041	0.037	0.036
Fe ⁺³	0.048	0.096	0.101	0.048	0.035	0.100	0.074	0.033	0.029	0.039	0.022	0.053	0.057	0.059
Mg	0.780	0.814	0.749	0.692	0.702	0.723	0.728	0.738	0.793	0.709	0.708	0.723	0.732	0.748
Fe ⁺²	0.187	0.180	0.190	0.245	0.252	0.184	0.204	0.252	0.194	0.257	0.248	0.202	0.229	0.220
Mn	0.005	0.007	0.006	0.006	0.006	0.006	0.006	0.006	0.005	0.007	0.005	0.004	0.006	0.005
Ca	0.819	0.804	0.852	0.850	0.850	0.868	0.853	0.840	0.843	0.870	0.867	0.884	0.880	0.872
Na	0.034	0.035	0.039	0.039	0.038	0.040	0.041	0.037	0.027	0.037	0.038	0.034	0.032	0.030
K	0.000	0.000	0.001	0.000	0.000	0.000	0.000	0.001	0.000	0.001	0.001	0.001	0.000	0.001
Z	2.000	2.000	2.000	2.000	2.000	2.000	2.000	2.000	2.000	2.000	2.000	2.000	2.000	2.000
XY	2.000	2.000	2.000	2.000	2.000	2.000	2.000	2.000	2.000	2.000	2.000	2.000	2.000	2.000
Ju ¹	0	0	0	0	0	0	0	0	0	0	0	0	0	0
Ac	3	3	3	4	3	4	3	3	2	4	2	2	4	4
Ti-Cats	5	4	4	6	5	5	4	4	4	4	4	4	4	4
Ti ₂ O ₆	0	0	0	0	0	0	0	0	0	0	0	0	0	0
Fe-Cats	2	3	7	1	1	6	4	1	1	0	0	3	2	0
Cats	7	5	2	6	6	3	4	5	6	4	6	5	3	3
Wo	34	35	37	36	37	37	37	38	37	39	40	39	40	40
En	40	39	39	34	35	38	37	37	40	35	36	37	37	38
Fs	8	7	7	12	12	6	9	12	8	13	12	9	10	9
Bu	0	0	1	1	1	1	1	1	0	1	0	0	0	0
%edge calc.	(99) ^o	(96)	(96)	(99)	(98)	(96)	(97)	(98)	(98) ^o	(99)	(97)	(98) ^o	(98)	(98)
"Wo"	45.9	44.7	47.6	47.6	47.1	48.9	47.7	45.9	46.1	47.4	47.6	48.8	47.8	47.4
"En"	43.6	45.3	41.8	38.7	38.9	40.7	40.8	40.3	38.6	40.0	38.8	40.0	39.8	40.6
"Fs"	10.5	10.0	10.6	13.7	14.0	10.4	11.5	13.8	14.0	11.2	13.6	11.2	12.4	12.0

* Calculated ferrous and ferric oxides based on XY + Z cations = 4. Total iron expressed as ferrous oxide is given in parentheses.
¹ Normalized end member compositions in per cent. The percentage of the composition calculated into end members is placed in parentheses.
^o Molecular percentages of ⁵⁶Feⁿ = Mg/R x 100, ⁵⁷Feⁿ = Fe + 2/R x 100, and ⁵⁸Feⁿ = Ca/R x 100 where R = Mg + Fe⁺² + Ca
 PH = phenocryst, GM = groundmass, C = core, R = rim

CLINOPYROXENES															
Sample Formation:	SE82-1-1 Edziza	SE63-6-1 Edziza	SE63-6-2 Edziza	SE66-1-1 Edziza	SE66-2-3 Edziza	SE66-3-1 Edziza	SE69-1-1 Edziza	SE72-1-3 Edziza	SE72-3-1 Edziza	SE72-3-2 Edziza	SE72-4-1 Edziza	SE72-4-2 Edziza	SE72-6-3 Edziza	SE141-A-6 Arctic Lake	SE132-1 Klastline
Type:	PH	PH	PH	GM	PH	PH	GM	GM	PHC	PHR	PH	PH	PH	GM	PH
SiO ₂	48.06	47.98	47.86	49.54	50.48	50.57	49.15	47.97	48.21	48.02	47.91	47.58	46.92	48.28	47.85
Al ₂ O ₃	0.30	0.22	0.45	0.43	0.95	0.98	0.83	0.23	0.21	0.34	0.28	0.22	0.30	3.69	5.97
Cr ₂ O ₃	0.00	0.01	0.01	0.00	0.00	0.00	0.01	0.02	0.01	0.00	0.00	0.00	0.00	0.00	0.20
TiO ₂	0.48	0.46	0.60	0.53	0.58	0.64	0.96	0.54	0.44	0.56	0.54	0.47	0.60	2.34	1.83
(Fe ₁₀₁ as FeO)	(28.71)	(29.32)	(29.77)	(23.02)	(16.21)	(16.33)	(25.01)	(30.43)	(29.48)	(28.91)	(29.29)	(29.63)	(29.28)	(10.70)	(6.70)
Fe ₂ O ₃	1.21	3.61	2.21	3.22	1.44	1.31	7.83	5.48	3.00	1.69	2.33	4.72	2.69	2.13	3.17
FeO	27.62	26.67	27.78	20.12	14.91	15.15	17.96	25.50	26.78	27.39	27.19	25.38	26.86	8.78	5.85
MnO	0.97	0.90	0.99	0.77	0.61	0.62	0.74	1.12	0.88	0.95	0.95	0.92	0.99	0.26	0.19
MgO	0.29	0.05	0.38	3.65	9.07	9.11	0.89	0.16	0.06	0.22	0.13	0.06	0.26	12.03	13.15
CaO	20.23	19.59	20.21	19.74	21.33	21.01	15.78	18.03	19.49	20.36	20.00	19.37	19.71	20.58	20.93
Na ₂ O	0.61	1.08	0.52	1.50	0.40	0.44	4.11	1.66	0.81	1.14	0.81	1.31	0.66	0.61	0.54
K ₂ O	0.01	0.00	0.00	0.02	0.00	0.02	0.02	0.04	0.00	0.01	0.00	0.00	0.00	0.00	0.02
Total	99.78	100.57	101.01	99.52	99.77	99.85	98.28	100.75	100.22	100.20	100.14	100.03	98.99	98.75	99.70
Formula based on 6 oxygens															
Si	1.984	1.968	1.957	1.984	1.956	1.957	1.993	1.960	1.980	1.975	1.973	1.959	1.958	1.843	1.790
Al	0.015	0.011	0.022	0.016	0.043	0.043	0.007	0.011	0.010	0.016	0.014	0.011	0.015	0.157	0.210
Fe ³⁺	0.002	0.022	0.021	0.000	0.001	0.000	0.000	0.029	0.010	0.009	0.014	0.030	0.027	0.000	0.000
Al	0.000	0.000	0.000	0.004	0.000	0.002	0.033	0.000	0.000	0.000	0.000	0.000	0.000	0.009	0.053
Cr	0.000	0.000	0.000	0.000	0.000	0.000	0.000	0.001	0.000	0.000	0.000	0.000	0.000	0.000	0.006
Ti	0.015	0.014	0.018	0.016	0.017	0.019	0.029	0.017	0.014	0.017	0.017	0.015	0.019	0.067	0.052
Fe ²⁺	0.036	0.090	0.047	0.097	0.041	0.038	0.239	0.140	0.083	0.044	0.083	0.116	0.058	0.061	0.089
Mg	0.018	0.003	0.023	0.218	0.524	0.526	0.054	0.010	0.004	0.014	0.008	0.004	0.016	0.685	0.733
Fe ²⁺	0.953	0.915	0.950	0.674	0.483	0.490	0.609	0.871	0.920	0.942	0.936	0.874	0.938	0.280	0.183
Mn	0.034	0.031	0.034	0.026	0.020	0.020	0.025	0.039	0.031	0.033	0.033	0.032	0.035	0.008	0.005
Ca	0.895	0.861	0.886	0.847	0.885	0.871	0.686	0.789	0.858	0.897	0.882	0.855	0.881	0.842	0.839
Na	0.049	0.086	0.041	0.116	0.030	0.033	0.323	0.132	0.091	0.093	0.065	0.105	0.053	0.045	0.039
K	0.001	0.000	0.000	0.001	0.000	0.001	0.001	0.002	0.000	0.001	0.000	0.000	0.000	0.002	0.001
Z	2.000	2.000	2.000	2.000	2.000	2.000	2.000	2.000	2.000	2.000	2.000	2.000	2.000	2.000	2.000
XY	2.000	2.000	2.000	2.000	2.000	2.000	2.000	2.000	2.000	2.000	2.000	2.000	2.000	2.000	2.000
Jd ³	0	0	0	0	0	0	2	0	0	0	0	0	0	0	0
Ac	3	8	5	10	4	4	25	13	7	4	5	11	5	5	3
Ti-Cals	0	0	1	1	2	2	0	0	0	0	0	0	0	7	5
Ti(Si) ₂ O ₆	1	1	1	1	0	0	3	2	1	1	2	1	2	0	0
Fe-Cals	1	1	0	0	0	0	0	1	1	0	1	1	1	1	6
Cals	0	0	0	0	0	0	1	1	1	0	1	1	0	1	1
Wo	45	43	44	43	43	43	35	40	43	45	43	42	43	37	35
En	1	0	1	11	26	26	2	0	0	0	0	0	1	34	37
Fs	48	46	47	33	24	24	31	43	47	48	48	44	46	14	7
Bu	1	1	1	1	1	1	1	1	1	1	1	1	2	1	1
%age calc.	(98)	(98)	(99)	(99)	(99)	(98)	(97)	(98)	(98)	(98)	(98)	(98)	(98)	(99)	(96)*
"Wo"	47.9	48.4	47.7	48.7	46.8	46.2	47.2	48.2	48.2	48.4	48.3	49.3	48.0	46.6	47.8
"En"	1.0	0.2	1.2	12.5	27.7	27.7	0.6	0.2	0.2	0.7	0.4	0.2	0.9	37.9	41.8
"Fs"	51.1	51.4	51.1	38.8	25.5	26.0	52.2	51.6	51.6	50.9	51.3	50.5	51.1	15.5	10.4

* Calculated ferrous and ferric oxides based on XY + Z cations = 4. Total iron expressed as ferrous oxide is given in parentheses.
 † Normalized end member compositions in per cent. The percentage of the composition calculated into end members is placed in parentheses.
 ‡ In sample SE132-1: Na/Cr₂O₆ = 1%; SE132-3: Na/Cr₂O₆ = 2%.
 § Molecular percentages of "En" = Mg/R x 100, "Fs" = Fe²⁺/R x 100, and "Wo" = Ca/R x 100 where R = Mg + Fe²⁺ + Ca
 PH = phenocryst, GM = groundmass, C = core, R = rim

CLINOPYROXENES

Sample: Formation:	SE132-2 Klastline	SE132-3 Klastline	SE132-4 Klastline	SE132-5 Klastline	SE132-6 Klastline	SE132-3-1 Klastline	SE132-3-2 Klastline	SE74-1-1 Kakiddi	SE74-1-2 Kakiddi	SE74-3-1 Kakiddi	SE74-3-2 Kakiddi	SE142-B-4 Kakiddi	SE142-B-6 Kakiddi	SE142-D-9 Kakiddi	SE142-E-10 Kakiddi	
Type:	PH	PH	PH	PH	PH	PHR	PHC	GM	GM	PHR	PHC	GM	GM	PHC	GM	
SiO ₂	49.64	49.15	50.48	49.97	49.19	48.75	49.55	47.94	47.50	48.18	48.41	48.20	48.18	48.39	48.27	
Al ₂ O ₃	5.64	4.54	3.03	5.07	5.01	5.11	3.95	0.42	0.31	0.62	0.36	0.70	0.52	0.83	0.38	
Cr ₂ O ₃	0.61	0.02	0.00	0.23	0.35	0.31	0.00	0.00	0.01	0.00	0.00	0.01	0.00	0.00	0.00	
TiO ₂	1.12	1.71	1.26	1.27	1.73	1.78	1.65	0.77	0.67	0.52	0.40	0.59	0.53	0.52	0.52	
(Fe _{Tot} as FeO)	(6.43)	(9.05)	(9.59)	(7.03)	(7.45)	(8.14)	(8.96)	(29.24)	(30.27)	(26.46)	(28.31)	(24.17)	(25.28)	(26.40)	(26.67)	
Fe ₂ O ₃	3.72	3.33	3.47	2.98	2.56	0.54	1.13	3.89	4.59	2.14	2.63	4.41	4.60	2.57	4.57	
FeO*	0.11	0.17	0.20	0.11	0.14	0.13	0.18	25.74	26.14	24.53	25.94	20.20	21.14	24.09	22.56	
MnO	14.83	13.69	14.05	14.62	14.08	12.69	12.85	1.16	1.29	0.91	0.87	0.78	0.99	0.81	0.70	
MgO	22.04	21.28	0.48	21.98	21.50	21.46	21.48	18.14	15.19	20.56	20.08	20.70	20.03	20.21	20.00	
CaO	0.40	0.52	0.48	0.47	0.52	0.43	0.47	1.26	0.88	1.04	0.53	0.53	0.55	0.55	0.99	
Na ₂ O	0.00	0.00	0.01	0.01	0.01	0.00	0.00	0.03	0.00	0.00	0.00	0.01	0.01	0.00	0.01	
K ₂ O	0.00	0.00	0.01	0.01	0.01	0.00	0.00	0.03	0.00	0.00	0.00	0.01	0.01	0.00	0.01	
Total	101.12	100.47	100.93	101.06	100.24	98.85	99.20	100.43	98.40	100.04	100.22	100.71	100.34	100.76	100.61	
Formula based on 6 oxygens																
Si	1.812	1.825	1.868	1.824	1.821	1.839	1.867	1.957	1.980	1.960	1.980	1.920	1.937	1.947	1.945	
Al	0.188	0.175	0.132	0.172	0.179	0.161	0.133	0.020	0.015	0.030	0.017	0.033	0.025	0.039	0.018	
Fe ⁺³	0.000	0.000	0.000	0.000	0.000	0.000	0.000	0.023	0.005	0.011	0.003	0.047	0.039	0.013	0.037	
Al	0.055	0.024	0.000	0.047	0.039	0.067	0.042	0.000	0.000	0.000	0.000	0.000	0.000	0.000	0.000	
Cr	0.018	0.001	0.000	0.006	0.010	0.009	0.000	0.000	0.000	0.000	0.000	0.000	0.000	0.000	0.000	
Ti	0.031	0.048	0.035	0.035	0.048	0.050	0.047	0.024	0.021	0.016	0.012	0.018	0.016	0.016	0.016	
Fe ⁺³	0.083	0.093	0.097	0.082	0.071	0.016	0.032	0.097	0.139	0.055	0.078	0.086	0.100	0.064	0.102	
Mg	0.807	0.758	0.807	0.777	0.777	0.714	0.722	0.666	0.643	0.630	0.630	0.272	0.207	0.167	0.156	
Fe ⁺²	0.114	0.188	0.200	0.133	0.159	0.241	0.250	0.879	0.911	0.834	0.887	0.673	0.711	0.811	0.760	
Mn	0.003	0.005	0.006	0.003	0.004	0.004	0.006	0.040	0.046	0.031	0.030	0.026	0.034	0.028	0.024	
Cu	0.862	0.846	0.852	0.862	0.853	0.868	0.867	0.794	0.678	0.896	0.880	0.884	0.863	0.871	0.864	
Na	0.028	0.037	0.034	0.033	0.037	0.032	0.034	0.100	0.159	0.046	0.082	0.041	0.069	0.043	0.077	
K	0.000	0.000	0.001	0.001	0.001	0.000	0.000	0.002	0.002	0.000	0.000	0.001	0.001	0.000	0.001	
Z	2.000	2.000	2.000	2.000	2.000	2.000	2.000	2.000	2.000	2.000	2.000	2.000	2.000	2.000	2.000	
XY	2.000	2.000	2.000	2.000	2.000	2.000	2.000	2.000	2.000	2.000	2.000	2.000	2.000	2.000	2.000	
Jd [†]	0	0	0	0	0	0	0	0	0	0	0	0	0	0	0	
Ac	0	3	5	2	3	2	3	10	14	6	8	9	10	6	10	
Ti-Cats	3	5	4	3	5	5	5	1	1	1	1	1	1	2	1	
TiSi ₂ O ₆	0	0	0	0	0	0	0	0	0	0	0	0	0	0	0	
Fe-Cats	8	6	5	6	4	0	0	0	0	0	0	0	0	0	0	
Cats	5	2	0	5	4	6	3	0	0	0	0	0	0	0	0	
Wo	37	37	38	37	37	38	40	39	34	44	44	45	43	43	43	
En	42	39	38	41	40	36	36	3	2	6	1	13	10	8	8	
Fs	3	7	9	5	6	12	12	44	46	40	45	30	33	40	36	
Bu	0	1	1	0	0	0	1	2	2	2	1	1	2	1	1	
%age calc.	(95) [*]	(97)	(99)	(97) [*]	(98) [*]	(98) [*]	(99)	(98)	(98)	(98)	(98)	(96)	(97)	(98)	(98)	
¹¹ W ₀ ¹¹	48.4	47.2	46.6	48.1	47.7	47.6	47.2	45.6	41.6	48.4	49.0	48.3	48.5	47.1	48.5	
¹¹ En ¹¹	45.2	42.3	42.4	44.5	43.4	39.2	39.2	3.8	2.6	6.5	1.7	14.9	11.6	9.0	8.8	
¹¹ Fs ¹¹	6.4	10.5	11.0	7.4	8.9	13.2	13.6	50.6	55.8	45.1	49.3	36.8	39.9	43.9	42.7	

* Calculated ferrous and ferric oxides based on XY + Z cations = 4. Total iron expressed as ferrous oxide is given in parentheses.
[†] Normalized end member compositions in per cent. The percentage of the composition calculated into end members is placed in parentheses.
¹¹ NaCrSi₂O₆ = 1%
¹¹ Molecular percentages of ¹¹En¹¹ = Mg/R x 100, ¹¹Fs¹¹ = Fe⁺²/R x 100, and ¹¹Wo¹¹ = Ca/R x 100 where R = Mg + Fe⁺² + Ca
PH = phenocryst, GM = groundmass, C = core, R = rim

CLINOPYROXENES															
Sample:	SE2-4-1	SE2-4-2	SE3-2-4	SE3-2-5	SE4-2-1	SE4-2-2	SE7-2-1	SE7-7-1	SE7-7-2	SE10-1-1	SE10-1-2	SE11-3-1	SE11-3-2	SE11-3-3	SE75-2-2
Formation:	Big Raven	Big Raven	Big Raven	Big Raven	Big Raven	Big Raven	Big Raven	Big Raven	Big Raven	Big Raven	Big Raven	Big Raven	Big Raven	Big Raven	Edziza
Type:	PHR	PHC	PHR	PHC	PHR	PHR	PH	PHC	PHR	PHC	PHR	PHR	PH	PHC	Nodule
SiO ₂	46.51	51.06	49.95	49.21	50.57	50.20	46.73	46.32	45.96	48.52	48.07	50.31	50.52	50.57	50.63
Al ₂ O ₃	6.00	2.45	3.62	4.20	3.40	3.92	6.96	7.89	8.60	4.25	4.38	3.24	3.25	3.13	1.18
Cr ₂ O ₃	0.10	0.10	0.00	0.01	0.34	0.51	0.02	0.03	0.01	0.00	0.03	0.00	0.02	0.00	0.00
TiO ₂	3.12	1.23	1.45	1.82	0.98	1.03	2.01	2.42	2.63	1.80	1.78	1.22	1.26	1.24	0.28
(Fe ^{tot} as FeO)	(10.69)	(10.33)	(8.96)	(8.77)	(7.58)	(7.27)	(10.52)	(9.17)	(9.25)	(8.26)	(8.57)	(10.72)	(9.84)	(9.92)	(18.22)
Fe ₂ O ₃	2.51	1.61	1.94	1.97	1.80	2.14	3.46	3.21	3.33	3.53	3.73	2.09	1.36	2.12	2.12
FeO	8.43	8.88	7.21	7.00	5.96	5.34	7.41	6.28	6.25	5.08	5.21	8.84	8.62	8.21	16.31
MnO	0.16	0.26	0.18	0.18	0.16	0.16	0.21	0.18	0.18	0.15	0.18	0.31	0.28	0.27	0.84
MgO	11.74	14.58	13.44	13.22	14.81	14.77	11.33	12.09	11.78	13.47	13.27	12.50	12.94	12.94	7.18
CaO	20.75	19.90	21.50	21.43	21.27	21.32	20.34	20.35	20.29	21.94	21.61	21.28	21.20	21.49	21.78
Na ₂ O	0.50	0.33	0.46	0.49	0.34	0.39	0.80	0.75	0.84	0.48	0.50	0.55	0.52	0.54	0.63
K ₂ O	0.00	0.00	0.00	0.00	0.00	0.00	0.03	0.00	0.00	0.02	0.01	0.01	0.00	0.00	0.00
Total	99.82	100.40	99.75	99.53	99.63	99.78	99.30	99.52	99.87	99.24	98.77	100.33	99.97	100.29	100.95
Formula based on 6 oxygens															
Si	1.759	1.900	1.869	1.846	1.880	1.862	1.768	1.739	1.720	1.823	1.817	1.885	1.892	1.889	1.958
Al	0.241	0.100	0.131	0.154	0.120	0.138	0.232	0.261	0.280	0.177	0.183	0.115	0.108	0.111	0.042
Fe ⁺³	0.000	0.000	0.000	0.000	0.000	0.000	0.000	0.000	0.000	0.000	0.000	0.000	0.000	0.000	0.000
Al	0.026	0.007	0.028	0.032	0.029	0.034	0.079	0.088	0.099	0.011	0.012	0.028	0.036	0.027	0.012
Cr	0.003	0.003	0.000	0.000	0.010	0.015	0.001	0.001	0.000	0.000	0.001	0.000	0.001	0.000	0.000
Ti	0.089	0.034	0.041	0.051	0.027	0.029	0.068	0.074	0.074	0.051	0.051	0.034	0.036	0.035	0.008
Fe ⁺³	0.072	0.045	0.055	0.056	0.050	0.060	0.098	0.091	0.094	0.100	0.106	0.059	0.038	0.053	0.062
Mg	0.662	0.809	0.750	0.739	0.821	0.817	0.939	0.939	0.657	0.754	0.748	0.698	0.722	0.720	0.414
Fe ⁺²	0.267	0.276	0.226	0.220	0.185	0.166	0.234	0.197	0.094	0.160	0.165	0.277	0.270	0.256	0.527
Mn ⁺	0.005	0.008	0.006	0.006	0.005	0.005	0.007	0.006	0.006	0.005	0.006	0.010	0.009	0.009	0.028
Ca	0.841	0.793	0.862	0.861	0.847	0.847	0.825	0.818	0.814	0.883	0.875	0.853	0.851	0.860	0.902
Na	0.037	0.024	0.033	0.036	0.024	0.028	0.059	0.055	0.061	0.035	0.037	0.040	0.038	0.039	0.047
K	0.000	0.000	0.000	0.000	0.000	0.000	0.001	0.000	0.000	0.001	0.001	0.001	0.000	0.000	0.000
Z	2.000	2.000	2.000	2.000	2.000	2.000	2.000	2.000	2.000	2.000	2.000	2.000	2.000	2.000	2.000
XY	2.000	2.000	2.000	2.000	2.000	2.000	2.000	2.000	2.000	2.000	2.000	2.000	2.000	2.000	2.000
Jd ⁺	0	0	0	0	0	0	0	0	0	0	0	0	0	0	0
Ac	4	2	3	4	2	1	7	6	5	3	4	3	4	3	5
Ti-Cats	9	3	4	5	3	3	6	7	7	5	5	3	4	3	1
Ti(Si) ₂ O ₆	0	0	0	0	0	0	0	0	0	0	0	0	0	0	0
Fe-Cats	3	3	2	2	3	5	3	3	4	7	7	3	0	2	1
Cats	3	1	3	3	3	3	8	9	10	1	1	3	0	2	1
Wo	34	36	39	38	38	38	32	31	30	39	38	39	38	39	44
En	33	41	37	37	41	42	32	34	33	39	38	35	36	36	20
Fs	13	13	11	10	8	6	9	9	10	6	6	13	14	13	26
Bu	1	1	1	1	1	1	1	1	1	0	1	1	1	1	2
%age calc.	(98)	(98)	(98)	(99)	(98)*	(97)*	(98)	(98)	(98)	(95)	(95)	(98)	(99)	(99)	(98)
"Wo"	47.5	42.2	46.9	47.3	45.7	46.3	48.6	48.3	48.9	49.1	49.0	46.7	46.2	46.8	49.0
"En"	37.4	43.1	40.8	40.6	44.3	44.6	37.6	40.0	39.4	42.0	41.8	38.2	39.2	39.2	22.4
"Fs"	15.1	14.7	12.3	12.1	10.0	9.1	13.8	11.7	11.7	8.9	9.2	15.1	14.6	14.0	28.6

* Calculated ferrous and ferric oxides based on XY + Z cations = 4. Total iron expressed as ferrous oxide is given in parentheses.
 † Normalized end member compositions in per cent. The percentage of the composition calculated into end members is placed in parentheses.
 ‡ NaCrSi₂O₆ = 1%
 § Molecular percentages of "En" = Mg/R x 100, "Fs" = Fe⁺²/R x 100, and "Wo" = Ca/R x 100 where R = Mg + Fe⁺² + Ca
 PH = phenocryst, GM = groundmass, C = core, R = rim

CLINOPYROXENES

Sample: SE75-4-1 SE79-1-4 SE79-1-5 SE79-2-2 SE79-2-2 SE79A-1-1
 Formation: Edziza Nodule Nodule Nodule Nodule Edziza Nodule Edziza Nodule

Type:	SE75-4-1 Edziza	SE79-1-4 Nodule	SE79-1-5 Nodule	SE79-2-2 Nodule	SE79-2-2 Edziza	SE79-2-2 Nodule	SE79A-1-1 Edziza	SE79A-1-1 Nodule
SiO ₂	50.21	50.51	50.01	50.85	50.91	50.71	50.71	50.71
Al ₂ O ₃	1.23	4.42	4.65	4.00	4.29	4.18	4.18	4.18
Cr ₂ O ₃	0.01	0.35	0.40	0.35	0.38	0.38	0.38	0.38
TiO ₂	0.23	1.29	1.02	0.85	0.97	1.03	1.03	1.03
(Fe _{Tot} as FeO)	(18.99)	(7.44)	(7.22)	(6.78)	(7.06)	(7.06)	(7.06)	(7.06)
Fe ₂ O ₃	2.41	2.21	1.62	0.70	0.00	2.31	2.31	2.31
FeO	16.82	7.25	5.76	6.15	7.06	4.98	4.98	4.98
MnO	0.84	0.15	0.12	0.13	0.12	0.13	0.13	0.13
MgO	6.22	14.42	14.36	14.75	14.40	14.79	14.79	14.79
CaO	21.68	20.87	21.41	21.22	21.21	21.53	21.53	21.53
Na ₂ O	0.80	0.40	0.39	0.39	0.38	0.52	0.52	0.52
K ₂ O	0.00	0.01	0.00	0.00	0.02	0.03	0.03	0.03
Total	100.45	99.78	99.74	99.44	99.60	100.59	100.59	100.59

Formula based on 6 oxygens

Si	1.960	1.874	1.855	1.887	1.889	1.863	1.863	1.863
Al	0.040	0.126	0.145	0.113	0.111	0.137	0.137	0.137
Fe ⁺ 3	0.000	0.000	0.000	0.000	0.000	0.000	0.000	0.000
Al	0.016	0.067	0.059	0.062	0.076	0.044	0.044	0.044
Cr	0.000	0.010	0.012	0.012	0.010	0.011	0.011	0.011
Ti	0.007	0.036	0.028	0.024	0.027	0.028	0.028	0.028
Fe ⁺ 3	0.071	0.006	0.045	0.020	0.000	0.064	0.064	0.064
Mg	0.362	0.792	0.794	0.816	0.796	0.810	0.810	0.810
Fe ⁺ 2	0.549	0.225	0.179	0.191	0.219	0.153	0.153	0.153
Mn	0.028	0.005	0.004	0.004	0.004	0.004	0.004	0.004
Ca	0.907	0.830	0.851	0.844	0.839	0.847	0.847	0.847
Na	0.060	0.029	0.028	0.028	0.027	0.037	0.037	0.037
K	0.000	0.001	0.000	0.000	0.001	0.001	0.001	0.001
Z	2.000	2.000	2.000	2.000	2.000	2.000	2.000	2.000
XY	2.000	2.000	2.000	2.000	2.000	2.000	2.000	2.000
Jd ¹	0	1	0	0	2	0	0	0
Ac	7	1	3	1	0	2	2	2
Tr-Cats	1	4	3	2	3	3	3	3
TiSi ₂ O ₆	0	0	0	0	0	0	0	0
Fe-Cats	0	0	2	1	0	4	4	4
Cats	2	5	6	6	5	4	4	4
Wo	44	37	37	38	38	38	38	38
En	18	41	40	42	41	41	41	41
Fs	27	10	8	9	10	7	7	7
Bu	1	0	0	0	0	0	0	0
%age calc.	(99)	(98) ^a	(98) ^b	(98) ^b	(99) ^b	(97) ^b	(97) ^b	(97) ^b
"Wo"	49.9	44.9	46.7	45.6	45.2	46.8	46.8	46.8
"En"	19.9	42.9	43.5	44.1	43.0	44.8	44.8	44.8
"Fs"	30.2	12.2	9.8	10.3	11.8	8.4	8.4	8.4

* Calculated ferrous and ferric oxides based on XY + Z cations = 4. Total iron expressed as ferrous oxide is given in parentheses.
 1 Normalized end member compositions in per cent. The percentage of the composition calculated into end members is placed in parentheses.
 " NaCrSi₂O₆ = 1%
 " Molecular percentages of "En" = Mg/R x 100, "Fs" = Fe⁺2/R x 100, and "Wo" = Ca/R x 100 where R = Mg + Fe⁺2 + Ca
 PH = phenocryst, GM = groundmass, C = core, R = rim

AMPHIBOLES

Sample Formation:	SE14-1-4 Armadillo	SE14-2-1 Armadillo	SE14-2-2 Armadillo	SE19-1-4 Armadillo	SE19-3-2 Armadillo	SE19-3-3 Armadillo	SE20-2-2 Armadillo	SE20-4-2 Armadillo	SE20-5-1 Armadillo	SE92-1-1 Spectrum	SE100-1-1 Spectrum	SE100-1-1 Spectrum	SE100-2-1 Spectrum	SE100-2-4 Spectrum	SE100-3-3 Spectrum
Type	PH	PH	PH	GM	GM	GM	GM	GM	GM	GM	GM	GM	GM	GM	GM
SiO ₂	50.38	50.98	50.70	50.81	50.72	49.94	50.39	50.47	50.71	50.49	48.85	49.35	49.08	49.28	49.25
Al ₂ O ₃	0.09	0.11	0.12	0.18	0.06	0.71	0.08	0.12	0.10	0.36	0.10	0.07	0.06	0.11	0.17
Cr ₂ O ₃	0.00	0.00	0.00	0.00	0.01	0.02	0.00	0.00	0.00	0.00	0.00	0.00	0.02	0.00	0.00
TiO ₂	0.11	0.14	0.10	1.24	0.12	0.15	0.14	0.33	0.15	0.00	0.19	0.23	0.13	0.17	0.23
(Fe ²⁺ as FeO)	(34.55)	(34.08)	(35.30)	(33.02)	(32.91)	(32.63)	(34.13)	(34.13)	(34.23)	(36.55)	(34.72)	(34.58)	(35.06)	(34.18)	(34.35)
FeO _{4*}	2.23	1.34	3.53	0.00	0.00	0.00	2.10	1.73	1.26	11.24	2.20	2.43	2.30	1.07	0.00
FeO ₃	32.54	32.87	32.12	33.02	32.91	32.63	32.54	32.57	33.10	26.44	32.56	32.53	32.99	33.22	34.35
MnO	0.85	0.81	0.79	0.80	0.79	0.73	0.85	0.85	0.80	0.90	1.17	1.20	1.15	1.16	1.20
MgO	0.00	0.02	0.01	0.02	0.01	0.01	0.04	0.14	0.03	0.01	0.00	0.00	0.00	0.01	0.02
CaO	0.35	0.36	0.59	1.28	0.90	0.84	0.84	1.08	0.81	2.46	2.79	2.39	2.91	2.47	3.19
Na ₂ O	9.38	9.16	9.12	8.85	8.42	8.91	8.87	8.57	8.86	5.67	7.25	7.64	7.38	7.65	7.54
K ₂ O	1.34	1.49	1.18	1.53	1.82	1.67	1.29	1.39	1.49	0.34	1.36	1.30	1.32	1.45	1.32
Total	97.27	97.28	98.26	97.35	96.14	95.74	97.13	97.25	97.31	97.91	96.48	97.14	97.34	96.59	97.27
Formula based on 23 oxygens															
Si	8.168	8.240	8.125	8.193	8.295	8.202	8.173	8.168	8.211	7.979	8.039	8.054	8.020	8.097	8.063
Al	0.000	0.000	0.000	0.000	0.000	0.000	0.000	0.000	0.000	0.021	0.000	0.000	0.000	0.000	0.000
Fe ²⁺	0.000	0.000	0.000	0.000	0.000	0.000	0.000	0.000	0.000	0.000	0.000	0.000	0.000	0.000	0.000
Al	0.017	0.021	0.023	0.034	0.012	0.137	0.015	0.023	0.019	0.046	0.019	0.014	0.012	0.021	0.033
Cr	0.000	0.000	0.000	0.000	0.001	0.003	0.001	0.000	0.000	0.000	0.001	0.000	0.003	0.000	0.000
Ti	0.013	0.017	0.012	0.150	0.015	0.018	0.017	0.040	0.018	0.000	0.024	0.028	0.016	0.021	0.028
Fe ³⁺	0.272	0.164	0.426	0.000	0.000	0.000	0.256	0.211	0.153	1.336	0.299	0.299	0.283	0.132	0.000
Mg	0.000	0.005	0.002	0.005	0.002	0.002	0.010	0.034	0.007	0.002	0.000	0.000	0.000	0.002	0.005
Fe ²⁺	4.412	4.443	4.305	4.452	4.501	4.482	4.427	4.408	4.482	3.484	4.481	4.440	4.508	4.565	4.703
Mn	0.117	0.111	0.107	0.109	0.109	0.106	0.100	0.116	0.110	0.120	0.163	0.166	0.159	0.161	0.166
Ca	0.061	0.062	0.101	0.155	0.224	0.165	0.146	0.187	0.140	0.416	0.492	0.418	0.510	0.435	0.560
Na	2.949	2.870	2.834	2.767	2.670	2.837	2.789	2.689	2.781	1.737	2.313	2.417	2.338	2.437	2.393
K	0.277	0.307	0.241	0.315	0.380	0.350	0.267	0.287	0.308	0.068	0.286	0.271	0.275	0.304	0.276
Z	8.168	8.240	8.125	8.193	8.295	8.202	8.173	8.168	8.211	8.000	8.039	8.054	8.020	8.097	8.063
Y	4.831	4.761	4.875	4.750	4.640	4.748	4.826	4.832	4.789	4.998	4.960	4.947	4.981	4.902	4.935
X	3.287	3.239	3.176	3.237	3.274	3.352	3.202	3.163	3.229	2.221	3.091	3.106	3.123	3.176	3.229
Na + K [†]	19.8	19.6	19.0	19.1	18.8	19.6	18.9	18.4	19.0	13.8	16.1	16.6	16.2	16.9	16.4
Si ^{IV} + Ca	50.2	50.7	50.2	50.6	51.2	50.3	50.4	50.5	50.6	51.3	50.0	49.8	49.7	50.1	49.7
(Al ^{IV} + Fe ²⁺ + Ti ⁴⁺)	30.0	29.7	30.8	30.3	30.0	30.1*	30.7	31.1	30.4	34.9	33.9	33.6	34.1	33.0	33.9
Mn + Mg + Ca [†]															
Al ^{IV} + Ca	0.061	0.062	0.101	0.155	0.224	0.165	0.146	0.187	0.140	0.437	0.492	0.418	0.510	0.435	0.560
Si ^{IV} + Na + K	11.364	11.417	11.200	11.275	11.345	11.389	11.229	11.144	11.300	9.784	10.638	10.742	10.633	10.838	10.732

* Calculated ferrous and ferric oxides based on Z + Y cations = 13. Total iron expressed as ferrous oxide is given in parentheses.

† Normalized cation totals in per cent based on 23 O

PH = phenocryst, GM = groundmass, C = core, R = rim

AMPHIBOLES

Sample: Formation:	SE100-4-2 Spectrum	SE100-4-3 Spectrum	SE100-5-1 Spectrum	SE100-6-1 Spectrum	SE63-6-3 Edziza	SE72-1-1 Edziza
Type:	GM	GM	GM	GM	PH	GM
SiO ₂	49.23	49.85	49.22	49.35	49.50	49.71
Al ₂ O ₃	0.19	0.06	0.10	0.15	0.10	0.18
Cr ₂ O ₃	0.00	0.02	0.00	0.00	0.01	0.00
TiO ₂	0.19	0.22	0.12	0.12	0.30	0.04
(Fe ₂ as FeO)	(34.67)	(34.90)	(34.61)	(34.18)	(34.94)	(35.05)
Fe ₂ O ₃ *	2.08	2.08	1.72	0.47	2.08	4.63
FeO	32.80	33.03	33.06	33.76	33.07	30.88
MnO	1.18	1.20	1.21	1.16	1.01	1.06
MgO	0.02	0.00	0.01	0.00	0.06	0.01
CaO	3.24	2.85	3.11	3.22	2.71	1.86
Ni ₂ O	6.87	7.26	7.07	7.18	7.27	7.54
K ₂ O	1.33	1.32	1.39	1.25	1.62	1.23
Total	97.13	97.89	97.01	96.66	97.73	97.14

Formula based on 23 oxygens

Si	8.038	8.070	8.057	8.102	8.042	8.060
Al	0.000	0.000	0.000	0.000	0.000	0.000
Fe ⁺³	0.000	0.000	0.000	0.000	0.000	0.000
Al	0.037	0.011	0.019	0.029	0.019	0.034
Cr	0.000	0.003	0.000	0.000	0.001	0.000
Ti	0.023	0.027	0.015	0.015	0.037	0.005
Fe ⁺²	0.255	0.253	0.212	0.058	0.254	0.565
Mn ₂	0.005	0.000	0.002	0.000	0.014	0.002
Fe ⁺²	4.479	4.472	4.526	4.635	4.493	4.187
Mn	0.163	0.164	0.168	0.161	0.139	0.146
Ca ^a	0.567	0.494	0.546	0.566	0.472	0.323
Na	2.175	2.279	2.244	2.286	2.290	2.370
K	0.277	0.273	0.290	0.262	0.336	0.254
Z	8.038	8.070	8.057	8.102	8.042	8.060
Y	4.962	4.930	4.942	4.898	4.954	4.939
X	3.019	3.046	3.080	3.114	3.098	2.947
Na ⁺ K ⁺	15.3	15.9	15.8	15.8	17.0	16.5
Si ^{IV} + Ca	50.2	50.3	50.1	50.3	49.6	50.5
(Al ^{IV} + Fe ⁺ Ti ⁺ + Mn ⁺ Mg ⁺ Ca)	34.5	33.8	34.1	33.9	33.4	33.0
Al ^{IV} + Ca	0.567	0.494	0.546	0.566	0.472	0.323
Si ⁺ Na ⁺ K	10.490	10.622	10.591	10.650	10.804	10.684

* Calculated ferrous and ferric oxides based on Z + Y cations = 13. Total iron expressed as ferrous oxide is given in parentheses
 † Normalized cation totals in per cent based on 23 O
 PH = phenocryst, GM = groundmass, C = core, R = rim

AENIGMATITE											
Sample:	SE14-5.2	SE19-1.5	SE27-2.1	SE27-4.2	SE27-4.3	SE100-3.2	SE100-6.3	SE100-7.2	SE72-1.4		
Formation:	Armadiillo	Armadiillo	Armadiillo	Armadiillo	Armadiillo	Spectrum	Spectrum	Spectrum	Edziza		
Type:	PH	PHC	PHC	PHR	PHC	GM	PH	PH	GM		
SiO ₂	41.68	41.41	40.88	39.97	40.62	40.58	40.99	39.91	41.09		
Al ₂ O ₃	0.13	0.68	0.47	0.78	0.40	0.39	0.20	0.49	0.33		
Cr ₂ O ₃	0.00	0.01	0.00	0.00	0.01	0.00	0.00	0.00	0.00		
TiO ₂	8.27	9.29	9.10	9.22	8.94	7.66	7.34	8.19	7.58		
(Fe _{tot} as FeO)	(42.32)	(41.86)	(41.40)	(40.65)	(40.71)	(42.02)	(41.01)	(40.99)	(42.13)		
Fe ₂ O ₃ *	1.72	0.20	0.61	0.00	0.11	1.74	0.44	0.69	2.78		
FeO	40.77	41.68	40.85	40.65	40.61	40.45	40.61	40.37	39.63		
MnO	0.81	0.75	0.74	0.72	0.71	0.74	0.87	0.80	0.86		
MgO	0.00	0.03	0.05	0.03	0.05	0.01	0.00	0.01	0.03		
CaO	0.21	0.65	0.42	0.70	0.35	0.43	0.23	0.40	0.40		
Na ₂ O	7.45	7.24	7.28	7.14	7.24	7.60	7.71	7.56	7.19		
K ₂ O	0.03	0.01	0.00	0.00	0.02	0.00	0.01	0.06	0.05		
Total	101.07	101.95	100.41	99.21	99.06	99.60	98.40	98.48	99.94		
Formula based on 40 oxygens											
Si	11.890	11.707	11.734	11.627	11.810	11.793	12.029	11.736	11.855		
Al	0.044	0.227	0.159	0.267	0.137	0.134	0.000	0.170	0.112		
Cr ⁺³	0.000	0.002	0.002	0.000	0.002	0.000	0.000	0.000	0.000		
Fe ⁺³	0.066	0.043	0.104	0.000	0.024	0.073	0.000	0.095	0.033		
Al	0.000	0.000	0.000	0.000	0.000	0.000	0.069	0.000	0.000		
Ti	1.774	1.975	1.964	2.017	1.955	1.674	1.620	1.811	1.644		
Fe ⁺³	0.303	0.000	0.028	0.000	0.000	0.308	0.098	0.058	0.570		
Mg ⁺²	0.000	0.013	0.021	0.013	0.022	0.004	0.000	0.004	0.013		
Fe ⁺²	9.726	9.854	9.806	9.889	9.874	9.831	9.967	9.927	9.562		
Mn	0.196	0.180	0.180	0.177	0.175	0.182	0.216	0.199	0.210		
Ca	0.064	0.197	0.129	0.218	0.109	0.134	0.072	0.126	0.124		
Na	4.120	3.968	4.052	4.027	4.081	4.282	4.387	4.310	4.022		
K	0.011	0.004	0.000	0.000	0.007	0.000	0.004	0.022	0.018		
Z	12.000	11.979	11.999	11.894	11.973	12.000	12.029	12.001	12.000		
Y	11.999	12.022	11.999	12.096	12.026	11.999	11.970	11.999	11.999		
X	4.195	4.169	4.181	4.235	4.197	4.416	4.463	4.458	4.164		

* Calculated ferrous and ferric oxides based on Z + Y cations = 24. Total iron expressed as ferrous oxide is given in parentheses.

PH = phenocryst, GM = groundmass, C = core, R = rim

OLIVINES

Sample Formation:	SE31-2-1 Raspberry	SE36-1-1 Raspberry	SE36-1-2 Raspberry	SE36-1-3 Raspberry	SE131-4-2 Little Iskut	SE107-4-2 PHR	SE107-4-3 PHC	SE115-1-3 GM	SE115-1-4 GM	SE115-2-1 PHR	SE115-2-2 PHC	SE120-1-1 PHC	SE123-2-1 PHR	SE123-2-2 PHC	SE125-1-1 PHR
Type:	PH	PH	PH	PH	PH	PHR	PHC	GM	GM	PHR	PHC	PHC	PHR	PHC	PHR
SiO ₂	38.46	38.87	38.95	38.19	30.04	38.29	38.08	35.40	35.32	35.91	37.23	38.59	37.88	38.07	37.15
Al ₂ O ₃	0.00	0.10	0.05	0.00	0.00	0.06	0.04	0.03	0.00	0.00	0.16	0.05	0.07	0.05	0.02
Cr ₂ O ₃	0.00	0.00	0.00	0.00	0.00	0.00	0.00	0.00	0.00	0.00	0.00	0.00	0.00	0.00	0.00
TiO ₂	0.01	0.04	0.05	0.03	0.08	0.02	0.02	0.05	0.09	0.05	0.00	0.04	0.03	0.01	0.04
Fe ₂ * Fe ₃ *	0.00	0.00	0.00	0.00	0.00	0.00	0.00	0.00	0.00	0.00	0.00	0.00	0.00	0.00	0.00
FeO**	22.20	20.51	20.79	20.66	65.25	23.27	23.83	39.42	41.24	36.83	29.30	20.09	23.89	24.23	29.76
MnO	0.25	0.26	0.26	0.25	3.03	0.27	0.28	0.79	0.87	0.70	0.37	0.25	0.25	0.29	0.46
MgO	35.44	40.64	40.67	40.37	1.03	37.95	37.46	24.59	23.42	26.81	33.29	40.59	37.06	37.42	32.88
CaO	0.29	0.30	0.28	0.31	0.54	0.22	0.21	0.42	0.44	0.33	0.19	0.24	0.21	0.23	0.34
NiO	0.13	0.09	0.10	0.13	0.00	0.10	0.13	0.00	0.03	0.00	0.03	0.14	0.10	0.10	0.07
Total	100.78	100.81	101.15	100.25	99.97	100.18	100.05	100.70	101.41	100.63	100.57	99.99	99.49	100.40	100.72
Formula based on 4 oxygens															
Si	0.993	0.995	0.994	0.985	1.006	0.999	0.998	1.000	0.999	1.000	0.997	0.994	0.999	0.996	0.997
Al	0.000	0.003	0.002	0.009	0.000	0.002	0.001	0.001	0.000	0.000	0.005	0.002	0.002	0.002	0.001
Ti	0.000	0.001	0.001	0.001	0.002	0.000	0.000	0.001	0.002	0.001	0.000	0.001	0.001	0.000	0.001
Fe ²⁺	0.000	0.000	0.000	0.000	0.000	0.000	0.000	0.000	0.000	0.000	0.000	0.000	0.000	0.000	0.000
Mg	1.518	1.550	1.548	1.552	0.051	1.476	1.464	1.035	0.988	1.113	1.328	1.559	1.457	1.460	1.315
Fe ³⁺	0.479	0.439	0.444	0.446	1.827	0.508	0.522	0.931	0.976	0.858	0.656	0.433	0.527	0.530	0.668
Mn	0.006	0.006	0.006	0.006	0.086	0.006	0.006	0.019	0.021	0.016	0.008	0.006	0.006	0.006	0.010
Ca	0.008	0.008	0.008	0.009	0.019	0.006	0.006	0.013	0.013	0.010	0.006	0.007	0.006	0.006	0.010
Ni	0.003	0.002	0.002	0.003	0.000	0.002	0.003	0.000	0.001	0.000	0.006	0.003	0.002	0.002	0.002
Cr	0.000	0.000	0.000	0.000	0.000	0.000	0.000	0.000	0.001	0.000	0.001	0.003	0.002	0.002	0.002
Z	0.993	0.995	0.994	0.985	1.006	0.999	0.998	1.000	0.999	1.000	0.997	0.994	0.999	0.996	0.997
X	2.014	2.005	2.011	2.026	1.983	2.000	2.002	2.000	2.001	1.998	2.004	2.011	2.001	2.006	2.007
Fe	76.0	77.9	77.7	77.7	2.7	74.4	73.7	52.6	50.3	56.5	66.9	78.3	73.4	73.4	66.3
Fa	24.0	22.1	22.3	22.3	97.3	25.6	26.3	47.4	49.7	43.5	33.1	21.7	26.6	26.6	33.7

* Total iron given as FeO
 PH = phenocryst, GM = groundmass, C = core, R = rim

OLIVINES

Sample: Formation:	SE125-1-2 Nido	SE125-2-2 Nido	SE125-2-3 Nido	SE125-6-1 Nido	SE125-6-2 Nido	SE84-2-2 Pyramid	SE51-1-1 Ice Peak	SE51-1-2 Ice Peak	SE51-1-3 Ice Peak	SE136-3-1 Pillow Ridge	SE136-3-2 Pillow Ridge	SE137-1-1 Pillow Ridge	SE137-1-2 Pillow Ridge	SE137-2-1 Pillow Ridge	SE137-2-2 Pillow Ridge
Type:	PHC	GM	GM	PH	PH	PHC	PHR	PHC	PHC	PHR	PHC	PHC	PHC	PHR	PHC
SiO ₂	38.64	36.59	36.51	36.39	36.07	31.53	37.92	38.18	37.78	38.85	38.75	39.20	39.80	39.33	39.51
Al ₂ O ₃	0.02	0.07	0.00	0.00	0.00	0.00	0.00	0.01	0.02	0.05	0.03	0.06	0.05	0.24	0.10
Cr ₂ O ₃	0.03	0.07	0.06	0.05	0.04	0.01	0.02	0.03	0.04	0.03	0.02	0.00	0.00	0.00	0.00
TiO ₂	0.00	0.00	0.00	0.00	0.00	0.00	0.00	0.00	0.00	0.02	0.03	0.02	0.02	0.03	0.01
Fe ₂ O ₃ *	22.67	31.80	33.48	35.34	35.97	59.85	23.73	24.63	24.79	20.18	20.29	17.01	16.96	17.78	16.75
MnO	0.26	0.53	0.59	0.49	0.53	2.32	0.30	0.32	0.31	0.26	0.26	0.22	0.22	0.22	0.22
MgO	38.77	30.38	29.60	28.72	28.02	6.44	38.56	37.71	37.94	39.95	40.32	42.56	42.35	41.99	42.70
CaO	0.21	0.44	0.44	0.27	0.27	0.21	0.30	0.28	0.29	0.29	0.24	0.22	0.27	0.27	0.24
NiO	0.15	0.08	0.00	0.01	0.02	0.00	0.11	0.12	0.08	0.00	0.00	0.20	0.22	0.25	0.25
Total	100.75	99.96	100.68	101.27	100.92	100.36	100.94	101.28	101.25	99.65	99.94	99.59	99.89	100.11	99.78
Formula based on 4 oxygens															
Si	0.999	1.001	0.999	0.998	0.996	1.010	0.986	0.992	0.984	1.004	0.999	0.999	1.010	1.000	1.003
Al	0.001	0.002	0.000	0.000	0.000	0.000	0.000	0.000	0.001	0.002	0.001	0.002	0.002	0.007	0.003
Ti	0.001	0.001	0.001	0.001	0.001	0.000	0.000	0.001	0.001	0.000	0.001	0.000	0.000	0.001	0.000
Fe ⁺³	0.000	0.000	0.000	0.000	0.000	0.000	0.000	0.000	0.000	0.000	0.000	0.000	0.000	0.000	0.000
Mg	1.494	1.238	1.207	1.173	1.154	0.307	1.494	1.461	1.473	1.538	1.549	1.621	1.601	1.592	1.616
Fe ⁺²	0.490	0.727	0.766	0.810	0.831	1.603	0.516	0.535	0.540	0.436	0.437	0.363	0.360	0.378	0.356
Mn	0.006	0.012	0.014	0.011	0.012	0.063	0.007	0.007	0.007	0.006	0.006	0.005	0.005	0.005	0.005
Ca	0.006	0.013	0.013	0.008	0.008	0.007	0.008	0.008	0.008	0.008	0.007	0.006	0.007	0.007	0.007
Ni	0.003	0.002	0.000	0.000	0.000	0.000	0.002	0.002	0.002	0.000	0.000	0.004	0.004	0.005	0.005
Cr															
Z	0.999	1.001	0.999	0.998	0.996	1.010	0.986	0.992	0.984	1.004	0.999	0.999	1.010	1.000	1.003
X	2.001	1.995	2.001	2.003	2.006	1.980	2.027	2.014	2.032	1.991	2.001	2.001	3.980	1.995	1.992
Fo	75.3	63.0	61.2	59.2	58.1	16.1	74.3	73.2	73.2	77.9	78.0	81.7	81.6	80.8	82.0
Fa	24.7	37.0	38.8	40.8	41.9	83.9	25.7	26.8	26.8	22.1	22.0	18.3	18.4	19.2	18.0

* Total iron given as FeO

PH = phenocryst, GM = groundmass, C = core, R = rim

OLIVINES

Sample:	SE66-4-1	SE139-1-1	SE139-1-2	SE141-A-1	SE141-B-5	SE141-C-9	SE132-4-1	SE132-4-2	SE132-4-5	SE132-5-1	SE2-1-1	SE2-1-2	SE2-5-1	SE2-5-2	SE3-5-1
Formation:	Edziza	Arctic Lake	Arctic Lake	Arctic Lake	Arctic Lake	Arctic Lake	Klastline	Klastline	Klastline	Klastline	Big Raven	Big Raven	Big Raven	Big Raven	Big Raven
Type:	PHC	PHC	GM	PHC	PHC	PHC	PHR	PHC	GM	PHC	PHR	PHC	PHR	PHC	PHC
SiO ₂	31.55	40.17	37.77	36.18	37.62	34.49	37.89	39.16	36.93	39.56	37.53	37.92	38.35	38.05	37.25
Al ₂ O ₃	0.00	0.02	0.47	0.01	0.08	0.01	0.06	0.04	0.04	0.06	0.03	0.04	0.00	0.04	0.01
Cr ₂ O ₃	0.00	0.03	0.02	0.00	0.00	0.00	0.01	0.01	0.05	0.02	0.05	0.03	0.03	0.01	0.02
TiO ₂	0.04	0.01	0.02	0.00	0.00	0.07	0.00	0.00	0.00	0.00	0.00	0.00	0.00	0.00	0.00
Fe ₂ O ₃ *	0.00	0.00	0.00	0.00	0.00	0.00	0.00	0.00	0.00	0.00	0.00	0.00	0.00	0.00	0.00
FeO**	55.51	14.89	23.35	32.30	23.63	38.80	28.20	20.87	31.32	20.56	23.07	21.13	23.25	22.06	29.16
MnO	2.23	0.18	0.30	0.51	0.30	0.73	0.47	0.27	0.51	0.25	0.35	0.26	0.31	0.30	0.46
MgO	9.49	44.60	38.30	30.62	37.78	25.01	33.54	38.38	30.43	39.83	39.34	40.88	38.95	39.46	33.82
CaO	0.56	0.23	0.28	0.29	0.26	0.35	0.34	0.33	0.35	0.30	0.31	0.30	0.34	0.33	0.28
NiO	0.00	0.00	0.00	0.05	0.09	0.00	0.09	0.04	0.04	0.13	0.12	0.13	0.07	0.11	0.07
Total	99.38	100.13	100.51	99.96	99.76	99.46	100.60	99.15	99.67	100.71	100.80	100.69	101.30	100.36	101.07
Si	1.000	1.006	0.984	0.992	0.990	0.987	1.008	1.019	1.009	1.011	0.976	0.977	0.990	0.987	0.993
Al	0.000	0.001	0.014	0.000	0.002	0.000	0.002	0.001	0.001	0.002	0.001	0.001	0.000	0.001	0.000
Th + 3	0.000	0.000	0.000	0.000	0.000	0.002	0.000	0.000	0.000	0.000	0.000	0.000	0.000	0.000	0.000
Fe + 3	0.448	1.664	1.487	1.252	1.481	1.066	1.330	1.489	1.239	1.518	1.525	1.570	1.499	1.526	1.343
Fe + 2	1.471	0.312	0.508	0.741	0.520	0.928	0.628	0.454	0.716	0.440	0.502	0.455	0.502	0.479	0.650
Mn	0.060	0.004	0.007	0.012	0.007	0.018	0.011	0.006	0.012	0.005	0.008	0.006	0.007	0.007	0.010
Ca	0.019	0.006	0.008	0.008	0.007	0.011	0.010	0.009	0.010	0.008	0.009	0.008	0.009	0.009	0.008
Ni	0.000	0.000	0.000	0.001	0.002	0.000	0.002	0.002	0.001	0.003	0.002	0.003	0.002	0.002	0.002
Cr	0.000	0.000	0.000	0.000	0.000	0.000	0.000	0.000	0.000	0.000	0.000	0.000	0.000	0.000	0.000
Z	1.000	1.006	0.984	0.992	0.990	0.987	1.008	1.019	1.009	1.011	0.976	0.977	0.990	0.987	0.993
X	1.999	1.987	2.024	2.014	2.019	2.025	1.983	1.961	1.980	1.976	2.048	2.044	2.020	2.024	2.013
Fe	23.4	84.2	74.5	62.8	74.0	53.5	68.0	76.6	63.4	77.5	75.2	77.5	74.9	76.1	67.4
Fa	76.6	15.8	25.5	37.2	26.0	46.5	32.0	23.4	36.6	22.5	24.8	22.5	25.1	23.9	32.6

Formula based on 4 oxygens

* Total iron given as FeO
PH = phenocryst, GM = groundmass, C = core, R = rim

OLIVINES

Sample Formation:	SE3-5-2		SE3-5-3		SE4-3-1		SE4-3-2		SE7-4-1		SE7-4-2		SE7-5-1		SE7-5-2		SE10-1-3		SE10-2-1		SE10-2-2		SE10-2-3		SE10-2-3		SE11-2-1		SE76-1-2			
	Big Raven	PHR	Big Raven	PHR	Big Raven	PHR	Big Raven	PHR	Big Raven	PHR	Big Raven	PHC	Big Raven	PHR	Big Raven	PHC	Big Raven	PH	Big Raven	PHR	Big Raven	PHC	Big Raven	PHC	Big Raven	PHC	Big Raven	PH	Big Raven	Edziza	Nodule	
SiO ₂	36.24	0.00	36.02	0.00	38.54	0.02	38.64	0.04	39.81	0.03	40.11	0.04	39.57	0.04	39.37	0.03	37.12	0.03	37.49	0.01	39.51	0.02	39.67	0.03	39.46	0.04	38.87	0.01	38.93	0.03		
Al ₂ O ₃	0.00																															
Cr ₂ O ₃	0.04	0.04	0.04	0.04	0.00	0.00	0.00	0.00	0.00	0.00	0.00	0.00	0.00	0.00	0.00	0.00	0.03	0.03	0.06	0.06	0.04	0.04	0.02	0.02	0.01	0.01	0.01	0.01	0.02	0.02		
TiO ₂	0.00		0.00		0.00		0.03		0.02		0.00		0.02		0.04		0.02		0.00		0.00		0.00		0.00		0.00		0.00			
Fe ₂ O ₃ *	30.15	0.00	32.60	0.00	19.25	0.00	18.68	0.00	17.85	0.00	14.56	0.00	17.63	0.00	14.44	0.00	26.07	0.00	29.72	0.00	17.90	0.00	20.13	0.00	20.34	0.00	22.44	0.00	22.07	0.00		
FeO*	0.47	0.55	0.74	0.55	0.27	0.23	0.23	0.24	0.24	0.24	0.15	0.25	0.25	0.25	0.19	0.36	0.51	0.36	0.51	0.27	0.21	0.21	0.27	0.27	0.27	0.27	0.27	0.27	0.28	0.27		
MnO	32.68	30.76	30.76	30.76	42.22	42.27	42.27	42.27	42.11	42.11	45.15	41.31	41.31	41.31	44.54	37.27	32.40	37.27	32.40	42.71	42.71	42.71	40.97	41.06	41.06	39.13	39.13	39.53	39.53			
MgO	0.25	0.27	0.27	0.27	0.30	0.32	0.32	0.32	0.30	0.30	0.26	0.28	0.28	0.28	0.24	0.27	0.34	0.27	0.34	0.22	0.16	0.16	0.16	0.16	0.16	0.16	0.29	0.31	0.31	0.31		
CaO	0.04	0.05	0.05	0.05	0.13	0.16	0.16	0.16	0.22	0.22	0.30	0.27	0.27	0.27	0.25	0.12	0.12	0.12	0.12	0.25	0.25	0.25	0.25	0.21	0.21	0.21	0.10	0.09	0.09	0.09		
NiO	99.87	100.29	100.29	100.29	100.73	100.37	100.37	100.37	100.58	100.58	100.57	99.37	99.37	99.37	99.10	101.17	100.65	101.17	100.65	100.87	100.87	100.87	101.50	101.55	101.55	101.12	101.12	101.12	101.12	101.12		
Total																																

Formula based on 4 oxygens

Si	0.985	0.987	0.983	0.986	1.007	1.000	1.013	0.997	0.975	1.006	0.998	1.005	1.000	1.000	1.000	1.000	1.000	1.000	1.000	1.000	1.000	1.000	1.000	1.000	1.000	1.000	1.000	1.000	1.000	1.000	0.988	
Al	0.000	0.000	0.000	0.001	0.001	0.001	0.001	0.001	0.001	0.001	0.001	0.001	0.001	0.001	0.001	0.001	0.001	0.001	0.001	0.001	0.001	0.001	0.001	0.001	0.001	0.001	0.001	0.001	0.001	0.001	0.001	0.001
Ti	0.000	0.001	0.001	0.000	0.000	0.000	0.000	0.000	0.000	0.000	0.000	0.000	0.000	0.000	0.000	0.000	0.000	0.000	0.000	0.000	0.000	0.000	0.000	0.000	0.000	0.000	0.000	0.000	0.000	0.000	0.000	0.000
Fe ⁺³	0.000	0.000	0.000	0.000	0.000	0.000	0.000	0.000	0.000	0.000	0.000	0.000	0.000	0.000	0.000	0.000	0.000	0.000	0.000	0.000	0.000	0.000	0.000	0.000	0.000	0.000	0.000	0.000	0.000	0.000	0.000	0.000
Mg ⁺²	1.324	1.256	1.256	1.608	1.588	1.678	1.576	1.681	1.459	1.295	1.608	1.576	1.576	1.576	1.681	1.459	1.295	1.459	1.295	1.608	1.608	1.608	1.547	1.552	1.552	1.500	1.500	1.511	1.511	1.511	1.511	
Fe	0.685	0.747	0.411	0.399	0.378	0.304	0.377	0.306	0.572	0.667	0.304	0.377	0.377	0.377	0.306	0.572	0.667	0.572	0.667	0.378	0.378	0.378	0.426	0.431	0.431	0.483	0.483	0.473	0.473	0.473	0.473	
Mn	0.011	0.013	0.013	0.005	0.005	0.003	0.005	0.004	0.008	0.005	0.003	0.005	0.005	0.005	0.004	0.008	0.010	0.008	0.010	0.004	0.004	0.004	0.006	0.006	0.006	0.006	0.006	0.006	0.006	0.006	0.006	
Ca	0.007	0.008	0.008	0.009	0.008	0.007	0.008	0.007	0.008	0.008	0.007	0.008	0.008	0.008	0.007	0.008	0.010	0.008	0.010	0.006	0.006	0.006	0.004	0.004	0.004	0.004	0.004	0.004	0.004	0.004	0.004	
Ni	0.001	0.001	0.001	0.003	0.004	0.006	0.006	0.005	0.004	0.004	0.006	0.006	0.006	0.006	0.005	0.004	0.003	0.004	0.003	0.005	0.005	0.005	0.005	0.005	0.005	0.005	0.005	0.005	0.005	0.005	0.005	0.005
Cr	0.000	0.000	0.000	0.000	0.000	0.000	0.000	0.000	0.000	0.000	0.000	0.000	0.000	0.000	0.000	0.000	0.000	0.000	0.000	0.000	0.000	0.000	0.000	0.000	0.000	0.000	0.000	0.000	0.000	0.000	0.000	0.000
Z	0.985	0.987	0.983	0.986	1.007	1.000	1.013	0.997	0.975	1.006	0.998	1.005	1.000	1.000	1.000	1.000	1.000	1.000	1.000	1.000	1.000	1.000	1.000	1.000	1.000	1.000	1.000	1.000	1.000	1.000	1.000	0.988
X	2.029	2.026	2.026	2.026	1.984	1.999	1.973	2.004	2.049	1.988	1.999	1.973	1.973	1.973	2.004	2.049	1.988	2.049	1.988	2.003	2.003	2.003	1.989	1.998	1.998	1.999	1.999	1.999	1.999	1.999	1.999	2.001
Fe	65.9	62.7	62.7	80.1	80.8	84.7	80.7	84.6	71.8	66.0	81.0	81.0	81.0	81.0	84.6	71.8	66.0	81.0	81.0	81.0	81.0	81.0	78.4	78.2	78.2	75.7	75.7	76.2	76.2	76.2	76.2	
Fa	34.1	37.3	37.3	19.9	19.2	15.3	19.3	15.4	28.2	34.0	19.0	19.0	19.3	19.3	15.4	28.2	34.0	34.0	34.0	19.0	19.0	19.0	21.6	21.8	21.8	24.3	24.3	24.3	24.3	24.3	24.3	

* Total iron given as FeO

PH = phenocryst, GM = groundmass, C = core, R = rim

OLIVINES

Sample: Formation:	SE76-2-2		SE79-2-1		SE79-2-1		SE79-2-3		SE79A-5-1		SE79A-5-2	
	Edziza	Nodule	Edziza	Nodule	Edziza	Nodule	Edziza	Nodule	Edziza	Nodule	Edziza	Nodule
Type:												
SiO ₂	38.78	38.45	38.27	38.90	38.95	38.95	39.21	39.22	39.21	39.22	39.22	39.22
Al ₂ O ₃	0.03	0.02	0.02	0.02	0.02	0.02	0.02	0.02	0.02	0.02	0.02	0.00
Cr ₂ O ₃	0.00	0.01	0.01	0.00	0.00	0.00	0.00	0.00	0.00	0.00	0.00	0.00
TiO ₂	0.00	0.01	0.02	0.05	0.02	0.01	0.01	0.01	0.01	0.01	0.00	0.00
Fe ₂ O ₃ *	0.00	0.00	0.00	0.00	0.00	0.00	0.00	0.00	0.00	0.00	0.00	0.00
FeO*	22.27	21.97	20.59	21.04	20.90	20.90	20.70	21.09	20.70	21.09	21.09	21.09
MnO	0.28	0.25	0.28	0.27	0.26	0.27	0.27	0.27	0.27	0.27	0.27	0.27
MgO	39.37	39.01	39.39	39.68	39.71	39.71	40.15	40.11	40.15	40.11	40.11	40.11
CaO	0.28	0.29	0.30	0.26	0.30	0.30	0.32	0.33	0.32	0.33	0.33	0.33
NiO	0.06	0.00	0.00	0.10	0.07	0.07	0.10	0.08	0.10	0.08	0.08	0.08
Total	101.07	100.01	98.88	100.32	100.23	100.23	100.78	101.10	100.78	101.10	101.10	101.10

Formula based on 4 oxygens

	Si	Al	Ti	Fu ⁺ 3	Mn	Fe ⁺ 2	Mn	Cu	Ni	Cr	Z	X	Fo	Fa
Si	0.998													
Al	0.001	0.001	0.001	0.001	0.001	0.001	0.001	0.001	0.001	0.001	0.001	0.001	0.001	0.001
Ti	0.000	0.000	0.000	0.000	0.000	0.000	0.000	0.000	0.000	0.000	0.000	0.000	0.000	0.000
Fu ⁺ 3	0.000	0.000	0.000	0.000	0.000	0.000	0.000	0.000	0.000	0.000	0.000	0.000	0.000	0.000
Mn	1.509	1.510	1.534	1.524	1.524	1.524	1.524	1.524	1.524	1.524	1.524	1.524	1.524	1.524
Fe ⁺ 2	0.479	0.477	0.450	0.453	0.450	0.453	0.450	0.451	0.450	0.451	0.451	0.451	0.451	0.451
Mn	0.006	0.006	0.006	0.006	0.006	0.006	0.006	0.006	0.006	0.006	0.006	0.006	0.006	0.006
Cu	0.008	0.008	0.008	0.007	0.008	0.007	0.008	0.007	0.008	0.007	0.008	0.007	0.008	0.007
Ni	0.001	0.000	0.000	0.002	0.000	0.002	0.000	0.002	0.000	0.002	0.000	0.002	0.000	0.002
Cr	0.000	0.000	0.000	0.000	0.000	0.000	0.000	0.000	0.000	0.000	0.000	0.000	0.000	0.000
Z	0.998	0.999	1.000	1.002	1.004	1.002	1.004	1.004	1.004	1.004	1.004	1.004	1.002	1.002
X	2.004	2.002	1.999	1.994	1.992	1.994	1.992	1.993	1.992	1.993	1.992	1.993	1.996	1.996
Fo	75.9	76.0	77.3	77.1	77.2	77.1	77.2	77.6	77.2	77.6	77.2	77.6	77.2	77.2
Fa	24.1	24.0	22.7	22.9	22.8	22.9	22.8	22.4	22.8	22.4	22.8	22.4	22.8	22.8

* Total iron given as FeO
PH = phenocryst, GM = groundmass, C = core, R = rim

FELDSPARS																
Sample:	SE31-1-1	SE31-1-2	SE31-3-4	SE31-3-5	SE32-1-4	SE32-1-5	SE32-2-1	SE32-2-2	SE32-2-3	SE36-2-1	SE36-2-2	SE128-1-2	SE128-4-3	SE128-4-3	SE131-3-1	
Formation:	Raspberry	Raspberry	Raspberry	Raspberry	Raspberry	Raspberry	Raspberry	Raspberry	Raspberry	Raspberry	Raspberry	Little Iskut	Little Iskut	Little Iskut	Little Iskut	
Type:	PHR	PHC	GM	GM	GM	GM	PHR	PHC	PHC	GM	GM	PHR	GM	GM	PHC	
SiO ₂	52.43	50.79	52.89	52.49	51.70	53.68	52.01	52.65	51.93	50.79	51.73	62.31	65.48	65.48	62.36	
Al ₂ O ₃	29.56	31.09	28.95	29.42	30.17	28.92	29.38	29.39	30.00	30.84	30.54	21.96	19.55	19.55	21.98	
TiO ₂																0.05
Fe ₂ O ₃ *	0.63	0.53	0.71	1.03	0.62	0.75	0.66	0.38	0.37	0.64	0.59	0.30	0.63	0.63	1.11	1.11
FeO	0.00	0.00	0.00	0.00	0.00	0.00	0.00	0.00	0.00	0.00	0.00	0.00	0.00	0.00	0.00	0.00
MnO																0.03
CaO	12.27	14.12	11.96	12.57	13.06	11.77	12.67	12.50	13.11	13.96	13.50	3.94	1.36	1.36	1.37	4.90
Na ₂ O	4.36	3.56	4.85	4.22	3.94	4.68	4.06	4.39	3.99	3.61	3.90	6.91	7.12	7.12	7.08	7.11
K ₂ O	0.24	0.13	0.30	0.22	0.28	0.36	0.26	0.28	0.19	0.17	0.19	3.14	4.87	4.87	4.22	2.18
Total	99.49	100.22	99.66	99.95	99.77	100.16	99.04	99.59	99.59	100.01	100.45	98.59	99.04	99.04	98.83	99.72
Formula based on 8 oxygens																
Si	2.392	2.311	2.411	2.388	2.358	2.430	2.386	2.400	2.369	2.317	2.345	2.820	2.947	2.947	2.800	2.800
Al	1.589	1.667	1.556	1.577	1.622	1.543	1.589	1.579	1.613	1.658	1.632	1.171	1.037	1.037	1.161	1.161
Fe + 3	0.022	0.018	0.024	0.035	0.021	0.026	0.023	0.013	0.013	0.022	0.020	0.010	0.021	0.021	0.037	0.037
Ti																
Fe + 2	0.000	0.000	0.000	0.000	0.000	0.000	0.000	0.000	0.000	0.000	0.000	0.000	0.000	0.000	0.000	0.000
Mn																
Ca	0.600	0.688	0.584	0.613	0.638	0.571	0.623	0.611	0.641	0.682	0.656	0.191	0.066	0.066	0.095	0.235
Ni	0.386	0.314	0.429	0.372	0.348	0.411	0.361	0.388	0.353	0.319	0.343	0.606	0.621	0.621	0.619	0.618
K	0.014	0.008	0.017	0.013	0.016	0.021	0.015	0.016	0.011	0.010	0.011	0.181	0.280	0.280	0.243	0.125
Z	4.003	3.986	3.991	4.000	4.001	3.999	3.998	3.992	3.995	3.997	3.997	4.001	4.005	4.005	3.998	3.998
X	1.000	1.010	1.030	0.998	1.002	1.003	0.999	1.015	1.005	1.011	1.010	0.978	0.968	0.968	0.981	0.981
Ab	38.6	31.1	41.6	37.3	34.7	41.0	36.1	38.2	35.1	31.6	34.0	62.0	64.3	64.3	63.1	63.1
An	60.0	68.2	56.7	61.4	63.5	56.9	62.4	60.2	63.8	67.4	64.9	19.5	6.8	6.8	24.1	24.1
Or	1.4	0.7	1.7	1.3	1.6	2.1	1.5	1.6	1.1	1.0	1.1	18.5	28.9	28.9	12.8	12.8

* Total iron given as Fe₂O₃

PH = phenocryst, GM = groundmass, C = core, R = rim

FELDSPARS

Sample: Formation:	SE131-3-2		SE131-5-2		SE-14-4-1		SE14-4-2		SE15-3-1		SE15-3-2		SE19-2-1		SE19-2-2		SE20-10-1		SE20-10-2		SE20-10-3		SE27-1GD		SE27-3-2		SE27-3-3		SE27-4-1		
	Little PHR	Iskut PHR	Little GM	Iskut GM	PHR	Armadiño PHR	PHC	Armadiño PHC	PHR	Armadiño PHR	PHC	Armadiño PHC	PHR	Armadiño PHR	PHC	Armadiño PHC	PHR	Armadiño PHR	PH	Armadiño PH	GM	Armadiño GM	PHR	Armadiño PHR	PHC	Armadiño PHC	PH	Armadiño PH			
SiO ₂	63.27		60.79		67.19	66.59	66.58	67.51	67.55	66.92	67.09	68.10	66.35	66.75	67.07	67.18					18.02	18.02	18.56	18.56	67.07	67.07	67.18	67.18	18.14	18.14	
Al ₂ O ₃	21.17		23.89		18.05	19.00	19.14	18.28	18.20	18.23	18.18	18.66	18.02	18.56	18.51	18.56															
TiO ₂	0.03		0.06		0.00	0.00	0.00	0.00	0.00	0.00	0.00	0.00	0.00	0.00	0.00	0.00															
Fe ₂ O ₃ *	0.47		0.42		0.73	0.34	0.28	0.53	0.72	0.71	0.65	0.59	1.18	0.62	0.46	1.17															
FeO	0.00		0.00		0.00	0.00	0.00	0.00	0.00	0.00	0.00	0.00	0.00	0.00	0.00	0.00															
MnO	0.00		0.00		0.00	0.00	0.00	0.00	0.00	0.00	0.00	0.00	0.00	0.00	0.00	0.00															
CaO	2.96		6.46		6.05	0.27	0.27	0.01	0.00	0.06	0.06	0.10	0.10	0.10	0.13	0.07															
Na ₂ O	7.24		7.22		6.79	7.33	6.98	7.14	6.48	6.97	7.12	7.14	6.50	7.53	7.49	6.99															
K ₂ O	3.75		0.90		7.38	6.55	7.16	7.50	7.41	7.22	7.00	7.05	2.63	6.11	6.24	7.14															
Total	98.89		99.74		100.19	100.08	100.74	100.34	100.36	100.11	100.10	101.64	99.78	99.67	99.90	100.69															
Si	2.858		2.719		3.012	2.981	2.977	3.017	3.017	3.003	3.007	3.004	2.996	2.995	3.002	3.000															
Al	1.127		1.259		0.954	1.002	1.009	0.963	0.958	0.964	0.960	0.970	0.959	0.981	0.976	0.955															
Fe + 3	0.016		0.014		0.025	0.012	0.009	0.018	0.024	0.024	0.022	0.020	0.040	0.021	0.016	0.039															
Ti	0.001		0.002		0.000	0.000	0.000	0.000	0.000	0.000	0.000	0.000	0.000	0.000	0.000	0.000															
Fe + 3	0.000		0.000		0.000	0.000	0.000	0.000	0.000	0.000	0.000	0.000	0.000	0.000	0.000	0.000															
Fe + 2	0.000		0.000		0.000	0.000	0.000	0.000	0.000	0.000	0.000	0.000	0.000	0.000	0.000	0.000															
Mn	0.000		0.000		0.000	0.013	0.013	0.001	0.000	0.003	0.003	0.005	0.005	0.005	0.006	0.003															
Ca	0.143		0.310		0.002	0.836	0.802	0.564	0.561	0.806	0.619	0.611	0.569	0.655	0.650	0.603															
Ni	0.634		0.626		0.590	0.374	0.411	0.408	0.422	0.413	0.400	0.397	0.440	0.350	0.356	0.407															
K	0.216		0.051		0.422	0.395	0.408	0.428	0.422	0.413	0.400	0.397	0.440	0.350	0.356	0.407															
Z	4.001		3.992		3.991	3.995	3.990	3.998	3.999	3.991	3.989	3.994	3.995	3.997	3.994	3.994															
X	0.994		0.989		1.014	1.023	1.016	0.993	0.983	1.022	1.022	1.013	1.014	1.010	1.012	1.015															
Ab	63.8		63.4		58.2	62.2	59.2	56.8	57.1	59.3	60.5	60.3	56.1	64.9	64.2	59.6															
An	14.4		31.4		0.2	1.3	0.3	1.3	0.0	0.3	0.3	0.5	0.5	0.5	0.6	0.3															
Or	21.8		5.2		41.6	36.5	40.5	39.8	42.9	40.4	39.2	39.2	43.4	34.6	35.2	40.1															

Formula based on 8 oxygens

* Total iron given as Fe₂O₃
 PH = phenocryst, GM = groundmass, C = core, R = rim

FELDSPARS

Sample: SE120-2-4	SE123-1-1	SE123-1-3	SE123-3-4	SE123-3-5	SE123-3-6	SE123-4-1	SE123-4-2	SE123-4-3	SE125-3-1	SE125-3-2	SE125-3-3	SE125-5-4	SE125-7-1	SE125-7-2
Formation:	Nido	Nido	Nido	Nido	Nido	Nido	Nido	Nido	Nido	Nido	Nido	Nido	Nido	Nido
Type:	PHR	PHC	GM	GM	GM	PHR	PHC	PHC	PHC	PHR	PHR	PHC	PH	PH
SiO ₂	51.74	53.23	52.10	53.09	52.79	52.33	56.86	52.43	53.46	53.84	54.19	53.99	54.73	53.51
Al ₂ O ₃	29.51	28.95	29.91	29.03	29.12	29.93	26.65	29.57	28.55	28.24	28.56	28.77	29.17	28.50
TiO ₂	0.57	0.41	0.76	0.86	0.87	0.67	0.38	0.50	0.24	0.27	0.27	0.24	0.28	0.33
Fe ₂ O ₃ *	0.00	0.00	0.00	0.00	0.00	0.00	0.00	0.00	0.00	0.00	0.00	0.00	0.00	0.00
MnO	12.71	11.23	12.73	11.61	12.07	12.72	8.64	12.29	11.28	10.84	10.97	11.14	11.16	11.20
CaO	4.21	4.98	4.24	4.78	4.40	3.90	6.08	4.40	5.05	5.21	5.08	5.16	5.25	5.04
Na ₂ O	0.27	0.33	0.25	0.28	0.29	0.25	0.78	0.41	0.28	0.36	0.29	0.31	0.24	0.27
K ₂ O	99.01	99.13	99.99	99.65	99.54	99.80	99.39	99.60	98.86	98.76	99.36	99.61	100.83	98.85
Total														

Formula based on 8 oxygens

Si	2.333	2.431	2.370	2.417	2.407	2.380	2.571	2.391	2.446	2.464	2.463	2.451	2.452	2.449
Al	1.844	1.558	1.604	1.558	1.565	1.604	1.420	1.590	1.540	1.523	1.530	1.539	1.540	1.537
Fe + 3	0.018	0.020	0.026	0.030	0.030	0.023	0.013	0.017	0.008	0.009	0.009	0.008	0.009	0.011
Ti	0.000	0.000	0.000	0.000	0.000	0.000	0.000	0.000	0.000	0.000	0.000	0.000	0.000	0.000
Fe + 2	0.000	0.000	0.000	0.000	0.000	0.000	0.000	0.000	0.000	0.000	0.000	0.000	0.000	0.000
Mn	0.673	0.550	0.621	0.566	0.590	0.620	0.419	0.601	0.553	0.532	0.534	0.542	0.536	0.549
Ca	0.331	0.441	0.374	0.422	0.389	0.344	0.533	0.389	0.448	0.462	0.448	0.454	0.456	0.447
Ni	0.007	0.016	0.015	0.016	0.017	0.015	0.045	0.024	0.016	0.021	0.017	0.018	0.014	0.016
K	3.995	4.003	4.000	4.005	4.002	4.007	4.004	3.998	3.994	3.996	4.002	3.998	4.001	3.997
Z	1.011	1.017	1.010	1.004	0.996	0.979	0.997	1.014	1.017	1.015	0.999	1.014	1.006	1.012
X														
Ab	32.7	36.9	37.1	42.0	39.1	35.1	53.5	38.4	44.0	45.5	44.8	44.8	45.4	44.2
An	66.6	54.4	61.5	56.4	59.2	63.4	42.0	59.3	54.4	52.4	53.5	53.4	53.3	54.2
Or	0.7	1.9	1.4	1.6	1.7	1.5	4.5	2.3	1.6	2.1	1.7	1.8	1.4	1.6

* Total iron given as Fe₂O₃
 PH = phenocryst, GM = groundmass, C = core, R = rim

FELDSPARS

Sample: Formation:	SE125-7-2 Nido	SE92-2-3	SE93-1-1	SE94-1-1	SE94-1-2	SE94-3-3	SE98-3-1	SE98-3-2	SE98-3-3	SE100-1-2	SE100-1-3	SE100-1-4	SE102-1-1	SE103-2-3	SE103-2-4
Type:	PH	PH	PH	PHR	PHC	GM	PHR	PHC	GM	GM	PHR	PHC	PHC	PH	GM
SiO ₂	53.55	66.73	67.18	68.05	67.49	67.00	67.52	67.49	67.65	67.36	67.17	66.90	67.08	66.82	66.51
Al ₂ O ₃	28.84	17.38	18.43	18.44	18.45	18.27	18.69	18.52	17.94	18.48	18.88	18.72	18.85	18.54	17.97
TiO ₂	0.29	1.40	0.39	0.68	0.63	1.31	0.49	0.69	1.31	0.54	0.28	0.26	0.27	0.76	1.54
Fe ₂ O ₃ *	0.00	0.00	0.00	0.00	0.00	0.00	0.00	0.00	0.00	0.00	0.00	0.00	0.00	0.00	0.00
FeO*	11.36	0.01	0.06	0.02	0.01	0.09	0.06	0.05	0.04	0.49	0.15	0.15	0.08	0.02	0.03
MnO	5.06	6.30	7.03	7.37	7.33	7.58	7.50	7.54	7.61	7.07	7.44	7.19	6.71	7.70	7.68
CaO	0.27	7.41	6.49	7.37	6.17	5.61	5.90	5.84	5.73	6.35	5.88	6.32	7.09	5.97	5.53
Na ₂ O	99.37	99.23	99.58	100.69	100.08	99.86	100.16	100.13	100.28	100.29	99.80	99.54	100.08	99.81	99.26
Total															
Si	2.439	3.023	3.013	3.015	3.010	2.998	3.005	3.006	3.014	3.003	2.989	3.001	3.000	2.994	2.997
Al	1.548	0.928	0.974	0.963	0.970	0.963	0.980	0.972	0.942	0.971	0.994	0.990	0.993	0.979	0.954
Fe + 3	0.010	0.048	0.013	0.023	0.021	0.044	0.016	0.023	0.044	0.018	0.009	0.009	0.009	0.026	0.052
Ti	0.000	0.000	0.000	0.000	0.000	0.000	0.000	0.000	0.000	0.000	0.000	0.000	0.000	0.000	0.000
Fe + 2	0.000	0.000	0.000	0.000	0.000	0.000	0.000	0.000	0.000	0.000	0.000	0.000	0.000	0.000	0.000
Mn	0.554	0.001	0.003	0.001	0.001	0.004	0.003	0.002	0.002	0.023	0.007	0.007	0.004	0.001	0.001
Ca	0.447	0.553	0.611	0.633	0.634	0.658	0.647	0.651	0.657	0.611	0.644	0.625	0.582	0.669	0.671
Ni	0.016	0.428	0.371	0.347	0.351	0.320	0.335	0.332	0.326	0.361	0.335	0.362	0.404	0.341	0.318
K	3.997	3.999	4.000	4.001	4.001	4.005	4.001	4.001	4.000	3.992	4.002	4.000	4.002	3.999	4.003
Z	1.017	0.982	0.985	0.981	0.986	0.982	0.985	0.985	0.985	0.995	0.986	0.994	0.990	1.011	0.990
Ab	44.0	56.3	62.0	64.6	64.3	67.0	65.7	66.1	66.7	61.4	65.3	62.9	58.8	66.2	67.7
An	54.5	0.1	0.3	0.1	0.1	0.4	0.3	0.2	0.2	2.3	0.7	0.7	0.4	0.1	0.2
Or	1.5	43.6	37.7	35.3	35.6	32.6	34.0	33.7	33.1	36.3	34.0	36.4	40.8	33.7	32.1

Formula based on 8 oxygens

* Total iron given as Fe₂O₃
PH = phenocryst, GM = groundmass, C = core, R = rim

FELDSPARS

Sample:	SE103-2-4	SE104-1-1	SE82-3-1	SE82-4-2	SE82-4-3	SE85-1-1	SE85-1-2	SE85-1-3	SE85-1-4	SE85-1-5	SE85-2-1	SE85-2-3	SE85-2-4	SE41-3-6	SE41-3-7
Formation:	Spectrum	Spectrum	Pyramid	Pyramid	Pyramid	Pyramid	Pyramid	Pyramid	Pyramid	Pyramid	Pyramid	Pyramid	Pyramid	Ice Peak	Ice Peak
Type:	GM	PH	PHC	PH	PHC	PH	PH	PH	PH	PHR	PH	PH	PH	PHR	PHC
SiO ₂	67.04	67.48	67.18	67.62	67.79	61.27	61.51	65.78	66.48	66.27	58.74	62.67	63.31	53.16	51.36
Al ₂ O ₃	17.88	18.21	18.74	17.84	17.97	23.40	23.32	19.13	19.08	19.20	26.59	23.16	22.87	29.61	30.97
TiO ₂	1.82	0.83	0.20	0.77	0.64	0.18	0.20	0.09	0.16	0.13	0.27	0.22	0.23	0.72	0.64
Fe ₂ O ₃ *	0.00	0.00	0.00	0.00	0.00	0.00	0.00	0.00	0.00	0.00	0.00	0.00	0.00	0.00	0.00
FeO	0.06	0.01	0.09	0.01	0.01	5.27	5.26	0.67	0.61	0.78	8.51	4.83	4.55	12.38	14.00
MnO	7.73	6.58	6.96	6.62	6.85	7.78	7.69	5.13	5.17	5.78	6.44	7.72	7.92	4.45	3.62
Na ₂ O	5.66	7.24	6.94	6.85	6.54	1.24	1.34	8.72	8.55	7.49	0.71	1.74	1.66	0.27	0.21
K ₂ O	100.19	100.35	100.11	99.71	99.80	99.14	99.32	99.52	100.05	99.65	101.26	100.34	100.54	100.59	100.80
Total															
Si	2.998	3.014	3.003	3.032	3.032	2.752	2.758	2.978	2.988	2.981	2.602	2.781	2.799	2.400	2.324
Al	0.942	0.959	0.987	0.943	0.947	1.239	1.232	1.021	1.011	1.018	1.388	1.211	1.192	1.575	1.651
Fe ⁺³	0.061	0.028	0.007	0.026	0.022	0.006	0.007	0.003	0.005	0.004	0.009	0.007	0.008	0.025	0.022
Ti	0.000	0.000	0.000	0.000	0.000	0.000	0.000	0.000	0.000	0.000	0.000	0.000	0.000	0.000	0.000
Fe ⁺²	0.000	0.000	0.000	0.000	0.000	0.000	0.000	0.000	0.000	0.000	0.000	0.000	0.000	0.000	0.000
Mn	0.670	0.570	0.603	0.001	0.001	0.254	0.263	0.033	0.029	0.038	0.404	0.230	0.216	0.599	0.679
Ca	0.003	0.001	0.004	0.575	0.594	0.678	0.669	0.450	0.451	0.504	0.553	0.664	0.679	0.390	0.318
Ni	0.323	0.413	0.396	0.392	0.373	0.071	0.077	0.504	0.490	0.430	0.040	0.099	0.094	0.016	0.012
K	4.001	4.001	3.997	4.001	4.001	3.997	3.997	4.002	4.004	4.003	3.999	3.999	3.999	4.000	3.997
Z	0.996	0.984	1.003	0.968	0.968	1.003	0.999	0.987	0.970	0.972	0.997	0.993	0.989	1.005	1.009
X															
Ab	67.3	57.9	60.2	59.4	61.4	67.6	67.0	45.7	46.5	51.9	55.5	67.0	68.7	38.8	31.5
An	0.3	0.1	0.4	0.1	0.1	25.3	25.3	3.3	3.0	3.9	40.5	23.1	21.8	59.6	67.3
Or	32.4	42.0	39.4	40.5	38.5	7.1	7.7	51.0	50.5	44.2	4.0	9.9	9.5	1.6	1.2

Formula based on 8 oxygens

* Total iron given as Fe₂O₃
 PH = phenocryst, GM = groundmass, C = core, R = rim

FELDSPARS															
Sample:	SE44-1-4	SE44-4-1	SE44-4-2	SE46-1-1	SE46-1-2	SE51-2-1	SE51-2-2	SE51-2-3	SE51-2-4	SE135-2-1	SE135-2-2	SE135-2-3	SE136-1-1	SE136-1-2	SE136-2-3
Formation:	Ice Peak	Ice Peak	Ice Peak	Ice Peak	Ice Peak	Ice Peak	Ice Peak	Ice Peak	Ice Peak	Pillow Ridge PHR	Pillow Ridge PHC	Pillow Ridge PHC	Pillow Ridge PHR	Pillow Ridge PHC	Pillow Ridge GM
Type:	GM	PHR	PHC	PHR	PHC	PHR	PH	PHR	PHC	PHR	PHC	PHC	PHR	PHC	
SiO ₂	67.28	66.97	66.29	62.83	55.83	52.19	51.52	52.72	52.68	54.35	53.82	53.32	50.85	49.54	53.06
Al ₂ O ₃	19.21	19.73	19.61	22.47	27.40	29.04	30.02	29.64	29.77	28.41	28.18	28.09	30.18	31.08	28.66
TiO ₂															
Fe ₂ O ₃ *	0.64	0.24	0.18	0.74	0.35	0.58	0.59	0.57	0.60	0.49	0.47	0.46	0.09	0.05	0.13
FeO	0.00	0.00	0.00	0.00	0.00	0.00	0.00	0.00	0.00	0.00	0.00	0.00	0.00	0.00	0.00
MnO															
CaO	0.34	0.79	0.66	4.53	10.05	11.98	12.96	12.54	12.93	12.09	12.17	12.21	14.80	15.59	13.04
Na ₂ O	7.26	7.33	6.81	7.70	5.60	4.53	4.01	4.25	4.23	4.52	4.63	4.55	3.33	2.77	4.21
K ₂ O	6.39	5.89	6.57	1.77	0.43	0.29	0.26	0.25	0.23	0.31	0.31	0.30	0.18	0.15	0.28
Total	101.12	100.95	100.12	100.04	99.66	98.61	99.36	99.97	100.44	100.17	99.58	98.93	99.90	99.69	100.17
Si	2.978	2.963	2.964	2.798	2.524	2.403	2.359	2.394	2.384	2.453	2.447	2.441	2.323	2.274	2.408
Al	1.002	1.029	1.033	1.179	1.460	1.576	1.620	1.586	1.588	1.511	1.510	1.516	1.625	1.682	1.533
Fe + 3	0.021	0.008	0.006	0.025	0.012	0.020	0.020	0.020	0.020	0.017	0.016	0.016	0.016	0.018	0.027
Ti	0.000	0.000	0.000	0.000	0.000	0.000	0.000	0.000	0.000	0.000	0.000	0.000	0.003	0.002	0.004
Fe + 2	0.000	0.000	0.000	0.000	0.000	0.000	0.000	0.000	0.000	0.000	0.000	0.000	0.000	0.000	0.000
Mn															
Ca	0.016	0.038	0.032	0.216	0.487	0.591	0.636	0.610	0.627	0.585	0.593	0.599	0.724	0.767	0.634
Ni	0.623	0.629	0.590	0.665	0.491	0.404	0.356	0.374	0.371	0.396	0.408	0.404	0.295	0.247	0.370
K	0.361	0.333	0.375	0.101	0.025	0.017	0.015	0.015	0.013	0.018	0.018	0.018	0.011	0.009	0.016
Z	4.001	4.000	4.003	4.002	3.996	3.999	3.999	4.000	3.992	3.981	3.973	3.973	3.964	3.974	3.968
X	1.000	1.000	0.997	0.982	1.003	1.012	1.007	0.999	1.011	0.999	1.020	1.021	1.033	1.025	1.024
Ab	62.3	62.9	59.2	67.8	49.0	40.0	35.4	37.4	36.7	39.6	40.0	39.6	28.6	24.1	36.3
An	1.6	3.8	3.2	22.0	48.5	58.3	63.1	61.1	62.0	58.6	58.2	58.7	70.4	75.0	62.1
Or	36.1	33.3	37.6	10.2	2.5	1.7	1.5	1.5	1.3	1.8	1.8	1.7	1.0	0.9	1.6

Formula based on 8 oxygens

* Total iron given as Fe₂O₃

PH = phenocryst, GM = groundmass, C = core, R = rim

FELDSPARS

Sample:	SE72-1.5*	SE72-6.4	SE139-1-3	SE139-1-4	SE139-2-2	SE139-3-3	SE141-A-2	SE141-A-3	SE141-B-4	SE141-C-10	SE132-2-1	SE132-2-2	SE132-2-3	SE132-4-6	SE132-5-2
Formation:	Edziza	Edziza	Arctic Lake GM	Arctic Lake GM	Arctic Lake GM	Arctic Lake GM	Arctic Lake PHC	Arctic Lake PHR	Arctic Lake PHC	Arctic Lake PH	Klastline PHR	Klastline PHC	Klastline GM	Klastline GM	Klastline PHR
Type:	GM	PH	GM	GM	GM	GM	PHC	PHR	PHC	PH	PHR	PHC	GM	GM	PHR
SiO ₂	66.13	66.88	51.19	52.10	52.67	51.35	54.14	51.67	51.98	50.52	53.86	48.37	53.16	53.67	56.68
Al ₂ O ₃	18.58	18.96	29.03	29.56	29.23	29.08	29.14	30.83	31.40	31.99	28.87	33.48	29.83	29.10	27.35
TiO ₂	0.00	0.00	0.10	0.10	0.12	0.12	0.01	0.15	0.11	0.06	0.15	0.08	0.12	0.16	0.17
Fe ₂ O ₃ *	0.51	0.30	0.61	0.52	0.61	0.56	0.32	0.74	0.70	0.68	0.97	0.79	0.79	0.72	0.58
FeO*	0.00	0.00	0.00	0.00	0.00	0.00	0.00	0.00	0.00	0.00	0.00	0.00	0.00	0.00	0.00
MnO	0.73	0.19	13.42	13.33	13.37	13.48	11.40	13.37	13.61	13.95	11.36	15.89	12.05	11.32	9.31
CaO	8.02	7.51	3.95	3.98	4.14	3.96	4.95	3.81	3.60	3.39	4.78	2.30	4.52	4.62	5.22
Ni ₂ O	5.20	5.95	0.25	0.25	0.25	0.25	0.37	0.28	0.27	0.25	0.42	0.12	0.35	0.39	0.72
K ₂ O	99.17	99.79	98.55	99.84	100.39	98.82	100.33	100.85	101.67	100.84	100.41	100.84	100.82	99.98	100.03
Total															
Si	2.980	2.991	2.366	2.373	2.386	2.367	2.440	2.333	2.327	2.285	2.429	2.196	2.394	2.428	2.545
Al	0.987	0.999	1.581	1.587	1.561	1.580	1.548	1.641	1.657	1.705	1.534	1.792	1.583	1.551	1.447
Fe + 3	0.017	0.010	0.021	0.018	0.021	0.019	0.011	0.025	0.024	0.023	0.033	0.021	0.027	0.024	0.020
Ti	0.000	0.000	0.004	0.003	0.004	0.004	0.000	0.005	0.004	0.002	0.005	0.003	0.004	0.005	0.006
Fe + 3	0.000	0.000	0.000	0.000	0.000	0.000	0.000	0.000	0.000	0.000	0.000	0.000	0.000	0.000	0.000
Fe + 2	0.000	0.000	0.000	0.000	0.000	0.000	0.000	0.000	0.000	0.000	0.000	0.000	0.000	0.000	0.000
Mn	0.035	0.009	0.665	0.650	0.649	0.666	0.551	0.647	0.653	0.676	0.549	0.773	0.581	0.549	0.448
Ca	0.701	0.651	0.354	0.351	0.364	0.354	0.433	0.334	0.313	0.297	0.418	0.203	0.395	0.405	0.454
Ni	0.299	0.339	0.015	0.015	0.014	0.015	0.021	0.016	0.015	0.014	0.024	0.007	0.020	0.023	0.041
K	3.984	4.000	3.968	3.978	3.968	3.966	3.999	3.999	4.008	4.013	3.996	4.009	4.004	4.003	4.012
Z	1.035	0.999	1.038	1.019	1.031	1.039	1.005	1.002	0.985	0.989	0.996	0.986	1.000	0.982	0.949
X															
Ab	67.7	65.1	34.3	34.6	35.4	34.2	43.1	33.5	31.9	30.1	42.2	20.6	39.6	41.5	48.1
An	3.4	0.9	64.3	64.0	63.2	64.4	54.8	64.9	66.5	68.4	55.4	78.7	58.4	56.2	47.5
Or	28.9	34.0	1.4	1.4	1.4	1.4	2.1	1.6	1.6	1.5	2.4	0.7	2.0	2.3	4.4

Formula based on 8 oxygens

* Total iron given as Fe₂O₃
PH = phenocryst, GM = groundmass, C = core, R = rim

FELDSPARS

Sample:	SE132-5-3	SE74-1-3	SE74-1-4	SE74-2-1	SE74-2-2	SE142-A-1	SE142-A-2	SE142-A-3	SE142-B-5	SE142-B-7	SE142-C-8	SE2-3-1	SE2-3-2	SE2-3-3	SE2-3-4
Formation:	Klastline	Kakiddi	Kakiddi	Kakiddi	Kakiddi	Kakiddi	Kakiddi	Kakiddi	Kakiddi	Kakiddi	Kakiddi	Big Raven	Big Raven	Big Raven	Big Raven
Type:	PHC	GM	GM	PHR	PHC	PHC	PHR	GM	GM	GM	PHC	PHR	PHR	PHC	GM
SiO ₂	47.64	66.84	66.38	66.98	67.00	67.05	66.20	65.93	65.53	65.83	67.01	52.52	52.49	51.36	53.79
Al ₂ O ₃	33.53	19.01	19.21	19.14	18.93	19.85	19.76	20.28	20.26	20.95	20.18	29.09	29.28	29.98	27.94
TiO ₂	0.05	0.00	0.00	0.00	0.00	0.01	0.04	0.07	0.06	0.09	0.04	0.00	0.00	0.00	0.00
Fe ₂ O ₃ *	0.51	1.27	1.27	0.29	0.27	0.19	0.28	0.33	0.28	0.27	0.20	0.94	0.70	0.71	0.97
FeO	0.00	0.00	0.00	0.00	0.00	0.00	0.00	0.00	0.00	0.00	0.00	0.00	0.00	0.00	0.00
MnO	16.22	0.75	1.17	0.49	0.25	0.34	0.41	0.79	0.53	1.17	0.39	12.96	12.92	13.44	11.14
CaO	2.08	7.56	7.92	7.22	6.99	6.60	6.84	7.31	7.32	7.75	6.99	4.33	4.44	4.15	5.12
Na ₂ O	0.13	5.19	4.55	6.17	6.68	6.61	6.08	4.93	5.59	4.07	5.12	0.28	0.31	0.26	0.42
K ₂ O	100.16	100.55	100.50	100.29	100.12	100.65	99.61	99.64	99.55	100.13	100.93	100.12	100.14	99.90	99.38
Total															
Si	2.179	2.969	2.950	2.984	2.993	2.973	2.964	2.941	2.937	2.917	2.960	2.390	2.388	2.346	2.456
Al	1.808	0.995	1.006	1.005	0.997	1.037	1.043	1.066	1.070	1.094	1.051	1.560	1.570	1.614	1.503
Fe + 3	0.018	0.040	0.043	0.010	0.009	0.006	0.009	0.011	0.009	0.009	0.007	0.032	0.024	0.024	0.033
Ti	0.002	0.000	0.000	0.000	0.000	0.000	0.001	0.002	0.002	0.003	0.001	0.000	0.000	0.000	0.000
Fe + 2	0.000	0.000	0.000	0.000	0.000	0.000	0.000	0.000	0.000	0.000	0.000	0.000	0.000	0.000	0.000
Mn	0.795	0.036	0.056	0.023	0.012	0.016	0.020	0.038	0.025	0.056	0.018	0.632	0.630	0.658	0.545
Ca	0.185	0.651	0.683	0.624	0.605	0.567	0.594	0.632	0.636	0.666	0.599	0.382	0.392	0.368	0.453
Ni	0.008	0.294	0.258	0.351	0.381	0.374	0.347	0.281	0.320	0.230	0.345	0.016	0.018	0.015	0.024
K	4.005	4.004	3.999	3.999	3.989	4.016	4.016	4.018	4.016	4.020	4.018	3.982	3.982	3.984	3.992
Z	0.990	0.981	0.997	0.998	0.998	0.957	0.962	0.953	0.983	0.955	0.963	1.030	1.040	1.041	1.022
Ab	18.7	66.4	68.5	62.5	60.7	59.3	61.8	66.5	64.8	70.0	62.2	37.1	37.7	35.3	44.3
An	80.5	3.6	5.6	2.3	1.2	1.7	2.0	4.0	2.6	5.8	1.9	61.3	60.6	63.2	53.3
Or	0.8	30.0	25.9	35.2	38.1	39.0	36.2	29.5	32.6	24.2	35.9	1.6	1.7	1.5	2.4

Formula based on 8 oxygens

* Total iron given as Fe₂O₃
PH = phenocryst, GM = groundmass, C = core, R = rim

FELDSPARS

Sample: Formation:	SE3-4-1		SE3-4-2		SE3-4-3		SE3-5-7		SE3-5-8		SE3-5-9		SE4-1-1		SE4-1-2		SE4-1-3		SE7-1-1		SE7-1-2		SE7-1-3		SE7-2-3A		SE7-2-3B		SE7-6-1		
	Big Raven	PHR	Big Raven	PHC	Big Raven	GM	Big Raven	PHR	Big Raven	PHC	Big Raven	GM	Big Raven	PHC	Big Raven	PH	Big Raven	PHR	Big Raven	PHR	Big Raven	PH	Big Raven	PHC	Big Raven	GM	Big Raven	GM	Big Raven	GM	
SiO ₂	54.07	49.24	54.66	56.12	54.01	60.12	50.64	51.26	51.20	50.94	55.81	50.12	55.87	50.94	55.81	50.12	55.87	50.94	50.94	50.94	55.81	50.12	55.87	50.94	50.12	50.66	50.76	50.66	50.76		
Al ₂ O ₃	28.30	31.48	27.92	26.88	28.39	22.68	31.43	30.72	30.89	29.97	26.80	29.45	26.73	29.97	26.80	29.45	26.73	29.97	29.97	29.97	26.80	29.45	26.73	29.97	29.45	29.87	29.98	29.87	29.98		
TiO ₂	0.70	0.58	0.80	0.45	0.62	1.22	0.53	0.55	0.57	0.76	0.38	1.40	0.36	0.76	0.38	1.40	0.36	0.76	0.76	0.76	0.38	1.40	0.36	0.76	1.40	0.85	0.70	0.85	0.70		
Fe ₂ O ₃ *	0.00	0.00	0.00	0.00	0.00	0.00	0.00	0.00	0.00	0.00	0.00	0.00	0.00	0.00	0.00	0.00	0.00	0.00	0.00	0.00	0.00	0.00	0.00	0.00	0.00	0.00	0.00	0.00	0.00		
FeO*	11.41	15.57	11.04	9.58	11.50	5.92	14.56	14.01	14.22	13.74	9.46	13.23	9.57	13.74	9.46	13.23	9.57	13.74	13.74	13.74	9.46	13.23	9.57	13.74	13.23	13.77	13.58	13.77	13.58		
MnO	4.76	3.03	5.40	5.89	5.07	6.94	3.19	3.64	3.51	3.85	5.92	4.22	5.89	3.85	5.92	4.22	5.89	3.85	3.85	3.85	5.92	4.22	5.89	3.85	4.22	3.77	3.84	3.77	3.84		
Na ₂ O	0.45	0.18	0.62	0.62	0.48	3.41	0.14	0.13	0.16	0.27	0.65	0.51	0.62	0.27	0.65	0.51	0.62	0.27	0.27	0.27	0.65	0.51	0.62	0.27	0.51	0.29	0.33	0.29	0.33		
K ₂ O	99.69	100.08	100.34	99.54	100.07	100.29	100.49	100.31	100.55	99.53	99.02	98.93	99.04	99.53	99.02	98.93	99.04	99.53	99.53	99.53	99.02	98.93	99.04	99.53	98.93	99.21	99.21	99.21	99.19		
Total																															
Formula based on 8 oxygens																															
Si	2.456	2.257	2.472	2.542	2.449	2.718	2.299	2.329	2.322	2.337	2.541	2.325	2.543	2.337	2.541	2.325	2.543	2.337	2.337	2.337	2.541	2.325	2.543	2.337	2.325	2.334	2.334	2.336	2.336		
Al	1.515	1.701	1.483	1.435	1.517	1.208	1.682	1.645	1.651	1.621	1.438	1.610	1.434	1.621	1.438	1.610	1.434	1.621	1.621	1.621	1.438	1.610	1.434	1.621	1.610	1.622	1.622	1.626	1.626		
Fe ⁺³	0.024	0.020	0.027	0.015	0.021	0.042	0.018	0.019	0.020	0.026	0.013	0.049	0.012	0.026	0.013	0.049	0.012	0.026	0.026	0.026	0.013	0.049	0.012	0.026	0.049	0.030	0.030	0.024	0.024		
Ti	0.000	0.000	0.000	0.000	0.000	0.000	0.000	0.000	0.000	0.000	0.000	0.000	0.000	0.000	0.000	0.000	0.000	0.000	0.000	0.000	0.000	0.000	0.000	0.000	0.000	0.000	0.000	0.000	0.000		
Fe ⁺²	0.000	0.000	0.000	0.000	0.000	0.000	0.000	0.000	0.000	0.000	0.000	0.000	0.000	0.000	0.000	0.000	0.000	0.000	0.000	0.000	0.000	0.000	0.000	0.000	0.000	0.000	0.000	0.000	0.000		
Mn	0.555	0.765	0.535	0.465	0.559	0.287	0.708	0.682	0.691	0.676	0.462	0.658	0.467	0.676	0.462	0.658	0.467	0.676	0.676	0.676	0.462	0.658	0.467	0.676	0.658	0.680	0.680	0.670	0.670		
Ca	0.419	0.269	0.474	0.517	0.446	0.608	0.281	0.321	0.309	0.342	0.523	0.380	0.520	0.342	0.523	0.380	0.520	0.342	0.342	0.342	0.523	0.380	0.520	0.342	0.380	0.337	0.343	0.337	0.343		
Ni	0.026	0.010	0.036	0.036	0.028	0.197	0.008	0.008	0.009	0.016	0.038	0.009	0.036	0.016	0.038	0.009	0.036	0.016	0.016	0.016	0.038	0.009	0.036	0.016	0.036	0.017	0.017	0.019	0.019		
K	3.995	3.978	3.982	3.992	3.987	3.968	3.999	3.993	3.993	3.984	3.992	3.984	3.989	3.984	3.992	3.984	3.989	3.984	3.984	3.984	3.992	3.984	3.989	3.984	3.984	3.986	3.986	3.986	3.986		
Z	1.000	1.044	1.045	1.018	1.033	1.092	0.997	1.011	1.009	1.034	1.023	1.068	1.023	1.034	1.023	1.068	1.023	1.034	1.034	1.034	1.023	1.068	1.023	1.034	1.068	1.034	1.034	1.034	1.034		
X																															
Ab	41.9	25.8	45.4	50.8	43.2	55.7	28.2	31.7	30.6	33.1	51.1	35.6	50.9	33.1	51.1	35.6	50.9	33.1	33.1	33.1	51.1	35.6	50.9	33.1	35.6	32.6	33.2	33.2	33.2		
An	55.5	73.2	51.2	45.7	54.1	26.3	71.0	67.5	68.5	65.4	45.2	61.6	45.6	65.4	45.2	61.6	45.6	65.4	65.4	65.4	45.2	61.6	45.6	65.4	61.6	65.8	64.9	64.9	64.9		
Or	2.6	1.0	3.4	3.5	2.7	18.0	0.8	0.8	0.9	1.5	3.7	2.8	3.5	1.5	3.7	2.8	3.5	1.5	1.5	1.5	3.7	2.8	3.5	1.5	2.8	1.6	1.9	1.9	1.9		

* Total iron given as Fe₂O₃

PH = phenocryst, GM = groundmass, C = core, R = rim

FELDSPARS

Sample: Formation.	SE7-6-2		SE10-4-1		SE10-4-2		SE10-4GD		SE11-2-2		SE11-4-1		SE11-4-2		SE11-4-3		SE11-5-5		SE75-1-4		SE75-2-5		SE76-1-3		SE76-4-3		SE76-4-4	
	Big Raven	PH	Big Raven	PHR	Big Raven	PHC	Big Raven	GM	Big Raven	GM	Big Raven	PHR	Big Raven	PH	Big Raven	PHC	Big Raven	GM	Edziza	Nodule	Edziza	Nodule	Edziza	Nodule	Edziza	Nodule	Edziza	Nodule
SiO ₂	56.16		52.35		54.54		52.44		52.94		54.62		49.42		50.41		53.49		65.76		65.64		49.42		48.43		49.34	
Al ₂ O ₃	27.04		28.92		27.78		29.07		28.52		27.96		31.17		30.93		28.73		19.84		19.80		31.02		32.33		31.32	
TiO ₂	0.34		0.75		0.40		0.80		0.85		0.57		0.72		0.62		0.95		0.19		0.16		0.46		0.53		0.59	
Fe ₂ O ₃ *	0.00		0.00		0.00		0.00		0.00		0.00		0.00		0.00		0.00		0.00		0.00		0.00		0.00		0.00	
MnO	9.51		12.15		10.50		12.33		11.84		10.80		14.80		14.45		12.52		1.15		1.23		14.29		15.53		14.47	
CaO	5.98		4.70		5.66		4.65		4.84		5.42		3.21		3.53		4.59		6.95		6.82		3.31		2.87		3.27	
Na ₂ O	0.65		0.39		0.49		0.36		0.42		0.49		0.23		0.22		0.38		5.80		5.98		0.10		0.09		0.12	
K ₂ O	99.68		99.26		99.37		99.65		99.41		99.86		99.55		100.16		100.66		99.69		99.63		98.60		99.78		99.11	
Total																												
Formula based on 8 oxygens																												
Si	2.540		2.400		2.483		2.396		2.421		2.476		2.274		2.301		2.418		2.948		2.947		2.288		2.226		2.276	
Al	1.441		1.563		1.491		1.565		1.537		1.494		1.690		1.664		1.531		1.048		1.048		1.693		1.751		1.702	
Fe ⁺³	0.012		0.026		0.014		0.028		0.029		0.019		0.025		0.021		0.032		0.006		0.005		0.016		0.018		0.020	
Ti	0.000		0.000		0.000		0.000		0.000		0.000		0.000		0.000		0.000		0.000		0.000		0.000		0.000		0.000	
Fe ⁺²	0.000		0.000		0.000		0.000		0.000		0.000		0.000		0.000		0.000		0.000		0.000		0.000		0.000		0.000	
Mn	0.461		0.597		0.512		0.604		0.580		0.525		0.730		0.707		0.606		0.055		0.059		0.709		0.765		0.715	
Ca	0.524		0.418		0.500		0.412		0.429		0.476		0.286		0.312		0.402		0.604		0.594		0.297		0.256		0.292	
Ni	0.038		0.023		0.028		0.021		0.024		0.028		0.014		0.013		0.022		0.332		0.342		0.006		0.005		0.007	
K	3.993		3.989		3.988		3.989		3.987		3.989		3.989		3.986		3.981		4.002		4.000		3.997		3.995		3.998	
Z	1.023		1.038		1.040		1.037		1.033		1.029		1.030		1.032		1.030		0.991		0.995		1.012		1.026		1.014	
X	51.3		40.3		48.0		39.8		41.5		46.3		27.8		30.3		39.0		60.9		59.7		29.4		24.9		28.8	
Ab	45.0		57.5		49.3		58.2		56.1		50.9		70.9		68.5		58.9		5.6		5.9		70.0		74.6		70.5	
An	3.7		2.2		2.7		2.0		2.4		2.8		1.3		1.2		2.1		33.5		34.4		0.6		0.5		0.7	

* Total iron given as Fe₂O₃
 PH = phenocryst, GM = groundmass, C = core, R = rim

FELDSPARS

Sample: Formation:	SE79A-2-1		SE140-A-2		SE140-B-4		SE140-C-6		SE140-C-7	
	Edziza	Nodule	Edziza	Xenolith	Edziza	Xenolith	Edziza	Xenolith	Edziza	Xenolith
Type:										
SiO ₂	49.70	49.71	65.61	65.68	65.66	65.66	65.66	65.66	66.09	66.09
Al ₂ O ₃	31.26	30.92	20.36	20.24	20.83	20.83	20.40	20.83	20.40	20.40
TiO ₂	0.00	0.00	0.06	0.05	0.02	0.02	0.02	0.02	0.03	0.03
Fe ₂ O ₃ *	0.48	0.51	0.19	0.26	0.20	0.20	0.18	0.20	0.18	0.18
FeO*	0.00	0.00	0.00	0.00	0.00	0.00	0.00	0.00	0.00	0.00
MnO	14.64	14.63	1.45	1.23	1.52	1.52	1.29	1.52	1.29	1.29
CaO	3.02	3.09	6.03	5.79	6.07	6.07	5.79	6.07	5.79	5.79
K ₂ O	0.11	0.09	5.04	6.58	5.92	5.92	6.56	5.92	6.56	6.56
Total	99.21	98.95	99.74	99.83	100.22	100.22	100.34	100.22	100.34	100.34
Formula based on 8 oxygens										
Si	2.287	2.294	2.936	2.941	2.923	2.923	2.943	2.923	2.943	2.943
Al	1.695	1.681	1.074	1.068	1.093	1.093	1.070	1.093	1.070	1.070
Fe ⁺³	0.017	0.018	0.006	0.009	0.007	0.007	0.006	0.007	0.006	0.006
Ti	0.000	0.000	0.002	0.002	0.001	0.001	0.001	0.001	0.001	0.001
Fe ⁺²	0.000	0.000	0.000	0.000	0.000	0.000	0.000	0.000	0.000	0.000
Fe ⁺²	0.000	0.000	0.000	0.000	0.000	0.000	0.000	0.000	0.000	0.000
Mn	0.722	0.723	0.070	0.059	0.072	0.072	0.061	0.072	0.061	0.061
Ca	0.269	0.276	0.523	0.503	0.524	0.524	0.500	0.524	0.500	0.500
Ni	0.006	0.005	0.345	0.376	0.336	0.336	0.373	0.336	0.373	0.373
K										
Z	3.999	3.993	4.016	4.018	4.023	4.023	4.019	4.023	4.019	4.019
X	0.997	1.004	0.938	0.938	0.932	0.932	0.934	0.932	0.934	0.934
Ab	27.0	27.5	55.8	53.6	56.2	56.2	53.5	56.2	53.5	53.5
An	72.4	72.0	7.4	6.3	7.8	7.8	6.6	7.8	6.6	6.6
Or	0.6	0.5	36.8	40.1	36.0	36.0	39.9	36.0	39.9	39.9

* Total iron given as Fe₂O₃
 PH = phenocryst, GM = groundmass, C = core, R = rim

OPAQUE OXIDES

Sample:	SE31-4-5	SE32-1-3	SE44-1-1	SE44-1-3	SE46-2-3	SE46-2-4	SE66-4-2	SE74-3-3	SE3-2-2	SE3-2-3	SE10-3-1	SE10-3-2	SE11-5-3	SE11-5-4	SE75-4-2	SE77-1-3
Formation:	Raspberry	Raspberry	Ice Peak	Ice Peak	Ice Peak	Ice Peak	Edziza	Edziza	Big Raven	Big Raven	Big Raven	Big Raven	Big Raven	Big Raven	Edziza	Edziza
Type:	PH	GM	PHC	PHR	GM	GM	PH	GM	PHC	PHR	PHC	PHR	PHC	PHC	Nodule	Nodule
SiO ₂	0.11	0.12	0.23	0.35	0.15	0.18	0.28	0.23	0.08	0.15	0.06	0.08	0.14	0.14	0.23	0.22
TiO ₂	51.16	52.06	13.29	12.82	23.55	24.08	20.06	17.14	49.77	28.30	49.40	49.47	23.11	23.25	16.30	23.39
Al ₂ O ₃	0.04	0.08	0.92	0.83	1.40	1.23	0.56	0.48	0.41	2.03	0.47	0.46	3.16	3.15	1.75	2.74
Cr ₂ O ₃	0.04	0.04	0.02	0.02	0.10	0.17	0.00	0.02	0.02	0.15	0.01	0.02	0.00	0.00	0.00	0.02
FeO*	46.58	44.04	79.10	77.53	70.94	70.23	72.18	75.44	44.05	64.65	44.38	44.58	65.70	65.64	75.86	67.35
MnO	0.51	0.60	0.90	0.93	0.91	0.93	0.96	0.93	0.49	0.62	0.49	0.48	0.49	0.51	1.00	0.55
MgO	2.00	3.25	0.17	0.12	0.81	0.77	0.25	0.13	4.36	2.91	4.19	4.24	3.93	4.00	0.48	3.51
CaO	0.05	0.04	0.01	0.00	0.18	0.13	0.02	0.13	0.05	0.03	0.02	0.04	0.03	0.00	0.02	0.02
Total	100.49	100.23	94.64	92.50	98.04	97.72	94.31	94.50	99.23	98.84	99.05	99.37	96.57	96.69	95.64	97.80

Formula based analyses

Ulvospinel Basis:

Fe ₂ O ₃	-	-	42.29	40.08	22.07	20.76	27.03	33.38	-	13.15	-	-	21.57	21.42	34.57	21.97
FeO	-	-	40.91	41.46	51.08	51.55	47.86	45.40	-	52.82	-	-	46.29	46.36	44.76	47.58
Total	-	-	98.74	96.52	100.25	99.80	97.02	97.85	-	100.16	-	-	98.73	98.84	99.10	100.00

Ilmenite Basis:

Fe ₂ O ₃	3.36	2.56	49.97	48.93	37.89	36.97	40.64	45.01	5.36	32.14	5.58	5.75	37.09	37.04	45.63	37.75
FeO	43.55	41.73	34.14	33.50	36.84	36.97	35.61	34.94	39.23	35.73	39.36	39.41	32.33	32.31	34.80	33.38
Total	100.83	100.49	99.65	97.40	101.84	101.42	98.38	99.01	99.77	102.06	99.61	99.95	100.29	100.40	100.21	101.58

PH = phenocryst, GM = groundmass, C = core, R = rim

* Total iron expressed as FeO

APPENDIX 2

Whole-rock chemistry

Sample	AR51	AR71	AR83	AR87	AR2636	AR2656	AR2667	AR2668	AR2870	AR2878	AR2881	AR2883	AR2884	AR2885	AR2894	AR2896	BR9	BR61	BR67	BR920	CH37	CH41
SiO ₂	70.60	46.40	70.10	72.10	45.60	44.40	47.80	48.00	79.70	78.60	78.00	76.70	77.50	46.10	66.60	66.80	47.90	50.60	48.40	47.60	46.80	48.40
TiO ₂	0.34	3.14	0.25	0.38	3.29	4.05	2.40	2.45	0.32	0.34	0.33	0.07	0.32	3.16	0.37	0.23	2.49	2.09	2.04	1.44	2.66	2.84
Al ₂ O ₃	12.80	14.50	15.40	10.80	14.60	13.00	13.80	13.90	8.90	8.40	8.80	8.80	8.40	13.90	14.30	15.10	15.70	16.90	16.80	13.80	16.50	17.10
Fe ₂ O ₃	3.80	4.90	1.70	3.50	2.40	5.80	3.00	2.10	2.70	3.10	1.70	1.40	1.00	5.90	1.50	2.20	1.60	1.10	0.90	0.21	4.90	2.90
FeO	0.0	8.60	0.50	2.70	11.10	9.20	10.40	10.40	1.90	1.50	2.80	3.10	3.40	8.00	4.00	1.90	10.40	8.80	9.90	1.20	7.20	9.00
MnO	0.11	0.18	0.01	0.10	0.19	0.28	0.40	0.30	0.04	0.05	0.08	0.0	0.07	0.15	0.15	0.11	0.19	0.16	0.16	0.19	0.18	0.16
MgO	0.27	6.09	0.39	0.27	5.50	3.40	1.60	1.80	0.30	0.40	0.40	0.40	0.30	6.90	0.40	0.30	6.48	5.08	7.54	16.00	6.53	5.50
CaO	0.16	9.51	0.21	0.45	10.20	9.10	6.80	7.30	0.30	0.30	0.20	0.30	0.30	8.10	1.50	1.40	9.58	8.28	10.90	6.70	9.71	7.76
NaO	5.50	3.20	6.10	3.70	2.80	2.80	3.50	3.60	4.10	4.40	4.50	4.90	5.40	2.90	5.40	5.50	3.50	4.30	3.00	3.00	3.00	4.00
K ₂ O	4.90	0.79	5.53	4.91	0.80	1.20	2.20	2.30	3.30	3.20	3.20	3.20	3.10	0.80	4.70	4.90	1.20	1.91	0.69	9.00	1.09	1.56
P ₂ O ₅	0.06	0.35	0.05	0.04	0.35	1.74	1.08	1.12	0.0	0.0	0.0	0.0	0.0	0.40	0.02	0.05	0.46	0.45	0.26	0.0	0.54	0.54
H ₂ O	0.0	0.20	0.0	0.0	0.30	2.20	5.50	4.80	0.0	0.0	0.10	1.00	0.0	0.0	1.00	0.0	0.0	0.0	0.0	0.0	0.0	0.0
CO ₂	0.60	2.00	0.40	0.70	1.30	2.70	1.90	1.10	0.90	0.70	0.60	0.0	0.30	3.50	0.50	0.90	0.10	0.30	0.0	0.0	0.50	0.80
Ba (ppm)	n.d.	<Det	n.d.	n.d.	n.d.	n.d.	n.d.	n.d.	n.d.	n.d.	n.d.	n.d.	<Det	n.d.	n.d.	514	n.d.	n.d.	<Det	n.d.	n.d.	176
Rb	n.d.	<Det	n.d.	n.d.	n.d.	n.d.	n.d.	n.d.	130	n.d.	n.d.	n.d.	124	n.d.	n.d.	91	n.d.	n.d.	<Det	n.d.	n.d.	19
Sr	4	56	<Det	2	45	34	24	11.	2	<Det	3	n.d.	<Det	50.	2	2	51	23	53	19	117	93
Y	n.d.	16	n.d.	n.d.	n.d.	n.d.	n.d.	n.d.	76	n.d.	n.d.	n.d.	63	n.d.	n.d.	33	n.d.	n.d.	15	n.d.	n.d.	21
Cr	<Det.	50	<Det.	<Det.	23	<Det.	2	<Det.	<Det.	<Det.	<Det.	<Det.	3	22	2	2	92	49	13	131	77	21
Ni	<Det.	31	<Det.	<Det.	30	6	<Det.	<Det.	<Det.	<Det.	<Det.	<Det.	<Det.	22	22	<Det.	42	27	49	403	64	28
Co	<Det.	24	<Det.	<Det.	23	21	13	11.	<Det.	<Det.	<Det.	n.d.	<Det.	22	<Det.	<Det.	25	18	26	57	26	29
Cu	<Det.	35	2	<Det.	44	20	35	14.	2	2	n.d.	<Det.	23	3	5	55	42	38	38	42	24	
Zn	172	80	188	220	79	90	73	77.	195	145	130	n.d.	22	85	137	86	84	73	61	76	70	92
V	12.	159	<Det.	3	117	65	16	15	3.	3	6.	n.d.	<Det.	134	<Det.	<Det.	119	64	61	56	98	130
Cd	<Det.	3	<Det.	<Det.	4	3	4	3.	<Det.	<Det.	3	n.d.	<Det.	2	<Det.	<Det.	3	3	3	4	3	4
La	97	9	33	52	9.	22	25	26.	157	28	187.	n.d.	3	16	54	94	18.	20	7	6	20	25
Th	7	<Det.	9	9	<Det.	<Det.	<Det.	<Det.	6	8.	3	n.d.	<Det.	<Det.	<Det.	9	<Det.	<Det.	<Det.	<Det.	<Det.	<Det.

Sample	EZ1	EZ4	EZ7	EZ12	EZ15	EZ68	IP2	IP11	IP21	IP45	IP72	IP75	IP89	IP2640	IP2646	IP2648	IP2679	IP2680	IP2681	IP2684	IP2687	KI92
SiO ₂	62.90	60.70	57.00	60.70	62.30	63.00	59.40	61.50	56.50	54.00	59.80	46.80	52.90	48.30	47.10	45.60	53.70	56.30	51.70	49.30	46.60	46.10
TiO ₂	0.50	0.43	1.28	0.45	0.65	0.43	0.39	0.52	1.28	1.40	0.62	3.15	1.72	2.09	2.24	2.19	1.74	1.08	2.16	2.53	2.93	2.68
Al ₂ O ₃	14.80	15.00	16.20	15.30	16.90	15.30	19.20	16.90	17.40	16.40	17.50	15.40	18.70	17.90	15.90	16.10	17.10	17.10	17.10	16.00	15.90	16.50
Fe ₂ O ₃	4.80	3.00	1.40	3.70	2.90	3.70	2.70	2.60	2.10	1.40	2.60	1.50	4.80	4.90	4.90	7.40	2.90	2.90	3.00	9.20	3.20	2.40
FeO	3.00	5.10	6.60	4.40	2.70	3.80	2.00	3.50	5.90	7.10	3.50	10.50	3.30	6.40	4.80	5.70	5.00	6.20	3.60	9.20	9.00	9.10
MnO	0.21	0.23	0.20	0.21	0.15	0.18	0.11	0.15	0.17	0.20	0.14	0.18	0.09	0.12	0.13	0.13	0.16	0.17	0.19	0.17	0.15	0.20
MgO	0.28	0.43	1.46	0.37	0.73	0.25	0.48	0.51	1.64	1.89	0.63	4.92	1.96	5.20	5.10	4.80	2.10	1.60	2.30	3.90	6.80	5.34
CaO	1.57	1.72	3.85	1.67	1.48	1.19	1.65	1.62	3.54	4.76	2.03	9.58	6.57	9.80	11.20	10.90	5.80	4.60	6.30	8.60	8.40	9.87
NaO	6.60	6.20	5.40	7.70	6.60	7.10	7.50	6.40	6.40	5.90	6.60	3.30	4.70	3.60	2.70	2.90	4.70	5.30	5.10	3.90	3.80	3.30
K ₂ O	5.13	4.94	4.09	5.03	5.78	4.68	5.17	5.61	4.18	3.54	5.24	0.87	2.76	0.90	0.90	0.90	2.70	2.10	2.80	1.60	1.40	1.15
P ₂ O ₅	0.08	0.07	0.37	0.12	0.14	0.06	0.13	0.11	0.31	0.44	0.14	0.39	0.37	0.30	0.30	0.30	0.38	0.16	0.53	0.78	0.49	0.45
H ₂ O	0.0	0.0	1.80	0.0	0.0	0.0	0.0	0.0	0.10	2.70	0.0	1.70	0.0	0.0	1.40	0.70	1.90	1.90	1.50	0.90	0.0	1.50
CO ₂	0.40	1.50	0.20	0.20	0.30	0.70	0.40	0.50	0.50	0.70	0.70	1.70	2.40	1.30	0.80	1.80	0.70	0.80	0.70	0.50	0.30	1.30
Ba (ppm)	n.d.	148	n.d.	n.d.	n.d.	n.d.	n.d.	<Det.	678	n.d.	n.d.	<Det.	n.d.	n.d.	n.d.	n.d.	703	<Det.	n.d.	n.d.	n.d.	<Det.
Rb	n.d.	90	n.d.	n.d.	n.d.	n.d.	n.d.	66	53	n.d.	n.d.	n.d.	n.d.	n.d.	n.d.	n.d.	n.d.	n.d.	n.d.	n.d.	n.d.	n.d.
Sr	<Det.	3.	16.	<Det.	<Det.	2.	3.	<Det.	14	21.	8.	55.	128.	107.	n.d.	87.	28.	26.	23.	38.	40.	70.
Y	n.d.	45	n.d.	n.d.	n.d.	n.d.	n.d.	27	30	n.d.	n.d.	16	n.d.	n.d.	n.d.	n.d.	23	30	n.d.	n.d.	n.d.	19
Cr	<Det.	2	7.	<Det.	<Det.	<Det.	<Det.	<Det.	9	22.	<Det.	49	40	34	<Det.	8.	20	24.	5	18.	52.	54
Ni	<Det.	<Det.	3.	<Det.	<Det.	<Det.	<Det.	<Det.	5	12	<Det.	24	14	44	<Det.	34	11.	13	4	10	63	30
Co	<Det.	<Det.	5.	<Det.	<Det.	<Det.	<Det.	6	7	<Det.	21.	8.	21	n.d.	23.	11.	5.	10.	10.	26.	24	
Cu	8	7.	10.	8.	9.	4.	9	8	14	16	9	32	24	31	n.d.	66	20.	39.	24.	21.	42.	38.
Zn	134	198	95	114.	93	242	82	95	114	104.	103	78	89	53	n.d.	58.	88.	108.	83	48.	63.	77
V	<Det.	<Det.	24	<Det.	<Det.	2	<Det.	<Det.	35	26	5	138	70	55	n.d.	46	57.	37.	51	53.	83.	126
Cd	<Det.	<Det.	2	<Det.	<Det.	<Det.	<Det.	<Det.	2	2	2	3	3	2	n.d.	2	2.	2	2	<Det.	2	4
La	66	74.	29	80.	42	90	41	46	43	39	44	9	39	9	n.d.	13	25.	36.	34	20.	20.	13
Th	6	8	<Det.	4	4	5	8	5	4	3	6	<Det.	5	<Det.	n.d.	<Det.	<Det.	<Det.	2	<Det.	<Det.	<Det.

Sample	KI99	KI100	KK6	KK19	KK2877	KI62	Ko2886	LI48	LI55	LI58	LI81	NI23	NI39	NI42	NI43	NI44	NI46	NI73	NI91	NI2651	NI2655	NI2669
SiO ₂	46.40	45.90	61.90	57.70	63.20	52.40	47.20	51.20	48.80	51.90	50.30	45.60	45.70	46.20	46.30	49.10	48.70	45.60	47.40	46.60	46.30	45.80
TiO ₂	2.88	2.4																				

APPENDIX 2 (cont.)

Sample	NI2673	NI2675	NI2676	NI2677	PR59	PY13	PY25	PY95	PY96	PY98	RA36	RA52	RA54	RA56	RA57	RA77	RA78	RA80	RA2662	RA2664	SP17	SP26
SiO ₂	46.60	43.90	44.70	45.60	47.20	73.70	74.20	73.60	74.80	73.20	45.00	47.60	46.00	46.10	46.90	45.30	49.40	46.00	46.50	46.50	75.30	74.90
TiO ₂	3.06	3.14	3.18	2.44	1.90	0.14	0.14	0.38	0.14	0.40	3.36	2.49	3.01	2.27	2.44	3.10	2.30	2.84	2.59	3.01	0.17	0.17
Al ₂ O ₃	15.60	15.20	15.50	18.20	16.20	12.60	12.80	9.70	12.50	10.10	16.20	16.50	16.40	16.20	16.20	16.10	18.30	17.00	16.20	18.70	11.50	11.70
Fe ₂ O ₃	0.90	3.40	4.00	3.10	3.10	0.90	0.70	1.50	2.20	4.30	3.60	3.30	5.20	3.70	1.70	2.50	4.00	2.80	2.20	3.50	1.10	0.60
FeO	11.70	9.80	9.50	8.00	8.40	1.40	1.60	3.70	0.30	1.50	9.60	8.00	7.70	8.10	10.10	10.50	6.50	8.90	10.00	7.80	1.50	2.00
MnO	0.20	0.21	0.20	0.17	0.18	0.03	0.04	0.10	0.30	0.09	0.17	0.15	0.21	0.23	0.21	0.19	0.16	0.18	0.19	0.17	0.05	0.05
MgO	3.40	3.80	4.30	4.30	7.53	0.32	0.16	0.26	0.18	0.30	6.41	6.66	3.24	6.91	5.75	4.99	2.89	4.84	2.70	2.60	0.13	0.17
CaO	7.20	8.90	8.20	9.80	10.70	0.30	0.31	0.31	0.07	0.29	8.23	8.96	8.10	8.80	9.02	8.96	7.83	8.97	7.70	8.70	0.26	0.28
NaO	4.10	3.60	3.80	3.50	2.80	5.20	5.50	5.30	4.90	3.90	3.00	3.10	3.90	2.70	2.80	3.20	4.10	3.20	3.70	3.60	4.40	4.70
K ₂ O	1.80	1.40	1.50	1.10	0.66	4.52	4.60	4.42	4.57	4.52	1.31	1.11	1.39	0.93	0.99	1.17	1.67	1.26	2.00	1.30	4.49	4.52
P ₂ O ₅	0.58	0.57	0.55	0.31	0.24	0.02	0.03	0.05	0.05	0.04	0.46	0.40	0.62	0.35	0.34	0.49	0.81	0.47	1.19	0.50	0.04	0.04
H ₂ O	4.10	4.70	3.90	3.20	0.50	0.0	0.0	0.0	0.0	0.0	0.0	0.0	2.70	1.00	3.10	2.20	1.20	2.10	3.80	3.20	0.0	0.0
CO ₂	1.30	1.30	0.90	1.20	0.20	0.10	0.20	0.50	0.0	1.30	2.60	1.90	1.30	3.20	0.80	1.80	1.00	2.10	1.20	1.00	0.10	0.10
Ba (ppm)	nd	nd	nd	nd	nd	nd	nd	nd	3	<Det	nd	44	nd	nd	nd	nd	nd	nd	nd	nd	nd	<Det
Rb	nd	nd	nd	nd	nd	nd	nd	nd	25	123	nd	2	nd	nd	nd	nd	nd	nd	nd	nd	nd	199
Sr	41	128	48	90	75	<Det	<Det	<Det	<Det	3	219	120	73	172	123	71	77	85	48	75	<Det	<Det
Y	nd	nd	nd	nd	nd	nd	nd	nd	nd	35	nd	16	nd	nd	nd	nd	nd	nd	nd	nd	nd	69
Cr	<Det	4	2	13	28	<Det	<Det	<Det	<Det	<Det	34	60	6	40	10	12	3	23	2	5	<Det	<Det
Ni	2	9	10	20	79	<Det	<Det	<Det	2	<Det	34	38	14	32	26	24	7	25	5	10	<Det	<Det
Co	20	24	25	24	29	<Det	<Det	<Det	nd	<Det	29	28	28	29	30	35	17	25	17	24	<Det	<Det
Cu	23	46	36	39	63	<Det	<Det	<Det	nd	<Det	28	25	23	21	16	31	18	26	26	41	2	<Det
Zn	88	90	82	74	66	3	7	5	19	138	82	88	79	78	111	79	66	73	73	79	5	4
V	49	84	86	92	62	<Det	<Det	<Det	nd	6	134	129	105	106	65	93	44	93	24	76	<Det	<Det
Cd	5	5	4	4	3	<Det	<Det	<Det	nd	<Det	4	3	3	3	2	4	3	4	4	3	<Det	<Det
La	25	18	20	12	10	<Det	<Det	<Det	nd	37	17	16	21	14	13	12	21	14	26	16	2	<Det
Th	<Det	<Det	<Det	<Det	<Det	<Det	<Det	<Det	nd	10	<Det	<Det	<Det	<Det	<Det	<Det	<Det	<Det	<Det	<Det	<Det	<Det

Sample	SP28	SP29	SP31	SP32	SP34	SP2872	SP88
SiO ₂	62.40	75.70	68.30	69.60	66.40	71.90	59.90
TiO ₂	0.64	0.18	0.51	0.37	0.61	0.50	0.27
Al ₂ O ₃	14.40	12.10	12.80	13.40	13.50	8.60	18.00
Fe ₂ O ₃	4.70	1.70	5.30	2.20	4.40	4.20	1.20
FeO	3.70	0.0	1.50	2.40	3.10	3.20	3.40
MnO	0.20	0.0	0.21	0.11	0.14	0.11	0.13
MgO	0.32	0.27	0.45	0.23	0.26	0.60	0.61
CaO	1.36	0.23	0.66	0.62	0.60	0.70	1.09
NaO	7.10	3.00	6.20	6.10	5.90	5.00	8.30
K ₂ O	4.80	4.87	4.43	4.99	4.66	3.20	5.18
P ₂ O ₅	0.10	0.04	0.06	0.05	0.06	0.05	0.09
H ₂ O	0.0	0.0	0.0	0.0	0.0	0.0	0.0
CO ₂	0.40	0.90	0.30	0.20	0.50	1.90	1.30
Ba (ppm)	nd	<Det	nd	nd	<Det	nd	nd
Rb	nd	222	nd	nd	119	nd	nd
Sr	<Det	<Det	2	<Det	<Det	8	2
Y	nd	71	nd	nd	50	nd	nd
Cr	<Det	<Det	2	<Det	<Det	<Det	2
Ni	<Det	<Det	<Det	<Det	<Det	<Det	<Det
Co	<Det	<Det	<Det	<Det	<Det	<Det	<Det
Cu	3	<Det	<Det	2	5	3	3
Zn	80	80	205	64	224	242	36
V	<Det	<Det	4	<Det	<Det	3	3
Cd	<Det	<Det	<Det	<Det	<Det	<Det	<Det
La	66	194	99	114	89	195	22
Th	2	5	12	7	3	5	2

APPENDIX 3

Rare-earth elements

Sample No.	La ppm	Nd ppm	Sm ppm	Ce ppm	Lu ppm	Eu ppm	Yb ppm	Tb ppm
11	46	40	11.1	84	1.0	1	3	1
21	48	25	12.5	82	1.0	4	3	2
26	93	65	25.1	182	2.0	<1	10	3
29	155	130	34.2	234	2.0	1	9	4
32	102	95	28.0	189	1.0	2	9	4
36	19	20	7.9	38	<1.0	3	1	1
48	25	20	9.9	53	<1.0	3	2	1
67	11	5	5.2	17	<1.0	1	1	1
68	103	75	25.9	201	1.0	3	8	4
2679	33	15	10.2	54	<1.0	3	2	3

APPENDIX 4a

HotSpring data (Physical and Geochemical Data)

Sample	Location(1)	Temp. (°C)	Flow(2) (L/s)	EC(3) (S/cm)			Field pH	Lab	Eh(4) (mV)	DO(5) (mg/L)	HS(6) (mg/L)	SiO ₂										
				Field	Lab	Field						HCO ₃ (7)	SO ₄ (8)	Cl	F	Br	Na*	K*	Ca ²⁺ *	Mg ²⁺ *	Total	Reac.
E1	Eiwyn HotSpring Vent #1	19.5	0.3	1805	1680	6.19	6.82	-10	7.35	LD	1374	1.02	36.6	0.31	LD	345	29	71.8	60.6	83.4	-	2005
E2	Eiwyn HotSpring Vent #2	29.0	0.3	2300	2772	6.06	6.64	-75	2.3	LD	2126	1.93	68.3	0.19	LD	501	41	122	102	118	-	3083
E3	Eiwyn Spring Vent #5	36.0	0.1	2780	2976	6.01	7.14	-100	0.8	LD	2512	0.62	51.0	0.25	LD	659	49	126	104	134	63.2	3639
T1	Taweh HotSpring Man Vent	45.9	0.3	3005	3288	6.59	6.71	-150	0.6	LD	2455	1.78	61.2	0.16	LD	529	62	171	136	144	61.7	3469
T2	Taweh Mushroom	43.0	0.3	3000	3240	6.75	6.77	-130	1.3	LD	2401	1.83	63.2	0.11	LD	529	63	170	138	144	-	3516
I3	Taweh South HotSpring	46.0	0.3	2900	2916	6.31	6.72	-103	0.9	LD	2088	1.59	58.2	0.09	LD	444	54	143	116	122	-	3033
MC1	Moss Creek HotSpring Vent #1	42.5	0.5	2400	2160	6.20	7.40	-260	0.11	2.5	441	150	209	1.7	LD	190	18	138	20.4	44.5	43.8	1216
ML1	Moss Lake Spring	13.0	0.01	4800	4416	6.69	6.54	+115	4.65	LD	2243	560	526	0.38	LD	950	44	361	94.7	51.8	-	4858
Detection Limits												1	0.05	0.1	0.05	0.03	0.2	0.2	0.05	0.005	1	1

Al	As	Ba	B	Co	Cr	Cu	Total	Diss	Hg	Li	Total	Diss	Mo	Ni	Pb	Sb	Se	Sr	Ti	Zn	Mr	
																					Fe	Mr
0.14	0.0027	0.116	0.96	LD	LD	LD	1.06	0.009	LD	0.35	0.032	0.029	0.02	LD	LD	LD	LD	0.0008	0.384	0.002	LD	LD
0.16	0.0038	0.197	1.34	LD	0.004	LD	1.01	0.97	0.00010	0.53	0.14	0.115	LD	LD	LD	LD	LD	0.002	0.634	LD	LD	LD
0.17	0.0081	0.295	1.73	LD	0.004	LD	2.50	1.0	0.00005	0.66	0.068	0.058	0.02	0.01	LD	0.07	0.0007	0.684	LD	LD	LD	LD
0.16	0.019	0.405	1.34	LD	0.004	LD	4.51	0.97	0.00006	0.56	0.057	0.115	LD	LD	LD	LD	0.002	1.30	LD	LD	LD	LD
0.16	0.018	0.389	2.16	LD	0.004	0.007	2.50	1.37	0.00005	0.58	0.037	0.038	LD	LD	LD	LD	LD	1.24	LD	LD	LD	LD
0.17	0.015	0.342	1.82	0.01	0.004	0.005	5.07	2.31	LD	0.48	0.21	0.233	LD	LD	LD	LD	LD	0.0001	1.06	LD	LD	LD
0.34	0.024	0.073	13.8	LD	LD	LD	LD	LD	LD	0.31	0.17	0.152	LD	LD	LD	LD	LD	0.0007	2.85	LD	0.007	LD
0.25	0.0006	0.016	0.92	0.01	0.005	0.011	7.10	LD	0.0010	1.11	0.42	0.072	LD	LD	0.002	LD	LD	0.0002	9.74	LD	LD	LD
0.05	0.2	0.001	0.01	0.01	0.002	0.005	0.002	0.003	0.00005	0.05	0.001	0.001	0.01	0.01	0.001	0.05	0.0001	0.0001	0.001	0.001	0.005	0.005

- NOTES
1. See Figure 189.
 2. Estimated visually in field.
 3. Electrical conductivity.
 4. Oxidation reduction potential (Redox, in millivolts).
 5. Dissolved oxygen.
 6. Sulphide (AS HS⁻ or H₂S) measured by colour matching test solution.
 7. Total alkalinity expressed as bicarbonate. Titration done in field.

APPENDIX 4b

HotSpring data (Isotope Data)

Sample	Date/Time	Location	Elevation (ft. asl)	Estimated Flow (L/s)	Temp (°C)	Oxygen-18 (‰ SNOW)	Deuterium (‰ SNOW)	Tritium ⁽¹⁾ (TU)	¹³ C (DIC)	¹³ C ⁽²⁾ (CO ₂)	log pCO ₂
E1	83-08-09/14:00	Elwyn HotSpring Vent #1	4700	0.3	19.5	-20.7	-166	12.6	-0.8	-5.0	-0.49
E2	83-08-09/20:28	Elwyn HotSpring Vent #2	4720	0.3	29.0	-22.0	-161	4.5	-1.9	-5.5	0.23
E3	83-08-10/21:18	Elwyn HotSpring Vent #3	4680	0.1	36.0	-21.8	-174	3.0	-1.2	-4.4	0.39
E4	83-08-10/15:30	Elwyn HotSpring Vent #4	4660	0.1	27.0	-21.9	-171	ND ± 8			
E5	83-08-11/09:10	Elwyn HotSpring Vent #5	4540	0.1	28.8	-21.8	-171	ND ± 8			
E6	83-08-09/18:33	Elwyn Cold Spring #1	4700	0.05	6.0	-20.0	-160	-			
E7	83-08-10/13:04	Elwyn Cold Spring #2	5700	0.1	8.0	-21.5	-163	-			
E8	83-08-09/19:15	Elwyn Creek #1	5400	-	-	-20.2	-165	-			
E9	83-08-10/12:08	Elwyn Creek #2	5400	-	-	-20.3	-164	-			
E10	83-08-10/12:33	Elwyn Creek #3	5650	-	-	-21.9	-164	-			
E11	83-08-10/15:45	Elwyn Creek #4	6500	-	-	-21.8	-168	-			
E12	83-08-10/15:30	Elwyn Glacier #1	6900	-	-	-28.4	-225	-			
E13	83-08-10/15:40	Elwyn Glacier #2	6600	-	-	-22.1	-172	-			
E14	83-08-10/10:00	Elwyn Precipitation	4700	-	-	-16.1	-142	-			
T1	83-08-14/18:42	Taweh HotSpring Main Vent	4400	0.2	45.9	-22.0	-171	6.3	-2.4	-6.7	-0.14
T2	83-08-14/16:56	Taweh HotSpring Mushroom	4400	0.3	43.0	-21.9	-174	5.8	-1.3	-6.2	-0.33
T3	83-08-14/13:33	Taweh South HotSpring	4400	0.1	46.0	-22.0	-172	5.7	-2.0	-5.6	0.08
T4	83-08-14/14:18	Taweh HotSpring Vent #4	4400	0.5	45.1	-22.1	-170	-			
T5	83-08-14/17:11	Taweh Upper Spring #5	4500	0.05	30.1	-21.9	-170	-			
T6	83-08-14/17:39	Taweh Upper Spring #6	4600	0.08	20.0	-21.8	-170	-			
T7	83-08-14/11:30	Taweh East Spring #7	4480	0.05	25.1	-21.8	-176	-			
T8	83-08-13/12:35	Taweh East Spring #8	4540	0.1	21.0	-21.7	-173	8 ± 8			
T9	83-08-12/13:20	Taweh Cold Spring #1	5640	0.1	0.5	-19.2	-152	-			
T10	83-08-13/11:11	Taweh Cold Spring #2	4900	0.2	< 5.0	-21.3	-165	18 ± 8			
T11	83-08-12/14:02	Taweh Creek #1	5780	-	-	-18.6	-150	-			
T12	83-08-12/15:51	Taweh Creek #2	6300	-	-	-19.5	-165	-			
T13	83-08-12/20:10	Taweh Creek #3	6100	-	-	-21.5	-178	-			
T14	83-08-13/10:08	Taweh Creek #4	5240	-	-	-21.4	-170	-			
T15	83-08-15/07:20	Taweh Creek #7	4420	-	-	-20.6	-169	-			
T16	83-08-14/19:33	Taweh Creek #8	4400	-	-	-20.5	-165	32.9			
T17	83-08-12/18:54	Taweh Glacier #1	6900	-	-	-19.9	-159	-			
T18	83-08-12/19:46	Taweh Glacier #2	6400	-	-	-20.2	-163	-			
MC1	83-08-15/10:13	Mess Creek HotSpring #1	2350	0.5	42.5	-20.4	-164	10.7	-5.2	-8.70	-0.49
MC2	83-08-15/10:46	Mess Creek HotSpring #2	2350	0.5	42.5	-20.7	-157	-			
MC3	83-08-15/13:12	Mess Creek	2340	-	-	-19.2	-148	-			
MC4	83-08-15/14:13	Mess Creek Inflow (West)	2330	-	-	-19.2	-154	-			
MC5	83-08-15/17:00	Mess Creek Inflow (East)	2330	-	-	-19.5	-154	-			
ML1	83-08-17/13:27	Mess Lake Spring #1	2520	0.01	13.0	-18.6	-166	5.1	-1.2	-7.68	-0.49
ML2	83-08-17/17:32	Mess Lake Spring #3	2500	0.01	14.0	-19.0	-163	-			
ML3	83-08-17/18:41	Mess Lake	2250	-	-	-18.8	-147	-			

NOTES: 1. Values determined by direct counting are shown with confidence limits. All others are determined by enriched tritium method. 1 TU = 1 ³H per 10¹⁸ ¹H.
2. ¹³C (CO₂) calculated for CO₂ gas in isotopic equilibrium with DIC.

ND = Not Detected

APPENDIX 4c

Gas Analyses

Gas Samples	O ₂	N ₂	CO ₂	CH ₄	SO ₂	H ₂
T1	0.48	2.81	97.0	<0.2	<0.05	<0.2
T2	0.23	0.77	97.7	"	"	"
T3	0.43	2.30	96.8	"	"	"
ML4	0.23	4.64	93.7	"	"	"
MC1A	1.93	84.5	13.0	"	"	"
MC1B	5.65	83.7	12.0	"	"	"
MC1	1.17	4.14	92.2	"	"	"
E1	1.68	1.86	94.6	"	"	"

All results reported as total percent.

APPENDIX 5

Source of Geographic Names

When this study was begun only a few of the physiographic features within the Mount Edziza Volcanic Complex bore geographic names. Names added to the map by the author were drawn from three main sources:

1. Local usage (unofficial names used by local people)
2. Field use (names applied for convenience during our initial field mapping)
3. Native (Tahltan) words, names or references to folklore

My main sources of Tahltan words and folklore were:

1. "A Grammar and Dictionary of the Language Spoken by the Tahltans on the Stikine River, B.C., A Tribe belonging to the Tinne Branch of North American Indians", by Charles Francis Palgrave (1868-1955), University of Chicago Library 1957.
2. "The Tahltan Indians" by G.T. Emmons, University of Pennsylvania Museum of Anthropological Publications, v. IV, no. 1, 1911.

LIST OF NEW NAMES

Arctic Plateau

After Arctic lake.

Both of the above are in common local usage.

Local usage

Artifact Creek, Ridge

Piles of chips left from the manufacture of obsidian tools and points by early Tahltan hunters are abundant in this area.

Field use

Big Raven Plateau

In Tahltan mythology, Cheskea Cho – the Big Raven was the form commonly assumed by the creator of man.

Emmons, p. 117

Cache Hill

This was the site of an air drop of food and equipment.

Field use

Camp Hill

This was the location of our first high camp from which systematic mapping was begun in 1965.

Field use

Cartoona Peak

Cartoona was an old Tahltan Shaman at the time of Emmons, visit to the Stikine area in 1904-6.

Emmons, p. 112

Chachani Creek

Several occurrences of copper mineralization were found along this tributary of Ball Creek. Name is Tahltan for copper.

Palgrave, p. 74.

Chalkima Creek

This creek terminates in a maze of beaver ponds.

Name is from Tahltan for beaver (Cha) and house (Kima).

Palgrave, p. 73, p. 160.

Destell Pass

This narrow rock cleft provides access between the broad upland valleys of Raspberry and "Artifact" creeks, both of which abound in game and evidence of early human habitation. destell is Tahltan for "going to camp".

Palgrave, p. 82.

Esja Peak and Hoyaa Peak

In 1956, while backpacking along this ridge to a camp on Bourgeaux Creek my assistant thought he suffered a heart attack and refused to go on, thus precipitating a rather traumatic search.

The Tahltan expression: "esja hoyaa" means – my heart is ailing.

Palgrave Gram. p. 16-19.

Eve Cone

After Eve Brown, the native woman who survived the snow slide that killed Jonny Edzertza and Hank Williams.

The name has been used locally for many years and, although Eve Brown is still living, the name has been used extensively in the literature.

See Beautiful B.C. Spring 1974, p. 41.

Exile Hill

An extension of the Wetalth (outcast people) theme. See also Nahta Cone and Outcast Hill.

Emmons, p. 22

Flyin Creek and Walkout Creek

In 1954, Herman Peterson, a well known bush pilot from Atlin mistook this drainage for Raspberry Pass and flew in under a low overcast. Unable to turn out of the narrow valley he crashed in the head of "Walkout Creek" and made his way back to Telegraph Creek on foot.

Field use.

Gerlib Creek

After Robert Gerlib, a student who worked with me in this area in 1958 and who, the following year, was killed in a mining accident.

Field use.

Gnu Butte

Field name used throughout our survey because of the resemblance of this flat-topped hill to those in parts of Africa.

Field use.

Hoia Bluff

Tahltan word for Sunset. Feature is a prominent west facing lookout.

Palgrave, p. 170.

Ice Peak

Mount Edziza was (and still is) known to the local Indians as "Ice Mountains". The name is preserved but restricted to the prominent ice covered south peak.

Local usage.

Idiji Glacier

Tahltan word for "it thunders", and appropriate name for this very active glacier.

Palgrave, p. 102.

Kadeya Creek

In 1956 one of my assistants precipitated a helicopter search by mistakenly following the wrong tributary of this creek, thus failing to show up at camp. The name is the Tahltan word "go after" (in search of).

Palgrave, p. 106.

Kaia Bluff

Tahltan word for Sunrise. Feature is a prominent east facing lookout.

Palgrave, p. 107, p. 170.

Kana Cone

This is a nested cinder cone in which the red, oxidized cinders of the inner cone appear hot.

"Kana" is the Tahltan word for "embers".

Palgrave, p. 150.

Kenda Cone (104G/10)

Tahltan word for Moose.

Palgrave, p. 109.

Kitsu Creek, Plateau, Peak

Tahltan word for "northern lights" (Aurora).

Palgrave, p. 114.

Kounugu Lake, Mountain

In Tahltan folklore Kounugu was guardian of fresh water, "who slept throughout the day on top of the well that contained his treasure".

Emmons, G.T., p. 118.

Kuno Peak

After Hisashi Kuno (deceased), a famous Japanese volcanologist and teacher who visited this area with me in 1966.

Field use.

Little Arctic Lake (104G/7)

As opposed to (Big) Arctic Lake, both on the same plateau. This name is already in use among locals and pilots.

Local usage.

Mess Creek Escarpment

After Mess Creek. The steep cliffs of this escarpment expose some of the best sections of volcanic stratigraphy. It is thus frequently referred to, making a formal name desirable.

Field usage.

Nagha Creek, Glacier

Tahltan for Wolverine;

So named because of regular visits by a wolverine to a sheep carcass on the ice during the time of our survey.

Palgrave, p. 126.

Nahta Cone

This feature is actually a cluster of small conelets. It is named after the last seven survivors of the WETALTH people, called Nahta.

Emmons, G.T., p. 22.

Nanook Dome (104G/10)

This word, of Tlingit origin, was adopted by the Tahltan for the hereditary head of the family.

Emmons, p. 18.

Nido Creek (104G/10, 104G/9W)

Nido is an archaic Tahltan word for "white man". Proposed for this creek because it is the location of a group of mineral claims which, because they were staked before the area was given park status, are still being actively explored by a mining group.

Palgrave, p. 129.

Obsidian Ridge (104G/7)

A source of high quality obsidian collected by early Tahltans for tool making.

Field use.

Ornostay Bluff and Koosick Bluff

According to tribal history part of the Tahltan population set out by canoe down the Stikine to find a new home on the coast. Their way was blocked by a glacier across the river but two very old women, ORNOSTAY and KOOSICK, volunteered to float under the ice bridge.

Emmons, p. 15.

Outcast Hill

An extension of the Wetalth (outcast people) theme. See also Nahta Cone and Exile Hill.

Emmons, p. 22.

180 Lake

Named by pilots because it is large enough for safe operation of the Cessna 180 float plane.

Local usage.

Pillow Ridge

The ridge is a subaqueous pile of pillow lava providing classic exposures of pillows.

Field use.

Sezill Creek

This tributary of Taweh Creek is the site of a large group of hot springs.

The name is Tahltan for "it is hot".

Palgrave, p. 132.

Shaman Creek

Shamanism was a common practice among early Tahltans.

Emmons, p. 112.

Sidas Cone

This feature is a distinctive breached cinder cone that has been cut into two symmetrical halves. Sidas is the Tahltan word for cut (oneself with a knife).

Palgrave, p. 133.

Sorcery Creek

An extension of the Witch Doctor theme (i.e. Shaman Creek, Cartoona Peak, Witch Spirit Lake).

Emmons, p. 112.

Stewbomb Creek

To commemorate the explosion of a pressure cooker full of stew in our tent while camped on this creek.

Field use.

Tadeda Peak

This brightly colored rhyolite peak has three prominent orange spots which resemble eyes. The proposed name is from the Tahltan words "Tade" (three) and "Da" (eye).

Palgrave, p. 135, p. 76.

Tadekho Creek, Hill

We were forced to move our camp from the head of this creek by a sow grizzly and two curious cubs.

Proposed name is from Tahltan "Tade" (three) and "Kho" (Grizzly bear).

Palgrave, p. 135, p. 148.

Tenchen Creek, Glacier

The glacier in this valley, though still active, is completely covered by rock debris fallen from the steep headwall and bounding spurs. Name is from the Tahltan words "Ten" (ice) and "Chen" (dirty).

Palgrave, p. 74, p. 138.

Tencho Glacier

This is the largest single glacier on the Mount Edziza Volcanic Complex. The name is from Tahltan words for big or great (cho) and ice (ten).

Palgrave, p. 75, p. 138.

Tennaya Creek, Glacier

Our field name for these features was "Ice Fall" Creek and Glacier because of the spectacular Ice Fall at the head of the valley.

Name is from Tahltan for ice (ten) and 'be come down' (naya).

Palgrave, p. 128, p. 138.

Tennena Cone

This feature is a symmetrical, subglacial volcanic cone almost completely surrounded by ice.

The name is from the Tahltan words for ice (ten) and bridge (nena). (see also ORNOSTAY and KOOSICK).

Palgrave, p. 128, p. 138.

The Ash Pit

A conical explosion crater filled with fine black volcanic ash.

Field usage.

The Pyramid

From any angle this white symmetrical lava dome resembles a pyramid.

Field usage.

Tsecha Creek

This creek heads in an area covered by loose black cinders and ash from Williams Cone.

The name is from the Tahltan words Tse (rock) and Cha (rain).

Palgrave, p. 139, p. 73.

Tsekone Ridge

This prominent, black ridge was formed by a subglacial volcanic eruption. The name is Tahltan for the native sweat-bath of woven willows. The literal translation is "stone fire".

Palgrave, p. 140.

Wetalth Ridge

This isolated ridge on the "Arctic Plateau" is named after a small, wandering and exploited group of outcasts from the Tahltan.

Emmons, G.T., p. 22.

Williams Cone

This feature, a prominent cinder cone, is the site of the snow slide that killed Jonny Edzertza and his companion Hank Williams.

Field use.

Witch Spirit Lake

An extension of the Shaman theme.

Emmons, p. 112.

Yeda Peak, Creek

Tahltan word for "the great bear" (Dipper) constellation.

Palgrave, p. 144.

Yagi Ridge

Yagi is the Japanese word for mountain goat, which abound in this area. It is also the name of a famous Japanese volcanologist and teacher who traversed this ridge with me during a visit to Canada.

Field use.

